

THE UNIVERSITY OF HULL

Development and Evaluation of CXCR4 Receptor Targeted Probes for Medical Imaging Applications



being a Thesis submitted for the Degree of
Doctor of Philosophy in the University of Hull

By

Rhiannon Elizabeth Lee, MChem (Hons)

November 2017

I. Abstract

The chemokine receptor CXCR4 has been shown to be overexpressed in over 23 different types of cancers, making it an attractive target for therapeutic and imaging agents. Molecular imaging techniques, such as positron emission tomography (PET) and single photon emission tomography (SPECT), are being used for the development of CXCR4 receptor targeted cancer diagnostic agents. This work exploits the properties of tetraazamacrocycles and their known affinity for the chemokine receptor CXCR4. The inclusion of copper-64, gallium-68, fluorine-18, technetium-99m and optical probes allows the high affinity macrocyclic compounds to be developed as imaging agents.

Copper-64 labelled CXCR4 targeted PET tracers have been reported in the literature (AMD3100 and AMD3465), however, they suffer from transchelation and loss of the radiolabel *in vivo*. Novel tetraazamacrocyclic tracers [⁶⁴Cu][Cu5(OAc)](OAc) and [⁶⁴Cu][Cu₂5(OAc)₂](OAc)₂ were produced in a decay corrected RCY of 41.6 ± 4.6% and 75.4 ± 1.5%. Calcium signalling assays gave an IC₅₀ value of 60 nM and 4 nM, respectively. *In vitro* cell binding experiments showed that [⁶⁴Cu][Cu5(OAc)](OAc) had a higher affinity for the CXCR4 receptor when compared to other CXCR4 imaging tracers. *In vivo* experiments carried out in mice revealed the tracer [⁶⁴Cu][Cu5(OAc)](OAc) to be specific to CXCR4 with an 8-fold higher uptake seen in the CXCR4 positive cell lines compared to the negative; (23.6 ± 2.7; 3.0 ± 0.5 respectively). Importantly no liver uptake was seen when a blocking dose was administered, indicating the improved stability of the CB cyclam structure.

Several approaches for developing a novel gallium-68 CXCR4 targeted PET tracer were investigated. *In vitro* and *in vivo* data showed that the inclusion of DOTAGA in [Zn₂29(OAc)₂](OAc)₂ resulted in a decrease in affinity. Alternative PEG chain spacer and pretargeted approaches were investigated to overcome this issue. A THP analogue of Pentixafor (**P5**) was synthesised and radiolabelled in a 76.8% decay corrected RCY. *In vivo* studies were carried out and showed that the lipophilicity of the THP moiety is detrimental to the biodistribution of the tracer. Inorganic radiofluorination was attempted for the synthesis of fluorine-18 labelled CXCR4 targeting PET probes; with the antagonist [Zn₂AlF43(OAc)₂](OAc)₂ showing high affinity towards the receptor (IC₅₀ = 20 nM).

Novel CXCR4 targeted SPECT tracers such as [^{99m}Tc][Cu₂Tc51(OAc)₂](OAc)₂ (IC₅₀ = 16 nM) were synthesised and radiolabelled at up to 46.0% RCY. Optical imaging CXCR4 probes were also developed including a novel aza-BODIPY labelled peptide (**P7**). The antagonist maintained high affinity (IC₅₀ = 42 nM) towards the CXCR4 receptor with initial confocal experiments indicating that the NIR probe is worthy of further investigation.

II. Acknowledgments

I would like to thank Professor Steve Archibald for his ongoing support during my PhD as my primary supervisor, and Dr Chris Cawthorne, my secondary supervisor. I would also like to thank Dr Juozas Domarkas for his expertise, patience and wisdom, as well as always having a cup of tea ready in my hour of need!

I would also like to thank all members of the Archibald group, past and present, and friends I have made along the way (Andrea, Alicija, Becky, Britney, Cecilia, Ellis, Fada, Farah, George, Guy, Hannah, Hayley, Isaline, James, Jordan, Michelle, Miffy, Mitch, Peter, Tom, Tahani, Shubhanchi, and Zainab); for all their help and support. There are many people whose direction, advice, support and friendship has proved invaluable along the way. In particular, a big thank you to the talented biologists who I have been fortunate to work with, Cecilia, Shubhanchi and James, all of whom have increased my understanding and have contributed to the work presented here. I have been extremely fortunate to have wonderful Master's and summer students (Peter, George, Anne, Kati and Brad) who's contributions have always been valuable.

A huge thank you is also owed to Zainab Ali-Ali, Rebecca Hargreaves and Miffy Cheng who have supplied me with some of the compounds reported herein. I wish to thank Carol Kennedy for performing all my CHN analysis. I wish to thank the people involved in conducting MS analysis on my samples: EPSRC National Mass Spectrometry Service Centre and Dr Kevin Welham (Hull). I would like to acknowledge Prof. Dominique Schol's group in Belgium for performing biological assays on my compounds.

Finally, I would like to show my appreciation to my friends and family, as without them this achievement would not have been possible. Firstly, a big thank you to Georgia; the balloon to my rock, for your constant unwavering support and positivity. Thank you also to my brother Joshua, for making me laugh when I needed it. I would also like to thank my parents who were by my side in helping me overcome every obstacle. Without your patience, support and determination I would have never have been able to master my dyslexia and excel in academia, therefore, this is as much your achievement as it is mine (even though after 3 years you still do not know what I do!).

A tremendous thank you is also owed to Mark, for believing and supporting me throughout this PhD and beyond. Thank you for listening to me discuss my work in the dead of night, thank you for comforting me when it all went wrong, thank you for celebrating with me when it went right and thank you most importantly for loving me. I love you.

III. Risk assessment

All experiments were carried out in accordance with the University of Hull's Health and Safety guidance. All full COSHH and risk assessment was carried out for each new experiment, signed by the participating student, supervisor (Professor S. Archibald) and the departmental safety officer (Dr T. McCreedy) before any practical work was undertaken.

IV. Abbreviations

λ	Wavelength
λ_{\max}	Maximum Wavelength
λ_{\min}	Minimum Wavelength
λ_{abs}	Maximum Absorption
λ_{em}	Emission Wavelength
[¹⁸ F]FDG	[¹⁸ F]2-deoxy-2-fluoro-glucose
α	Alpha Particle
Å	Angstrom
ADME	Absorption, Distribution, Metabolism, and Excretion
AIBN	Azobisisobutyronitrile
AIDS	Acquired Immune Deficiency Syndrome
Alloc	Allyloxycarbonyl
AMD3100	1,1-[1,4-Phenylenebis(methylene)]bis [1,4,8,11-tetraazacyclotetradecane]
AMBA	4-(Aminomethyl)benzoic acid
Arg	Arginine
Asp	Aspartic Acid
AzMBA	4-(Azidomethyl)benzoic acid
β^-	Electron (beta minus)
β^+	Positron (beta plus)
BFC	Bifunctional Chelator
Boc	<i>tert</i> -Butyloxycarbonyl
BODIPY	Boron dipyrromethene difluoride
BP	Boiling point
br	Broad signal
c	Concentration
CB	Cross-bridged
CC ₅₀	Cytotoxic Concentration required to reduce a population by 50%
Cit	Citrulline
COPD	Chronic Obstructive Pulmonary Disease
COSHH	Control of Substances Hazardous to Health
CT	Computed Tomography
Cyclam	1,4,8,11-Tetraazacyclotetradecane
Cylen	1,4,7,10-Tetraazacyclododecane

Cys	Cysteine
δ	Chemical shift
<i>d</i>	Day
d	Doublet
DBU	1,8-Diazabicyclo(5.4.0)undec-7-ene
DCM	Dichloromethane
DFO	Desferrioxamine B
dd	Double doublet
Ddp	N-[1-(4,4-Dimethyl-2,6-dioxo-cyclohexylidene)ethyl]
DIPEA	N,N-Diisopropylethylamine
DMF	N,N'-Dimethylformamide
DMSO	Dimethylsulfoxide
DOTA	1,4,7,10-tetraazacyclododecane-1,4,7,10-tetraacetic acid
DOTAGA	2-(4,7,10-tris(carboxymethyl)-1,4,7,10-tetraazacyclododecan-1-yl)pentanedioic acid
DPAA	Diphenylarsinic acid
dt	Double triplet
DTPA	Diethylenetriaminepentaacetic Acid
ϵ	Molar Absorptivity Coefficient
EC ₅₀	Effective concentration required to reduce an effect by 50%
EDTA	2-((2-[Bis(carboxymethyl)amino]ethyl)(carboxymethyl)amino)acetic acid
EGFR	Epidermal growth factor receptor
ESI	Electrospray ionisation
EtOH	Ethanol
FACS	Fluorescence activated cell sorting
FDA	Food and Drug Administration
FDG	2-Deoxy-2-fluoro-D-glucose
FITC	Fluorescein Isothiocyanate
Fmoc	Fluorenylmethyloxycarbonyl Chloride
Φ_f	Fluorescence Quantum Yield
γ	Gamma
Glu	Glutamic Acid
Gly	Glycine
h	Hour
HATU	1-[Bis(dimethylamino)methylene]-1H-1,2,3-triazolo[4,5-b]pyridinium 3-oxid hexafluorophosphate

HBTU	O-(benzotriazol-1-yl)-N,N,N',N'-tetramethyluronium hexafluorophosphate
HEPES	4-(2-Hydroxyethyl)-1-piperazineethanesulfonic acid
HILC	Hydrophilic Interaction Liquid Chromatography
HFIP	Hexafluoro-2-propanol
His	Histidine
HIV	Human immunodeficiency virus
HPLC	High Performance Liquid Chromatography
HRMS	High Resolution Mass Spectrometry
HSC	Haematopoietic Stem Cell
HYNIC	Hydrazinonicotinamide
IBD	Inflammatory Bowel Disease
IC ₅₀	Concentration required to inhibit binding by 50%
ID/g	Incubated Dose per Gram
IIDA	Inverse-demand Diels-Alder
IGC	Indocyanine Green
<i>J</i>	Coupling constant
kDa	Kilodaltons
keV	Kiloelectronvolts
Lys	Lysine
M	Molar
m	Multiplet
Me	Methyl
mAb	Monoclonal Antibodies
MB	Methylene Blue
MBq	Megabecquerel (10 ⁶ Bq)
MeV	Megaelectronvolts
MHz	Megahertz
Mm	Millimetres
μM	Micromolar
μmol	Micromolar
MRI	Magnetic Resonance Imaging
MS	Mass Spectrometry
MTBE	Methyl <i>tert</i> -butyl Ether
n	Neutron
Nal	Naphthylalanine
NBS	N-Bromosuccinimide

NIR	Near Infrared
NHS	N-hydroxysuccinimide
nm	Nanometres
nM	Nanomolar
NMP	N-Methyl-2-pyrrolidone
NMR	Nuclear Magnetic Resonance
NODA	1,4,7-triazacyclononane-1,4-diacetate
NOTA	1,4,7-triazacyclononane-1,4,7-triacetic acid
OI	Optical Imaging
Orn	Ornithine
p	Proton
Pbf	Pentamethyl-2,3-dihydrobenzofuran-5-sulfonyl
PBS	Phosphate buffer solution
PEG	Polyethyleneglycol
PET	Positron Emission Tomography
pm	Picometers
ppm	Parts per million
Pro	Proline
q	Quartet
RA	Rheumatoid Arthritis
RBC	Red Blood Cell
RCY	Radiochemical yield
RDG	Arginine-Glycine-Aspartate
R _f	Retention factor
RT	Room temperature
s	Singlet
S ₀	Ground state
SB	Side-bridged
SCLC	Small Cell Lung Cancer
SDF-1	Stromal Cell-derived Factor 1 (CXCL12)
sec	Second
SEM	Standard Error of the Mean
SM	Starting material
SOD	Superoxide Dismutase
SPR	Surface Plasmon Resonance
SPAAC	Strain-Promoted Alkyne-Azide Cycloaddition

SPECT	Single Positron Emission Computed Tomography
SSR2	Signal Sequence Receptor 2
SSR3	Signal Sequence Receptor 3
SSR5	Signal Sequence Receptor 5
SUV	Standardised Uptake Value
t	Triplet
TEA	Triethylamine
TE2A	4,11-bis(Carboxymethyl)-1,4,8,11-tetraazabicyclo[6.6.2]hexadecane
TETA	1,4,8,11-Tetraazacyclotetradecane-1,4,8,11-tetraacetic acid
TFA	Trifluoroacetic Acid
THF	Tetrahydrofuran
THP	Tris(hydroxypyridinone)
Thr	Threonine
TLC	Thin Layer Chromatography
TRAP	1,4,7-Triazacyclononane-1,4,7-tris[methyl(2-carboxyethyl)phosphinic acid]
Trt	Trityl
TM	Transmembrane
Tyr	Tyrosine
UK	United Kingdom
US	Ultrasound
USA	United States of America
UV	Ultra-Violet
UV-vis	Ultra-Violet-visible

V. LIST OF FIGURES

Figure 1. Toshiba Celesteion PET-CT system. (Reproduced from Toshiba America Medical Systems). ⁷	3
Figure 2. Diagram showing the principle involved in undertaking a PET scan.	4
Figure 3. Molecular structure of radiotracer [¹⁸ F]-fluorodeoxyglucose (FDG).	5
Figure 4. Periodic table where shaded elements represent radionuclides with uses or identified potential for imaging and therapy; γ -emitters (pink) for SPECT, β^+ emitters (purple) for PET and β^- , α and auger-emitting radioisotopes (orange). (Inspired by figure reported by Blower <i>et al.</i>). ¹⁴	6
Figure 5: The process of production of PET radiotracers. From top the generation of a radioisotope via commercial generator or cyclotron; radiolabelling the chelator inside a hot cell; purification of the radiotracer; administration of the radiotracer; scanning and generation of a processed PET image.	10
Figure 6: Nuclear decay characteristics of germanium-68 to gallium-68.	12
Figure 7: Diagram showing how macrocyclic and acyclic chelators encapsulate radiometal ions.	16
Figure 8: Common derivative BFCs of DOTA.	19
Figure 9: Structures of derivatives of TETA.	21
Figure 10: Diagram showing the sub-classes of chemokine receptors, their ligands and their association to disease. The receptors for the CXC subclass are shown in blue, the receptors for the CC subclass are shown in red and the receptors for the C and CX3C class are shown in green. (Inspired by figures reported by Wells <i>et al.</i> and Proudfoot <i>et al.</i>). ^{112, 113}	23
Figure 11: Schematic representation of the seven transmembrane helices of the CXCR4 receptor. Amino acids shaded red (Asp171, Asp262 ect.) shown to be key site for binding. (Reproduced from Fruehauf <i>et al.</i>). ¹¹⁶	24
Figure 12: Imaging showing chemokine receptors CCR5 and CXCR4 are the two possible co-receptors for HIV entry. (Image reproduced from Liang <i>et al.</i>). ¹²³	25
Figure 13: Schematic representation of the interaction between CXCR4 and a radiolabelled imaging agent.	27
Figure 14: Structure of T140 and radiolabelled derivative.	28
Figure 15: Structures of T140 radiolabelled derivatives for PET imaging.	30
Figure 16: Structures of FC131 and Pentixafor (CPCR4.2 DOTA) derivative.	31
Figure 17: Example of high tumour-to-background ratios in multiple-myeloma patient. Shown are maximum-intensity projections (A, left; B, right) as well as trans axial slices 40 (A) and 236 (B) minutes after injection with [⁶⁸ Ga]Pentixafor. (Reproduced from Herrmann <i>et al.</i>). ¹⁷¹	32
Figure 18: Structures of novel CXCR4 antagonist target compounds that are synthesised in this work and tested <i>in vivo</i>	34
Figure 19: Timeline of the discoveries that shaped the development of AMD3100 and its uses.	37
Figure 20. Structures involved in the discovery process of AMD3100.	38
Figure 21. Diagram showing AMD3100 interactions in the CXCR4 receptor. (Reproduced from Pérez-Nueno <i>et al.</i>). ¹⁷⁹	38
Figure 22: The six configurations of metal-cyclam complexes.	40
Figure 23: Structures of radiolabelled AMD3100.	41
Figure 24: PET/CT scan of mice bearing both CXCR4-positive and CXCR4-negative tumours (hollow arrow and solid arrow respectively). B = bladder; K = kidney; L = liver. A: Mouse injected only with copper-64 AMD3100. B: Blocking study in which mouse was injected first with AMD3100, then with [⁶⁴ Cu][CuAMD3100] ²⁺ . C: Biodistribution study in which [⁶⁴ Cu]CuCl ₂ was injected into the mouse. (Reproduced from Nimmagadda <i>et al.</i>). ¹⁸⁹	42
Figure 25. Structure of mono-macrocyclic radiolabelled derivatives AMD3465.	43
Figure 26: A: PET scan of mouse bearing CXCR4-positive tumour on right shoulder and CXCR4-negative tumour on left shoulder after injection with [⁶⁴ Cu]CuL9 ²⁺ . B: Blocking dose of [CuAMD3465] ²⁺ followed by [⁶⁴ Cu]CuL9 ²⁺ . C: Biodistribution study in which [⁶⁴ Cu]CuCl ₂ was injected into the mouse. (Reproduced from De Silva <i>et al.</i>). ¹⁹⁵	44
Figure 27: Structure and geometry of side-bridged (SB) cyclam & cross-bridge (CB) cyclam.	45

Figure 28: Cross bridged restricted macrocycles ligands that were complexed with zinc and copper (reproduced from Maples et al.). ²⁰²	45
Figure 29: Structure of unlabelled mono-macrocycle configurational constricted derivatives of AMD3465.	46
Figure 30: A) PET/CT Scan with [⁶⁴ Cu][Cu L17] ²⁺ (left), and AMD3465 blocking dose followed by [⁶⁴ Cu][Cu L20] ²⁺ (right); B) PET/CT Scan with [⁶⁴ Cu][Cu L21] ²⁺ (left), and AMD3465 blocking dose followed by [⁶⁴ Cu][Cu L18] ²⁺ , C) PET/CT Scan with [⁶⁴ Cu]AMD3465, 18. Filled arrow, U87-CXCR4 tumour (right); unfilled arrow, control U87 tumour (left); L – liver, K – kidney, I – intestines. (Reproduced from Woodard et al.). ²⁰³	46
Figure 31: Ortho-, meta- and para- derivatives (L19-28) of bis-azamacrocycles with determined EC ₅₀ values determined from anti-HIV infection assays, (reproduced from Bridger et al. and Tanaka et al.). ^{187, 204}	48
Figure 32: Configurationally restricted macrocycles and metal derivatives synthesised by the Archibald group. ^{199, 200, 205, 206}	49
Figure 33: A) Structure of CB para-bis tetraazamacrocycle, 5 , and the bis-copper derivative [Cu ₂ 5 (OAc) ₂](OAc) ₂ ; B) Representation of binding of [Cu ₂ 5 (OAc) ₂](OAc) ₂ with two Aspartate ligands on CXCR4 receptor.	49
Figure 34: Investigation of the receptor residence time of AMD3100 and derivatives. [Cu ₂ 5 (OAc) ₂](OAc) ₂ , (blue) shows the highest receptor residence time. ¹⁹⁸	50
Figure 35: Structures of copper-64 radiolabelled CB macrocycles of chelator 5	50
Figure 36: Structure of various transitional metal complexes of CXCR4 antagonist 5 , 8 and 9	53
Figure 37: Structures of cyclopentapeptides CPCR4.2 (P2) and structure of P3 includes an azide group for subsequent click chemistry.	54
Figure 38: Synthetic route for azide peptide P2 , (CPCR4.2 azide) using resin synthesis. Alternatively for the synthesis of P3 , instead of spacer AzMBA being used; AMBA was used instead.	56
Figure 39: HPLC chromatograph of the chelation of P4 with gallium(III) nitrate.	58
Figure 40: Structures of cyclam based BFC for complexation with copper-64.	61
Figure 41: A) Radio-TLC (neutral alumina, eluting in MeOH:H ₂ O 95:5 with excess NaCl) for [⁶⁴ Cu][Cu 5 (OAc)](OAc); B) Radio-HPLC trace for [⁶⁴ Cu][Cu 5 (OAc)](OAc).	63
Figure 42: Radio-TLC's taken for the formation of [⁶⁴ Cu][Cu ₂ 5 (OAc) ₂](OAc) ₂ after one hour and three hours; (neutral alumina, eluting in MeOH:H ₂ O 95:5 with excess NaCl).	65
Figure 43: Radio- HPLC chromatograph of [⁶⁴ Cu][Cu 8 (OAc)](OAc).	66
Figure 44: Radio-HPLC chromatograph of [⁶⁴ Cu][Cu 9 (OAc)](OAc).	67
Figure 45: Radio-HPLC chromatograph of [⁶⁸ Ga][Ga P4].	68
Figure 46: CXCR4 expression in A) U87-CXCR4 vs U87 cells and B) MM1.S vs Jurkat as determined by flow cytometry (data collected by Ms. Cecilia Miranda).	69
Figure 47: PET scan of mouse showing mice bearing CXCR4-positive U87-CXCR4 tumours (left) and CXCR4-negative U87 tumours (middle) 90 min after injection of tracer [⁶⁴ Cu][Cu 5 (OAc)](OAc). A blocking study of a CXCR4-positive tumour in which [Cu ₂ 5 (OAc) ₂](OAc) ₂ , was injected followed by tracer [⁶⁴ Cu][Cu 5 (OAc)](OAc).	72
Figure 48: HPLC traces of antagonist 5 and [Cu 5 (OAc)](OAc) run in gradient from 20 mM sodium acetate pH 5 (5%-80%, 30 min) and ethanol.	74
Figure 49: HPLC traces of antagonist [Cu 5 (OAc)](OAc) and [Cu ₂ 5 (OAc) ₂](OAc) ₂ run in gradient from 20 mM sodium acetate pH 3 (5%-80%, 30 min) and ethanol.	75
Figure 50: AMD3100 derivative with inclusion of a PEG chain on the xylyl group for labelling with gallium-68. ⁵³	80
Figure 51: The process of pretargeted PET imaging in a mouse model. Where the blue circle represents the targeting moiety (in this case identified as a CXCR4 antagonist).	83
Figure 52: Pretargeting componets: Tetrazine-DOTA (L48) and trans-cyclooctene-NHS (L49).	83

Figure 53: Small animal SPECT-CT image of live mice bearing colon carcinoma xenograft. a) CC49-TCO followed 24 hours later by [¹¹¹ In][InL17]; b) CC49 (100 mg) followed one day later by [¹¹¹ In][InL17 and c) Rtx-[TCOIn]-1;. (Reproduced from Rossin <i>et al.</i>). ²⁵⁴	84
Figure 54: Examples of the target structures of the gallium-68 CXCR4 antagonist designed and evaluated herein. Both a direct and a pretargeted approach were investigated.	85
Figure 55: The alternative methods for synthesis and radiolabelling of azamacrocyclic CXCR4 antagonists.	86
Figure 56: Structures of DO3A, [Cu25] and radiolabelled [⁶⁸ Ga][Ga25].	87
Figure 57: Plot of log[concentration] versus the percentage of radiolabelling with gallium-68 achieved with the DO3A or [Cu25] starting material.	88
Figure 58: Library of metal complexes formed with zinc(II), copper(II) and nickel(II).....	90
Figure 59: Structures of DOTAGA containing compounds 26 and 27	91
Figure 60: Non-radioactive analogues of compounds 27 and [Zn27(OAc)](OAc) with gallium(III) nitrate.	92
Figure 61: A) Radio-TLC illustrating free ⁶⁸ Ga, in 0.1 M citric acid/trisodium citrate 1:1 buffer; B) Radio-TLC illustrating 100% labelling of ⁶⁸ Ga[4], in 0.1 M citric acid/trisodium citrate 1:1 buffer; C) Graph showing effect of temperature on radiolabelling yield of ligand 27 , (n=3).	95
Figure 62: Graph showing effect of concentration on labelling yield with [⁶⁸ Ga][Ga27].	96
Figure 63: Radio-HPLC chromatograph of [⁶⁸ Ga][GaCu ₂ 29(OAc) ₂](OAc) ₂	99
Figure 64: Effect of varying the concentration of 29 on the labelling yield with gallium-68, (n=3).	99
Figure 65: Cell binding of [⁶⁸ Ga][GaZn ₂ 29(OAc) ₂](OAc) ₂ in U87, U87-CXCR4 and Jurkat cells, data is represented as percentage of incubated dose. Data presented as mean ± standard deviation. % ID = percentage incubated dose. (n=3) (data collected by Ms. Cecilia Miranda).	102
Figure 66: Cell binding of [⁶⁸ Ga][GaP4] in U87-CXCR4 and U87, data is represented as percentage of incubated dose. % ID = percentage incubated dose. (n=3) (data collected by Ms. Cecilia Miranda).	103
Figure 67: Comparison of [⁶⁸ Ga][GaZn ₂ 29(OAc) ₂](OAc) ₂ (black) and [⁶⁸ Ga][GaP4] (orange) uptake in MM1.s tumours expressing low levels of CXCR4. A, B: Time activity curves showing tumour uptake of [⁶⁸ Ga][GaZn ₂ 29(OAc) ₂](OAc) ₂ and [⁶⁸ Ga][GaP4]. C, D) Time activity curves showing liver uptake of [⁶⁸ Ga][GaZn ₂ 29(OAc) ₂](OAc) ₂ 7 and [⁶⁸ Ga][GaP4] (n=3). E) and F): Representative coronal PET/CT image of [⁶⁸ Ga][GaZn ₂ 29(OAc) ₂](OAc) ₂ and [⁶⁸ Ga]Pentixafor uptake in MM.1S tumour-bearing CD-1 nude mice (90 minutes post injection). (Data collected by Ms. Cecilia Miranda).	104
Figure 68: Representative coronal PET/CT image of [⁶⁸ Ga]gallium citrate] scan in wild type nude mice (10 MBq, 90 minutes post injection).	105
Figure 69: Structure of extended mono- copper antagonist; [Cu31(OAc)](OAc)	107
Figure 70: Structures of metal complexes [Cu ₂ 34(OAc) ₂](OAc) ₂ and [Zn ₂ 34(OAc) ₂](OAc) ₂	109
Figure 71: Radio HPLC trace of [⁶⁸ Ga][Ga34], run in acidic conditions after 3 hr.	109
Figure 72: Structure of [Cu ₂ 37(OAc) ₂](OAc) ₂	112
Figure 73: Radio-HPLC trace for the attempted radiolabelling of [⁶⁸ Ga][Ga38].	114
Figure 74: Structures of the alternative TCO and tetrazine click components 39 and 40	115
Figure 75: Structure of THP conjugated CPC4.2 P2 peptide (a Pentixafor analogue)	116
Figure 76: Radio HPLC trace of [⁶⁸ Ga][GaP5]	117
Figure 77: PET scan of [⁶⁸ Ga][GaP4] (A -left) and [⁶⁸ Ga][GaP5] (B - right) uptake in MM.1S tumour-bearing CD-1 nude mice (coronal maximum intensity projections at 46-66 minutes). (Data collected by Dr. C. Cawthorne).....	118
Figure 78: Dynamic tumour time activity curves acquired during 90 mins in mice (SUV _{max}). A) (left) injected with [⁶⁸ Ga][GaP4]; B) (right) injected with [⁶⁸ Ga][GaP5]. Experiments carried out in two mice (a00456 and a00457).	119
Figure 79: Future structure of antagonist L36 , formed from the IDDA reaction between 39 and 40	121
Figure 80: Proposed structure for gallium-68 bis-macrocylic antagonists.	122

Figure 81: Various techniques used for radiolabelling radiopharmaceuticals with fluorine-18 (image adapted from that reported by Cole <i>et al.</i>). ²⁸⁹	124
Figure 82: PET/CT images of MCF-7 tumour-bearing mice using [¹⁸ F][AIFL52] and [¹⁸ F][AIFL53]; scans taken after 60 mins in mice bearing MCF-7 tumours. (Reproduced from Da Pieve <i>et al.</i>) ³⁰⁰	127
Figure 83: a) Representative photograph (left) and PET image (right) of a mouse bearing tumours with different amounts of CHO-CXCR4 cells (20, 40, 60 and 80%) at 1 hr post-injection of [¹⁸ F][AIFNOTA-T140]. B) Western blot of CXCR4 expression by tumours generated by increasing proportion of CHO-CXCR4 cells. (Reproduced from Yan <i>et al.</i>) ³¹²	128
Figure 84: Structures of adapted Pentixafor peptide of Al[¹⁸ F] labelling ; L54 , NODA-Pentixather and L55 , NODA-NCS-Pentixather.	129
Figure 85: Structure of target molecule radiolabelled via aluminium radiofluorination.	130
Figure 86: Structure of compound 42 and the non-radioactive standard [AIF 42].	131
Figure 87: Trial reaction using benzyl-NODA, 42 , to optimise radiolabelling conditions with [¹⁸ F]AIF complex.....	132
Figure 88: Comparative study of labelling compound 42 with [¹⁸ F]AIF with and without the presence of ethanol (n = 4).....	134
Figure 89: Radio-HPLC trace of compound [¹⁸ F][AIF 42]......	136
Figure 90: Effect on radiolabelling yield by varying the volume of AlCl ₃ stock added to each reaction, (n = 3).	136
Figure 91: Graph showing the effect of varying the concentration of benzyl-NODA-amide, 42 on radiolabelling yield, (n = 3).....	137
Figure 92: Graph showing the effect of temperature and concentration on radiolabelling yields of compound 42 , (n = 3).....	138
Figure 93: Structure of compound 43 metal derivatives.	140
Figure 94: Radio-TLC trace of [¹⁸ F][Cu ₂ AIF43(OAc) ₂](OAc) ₂ showing ca. 2% radiolabelling yield.....	141
Figure 95: Radio-HPLC trace of [¹⁸ F][AIF 43].	142
Figure 96: Potential alternative radiotracers that can be formed for compound 43 , [Cu ₂ 43 (OAc) ₂](OAc) ₂ and [Zn ₂ 43 (OAc) ₂](OAc) ₂ with copper-64 for high affinity antagonists of the CXCR4 receptor.	147
Figure 97: Structures of imaging moieties <i>fac</i> -[^{99m} Tc]((CO) ₃ TACN) ⁺ , <i>fac</i> -[^{186/188} Re][Re(CO) ₃ TACN] ⁺ ..	150
Figure 98: Crystal structure of <i>fac</i> -[^{99m} Tc][Tc(O) ₃ TACN] ⁺ . Hydrogen atoms omitted for clarity. (Reproduced from Braband <i>et al.</i>). ³⁵⁹	152
Figure 99: CXCR4 imaging in PC-3 tumour xenografts bearing mice with [^{99m} Tc][TcAMD3100]. A) SPECT image of [^{99m} Tc]AMD3100 and B) digital image of control animal. C) SPECT image after administration of a blocking dose of AMD3100 (20 mg/kg). D) Digital image of the blocked mice. Arrow indicates the tumour. (Reproduced from Hartimath <i>et al.</i>). ³³²	154
Figure 100: Schematic representations for the design of CXCR4 specific SPECT tracers and example of structure of target molecule.....	155
Figure 101: Structures of metal complexation of compound 51 copper(II) and zinc(II); [Cu ₂ 51 (OAc) ₂](OAc) ₂ , and [Zn ₂ 51 (OAc) ₂](OAc) ₂ , respectively.	161
Figure 102: Structure of rhenium cold standards of compound 49 , and of the metal complex of compound 51	163
Figure 103: Graph showing the UV HPLC trace of compound [Re(CO) ₃ 51] ⁺ eluting at 10 min 20 sec.	163
Figure 104: A) Graph showing the overlay HPLC chromatographs of ^{99m} Tc(VII) (green), ^{99m} Tc(I) (purple) species. B) Schematic representation of the radio-TLC of the separation of the of ^{99m} Tc(VII) (green), ^{99m} Tc(I) (purple) species, carried out in saline solution.	164
Figure 105: Radio-HPLC chromatograph of compound [^{99m} Tc][Tc(CO) ₃ 44] ⁺ eluting at 10 min and 20 sec.	165
Figure 106: The effect of varying the concentration (M) of compound 44 on radiolabelling efficiency (n = 3).	167

Figure 107: Radio-HPLC of compound $[^{99m}\text{Tc}][\text{Tc}(\text{CO})_3\mathbf{49}]^+$ taken after 3 hours stability in PBS solution at 37°C.....	168
Figure 108: Structure of technetium-99m radiolabelled compound 51 and bis-copper derivative... 169	169
Figure 109: Radio-HPLC trace of compound $[^{99m}\text{Tc}][\text{Tc}(\text{CO})_3\mathbf{51}]^+$ taken after 3 hours in PBS solution at 37°C.....	170
Figure 110: Radio-HPLC of compound $[^{99m}\text{Tc}][\text{Cu}_2\text{Tc}(\text{CO})_3\mathbf{51}(\text{OAc})_2](\text{OAc})_2^+$ taken after three hours stability in acidic (0.1% TFA) solution at 37°C.....	171
Figure 111: Visualisation of subcutaneous tumours in mice with CXCL12-IRDye800. MCF-7 breast tumour (yellow arrow) and A764 glioma cells (blue arrow) were implanted subcutaneously into the right and left flank respectively. (Reproduced from Meincke <i>et al.</i>). ³⁹⁷	178
Figure 112: A schematic diagram of the fluorescently coupled peptide-conjugates derived for Ac-TZ14011 that have been investigated as optical probes for CXCR4. R1 and R2 indicate the sites of modification outlined in table 24. ³⁹⁹⁻⁴⁰¹	179
Figure 113: Confocal images of 0.1 μM of Ac-TZ14011-FITC distribution in live MDAMB231 and MDAMB231 ^{CXCR4+} tumour cells. (Reproduced from Van de Berg <i>et al.</i>). ⁴⁰⁰	181
Figure 114: Structures of FC131 and bivalent derivatives. ^{405, 407}	182
Figure 115: FACS analysis of MDA-MB-231 cells alone (red), incubated with a 100 nM (blue) and 1000 nM (green) dose of FC131-TexRed for 60 min at 37°C (A), fluorescence microscopy images of MDA-MB-231 cells after incubation with FC131-TexRed(B), co-localization with DAPI (C) (Reproduced from Nomura <i>et al.</i>). ⁴⁰⁷	183
Figure 116: Confocal images for PepR-NIR750 and dye alone (NIR-750) showing binding to B16-CXCR4 tumour cells (Reproduced from Santagata <i>et al.</i>). ⁴⁰⁹	183
Figure 117: Structures of side-bridge cyclam RITC containing CXCR4 antagonists synthesised by Khan <i>et al.</i> ⁴¹⁵	184
Figure 118: Structures of anthracenyl derivatives of AMD3100 and its metal complexes synthesised by Knight <i>et al.</i> ⁴¹⁶	184
Figure 119: Structures of the fluorescent macrocycles synthesised by Oltmanns <i>et al.</i> ⁴¹⁴	185
Figure 120: Structure of AMD3100 BODIPY containing metal complex derivatives. ⁵³	186
Figure 121: Structures of target molecules to be developed for OI of the CXCR4 receptor.	187
Figure 122: Library of configurational restricted fluorescent mono-macrocycles conjugated to rhodamine or fluorescein.	188
Figure 123: Library of configurationally restricted fluorescent bis-macrocycles.	189
Figure 124: Structures of BODIPY-CPCR4.2 conjugates P6 and P7	192
Figure 125: Absorption (blue line) and emission (red line) spectra of P7 . (Date collected by Ms. Miffy Cheng).	193
Figure 126: Flow cytometric histogram plots for binding of 12G5 mAb in competition with peptide P7 at varying concentrations in Jurkat cells.....	194
Figure 128: CXCR4 expression in U87-CXCR4 vs U87 cells as determined by flow cytometry.	195
Figure 129: Confocal microscopy images of peptide P7 in U87-CXCR4 cells at 5 and 10 μM	196
Figure 130: Summary of different modalities for imaging the CXCR4 receptor and examples of antagonists investigated.....	201
Figure 131: Structures of some of the other library of configurationally restricted bis-tetraazamacrocycles CXCR4 antagonists synthesised by the Archibald research group. ^{257, 438}	207
Figure 132: Proposed therapeutic and imaging agents that could be synthesised with the azide CXCR4 peptide P3	208
Figure 133: Confocal microscopy Z-stack (20-slices) images of peptide P7 (10 μM) in U87-CXCR4 cells.	362
Figure 134: Confocal microscopy images of peptide P7 in U87 and U87-CXCR4 cell, along with a control autofluorescence image of cells alone.	363
Figure 135: Confocal images of competition/blocking experiment of peptide P7 with $[\text{Cu}_2\mathbf{5}(\text{OAc})_2](\text{OAc})_2$ in U87 CXCR4 cells.	363

VII. LIST OF TABLES

Table 1: Comparison of <i>in vivo</i> imaging techniques currently used in medical imaging. ³⁻⁵	0
Table 2: Details of the different properties and production method of common radioisotopes in nuclear imaging. ¹⁵	7
Table 3: Table listing some of the generator pairs and half-lives. ¹⁹	8
Table 4: Key emission for copper-60, copper-61, copper-62 and copper-64. For β^+ energies determined as average of end-point energies, weighted by intensity. ⁴⁰	14
Table 5: Average bond dissociation energies and bond length for common radiofluorination approaches. ⁴⁷	15
Table 6: DOTA BFC with relevant radiometal ion, labelling conditions, thermodynamic stability constants ($\log K_{ML}$) and coordination geometries. * Indicates that the donor set is dependent on the metal.	19
Table 7: TETA, and NOTA BFC with relevant radiometal ion, labelling conditions, thermodynamic stability constants ($\log K_{ML}$) and coordination geometries.	20
Table 8: THP acyclic BFC with relevant radiometal ion and labelling conditions	22
Table 9: Different cancers showing an overexpression of chemokine receptors.....	26
Table 10: Summary of biological assay data generated for CXCR4 antagonist determined by antibody displacement in Jurkat cells and calcium signalling in U87-CXCR4 cells. ^a represents data taken from past work carried out by the Archibald group.....	59
Table 11: Reaction conditions used for the labelling of tetraazamacrocyclic ligands with copper-64.62	62
Table 12: Binding of tracers to U87-CXCR4 and U87 cells. Each cell line was incubated with 37 KBq of tracer. ($n = 3$) (Biological data collected by Ms. Cecília Miranda).	69
Table 13: Blocking experiments carried out with 37 KBq of $[^{64}\text{Cu}][\text{Cu}_5(\text{OAc})](\text{OAc})$ were cells were blocked prior to incubation with CXCR4 antagonists. ($n = 1$) (Biological data collected by Ms. Cecília Miranda).....	71
Table 14: Gallium-68 novel PET tracers in clinical evaluation.	79
Table 15: Summary of biological assay data generated for CXCR4 antagonist determined by antibody displacement in Jurkat cells and calcium signalling in U87-CXCR4 cells. ^a represents data taken from past work carried out by the Archibald group.....	93
Table 16: Radiochemical properties of tracers $[^{68}\text{Ga}][\text{Ga}29]$, $[^{68}\text{Ga}][\text{GaCu}_229(\text{OAc})_2](\text{OAc})_2$ and $[^{68}\text{Ga}][\text{GaCu}_229(\text{OAc})_2](\text{OAc})_2$	100
Table 17: Summary of biological assay data generated for CXCR4 antagonist determined by antibody displacement in Jurkat cells and calcium signalling in U87-CXCR4 cells. ^a indicates data taken from past work carried out by the Archibald group.....	101
Table 18: Summary of biological assay data generated for CXCR4 antagonist determined by antibody displacement in Jurkat cells and calcium signalling in U87-CXCR4 cells (* indicates crude sample mixture, not purified by HPLC).....	110
Table 19: Reaction conditions trailed for the labelling of antagonists $[\text{Cu}_243(\text{OAc})_2](\text{OAc})_2$ and 43 with aluminium fluoride-18.	141
Table 20: Table showing the IC_{50} values determined in the calcium signalling assay for macrocyclic compounds. ^a Concentration required to reduce the level of Ca^{2+} ions observed during a 'normal' signalling process by 50% (IC_{50}) in U87-CXCR4 cells.	143
Table 21: Radioisotopes used for different clinical studies by SPECT imaging and their properties.	149
Table 22: Table showing the variations in yield using different buffers and pH values ($n=1$).....	166
Table 23: Table showing the IC_{50} values determined by for bis-macrocyclic compounds. Concentration required to reduce the level of Ca^{2+} ions observed during a 'normal' signalling process by 50% (IC_{50}) in U87-CXCR4 cells.	172
Table 24: Biological activity of fluorescently labelled T140 analogues. ^a IC_{50} values obtained with $[^{125}\text{I}]\text{CXCL12}$ on CHO cells unless otherwise stated; ^b IC_{50} values obtained with $[^{125}\text{I}]\text{CXCL12}$ on HeLa-CD4-CCR5 cells. ^{399, 401}	180

Table 25: Emission and excitation wavelengths of the fluorescent macrocyclic compounds.....	190
Table 26: Photophysical properties of the BODIPY starting material and peptide P7 in PBS at 298K.	193
Table 27: IC ₅₀ values of Pentixafor peptide and aza-BODIPY derivatives. Concentration required to reduce the level of Ca ²⁺ ions observed during a 'normal' signalling process by 50% (IC ₅₀) in U87- CXCR4 cells.	194
Table 28: Copper-64 radiolabelling conditions and information.....	352
Table 29: Gallium-68 radiolabelling conditions and information.	353
Table 30: Fluorine-18 radiolabelling conditions and information.	355
Table 31: Technetium-99m radiolabelling conditions and information.	356

VII. LIST OF SCHEMES

Scheme 1: Synthesis of cross bridge functionalised bis macrocycle	51
Scheme 2: Synthesis route of AMD3100, 8	52
Scheme 3: Synthesis of DO3A conjugated P4	57
Scheme 4: First example of a IDDA reaction reported in 1959 by Carboni and Lindsey.	82
Scheme 5: The IDDA reaction between a 1,2,4,5-tetrazine and a strained trans-cyclooctene dienophile.	82
Scheme 6: Synthetic route for the synthesis of the mono-macrocycles 1 (side bridge) and 2 (cross bridge).....	89
Scheme 7: Synthetic route for the synthesis of the bis-macrocycle 23 and 24	97
Scheme 8: Scheme showing the synthesis of tracers $[\text{Cu}_2\mathbf{29}(\text{OAc})_2](\text{OAc})_2$ and $[\text{Zn}_2\mathbf{29}\text{OAc}]_2(\text{OAc})_2$	98
Scheme 9: Attempted scheme for the synthesis of the extended pegylated antagonist 32	106
Scheme 10: Synthesis of PEG containing compound 34	108
Scheme 11: The synthesis of <i>trans</i> -cyclooctene compound 35	111
Scheme 12: The attempted reaction to produce $[\text{natGa}][\text{Ga}\mathbf{38}]$	113
Scheme 13: Synthesis of $[\text{F}^{18}]\text{AlF}$ NODA complexes L50 and L51 . ^{297, 298}	126
Scheme 14: Synthetic pathway for the formation of compound 43	139
Scheme 15: Attempted ring-opening of diglycolic anhydride and benzyl amine TACN derivative. ...	156
Scheme 16: Attempted synthesis of antagonist with benzyl amine TACN chelated group.	157
Scheme 17: Pathway used for the successful synthesis of compound 49	158
Scheme 18: Route for the synthesis of the TACN conjugated bis-macrocycle antagonist, 51	160
Scheme 19: Scheme showing the synthesis of $[\text{99mTc}(\text{OH}_2)_3(\text{CO})_3]^+$ from $\text{Na}^{99\text{m}}\text{TcO}_4$, followed by labelling with TACN-benzyl amine	164
Scheme 20: Alternative radiolabelling procedure for $[\text{Cu}\mathbf{5}(\text{OAc})](\text{OAc})$ with copper-64 to form $[\text{64Cu}][\text{Cu}_2\mathbf{5}(\text{OAc})_2](\text{OAc})_2$	208

Contents	
I. Abstract.....	ii
II. Acknowledgments.....	iii
III. Risk assessment	iv
IV. Abbreviations.....	v
Chapter One.....	1
Introduction	1
1.1 Medical imaging.....	2
1.1.1 The origins of nuclear medicine.....	2
1.1.2 Medical imaging technologies	2
1.1.3 Positron Emission Tomography (PET) imaging	3
1.1.4 Physical principles of PET	4
1.2 Designing a PET imaging agent	5
1.2.1 Key parameters for consideration in the design of a PET imaging agent.....	5
1.2.2 Radionuclides used in molecular imaging.....	6
1.2.3 Production of a radionuclide.....	8
1.2.3.1 Production of radiometals from a generator.....	8
1.2.3.2 Generation of radiometals from a cyclotron	8
1.2.3.3 Process of generation of radiotracer	9
1.3 Key aspects of radiopharmaceutical chemistry	11
1.3.1 Gallium-68.....	11
1.3.1.1 Chemical properties of gallium	11
1.3.1.2 Properties of gallium radioisotopes.....	11
1.3.1.3 Production of gallium-68 from generators	12
1.3.2 Copper-64.....	13
1.3.2.1 Chemical properties of copper	13
1.3.2.2 Properties of copper radioisotopes	13
1.3.2.3 Production of copper-64.....	14
1.3.3 Fluorine-18	15
1.3.3.1 Chemical properties of fluorine-18.....	15
1.3.3.2 Radiochemical properties of fluorine-18	15
1.3.3.3 Production of fluorine-18.....	15
1.4 Labelling with radiometal isotopes.....	16
1.4.1 Bifunctional chelators (BFCs)	16
1.4.2 The macrocyclic effect.....	17
1.4.3 Design of a chelator for radiometals	17
1.4.4 Commonly used chelators and their compatibility with radiometals	18
1.4.4.1 DOTA as a radiometal chelator	18

1.4.4.2 TETA as a radiometal chelator	20
1.4.4.3 NOTA as a radiometal chelator	21
1.4.4.4 TRAP as a radiometal chelator	21
1.4.4.5 DTPA.....	22
1.4.4.6 THP	22
1.4.4.7 DFO.....	22
1.5 Chemokines and the CXCR4 chemokine receptor	23
1.5.1 Biological role of chemokines and chemokine receptors	23
1.5.2 CXCR4 chemokine receptor	24
1.5.3 Role of the CXCR4 chemokine receptor in diseases	25
1.5.3.1 Role of CXCR4 in Human Immunodeficiency Virus	25
1.5.3.2 Role of CXCR4 in cancer	26
1.6 Development of PET tracers for CXCR4 imaging.....	27
1.6.1 Peptides as CXCR4 imaging probes.....	27
1.6.1.1 T140 and its derivatives	27
1.6.1.2. Cyclopentapeptides as CXCR4 imaging probes.....	31
1.7 Research aims	34
1.6 Summary	35
Chapter Two.....	36
Synthesis and radiolabelling of CXCR4 antagonists with copper-64 for PET imaging	36
2.1.3 AMD3100 derivatives as imaging agents.....	40
Chapter Three	78
Synthesis and radiolabelling of CXCR4 antagonists with gallium-68 for PET imaging.....	78
3.1 Previous research and development of gallium-68 radiotracers	79
3.1.1 Gallium-68 tracers for imaging CXCR4.....	79
3.2 Direct and pretargeted imaging.....	81
3.2.1 Direct approach and alternatives.....	81
3.2.2 Click chemistry approach	81
3.3 Proposed strategy for tetraazamacrocyclic CXCR4 antagonist click derivatives	85
3.4 Design and functionalisation of tetraazamacrocyclic CXCR4 antagonists	86
3.4.1 Position of attachment and order of reactions	86
3.4.2 Competition radiolabelling results.....	87
3.5 Synthesis of tetraazamacrocycles conjugated to a BFC.....	89
3.5.1 Synthesis of the mono-macrocyclic gallium compounds	89
3.6 <i>In vitro</i> testing of the mono-tetraazamacrocyclic compounds	93
3.7 Development of radiolabelling conditions for mono-cyclam DOTAGA compounds	95
3.8 Synthesis of the bis-cyclam/cyclen BFC conjugates and gallium radiolabelling	97
3.8.1 Synthesis of the first and second generation of bis-cyclam/cyclen compounds.....	97

3.8.2 Developing radiolabelling conditions for bis-cyclam/cylen DOTAGA compounds	99
3.9 <i>In vitro</i> CXCR4 binding assays of tetraazamacrocycles	101
3.9.1 Calcium signalling assay	101
3.9.2 CXCR4 expressing cell binding assay with radiotracers	102
3.10 <i>In vivo</i> comparison of [⁶⁸ Ga][GaZn ₂ 29 (OAc) ₂](OAc) ₂	104
3.11 Second generation of DOTAGA conjugated macrocyclic compounds	106
3.11.1 Incorporation of PEG linker between the CXCR4 binding component and the BFC.....	106
3.11.2 Pretargeted <i>in vivo</i> click chemistry CXCR4 antagonists	111
3.12 Tripodal tris(hydroxypyridinone) chelator conjugated CXCR4 binding peptide	116
3.12.1 Synthetic of a THP Pentixafor analogue.....	116
3.12.2 Radiolabelling of the THP-Pentixafor analogue with gallium-68.....	117
3.12.3 <i>In vivo</i> validation of P5	118
3.13 Conclusion.....	120
3.14 Future work.....	121
Chapter 4.....	123
Development of imaging probes for the CXCR4 chemokine receptor labelled with fluorine-18.....	123
4.1 Previously developed strategies and current state-of-the-art	124
4.1.1 Aluminium radiofluorination	125
4.1.2 Fluorine-18 labelled probes for imaging the CXCR4 chemokine receptor	128
4.2 Proposed strategy	130
4.2.1 Synthesis of a test compound.....	131
4.3 Optimisation of radiofluorination conditions using the test compound.....	132
4.3.1 Reaction pH and buffer	133
4.3.2 Effect of the addition of co-solvents.....	133
4.3.3 Optimisation of the concentration of the AlCl ₃ stock.....	135
4.3.4 Optimisation of the concentration of the chelator.....	137
4.3.5 Optimisation of temperature.....	138
4.3.6 Overall optimised conditions and stability	139
4.4 Synthesis of high affinity CXCR4 antagonists for fluorine-18 labelling.....	139
4.4.1 Synthesis of bis-tetraazamacrocycle NODA-amide and metal containing derivatives.....	139
4.4.2 Attempted radiolabelling of bis-tetraazamacrocycle antagonists.....	141
4.5 <i>In vitro</i> CXCR4 binding assays.....	143
4.6 Conclusion.....	145
4.7 Future work.....	146
Chapter Five	148
Synthesis and radiolabelling of CXCR4 antagonists with technetium-99m for SPECT imaging	148
5.1 Previously developed strategies and current state-of-the-art	149
5.1.1 Technetium and rhenium isotopes	149

5.1.2 SPECT tracers to target the CXCR4 receptor.....	152
5.2 Synthetic strategy for next generation ^{99m} Tc tracers.....	155
5.2.1 Mono-macrocyclic CXCR4 antagonists conjugated to TACN.....	156
5.2.2 Bis-macrocyclic TACN conjugated CXCR4 receptor antagonists.....	159
5.3 Radiolabelling with technetium-99m.....	163
5.3.1 Introduction and past strategies.....	163
5.3.2 Preparation of technetium-99m tricarbonyl.....	164
5.3.3 Optimisation of radiolabelling conditions for 44	165
5.3.4 Radiolabelling of 49	168
5.3.5 Radiolabelling of 51 and its derivatives.....	169
5.4 <i>In vitro</i> CXCR4 receptor binding studies.....	172
5.5 Conclusion.....	174
5.6 Future work.....	175
Chapter Six.....	176
Synthesis of fluorescent dye labelled CXCR4 imaging probes.....	176
6. Strategy for optical probe design and current state-of-the-art in CXCR4 optical imaging.....	177
6.1 Introduction to optical imaging.....	177
6.2 Overview of optical imaging probes for the the CXCR4 receptor.....	177
6.2.1 Optical imaging probes to target CXCR4 derived from CXCL12.....	177
6.2.2 Optical imaging probes to target CXCR4 derived from peptides.....	179
6.2.3 Optical imaging probes derived from small molecule antagonists of CXCR4.....	183
6.3 Proposed strategy to synthesise azamacrocyclic CXCR4 binding compounds conjugated to fluorescent dyes.....	187
6.4 Synthesis of library of fluorophore macrocyclic compounds.....	187
6.4.1 Mono-macrocyclic fluorescent compounds.....	187
6.4.2 Bis-configurational constricted library of fluorescent compounds.....	189
6.5 Strategy to synthesise CXCR4 binding peptides conjugated to a near-IR emitting dye.....	191
6.5.1 Proposed strategy to produce CXCR4.2 conjugates with aza-BODIPY.....	191
6.5.2 Synthesis of the aza-BODIPY conjugated peptide.....	192
6.5.3 <i>In vitro</i> CXCR4 binding assays for the aza-BODIPY peptide conjugate.....	194
6.6 Conclusion.....	198
6.7 Future work.....	199
Chapter Seven.....	200
Conclusion.....	200
7. Conclusion.....	201
7.1 Overview.....	201
7.2 Main achievements in this work.....	202
7.3 Wider context and applicability of some aspects of the research.....	204

Chapter Eight	205
Future Work	205
8. Future work.....	206
8.1 Short-term goals	206
8.2 Long-term goals	207
8.2.1 Synthesis	207
8.2.2 Radiolabelling and Biological validation	208
Chapter Nine	210
Experimental	210
9.1. General Method.....	211
9.1.1 General notes.....	211
9.1.2 NMR spectroscopy	211
9.1.3 Mass Spectrometry	211
9.1.4 Elementary analysis	211
9.1.5 Radio-Thin layer chromatography (Radio-TLC).....	211
9.1.6 UV-visible Spectroscopy.....	211
9.1.7 Fluorescence Spectroscopy.....	211
9.1.8 Materials	212
9.2 HPLC purification.....	213
9.2.1 Analytical.....	213
9.2.2 Semi-preparative.....	216
9.3 Compound Synthesis.....	220
9.3.1 Synthesis of <i>cis</i> -3,5,8,10-tetraazaperhydropyrene (1) and <i>cis</i> -13-1,4,7,10-tetraazatetracyclo[5.5.1.0 ^{4,14} 0 ^{10,13}]tetradecane (2)	220
9.3.2 Synthesis of <i>cis</i> -3,3'-(1,4-phenylenebis(methylene))-bis(decahydro-3,5,8,10-tetraazapyrenim) dibromide (3)	222
9.3.3 Synthesis of 3-(4(8-methyl- <i>cis</i> -decahydro-(5,10-diaza-bicyclo[6.6.2]hexadeco-11-ylmethyl)-benzyl)-1,4,8,11-tetraaza-bicyclo[6.6.2]-hexadecane (4).....	223
9.3.4 Synthesis of 1,4-bis((11-methyl-1,4,8,11-tetraazabicyclo[6.6.2]hexadecan-4-yl)methyl)benzene (5).....	224
9.3.5 Synthesis of mono metal complexes of ligand 1,4-bis((11-methyl-1,4,8,11-tetraazabicyclo[6.6.2]hexadecan-4-yl)methyl)benzene ([Ni 5 (OAc)](OAc), [Cu 5 (OAc)](OAc), and [Zn 5 (OAc)](OAc)).....	225
9.3.6 Synthesis of bis copper complexes of ligand 1,4-bis((11-methyl-1,4,8,11-tetraazabicyclo[6.6.2]hexadecan-4-yl)methyl)benzene ([Cu ₂ 5 (OAc) ₂](OAc) ₂)	227
9.3.7 Synthesis of 1,4,8-tris(<i>tert</i> -butoxycarbonyl)-1,4,8,11-tetraazacyclotetradecane (6).....	228
9.3.8 Synthesis of hexa- <i>tert</i> -butyl-11,11'-(1,4-phenylenebis(methylene))bis(1,4,8,11-tetraazacyclotetradecane-1,4,8-tricarboxylate (7)).....	229
9.3.9 Synthesis of 1,1'-(1,4-phenylenebis(methylene))bis-1,4,8,11-tetraazacyclotetradecane octahydrochloride (8)	230

9.3.10 Synthesis of mono metal complexes of 1,1'-(1,4-phenylenebis(methylene))bis(1,4,8,11-tetraazacyclotetradecane) ([Ni 8 (OAc)](OAc), [Cu 8 (OAc)](OAc) and [Zn 8 (OAc)](OAc)).....	231
9.3.11 Synthesis of copper complexed AMD3465 hexahydrobromide ([Cu 9 (OAc)](OAc))	233
9.3.12 Synthesis of 3a-(4-(bromomethyl)benzyl)-decahydro-3a,5a,8a,10a-tetraaza-pyrenium bromide (10)	234
9.2.13 Synthesis of 1-(4-cyanobenzyl)-1,4,8,11 tetraazabicyclo[10.2.2]-hexadecane (11).....	235
9.3.14 Synthesis of 1-(4-aminomethylbenzyl)-1,4,8,11-tetraazabicyclo[10.2.2]-hexadecane (12)	237
9.3.15 Synthesis of metal complexes of ligands 1-(4-aminomethylbenzyl)-1,4,8,11-tetraazabicyclo[10.2.2]-hexadecane ([Ni 12 (OAc)](OAc), [Cu 12 (OAc)](OAc) and [Zn 12 (OAc)](OAc)	238
9.3.16 Synthesis of 3a-(4-cyanobenzyl)-8a-(methyl)-decahydro-3a,5a,8a,10a-tetraaza-pyrenium diiodide (13).....	240
9.3.17 Synthesis of 1-(4-cyanobenzyl)-8-(methyl)-1,4,8,11-tetraazabicyclo[6.6.2]-hexadecane (14).....	241
9.3.18 Synthesis of 1-(4-aminomethylbenzyl)-8-(methyl)-1,4,8,11-tetraazabicyclo[6.6.2]-hexadecane (15).....	242
9.3.19 Synthesis of metal complexes of ligands 1-(4-aminomethylbenzyl)-8-(methyl)-1,4,8,11-tetraazabicyclo[6.6.2]hexadecane ([Ni 15 (OAc)](OAc), [Cu 15 (OAc)](OAc) and [Zn 15 (OAc)](OAc))	243
9.3.20 Synthesis of 3a-(4-(bromomethyl)benzyl)dodecahydro-6H-3a,5a,8a,10a-tetraazapyren-3a-ium bromide (16)	245
9.3.21 Synthesis of 2a-(4-nitrobenzyl)-decahydro-2a,4a,6a,8a-tetraaza-pyrenium bromide (17), and 2a-(4-cyanobenzyl)-decahydro-2a,4a,6a,8a-tetraaza-pyrenium bromide (18).....	246
9.3.23 Synthesis of 2a-(4-nitrobenzyl)-6a-(4-((decahydro-3a,5a,8a,10a-tetraaza-pyren-3a-ium)methyl)benzyl) tribromide (19), and 2a-(4-cyanobenzyl)-6a-(4-((decahydro-3a,5a,8a,10a-tetraaza-pyren-3a-ium)methyl)benzyl)-decahydro-2a,4a,6a,8a-tetraazapyrenium tribromide (20)	248
9.3.24 Synthesis of 1-(4-nitrobenzyl)-7-(4-((1,4,8,11-tetraazabicyclo[10.2.2]hexadecane)methyl)benzyl)-1,4,7,10-tetraazabicyclo[5.5.2]dodecane (21), and 1-(4-cyanobenzyl)-7-(4-((1,4,8,11-tetraazabicyclo[10.2.2]hexadecane)methyl)benzyl)-1,4,7,10-tetraazabicyclo[5.5.2]dodecane (22)	250
9.3.25 Synthesis of metal complexes of 1-(4-(aminomethyl)benzyl)-7-(4-((1,4,8,11-tetraazabicyclo[10.2.2]hexadecane)methyl)benzyl)-1,4,7,10-tetraazabicyclo[5.5.2]dodecane ([Ni 22 (OAc) ₂](OAc) ₂ , [Cu 22 (OAc) ₂](OAc) ₂ and [Zn 22 (OAc) ₂](OAc) ₂)	252
9.3.26 Synthesis of 1-(4-aminobenzyl)-7-(4-((1,4,8,11-tetraazabicyclo[10.2.2]hexadecane)methyl)benzyl)-1,4,7,10-tetraazabicyclo[5.5.2]dodecane (23)	254
9.3.27 Synthesis of metal complexes of 1-(4-(aminomethyl)benzyl)-7-(4-((1,4,8,11-tetraazabicyclo[10.2.2]hexadecane)methyl)benzyl)-1,4,7,10-tetraazabicyclo[5.5.2]dodecane ([Cu 23 (OAc) ₂](OAc) ₂ and [Zn 23 (OAc) ₂](OAc) ₂)	255
9.3.28 Synthesis of 1-(4-(aminomethyl)benzyl)-7-(4-((1,4,8,11-tetraazabicyclo[10.2.2]hexadecane)methyl)benzyl)-1,4,7,10-tetraazabicyclo[5.5.2]dodecane (24)	257

9.3.29 Synthesis of metal complexes of 1-(4-(aminomethyl)benzyl)-7-(4-((1,4,8,11-tetraazabicyclo[10.2.2]hexadecane)methyl)benzyl)-1,4,7,10-tetraazabicyclo[5.5.2]dodecane ([Cu ₂ 24 (OAc) ₂](OAc) ₂ and [Zn ₂ 24 (OAc) ₂](OAc) ₂).....	258
9.3.30 Synthesis of 2,2',2''-(1,4,7,10-tetraazacyclododecane-1,4,7-triyl)triacetic acid copper(II) acetate ([Cu 25])	260
9.3.31 Synthesis of 2,2',2''-(10-(4-((4-((1,5,8,12-tetraazabicyclo[10.2.2]hexadecan-5-yl)methyl)benzyl)amino)-1-carboxy-4-oxobutyl)-1,4,7,10-tetraazacyclododecane-1,4,7-triyl)triacetic acid (26).....	261
9.3.32 Synthesis of metal complexes of 2,2',2''-(10-(4-((4-((1,5,8,12-tetraazabicyclo[10.2.2]hexadecan-5-yl)methyl)benzyl)amino)-1-carboxy-4-oxobutyl)-1,4,7,10-tetraazacyclododecane-1,4,7-triyl)triacetic acid ([Ni 26 (OAc)](OAc), [Cu 26 (OAc)](OAc), and [Zn 26 (OAc)](OAc)).....	262
9.3.33 Synthesis of 2,2',2''-(10-(1-carboxy-4-((4-((11-methyl-1,4,8,11-tetraazabicyclo[6.6.2]hexadecan-4-yl)methyl)benzyl)amino)-4-oxobutyl)-1,4,7,10-tetraazacyclododecane-1,4,7-triyl)triacetic acid (27).....	264
9.3.34 Synthesis of 2,2',2''-(10-(1-carboxy-4-((4-((11-methyl-1,4,8,11-tetraazabicyclo[6.6.2]hexadecan-4-yl)methyl)benzyl)amino)-4-oxobutyl)-1,4,7,10-tetraazacyclododecane-1,4,7-triyl)triacetic acid metal derivatives ([Cu] 27 and [Zn] 27)	265
9.3.35 Synthesis of 2,2',2''-(10-(1-carboxy-4-((4-((11-methyl-1,4,8,11-tetraazabicyclo[6.6.2]hexadecan-4-yl)methyl)benzyl)amino)-4-oxobutyl)-1,4,7,10-tetraazacyclododecane-1,4,7-triyl)triacetic acid (27) with gallium(III) to form ([^{nat} Ga 27]).....	267
9.3.36 Synthesis of metal complexes of 2,2',2''-(10-(1-carboxy-4-((4-((11-methyl-1,4,8,11-tetraazabicyclo[6.6.2]hexadecan-4-yl)methyl)benzyl)amino)-4-oxobutyl)-1,4,7,10-tetraazacyclododecane-1,4,7-triyl)triacetic acid zinc(II) acetate ([Zn 27 (OAc)](OAc)) with gallium(III) to form ([^{nat} GaZn 27 (OAc)](OAc))	268
9.3.37 Attempted synthesis of 2,2',2''-(10-(4-((4-((10-(4-((1,5,8,12-tetraazabicyclo[10.2.2]hexadecan-5-yl)methyl)benzyl)-1,4,7,10-tetraazabicyclo[5.5.2]tetradecan-4-yl)methyl)phenyl)amino)-1-carboxy-4-oxobutyl)-1,4,7,10-tetraazacyclododecane-1,4,7-triyl)triacetic acid (28).....	269
9.3.38 Attempted synthesis of 2,2',2''-(10-(4-((4-((10-(4-((1,5,8,12-tetraazabicyclo[10.2.2]hexadecan-5-yl)methyl)benzyl)-1,4,7,10-tetraazabicyclo[5.5.2]tetradecan-4-yl)methyl)phenyl)amino)-1-carboxy-4-oxobutyl)-1,4,7,10-tetraazacyclododecane-1,4,7-triyl)triacetic acid metal complexes ([Cu ₂ 28 (OAc) ₂](OAc) ₂ and [Zn ₂ 28 (OAc) ₂](OAc) ₂).....	270
9.3.39 Synthesis of 2,2',2''-(10-(4-((4-((10-(4-((1,5,8,12-tetraazabicyclo[10.2.2]hexadecan-5-yl)methyl)benzyl)-1,4,7,10-tetraazabicyclo[5.5.2]tetradecan-4-yl)methyl)benzyl)amino)-1-carboxy-4-oxobutyl)-1,4,7,10-tetraazacyclododecane-1,4,7-triyl)triacetic acid (29).....	272
9.3.40 Synthesis of 2,2',2''-(10-(4-((4-((10-(4-((1,5,8,12-tetraazabicyclo[10.2.2]hexadecan-5-yl)methyl)benzyl)-1,4,7,10-tetraazabicyclo[5.5.2]tetradecan-4-yl)methyl)benzyl)amino)-1-carboxy-4-oxobutyl)-1,4,7,10-tetraazacyclododecane-1,4,7-triyl)triacetic acid metal complexes ([Cu ₂ 29 (OAc) ₂](OAc) ₂ and [Zn ₂ 29 (OAc) ₂](OAc) ₂).....	273
9.3.41 Synthesis of metal complexes of 2,2',2''-(10-(4-((4-((10-(4-((1,5,8,12-tetraazabicyclo[10.2.2]hexadecan-5-yl)methyl)benzyl)-1,4,7,10-tetraazabicyclo[5.5.2]tetradecan-4-yl)methyl)benzyl)amino)-1-carboxy-4-oxobutyl)-1,4,7,10-tetraazacyclododecane-1,4,7-triyl)triacetic acid of (29) with gallium(III) nitrate to form ([^{nat} Ga 29]).....	275

9.3.42	Synthesis of metal complexes of 2,2',2''-(10-(4-((10-(4-((1,5,8,12-tetraazabicyclo[10.2.2]hexadecan-5-yl)methyl)benzyl)-1,4,7,10-tetraazabicyclo[5.5.2]tetradecan-4-yl)methyl)benzyl)amino)-1-carboxy-4-oxobutyl)-1,4,7,10-tetraazacyclododecane-1,4,7-triyl)triacetic acid of $[\text{Cu}_2\mathbf{29}(\text{OAc})_2](\text{OAc})_2$ and $[\text{Zn}_2\mathbf{29}(\text{OAc})_2](\text{OAc})_2$ with gallium(III) nitrate to form $[\text{natGaCu}_2\mathbf{29}(\text{OAc})_2](\text{OAc})_2$, and $[\text{natGaZn}_2\mathbf{29}(\text{OAc})_2](\text{OAc})_2$	276
9.3.43	Synthesis of (9H-fluoren-9-yl)methyl(1-(4-((11-methyl-1,4,8,11-tetraazabicyclo[6.6.2]hexadecan-4-yl)methyl)phenyl)-3-oxo-6,9,12,15,18-pentaoxa-2-azaicosan-20-yl)carbamate (30).....	278
9.3.44	Synthesis of (9H-fluoren-9-yl)methyl(1-(4-((11-methyl-1,4,8,11-tetraazabicyclo[6.6.2]hexadecan-4-yl)methyl)phenyl)-3-oxo-6,9,12,15,18-pentaoxa-2-azaicosan-20-yl)carbamate copper(II) acetate $[\text{Cu}\mathbf{30}(\text{OAc})](\text{OAc})$	279
9.3.45	Synthesis of 1-amino-N-(4-((11-methyl-1,4,8,11-tetraazabicyclo[6.6.2]hexadecan-4-yl)methyl)benzyl)-3,6,9,12,15-pentaoxaoctadecan-18-amide (31).....	280
9.3.46	Synthesis of 1-amino-N-(4-((11-methyl-1,4,8,11-tetraazabicyclo[6.6.2]hexadecan-4-yl)methyl)benzyl)-3,6,9,12,15-pentaoxaoctadecan-18-amide copper(II) acetate $[\text{Cu}_2\mathbf{31}(\text{OAc})](\text{OAc})$	281
9.3.47	Attempted synthesis of 2,2',2''-(10-(25-carboxy-1-(4-((11-methyl-1,4,8,11-tetraazabicyclo[6.6.2]hexadecan-4-yl)methyl)phenyl)-3,22-dioxo-6,9,12,15,18-pentaoxa-2,21-diazapentacosan-25-yl)-1,4,7,10-tetraazacyclododecane-1,4,7-triyl)triacetic acid (32).....	282
9.3.48	Synthesis of 2,2',2''-(10-(1-carboxy-4,21-dioxo-2,8,11,14,17-pentaoxa-5,20-diazadocosan-22-yl)-1,4,7,10-tetraazacyclododecane-1,4,7-triyl)triacetic acid (33).....	283
9.3.49	Synthesis of 2,2',2''-(10-(1-(4-((10-(4-((1,5,8,12-tetraazabicyclo[10.2.2]hexadecan-5-yl)methyl)benzyl)-1,4,7,10-tetraazabicyclo[5.5.2]tetradecan-4-yl)methyl)phenyl)-3,7,24-trioxo-5,11,14,17,20-pentaoxa-2,8,23-triazapentacosan-25-yl)-1,4,7,10-tetraazacyclododecane-1,4,7-triyl)triacetic acid (34).....	284
9.3.50	Attempted synthesis of metal complexes of 2,2',2''-(10-(1-(4-((10-(4-((1,5,8,12-tetraazabicyclo[10.2.2]hexadecan-5-yl)methyl)benzyl)-1,4,7,10-tetraazabicyclo[5.5.2]tetradecan-4-yl)methyl)phenyl)-3,7,24-trioxo-5,11,14,17,20-pentaoxa-2,8,23-triazapentacosan-25-yl)-1,4,7,10-tetraazacyclododecane-1,4,7-triyl)triacetic acid $[\text{Cu}_2\mathbf{34}(\text{OAc})_2](\text{OAc})_2$ and $[\text{Zn}_2\mathbf{34}(\text{OAc})_2](\text{OAc})_2$	285
9.3.51	Synthesis of (E)-2,2',2''-(10-(1-carboxy-4-((3-(((cyclooct-4-en-1-yloxy)carbonyl)amino)propyl)amino)-4-oxobutyl)-1,4,7,10-tetraazacyclododecane-1,4,7-triyl)triacetic acid (35).....	287
9.3.52	Synthesis of metal complexes of (E)-2,2',2''-(10-(1-carboxy-4-((3-(((cyclooct-4-en-1-yloxy)carbonyl)amino)propyl)amino)-4-oxobutyl)-1,4,7,10-tetraazacyclododecane-1,4,7-triyl)triacetic acid (35) with gallium(III) to form $[\text{natGa}\mathbf{35}]$	288
9.3.53	Synthesis of N-(4-((11-methyl-1,4,8,11-tetraazabicyclo[6.6.2]hexadecan-4-yl)methyl)benzyl)-1-((6-(p-tolyl)-1,2,4,5-tetrazin-3-yl)oxy)-3,6,9,12-tetraoxapentadecan-15-amide (36).....	289
9.3.54	Attempted synthesis of N1-(4-((10-(4-((1,5,8,12-tetraazabicyclo[10.2.2]hexadecan-5-yl)methyl)benzyl)-1,4,7,10-tetraazabicyclo[5.5.2]tetradecan-4-yl)methyl)benzyl)-N19-(4-(6-methyl-1,2,4,5-tetrazin-3-yl)benzyl)-4,7,10,13,16-pentaoxononadecanediamide copper(II) acetate $[\text{Cu}_2\mathbf{37}(\text{OAc})_2](\text{OAc})_2$	290
9.3.55	Attempted syntheses of 2-(4-(1-carboxy-4-((3-(((1-(1-(4-((11-methyl-1,4,8,11-tetraazabicyclo[6.6.2]hexadecan-4-yl)methyl)phenyl)-3-oxo-6,9,12,15-tetraoxa-2-azaheptadecan-17-yl)oxy)-4-(p-tolyl)-2,4a,5,6,7,8,9,10-octahydrocycloocta[d]pyridazin-6-	

yl)oxy)carbonyl)amino)propyl)amino)-4-oxobutyl)-7,10-bis(carboxymethyl)-1,4,7,10-tetraazacyclododecan-1-yl)acetate (38)	291
9.3.56 Attempted syntheses of gallium metallated 2-(4-(1-carboxy-4-((3-(((1-((1-(4-((11-methyl-1,4,8,11-tetraazabicyclo[6.6.2]hexadecan-4-yl)methyl)phenyl)-3-oxo-6,9,12,15-tetraoxa-2-azaheptadecan-17-yl)oxy)-4-(p-tolyl)-2,4a,5,6,7,8,9,10-octahydrocycloocta[d]pyridazin-6-yl)oxy)carbonyl)amino)propyl)amino)-4-oxobutyl)-7,10-bis(carboxymethyl)-1,4,7,10-tetraazacyclododecan-1-yl)acetate ([^{nat} Ga 38]).....	292
9.3.57 Synthesis of (<i>E</i>)-cyclooct-4-en-1-yl(4-((10-(4-((1,5,8,12-tetraazabicyclo[10.2.2]hexadecan-5-yl)methyl)benzyl)-1,4,7,10-tetraazabicyclo[5.5.2]tetradecan-4-yl)methyl)benzyl)carbamate (39)	293
9.3.58 Synthesis of 2,2',2''-(10-(16-carboxy-1-(4-(6-methyl-1,2,4,5-tetrazin-3-yl)phenoxy)-13-oxo-3,6,9-trioxa-12-azahexadecan-16-yl)-1,4,7,10-tetraazacyclododecane-1,4,7-triyl)triacetic acid (40).....	294
9.3.59 Synthesis of deprotected tris(hydroxypyridinone)-phenyl isothiocyanate (41)	295
9.3.60 Synthesis of 2,2'-(7-(2-(benzylamino)-2-oxoethyl)-1,4,7-triazonane-1,4-diyl)diacetic acid (42)	296
9.3.61 Aluminium fluoride complexation with 2,2'-(7-(2-(benzylamino)-2-oxoethyl)-1,4,7-triazonane-1,4-diyl)diacetic acid with aluminium chloride ([AlF] 42).....	297
9.3.62 Synthesis of 2,2'(7-(2-((4-((10-(4-((1,5,8,12-tetraazabicyclo[10.2.2]hexadecan-5-yl)methyl)benzyl)-1,4,7,10-tetraazabicyclo[5.5.2]tetradecan-4-yl)methyl)benzyl)amino)-2-oxoethyl)-1,4,7-triazonane-1,4-diyl)diacetic acid (43).....	298
9.3.63 Aluminium fluoride complexation of 2,2'-(7-(2-((4-((10-(4-((1,5,8,12-tetraazabicyclo[10.2.2]hexadecan-5-yl)methyl)benzyl)-1,4,7,10-tetraazabicyclo[5.5.2]tetradecan-4-yl)methyl)benzyl)amino)-2-oxoethyl)-1,4,7-triazonane-1,4-diyl)diacetic acid with aluminium fluoride ([AlF] 43)	299
9.3.64 Synthesis of 2,2'-(7-(2-((4-((10-(4-((1,5,8,12-tetraazabicyclo[10.2.2]hexadecan-5-yl)methyl)benzyl)-1,4,7,10-tetraazabicyclo[5.5.2]tetradecan-4-yl)methyl)benzyl)amino)-2-oxoethyl)-1,4,7-triazonane-1,4-diyl)diacetic acid with copper or zinc acetate ([Cu ₂ 43 (OAc) ₂](OAc) ₂ and [Zn ₂ 43 (OAc) ₂](OAc) ₂).....	300
9.3.65 Aluminium fluoride complexation of 2,2'-(7-(2-((4-((10-(4-((1,5,8,12-tetraazabicyclo[10.2.2]hexadecan-5-yl)methyl)benzyl)-1,4,7,10-tetraazabicyclo[5.5.2]tetradecan-4-yl)methyl)benzyl)amino)-2-oxoethyl)-1,4,7-triazonane-1,4-diyl)diacetic acid with copper or zinc acetate ([Cu ₂ AlF 43 (OAc) ₂](OAc) ₂ and [Zn ₂ AlF 43 (OAc) ₂](OAc) ₂).....	302
9.3.66 Synthesis of (4-((1,4,7-triazonan-1-yl)methyl)phenyl)methanamine (44).....	304
9.3.67 Attempted synthesis of 2-(2-((4-((1,4,7-triazonan-1-yl)methyl)benzyl)amino)-2-oxoethoxy)acetic acid (45)	305
9.3.68 Synthesis of 2-(2-((4-((11-methyl-1,4,8,11-tetraazabicyclo[6.6.2]hexadecan-4-yl)methyl)benzyl)amino)-2-oxoethoxy)acetic acid (46)	306
9.3.69 Synthesis 2-(2-((4-((4,7-bis(<i>tert</i> -butoxycarbonyl)-1,4,7-triazonan-1-yl)methyl)benzyl)amino)-2-oxoethoxy)acetic acid (47)	307
9.3.70 Synthesis of di- <i>tert</i> -butyl 7-(4-((2-(2-((4-((11-methyl-1,4,8,11-tetraazabicyclo[6.6.2]hexadecan-4-yl)methyl)benzyl)amino)-2-oxoethoxy)acetamido)methyl)benzyl)-1,4,7-triazonane-1,4-dicarboxylate (48)	308
9.3.71 Synthesis of N-(4-((1,4,7-triazonan-1-yl)methyl)benzyl)-2-(2-((4-((11-methyl-1,4,8,11-tetraazabicyclo[6.6.2]hexadecan-4-yl)methyl)benzyl)amino)-2-oxoethoxy)acetamide (49)	310

9.3.72	Synthesis of the rhenium complexation of N-(4-((1,4,7-triazonan-1-yl)methyl)benzyl)-2-(2-((4-((11-methyl-1,4,8,11-tetraazabicyclo[6.6.2]hexadecan-4-yl)methyl)benzyl)amino)-2-oxoethoxy)acetamide ([Re(CO) ₃ 49] ⁺)	312
9.3.73	Synthesis of di- <i>tert</i> -butyl-7-(4-((2-(2-((4-((10-(4-((1,5,8,12-tetraazabicyclo[10.2.2]hexadecan-5-yl)methyl)benzyl)-1,4,7,10-tetraazabicyclo[5.5.2]tetradecan-4-yl)methyl)benzyl)amino)-2-oxoethoxy)acetamido)methyl)benzyl)-1,4,7-triazonane-1,4-dicarboxylate (50)	313
9.3.74	Synthesis of N-(4-((1,4,7-triazonan-1-yl)methyl)benzyl)-2-(2-((4-((10-(4-((1,5,8,12-tetraazabicyclo[10.2.2]hexadecan-5-yl)methyl)benzyl)-1,4,7,10-tetraazabicyclo[5.5.2]tetradecan-4-yl)methyl)benzyl)amino)-2-oxoethoxy)acetamide (51).....	314
9.3.75	Synthesis of the rhenium complexation of N-(4-((1,4,7-triazonan-1-yl)methyl)benzyl)-2-(2-((4-((10-(4-((1,5,8,12-tetraazabicyclo[10.2.2]hexadecan-5-yl)methyl)benzyl)-1,4,7,10-tetraazabicyclo[5.5.2]tetradecan-4-yl)methyl)benzyl)amino)-2-oxoethoxy)acetamide ([Re(CO) ₃ 51] ⁺)	315
9.3.76	Synthesis of metal complexes of di- <i>tert</i> -butyl-7-(4-((2-(2-((4-((10-(4-((1,5,8,12-tetraazabicyclo[10.2.2]hexadecan-5-yl)methyl)benzyl)-1,4,7,10-tetraazabicyclo[5.5.2]tetradecan-4-yl)methyl)benzyl)amino)-2-oxoethoxy)acetamido)methyl)benzyl)-1,4,7-triazonane-1,4-dicarboxylate ([Cu ₂ 50 (OAc) ₂](OAc) ₂ and [Zn ₂ 50 (OAc) ₂](OAc) ₂).....	316
9.3.77	Synthesis of metal complexes of N-(4-((1,4,7-triazonan-1-yl)methyl)benzyl)-2-(2-((4-((10-(4-((1,5,8,12-tetraazabicyclo[10.2.2]hexadecan-5-yl)methyl)benzyl)-1,4,7,10-tetraazabicyclo[5.5.2]tetradecan-4-yl)methyl)benzyl)amino)-2-oxoethoxy)acetamide ([Cu ₂ 51 (OAc) ₂](OAc) ₂ and [Cu ₂ 51 (OAc) ₂](OAc) ₂)	318
9.3.78	Synthesis of the rhenium complexation of the metal complexed of N-(4-((1,4,7-triazonan-1-yl)methyl)benzyl)-2-(2-((4-((10-(4-((1,5,8,12-tetraazabicyclo[10.2.2]hexadecan-5-yl)methyl)benzyl)-1,4,7,10-tetraazabicyclo[5.5.2]tetradecan-4-yl)methyl)benzyl)amino)-2-oxoethoxy)acetamide ([Cu ₂ Re(CO) ₃ 51 (AcO) ₂](AcO) ₂) ⁺ and [Zn ₂ Re(CO) ₃ 51 (AcO) ₂](AcO) ₂) ⁺	320
9.3.79	Synthesis of N-(9-(4-(3-(4-((1,5,8,12-tetraazabicyclo[10.2.2]hexadecan-5-yl)methyl)benzyl)thioureido)-2-carboxyphenyl)-6-(diethylamino)-3H-xanthen-3-ylidene)-N-ethylethanaminium chloride (52)	322
9.3.80	Synthesis of N-(9-(4-(3-(4-((1,5,8,12-tetraazabicyclo[10.2.2]hexadecan-5-yl)methyl)benzyl)thioureido)-2-carboxyphenyl)-6-(diethylamino)-3H-xanthen-3-ylidene)-N-ethylethanaminium chloride metal derivatives ([Ni 52 (OAc)](OAc), [Cu 52 (OAc)](OAc), and [Zn 52 (OAc)](OAc)).....	323
9.3.81	Synthesis of 5-((4-((1,5,8,12-tetraazabicyclo[10.2.2]hexadecan-5-yl)methyl)benzyl)carbamoyl)-2-(6-hydroxy-3-oxo-3H-xanthen-9-yl)benzoic acid (53)	325
9.3.82	Synthesis of 5-((4-((1,5,8,12-tetraazabicyclo[10.2.2]hexadecan-5-yl)methyl)benzyl)carbamoyl)-2-(6-hydroxy-3-oxo-3H-xanthen-9-yl)benzoic acid metal derivatives, ([Cu 53 (OAc)](OAc), and [Zn 53 (OAc)](OAc)	326
9.3.83	Synthesis of N-(9-(2-carboxy-4-(3-(4-((11-methyl-1,4,8,11-tetraazabicyclo[6.6.2]hexadecan-4-yl)methyl)benzyl)thioureido)phenyl)-6-(diethylamino)-3H-xanthen-3-ylidene)-N-ethylethanaminium chloride (54)	328
9.3.84	Synthesis of N-(9-(2-carboxy-4-(3-(4-((11-methyl-1,4,8,11-tetraazabicyclo[6.6.2]hexadecan-4-yl)methyl)benzyl)thioureido)phenyl)-6-(diethylamino)-3H-xanthen-3-ylidene)-N-ethylethanaminium chloride metal derivatives ([Cu 54 (OAc)](OAc), and [Zn 54 (OAc)](OAc)).....	329

9.3.85	Synthesis of 2-(6-hydroxy-3-oxo-3H-xanthen-9-yl)-5-(2-((4-((11-methyl-1,4,8,11-tetraazabicyclo[6.6.2]hexadecan-4-yl)methyl)benzyl)amino)-2-oxoethyl)benzoic acid (55).....	331
9.3.86	Synthesis of 2-(6-hydroxy-3-oxo-3H-xanthen-9-yl)-5-(2-((4-((11-methyl-1,4,8,11-tetraazabicyclo[6.6.2]hexadecan-4-yl)methyl)benzyl)amino)-2-oxoethyl)benzoic acid metal derivatives ([Cu 55 (OAc)](OAc) and [Zn 55 (OAc)](OAc))	332
9.3.87	Synthesis of N-(9-(4-(3-(4-((10-(4-((1,5,8,12-tetraazabicyclo[10.2.2]hexadecan-5-yl)methyl)benzyl)-1,4,7,10-tetraazabicyclo[5.5.2]tetradecan-4-yl)methyl)benzyl)thioureido)-2-carboxyphenyl)-6-(diethylamino)-3H-xanthen-3-ylidene)-N-ethylethanaminium chloride (56)	334
9.3.88	Synthesis of N-(9-(4-(3-(4-((10-(4-((1,5,8,12-tetraazabicyclo[10.2.2]hexadecan-5-yl)methyl)benzyl)-1,4,7,10-tetraazabicyclo[5.5.2]tetradecan-4-yl)methyl)benzyl)thioureido)-2-carboxyphenyl)-6-(diethylamino)-3H-xanthen-3-ylidene)-N-ethylethanaminium chloride metal derivatives ([Cu ₂ 56 (OAc) ₂](OAc) ₂ and [Zn ₂ 56 (OAc) ₂](OAc) ₂)	335
9.3.89	Synthesis of 5-((4-((10-(4-((1,5,8,12-tetraazabicyclo[10.2.2]hexadecan-5-yl)methyl)benzyl)-1,4,7,10-tetraazabicyclo[5.5.2]tetradecan-4-yl)methyl)benzyl)carbamoyl)-2-(6-hydroxy-3-oxo-3H-xanthen-9-yl)benzoic acid (57).....	337
9.3.90	Synthesis of 5-((4-((10-(4-((1,5,8,12-tetraazabicyclo[10.2.2]hexadecan-5-yl)methyl)benzyl)-1,4,7,10-tetraazabicyclo[5.5.2]tetradecan-4-yl)methyl)benzyl)carbamoyl)-2-(6-hydroxy-3-oxo-3H-xanthen-9-yl)benzoic acid metal derivatives ([Cu ₂ 57 (OAc) ₂](OAc) ₂ and [Zn ₂ 57 (OAc) ₂](OAc) ₂).....	338
9.4	Peptide synthesis	340
9.4.1	Stages of peptide synthesis.....	340
9.4.2	Synthesis of protected CPCR4.2 AzMBA, (P1).....	342
9.4.3	Synthesis of deprotected CPCR4.2-AzMBA, (P2)	343
9.4.4	Synthesis of CPCR4.2-AMBA, (P3).....	344
9.4.5	Synthesis of CPCR4.2-AMBA-DOTA, (P4)	345
9.4.6	Synthesis of gallium Pentixafor, ([^{nat} Ga] P4)	346
9.4.7	Synthesis of CPCR4.2-AMBA conjugated with tris(hydroxypyridinone)-phenyl isothiocyanate (P5)	347
9.4.8	Complexation of P5 with gallium(III) nitrate.....	348
9.4.9	Attempted synthesis of CPCR4.2-AzMBA conjugated BODIPY (P6).....	349
9.4.10	Synthesis of CPCR4.2-AMBA conjugated BODIPY (P7).....	350
9.5	Radiolabelling conditions.....	351
9.5.1	Radiolabelling with copper-64	351
9.5.2	Radiolabelling with gallium-68.....	352
9.5.3	Radiolabelling with fluorine-18.....	354
9.5.4	Radiolabelling with technetium-99m.....	354
9.5.5	Radiolabelling and purification of ligands.....	352
9.5.6	Calculating the partition coefficient (LogP)	357
9.5.7	Stability studies in serum/PBS	357
9.5.8	Stability studies in apo-transferrin.....	357
9.5.9	Radiochemical decay corrected	357

9.5.10 Column recovery	357
9.6 Biological Experiments	359
9.6.1 <i>In vivo</i> experiments	359
9.6.2 Experimental for competition binding assay	359
9.6.3 Experimental for fluorescent ligand binding assays	360
9.6.4 Experimental for confocal microscopy	361
9.6.5 Experimental for determination of CXCR4 radioligand binding <i>in vitro</i>	361
10. Appendix	362
10.1 Z-stacking confocal images of peptide P7 in U87-CXCR4 cells.....	362
10.2 Comparison confocal images of peptide P7 in U87 and U87-CXCR4 cells.....	363
10.3 Confocal blocking images of peptide P7 in U87-CXCR4 cells treated with [Cu ₂ 5(OAc) ₂](OAc) ₂	363
11. References	364

Chapter One

Introduction

1.1 Medical imaging

1.1.1 The origins of nuclear medicine

“Nuclear medicine” as a medical speciality was recognised in 1946 following Sam Seidlin’s description of the successful use of radioactive iodine-131 in the treatment of patients with advanced thyroid cancer in the *Journal of the American Medical Association*.¹ By the mid-1950s, research into the clinical use of nuclear medicine had become wide-spread with increased understanding of the methods for detection of radioactivity. Benedict Cassen developed the first rectilinear scanner and Hal Anger’s scintillation camera helped expand the growing field of nuclear medicine.²

Now the field of nuclear medicine has dramatically changed our understanding of disease states by the use of localising radiotracers and tracking biochemical pathways. The information that can be gained by the use of radionuclides on a specific molecular pathway or disease process *in vivo* can be termed ‘molecular imaging’.

1.1.2 Medical imaging technologies

The first medical images of a human body were acquired over 100 years ago with the discovery of X-rays by Roentgen in 1895.³ For many decades diagnostic X-ray techniques dominated the field, until the early 1960’s when techniques such as ultrasound (US), computer tomography (CT) and then a decade later imaging techniques such as positron emission tomography (PET), magnetic resonance imaging (MRI), and optical imaging (OI).³

Medical imaging nowadays is crucial at all levels of healthcare, with most hospitals having a department dedicated to utilising at least two or three of these techniques. Table 1 offers a comparison of the most commonly used clinical diagnostic medical imaging techniques. US scanning is one of the most frequently used clinical imaging techniques. US works by using high energy sound waves to interrogate the interior of a living organism by measuring reflection of the waves, and thus does not use ionising radiation. CT uses high energy X-rays to obtain cross sectional pictures of the human body via attenuation. MRI is based on the principle of nuclear magnetic resonance (NMR) and gives environment dependent information on water protons in the body.³ OI uses light and is discussed in more detail in Chapter 6. Single-photon emission computed tomography (SPECT) and PET are techniques involving radiation emitting isotopes, which utilise gamma rays that are either directly produced or results from positron annihilation.

Technique	Resolution	Application	Advantages	Disadvantages
SPECT	6-8 mm	Functional imaging	<ul style="list-style-type: none"> - Multiple probe imaging numerous probes 	<ul style="list-style-type: none"> - Radiation exposure - Low spatial resolution
PET	4 mm	Metabolic, functional and molecular.	<ul style="list-style-type: none"> - High selectivity quantitative translational - Requires small dose of radioactive tracer - Signal is proportional to radiotracer injected - Can image physiological processes 	<ul style="list-style-type: none"> - Some radionuclides require expensive cyclotron - Low spatial resolution
MRI	1 mm	Anatomical, functional and molecular.	<ul style="list-style-type: none"> - High spatial resolution morphological and functional imaging 	<ul style="list-style-type: none"> - Low sensitivity - Long scans and post-processing time
CT	0.5 mm	Anatomical and functional.	<ul style="list-style-type: none"> - Fast detailed image in three-dimension - High contrast 	<ul style="list-style-type: none"> - Limited soft tissue contrast - High exposure to radiation
Ultrasound	300-500 μm	Anatomical and functional.	<ul style="list-style-type: none"> - Real time - No harmful radiation - Low cost 	<ul style="list-style-type: none"> - Low resolution - Limited to soft tissue contrast - Direct trade-off between imaging depth and spatial resolution - Operator dependent analysis
Optical Imaging	>0.3 μm	Physiological and molecular	<ul style="list-style-type: none"> - No harmful radiation - Low cost 	<ul style="list-style-type: none"> - Limited use ~10 cm depth - So far limited clinical use

Table 1: Comparison of *in vivo* imaging techniques currently used in medical imaging.³⁻⁵

1.1.3 Positron Emission Tomography (PET) imaging

Over the past decade the use of PET has increased in preclinical and clinical imaging facilities. In Europe, there was an estimated 21% increase in the number of PET and PET-CT scans between 2005 and 2010.⁶ The increasing use of this technique is due to the many technical advances that have been made to lower costs and to validate the advantages PET imaging can offer over other modalities particularly for cancer imaging. It is a non-invasive imaging that can be used to locate both primary and metastatic cancerous tumours with high sensitivity.⁴ A typical PET-CT scanner is shown in Figure 1, the combination of using both PET and CT is currently the most common. The patient is scanned during the same procedure with both devices and the images are subsequently combined, giving metabolic information via PET and anatomic information via CT. PET is a relatively expensive imaging technique, however, technological advances are being made to facilitate tracer production and cost effectiveness is being demonstrated in improved patient care.⁴

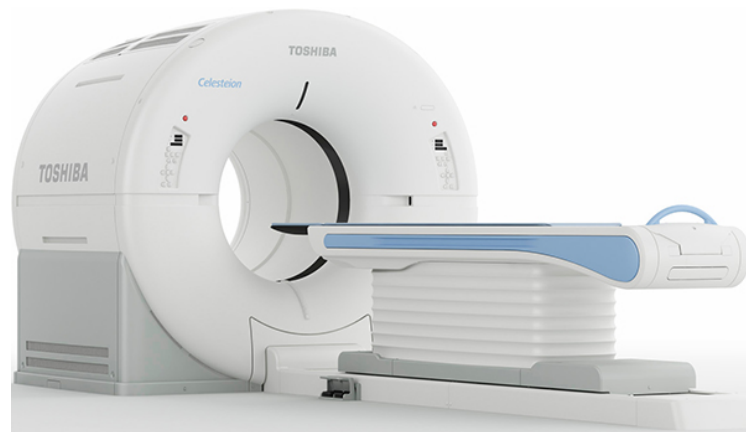


Figure 1. Toshiba Celesteion PET-CT system. (Reproduced from Toshiba America Medical Systems).⁷

1.1.4 Physical principles of PET

In 1928, Paul A.M. Dirac postulated the existence of a subatomic particle that was equal in mass to an electron but carried a positive charge instead.⁴ Carl Anderson in 1937 carried out cosmic ray experiments in which he used a cloud chamber and was able to observe the movement of these particles, which he named 'positrons'. Both received Nobel Prizes in Physics and their work contributed to the understanding of these particles, paving the way for their application in medical imaging.

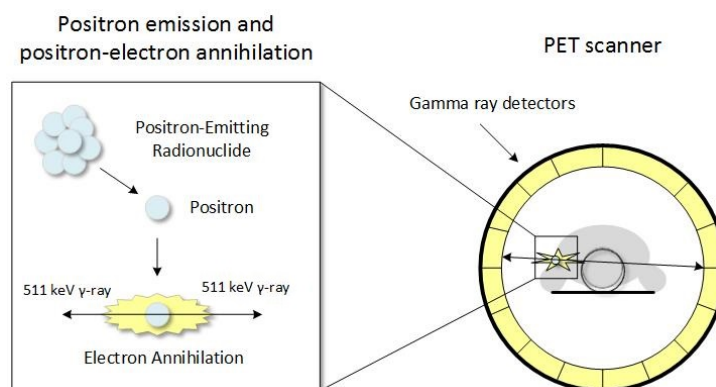


Figure 2. Diagram showing the principle involved in undertaking a PET scan.

The principle behind PET imaging involves the use of a neutron-deficient isotope that decays rapidly via the emission of a positron which then travels a short distance through surrounding tissue, (*ca.* less than 2 mm). During this time the positron is decelerating due to loss of kinetic energy until annihilation occurs when it collides with an electron, creating two 511 keV gamma rays to be emitted *ca.* 180° apart, see Figure 2.⁴ These gamma rays are then detected by scintillators and amplified by photomultiplier tubes that are arranged in a ring, surrounding the patient. Annihilation gamma rays are detected in coincidence and computer software calculations determine the origin where they were emitted in the patient's body.

1.2 Designing a PET imaging agent

1.2.1 Key parameters for consideration in the design of a PET imaging agent

Radiotracers can be designed to be either specific (e.g. binding to a receptor overexpressed in tumours) or non-specific (eg. H_2^{15}O and $^{13}\text{NH}_3$) for the study of metabolic processes. The most commonly used PET tracer is fluorine-18 labelled flurodeoxyglucose (^{18}F FDG), see Figure 3. FDG is an analogue of glucose; it is taken up in cancerous cells due to the Warburg effect. The Warburg effect is phenomenon where additional energy is produced in cancerous cells through increased oxygen-dependent glycolysis. FDG has been shown to be a powerful diagnostic agent, and is the most frequently used clinical PET tracer; it has been shown to have great success in diagnosing Hodgkin's disease, breast, colorectal and lung cancer.⁸ However, due to the non-specific nature of ^{18}F FDG it does accumulate in healthy cells, limiting its use in diagnosing tumours near other high metabolism tissues (e.g. brain).

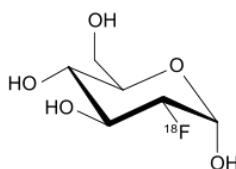


Figure 3. Molecular structure of radiotracer ^{18}F -flurodeoxyglucose (FDG).

Pharmacokinetic and pharmacodynamic properties are key when designing a tracer for PET imaging. Pharmacodynamics is the study of what a drug does to the body, for example bind to a specific targeted site, affinity, dissociation, whereas pharmacokinetics is what the body does to the drug.⁹ This refers to the absorption, bioavailability, distribution, metabolism and excretion (ADME) of the tracer. Of particular importance for a tracer is to avoid formation of metabolites as this changes the properties of the image and can cause a higher background signal.¹⁰

For the imaging of cancers, tracers must show high accumulation at the target site. Depending on the type of tracer (e.g. antibody, nanoparticle, peptide, organic compound) the interaction and penetration of the tumour can differ greatly. For example, properties of the tracer which effect target site accumulation can include whether the tracer is designed to be transported inside the cancerous cell or to bind to the surface of the cell. Tracers that have a high molecular weight such as antibodies and nanoparticles tend to show low tumour penetration. Therefore more time is needed before the scan, which can affect the selection of radioisotope.¹¹ In contrast, a low molecular weight tracer tends to have faster tissue penetration, so shorter lived radioisotopes are acceptable.

Clearance of an agent is also an important factor in achieving a high quality image. The unbound tracer needs to be excreted rapidly, otherwise the high background signal in the circulatory system can reduce image quality. Nevertheless, if the imaging agent is being cleared too rapidly, the tracer will suffer from poor tumour/ tissue uptake. Therefore, when designing imaging agents it is important to strike the right balance of accumulation and excretion properties.

1.2.2 Radionuclides used in molecular imaging

Some radioisotopes occur naturally but many more have been produced experimentally. This approach to produce radioactive isotopes was first reported in 1934 by Irene Curie (daughter of Marie and Pierre Curie) and Frederic Joliot, who generated radioactive isotopes from boron and aluminium targets through the bombardment with alpha particles from polonium.¹² Today, more than 2500 radioisotopes have been generated through the use of particle accelerators (such as cyclotrons) and nuclear reactors.¹³

The periodic table shows the following shaded elements:

- Orange (α and Auger-emitting):** Sc, Ti, V, Cr, Mn, Fe, Co, Ni, Cu, Zn, Ga, Ge, As, Se, Br, Kr, Rb, Sr, Y, Zr, Nb, Mo, Tc, Ru, Rh, Pd, Ag, Cd, In, Sn, Sb, Te, I, Xe, Cs, Ba, La, Ce, Pr, Nd, Pm, Sm, Eu, Gd, Tb, Dy, Ho, Er, Tm, Yb, Ac, Th, Pa, U, Np, Pu, Am, Cm, Bk, Cf, Es, Fm, Md, No.
- Purple (β⁺ emitters):** Na, Mg, K, Ca, Sc, Ti, V, Cr, Mn, Fe, Co, Ni, Cu, Zn, Ga, Ge, As, Se, Br, Kr, Rb, Sr, Y, Zr, Nb, Mo, Tc, Ru, Rh, Pd, Ag, Cd, In, Sn, Sb, Te, I, Xe, Cs, Ba, La, Ce, Pr, Nd, Pm, Sm, Eu, Gd, Tb, Dy, Ho, Er, Tm, Yb, Ac, Th, Pa, U, Np, Pu, Am, Cm, Bk, Cf, Es, Fm, Md, No.
- Pink (β⁻ emitters):** Na, Mg, K, Ca, Sc, Ti, V, Cr, Mn, Fe, Co, Ni, Cu, Zn, Ga, Ge, As, Se, Br, Kr, Rb, Sr, Y, Zr, Nb, Mo, Tc, Ru, Rh, Pd, Ag, Cd, In, Sn, Sb, Te, I, Xe, Cs, Ba, La, Ce, Pr, Nd, Pm, Sm, Eu, Gd, Tb, Dy, Ho, Er, Tm, Yb, Ac, Th, Pa, U, Np, Pu, Am, Cm, Bk, Cf, Es, Fm, Md, No.
- Yellow (γ emitters):** Na, Mg, K, Ca, Sc, Ti, V, Cr, Mn, Fe, Co, Ni, Cu, Zn, Ga, Ge, As, Se, Br, Kr, Rb, Sr, Y, Zr, Nb, Mo, Tc, Ru, Rh, Pd, Ag, Cd, In, Sn, Sb, Te, I, Xe, Cs, Ba, La, Ce, Pr, Nd, Pm, Sm, Eu, Gd, Tb, Dy, Ho, Er, Tm, Yb, Ac, Th, Pa, U, Np, Pu, Am, Cm, Bk, Cf, Es, Fm, Md, No.

* Lanthanide series

lanthanum 57	cerium 58	praseodymium 59	neodymium 60	promethium 61	europium 62	gadolinium 63	terbium 64	dysprosium 65	holmium 66	erbium 67	thulium 68	ytterbium 69
138.91	140.12	140.91	144.24	[145]	150.36	151.96	157.25	158.93	162.50	164.93	168.93	173.04
[227]	[232.04]	231.04	238.03	[237]	[244]	[243]	[247]	[247]	[251]	[252]	[257]	[259]

** Actinide series

actinium 89	thorium 90	protactinium 91	uranium 92	neptunium 93	plutonium 94	americium 95	curium 96	berkelium 97	californium 98	einsteinium 99	fermium 100	mendelevium 101	nobelium 102
[227]	[232.04]	231.04	238.03	[237]	[244]	[243]	[247]	[247]	[251]	[252]	[257]	[259]	[259]

Figure 4. Periodic table where shaded elements represent radionuclides with uses or identified potential for imaging and therapy; γ -emitters (pink) for SPECT, β^+ emitters (purple) for PET and β^- , α and Auger-emitting radioisotopes (orange). (Inspired by figure reported by Blower *et al.*)¹⁴

Radioisotopes are present in all groups of the periodic table (as shown in Figure 4, where all the shaded elements represent an isotope that is used or has been investigated for use as a therapeutic radiopharmaceuticals or imaging agents).¹⁴ These isotopes have a wide variety of properties (some of which are listed in Table 2). The important properties in medical imaging are: availability, production, radioactive half-life, chemical reactivity (including coordination chemistry for metals) and emitting species.

Table 2: Details of the different properties and production method of common radioisotopes in nuclear imaging.¹⁵

Isotope	Half life	Decay mode	Production Method
¹¹ C	20.3 min	β+ (100%), 961 keV	Cyclotron ¹⁴ N(p,α)/ ¹¹ C
¹⁸ F	110 min	β+ (97%), 873 keV	Cyclotron H ₂ ¹⁸ O (p,n)/ ¹⁸ F
⁶⁴ Cu	12.7 h	β+ (19%), 656 keV	Cyclotron ⁶⁴ Ni(p,n)/ ⁶⁴ Cu
⁶⁸ Ga	67.8 min	β+ (89%), 1880 keV	⁶⁸ Ge/ ⁶⁸ Ga generator
⁴⁴ Sc	3.9 h	γ, 1157 keV	⁴⁴ Ti/ ⁴⁴ Sc generator
¹¹¹ In	67.2 h	γ, 245 keV	Cyclotron ¹¹¹ Cd(p,n)/ ¹¹¹ In
^{99m} Tc	6.0 h	γ, 140 keV	Cyclotron, ⁹⁹ Mo/ ^{99m} Tc generator
⁸⁶ Y	14.7 h	β+ (33%), 1221 keV	Cyclotron ⁸⁶ Sr(p,n)/ ⁸⁶ Y
⁸⁹ Zr	78.5 h	β+ (23%), 897 keV	Cyclotron ⁸⁹ Y(p,n)/ ⁸⁹ Zr

The organic isotopes, carbon-11, nitrogen-13, oxygen-15, and fluorine-18, were initially used for the synthesis of direct analogue tracers, which are chemically identical to already approved pharmaceutical drugs or simple biologically relevant molecules. This approach has the advantage that tracer development is generally much quicker due to the fact that much of the work into the biological response, toxicity, optimising synthetic procedure, has already been investigated. However, it should not be taken for granted that the radiolabelled 'drug' versions will have an identical *in vivo* biodistribution or metabolic pathway. This approach is no longer limited to the 'organic' radionuclides, as there are now many papers in the literature using radiometals to track metal ion metabolism or form labelled version of metalloproteins.¹⁶

Another factor to consider with the 'organic' radionuclides is that they typically have very short half-lives compared to the radiometals. In addition, the inclusion of 'organic' radionuclides into tracer molecules can often be complex and time-consuming. In some cases the half-life is prohibitively short and so only rapidly occurring biological processes, such as blood flow, can be measured.¹⁷ [¹⁸F]FDG is not a natural organic molecule but has the balance of half-life and metabolic trapping which make it highly useful for PET imaging (section 1.2.1).

In recent years, PET emitting radiometals, such as copper-64, gallium-68, yttrium-86 and zirconium-89 have gained much attention in the design of potential imaging agents building on the use of SPECT isotopes technetium-99m and indium-111. This is in part due to the greater availability of radioisotopes produced by generators, nuclear reactors and cyclotrons. With the use of radiometals, chelators termed bifunctional chelators (BFCs) are required to bind to the metal and to link to a targeting group (discussed in section 1.2.4).

1.2.3 Production of a radionuclide

Radionuclides can be generated in one of three ways; from a generator, cyclotron (particle accelerator) or as a product of a nuclear reaction. Only the first two methods are viable for on-site routine clinical production of radiopharmaceuticals and are discussed in more detail below.

1.2.3.1 Production of radiometals from a generator

A radionuclide generator is a device that allows the separation of a daughter radionuclide formed by the decay of the parent radioisotope.¹⁸ These generally consist of the parent immobilised on a stationary phase in a shielded column with the daughter isotope periodically eluted by an ion exchange process. In-house generators are now frequently found in many research facilities and hospitals worldwide. Generators require less investment in infrastructure than cyclotrons and can provide access to PET scanning in locations without cyclotron access.

An important requirement of a radioisotope generator for routine use is a long half-life of the parent radioisotope. Table 3 below lists several of the most common generators used for PET and SPECT imaging and their half-lives. The specific example of the germanium/gallium-68 generator is discussed in more detail in section 1.3.1.3.

Table 3: Table listing some of the generator pairs and half-lives.¹⁹

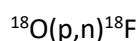
Generator System	Parent radionuclide		Daughter radionuclide	
	T½	Decay Mode	T½	Decay Mode
⁵² Fe/ ^{52m} Mn	8.28 h	β ⁺	21.1 min	β ⁺
⁶⁸ Ge/ ⁶⁸ Ga	270.8 d	Electron capture	67.8 min	β ⁺
⁷² Se/ ⁷² As	8.4 d	Electron capture	1.08 d	β ⁺
¹³⁴ Ce/ ¹³⁴ La	3.16 d	Electron capture	6.4 min	β ⁺
⁹⁹ Mo/ ^{99m} Tc	2.75 d	β ⁻	6.01 h	γ
¹¹⁸ Te/ ¹¹⁸ Sb	6.00 d	Electron capture	3.6 min	β ⁺

1.2.3.2 Generation of radiometals from a cyclotron

Cyclotrons produce radioisotopes through the bombardment of stable nuclei with high energy particles, such as protons (H⁺), deuterons (²H⁺) and alpha particles (⁴He²⁺). Charged particles must be accelerated to high kinetic energies to overcome the repulsive coulomb barrier of the target atom's nuclei. In Berkeley, California, in 1931, the first cyclotron had been developed by E. Lawrence. It involved a vacuum chamber between the poles of an electromagnet to allow for acceleration.¹³ The static magnetic field created by the electromagnetic causes the ions to travel in a circular path,

where the radius of the circle increases as the ions gain more kinetic energy. The cyclic pathway of these ions gave rise to the name 'cyclotron'.¹³

When the accelerating ions collide with the target nuclei, they undergo a nuclear reaction. An incident particle may leave the target nucleus after transferring/absorbing some of the energy. The specific reaction that occurs depends on the type and energy of the bombarding particles as well as composition of the target nuclei. For example the production of fluorine-18 is a cyclotron product; the production reaction is written as follows:



Nuclear reactions are described in this generic format **T(P,x)R**, where projectile (P) and the target (T) emit particle (x) to form the residual nucleus (R). Therefore; in the above example the target material is oxygen-18 and the bombarding particle is a proton (p). This reaction results in the emission of one neutron (n) creating the residue nucleus fluorine-18.²⁰

1.2.3.3 Process of generation of radiotracer

Figure 5 demonstrates the stages that are involved to produce a radiotracer and obtain a PET image. The radioisotope is obtained from either a cyclotron or a generator. The radioisotope is incorporated into the tracer. The compound must then be analysed by techniques such as high performance liquid chromatography (HPLC) and radio-thin layer chromatography (radio-TLC) before it can be administered *in vivo* (in some cases purification is necessary). For a cyclotron produced radionuclide, the half-life will determine possible transportation distances. For example, fluorine-18 tracers would not generally be delivered to a site more than one half-life away (*ca.* 2 hours). Previously mentioned (section 1.2.3.1) radioisotopes such as gallium-68 and technetium-99m can be produced on site via generators. Much work has been reported with the use of radiolabelling with generator produced isotopes through 'kits' which offers high convenience for local radiopharmacies.

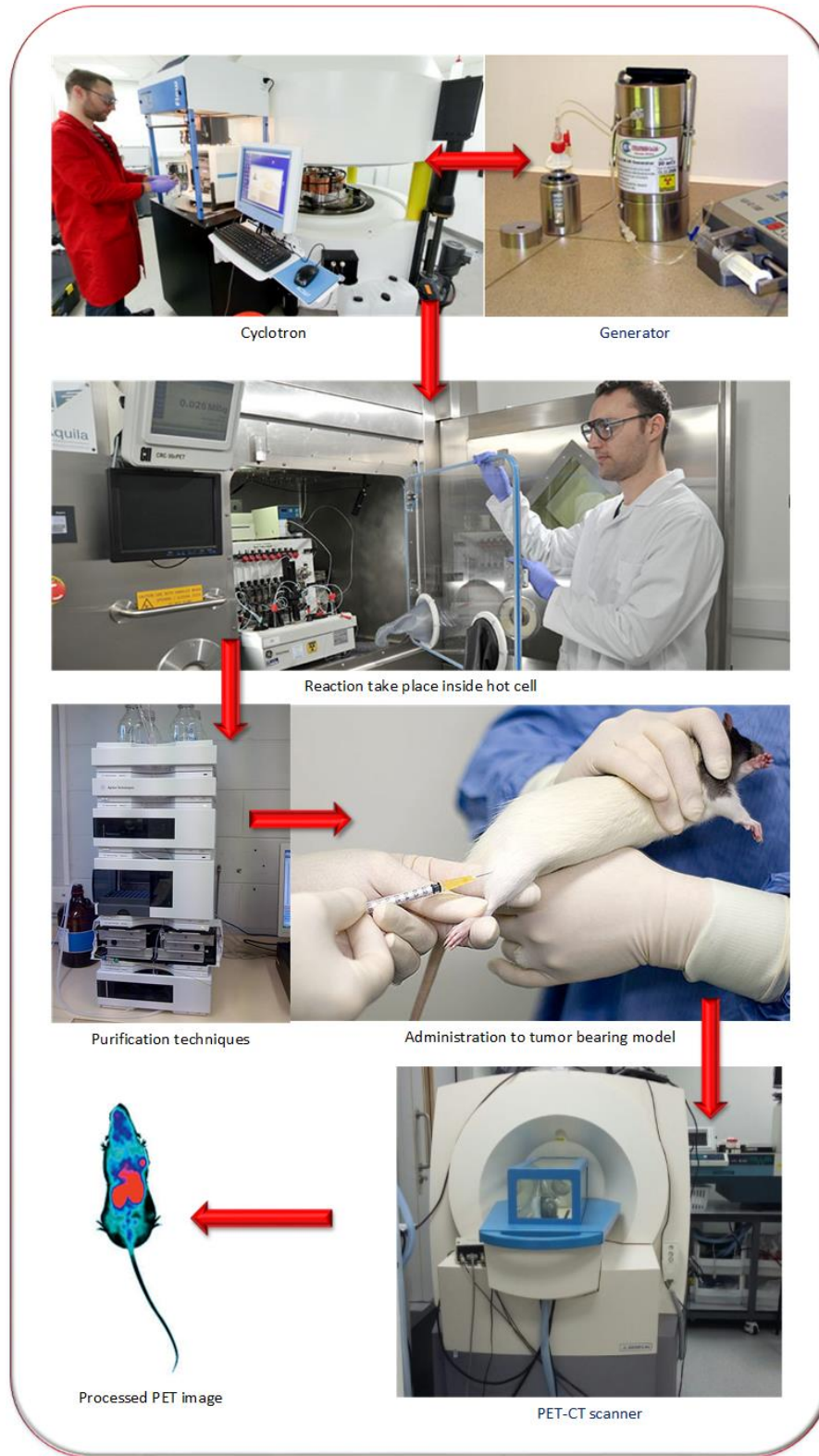


Figure 5: The process of production of PET radiotracers. From top the generation of a radioisotope via commercial generator or cyclotron; radiolabelling the chelator inside a hot cell; purification of the radiotracer; administration of the radiotracer; scanning and generation of a processed PET image.

1.3 Key aspects of radiopharmaceutical chemistry

As shown in Figure 4, there are a wide range of radionuclides available for functional imaging and therapy. The radioisotopes that are discussed in more detail in this section (gallium-68, copper-64 and fluorine-18) have been selected as having appropriate decay properties (emission and half-life) and chemical properties for the design of novel PET tracers.

1.3.1 Gallium-68

1.3.1.1 Chemical properties of gallium

Gallium is a group 13 post-transition metal of electronic configuration $[\text{Ar}]3d^{10}4s^24p^1$. Its chemistry in aqueous solution is limited to the +3 oxidation state, hydrolysing nearly completely at pH values close to neutral, readily forming highly insoluble amorphous $\text{Ga}(\text{OH})_3$. Therefore when radiolabelling with gallium-68 an acidic buffer (above pH 5) must be used to prevent formation of these insoluble hydroxo species.²¹

Gallium-68 has a small ionic radius of 47-62 pm,²² and can be described as a 'hard Lewis acid' resulting in strong bonds with ligands containing multiple anionic donors, such as oxygen and nitrogen.²³ It can coordinate with ligands forming a coordination sphere with 4-6 donor atoms.²⁴ The lower 4 and 5 coordination geometries are more susceptible to nucleophilic attack, particularly in physiological media. Thus when designing a BFC for gallium(III), with its d^{10} electron configuration, the six-coordinate geometry is the most stable (most commonly distorted octahedral). The hard character of the gallium(III) ion gives preference for hard donor atoms such as carboxylate-oxygens, amine-nitrogen's, hydroxamate-oxygens etc.

1.3.1.2 Properties of gallium radioisotopes

Gallium-68 is rapidly emerging as an attractive radionuclide for PET imaging applications. The three isotopes of gallium which are used in nuclear medicine are gallium-66, gallium-67 and gallium-68.⁶ Gallium-68 is the preferred positron emitter (89% positron emission), and half-life of 68 minutes. Additionally gallium-68 has a reasonable positron energy (1.92 MeV maximum²⁵) for PET imaging; if the energy is too high (e.g. bromine-76, 3.4 MeV maximum²⁶) the positron travels a relatively long distance before annihilation which reduces the resolution of the image acquired.²² Although this energy is suitable for PET imaging it is important to note that other radioisotopes such as copper-64 and zirconium-89 (653 and 902 keV, respectively²⁷) are even lower β^+ energy emitters.

1.3.1.3 Production of gallium-68 from generators

A major advantage of gallium-68 is that it can be produced easily in-house with reduced infrastructure using a germanium/gallium generator. Germanium-68 has a half-life of 270 days and decays to give gallium-68 with a half-life of 68 min, as shown in Figure 6. The generator is made of germanium-68 adsorbed on a stationary phase and loaded in a plastic or glass column.²⁸ This generator has the advantage that it can be eluted relatively frequently (usually twice a day), as the maximum yield is generated within a few hours.

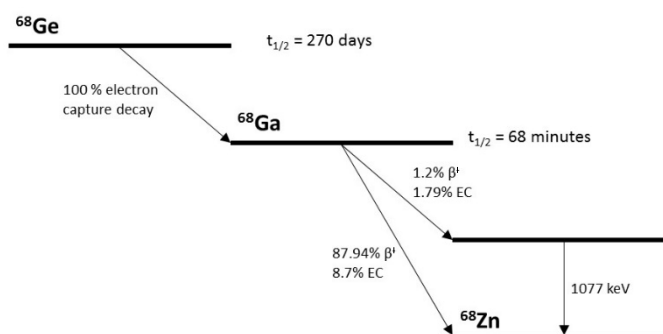


Figure 6: Nuclear decay characteristics of germanium-68 to gallium-68.

Modern gallium-68 generators produce ionic gallium, with four different commercially available columns currently available (iThemba, EZAG, ITG, Obninsk).²⁹ The column of the generator at the University of Hull which is made from tin dioxide, the eluent used is 0.6 M HCl, giving an optimum gallium yield of between 75-80% with only 0.0002% germanium breakthrough.¹⁸

Another advantage for use of $^{68}\text{Ge}/^{68}\text{Ga}$ generator system is that it has a long shelf life of ~ 1 year which allows easy mobilisation to hospital nuclear pharmacies regardless of their proximity to cyclotron or nuclear reactor production sites.

1.3.2 Copper-64

1.3.2.1 Chemical properties of copper

Copper is a group 11 transitional metal of electronic configuration $[\text{Ar}]3d^{10}4s^1$ and over the past decade has been shown to be a highly versatile radionuclide for PET imaging. Copper has a relatively small ionic radius between 57 pm and 73 pm (dependent on coordination geometry).²⁴ In contrast to gallium, several oxidation states are accessible for copper in the presence of suitable donor atoms, ranging from +1 to +3. In its lowest oxidation state, +1, copper has a diamagnetic d^{10} electronic configuration with no ligand field stabilisation energy. Copper(I) can be described as a soft acid and it is readily transformed into the copper(II) oxidation state, therefore is challenging to stabilise for radiopharmaceutical applications. Copper(II) has a d^9 electron configuration and forms square planar, trigonal pyramidal and distorted octahedral complexes, with donor atoms such as amine-N, imine-N, pyridine-N, carboxylate-O and thiol-S.^{22, 23} Due to the d^9 electronic configuration, copper(II) six coordinate complexes often exhibit Jahn-Teller distortion. Copper(III) is rarely seen in radiopharmaceuticals as it is hard to stabilise without strong π -donor atoms.

As a result, the use of copper in medical imaging focuses on copper(II). In designing a chelator for copper(II) it is crucial to have a BFC that will form stable complexes to minimise *in vivo* transchelation. These requirements map well onto azamacrocycles, which can be used to achieve high stability complexes. There is a wealth of literature investigating the use of macrocycles as bifunctional chelators (BFCs) for copper(II) (see section 1.4.4).^{30, 31} There is also continuing interest in the design of copper BFCs; with many review articles in this field.³²⁻³⁴ A key area of investigation has focussed on the cross-bridged cyclam as a possible solution (see section 2.5).³⁵⁻³⁸

1.3.2.2 Properties of copper radioisotopes

There are several radioactive isotopes of copper that are currently used with a range of half-lives ranging from 10 minutes (copper-62 generator produced) to 12.7 h (copper-64); shown in Table 4.³⁹ Although there are additional factors to consider in designing a copper radiopharmaceutical. For example, high-energy positron energy emitters such as copper-60, copper-61 and copper-62 give lower spatial resolution.

Table 4: Key emission for copper-60, copper-61, copper-62 and copper-64. For β^+ energies determined as average of end-point energies, weighted by intensity.⁴⁰

Nuclide	Half-life (min)	Radiation	Energy (KeV)	Intensity (%)	Reference
⁶⁰ Cu	23.4	β^+	2940	92	41
		γ	511, 467, 826, 1332	183, 4, 22, 88	
⁶¹ Cu	204.5	β^+	1159	62	42
		γ	511, 283, 589, 656	123, 12, 1, 11	
⁶² Cu	9.7	β^+	2925	93	43
		γ	511	155	
⁶⁴ Cu	761.9	β^+	657	17	44
		γ	511, 1346	35, 1	

Copper-64 is also attractive as a theranostic radionuclide as it is a beta- and Auger electron-emitter as well as positron emitter.¹⁴

1.3.2.3 Production of copper-64

Copper-64 can be effectively produced by both nuclear reactor-based and accelerator-based methods. One method of copper-64 production is the $^{64}\text{Zn}(n,p)^{64}\text{Cu}$ reaction in a nuclear reactor.²² However, the disadvantage of this method is the formation of the by-products zinc-65 which has a long half-life of 245 days. This combined with high cost and impracticality of production by a nuclear reactor limits the production of copper-64 by this method.

The more common production method of copper-64 is via the $^{64}\text{Ni}(p,n)^{64}\text{Cu}$ reaction on a biomedical cyclotron which was first proposed by Szelecsenyi *et al.*⁴⁵ The study showcased the feasibility of producing copper-64 with a small cyclotron. Subsequent studies by McCarthy *et al.* fine-tuned the procedure which is now used world-wide by researchers to produce copper-64.⁴⁶

1.3.3 Fluorine-18

1.3.3.1 Chemical properties of fluorine-18

Fluorine-18 is the most widely used isotope for PET imaging. Fluorine is a group 17 element with the electronic configuration $[\text{He}]2s^22p^5$. It is highly electronegative with a small radius of 42 pm.²³

It is most often incorporated into an imaging agent by the formation of a carbon-fluorine bond. However, this is not the only way fluorine can be introduced as boron, aluminium, phosphorus and silicon all have very high bonding energies with fluorine (shown in Table 5).

Table 5: Average bond dissociation energies and bond length for common radiofluorination approaches.⁴⁷

Bond	Bond dissociation energy (KJmol⁻¹)	Bond length (Å)
C-F	513.8 ± 10	1.35
Al-F	675	1.63
B-F	732	1.30
Si-F	576.4 ± 17	1.60
P-F	≤ 405	1.54

1.3.3.2 Radiochemical properties of fluorine-18

Fluorine-18 is a versatile positron-emitting radionuclide with a useful balance of properties. Decay of fluorine-18 is largely by positron emission (97%), with a low energy emission (maximum 0.635 MeV), thus the positrons have a short mean range (2.39 mm in water).⁴⁸ The moderate half-life of 109.7 minutes allows for more elaborate syntheses (compared to the organic radionuclides; carbon-11, oxygen-15). The half-life also allows for fluorine-18 radiopharmaceuticals to be distributed to locations distant from the cyclotron, hence, the popularity of fluorine based radiopharmaceuticals in clinical imaging.

Radiolabelling with fluorine-18, in general, can be carried out in one of two ways; either by nucleophilic or electrophilic substitution. There have been many excellent reviews written on the reaction chemistry of fluorine-18 and the future potential for novel radiotracer development.⁴⁹⁻⁵¹

1.3.3.3 Production of fluorine-18

Fluorine-18 is readily available from both particle accelerators and nuclear reactor, using a wide range of nuclear reactions. For practical purposes nearly all fluorine-18 is currently produced using a single nuclear reaction, $^{18}\text{O}(p,n)^{18}\text{F}$, where fluorine-18 is isolated as a fluoride ion in aqueous solution from oxygen-18 enriched water.

1.4 Labelling with radiometal isotopes

In the majority of cases to use radiometals in molecular imaging, the 'free' radiometal ion is sequestered from an aqueous solution using a chelator to form a complex that is stable in the biological system. Chelators used for this application are typically covalently linked to a biologically active targeting moiety. The different radiometals each have unique physicochemical characteristics, and so it is important to match the chelator to the radioisotope to ensure rapid complex formation and high stability.

1.4.1 Bifunctional chelators (BFCs)

BFCs for radiopharmaceuticals are designed to contain donor atoms to bind to a radiometal but also have a functional group that allows for linking to a biological targeting group. The design of a BFC depends on the radiometal and its properties, including preferred geometry, coordination number and oxidation state. Furthermore, the BFC must be non-toxic and should form both thermodynamically and kinetically stable complexes *in vivo*. The chelator radiolabelling process should be rapid, efficient and selective to give a straightforward preparation method for use in radiopharmacies. BFCs can be classified as either cyclic or acyclic which influences the way they encapsulate a radiometal, see Figure 7.



Figure 7: Diagram showing how macrocyclic and acyclic chelators encapsulate radiometal ions.

The structure and physicochemical properties of the radiometal-chelate complex will influence the pharmacokinetics of the radiotracer, with many radiometal complexes being highly hydrophilic. It has been observed that the chelation of the radiometals can have a dramatic effect on the biodistribution of the constructs.⁵²

1.4.2 The macrocyclic effect

Macrocyclic chelators form more kinetically stable complexes in comparison to their acyclic counterparts. When considering thermodynamics, macrocyclic chelators require less physical rearrangement during metal complex formation, as they inherently possess a degree of preorganisation, therefore the entropy penalty has already been paid.⁵³ In contrast, acyclic chelators undergo a more dramatic reorganisation of the physical orientation on complex formation to arrange donor atoms in the correct geometry. This causes a more significant decrease in entropy and as a result makes it more thermodynamically unfavourable.⁵⁴ This phenomenon is known as the macrocyclic effect, and is key consideration in designing a BFC.

However, acyclic chelators do have the advantage of more rapid kinetics of complex formation; resulting in faster radiolabelling at lower temperatures (e.g. acyclic chelators have been radiolabelled in 5 minutes at room temperature). Macrocyclic chelators often require much longer reaction times of 30-90 minutes at elevated temperature (60-95°C).

1.4.3 Design of a chelator for radiometals

The key properties when selecting a BFC for *in vivo* use are a combination of thermodynamic stability and kinetic inertness. These properties are represented by the formation constant ($K_{ML} = [ML]/[M][L]$) and the rate constant for the complex formation. The formation/stability constants can be measured for non-radioactive complexes by potentiometric titrations and provide an excellent starting point for selection of chelators, however it is challenging to fully represent the conditions and competing chelating ligands present in biological systems.

Transchelation experiments in model systems are also useful to determine whether the radiometal complex is suitable for *in vivo* studies, as this can include proteins and biological molecules which competitively bind to the metal ions. Tests can be carried out with relevant biological fluids, protein solutions or biomaterials, including blood serum, apo-transferrin and hydroxyapatite. The radiometal-BFC complex is incubated with the biorelevant solutions and the mixture analysed by HPLC or TLC to give an indication of the stability of the complex over time.

1.4.4 Commonly used chelators and their compatibility with radiometals

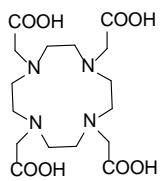
Chelator design has been a key part of radiopharmaceutical development and some examples of the most commonly applied chelators are presented in this section.

The tables below aim to provide a quick reference in comparing each chelator to commonly used radioisotopes. The categories of poor, okay and good have been used to describe the pairing of the radiometal with the chelator which is based on author's opinions on the general suitability of the chelator and specific radiometal. Factors such as radiolabeling condition and *in vivo/vitro* stability have been considered in the assignment of a rating. The assignment of good may suggest that the pairing of the chelator and radiometal are currently 'gold standard' used widely in the field, or that early work is looking promising. The assignment of okay indicates may indicate that although this pairing has been used successfully in the past for *in vivo* imaging that perhaps it has been surpassed by a new and superior chelator. The assignment of poor indicates that the chelator and radioisotope pair suffers from severe instability or radiolabeling problems.

1.4.4.1 DOTA as a radiometal chelator

DOTA (1,4,7,10-tetraazacyclododecane-1,4,7,10-tetraacetic acid, see Table 6) is one of the most commonly used chelators for complex formation with radiometals, and has been the 'gold standard' for the complexation of various radiometals (including gallium-68, indium-111, lutetium-177 and actinium-225). DOTA is not only widely used in nuclear imaging such as PET and SPECT, but is also applied in MRI and OI.

Table 6: DOTA BFC with relevant radiometal ion, labelling conditions, thermodynamic stability constants ($\log K_{ML}$) and coordination geometries. * Indicates that the donor set is dependent on the metal.

Bifunctional chelator	Radioisotopes	Labelling Efficiency	Radiolabelling conditions	Log K_{ML}	Reference
 DOTA, 1,4,7,10-tetraazacyclododecane-1,4,7,10-tetraacetic acid, donor set $N_4O_4^*$	$^{67/68}\text{Ga}^{3+}$	Okay	37-90°C, 10-30 min, pH 4.0 – 5.5	21.3	55-64
	$^{111}\text{In}^{3+}$	Good	37-90°C, 15-60 min, pH 4.0 – 6.0	23.9	55, 61, 64-67
	$^{64}\text{Cu}^{2+}$	Okay	25-90°C, 30-60 min, pH 5.5 – 6.5	22.2, 22.7	57, 66, 68-75
	$^{44/47}\text{Sc}^{3+}$	Good	95°C, 20-30 min, pH 4.0	27.0	76-78
	$^{177}\text{Lu}^{3+}$	Good	25-100°C, 15-90 min, pH 4.0 – 6.0	23.5, 21.6	67, 79

In 1976, Stetter and Frank were the first to report the complexation properties DOTA has with lanthanide and transition metal ions. Although DOTA is widely applied to complex metals in radiopharmaceuticals, it is not ideal for some metal ions, in particular copper(II) (copper-64) which does not form complexes of sufficient kinetic stability for *in vivo* use. The issues are different for gallium-68 where the slow kinetics of complex formation require elevated temperatures and longer reaction times. However, in general terms, the DOTA chelator offers a good balance of properties and its strength is its versatility as it can bind effectively to a wide variety of metal ions.^{38, 80-82}

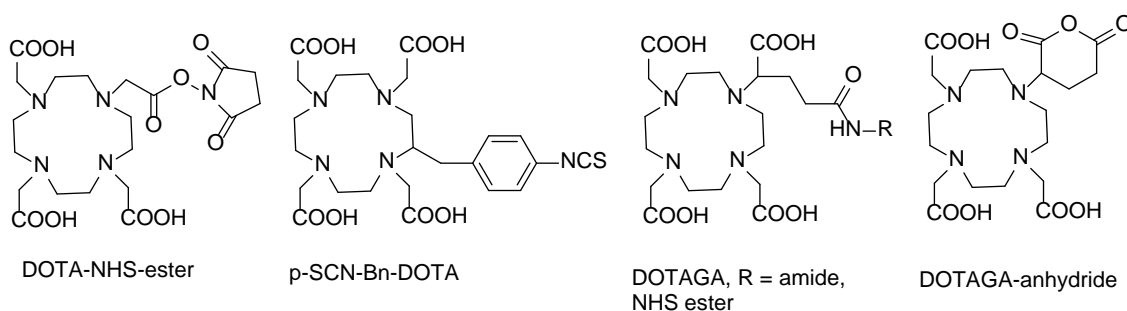
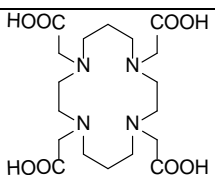
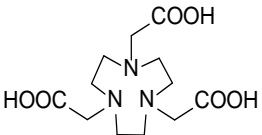


Figure 8: Common derivative BFCs of DOTA.

DOTA derivatives (see Figure 8) can take advantage of one of the unbound carboxylate acid arms in six coordinate complexes to allow for conjugation to a targeting moiety. For radiometals requiring an octadentate coordination sphere, using all of the carboxylate functional groups, C-functionalisation or branched pendant arms can be incorporated to provide the additional functional group required for conjugation.

1.4.4.2 TETA as a radiometal chelator

Table 7: TETA, and NOTA BFC with relevant radiometal ion, labelling conditions, thermodynamic stability constants ($\log K_{ML}$) and coordination geometries.

Bifunctional chelator	Radioisotopes	Labelling Efficiency	Radiolabelling conditions	Log K_{ML}	Reference	
	$^{67/68}\text{Ga}^{3+}$	Poor	-	19.74	83	
	$^{111}\text{In}^{3+}$	Poor	-	21.9	83	
	TETA, 1,4,8,11-tetraazacyclotetradecane-1,4,8,11-tetraacetic acid, donor set N_4O_4	$^{64}\text{Cu}^{2+}$	Okay	80°C, 30-60 min, pH 4.0 – 6.0	21.9, 21.6	84, 85
		$^{67/68}\text{Ga}^{3+}$	Good	25°C, 30-60 min, pH 4.0– 5.5	31.0	57, 64, 86-90
		$^{111}\text{In}^{3+}$	Okay	60-95°C, 20-30 min, pH 4.0-5.0	26.2	64, 83, 91-94
		$^{64}\text{Cu}^{2+}$	Good	80°C, 30-60 min, pH 5.5 – 6.5	21.6	95, 96
		$^{44/47}\text{Sc}^{3+}$	Okay	95°C, 20-30 min, pH 4.0	16.5	78
	$^{99\text{m}}\text{Tc}^{3+}$	Good	90°C, 30 min, pH 4.0 – 7.0		97	

1,4,8,11-Tetraazacyclotetradecane-1,4,8,11-tetraacetic acid (TETA, see Table 7) is an octadentate N_4O_4 macrocyclic chelator, based on the cyclam macrocycle, that has mainly been reported as a copper-64 chelator in PET radiotracer design. TETA is not very commonly used in research today as has been replaced by TETA derivatives such as SAR, CB-TE2A, CB-TE1A1P, CB-TE2P (see Figure 9). These derivatives form more kinetically stable complexes, and some can be radiolabelled with copper-64 at room temperature. Unlike DOTA, TETA has not been extensively

investigated with radiometals other than copper-64, however some attempts have been made to label it with gallium-68 and indium-111 (see Table 7).

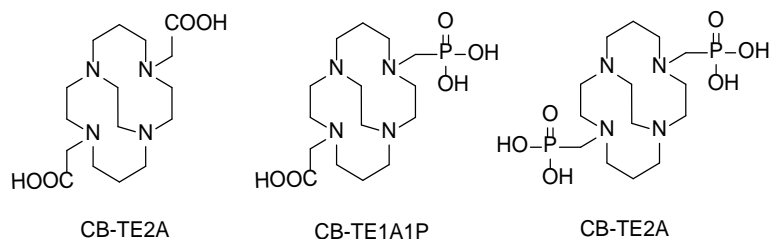


Figure 9: Structures of derivatives of TETA.

1.4.4.3 NOTA as a radiometal chelator

1,4,7-Triazacyclononane-1,4,7-triacetic acid, NOTA is a hexadentate N_3O_3 chelator and has been successfully used to chelate gallium-68 and copper-64 (see Table 7). With gallium-68, NOTA offers high radiolabelling yields under mild conditions (room temperature 30-60 min) and appropriate *in vivo* stability. NOTA is superior in radiolabelling properties and stability for copper-64 when compared to ethylenediaminetetraacetic acid (EDTA), DOTA, and TETA. As with previous examples, the structure of NOTA can be modified on the ring carbons or with a branched pendant arm to allow for the conjugation to the biological targeting moiety without disruption of the coordination sphere.

1.4.4.4 TRAP as a radiometal chelator

1,4,7-Triazacyclononane-1,4,7-tris[methyl(2-carboxyethyl)phosphinic acid], TRAP is a derivative of NOTA. The carboxylic acid arms of NOTA are replaced with phosphinic acid groups and it was originally reported more than twenty years ago by Parker *et al.*, who was the first to suggest the use of TRAP as a gallium-68 chelator.^{98, 99} TRAP can be radiolabelled efficiently at room temperature and very low pH (<1).^{100, 101} It has a formation constant ($\log K_{ML}$) of 26.3 and has been shown to be more specific in binding to gallium(III) over other competing metal ions than NOTA.¹⁰¹

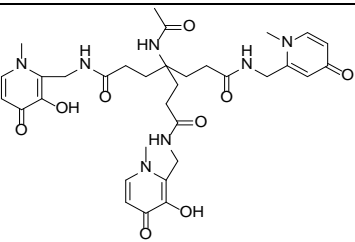
1.4.4.5 DTPA

Diethylenetriaminepentaacetic acid, DTPA is an acyclic chelator that has been used in radiochemistry for many years and can be radiolabelled with a wide range of radiometals.⁶ DTPA has been largely superseded by DOTA and NOTA as it suffers from poor *in vivo* stability in comparison, although some derivatives with a rigidified backbone have a good balance between rapid kinetics of complex formation and stability.¹⁰²

1.4.4.6 THP

Tris(hydroxypyridinone) ligands, THP (structure show in Table 8), are a relatively recent addition to the library of BFCs and have received a lot of attention as they can be radiolabelled with gallium-68 rapidly under mild conditions. Berry *et al.* labelled the BFC at room temperature over 5 min at pH 6.5.¹⁰³ This chelator has the potential for use in labelling of sensitive biomolecules with gallium-68 and, perhaps more importantly, the development of one-step kit like protocols for simplifying the radiolabelling procedures with gallium-68 to streamline clinical radiopharmacy production.

Table 8: THP acyclic BFC with relevant radiometal ion and labelling conditions

Bifunctional chelator	Radioisotopes	Labelling Efficiency	Radiolabelling conditions	Reference
	$^{67/68}\text{Ga}^{3+}$	Good	25°C, 5 min, pH 6.5	103-106
THP, tripodal tris(hydroxypyridinone) ligands; donor set O ₆	$^{89}\text{Zr}^{4+}$	Good (but low stability)	25°C, 10-15 min, pH 6-7	107

1.4.4.7 DFO

Desferrioxamine B, DFO, is clinically used for iron chelation therapy in patients presenting with excessive iron deposition in tissues and organs.¹⁰⁸ DFO has also been used with isotopes of gallium and zirconium for the development of radiotracers. DFO is the most commonly reported BFC for complex formation with zirconium-89 and has been studied *in vivo*. However, there are not yet any FDA-approved radiopharmaceuticals utilising zirconium-89. The gallium(III) DFO complex gives hexadentate (O₆) coordination in an octahedral geometry with a high stability constant (logK_{ML}) of 28.6.⁶

1.5 Chemokines and the CXCR4 chemokine receptor

1.5.1 Biological role of chemokines and chemokine receptors

The term chemokine is used to describe a large family of chemotactic cytokine proteins (see Figure 10). These proteins play several important roles in the body and are found in a range of cells in the immune system, central nervous system and endothelial cells.¹⁰⁹ They regulate the movement of cells, a process known as chemotaxis and consist of several small proteins in a size from 8-14 kDa. They can be divided into four categories C, CC, CXC, and CX3C depending on the position of the first two cysteine residues which are adjacent to the N-terminus.¹⁰⁹ To date at least 20 different chemokine receptors have been identified, with more than 50 chemokines found to influence a variety of biological processes.^{110, 111} The large number of chemokines, compared to the receptors implies the interaction of various ligands binding to several receptors, as shown in Figure 10.

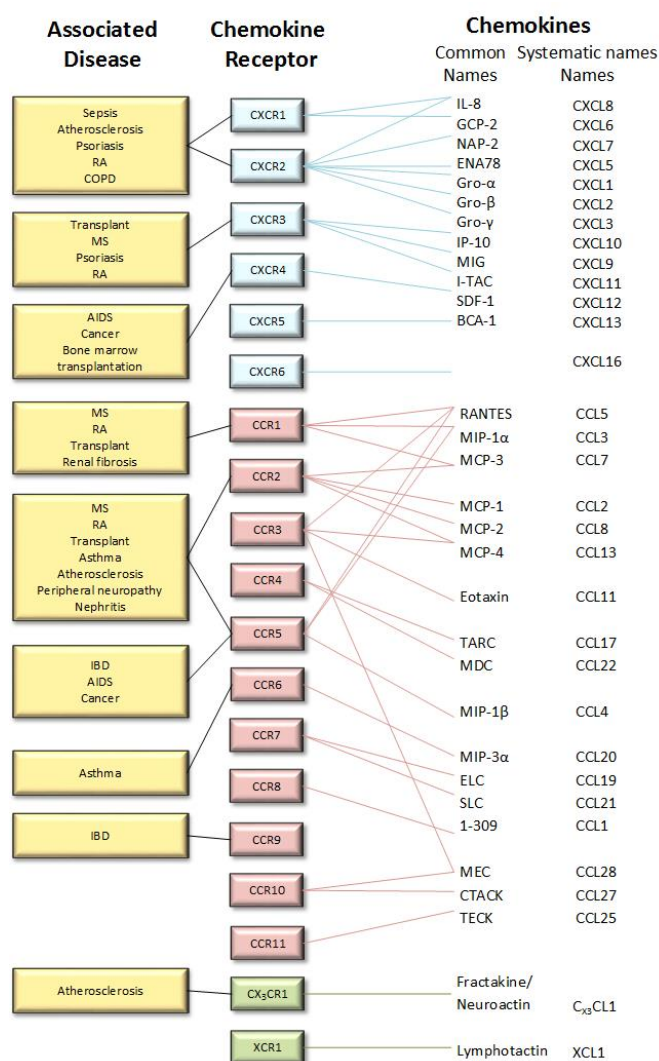


Figure 10: Diagram showing the sub-classes of chemokine receptors, their ligands and their association to disease. The receptors for the CXC subclass are shown in blue, the receptors for the CC subclass are shown in red and the receptors for the C and CX3C class are shown in green. (Inspired by figures reported by Wells *et al.* and Proudfoot *et al.*).^{112, 113}

1.5.2 CXCR4 chemokine receptor

CXCR4 is a seven transmembrane helix G-protein-coupled receptor consisting of 352 amino acids, roughly 40 kDa in size (structure seen in Figure 11). The receptor has only one endogenous ligand; the chemokine stromal cell-derived factor-1 (SDF-1), also known as CXCL12, which is a small protein containing ca. 70-90 amino acid residues with four conserved cysteines that form two disulfide bonds. Studies have shown that CXCL12 can also bind to the CXCR7 chemokine receptor linking the function of these two receptors.¹¹⁴ The CXCR4 receptor has emerged as one of the most studied chemokine receptors due to its role as a co-receptor for the entry of HIV into a cell and in the growth and spread of cancer.¹¹⁵

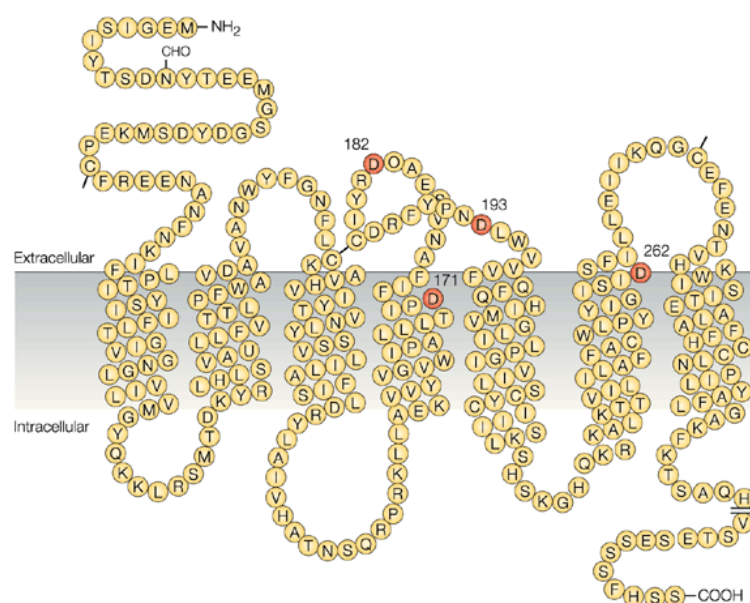


Figure 11: Schematic representation of the seven transmembrane helices of the CXCR4 receptor. Amino acids shaded red (Asp171, Asp262 ect.) shown to be key site for binding. (Reproduced from Fruehauf *et al.*).¹¹⁶

The CXCR4 receptor is rich in aspartate, histidine and tyrosine amino acids. Several of the aspartate residues surround the CXCL12 binding pocket. Their arrangement is unique to CXCR4, and although two of the aspartate residues (Asp¹⁷¹ and Asp²⁶²) are conserved in the CXCR3 receptor, the overall structural arrangements are different.¹¹⁷

CXCR4 is commonly expressed by adult bone marrow progenitor, hematopoietic, retinal pigment, endothelial, vascular smooth muscle, microglia, neuron and neuron stem cells.¹¹⁸ It is important in embryogenesis, neoangiogenesis, hematopoiesis and inflammation processes.¹¹⁹ If there is a fault or mutation in the CXCR4/CXCL12 interaction during the embryonic stages of development it leads to severe birth abnormalities including cardiac dysfunction and bone marrow defects.¹²⁰

1.5.3 Role of the CXCR4 chemokine receptor in diseases

Due to the involvement of CXCR4 and its natural ligand CXCL12 in a wide range of physiological and pathologic processes, there has been intensive biological, chemical, and pharmaceutical research into understanding the molecular mechanisms of chemokine-chemokine receptor interactions. The number of publications devoted to the topic of CXCR4 biological, radiopharmaceutical and clinical applications has dramatically increased in the past twenty years. Estimations based on PubMed reveal in the past ten years alone (2006 to 2016) there has been an approximate 70% increase in published papers on CXCR4.

CXCR4 has become an increasingly relevant topic of research due to the key role it plays in several life-threatening diseases. CXCR4 is implicated in human immunodeficiency virus (HIV)-I infection, normal hematopoietic and neural stem cell migration, cancer–stromal cell interaction, solid tumours, and inflammation/autoimmune diseases such as rheumatoid arthritis and allergic asthma.

1.5.3.1 Role of CXCR4 in Human Immunodeficiency Virus

The CXCR4 receptor has been shown to play a crucial role in the life cycle of HIV. Viral entry into a cell is mediated through the interaction of the HIV envelope protein (Env) and two receptors; CD4 and either CXCR4 or CCR5, (shown in Figure 12).^{121, 122} The virus infects and destroys the CD4+ T-lymphocytes thus causing a progressive state of immunodeficiency.¹¹⁵

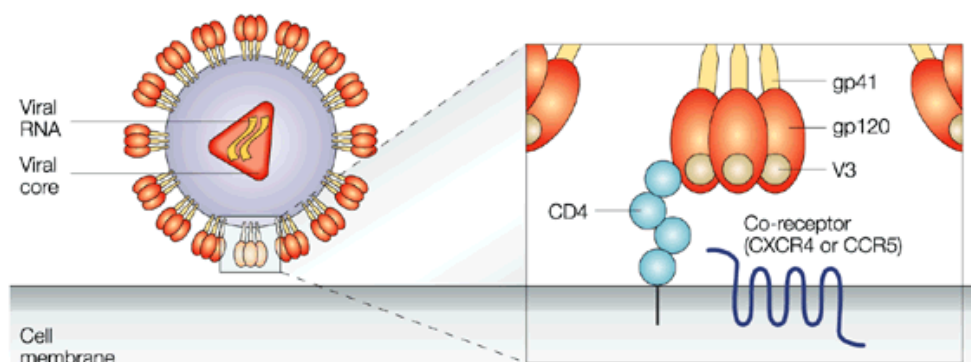


Figure 12: Imaging showing chemokine receptors CCR5 and CXCR4 are the two possible co-receptors for HIV entry. (Image reproduced from Liang *et al.*).¹²³

The work to discover CXCR4 antagonists which prevented the HIV virus entering cells was given an early boost as one of the effective anti-HIV drug candidates (from the 1990s) was discovered to act by blocking this pathway in the initial determination of the role of CXCR4 in HIV infection. The drug molecule is AMD3100, which was taken into clinical trials even before CXCR4 was confirmed to have a role in HIV infection. It is discussed in more detail in section 2.1.1. The

determination of the X-ray crystal structure of the CXCR4 receptor by Wu *et al.* in 2010 was also a key advance in enabling design of drug candidates that bind to the CXCR4 receptor.¹²⁴

1.5.3.2 Role of CXCR4 in cancer

Cancer is a disease caused by the unregulated division of abnormal cells in parts of the body. Cancer Research UK reports that cancer will affect 1 in 3 people in the UK, and every day more than *ca.* 1000 people will be diagnosed.¹²⁵ One of the key aims of research is to develop better methods for earlier diagnosis of cancer; as the earlier cancer is detected, the better the prognosis of the patient.

It is known that many cancers have a complex chemokine network that influences the immune-cell infiltration of a tumour, as well as tumour cell growth, migration, and angiogenesis. The CXCR4 receptor is one of the most over expressed chemokine receptors in cancers. It has been reported to be over expressed in 23 different types of cancers (Table 9 shows several cancers that up regulate chemokine receptors).¹¹⁹ Examples include breast cancer, ovarian cancer, prostate cancer, pancreatitis cancer, gastric cancer, melanoma, oesophageal carcinoma, lung cancer, head and neck cancer, bladder carcinoma, acute lymphoblastic leukaemia and chronic myelogenous leukemia.^{111, 118}

Table 9: Different cancers showing an overexpression of chemokine receptors.

Cancer	Chemokine receptor expressed
Breast	CXCR4, CCR7 ¹²⁶
Ovarian	CXCR4 ^{127, 128}
Prostate	CXCR4 ¹²⁹
Pancreas	CXCR4 ¹³⁰
Melanoma	CXCR4, CCR7, CCR10 ^{131, 132}
Brain	CXCR4 ^{111, 133}
Oesophageal	CXCR4, CCR10, CCR7, CCR9 ^{134, 135}
Lung	CXCR4 ¹³⁶
Head and Neck	CXCR4, CCR7 ¹³⁷
Bladder	CXCR4, CCR7, CXCR5 ^{138, 139}
Colorectal	CXCR3 ¹⁴⁰ , CXCR4 ^{141, 142}
Osteosarcoma	CXCR4, CCR7 ^{143, 144}
Neuroblastoma	CXCR4 ^{145, 146}
Acute Lymphoblastic Leukaemia	CXCR4, CXCR3 ^{147, 148}
Chronic myelogenous Leukemic	CXCR4, CXCR3, CXCR5 ¹⁴⁹
Renal cell carcinoma	CXCR4 ¹⁵⁰
Sort Tissue sarcomas	CXCR4 ¹⁵¹

Cancerous cells are thought to ‘hijack’ the CXCR4/CXCL12 axis to establish distant sites in organs for metastasis. Although there is still limited understanding about the mechanism of metastasis, it is not thought to be a random process. The CXCR4 receptor has been reported having high levels of expression in common sites of metastasis; such as the brain, bone marrow, liver, lymph nodes and lungs.¹⁵² Muller *et al.* showed that abrogation of the CXCR4/CXCL12 axis resulted in reduced metastatic burden in a variety of mouse models.¹²⁶ Up-regulation of the CXCR4 receptor has also been correlated with increased risk of metastasis, poor prognosis, tumour aggressiveness and increased chance of reoccurrence.¹⁰⁹

1.6 Development of PET tracers for CXCR4 imaging

Non-invasive imaging of CXCR4 would allow for a complementary diagnostic or prognostic biomarker for tumours expressing the CXCR4 receptor. The main areas of research into the development of a CXCR4 imaging agent utilise derivatives of T140 (peptide), FC131 (peptide) or AMD3100 (see section 2.1.1-3). Figure 13 shows a general concept that has been applied to develop a CXCR4 targeted PET tracer.

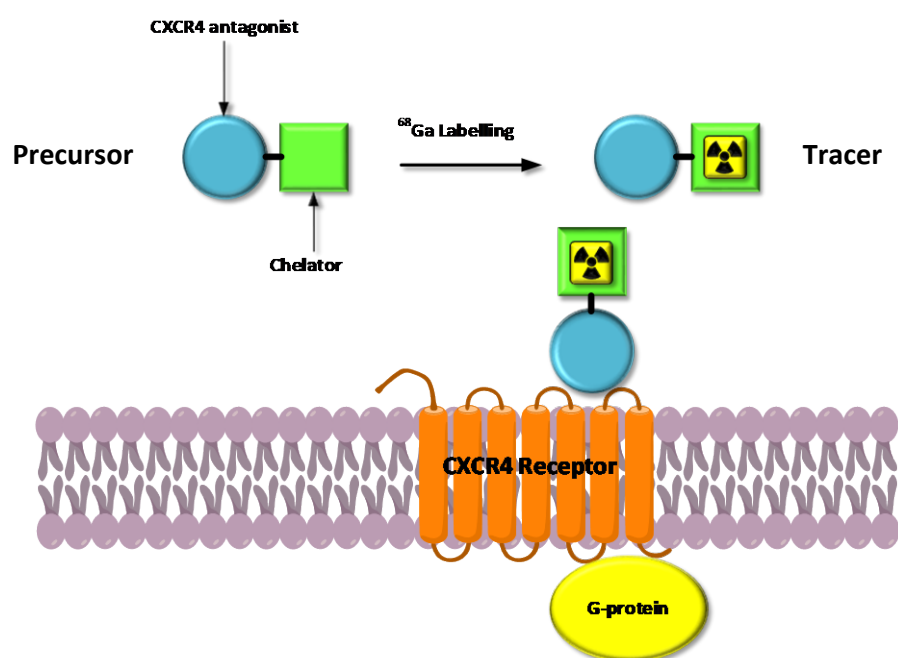


Figure 13: Schematic representation of the interaction between CXCR4 and a radiolabelled imaging agent.

1.6.1 Peptides as CXCR4 imaging probes

1.6.1.1 T140 and its derivatives

Many of the peptides used for CXCR4 imaging find their origins in work conducted by Nakashima *et al.* who were investigating horseshoe crab defence proteins tachyplesin and polyphemusin.¹⁵³ They screened many analogue peptides looking for anti-HIV activity and, of the

peptides synthesised, T140 (Arg¹-Arg²-Nal³-cyclo(Cys⁴-Tyr⁵-Arg⁶-Lys⁷-D-Lys⁸-Pro⁹-Tyr¹⁰-Arg¹¹-Cit¹²-Cys¹³)-Arg¹⁴, shown in Figure 14, **L1**) was revealed to be the most active for binding to CXCR4.

In 1998 this work was continued by Tamamura *et al.* who investigated this 14-residue peptide further.¹⁵⁴ Studies have shown that T140 binds to the CXCR4 receptor at the N- and C-terminus through four key residues (Arg², Nal³, Tyr⁵ and Arg¹⁴).¹⁵⁵ T140 derivatives form one of the most studied classes of CXCR4 antagonist as they have low nanomolar affinity and high specificity for the CXCR4 receptor. However, the high net charge on T140 caused cytotoxicity problems. Tamamura *et al.* later reported that changing some of the charged amino acid residues such as arginine or lysine to neutral L-citrulline can reduce the cytotoxicity issues, while still producing a highly stable and potent antagonist.¹⁵⁶

A further disadvantage of T140 is poor metabolic stability in serum, which led to many analogues being synthesised with modifications at each terminus to increase stability.¹⁵⁷ The most successful of these is Ac-TZ14011, with the carboxyl group protection via amidation on Arg¹.

The first use of T140 in a radiotracer construct was reported in 2006 by Hanaoka *et al.* who synthesised a CXCR4 targeting SPECT tracer by conjugating DTPA to AC-TZ14011 and radiolabelling with ¹¹¹In.¹⁵⁸ ¹¹¹In-DTPA-Ac-TZ14011 showed partial tumour uptake in nude mice bearing pancreatic tumours, as well as a significant difference in blocking studies (blocked with 10 mg/kg unlabelled TZ14011). However, the tracer was not suitable for further study as it also has high uptake in non-CXCR4 expressing organs.¹⁵⁸

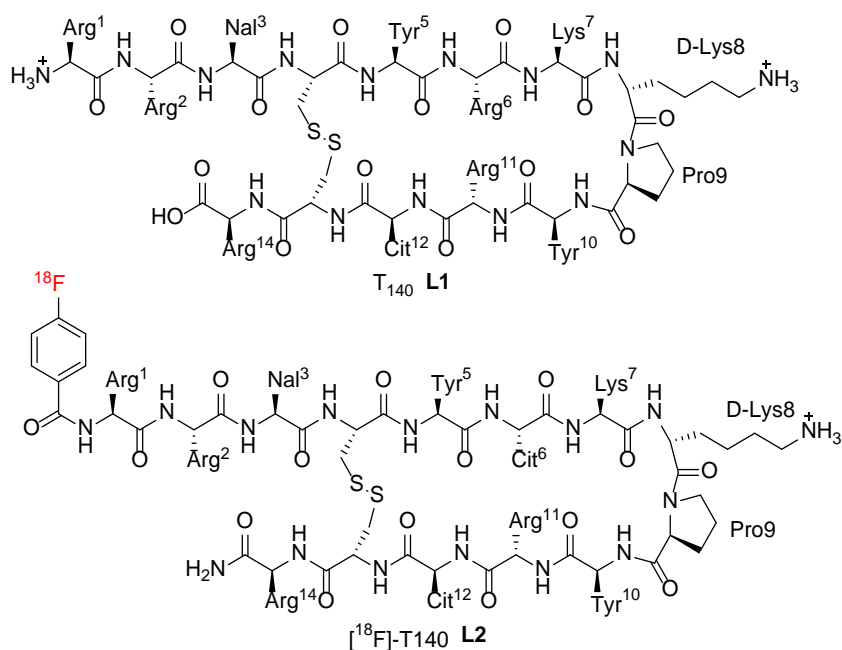


Figure 14: Structure of T140 and radiolabelled derivative.

Peptide **L2** (shown in Figure 14), [¹⁸F]-T140, was the first reported PET imaging agent derived from T140. It has a fluoro-benzyl group at the N-terminus, where the fluorine-18 radiolabel is incorporated.¹⁵⁹ *In vivo*, the tracer showed accumulation in CXCR4-expressing tumours (tumour-to-muscle ratio of 21.6), while no uptake was seen in CXCR4 negative tumours. Peptide **L2** did however have several drawbacks; the compound was only able to distinguish tumours of varying CXCR4 expression with a co-injection of the non-radioactive compound. Jacobson *et al.* proposed that without this co-injection the tracer would bind non-specifically to red blood cells (RBCs) to such an extent it would prevent the tracer from reaching the receptors in the tumour. The tracer was also both challenging to synthesise and to radiolabel, and so further development work was required.¹⁶⁰

In 2013, Zhang *et al.* investigated radiolabelling of Ac-TC14012, another T140 derivative, with fluorine-18.¹⁶¹ This was achieved via attachment to either a fluorobenzoate or fluoropropionate group at Lys-7. Both radiotracers showed higher accumulation, 4 or 5 fold increase in CXCR4-positive over CXCR4-negative tumour xenografts in mice.¹⁶¹ In contrast to the previous minimal binding to RBCs was observed, showing the influence of the C-terminal placement of the fluorobenzoate in peptides **L2** (and later **L5** and **L6**) in preventing non-specific binding.

Jacobson *et al.* also investigated other isotopes to allow facile radiolabelling of T140. The group synthesised T140 derivatives with the inclusion of DOTA or NOTA BFCs on the lysine group to radiolabel with copper-64 and gallium-68 (structures shown in Figure 15).¹⁶² The non-radioactive copper complexes of DOTA T140-NFB, **L3**, and NOTA-NFB, **L4**, gave IC₅₀ values of 68 and 138 nM respectively, which show a reduction in potency in comparison to T140 (2.5 nM).¹⁶² However, similar problems as before with binding to RBCs were observed, but the tracers were still able to positively identify the tumour (tumour-to-muscle ratio of *ca.* 5). There may also be issues with the use of a DOTA chelator for the copper-64 ion as radiometal release is likely to occur and be responsible for an increase in liver uptake (see section 1.4.4.1).

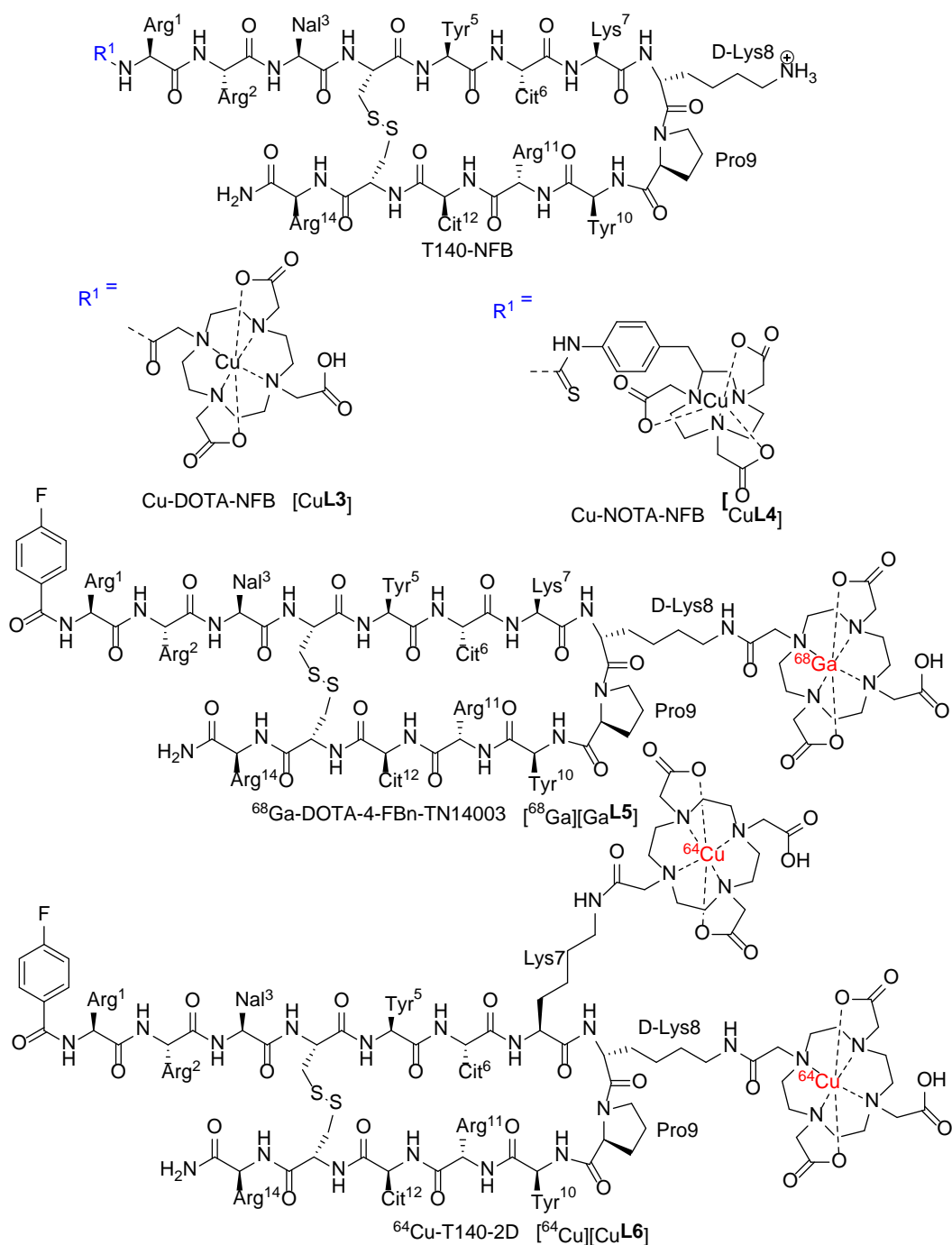


Figure 15: Structures of T140 radiolabelled derivatives for PET imaging.

^{68}Ga -DOTA-4-FBn-TN14003, [^{68}Ga][GaL5], was reported in 2012 by Hennrich *et al.* based on a very similar structure to 4-FBn-T140 reported by Jackson *et al.*, they also included a DOTA chelator at the D-Lys8 residue for gallium-68 radiolabelling.¹⁶³ *In vitro* IC₅₀ assays gave a value an approximately 2 nM for the Ga-DOTA peptide conjugate, which is promising as it matched that of 4-F-T140. However, no *in vivo* imaging data was reported for this compound.¹⁶³

Jacobson *et al.* investigated other copper-64 labelled peptide derivatives including [^{64}Cu][CuL6], with the inclusion of two DOTA BFCs attached to the peptide (see Figure 15).¹⁶⁴ [^{64}Cu][CuL6] was

reported to have an IC₅₀ value identical to T140. They reported higher uptake in the liver when compared to the ¹⁸F-T140 derivatives, and concluded this was due to transchelation of the radiometal. Tracer [⁶⁴Cu][CuL6] also needed to be co-injection with the non-radiolabelled peptide to prevent RBC binding, in line with the previous observations. [⁶⁴Cu][CuL6] has poor tumour uptake and low labelling stability, hence is not an ideal candidate for further investigation.

1.6.1.2. Cyclopentapeptides as CXCR4 imaging probes

Cyclopentapeptides have also been synthesised to produce PET tracers. The peptide FC131 (L7, shown in

Figure 16) has been radiolabelled in several ways; inclusion of DOTA for ⁶⁸Ga³⁺ labelling, reaction with *p*-fluorobenzaldehyde or by “click chemistry” with a Fluorine-18 precursor.¹⁶⁵⁻¹⁶⁸ FC131 has also been labelled with iodine-124 by Dijkgraaf *et al.* and although it had promising interaction with CXCR4,¹⁶⁹ high uptake in the liver and intestines was observed (tumour-to-liver and tumour-to-intestine ratios of 0.3 and 0.6 respectively), which was attributed to its high lipophilicity.^{169, 170}

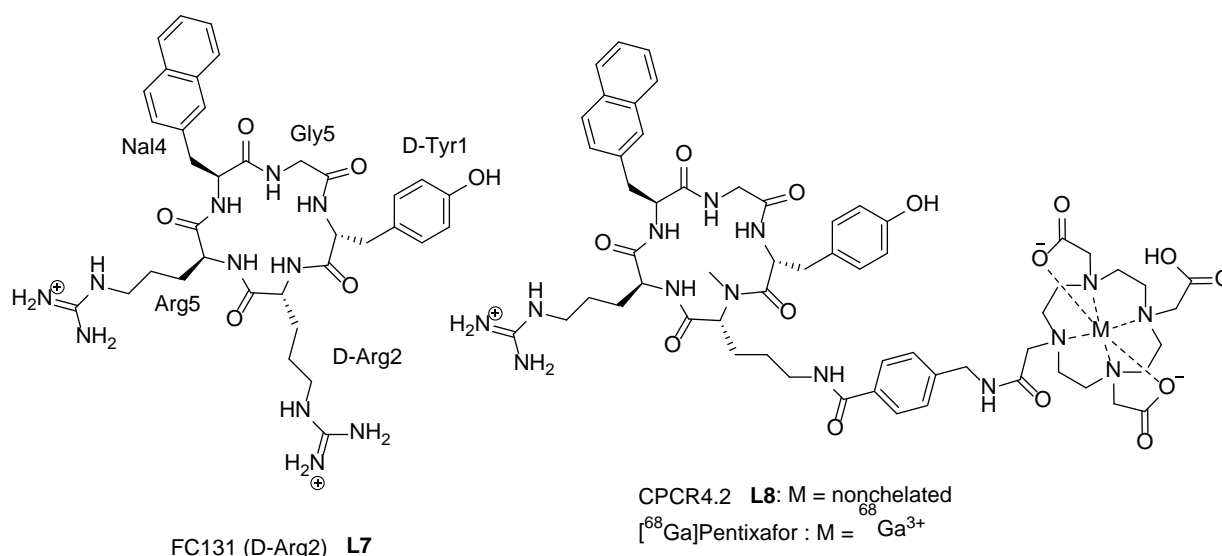


Figure 16: Structures of FC131 and Pentixafor (CPCR4.2 DOTA) derivative.

Gourni *et al.* reported the conjugation of the FC131 peptide to DOTA forming the derivative CPCR4.2, L8, and it was radiolabelled with gallium-68 to give [⁶⁸Ga]Pentixafor. The IC₅₀ value for the uncomplexed CPCR4-2, L8, was considerably higher than FC131 (150 and 4 nM respectively).¹⁶⁶ Intriguingly when complexed with gallium-68, [⁶⁸Ga]Pentixafor, the IC₅₀ decreased (5 nM) to give a more potent compound.¹⁶⁵ *In vivo* studies of Pentixafor in small cell lung cancer (OH1 h-SCLC) showed tumour specific uptake (SUV_{max} 2.1% ID/g), which could be validated though blocking experiments with AMD3100.¹⁶⁵

The success of this tracer in preclinical studies led to trials in human patients. In March 2015, Herrmann *et al.* reported the use of Pentixafor for imaging five multiple myeloma patients to assess

biodistribution and dosimetry.¹⁷¹ The results were very promising, detectable tumour uptake was seen in two of the five patients (consistent with 43% of multiple myeloma cases being CXCR4-positive, Figure 17) with high tumour-to-background ratios as well as the lack of toxicity and favourable imaging characteristics.¹⁷¹

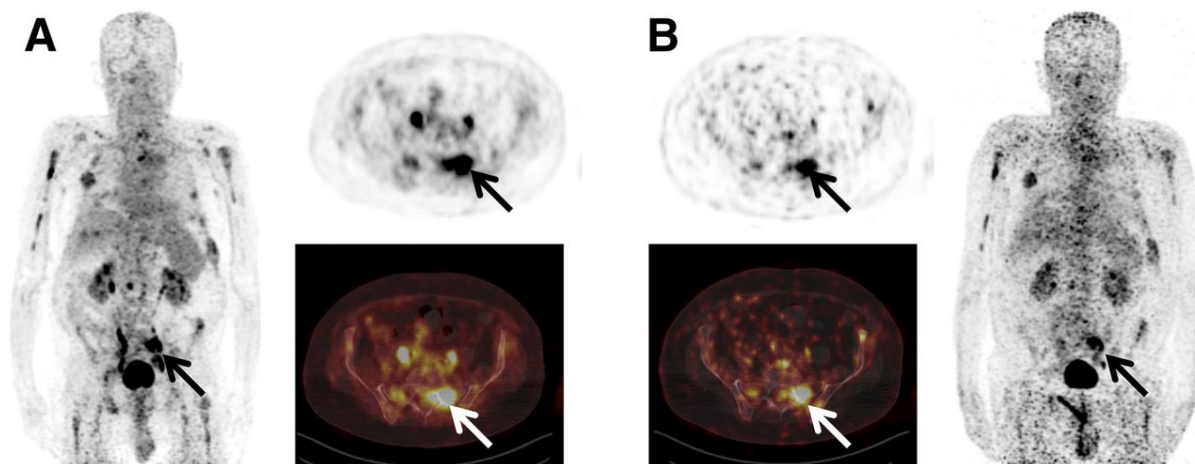


Figure 17: Example of high tumour-to-background ratios in multiple-myeloma patient. Shown are maximum-intensity projections (A, left; B, right) as well as trans axial slices 40 (A) and 236 (B) minutes after injection with [⁶⁸Ga]Pentixafor. (Reproduced from Herrmann *et al.*).¹⁷¹

The use of Pentixafor for CXCR4-targeted imaging in clinical trials is a milestone in the field of CXCR4 research. A further clinical trial imaging with [⁶⁸Ga]Pentixafor in fourteen patients was reported by the same group.¹⁷² The study compares the ability of tracers [⁶⁸Ga]Pentixafor and [¹⁸F]FDG to detect tumours. [⁶⁸Ga]Pentixafor was revealed to be better at detecting lesions in seven of the fourteen patients and comparable in three patients. In two patients [¹⁸F]FDG was judged to provide superior diagnostic information, and in the remaining two patients both tracers provided useful complementary information. This work does indicate a shortcoming in the application of Pentixafor as it failed to identify some CXCR4-positive tumours.

Recently Poschenrieder *et al.* looked at expanding on the library of metal-chelate conjugate derivatives of Pentixafor.¹⁷³ The paper reported on different BFCs (DOTA, DOTAGA, NOTA, NODAGA, DTPA and DFO-B) along with chelation to various non-radioactive metal ions (Ga³⁺, AlF²⁺, Zr⁴⁺, Cu²⁺, In³⁺, Lu³⁺, Y³⁺, and Bi³⁺). Each complex was assessed for CXCR4 binding affinity and as a result of this study, two constructs, Pentixafor-NOTA ([^{nat}Ga³⁺], IC₅₀ = 17.8 nM) and a Pentixafor-DOTA ([^{nat}Bi³⁺], IC₅₀ = 22.1 nM) were identified as potential CXCR4 targeting agents.¹⁷³ However, the gallium-NOTA Pentixafor tracer gave disappointing *in vivo* results.¹⁷⁴

Another recent paper from the same group reported the synthesis and labelling of the CXCR4 peptide used in Pentixafor with therapeutic radionuclides lutetium-177 and yttrium-90, to give [¹⁷⁷Lu]Pentixather and [⁹⁰Y]Pentixather.¹⁷⁵ This approach offers a theranostic combination of

isotopes where patients can be selected for response to the therapeutic isotope labelled agent with a scan using the PET isotope equivalent. Therapy response can also be tracked using the imaging radiotracer. The radiotherapeutic agents were administered to three patients along with stem cell therapy and chemotherapy. The paper reports that one patient went into complete remission, one showed a partial response and the third developed terminal sepsis. It is hard to conclude the extent of the effect of the therapeutic agents [¹⁷⁷Lu]-pentixather or [⁹⁰Y]-pentixather as the positive patient response could be due to the other therapies they underwent simultaneously but this shows that this approach is worthy of further investigation.

Peptides such as T140, CPCR4.2 and their derivatives have shown promise for the imaging of CXCR4 expression *in vivo*, and are at a relatively advanced stage of development: There are also recent advances in other classes of tracer, in particular those based on tetraazamacrocyclic constructs for binding to the CXCR4 receptor, which forms the basis for the research in this thesis.

1.7 Research aims

The main aims of this work are to synthesise, label (with radioisotope or optically active tags) and biologically validate tetraazamacrocyclic compounds and peptides as CXCR4 binding probes for medical imaging applications. This work largely builds upon previously reported results by the Archibald group that the inclusion of metal ions in configurationally restricted multi-tetraazamacrocyclic compounds enhances binding towards the CXCR4 chemokine receptor.

PET radioisotopes such copper-64, gallium-68 and fluorine-18 can be utilised for the development of novel CXCR4 specific imaging probes. *In vivo* validation in mice models is required to determine the potential of the antagonists, with a focus on the compounds shown in Figure 18.

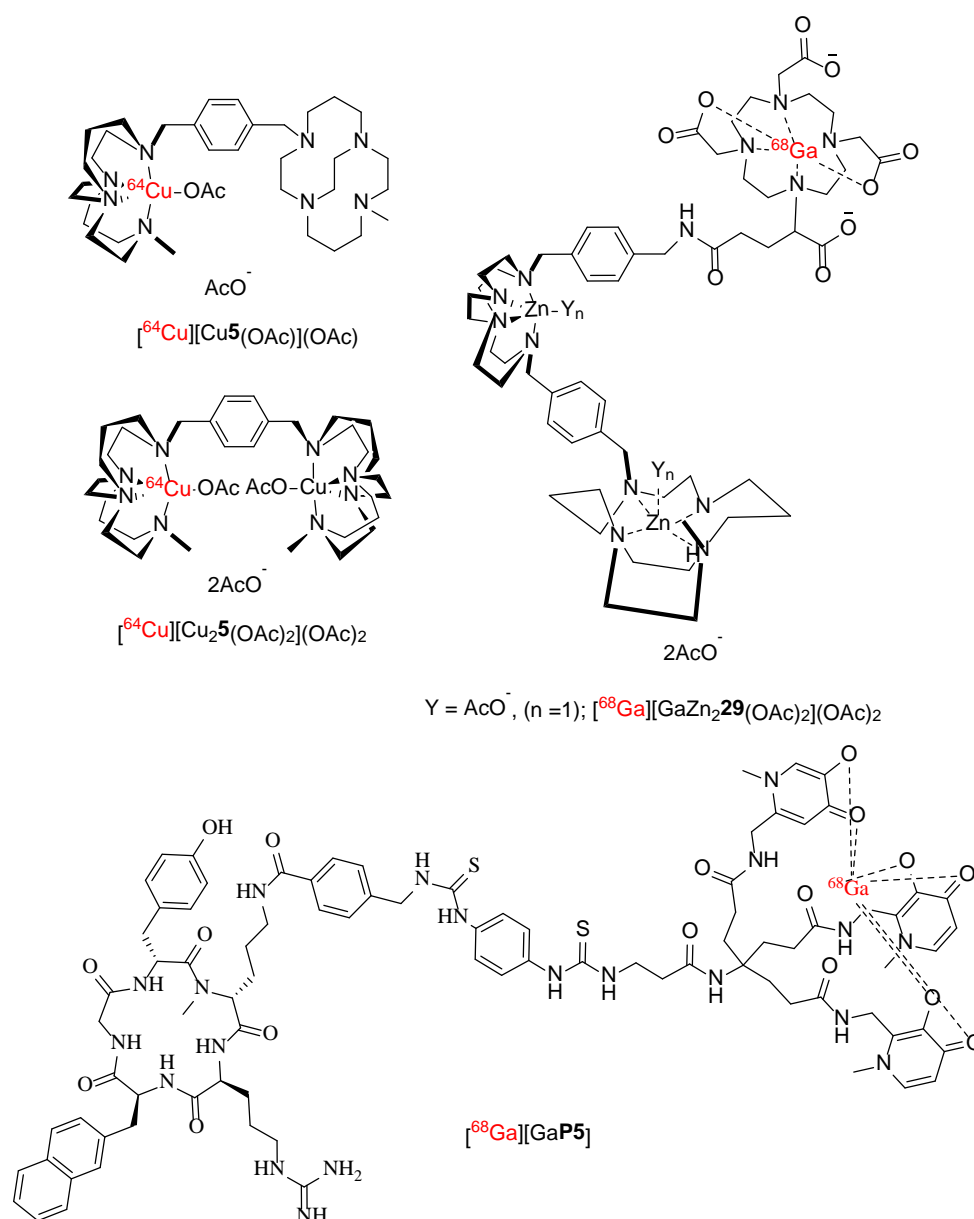


Figure 18: Structures of novel CXCR4 antagonist target compounds that are synthesised in this work and tested *in vivo*.

Novel technetium-99m labelled CXCR4 binding probes are also of interest for SPECT imaging, with *in vitro* validation to determine the most promising structures for future development *in vivo*. Fluorophores can be conjugated to the small molecules and peptides for the development of CXCR4 specific optical imaging. There is interest in novel NIR emitting dyes (e.g. aza-BODIPY) in the development of CXCR4 optical imaging probes.

1.6 Summary

There has been a dramatic increase over recent years in the development of target specific radiopharmaceuticals for cancer imaging. Although, the peptide Pentixafor reported by the Wester group has been clinically translated, there still remains a great deal of scope for further CXCR4 specific imaging agents; especially small molecule based compounds. This work investigates the development of high affinity CXCR4 antagonists for diagnostic applications. In chapter 2 the synthesis and biological investigation of copper-64 radiolabelled small tetraazamacrocycles is discussed. Chapter 3 outlines the synthesis of novel gallium-68 radiolabelled compounds, either by a direct or pretargeted approach. In chapter 4 the synthesis of inorganic (Al-F) radiolabelled fluorine-18 tetraazamacrocyclic compounds is discussed. Chapter 5 details the synthesis and biological testing of novel technetium-99m tetraazamacrocycles for SPECT imaging. Chapter 6 describes the development of a novel NIR dye conjugate CXCR4 binding peptide. The work is then summarised and concluded in chapter 7 with potential future work outlined in chapter 8.

Chapter Two

Synthesis and radiolabelling of
CXCR4 antagonists with
copper-64 for PET imaging

2.1 Previous research and development of small CXCR4 antagonists

2.1.1 Tetraazamacrocyclic CXCR4 antagonists (AMD3100)

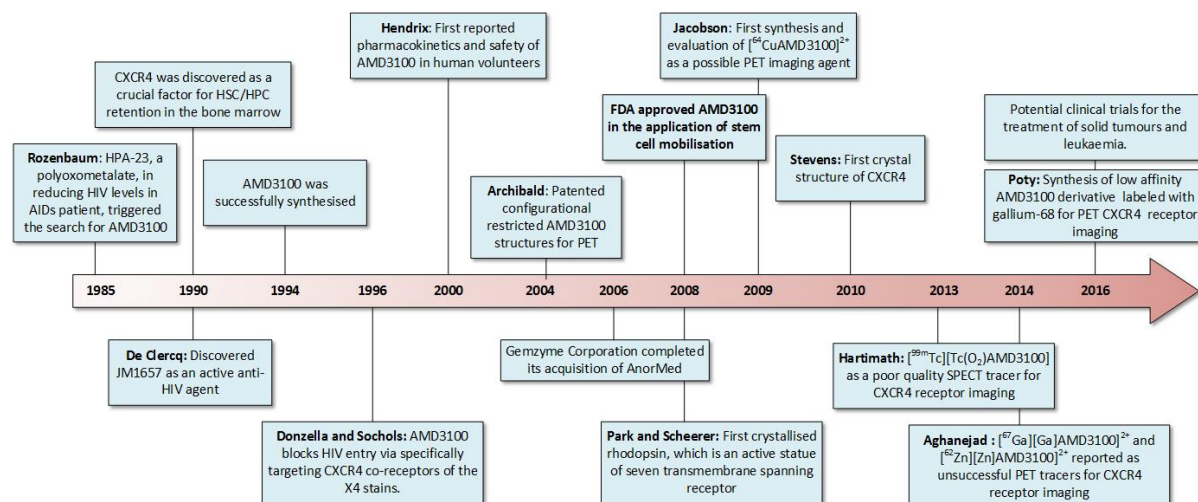


Figure 19: Timeline of the discoveries that shaped the development of AMD3100 and its uses.

The discovery of AMD3100 as a CXCR4 antagonist (see Figure 19) stemmed from the early 1980s search for drugs to combat the acquired immune deficiency syndrome (AIDS) epidemic. Rozenbaum *et al.* reported *in vivo* efficacy of a polyoxometalate (HPA-23), that inhibited HIV levels in patients with AIDS, triggering a screen of molecules that did not fit with traditional drug discovery; including porphyrins and tetraazamacrocycles.^{176, 177}

The potent use of tetraazamacrocycles as CXCR4 antagonists was discovered serendipitously in the 1980s. Erik De Clercq at the Rega Institute was screening a large library of compounds for anti-HIV activity, in collaboration with Johnson Matthey, and found an impurity in one sample of cyclam (JM1498) that had potent anti-HIV activity, with an EC_{50} of about 10 μg per mL.¹¹⁶ After further investigation it was discovered that this impurity consisted of two 14-membered tetraazamacrocyclic rings connected directly by a C-C bond, the impurity was labelled JM1657, see Figure 20. This led to the synthesis of a series of bis-cyclam analogues containing different linkers. JM3100 (later changed to AMD3100 when the development was transferred to a separate company AnorMED) was an analogue which consisted of the two cyclam rings with an aromatic linker, and had a 100 fold increase in potency in the anti-HIV assays.

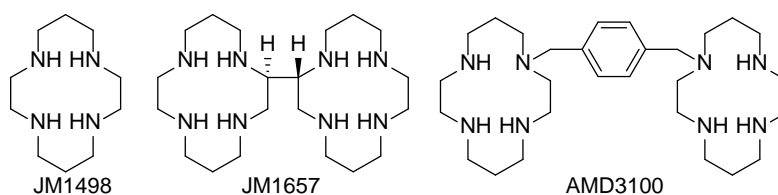


Figure 20. Structures involved in the discovery process of AMD3100.

The role of the CXCR4 chemokine receptor in the HIV infection cycle was not yet known at the time of AMD3100 discovery. Work carried out by De Clercq *et al.* indicated that AMD3100 inhibits the early, post-adsorption event in the HIV viral replication cycle, which is termed fusion/uncoating.¹¹⁶ De Clercq was proven to be correct as further research into AMD3100 showed a specific interaction with the CXCR4 receptor; shown to be a key co-receptor for the entry of the virus into the cell.¹⁷⁸

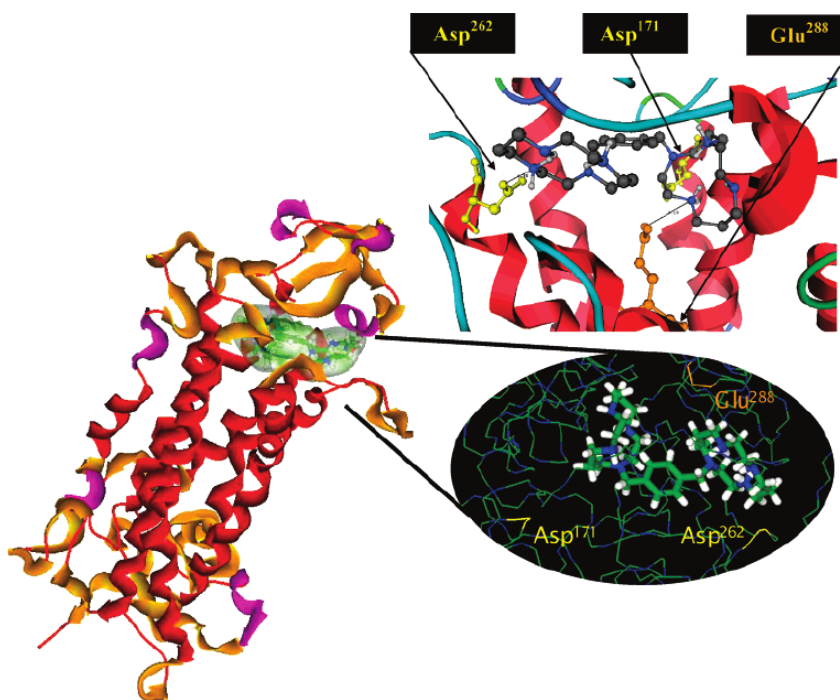


Figure 21. Diagram showing AMD3100 interactions in the CXCR4 receptor. (Reproduced from Pérez-Nueno *et al.*).¹⁷⁹

AMD3100 binds to the CXCR4 receptor via electrostatic interactions and hydrogen bonding between the positively charged protonated nitrogen atoms of the cyclam ring and the negatively charged carboxylates of the glutamate and aspartate amino acids of the receptor.⁵³ Site directed mutagenesis studies found that the amino acid residues Asp¹⁸¹, Asp¹⁸², Asp¹⁸⁷ and Asp¹⁹³ in extracellular loop two and, particularly, Asp¹⁷¹ and Asp²⁶² on transmembrane helix (TM)-IV and TM-VI (which are positioned at each end of the main ligand-binding crevice of the CXCR4 receptor) have a role in the ability of AMD3100 to block the binding of the chemokine ligand CXCL12 (as shown in Figure 21).¹⁸⁰⁻¹⁸²

AMD3100 was clinically tested as an anti-HIV drug, but the trial was not successful for a few reasons, mainly because it was entered into without screening the patients for their viral strain. This meant that patients with R5 (uses CCR5) viral strains that use the CCR5 chemokine receptor for cell entry were included in the cohort to be treated. There were also concerns with the low oral bioavailability of the compound which meant that it needs to be administered by injection. AMD3100 is now licenced by the FDA as Plerixafor, a Haematopoietic Stem Cell (HSC) mobilisation drug for use in non-Hodgkin's lymphoma and multiple myeloma patients.¹⁸³ The HSC mobilisation effects were noted in the patients in the initial clinical trial.

2.1.2 Synthesis of AMD3100 metal complexes

AMD3100 provided inspiration for the design of modified agents for binding to the CXCR4 receptor. The preorganisation of the cyclam macrocyclic framework and the availability of lone pairs of electrons make it an ideal framework for coordinating metal ions. It made sense to test the metal complexes of this compound to investigate the effects on the protein binding interaction.¹⁸⁴

AMD3100 has two cyclam rings that can coordinate to metal ions, each with four nitrogen donor atoms and the flexibility to coordinate in either a square planar arrangement or a folded tetradentate form. From a cation size perspective, the best match is with the first row transitional metals, with a focus on those with a 2+ charge and an ionic radius of less than 7 Å.¹⁸⁵ Gerlach *et al.* reported that the incorporation of metal ions, such as copper(II), zinc(II) or nickel(II), into the cyclam rings could dramatically enhance the binding affinity to the CXCR4 receptor. The inclusion of two zinc(II) ions into the cyclam rings of AMD3100 sees an increase in affinity to the CXCR4 receptor in an *in vitro* screening assay (AMD3100, $IC_{50} = 74$ nm; $[Zn_2AMD3100]^{4+}$, $IC_{50} = 12$ nM).¹⁸⁶ The increase in binding affinity is thought to be due to a coordinate bond that forms between the metal ion and the carboxylate functional group of the aspartate in the AMD3100 binding site of the CXCR4 receptor.¹⁸⁶ Gerlach *et al.* also synthesised a library of mono-copper(II), zinc(II), nickel(II) coordinated AMD3100 derivatives. They appeared to show in some cases that the mono-metal compounds showed equal affinity to the bis-metallated, therefore, attributed the increase in affinity to only one of the metal ions, although later studies indicate that this may not be entirely correct.¹⁸⁶

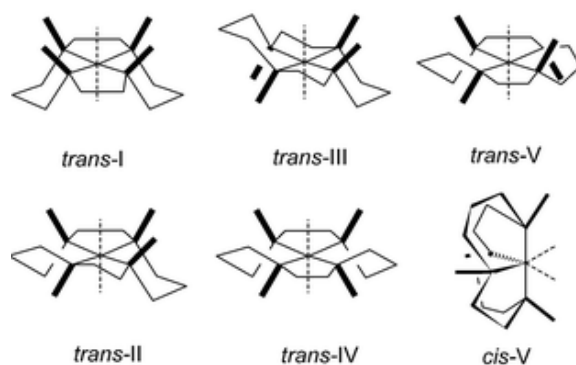


Figure 22: The six configurations of metal-cyclam complexes.

The group also indicated the possible geometries of the AMD3100 metal complexes based on the extensive work already carried out characterising cyclam complexes. The zinc(II) complex is likely to form a complex with either a square pyramidal or an octahedral geometry.¹⁸⁶ However, AMD3100 copper(II) complexes can form a wider variety of geometries from four-coordinate square planar geometry to five or six coordinate geometries (Figure 22).¹⁸⁷ The formation of metal complexes with AMD3100 causes the nitrogens of the cyclam rings to become chiral, giving rise to six possible different configurations for each cyclam. In general, the most thermodynamically stable configurations are the folded (cis-V) and planar (trans-III) configurations but this can vary with different metal ions, solvent and counter anions.¹²³

2.1.3 AMD3100 derivatives as imaging agents

Due to the affinity of AMD3100 towards CXCR4 there has been a great deal of research aimed at developing AMD3100 derivatives as PET imaging agents. Jacobson *et al.* were the first to successfully radiolabel AMD3100 with mono copper-64 to form $[^{64}\text{Cu}][\text{CuAMD3100}]^{2+}$ (Figure 23). In addition to copper-64 having beneficial radiochemical properties, the presence of the copper(II) ion complex with the macrocyclic ring may increase the binding affinity of AMD3100 to the CXCR4 receptor. Biodistribution studies of $[^{64}\text{Cu}][\text{CuAMD3100}]^{2+}$ were carried out in normal mice and showed high clearance from the blood; as well as uptake in CXCR4 expressing organs such as liver, kidneys and spleen.¹⁸⁸ This early study showed potential for copper-64 AMD3100 as a CXCR4 specific imaging agent.

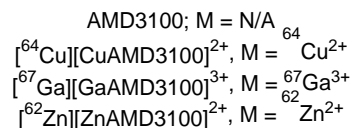
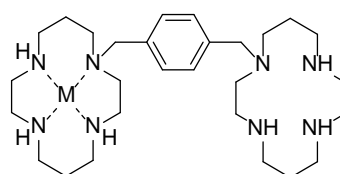


Figure 23: Structures of radiolabelled AMD3100.

A further more detailed study a few years later by Nimmagadda *et al.* tested $[^{64}\text{Cu}][\text{CuAMD3100}]^{2+}$ in various mouse xenograft models. The group reported that tracer accumulation was higher in over-expressing transfected CXCR4 glioblastoma cellular models (35% ID/g) compared to endogenous tissues or a low expressing CXCR4 xenograft tumour (see Figure 24). Furthermore, the group reported the use of $[^{64}\text{Cu}][\text{CuAMD3100}]^{2+}$ for imaging lung metastases in mice, which shows an increased level of CXCR4 expression compared to healthy lungs. However, high liver uptake (>40% ID/g) indicates that stability of the copper-64 in the cyclam ring may be problematic, although this was not fully investigated by the authors. This would limit the use of $[^{64}\text{Cu}][\text{CuAMD3100}]^{2+}$ as a PET tracer, as the signal could either be due to the CXCR4 binding complex or the released radioisotope.¹⁸⁹ It is expected that released copper-64 would ultimately end up in the liver with previous studies showing initial binding to ceruloplasmin in the blood followed by transfer to the liver and uptake into CuZn SOD.¹⁹⁰ To investigate the potential for copper transchelation, mice were also injected with $[^{64}\text{Cu}]\text{CuCl}_2$, which indicated that the uptake seen with $[^{64}\text{Cu}][\text{CuAMD3100}]^{2+}$ was not due to the transchelation of copper-64, although there is some uptake of the $[^{64}\text{Cu}]\text{CuCl}_2$ in the tumour.

This was also shown by Weiss *et al.* who reported that $[^{64}\text{Cu}][\text{CuAMD3100}]^{2+}$, showed high-uptake in non-targeted tissues, including the lungs, liver, spleen and kidneys. The group attempted a blocking study using unlabelled AMD3100, however, PET-CT scans still revealed a high signal in these organs, especially the liver. The group attempted to account for this by the possibility of $[^{64}\text{Cu}][\text{CuAMD3100}]^{2+}$ binding to another receptor, however, the most likely explanation is the transchelation of the copper(II) ion.¹⁹¹ This therefore hindered the clinical development of the copper-64 complex of AMD3100 as a PET imaging tracer.

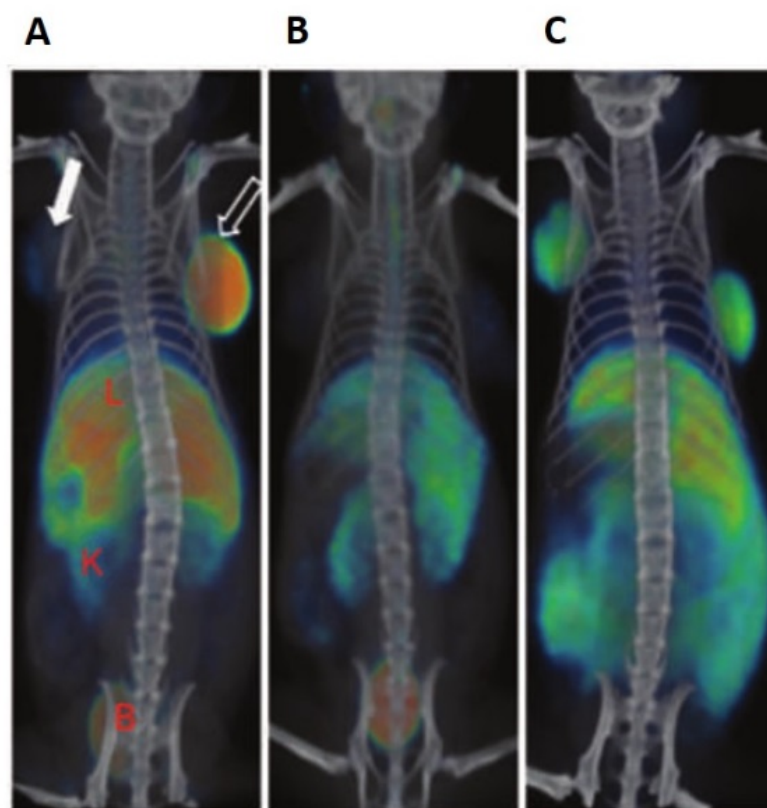


Figure 24: PET/CT scan of mice bearing both CXCR4-positive and CXCR4-negative tumours (hollow arrow and solid arrow respectively). B = bladder; K = kidney; L = liver. A: Mouse injected only with copper-64 AMD3100. B: Blocking study in which mouse was injected first with AMD3100, then with $[^{64}\text{Cu}][\text{CuAMD3100}]^{2+}$. C: Biodistribution study in which $[^{64}\text{Cu}]\text{CuCl}_2$ was injected into the mouse. (Reproduced from Nimmagadda *et al.*).¹⁸⁹

AMD3100 has also been radiolabelled with gallium-67, although it seems highly unlikely that this would form a stable complex. Aghanejad *et al.* reported the biodistribution of $[^{67}\text{Ga}][\text{GaAMD3100}]^{3+}$ (Figure 23) in wild type Sprague-Dawley rats.¹⁹² As with $[^{64}\text{Cu}][\text{CuAMD3100}]^{2+}$, considerable uptake in the spleen was observed. The group also imaged human breast carcinoma-bearing mice with $[^{67}\text{Ga}][\text{GaAMD3100}]^{3+}$ and reportedly accumulation of the radiotracer in the CXCR4 positive tumours 4 and 24 hours post-injection. However, no exact values or ratios are given for the tumour bearing animals, and the image quality is poor.¹⁹² Blocking studies were not carried out.

A further proof-of-principle study by the same group was also reported the same year; investigating radiolabelling of AMD3100 with the rarely used zinc-62 radioisotope which is also the parent isotope of copper-62.¹⁹³ $[^{62}\text{Zn}][\text{ZnAMD3100}]^{2+}$ was synthesised, although the details of the study and analysis were not of a high standard. The group claimed good stability in human serum for 24 hours at 37°C. However, as with all the radiolabelled analogues of AMD3100 investigated thus far, the biodistribution in rat models showed high uptake in liver, kidneys and spleen.¹⁹³ No *in vitro* data was reported on the affinity of $[^{62}\text{Zn}][\text{ZnAMD3100}]^{2+}$ towards CXCR4 and no blocking studies were performed, limiting the value of this work.

2.1.4 Tetraazamacrocyclic compounds for PET imaging

AMD3100 sparked a lot of interest in the synthesis and testing of small macrocyclic compounds to bind to the CXCR4 receptor. Gelach *et al.* explored the binding of cyclam to the CXCR4 receptor and discovered it was dependent on the Asp¹⁷¹ residue.¹⁸⁰ A series of mono-macrocyclic compounds were developed to build upon this. Of particular note is AMD3465 (shown in Figure 25), the compound structure consists of only the one macrocyclic ring and a N-pyridinylmethylene group.

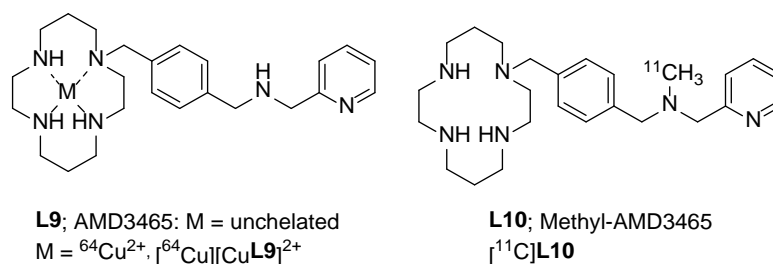


Figure 25. Structure of mono-macrocycle radiolabelled derivatives AMD3465.

AMD3465 has a high affinity for the CXCR4 receptor with an IC₅₀ value of 18 nM.¹⁹⁴ De Silva *et al.* formed a metal complex of AMD3465 with copper-64 to give the potential PET tracer [⁶⁴Cu][CuL9]²⁺. Mice bearing U87-CXCR4 tumours showed very high uptake (96.3% ID/g) even after 24 hours, when compared to the control tumours (3.0% ID/g).¹⁹⁵ Furthermore, the maximum tracer uptake showed a tumour-to-muscle ratio of 361 (versus 18 in low CXCR4 expressing tumours), see Figure 26.¹⁹⁵ Uptake of [⁶⁴Cu][CuL9]²⁺ could be blocked by the administration of non-radioactive copper(II) complex AMD3465 to demonstrate specificity for the CXCR4 receptor. However, as with [⁶⁴Cu][CuAMD3100]²⁺ after the administration of a blocking dose (Figure 26, B) the liver remains clearly visible. This is again likely to be due to the instability of the cyclam copper(II) complex releasing the copper-64 ion.

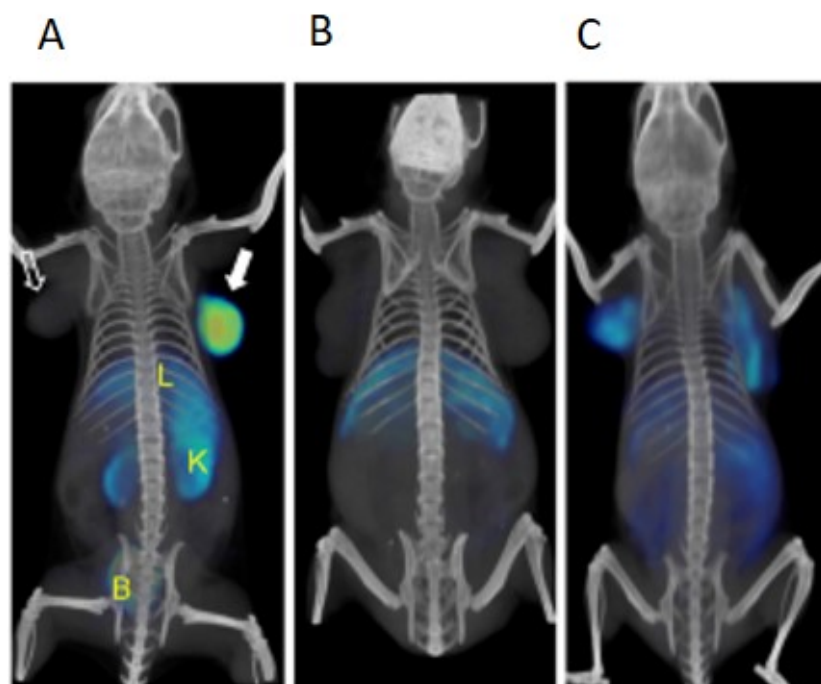


Figure 26: A: PET scan of mouse bearing CXCR4-positive tumour on right shoulder and CXCR4-negative tumour on left shoulder after injection with $[^{64}\text{CuL9}]^{2+}$. B: Blocking dose of $[\text{CuAMD3465}]^{2+}$ followed by $[^{64}\text{Cu}][\text{CuL9}]^{2+}$. C: Biodistribution study in which $[^{64}\text{Cu}]\text{CuCl}_2$ was injected into the mouse. (Reproduced from De Silva *et al.*).¹⁹⁵

More recently, Hartimath *et al.* radiolabelled AMD3465 with carbon-11 to form compound **L10** (Figure 25). The group prepared N- $[^{11}\text{C}]$ methyl-AMD3465 by the N-methylation of $[^{11}\text{C}]\text{CH}_3\text{OTf}$. They obtained compound, $[^{11}\text{C}]\text{L10}$, at *ca.* 60% radiochemical yield (RCY) in high purity.¹⁹⁶ N- $[^{11}\text{C}]$ methyl-AMD3465 showed good *in vitro* stability toward human liver microsomes and rat plasma. However, the methylation of the secondary amine in the linker between the cyclam macrocycle and the pyridine ring resulted in slightly lower binding affinity towards the CXCR4 receptor compared to AMD3465. Nonetheless, $[^{11}\text{C}]\text{L10}$ still has a lower IC_{50} (*ca.* 0.45 μM) than that of AMD3100 (*ca.* 1.5 μM). It should be noted that the *in vitro* assay used is not the same one reported previously for the other compounds, hence the higher values.¹⁹⁶ In 2017, the group also illustrated how $[^{11}\text{C}]\text{L10}$ could be used to investigate the relationship between amount of drug administered and the occupancy of the receptors *in vivo*.¹⁹⁷

2.1.5 Configurational restricted tetraazamacrocycles

Further development of the cyclam based CXCR4 imaging tracers has been attributed to the instability caused by the transchelation of copper-64 ion from the cyclam ring. Archibald and co-workers showed that the incorporation of an ethylene bridge could be achieved for bis-tetraazamacrocyclic complexes and filed a patent application for these compounds in 2004. The bridge between adjacent (side bridge, SB) and non-adjacent nitrogens (cross bridge, CB) in the tetraazamacrocyclic ring increases kinetic stability of transition metal complexes (Figure 27) and there is extensive previous characterisation of the related mono-macrocycle compounds from Busch, Weisman and Wong.¹⁹⁸⁻²⁰¹

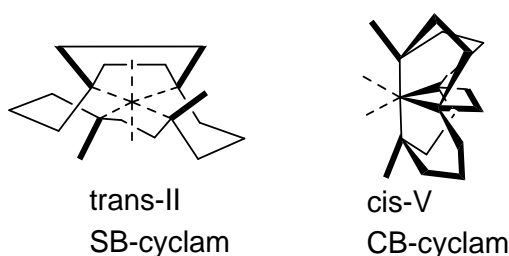


Figure 27: Structure and geometry of side-bridged (SB) cyclam & cross-bridge (CB) cyclam.

The restricted macrocycles become highly rigid and when complexed with a transition metal, form only one macrocycle configuration. As shown in Figure 27, the side bridge cyclam complex forms a *trans-II* configuration while the cross bridge cyclam complex forms a folded *cis-V* configuration. The metal complex fixed in the *cis-V* configuration provides high kinetic stability, even for the labile copper(II) complex. It is also suspected to provide an enhanced geometry for protein binding by coordinate bond formation with aspartate residues on the CXCR4 receptor.^{198, 202}

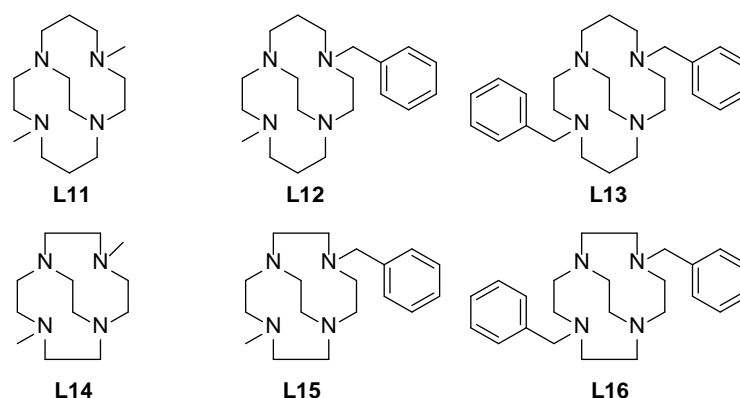


Figure 28: Cross bridged restricted macrocycles ligands that were complexed with zinc and copper (reproduced from Maples et al.).²⁰²

Archibald and co-workers went on to report a series of rigid cross-bridge bis-tetraazamacrocyclic transitional metal chelated antagonists which bind to CXCR4 with high affinity and long receptor residence times.¹⁹⁸ In 2016, Archibald and co-workers reported the binding affinity of mono-

tetraazamacrocyclic ligands (**L11-L16**, Figure 28) complexed with copper(II) and zinc(II) to further elucidate the bonding interaction.²⁰² The investigation found that the most potent antagonists were $[\text{CuL12}]^{2+}$, $[\text{ZnL13}]^{2+}$, $[\text{ZnL15}]^{2+}$, and $[\text{ZnL16}]^{2+}$, all having IC_{50} values below 20 nM, similar to that of AMD3100.²⁰² However, due to the single coordination bonding interaction for these molecules with the protein, they suffer from non-specific binding and would be likely to have a shorter residence time at the receptor, therefore making bis-macrocycle compounds are preferred.

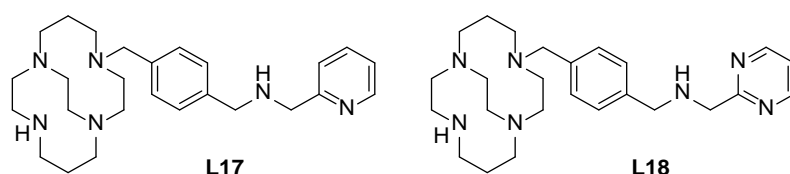


Figure 29: Structure of unlabelled mono-macrocycle configurational constricted derivatives of AMD3465.

Building on the work in the Archibald group, the theory on configurational restriction was exploited by Woodard *et al.* in 2014 with the formation of two configurationally restricted analogues of AMD3465, shown in Figure 29.²⁰³ The group radiolabelled the cross-bridged cyclam analogues of AMD3465 with copper-64 for imaging studies carried out in mice bearing U87-CXCR4 and control U87 tumours (see Figure 30). High accumulation was shown for both tracers $[\text{}^{64}\text{Cu}][\text{CuL17}]^{2+}$ and $[\text{}^{64}\text{Cu}][\text{CuL18}]^{2+}$ in the high expressing CXCR4 tumour model and was shown to be blockable by the non-radioactive analogue, see Figure 30. tumour-to-muscle ratios for $[\text{}^{64}\text{Cu}][\text{CuL17}]^{2+}$ and $[\text{}^{64}\text{Cu}][\text{CuL18}]^{2+}$ reached 61.10 ± 16.90 and 106.05 ± 17.19 respectively, while tumour-to-blood ratios reached 11.54 ± 2.17 and 28.08 ± 4.78 , respectively.²⁰³

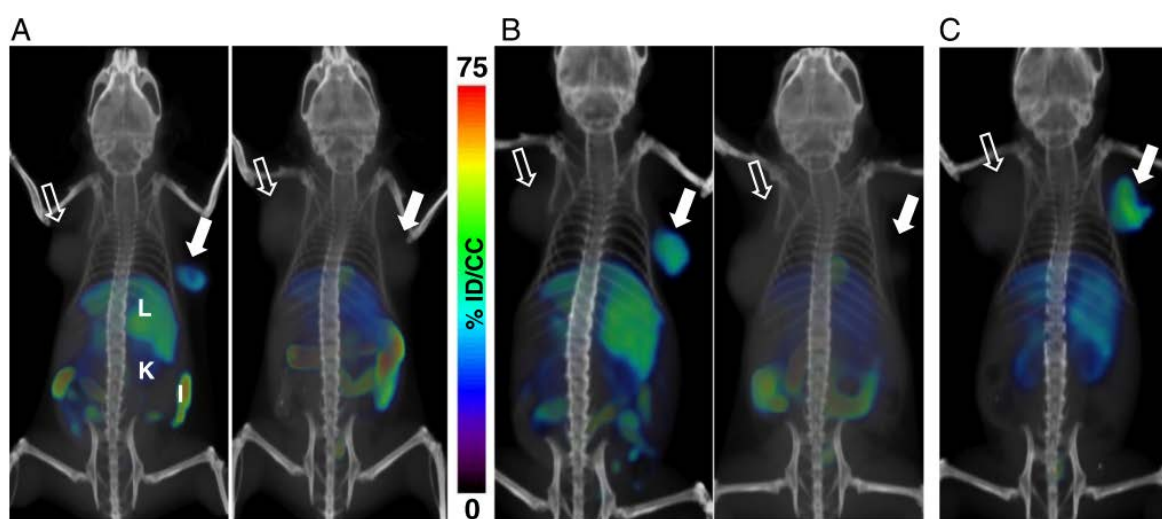


Figure 30: A) PET/CT Scan with $[\text{}^{64}\text{Cu}][\text{CuL17}]^{2+}$ (left), and AMD3465 blocking dose followed by $[\text{}^{64}\text{Cu}][\text{CuL20}]^{2+}$ (right); B) PET/CT Scan with $[\text{}^{64}\text{Cu}][\text{CuL21}]^{2+}$ (left), and AMD3465 blocking dose followed by $[\text{}^{64}\text{Cu}][\text{CuL18}]^{2+}$, C) PET/CT Scan with $[\text{}^{64}\text{Cu}]\text{AMD3465}$, 18. Filled arrow, U87-CXCR4 tumour (right); unfilled arrow, control U87 tumour (left); L – liver, K – kidney, I – intestines. (Reproduced from Woodard *et al.*).²⁰³

However, Woodard *et al.* reported the highest uptake of activity 90 minutes after injection in the liver ($84.72 \pm 9.78\%ID/g$) compared to only $18.61 \pm 2.29\%ID/g$ seen in the CXCR4 transfected tumours. The values detailed are higher than that previously reported by De Silva *et al.* labelling the non-configurational restricted precursor AMD3465, **L9**. The increased uptake seen in the liver would be expected if the tracer was not stable, and copper-64 was transchelating from the cyclam ring. These results are counterintuitive when compared to the literature discussed previously where it is shown that that configurationally restricted macrocycles increase stability for complex formation with metal ions such as copper(II). Therefore, the possibility of compounds **L17** and **L18** labelling out of the cavity of the macrocycle; resulting in a lower activation energy; may explain the unexpected poor *in vivo* stability. The authors acknowledge the concern of high liver uptake but do not offer any detailed explanation of its cause.

2.2 Key aspects of previous relevant research

The synthesis, radiolabelling and biological validation of configurationally restricted bis-tetraazamacrocycles with copper-64 was investigated in the work reported in this chapter. The bis-macrocycles are configurationally restricted with an ethylene bridge which forms either CB or SB macrocycles. This configurational restriction optimises binding to the CXCR4 receptor for metal complexes. Furthermore, in particular, metal complex formation with copper(II) offers high affinity antagonists for the CXCR4 receptor, allowing for the development of a specific CXCR4 imaging tracer using the copper-64 isotope. The compounds selected were based on the previous optimisation of the bis-macrocyclic antagonists.

2.2.1 Bis-linked tetraazamacrocycle antagonist

Variations in ring size (between 12-16), linkers (alkyl/aryl) and position (*ortho*-, *para*- and *meta*-) have all been investigated (without metal ions present) with a selection of examples shown in Figure 31. Bridger *et al.* synthesised ligands **L19-24** and found that the increase in ring size (12-14 membered) in both the *para*- and the *meta*- substituted bis-macrocycles there was an increase in CXCR4 affinity.²⁰⁴ However, this trend did not continue and for rings larger than 14 members there was a decrease in affinity. Bridger *et al.* reported the highest affinity with the 12 and 13 membered rings in the *meta*-positions (**L24**, $EC_{50} = 0.54 \mu M$; **L19**, $EC_{50} = 0.034 \mu M$), whilst the *para*-substituted derivative gave the highest affinity in the 14 membered rings (**L26**, $EC_{50} = 1.7 \mu M$).²⁰⁴

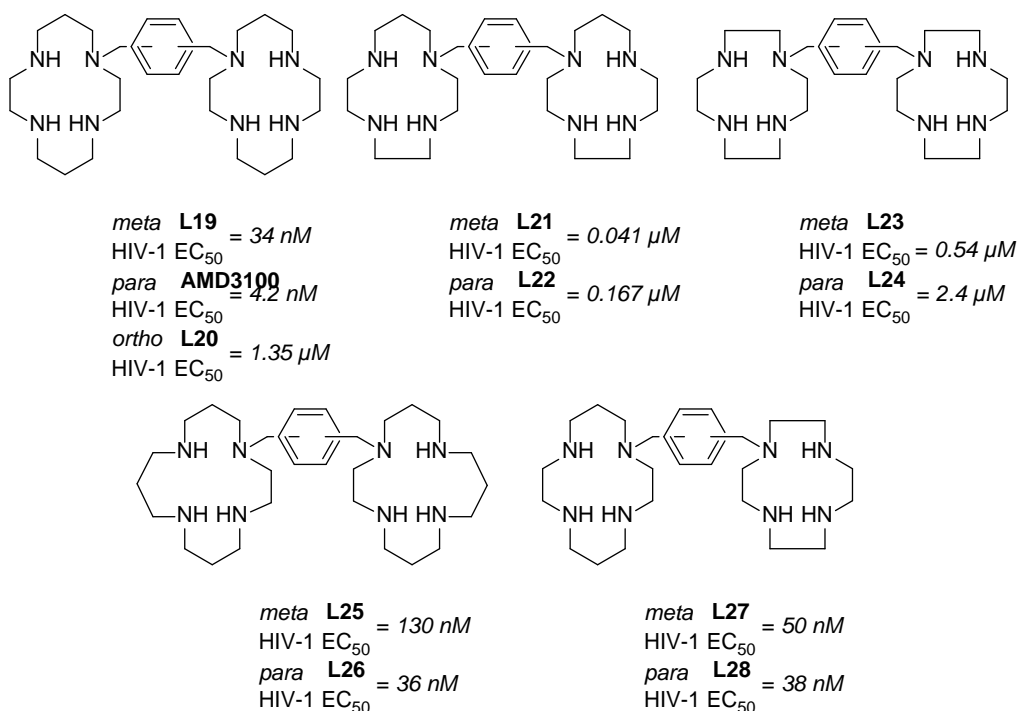


Figure 31: Ortho-, meta- and para- derivatives (**L19-28**) of bis-azamacrocycles with determined EC₅₀ values determined from anti-HIV infection assays, (reproduced from Bridger *et al.* and Tanaka *et al.*).^{187, 204}

Tanaka *et al.* expanded on this library of bis-macrocytic compounds altering the aza-containing group and reported on the effect this had on the affinity towards the CXCR4 receptor.¹⁸⁷ The group evaluated the affinity via a displacement assay where each ligand competed against [¹²⁵I]CXCL12 for the CXCR4 receptor in Jurkat cells, and also via anti-HIV infection assays. Results revealed that, in general, the bis-macrocytic compounds containing cyclen showed poorer affinity to the receptor. Results also showed that compounds with the *para*-xylyl linker generally showed higher inhibition over those with a *meta*-xylyl linker. From this group of compounds, the ligand AMD3100 was shown to be the best CXCR4 inhibitor in the anti-HIV infection assay, although the other *para*-xylyl compounds also had high affinity for the receptor, see Figure 31.¹⁸⁷

2.2.2 Bis-macrocycle metal complexes

As discussed in section 2.1.2; Gerlach *et al.* reported that the inclusion of a transition metal ion into the cyclam ring of AMD3100 enhanced its affinity towards the CXCR4 receptor.¹⁸⁶ Archibald and co-workers similarly reported the chelation of nickel(II) or zinc(II) into the configurational restricted SB bis-cyclam ligand **L29** (structure seen in Figure 32). Increased affinity for the CXCR4 was seen with EC₅₀ values of 14 nM and 2.5 nM seen for [Ni₂**L29**]⁴⁺ and [Zn₂**L29**]⁴⁺ respectively.^{199, 200}

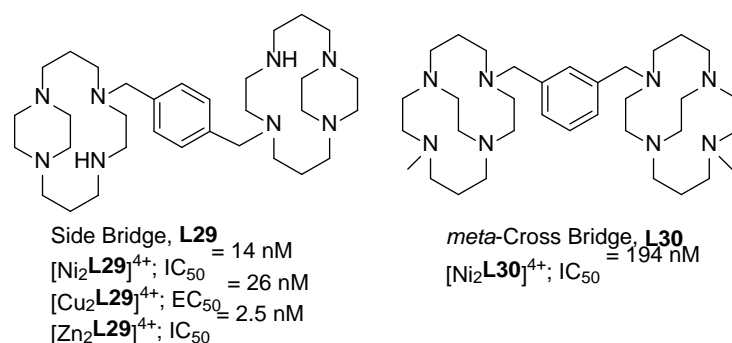


Figure 32: Configurationally restricted macrocycles and metal derivatives synthesised by the Archibald group.^{199, 200, 205, 206.}

Valk *et al.* revealed that the configurationally restricted ligand **L29** gave the highest CXCR4 affinity when complexed with two zinc(II) metals ($[\text{Zn}_2\text{L29}]^{4+}$), showing improved affinity compared to AMD3100 and the bis-zinc analogue of AMD3100.²⁰⁰ Smith *et al.* later reported a *meta*-CB bis macrocycle, **L30**, chelated to nickel(II) with the macrocycles in the meta positions on the xylyl group.

Tanaka *et al.* reported the zinc(II) and copper(II) complexes of all the ligands shown in Figure 31 and in general found the zinc(II) complexes to have higher affinity for the receptor.¹⁸⁷ For example, the unsymmetrical cyclam/cyclen ligands **L27** and **L28** have the highest affinity when complexed with zinc(II). $[\text{Zn}_2\text{L27}]^{4+}$ and $[\text{Zn}_2\text{L28}]^{4+}$ gave IC_{50} values of 11 and 8 nM, respectively which is comparable to AMD3100 and $[\text{Zn}_2\text{AMD3100}]^{4+}$.¹⁸⁷

2.3 Proposed strategy in this work

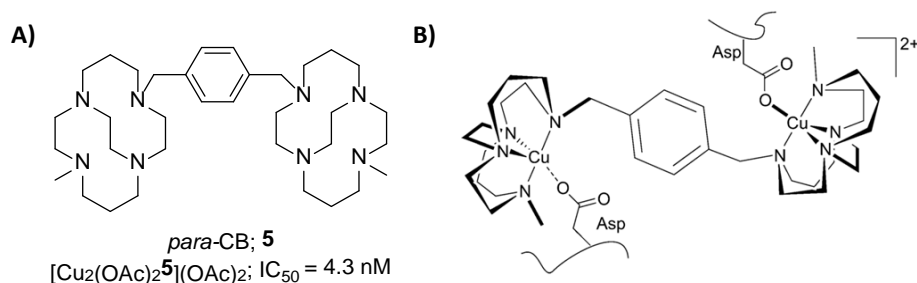


Figure 33: A) Structure of CB *para*-bis tetraazamacrocycle, **5**, and the bis-copper derivative $[\text{Cu}_2\mathbf{5}(\text{OAc})_2](\text{OAc})_2$; B) Representation of binding of $[\text{Cu}_2\mathbf{5}(\text{OAc})_2](\text{OAc})_2$ with two Aspartate ligands on CXCR4 receptor.

Previously the Archibald group has also reported the synthesis and preliminary *in vitro* validation of the *para*-xylyl cross bridged bis-tetraazamacrocycle antagonist, **5** (Figure 33, A).¹⁹⁸ $[\text{Cu}_2\mathbf{5}(\text{OAc})_2](\text{OAc})_2$ has a greater affinity than AMD3100 when tested in an anti-HIV-1 assay in MT-4 cells ($\text{IC}_{50} = 4.3 \text{ nM}$). The increase in activity was attributed to an increase in receptor residence time due to the optimised coordinate bonds that form between the positive copper(II) metal ion and the negatively charged aspartate ligands on the CXCR4 receptor (Figure 33, B). A receptor residence time assay was performed by antibody competition in a growing cell population, see Figure 34, and after 48 hours, inhibition is only seen with $[\text{Cu}_2\mathbf{5}(\text{OAc})_2](\text{OAc})_2$ and not with AMD3100 and $[\text{CuAMD3100}]$.

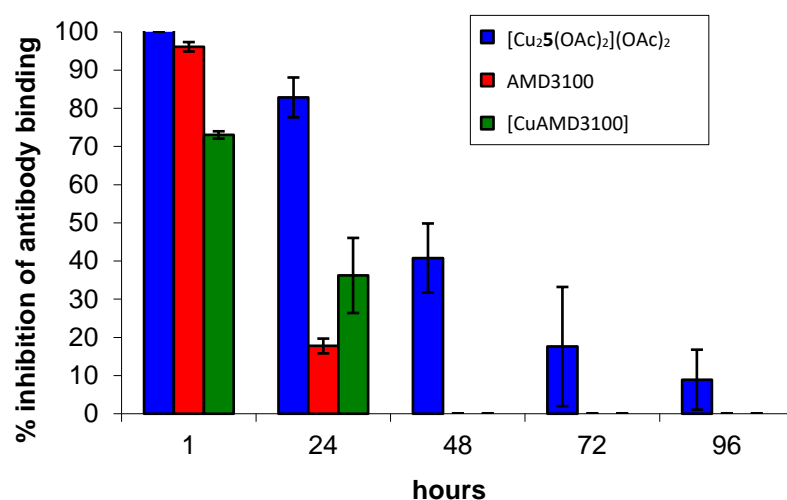


Figure 34: Investigation of the receptor residence time of AMD3100 and derivatives. [Cu₂₅(OAc)₂](OAc)₂, (blue) shows the highest receptor residence time.¹⁹⁸

It is apparent that the high affinity of [Cu₂₅(OAc)₂](OAc)₂ has some advantages over the other copper complexes previously investigated and the aim of this work is to investigate the use of these configurational restricted CB copper(II) complexes as imaging agents for tumours that overexpress the CXCR4 receptor. Both the mono-copper complex [⁶⁴Cu][Cu₅(OAc)](OAc) and bis-copper complex [⁶⁴Cu][Cu₂₅(OAc)₂](OAc)₂, (see Figure 35) were radiolabelled and purification methods developed. *In vivo* and *in vitro* validation was carried out and some of the previously reported CXCR4 tracers were resynthesised for direct comparison.

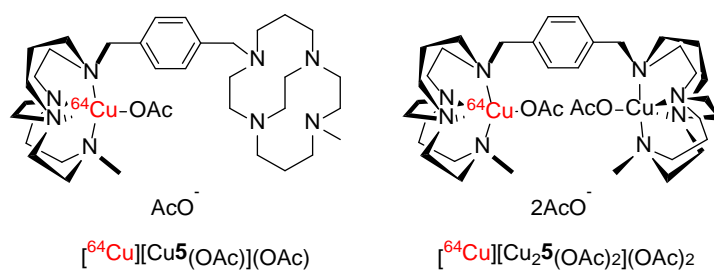
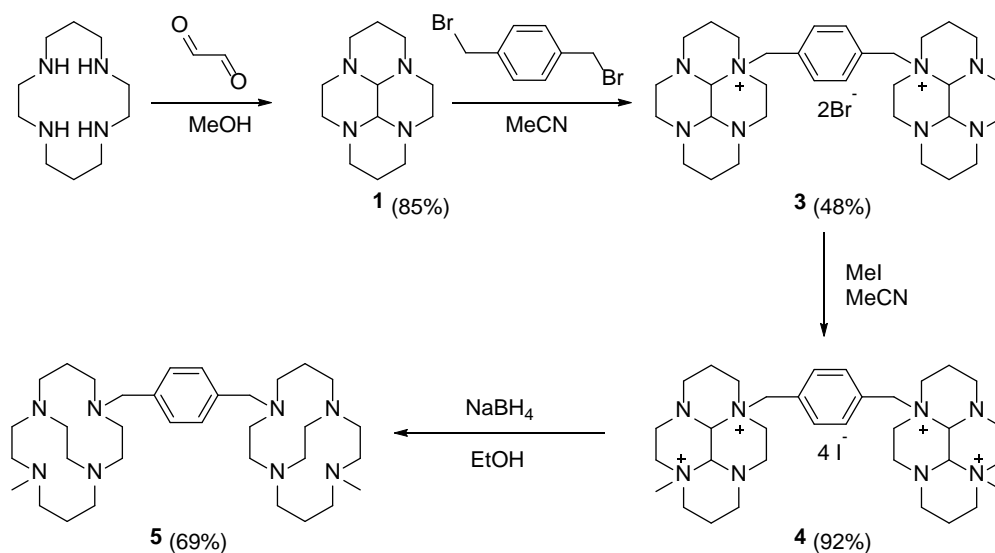


Figure 35: Structures of copper-64 radiolabelled CB macrocycles of chelator 5.

2.3.1 Synthesis of CB bis-tetraazamacrocycle

Scheme 1 shows the synthetic pathway used to produce **5**, which has been developed and further optimised from that reported by Khan *et al.*¹⁹⁸



Scheme 1: Synthesis of cross bridge functionalised bis macrocycle

The synthesis of the glyoxal bridged cyclam **1** was adapted from a procedure reported by Handel and Le Baccon.²⁰⁷ The reaction involves a condensation between the macrocycle and the bis-aldehyde, glyoxal. The reaction is temperature dependent, and as a result must be kept below -10°C during the period of the addition of the glyoxal to reduce the formation of polymeric product. The temperature was initially maintained via a salt-ice bath, however this was exchanged in later reactions for a dry ice/acetone bath as this provided more reliable temperature control.

The formation of compound **3** was also adapted from a procedure reported by Le Baccon *et al.*²⁰⁷ The bridged glyoxal cyclam **1** and bis-bromomethyl-benzene were both dissolved in dry acetonitrile and stirred together at room temperature for a week under argon. The long reaction time is to ensure the maximum yield of formation of the bis-macrocycle **3**.

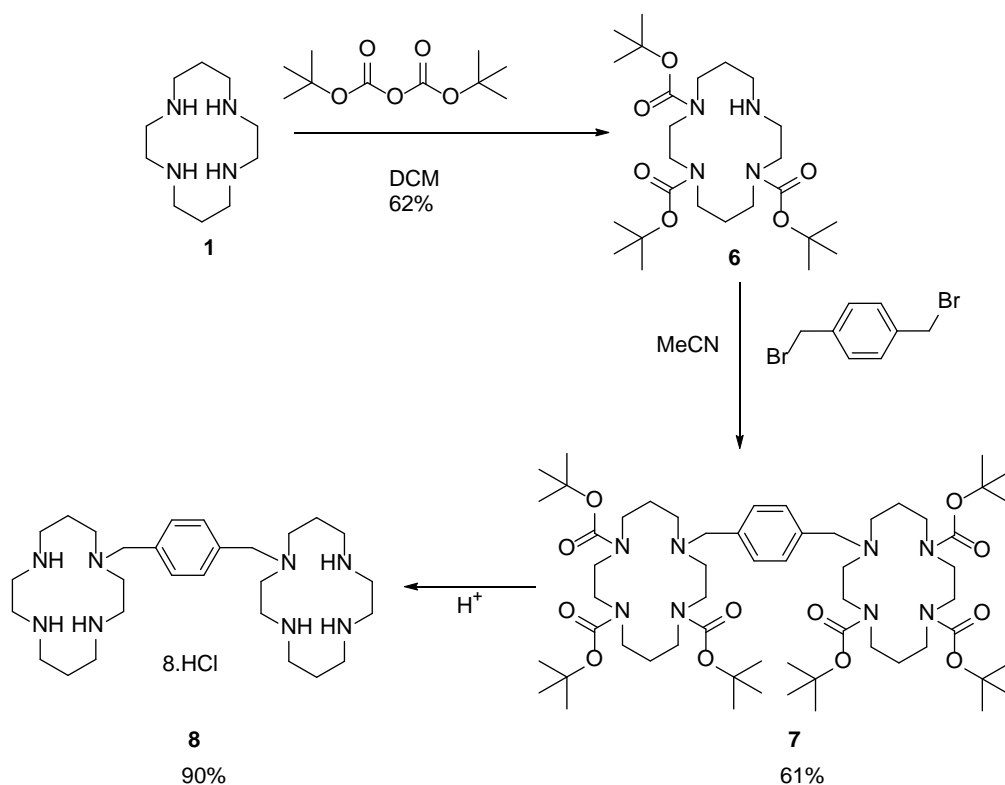
The procedure for formation of compound **4** followed that reported in the Archibald groups by Silversides *et al.*^{37, 199} In the prior synthesis of **5**, the macrocycle undergoes reductive ring cleavage in the presence of sodium borohydride, with the quaternary nitrogens cleaving consecutively.³⁷ However, this procedure requires a 14 day stir at room temperature, as well as 70 equivalents of sodium borohydride and analysis by NMR often shows low levels of impurity. The new method developed in this work adapted a procedure reported by another member of the Archibald group (Abdulwahaab *et al.*) which involved microwave heating with sodium borohydride.²⁰⁸ Full reduction

was achieved with 10 equivalents of sodium borohydride, heating at 90°C for 5 hours. Purification via extraction was carried out as previously reported.¹⁹⁸ The microwave method cut reaction time of that step down from 2 weeks to one day, and gave a pure compound which did not require further purification.

2.3.2 Synthesis of AMD3100

To allow for direct comparison of **5** with other radiolabelled CXCR4 antagonists reported in the literature, AMD3100, AMD3465 and Pentixafor were radiolabelled 'in house' (with AMD3100 and Pentixafor synthesised and AMD3465 purchased). This enabled all four tracers to be evaluated in the biological assays with high consistency, and scanned in the same xenograft models under identical conditions to allow direct comparisons.

There are several alternative ways of synthesising AMD3100, **8**, reported in the literature.^{204, 207, 209, 210} Either a tris-protected cyclam (i.e. tosyl, mesityl, or tert-butoxycarbonyl (boc)) or bridged cyclam, is reacted with α,α' -dibromo-*p*-xylene to form the bis-tetra-azamacrocycle, before being reduced or deprotected to form AMD3100. Due to the occurrence of polymerisation with the bridged cyclam method, the use of tris-protected cyclam is the higher yielding route. Therefore, as shown in Scheme 2, an adapted procedure of the reaction scheme reported by Bridger *et al.* was used to synthesise AMD3100.²⁰⁴



Scheme 2: Synthesis route of AMD3100, **8**.

The preparation of **6** was modified from a procedure reported by *et al.*²¹¹ Cyclam was added dropwise to three equivalents of di-*tert*-butyl dicarbonate in dry dichloromethane over a period of 2 hours, and then stirred at room temperature for 16 hours, after which the tris-boc cyclam product was purified from any mono-, bis- or tetra- side products by silica gel column chromatography. As the reaction was carried out on a large enough scale to continue, no further optimisation was carried out. Compound **8** was synthesised in high purity and good yield.

2.3.3 Metal complex formation of tetraazamacrocycles

For HPLC method development and *in vitro* validation it is essential to synthesise non-radioactive analogues of the radiopharmaceutical being investigated. Figure 36 shows the library of metal complexes that were synthesised from the corresponding metal acetate salts to allow HPLC conditions to be developed.

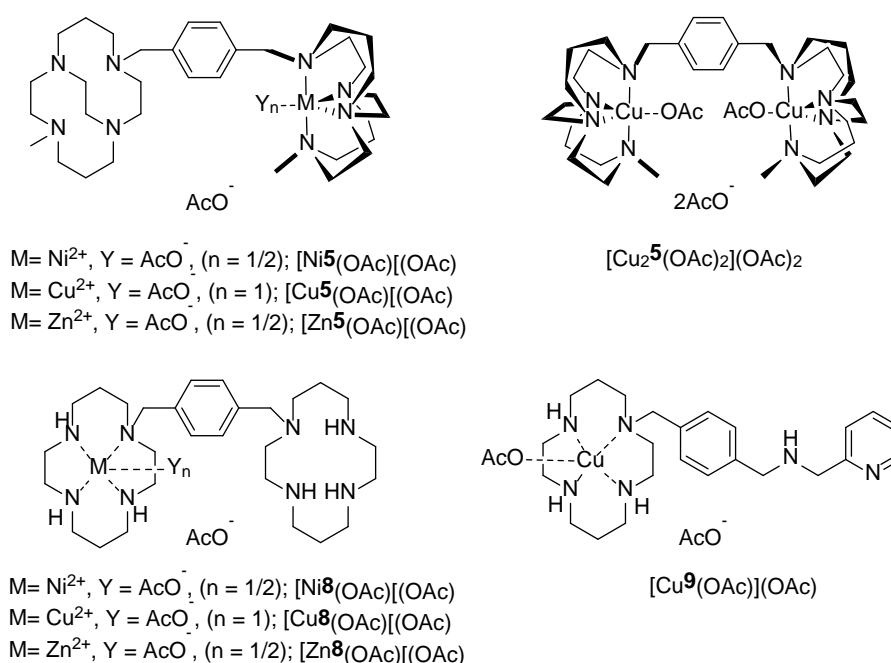


Figure 36: Structure of various transitional metal complexes of CXCR4 antagonist **5**, **8** and **9**.

The general procedure to form the metal containing derivatives involved the corresponding ligand being dissolved in dry methanol with the addition of the metal acetate dropwise as the solution is stirred.^{200, 212} Due to the increased activation energy needed for metal complexation of the cross bridge conformation it is necessary to reflux the reaction overnight, whereas the ligands **8** and **9** were stirred at RT for 8 hours.

Complexes were purified via size exclusion chromatography (Sephadex LH20) with each fraction collected analysed by mass spectrometry and the fractions with the expected molecular ions combined. This reduced yields relative to previous syntheses but resulted in the isolation of higher purity complexes.

2.3.4 Synthesis of Pentixafor

To allow a like-for-like comparison of the novel tracers made from **5**, synthesis of the clinically tested CXCR4 binding peptide Pentixafor was required (see section 1.6.1.2). This is available commercially but at a high price and the production of modified peptides would not be possible from the purchased compound. Gallium-68 Pentixafor has been widely investigated in clinical and preclinical studies but does have the limitation in preclinical studies that it only binds to human and not murine CXCR4. $[^{64}\text{Cu}][\text{Cu5}(\text{OAc})](\text{OAc})$ and $[^{64}\text{Cu}][\text{Cu5}(\text{OAc})_2](\text{OAc})_2$ have the advantage being able to image expression of both human and murine CXCR4 receptors, which allows for a wider range of preclinical studies, and the longer half-life may offer some imaging time-point advantages.

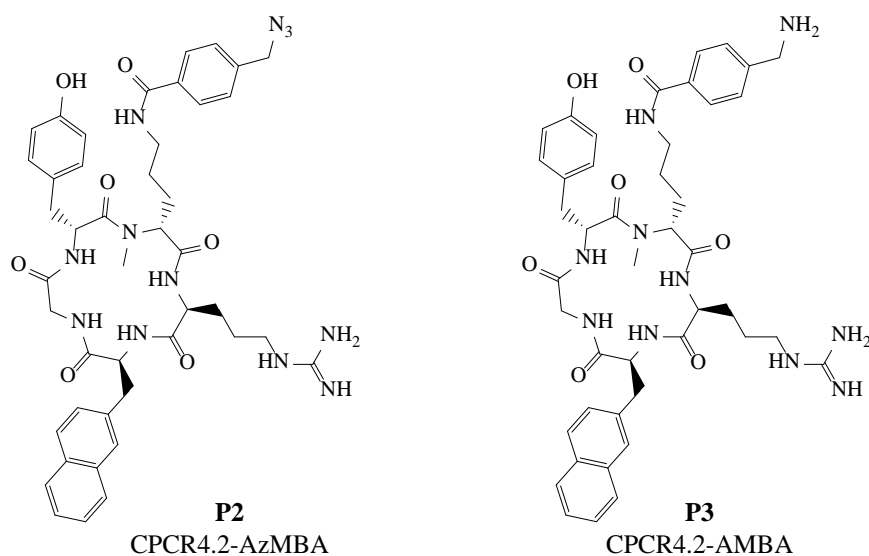


Figure 37: Structures of cyclopentapeptides CPCr4.2 (**P2**) and structure of **P3** includes an azide group for subsequent click chemistry.

Peptides **P2** and **P3** (structures shown in Figure 37) were synthesised using adapted procedures based on literature reports.^{213, 214} Both peptide **P2** and **P3** were synthesized manually by standard Fmoc-based solid-phase peptide synthesis, starting from preloaded Fmoc-Gly-2-Cl-Trt resin (0.54 mmol/g). All amino acid building blocks were N α -Fmoc-protected, and the following side chain protecting groups were used: pentamethyl-2,3-dihydrobenzofuran-5-sulfonyl (Pbf) for Arg; t-Bu for D-Tyr; and Alloc for Orn.

The synthesis of peptide **P2** and **P3** followed the same procedure up to the coupling of the spacer components. For peptide **P2**, 4-(azidomethyl)benzoic acid (AzMBA) was used, and for peptide **P3**, 4-(aminomethyl)benzoic acid (AMBA) was used as the spacer. Peptide **P2**, with the azide spacer is a novel derivative of the peptide framework. The addition of this azide moiety allows for other compounds including optical dyes to be conjugated with the peptide, (see section 6.5).

The resin was swollen in DCM and suspended in DMF. Before each coupling step, the terminal amine Fmoc protecting group was removed with 20% piperidine in DMF (1 min + 5 min). Amino acid couplings were performed using four equivalents of N- and side chain-protected amino acids activated by either *o*-(benzotriazol-1-yl)-N,N,N',N'-tetramethyluronium hexafluorophosphate (HBTU) or 1-[Bis(dimethylamino)methylene]-1H-1,2,3-triazolo[4,5-b]pyridinium 3-oxid hexafluorophosphate (HATU), in case of coupling on N-methylated Orn residue or on the γ -NH₂ of Orn, in presence of DIPEA in DMF.

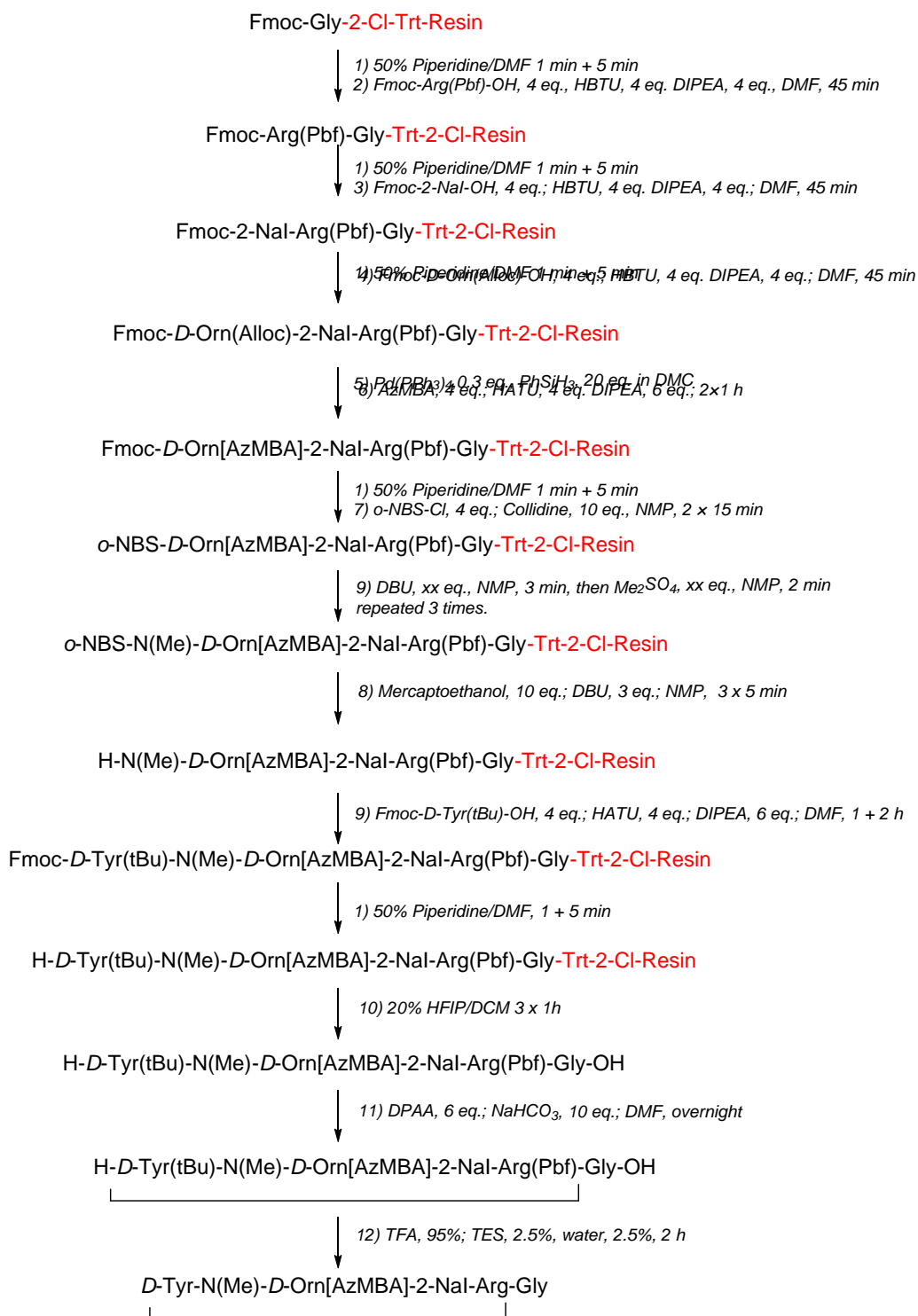


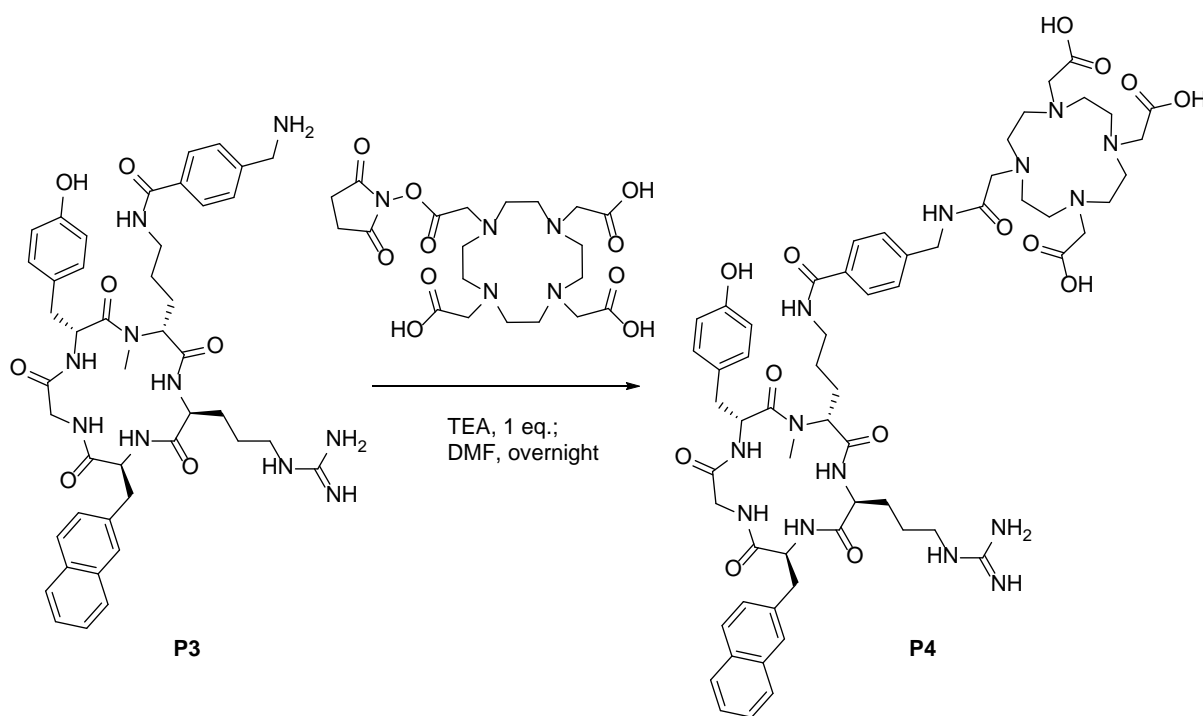
Figure 38: Synthetic route for azide peptide **P2**, (CPCR4.2 azide) using resin synthesis. Alternatively for the synthesis of **P3**, instead of spacer AzMBA being used; AMBA was used instead.

For the coupling of the CPCR4.2-AzMBA (**P2**) and CPCR4.2-AMBA (**P3**) moiety onto the *D*-Orn side chain the literature reports the use of Fmoc or N-[1-(4,4-dimethyl-2,6-dioxocyclohexylidene)ethyl] Dde protecting groups for the orthogonal protection of the amine group on the side chain of Orn.^{173, 213} Initially Dde was used, however, despite the literature report of full

deprotection after 1 hr,²¹³ this was only seen when the peptide was left stirring at room temperature overnight. Therefore, the protection strategy using the Alloc protecting group was employed. The advantage of Alloc was fast cleavage in the presence of tetrakis-triphenylphosphine palladium(0) and radical scavenger phenylsilane which does not affect the N α terminal Fmoc group.^{215, 216}

Fukuyama *et al.* were the first to develop on resin methylation using 4-nitrobenzenesulfonyl chloride (*o*-NBS-Cl).²¹⁷ The selective N-methylation of D-Orn shown in Figure 38 was performed using an adapted procedure reported by Biron *et al.* in 2006.²¹⁸ The reaction was carried out in N-methylpyrrolidone (NMP) as it allows for a faster reaction and has the advantage that no solvent change is need for the Fmoc deprotection.²¹⁸ Selective N-methylation was therefore achieved with *o*-NBS-Cl (4 eq) in the presence of collidine (10 eq) with 1,8-diazabicyclo(5.4.0)undec-7-ene (DBU) as a base. The reaction was shaken at room temperature for 15 min followed by the addition of 10 eq of dimethylsulfate for 2 min.

N-alkylated amines were acylated using HATU as racemization suppressant. Cleavage of the peptide from the TCP support was achieved by treating the peptidyl resin with a solution of diphenylarsinic acid (DPAA, 6 eq) and sodium bicarbonate (10 eq) in DMF shaken overnight at room temperature. Lastly for deprotection of acid-labile groups, TFA:triisopropylsilane:H₂O (95:2.5:2.5; v/v/v) was used. Mass spectrometry was used to confirm the desired peptide had formed, and the peptide was then purified by reverse phase semi-preparative HPLC.



Scheme 3: Synthesis of DO3A conjugated **P4**.

P3 was further reacted with 1.2 equivalents of NHS-DO3A. The reaction was stirred overnight with the addition of base (Scheme 3). The reaction was purified by reverse phase semi-preparative HPLC. A cold standard was synthesised using gallium(III) nitrate in which **P4** was dissolved in 0.2 M sodium acetate buffer (at pH 4.6) and heated at 60°C for 6 hours. The reaction showed 95% incorporation of the gallium, determined by integration of peaks on HPLC (see Figure 39).

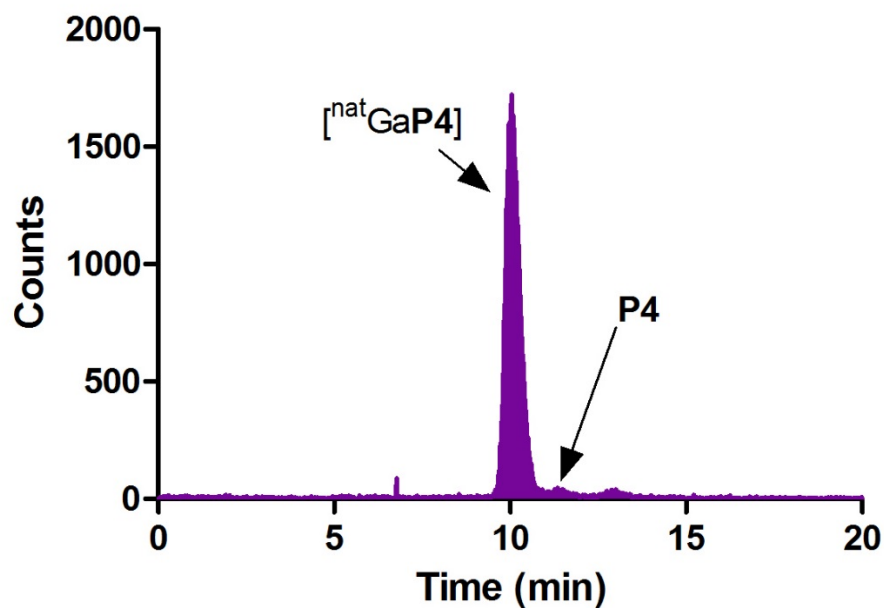


Figure 39: HPLC chromatograph of the chelation of **P4** with gallium(III) nitrate.

2.4 In vitro CXCR4 binding assay

In vitro studies were carried out on **5**, **8**, **9**, the metal complexes of the chelators and key peptide derivatives, to evaluate the binding affinity towards the CXCR4 receptor. The IC₅₀ of a chemokine receptor antagonist can be determined by its ability to block the chemokine-induced intracellular Ca²⁺ flux. All of the compounds were analysed by the research group of Prof Dominique Schols at the Rega Institute (KU Leuven) where the assay was originally developed. Table 10 shows the IC₅₀ values of the various CXCR4 antagonist discussed in the chapter.

Table 10: Summary of biological assay data generated for CXCR4 antagonist determined by antibody displacement in Jurkat cells and calcium signalling in U87-CXCR4 cells.^a represents data taken from past work carried out by the Archibald group.

Antagonist	Calcium Signalling IC ₅₀ /nM U87-CXCR4
5	>2000 ^a
[Cu 5 (OAc)](OAc)	60 ^a
[Cu ₂ 5 (OAc) ₂](OAc) ₂	4 ^a
8	175
[Cu 8 (OAc)](OAc)	75 ^a
9	4
P2	183
P3	4
[^{nat} Ga] P4	102

Antagonists [Cu₂**5**(OAc)₂](OAc)₂ and [Cu**5**(OAc)](OAc) were shown to have high affinity toward the CXCR4 receptor, both reporting lower IC₅₀ values than the previously published antagonist; AMD3100 (**8**) and Pentixafor ([^{nat}Ga]**P4**). The results highlight the potential of these small metal containing tetraazamacrocyclic antagonist as CXCR4 specific PET tracers.

As predicted the bis containing antagonist [Cu₂**5**(OAc)₂](OAc)₂ has a 15 fold higher affinity value, compared to the mono metal species [Cu**5**(OAc)](OAc) towards the CXCR4 receptor (4 nM to 60 nM respectively). This observation has also been confirmed via competitive binding FACS assays (data not shown).

Similarly, the inclusion of a metal ion resulting in higher affinity was also observed with antagonist **8** and [Cu**8**(OAc)](OAc). Table 10 shows *ca.* 2.3 fold increase in affinity with the inclusion of the copper(II) acetate ion; (175 nM to 75 nM respectively). This supports data reported by Jacobson *et al.* who investigated antagonists **8** and [Cu**8**(OAc)](OAc) ability to inhibit CXCL12 in Jurkat cell.¹⁸⁸ The group reported *ca.* 2.8 times increase in affinity upon the inclusion of the metal ion (IC₅₀ of 27.4 nM and 75.4 nM, respectively).¹⁸⁸

Although the data in Table 10 indicates that the inclusion of the azide moiety in **P2** (IC₅₀ = 183 nM) has a negative effect on the peptides affinity towards CXCR4 receptor compared to the amine containing derivative **P3** (IC₅₀ = 4 nM), this may be misleading. There is no explanation as to why this change in functional moiety would result in a drop in affinity. Further repeats and analyses are needed to investigate the presence of salt formation, as this could lead to inaccurate molecular masses being used in the IC₅₀ calculations, explaining the unexpected differences in values between the different peptides.

2.5 Radiolabelling optimisation

Copper-64 radiolabelling of tetraazamacrocyclic compounds has been well established in the literature, although there are few reports of labelling of bridged macrocycles without coordinating pendant arms. In section 1.4.4, the bifunctional chelators were discussed for many metal radioisotopes including copper-64.

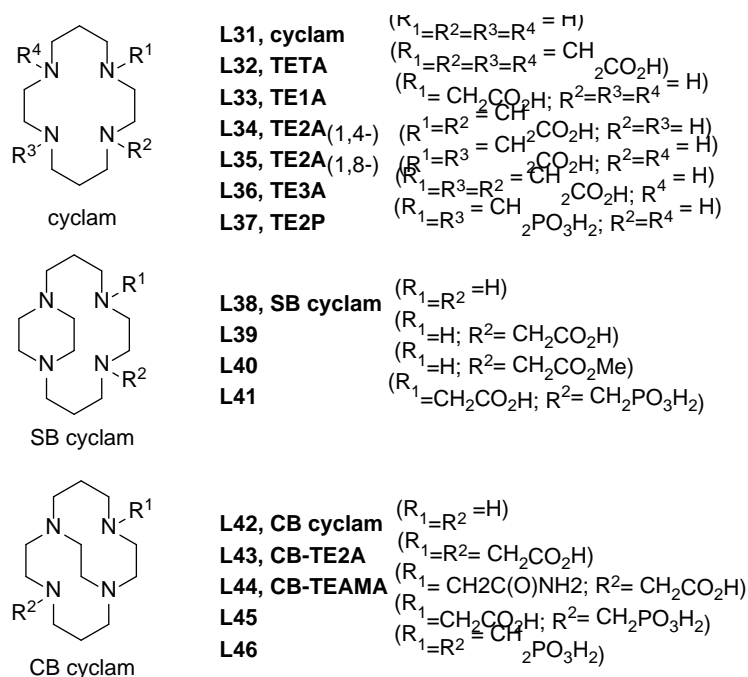


Figure 40: Structures of cyclam based BFC for complexation with copper-64.

The cavity of cyclam is good size match for copper(II) ions and in an effort to provide stable complexes *in vivo* tetraazamacrocyclic ligands such as cyclam have been investigated as copper-64 BFCs. Figure 40 shows a few of the key cyclam based structures that have been reported for the complex formation with copper-64. There have been several in-depth reviews evaluating tetraazamacrocyclic chelator complex formation with copper-64.^{24, 31, 33-35} Table 11 summarises the different conditions used for radiolabelling the structures depicted in Figure 40.

Pandya *et al.* report that **L35** (TE2A) with the addition of two carboxylic pendant arms showed improved stability *in vivo* compared to **L32** (TETA). Transchelation stability of the two copper-64 complexes was determined by rat biodistribution where [⁶⁴Cu][Cu**L35**]²⁺ showed lower kidney and liver uptake than [⁶⁴Cu][Cu**L32**]²⁺ after 24 hours post injection.

In a further attempt to improve stability of copper-64 chelates, researchers increased the rigidity of the cyclam, as discussed in section 2.1.5. Weisman initially synthesised the cross bridged cyclam structure, Busch then synthesised and demonstrated the stability of metal complexes and Archibald reported the first bifunctional chelator of CBTE2A.^{82, 201, 219} **L42** with the inclusion of an

ethylene bridge between non-adjacent nitrogens was developed as a more stable alternative (**L38** – **L46**). However, the formation of $[^{64}\text{Cu}][\text{CuL42}]^{2+}$ requires high temperature (90°C) and long reaction time to achieve high radiochemical yields, which limits its use as a BFC. Since then there have been many variations to allow for conjugation, to increase stability and optimise biodistribution.^{36, 38, 199, 212,}

220-224

Table 11: Reaction conditions used for the labelling of tetraazamacrocyclic ligands with copper-64.

Ligand	Reagents	Temperature (°C)	Time (min)	Ref
L31	20 mM water, pH 5.5	RT	10	225
L32	20 mM water, pH 5.5	RT	30	225
L34	10 mM ligand in EtOH or 0.1M ammonium citrate, pH 6.5;	75	4 h	222
L37	0.1 M ammonium acetate, pH 5.5	RT	15	226
L38	5 mM water, pH 6.4	RT	20	225
L42	EtOH (10 mM ligand), 5 μL 1 M NaOH (in EtOH)	75	90	222
L43	EtOH (10 mM ligand) Cu(II)/L: 1:100 to 1:1	75	240	222
	0.1M ammonium citrate, pH 6.5, Cu(II)/L: 1:100 to 1:1	75	240	222
	Cs ₂ CO ₃ , EtOH (30 min pre-incubation)	75	30	227
RL44	0.1 M ammonium acetate, pH 8.0	95	30	228
RL46	0.1 M ammonium acetate, pH 8.1	RT	30	229

The main variations in the procedure for labelling cyclam BFCs with copper-64 are the copper(II) salt used and the pH of the reaction mixture. Woodard *et al.*, radiolabelled the CB cyclam at a basic pH (pH 8) with $[^{64}\text{Cu}][\text{CuCl}_2]$ at 95°C for an hour.²⁰³ Alternately, $[^{64}\text{Cu}][\text{CuCl}_2]$ can be converted to $[^{64}\text{Cu}][\text{Cu}(\text{OAc})_2]$ by heating in acetate buffer (pH 5.5) to generate the acetate salt prior to reaction with the chelator.¹⁸⁸

2.5.1 Copper-64 radiolabelling of bis-tetraazamacrocycle 5

Figure 35 shows the structures of mono $[^{64}\text{Cu}][\text{Cu5}(\text{OAc})](\text{OAc})$ and bis $[^{64}\text{Cu}][\text{Cu}_2\mathbf{5}(\text{OAc})_2](\text{OAc})_2$ tracers. For labelling of antagonist **5**, a solution of $[^{64}\text{Cu}][\text{Cu}(\text{OAc})_2]$ was used. The necessary volume of stock solution of compound **5** was added to the reaction to ensure the overall concentration was 0.5 mg/mL. The volume of copper-64 solution added was matched volume to volume (v/v) by the addition of buffer; 0.4 M sodium acetate (pH 7). The chelator and the radioisotope solution were then heated for 15 min at 90°C, after which the reaction was allowed to cool before being analysed by radio-TLC (Figure 41 A).

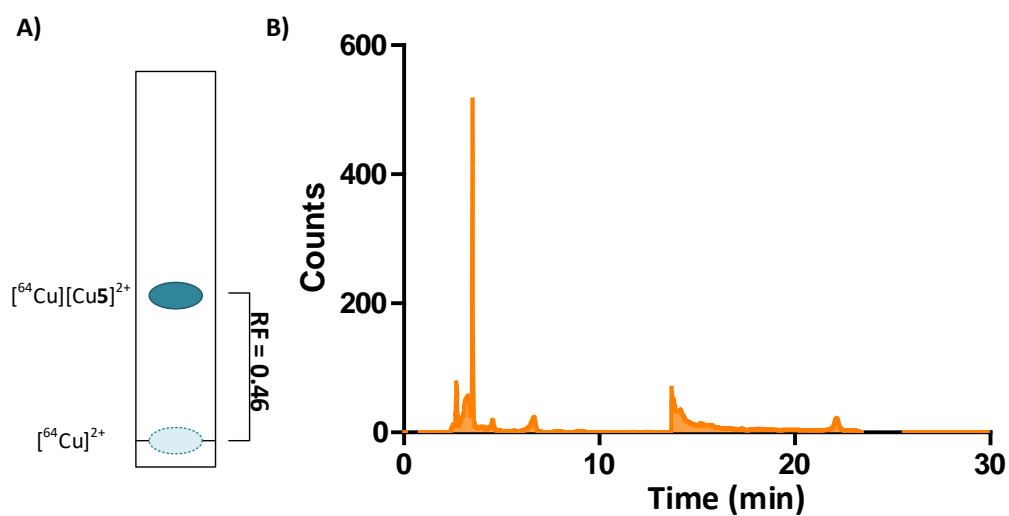


Figure 41: A) Radio-TLC (neutral alumina, eluting in MeOH:H₂O 95:5 with excess NaCl) for $[^{64}\text{Cu}][\text{Cu5}(\text{OAc})](\text{OAc})$; B) Radio-HPLC trace for $[^{64}\text{Cu}][\text{Cu5}(\text{OAc})](\text{OAc})$.

The development of HPLC-purification conditions for the separation of $[^{64}\text{Cu}][\text{Cu5}(\text{OAc})](\text{OAc})$ from the unlabelled chelator was challenging. The copper(II) ion in the CB-cyclam macrocycle has high affinity for anions and can exchange or carry them with the complex in the HPLC, meaning HPLC traces would often look very broad or contain multiple peaks. However, analysis via mass spectrometry reveals that these broad multiple peaks are the same cationic complex. Initial studies in the group with $[^{64}\text{Cu}][\text{Cu5}(\text{OAc})](\text{OAc})$ did not purify the labelled compound, however, this led to the presence of a large chelator impurity which has some affinity for the CXCR4 receptor.

Partial purification was achieved using HPLC conditions shown in Figure 41; B. Using a gradient consisting of initially 95% 20 mM sodium acetate (pH 3.5) and 5% ethanol (isocratic) for the first ten minutes before changing to 50:50. This produced narrow peaks rather than the broad peaks previously observed.

As seen with Figure 41 B, the first peak (< 3 min) in the radio-HPLC was determined to be free copper-64 (confirmed by TLC) and in the UV detector unreacted chelator **5** also eluted early. The peaks appearing between 3:30-5:00 min are attributed to [⁶⁴Cu][Cu**5**(OAc)](OAc), with lower intensity seen in the UV trace during this period. This was determined by running a TLC on this fraction which showed low levels of free copper and a R_f value 0.45, matching that of the cold. This HPLC fraction was combined with ethanol (0.5 mL) and dried using a flow of argon. The product was then dissolved in PBS, sterile filtered, and used for *in vitro* and *in vivo* experiments. Overall an average of 41.6 ± 4.6% decay corrected RCY (*n* = 4) was achieved after formulation. A partition coefficient of -2.38 ± 0.23 (octanol/water) was determined.

Upon further analysis of the re-injection of the peak collected at ~14 min, an identical HPLC trace was obtained as that shown in Figure 41. This was later confirmed by the injection of the non-radioactive analogue [Cu**5**(OAc)](OAc); with all peaks collected and analysed by mass spectrometry. Analysis revealed that the peaks that elute between 3:30-5:00 min have the same mass ions as the peak which elutes at 14 min. It is thought that the sudden shift in mobile phase causes the elution of further [Cu**5**(OAc)](OAc) retained on the column.

Although these HPLC conditions are not ideal, they do remove the majority of the unlabelled chelator which still has lower potency binding properties and can detrimentally effect the biological assays and *in vivo* imaging. Further development was undertaken to improve the separation of [⁶⁴Cu][Cu**5**(OAc)](OAc) and is discussed in section 2.8.

For the radiolabelling of [⁶⁴Cu][Cu₂**5**(OAc)₂](OAc)₂, a method involving the metal complex formation of purified [⁶⁴Cu][Cu**5**(OAc)](OAc) with non-radioactive copper(II) acetate was used. Purified [⁶⁴Cu][Cu**5**(OAc)](OAc) was dried under argon, before being re-suspended in 0.4 M sodium acetate (pH 7) buffer (ca. 60-100 µL). To this 1 µL of copper(II) acetate (1 mg/ml stock solution) was added to the reaction and heated at 100°C for 60 minutes. Radio-TLC was used to confirm the absence of free copper-64. A further 1 µL of copper(II) acetate (1 mg/ml stock solution) was then added to the reaction vial and it was left for a further 2 hours at 100°C to ensure the reaction was complete.

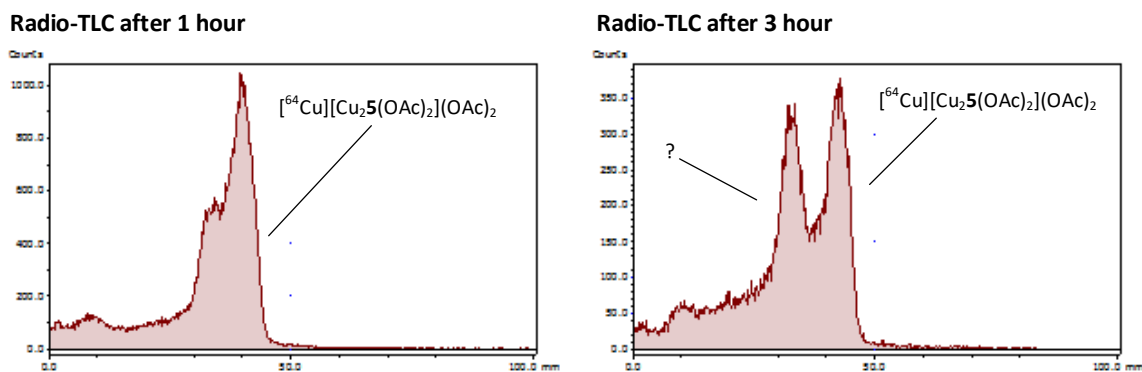


Figure 42: Radio-TLC's taken for the formation of $[^{64}\text{Cu}][\text{Cu}_2\mathbf{5}(\text{OAc})_2](\text{OAc})_2$ after one hour and three hours; (neutral alumina, eluting in MeOH:H₂O 95:5 with excess NaCl).

Comparison of radio-TLC taken after one hour and three hours of reaction show that, although no free copper-64 is seen, there is a splitting of the expected $[^{64}\text{Cu}][\text{Cu}_2\mathbf{5}(\text{OAc})_2](\text{OAc})_2$ peak (see Figure 42). It is unlikely that ligand **5** is degrading, as these small tetraazamacrocycles are extremely thermodynamically stable. It has previously been shown that $[^{64}\text{Cu}][\text{Cu}\mathbf{5}(\text{OAc})](\text{OAc})$ and $[^{64}\text{Cu}][\text{Cu}_2\mathbf{5}(\text{OAc})_2](\text{OAc})_2$ have similar retention times using these TLC conditions ($R_f = 0.46$). Further investigation using cold compounds and mass spectrometry is required to fully determine the species present but it thought that it may be again due to anion exchange, although isomers may also be being formed.

After the reaction period, with the addition of ethanol the reaction was dried using a flow of argon. The reaction was then formulated in PBS, biologically filtered, and used for *in vitro* and *in vivo* experiments. A much higher decay corrected RCY of $75.4 \pm 1.5\%$ ($n = 2$) was achieved for this reaction, as no purification was carried out. A loss of activity was observed when passing the tracer through the sterile filter. A partition coefficient of -2.45 ± 0.31 was determined, similar to that determined for $[^{64}\text{Cu}][\text{Cu}\mathbf{5}(\text{OAc})](\text{OAc})$. The reported logP value for $[^{64}\text{Cu}][\text{Cu}\mathbf{8}]$ is 0.52 which is higher than for the configurationally restricted analogues and is likely to be a reflection of increased number of available protonation sites (NH groups).¹⁸⁹

One potential issue is with the effectiveness of the initial purification of the radiolabelled compound, as no further purification was carried out on $[^{64}\text{Cu}][\text{Cu}_2\mathbf{5}(\text{OAc})_2](\text{OAc})_2$, if any chelator **5** would react with the non-radioactive copper(II) acetate to form the non-radioactive analogue $[\text{Cu}\mathbf{5}(\text{OAc})](\text{OAc})$ or $[\text{Cu}_2\mathbf{5}(\text{OAc})_2](\text{OAc})_2$. If this occurred, it would lower the specific activity of the tracer, which could be problematic for any *in vitro* and *in vivo* work carried out.

2.5.2 Copper-64 radiolabelling of AMD3100

Jacobson *et al.* previously reported the radiolabelling of AMD3100 with copper-64 in 0.4 ammonium acetate buffer (pH 5.5), stirring at RT for an hour.¹⁸⁸ This approach was modified to increase the temperature (60°C) to reduce reaction time. **8** was labelled using ~100 MBq of [⁶⁴Cu][Cu(OAc)₂] in 0.4 M sodium acetate (pH 7) buffer and heated for 15 min. Jacobson *et al.* did not carry out any purification on the radiolabelled AMD3100 for the *in vitro* and *in vivo* experiments they reported. However, in the later study by Nimmagadda *et al.* semi-preparative HPLC purification was carried out. Using their conditions it was reported that the labelled AMD3100 would elute between 20 to 22 minutes.¹⁸⁹

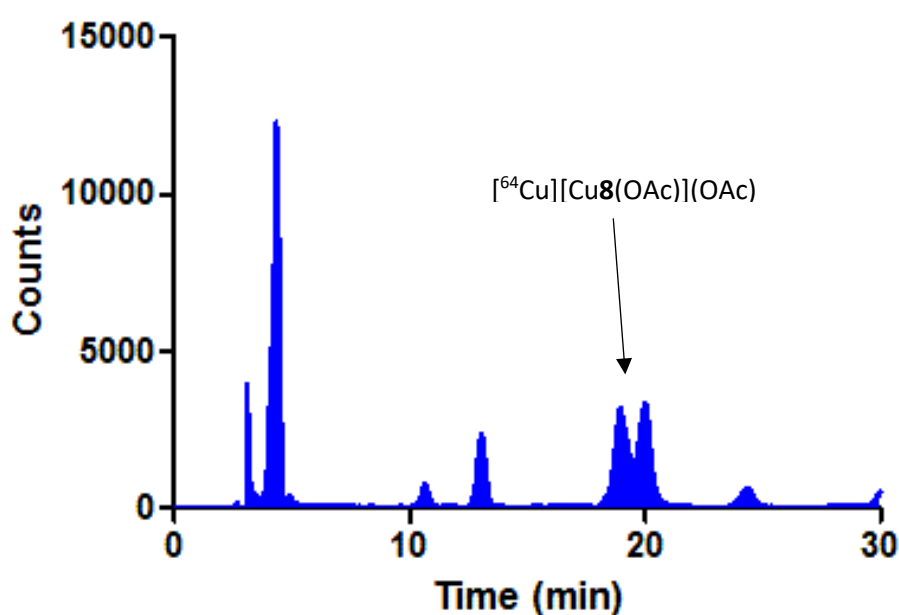


Figure 43: Radio- HPLC chromatograph of [⁶⁴Cu][Cu $\mathbf{8}$ (OAc)](OAc).

Figure 43 shows the HPLC trace obtained for [⁶⁴Cu][Cu $\mathbf{8}$ (OAc)](OAc). On comparison of Figure 43 to the radio-HPLC provide in the supplementary data by Nimmagadda *et al.* it is apparent that [⁶⁴Cu][Cu $\mathbf{8}$ (OAc)](OAc) had several radiolabelled impurities.¹⁸⁹ It is unlikely that these impurities are due to chelator decomposition using the elevated reaction temperature as AMD3100 is highly thermodynamically stable. It is most likely due to the presence of various protonation states as seen with [⁶⁴Cu][Cu $\mathbf{9}$ (OAc)](OAc).

Unfortunately, due to time restraints during these experiments full column recoveries could not be determined. However, crude analysis of the activity pre-injection and the activity collected did indicate that activity was possibly being retained on the column. Further method develop is need with increased washing time to alleviate this problem.

The peaks between 19-20 min were collected and formulated for *in vivo*. As a result of the purification a low RCY of 12.7% ($n=1$) was achieved. Due to the low yield obtained, further $[^{64}\text{Cu}][\text{Cu}8(\text{OAc})](\text{OAc})$ production was carried out at lower temperature with no HPLC purification for *in vitro* analyses.

2.5.3 Copper-64 radiolabelling of AMD3465

De Silva *et al.* were the first to publish the radiolabelling of AMD3465 with copper-64.¹⁹⁵ The group reported radiolabelling with $[^{64}\text{Cu}][\text{Cu}(\text{OAc})_2]$ in 0.1 M sodium acetate (pH 5.5) buffer heating the reaction at 55-60°C for 45 min. The reaction was then purified by reverse-phase HPLC. Radiolabelled AMD3465 elutes between 16-18 min.¹⁹⁵

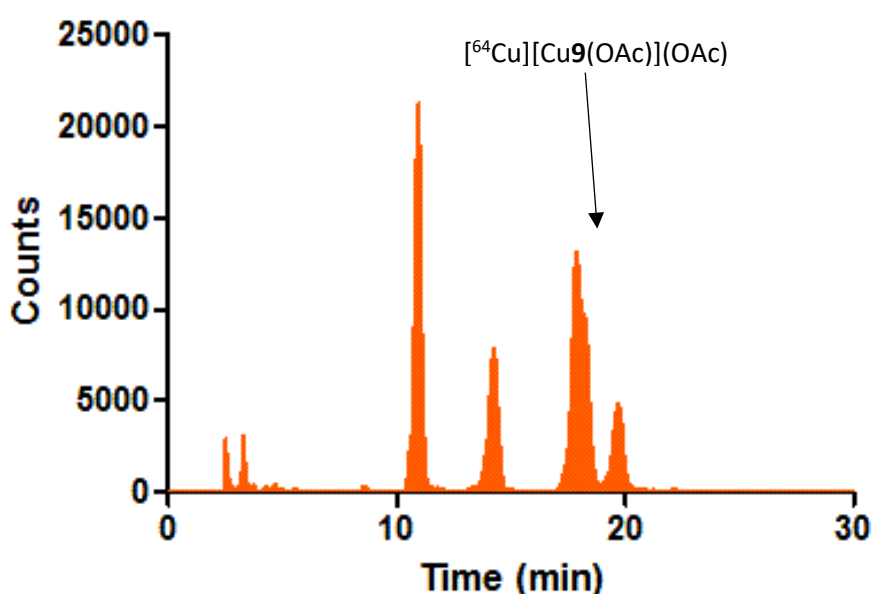


Figure 44: Radio-HPLC chromatograph of $[^{64}\text{Cu}][\text{Cu}9(\text{OAc})](\text{OAc})$.

Figure 44 shows the radio-HPLC obtained for radiolabelling of $[^{64}\text{Cu}][\text{Cu}9(\text{OAc})](\text{OAc})$, all peaks were collected with the largest peaks eluting at 11 min (22%) and 18 min (30%). The fractions eluting at 18 and 20 min were combined (for homogenous reasons and to allow enough activity for the planned *in vivo* and *in vitro* experiments) and formulated, all other peaks were discarded although some may also have been the desired compound. The complexity of the HPLC was surprising, as the AMD3465 was validated as pure (purchased from Toris) and the HPLC shown in the supplementary data by De Silva *et al.* shows only one broad peak at 16-18 min. The only variation was in the reaction time being reduced from 45 to 15 mins, however TLC analysis showed that complex formation was complete. An overall decay corrected RCY of 35.1% was achieved.

2.5.4 Gallium-68 radiolabelling of Pentixafor

$[^{68}\text{Ga}][\text{GaP4}]$ (Pentixafor) was selected for *in vivo* comparison in the tumour models. The procedure reported by Demmer *et al.* was modified for the radiolabelling of **P4**.²³⁰ Radiolabelling yields were shown to increase if the peptide was firstly solubilised in 20 μL of methanol before adding the 180 μL of HEPES (pH 3.5). The reaction was heated at 95°C for 10 minutes, before analysis by radio-TLC (0.1M sodium citric buffer, $[^{68}\text{Ga}][\text{GaP4}]$ staying at the baseline). Demmer *et al.* reported using an isocratic semi-preparative HPLC gradient (49% methanol: 51% 0.2 M ammonium acetate buffer), however this showed $[^{68}\text{Ga}][\text{GaP4}]$ and the unlabelled **P4** eluting together when attempted. Therefore, a gradient method, ranging from 40-55% methanol with 0.2 M ammonium acetate buffer, was developed. $[^{68}\text{Ga}][\text{GaP4}]$ (Figure 45) was shown to elute first at 12 min and 50 sec, while **P4** eluted later at 13 min and 45 sec.

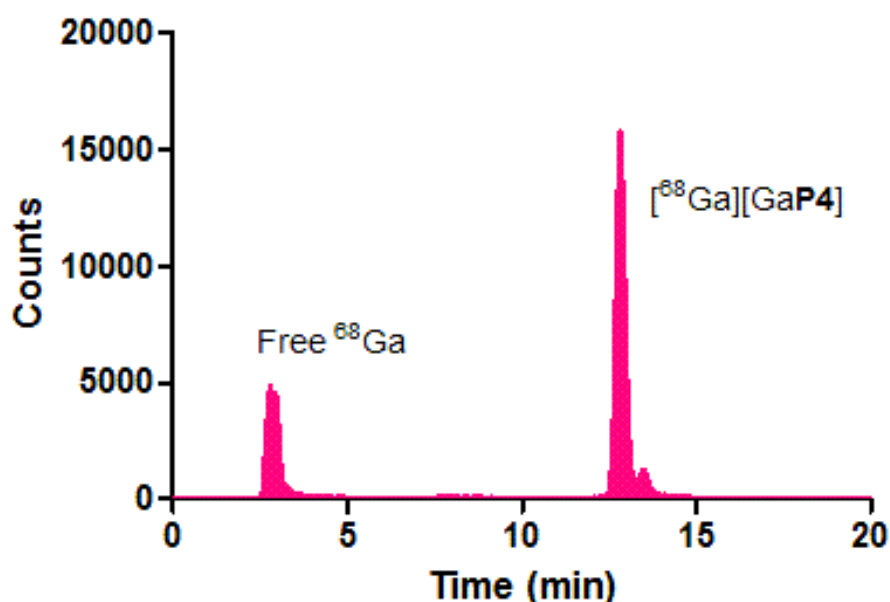


Figure 45: Radio-HPLC chromatograph of $[^{68}\text{Ga}][\text{GaP4}]$.

The radiochemical yield of the reaction varied and appeared to be dependent on the batch of **P4** which was used. 34.9% was the best decay corrected yield achieved after formulation, but this is still lower than the 50% decay corrected yield reported by Demmer *et al.* The lowest decay corrected yield seen was 0.9% with the TLC predictive of the yield after semi-preparative HPLC purification. The lower yields were attributed to the presence of potassium ions chelating with the DO3A, which was observed by mass spectrometry. The potassium ion-DO3A complex could be preventing the chelation to the gallium-68, therefore resulting in a reduced yield.

2.6 *In vitro* validation of radiolabelled tracer

Several cell lines of varying CXCR4 expression levels were used in the evaluation of the radiotracers. Expression levels of CXCR4 was determined in U87-CXCR4, Jurkat, MM.1S and U87 cells; using a CXCR4 monoclonal antibody (clone 12G5 PE). As shown in Figure 46, U87-CXCR4 and Jurkat cell lines were shown to have high expression levels of the CXCR4 receptor, while MM.1S showed low levels of expression and U87 showed no expression. Expression levels were also confirmed by immunohistochemistry staining (results not shown and all expression evaluation experiments were carried out by Ms. Cecília Miranda).²³¹

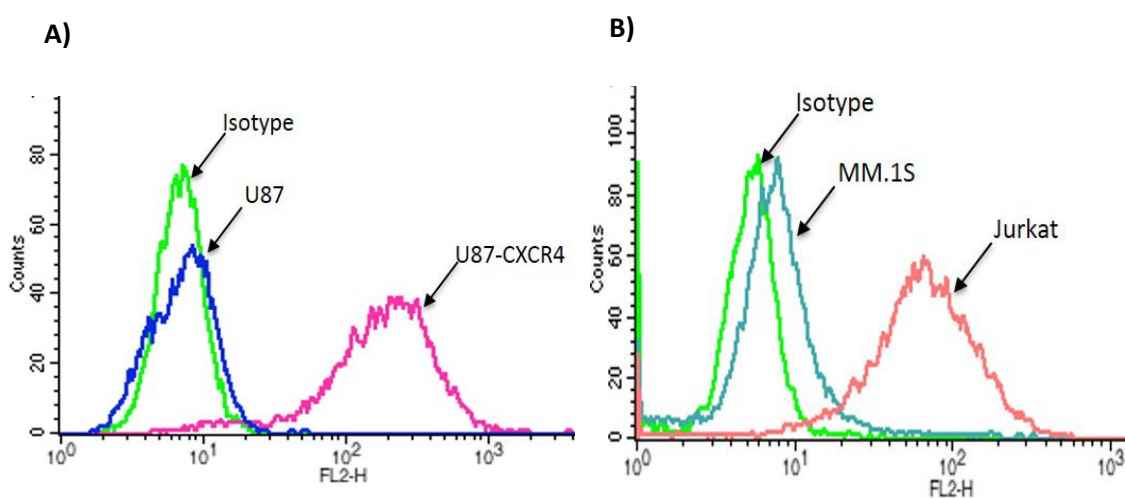


Figure 46: CXCR4 expression in A) U87-CXCR4 vs U87 cells and B) MM.1S vs Jurkat as determined by flow cytometry (data collected by Ms. Cecília Miranda).

In vitro cell binding assays were carried out with the radiolabelled compound to investigate the affinity of the tracers $[^{64}\text{Cu}][\text{Cu}5(\text{OAc})](\text{OAc})$, $[^{64}\text{Cu}][\text{Cu}_25(\text{OAc})_2](\text{OAc})_2$, $[^{64}\text{Cu}][\text{Cu}9(\text{OAc})](\text{OAc})$, $[^{64}\text{Cu}][\text{Cu}8(\text{OAc})](\text{OAc})$ and $[^{68}\text{Ga}][\text{GaP}4]$. The results are shown in Table 12.

Table 12: Binding of tracers to U87-CXCR4 and U87 cells. Each cell line was incubated with 37 KBq of tracer. ($n = 3$) (Biological data collected by Ms. Cecília Miranda).

Tracer	% Incubated dose in U87-CXCR4	% Incubated dose in U87	% Incubated dose in Jurkat	% Incubated dose in MM.1S
$[^{64}\text{Cu}][\text{Cu}5(\text{OAc})](\text{OAc})$	20.21 ± 5.78	0.66 ± 0.56	6.89 ± 1.72	5.00 ± 1.08
$[^{64}\text{Cu}][\text{Cu}_25(\text{OAc})_2](\text{OAc})_2$	10.0 ± 0.23	0.55 ± 0.2	4.8 ± 0.9	-
$[^{64}\text{Cu}][\text{Cu}8(\text{OAc})](\text{OAc})$	-	-	0.29 ± 0.14	-
$[^{64}\text{Cu}][\text{Cu}9(\text{OAc})](\text{OAc})$	-	-	1.79 ± 0.68	-
$[^{68}\text{Ga}][\text{GaP}4]$	5.36 ± 2.18	0.17 ± 0.04	3.17 ± 0.25	3.62 ± 1.34

Each cell line was incubated with 37 kBq /mL of the corresponding radiotracer at 4°C for 30 minutes in a binding buffer. After incubation, cells were washed four times and cell-associated radioactivity was determined in a gamma counter. Radioactivity values were converted into percentage of incubated dose. *In vitro* experiments were performed in triplicate and repeated three times. All experiment carried out by Ms. Cecília Miranda.²³¹ Percent incubated dose determined by dividing the radioactivity in the pellet by the total radioactivity (supernatant + pellet); full experimental detail described in section 9.6.5.

[⁶⁴Cu][Cu5(OAc)](OAc) was shown to have the highest percentage incubated dose binding of all five tracers in U87-CXCR4 cell (20.21 ± 5.78%). A *ca.* 31 fold reduction in binding affinity was seen for [⁶⁴Cu][Cu5(OAc)](OAc) in the CXCR4 negative cell line (U87, 0.66 ± 0.56%) which demonstrates the high affinity and specificity of the tracer towards CXCR4. In fact, the percentage incubate dose in all five cells lines of [⁶⁴Cu][Cu5(OAc)](OAc) correlated well with the expression levels determined in each cell line: U87-CXCR4>Jurkat>MM1.S>U87 cells.

Correlation with expression level in each cell line and percentage incubated dose was not observed for the tracer [⁶⁸Ga][GaP4] (Pentixafor) which saw higher uptake in the MM1.S cells over Jurkat cells. On comparing the percentage incubated dose of [⁶⁴Cu][Cu5(OAc)](OAc) and [⁶⁸Ga][GaP4] in both the U87-CXCR4 and U87 cells, [⁶⁴Cu][Cu5(OAc)](OAc) was shown to have a *ca.* 3.8 fold higher incubated percentage dose. This may indicate that [⁶⁴Cu][Cu5(OAc)](OAc) binds more effectively than [⁶⁸Ga][GaP4] (Pentixafor). This data agrees with the IC₅₀ data obtained for calcium signalling assays shown in Figure 10.

[⁶⁴Cu][Cu₂5(OAc)₂](OAc)₂ showed a much lower percentage incubated dose in U87-CXCR4 cells than [⁶⁴Cu][Cu5(OAc)](OAc), which was unexpected and does not correlate with the known affinity data. However, [⁶⁴Cu][Cu₂5(OAc)₂](OAc)₂ did prove to be specific to CXCR4 with *ca.* 18 times less binding seen in the CXCR4 negative cell line U87. One possible explanation for the observed reduction in affinity is the presence of the non-radioactive antagonist [Cu5(OAc)](OAc) (or the bis-copper compound) formed due to a contaminant of the chelator being present which could then form non-radioactive copper containing antagonists that would interfere with binding (discussed previously in Section 2.5.1).

To further investigate the affinity of [⁶⁴Cu][Cu5(OAc)](OAc), blocking studies were carried out in U87-CXCR4 and Jurkat cells. Each cell line was incubated with 20 µM of non-radioactive antagonists ([Cu5(OAc)](OAc), [Cu₂5(OAc)₂](OAc)₂, **8** and **9**) for 60 minutes at 4°C, before being washed three times in chilled buffer before incubation with [⁶⁴Cu][Cu5(OAc)](OAc). The results are shown in Table 13.

Table 13: Blocking experiments carried out with 37 KBq of [⁶⁴Cu][Cu5(OAc)](OAc) were cells were blocked prior to incubation with CXCR4 antagonists. (n = 1) (Biological data collected by Ms. Cecília Miranda).

Blocking compound	% Blocking in Jurkat cells	% Blocking in U87-CXCR4 cells
[Cu5(OAc)](OAc)	78.3	74.2
[Cu ₂ 5(OAc) ₂](OAc) ₂	92.1	87.9
8	37.9	-
9	-4.6	-

As shown in Table 13; blocking with non-radioactive [Cu₂5(OAc)₂](OAc)₂ gave the highest percentage blocking in both Jurkat and U87-CXCR4 cell line (92.1% and 87.9%, respectively) in line with the affinity of the compounds. The *in vitro* data collected on the non-radioactive derivatives shows that [Cu₂5(OAc)₂](OAc)₂ has a higher affinity for CXCR4 than [Cu5(OAc)](OAc). This is additional evidence to suggest that [⁶⁴Cu][Cu₂5(OAc)₂](OAc)₂ was not synthesised with a higher enough purity/ lower specific activity.

Both non-radioactive antagonists [Cu₂5(OAc)₂](OAc)₂ and [Cu5(OAc)](OAc) show higher percentage blocking (92.1% and 78.3%, respectively) than antagonist **8** (AMD3100, 37.9%), indication that both tracers have a higher affinity towards CXCR4 than compound **8**. Compound **9** (AMD3465) was unable to block the CXCR4 receptor, which may indicate that the compound is more easily displaced by the radiotracers than AMD3100.

2.7 *In vivo* validation

In vivo studies for [⁶⁴Cu][Cu₅(OAc)](OAc), were carried out in mice bearing U87-CXCR4 and U87 tumours. CD-1 nude mice were subcutaneously inoculated into the right flank with 5x10⁶ cells (expression shown in Figure 46), and tumours were allowed to grow until the tumour size reached 100-300 mm³. All preclinical scanning were carried out under Home Office License number 60/4549 held by Dr Chris Cawthorne, while data interpretation carried out by Ms. Cecilia De Miranda.

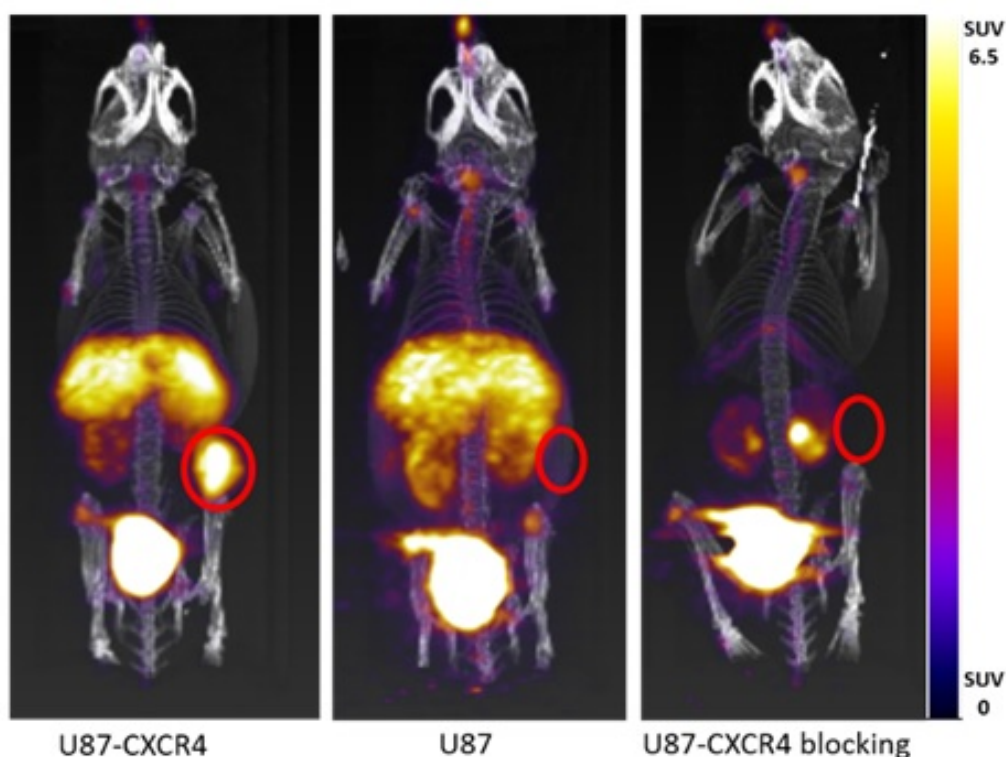


Figure 47: PET scan of mouse showing mice bearing CXCR4-positive U87-CXCR4 tumours (left) and CXCR4-negative U87 tumours (middle) 90 min after injection of tracer [⁶⁴Cu][Cu₅(OAc)](OAc). A blocking study of a CXCR4-positive tumour in which [Cu₂5(OAc)₂](OAc)₂, was injected followed by tracer [⁶⁴Cu][Cu₅(OAc)](OAc).

PET images acquired over 90 min showed greater accumulation of activity in U87-CXCR4 over U87 tumours; Figure 47. The tumour-to-muscle ratio at 90 min after injection of [⁶⁴Cu][Cu₅(OAc)](OAc), in U87-CXCR4 tumours (23.6 ± 2.7) increased 8-fold compared to U87 tumours (3.0 ± 0.5), demonstrating the high specificity of the tracer for the CXCR4 receptor. Strong uptake in the liver, bone marrow and bony growth plates was also observed, as expected due to the natural CXCR4 expression in these tissues. A blocking study using 10 mg/kg of the higher affinity cold antagonist ([Cu₅(OAc)](OAc), IC₅₀ = 4 nM) was administered an hour before [⁶⁴Cu][Cu₅(OAc)](OAc), to give a >92% reduction of radioactivity in the tumour. Highlighting the specificity of [⁶⁴Cu][Cu₅(OAc)](OAc) as a CXCR4 tracer.

It is worth noting that a pronounced reduction in liver uptake was seen in this blocking study, where in comparison to blocking study used by Nimmagadda *et al.* for tracer $[^{64}\text{Cu}8(\text{OAc})](\text{OAc})$, the liver is still clearly visible in the PET scan (see Figure 24), indicating considerable levels of radioactive uptake in the liver despite the receptors being blocked. In fact, the liver-to-muscle ratio of $[^{64}\text{Cu}][\text{Cu}8(\text{OAc})](\text{OAc})$ is reported as approximately 56:1, significantly higher than that of $[^{64}\text{Cu}][\text{Cu}5(\text{OAc})](\text{OAc})$, which is approximately 11:1. A possible explanation for this decreased ratio could be the increased stability of the complex $[^{64}\text{Cu}][\text{Cu}5(\text{OAc})](\text{OAc})$ and lack of free copper-64 ions, which would accumulate in the liver. This also contrasts with the data reported by Woodard *et al.*, as copper-64 binding in the cross-bridge cyclam unit of tracer $[^{64}\text{Cu}][\text{Cu}5(\text{OAc})](\text{OAc})$ did not show the same release of the metal ion as $[^{64}\text{Cu}][\text{Cu}8(\text{OAc})](\text{OAc})$ and $[^{64}\text{Cu}][\text{Cu}9(\text{OAc})](\text{OAc})$.²⁰³ These imaging experiments were repeated in Hull and the instability of the tracers *in vivo* was confirmed (data not shown).

2.8 Further development of HPLC conditions

In an attempt to increase the purity/specific activity of both the radiolabelled $[^{64}\text{Cu}][\text{Cu5}(\text{OAc})](\text{OAc})$ and $[^{64}\text{Cu}][\text{Cu}_2\mathbf{5}(\text{OAc})_2](\text{OAc})_2$ antagonists, alternative HPLC conditions were developed. The cold standards of antagonists **5**, $[\text{Cu5}(\text{OAc})](\text{OAc})$ and $[\text{Cu}_2\mathbf{5}(\text{OAc})_2](\text{OAc})_2$ were used for method development. The standards were purified by size exclusion chromatography and purity confirmed via elemental analysis. As the protonation state/pH is key to separation three different pH's of a 20 mM sodium acetate buffer were tested (pH 3, 5 and 7).

Using a neutral buffer (20 mM sodium acetate, pH 7) poor separation was achieved; with all three compounds running together and giving many broad peaks.

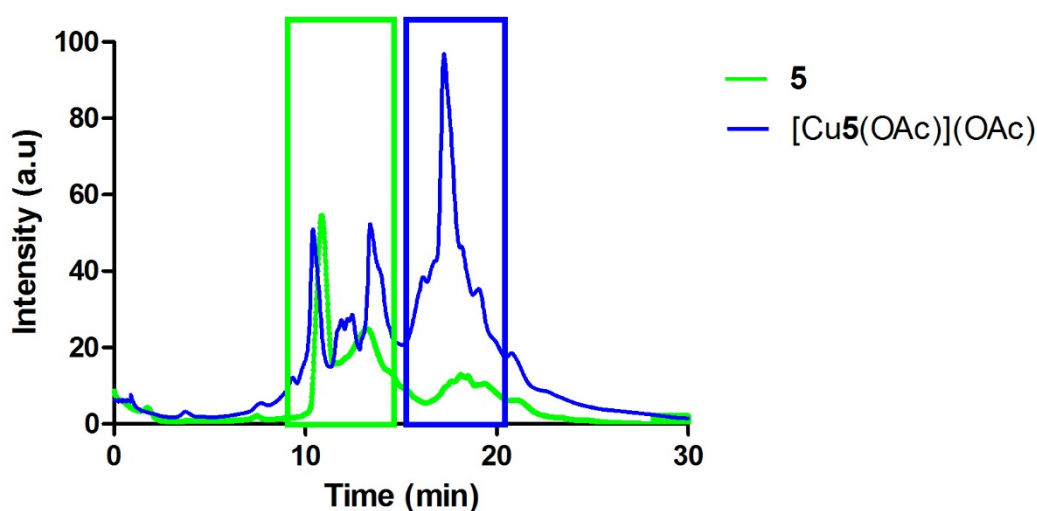


Figure 48: HPLC traces of antagonist **5** and $[\text{Cu5}(\text{OAc})](\text{OAc})$ run in gradient from 20 mM sodium acetate pH 5 (5%-80%, 30 min) and ethanol.

Figure 48 shows the HPLC trace that was observed for **5** and $[\text{Cu5}(\text{OAc})](\text{OAc})$ at pH 5. Interestingly the free ligand, **5**, did not run as a single peak, although it is possible that the configuration restricted cyclams could chelate with small ions (H^+ , sodium, potassium ect.) or be forming various protonated species. Mass spectra analyses revealed that all peaks that were observed in the green box corresponded to **5**, while the second large peak highlighted in the blue box, eluted between 17-18 min corresponds to the mono metal species $[\text{Cu5}(\text{OAc})](\text{OAc})$.

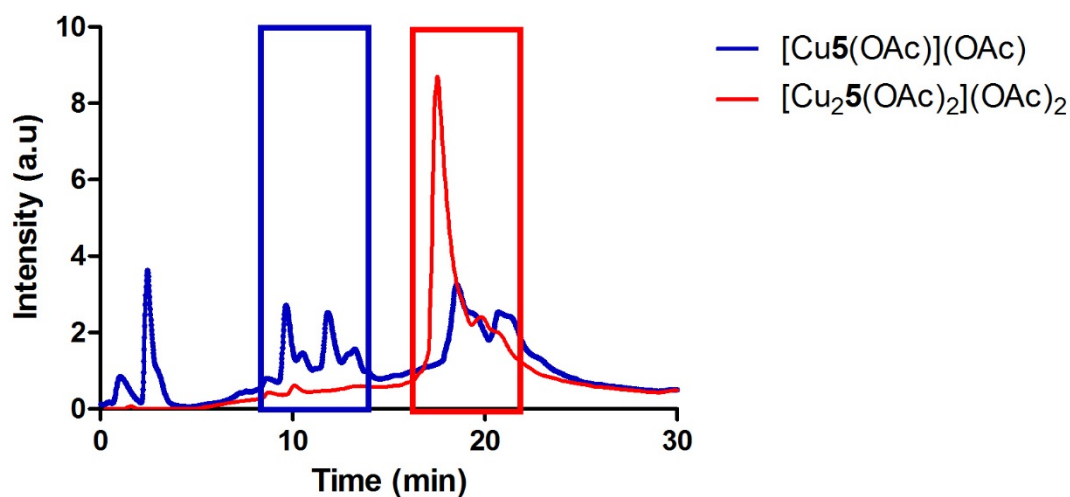


Figure 49: HPLC traces of antagonist $[\text{Cu}_5(\text{OAc})](\text{OAc})$ and $[\text{Cu}_{25}(\text{OAc})_2](\text{OAc})_2$ run in gradient from 20 mM sodium acetate pH 3 (5%-80%, 30 min) and ethanol.

Figure 49 shows the HPLC trace that gave the greatest peak separation for $[\text{Cu}_5(\text{OAc})](\text{OAc})$ and $[\text{Cu}_{25}(\text{OAc})_2](\text{OAc})_2$. The gradient elution was carried out at pH 3, and mass spectrometry analysis revealed that the compound collected in the peaks highlighted in the blue box showed masses corresponding to $[\text{Cu}_5(\text{OAc})](\text{OAc})$. While the peak shown in the red box that eluted later were shown to have masses that corresponded to $[\text{Cu}_{25}(\text{OAc})_2](\text{OAc})_2$.

These systems show a better separation than was previously achieved. More work is needed to develop these conditions with the radioactive analogues. However, initial results are promising for efficient high purity/ high specific activity tracers.

2.9 Conclusion

Although success has been reported in radiolabelling AMD3100 with copper-64; the application of the tracer is limited by the transchelation of the copper(II) ion. The Archibald group have reported the inclusion of an ethylene bridge between nitrogens on the cyclam ring increasing the stability when complexed with a second row transitional metal ion in bis-macrocyclic compounds.

Antagonist **5** was synthesised via a modified procedure that included the use of a microwave aided reduction which enabled a much shorter synthesis time and a higher purity product to be formed. Competitor tracers were also synthesised with Pentixafor (**P4**) and a novel azide derivate (**P3**) being produced via a modified procedure. These well-established CXCR4 tracers were used to validate the affinity of the novel copper-64 labelled analogues of antagonist **5**.

The radiotracer $[^{64}\text{Cu}][\text{Cu5}(\text{OAc})](\text{OAc})$ was radiolabelled and characterised with a $41.6 \pm 4.6\%$ RCY, and a partition coefficient of -2.38 ± 0.23 . *In vitro* cell binding experiments showed that $[^{64}\text{Cu}][\text{Cu5}(\text{OAc})](\text{OAc})$ had the highest affinity compared to all the other CXCR4 specific tracers tested (Table 12), although this may be due to the lower specific activity of the bis-copper tracer tested. *In vivo* dynamic PET/CT scans showed that $[^{64}\text{Cu}][\text{Cu5}(\text{OAc})](\text{OAc})$ was specific to CXCR4, with uptake in the CXCR4 positive tumour being 8 fold higher than that in the CXCR4 negative tumour (U87-CXCR4, $20.21 \pm 5.78\%$; U87, 3.0 ± 0.5). Importantly liver uptake also proved to be blockable proving that the copper-64 chelated complex is stable and no transchelation was observed. This issue has previously been problematic in the further development of copper-64 labelled AMD3100 and AMD3465 tracers.

The bis-copper analogue; $[^{64}\text{Cu}][\text{Cu}_2\mathbf{5}(\text{OAc})_2](\text{OAc})_2$, for which non-radioactive analogue has been shown by various *in vitro* experiments (see Table 10) to have a higher affinity towards the CXCR4 receptor than the mono-copper derivative; was formed. A RCY of after formulation of $75.4 \pm 1.5\%$ was achieved with no HPLC purification being carried out. A partition coefficient of -2.45 ± 0.31 , similar to $[^{64}\text{Cu}][\text{Cu5}(\text{OAc})](\text{OAc})$ was determined. However, *in vitro* and experiments completed with $[^{64}\text{Cu}][\text{Cu}_2\mathbf{5}(\text{OAc})_2](\text{OAc})_2$ did not show the expected increase in affinity towards the CXCR4 receptor relative to the mono-copper tracer. This could be caused by a relatively small amount of contamination of the unreacted chelator. The presence of **5**, could allow reaction with the added non-radioactive copper(II) acetate and reduce the specific activity of the tracer. This expected trend was confirmed both by *in vitro* and *in vivo* blocking studies where the non-radioactive $[\text{Cu}_2\mathbf{5}(\text{OAc})_2](\text{OAc})_2$ was able to prevent binding of $[^{64}\text{Cu}][\text{Cu5}(\text{OAc})](\text{OAc})$ to the CXCR4 receptor. Therefore alternative HPLC separation method development was carried to use in the synthesis of tracer $[^{64}\text{Cu}][\text{Cu}_2\mathbf{5}(\text{OAc})_2](\text{OAc})_2$ to improve the specific activity.

2.10 Future work

As previously mentioned more work is needed to develop an effective HPLC purification method for the tracers $[^{64}\text{Cu}][\text{Cu}_5(\text{OAc})](\text{OAc})$ and $[^{64}\text{Cu}][\text{Cu}_2\mathbf{5}(\text{OAc})_2](\text{OAc})_2$. Section 2.8 showed partial success in the development of HPLC conditions which could be used to purify the non-radioactive analogues of the two tracers, however, these conditions need to be further developed using the radioactive tracers.

Once high specific activity can be obtained $[^{64}\text{Cu}][\text{Cu}_2\mathbf{5}(\text{OAc})_2](\text{OAc})_2$, *in vivo* experiments can be carried out to assess the affinity and biodistribution. The presence of the two metal ions, as shown in Figure 34 will increase residence time at the receptor and this would provide an interesting comparison with the mono-copper compound, particularly at later imaging time points.

Chapter Three

Synthesis and radiolabelling of
CXCR4 antagonists with
gallium-68 for PET imaging

3.1 Previous research and development of gallium-68 radiotracers

Gallium-68 is one of the most widely studied radioisotopes in PET imaging, due to the ease of production from a generator and its convenient half-life of 68 mins, providing sufficient time for radiochemistry and scanning, but short enough that dosimetry for patients is not problematic. An area that has seen the widest use of gallium-68 PET tracers is imaging the somatostatin receptor with targeting peptides such as DOTATATE, DOTATOC and various derivatives.^{232, 233}

The first tracer of this class that was utilised for the clinical detection of malignancies was [⁶⁸Ga][GaDOTATOC] which has a high affinity for SSR2 and SSR3 and a low affinity for SSR5, making it an appropriate imaging agent for several different tumours.^{234, 235} However, [⁶⁸Ga][GaDOTATOC] suffers from limitations including non-specific uptake in organs such as the pancreas and pituitary glands.²³⁶ The preferred tracer for somatostatin receptor imaging is [⁶⁸Ga][GaDOTATATE] which has improved biodistribution and excretion characteristics.²³⁷

Table 14: Gallium-68 novel PET tracers in clinical evaluation.

Ligand	Antagonist category	Application	Reference
[⁶⁸ Ga][GaNOTA-NFB ⁽¹³⁾]	Peptide	Glioma or Breast Cancer	238
[⁶⁸ Ga][GaEDTMP ⁽¹⁵⁾]	Small molecule	Bone imaging	239
[⁶⁸ Ga][Ga-F(ab') ₂ -Trastuzumab]	Antibody fragment	Breast Cancer	240
[⁶⁸ Ga][GaPSMA]	Peptide	Prostate Cancer	241

In addition to the somatostatin receptor antagonists, several other gallium-68 based radiopharmaceuticals are currently undergoing clinical trials (see Table 14). Recently tracers such as PSMA and Pentixafor have shown how effective and convenient gallium-68 imaging agents can be. The reduced infrastructure requirements for generator use combined with the advances in chelator technology and growing use of tracer kit-preparation, are key factors in the predicted expansion of clinical imaging with gallium-68 tracers.

3.1.1 Gallium-68 tracers for imaging CXCR4

As discussed in Section 1.6.1.2; the peptide Pentixafor has shown the best clinical results as a CXCR4 specific PET imaging tracer. However, there are few alternative gallium-68 radiolabelled tracers reported in the literature for imaging of the CXCR4 receptor and there is interest in looking at alternative tracers for kit-like preparation or optimised receptor targeting.

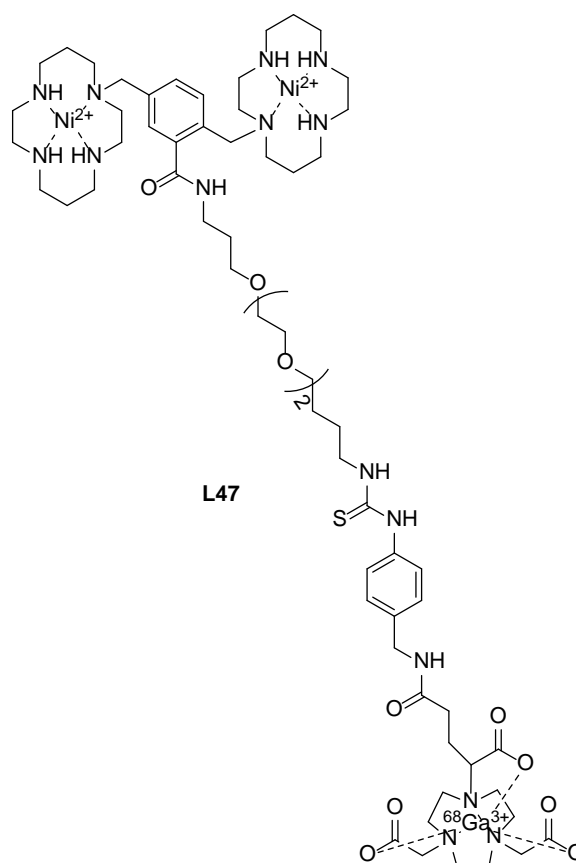


Figure 50: AMD3100 derivative with inclusion of a PEG chain on the xylonyl group for labelling with gallium-68.⁵³

One example of a gallium-68 CXCR4 small molecule tracer was reported concurrently to the work ongoing in (and in collaboration with) the Archibald group. The University of Burgundy group of Denat, Goze and co-workers synthesised a series of functionalised AMD3100 derivatives.⁵³ Poty *et al.* adapted the AMD3100 structure with the addition of a PEG chain on the central linking xylonyl group and attached DOTA or NOTA-GA to allow labelling with gallium-68.²⁴² Compound **L47** (see Figure 50) which showed the best IC_{50} (121 nM) of the compounds synthesised was evaluated *in vivo* in H69 tumour xenografts. However, scans with tracer **L47** were of poor quality with low accumulation seen in tumours. This may be due to the low specificity of **L47**, to the CXCR4 receptor. No uptake was observed in high expressing CXCR4 tissues such as the bony growth plates, as seen with other CXCR4 specific tracers. It has previously been shown by the Archibald group that modification of the xylonyl linker in AMD3100 derivatives can considerably lower the affinity for the CXCR4 receptor, although *ca.* 100 nM is still a reasonable affinity value to progress to *in vivo* testing.

3.2 Direct and pretargeted imaging

3.2.1 Direct approach and alternatives

The 'direct' approach involves the synthesis of radiotracers as shown in Chapter 2, where the moiety responsible for binding is directly conjugated to the BFC or moiety that is radiolabelled. This is the standard approach but has some limitations; particularly with larger biological molecules that are slow to clear. Alternative approaches are now being developed to utilise chemical reactions that are efficient enough to allow reaction between a targeting groups (bound to the target) and a radiolabelled group *in vivo*.

3.2.2 Click chemistry approach

The phrase 'click chemistry' was introduced by K. B. Sharpless in 1998, to describe reactions that were simple, fast, high yielding, produced only "inoffensive by-products", were widely applicable and did not require complicated purification methods.²⁴³ Reactions of this type have received a lot of interest from the pharmaceutical and materials industries. Several reactions have been identified and developed that meet Sharpless's initial criteria:

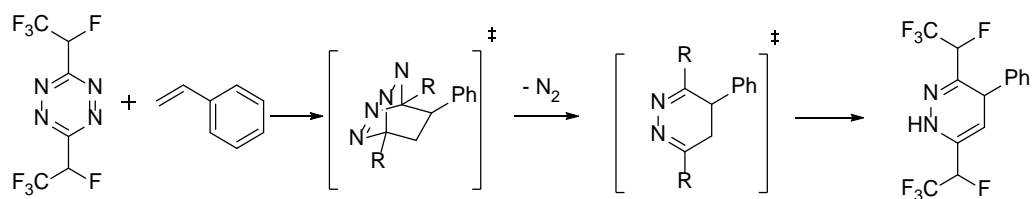
- Huisgen 1,3-dipolar cycloaddition
- The Staudinger-Bertozzi ligation
- Copper-Catalysed Azid-Alkyne Cycloaddition (CuAAC)
- Strain-promoted alkyne-azide cycloaddition (SPAAC)
- Inverse-demand Diels-Alder reaction (IDDA)

These click chemistry reactions have been used in many applications, and an excellent demonstration of their potential is in pretargeted imaging.²⁴⁴

3.2.2.1 Bioorthogonal reactions

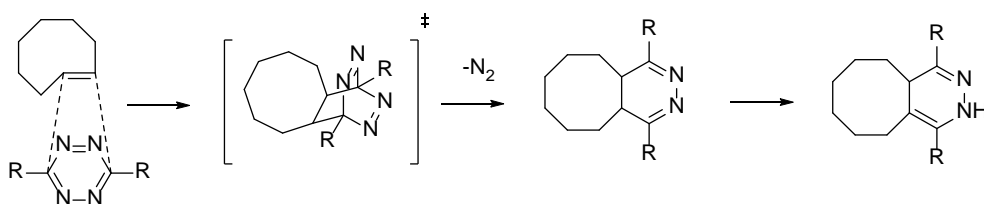
Bioorthogonal reactions are chemical reactions that can occur in a biological system without disrupting the 'native' biochemical processes. The participating compounds contain functional groups that are inert to all biological moieties, thus preventing them from reacting or interfering with the biological system.²⁴⁵ In the past decade these reactions have received a large amount of attention for their application to *in vivo* imaging.²⁴⁴ Bioorthogonal reactions utilise click chemistry, however not all click chemistry reactions are bioorthogonal.

The origins of the inverse-demand Diels-Alder reaction (IDDA) can be traced back to 1959 when it was first reported by Carboni and Lindsey who investigated the reaction between phenylstyrene and a fluorinated tetrazine, which was found to be exothermic and extremely rapid at room temperature (Scheme 4).²⁴⁶ This reaction was only of academic interest until nearly 50 years later in 2008 when Fox *et al.* described an adaptation as a bioorthogonal reaction.²⁴⁷



Scheme 4: First example of a IDDA reaction reported in 1959 by Carboni and Lindsey.

Fox *et al.* reported the reaction of tetrazine with a range of strained alkenes; of particular note was the reaction with (*E*)-trans-cyclooctene (TCO).²⁴⁸ The electron-rich dieneophile TCO reacts with the electron deficient tetrazine by the reverse-Diels-Alder [4+2] cycloaddition reaction to form an intermediate that rearranges with the release of nitrogen gas to form a stable dihydropyridazine compound (see Scheme 5).²⁴⁹



Scheme 5: The IDDA reaction between a 1,2,4,5-tetrazine and a strained trans-cyclooctene dienophile.

An important factor in the utility of this bioorthogonal reaction is that the modification of the two reacting moieties is easier and quicker than either the Staudinger-Betozzi ligation or the SPAAC reaction, and also the tetrazine moiety is more stable for long term storage.^{247, 250} TCO-tetrazine IDDA bioorthogonal reactions show rates of reaction up to 5 orders of magnitude greater than that of the SPAAC reaction and 7 orders of magnitude greater than the Staudinger-Betozzi ligation.²⁴⁷ The reaction has been reported to occur at an extremely fast rate ($k_2 = 3.5 \times 10^5 \text{ M}^{-1}\text{s}^{-1}$ in MeOH/water (9/1)²⁵¹), and proceeds in high yield in organic solvents, aqueous, buffer, and cell media solutions.²⁴⁸ For these reasons the TCO-tetrazine IDDA bioorthogonal reactions was selected for use in this work.

3.2.2.2 Pretargeted approaches in PET imaging

The principles of pretargeted PET imaging are shown in Figure 51. It is a two-step approach, where firstly a non-radiolabelled molecule with a reactive tag (TCO or tetrazine) is injected into the patient, there is a delay of the appropriate time for the molecule to reach the tissues/tumour and bind to the biological target as well as clearance of the unbound compound from the system. Next, a radiolabelled moiety (small molecule) is injected with the complimentary reactive tag, which will rapidly and selectively react with the tag on the pretargeted molecule at the receptor. Once again there is a waiting period to allow for the molecule to diffuse to the target and unreacted compound to clear.²⁴⁴ The image is then acquired in the scanner.

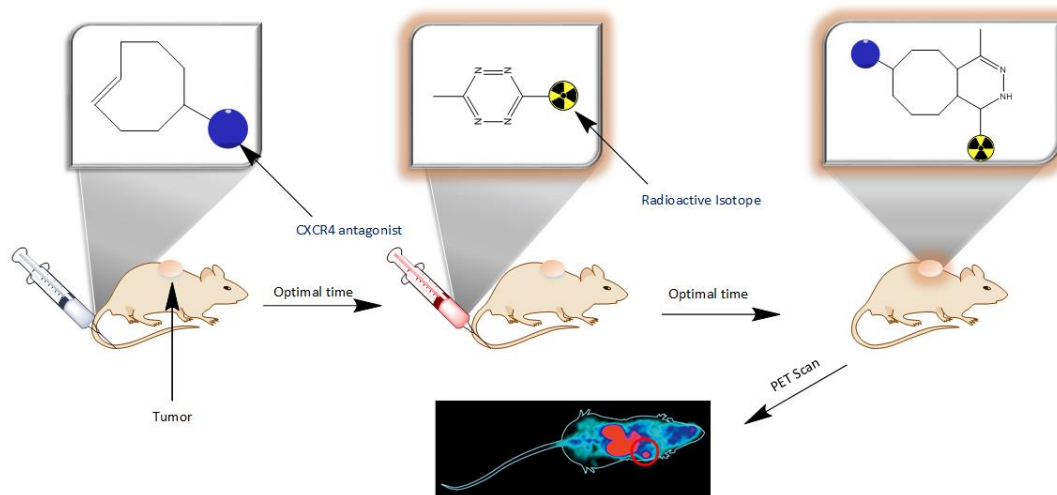


Figure 51: The process of pretargeted PET imaging in a mouse model. Where the blue circle represents the targeting moiety (in this case identified as a CXC4 antagonist).

This technique allows the use of radioisotopes with a shorter half-life that would not be suitable for direct imaging with targeting biological molecules (e.g. antibodies).²⁵² Peptides can also be used as targeting moieties and superior tumour-to-blood ratios achieved with the greater clearance time.²⁵²

In the past five years there have been a number of papers published outlining the use of the TCO-tetrazine click reaction in PET imaging. In 2010 Rossin *et al.* published a landmark study where they reported a tumour pretargeted approach between tetrazine-DOTA derivative (**L48**, Figure 52) radiolabelled with ¹¹¹In and TCO (**L49**) conjugated to anti-TAG72 Mab.²⁵³ The TAG72 antigen was chosen by the group as it had reported to be expressed in a variety of cancer cell lines.

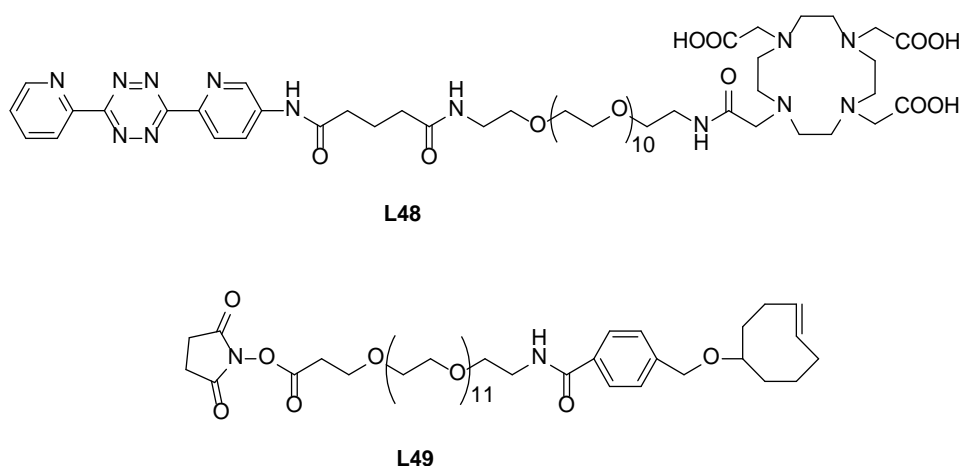


Figure 52: Pretargeting components: Tetrazine-DOTA (**L48**) and trans-cyclooctene-NHS (**L49**).

Rossin *et al.* went on to test the reaction *in vivo*, where compound **L49** was conjugated to mAb-CC49 and administered to mice bearing colon cancer xenografts, followed 24 hours later by an injection of 3.4 mol equivalents of compound [¹¹¹In][In**48**]. The resulting SPECT-CT scan (see Figure 53) showed the expected localisation of radioactivity in the tumour. Only low levels of radioactivity were detected in non-targeted organs or in the blood due to the rapid excretion into the urinary tract via the kidneys.²⁵³

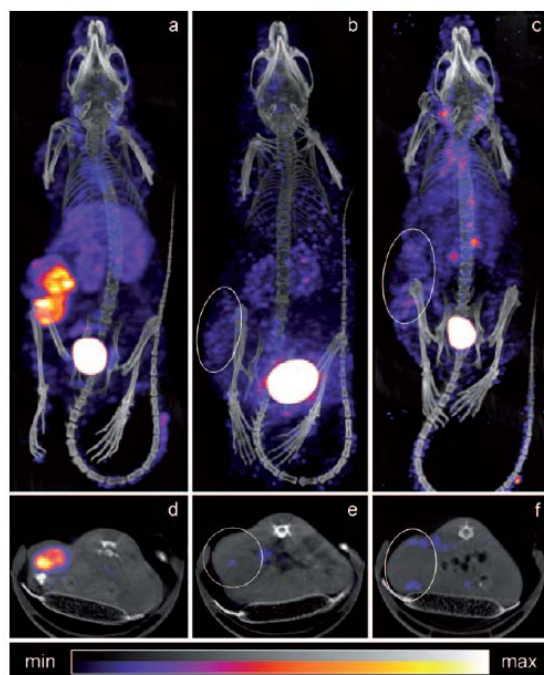
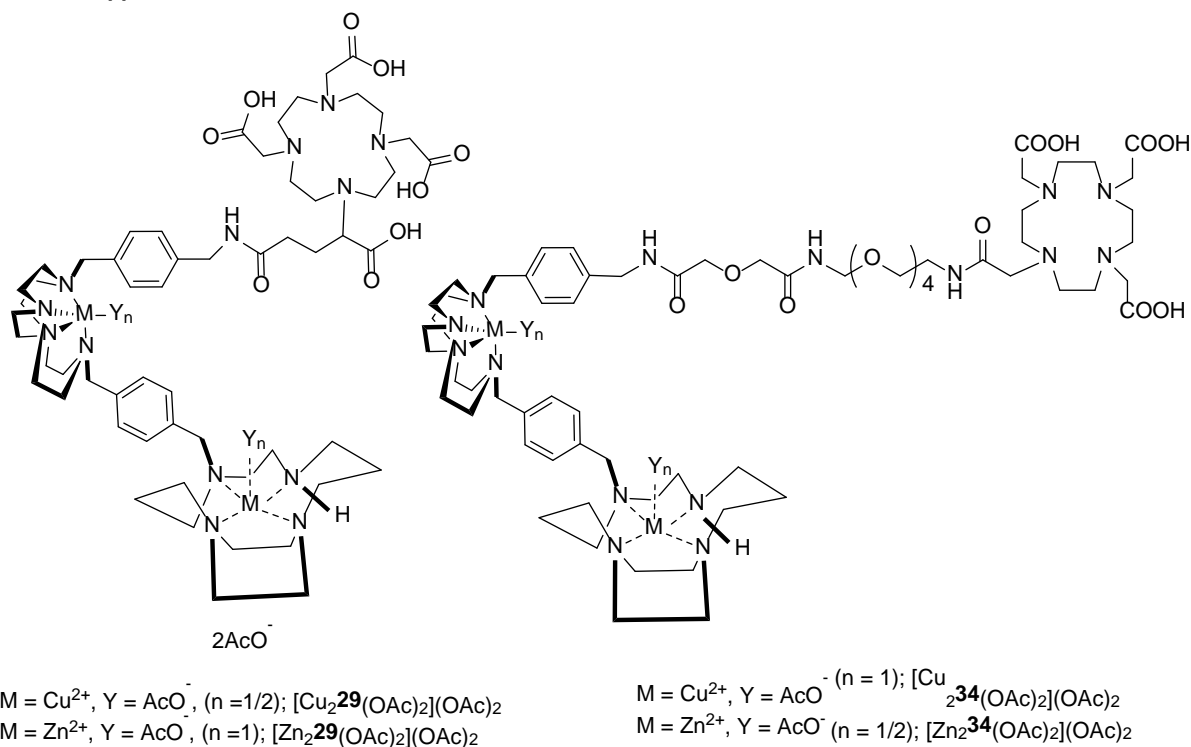


Figure 53: Small animal SPECT-CT image of live mice bearing colon carcinoma xenograft.a) CC49-TCO followed 24 hours later by [¹¹¹In][In**L17**]; b) CC49 (100 mg) followed one day later by [¹¹¹In][In**L17** and c) Rtx-[TCOIn]-1;. (Reproduced from Rossin *et al.*).²⁵⁴

3.3 Proposed strategy for tetraazamacrocyclic CXCR4 antagonist click derivatives

As discussed in chapter two, configurationally restricted tetraazamacrocyclic ligand complexes with transitional metals can be used to form antagonists that bind to CXCR4 with high affinity and long residence times.¹⁹⁸ Therefore the work reported herein aims to develop these high affinity antagonists with the inclusion of a BFC to allow for radiolabelling with gallium-68 and to extend this to include a pretargeted approach.

Direct Approach:



Pretargeted Approach:

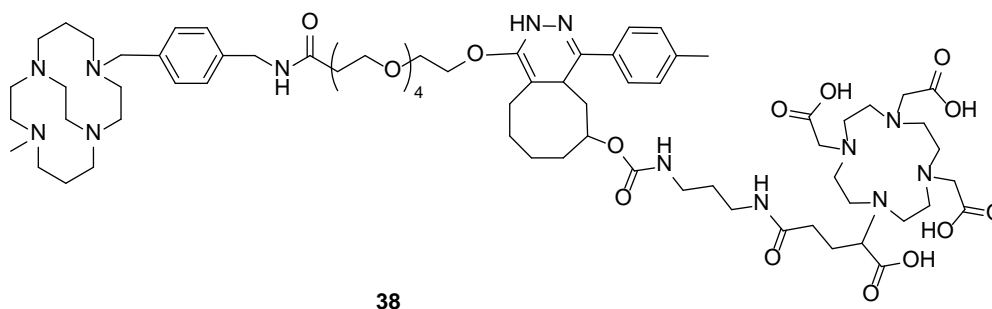


Figure 54: Examples of the target structures of the gallium-68 CXCR4 antagonist designed and evaluated herein. Both a direct and a pretargeted approach were investigated.

Figure 54 shows some of the proposed molecular structures that would allow radiolabelling with gallium-68 and are investigated in this chapter. Both a 'direct' and a 'pretargeted' approach to tracer design were investigated.

3.4 Design and functionalisation of tetraazamacrocyclic CXCR4 antagonists

3.4.1 Position of attachment and order of reactions

Initially two different routes to synthesise the radiolabelled CXCR4 antagonist were investigated, both routes utilise the same reactions and BFC, but in a different order (see Figure 55). The first approach (red arrows, Figure 55) involves the azamacrocycle transition metal complex being formed prior to conjugation to the BFC and radiolabelling. Alternatively (green arrows, Figure 55), the conjugation of the ligand and the BFC can be carried out; followed by the metal complex formation but this will result in the transition metal also binding into the BFC cavity; and so the gallium-68 will need to displace this metal ion in the radiolabelling process.

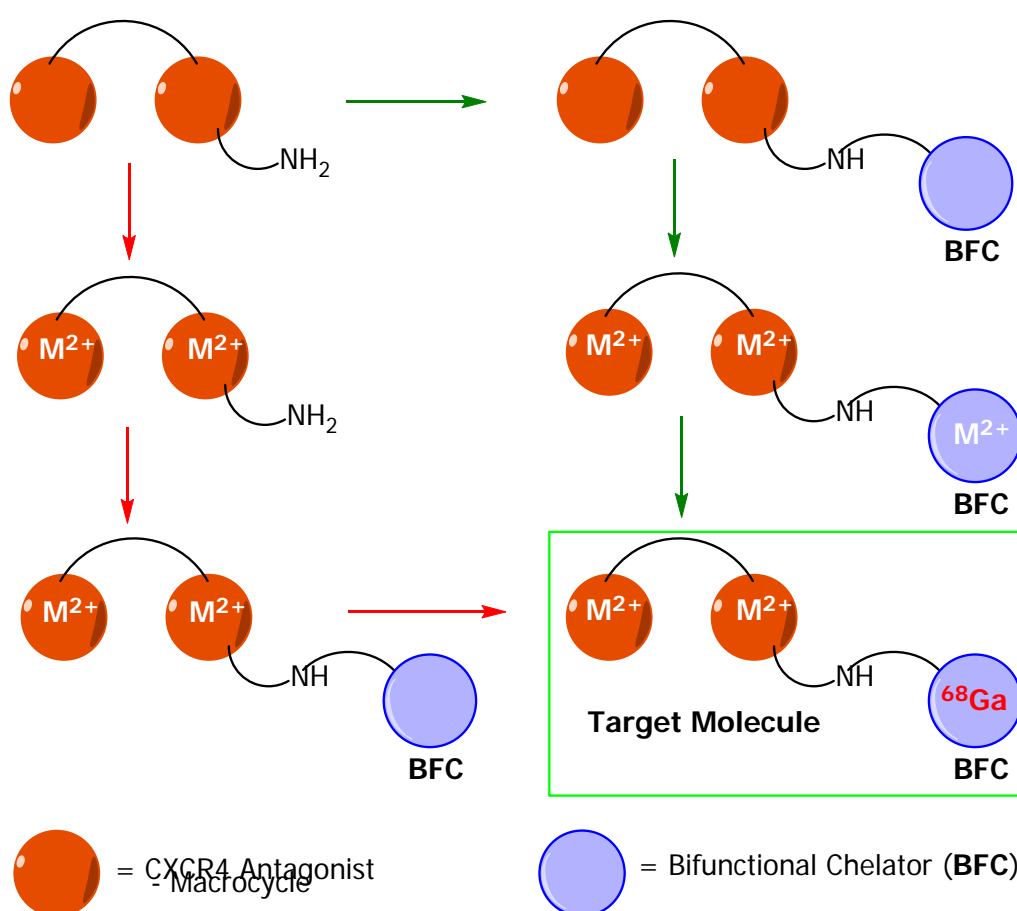


Figure 55: The alternative methods for synthesis and radiolabelling of azamacrocyclic CXCR4 antagonists.

The second approach is preferable from a synthesis and analysis perspective as it is easier to react and analyse the precursor compound in the absence of the transition metal ions. The metal ion can cause various charged species to appear and can exchange counterions giving more complex MS spectra. Additionally, paramagnetic transitional metals prevent NMR analysis. Therefore, a proof of principle experiment was carried out to determine if the gallium-68 could compete effectively with a

transitional metal in a BFC and give reasonable labelling yields. The DO3A complex with copper(II) was used as a model for the BFC and labelling reactions attempted with gallium-68 (see Figure 56).

3.4.1.1 DO3A stability competition assay

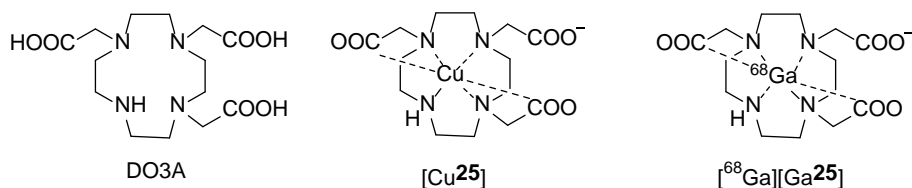


Figure 56: Structures of DO3A, [Cu25] and radiolabelled [⁶⁸Ga][Ga25].

The stability constants of the Ga(III)-DOTA and related complexes have been determined. In a review article Price *et al.* summarised the reported stability constants ($K_{ML} = [ML]/[M][L]$) for the chelator DOTA with various radiometal ions. The logK values for copper(II) range from 22.2 – 22.7, while gallium(III) has a lower value of 21.3.⁶ Therefore, the thermodynamics appear to be unfavourable for DOTA, however this may not be the same for DO3A and variations in measurement conditions could account for the difference. Kinetic factors could also be important and so it is worth testing the chemistry under radiolabelling conditions to see if the reaction occurs.

3.4.2 Competition radiolabelling results

To determine the optimal concentration for labelling of DO3A with gallium-68 a concentration curve was determined using different concentrations of the chelator. Labelling was carried out in 0.2 M sodium acetate (pH 4.6) with 10-25 MBq of gallium-68 and heated at 95°C for 30 minutes. The reaction was monitored by radio-TLC, with free gallium-68 having an R_f value of 1, while the labelled [⁶⁸Ga][Ga25] has an R_f value of 0.3.

Figure 57 shows the concentration curve seen when labelling DO3A with gallium-68. DO3A was labelled at the lowest concentration tested of *ca.* 20.0 μ M in quantitative yields.

To determine if the inclusion of a transitional metal such as copper would effect labelling, the same experiment was carried out with [Cu25] to determine if it could be labelled with gallium-68 under the same conditions. However, as predicted quantitative radiolabelling was not achieved, with only partial radiolabelling to form [⁶⁸Ga][Ga25] (>14%, Figure 57) observed at high concentrations.

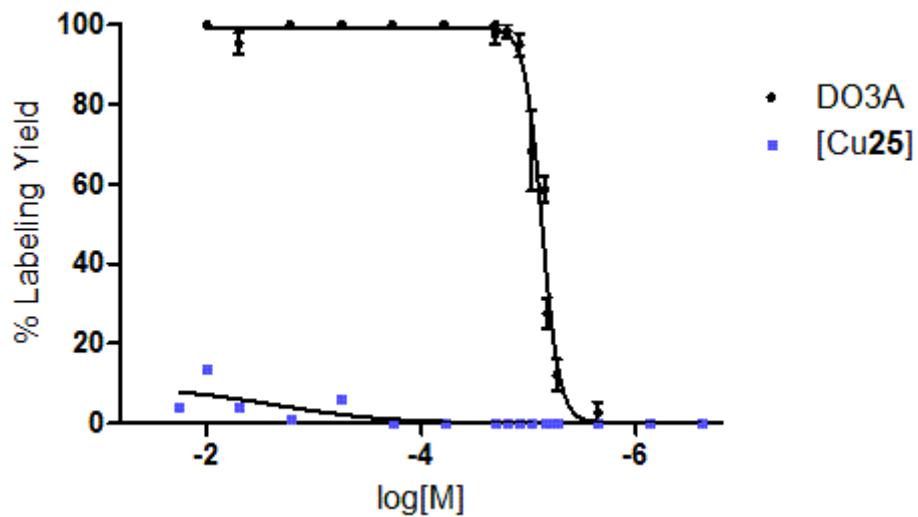


Figure 57: Plot of log[concentration] versus the percentage of radiolabelling with gallium-68 achieved with the DO3A or [Cu25] starting material.

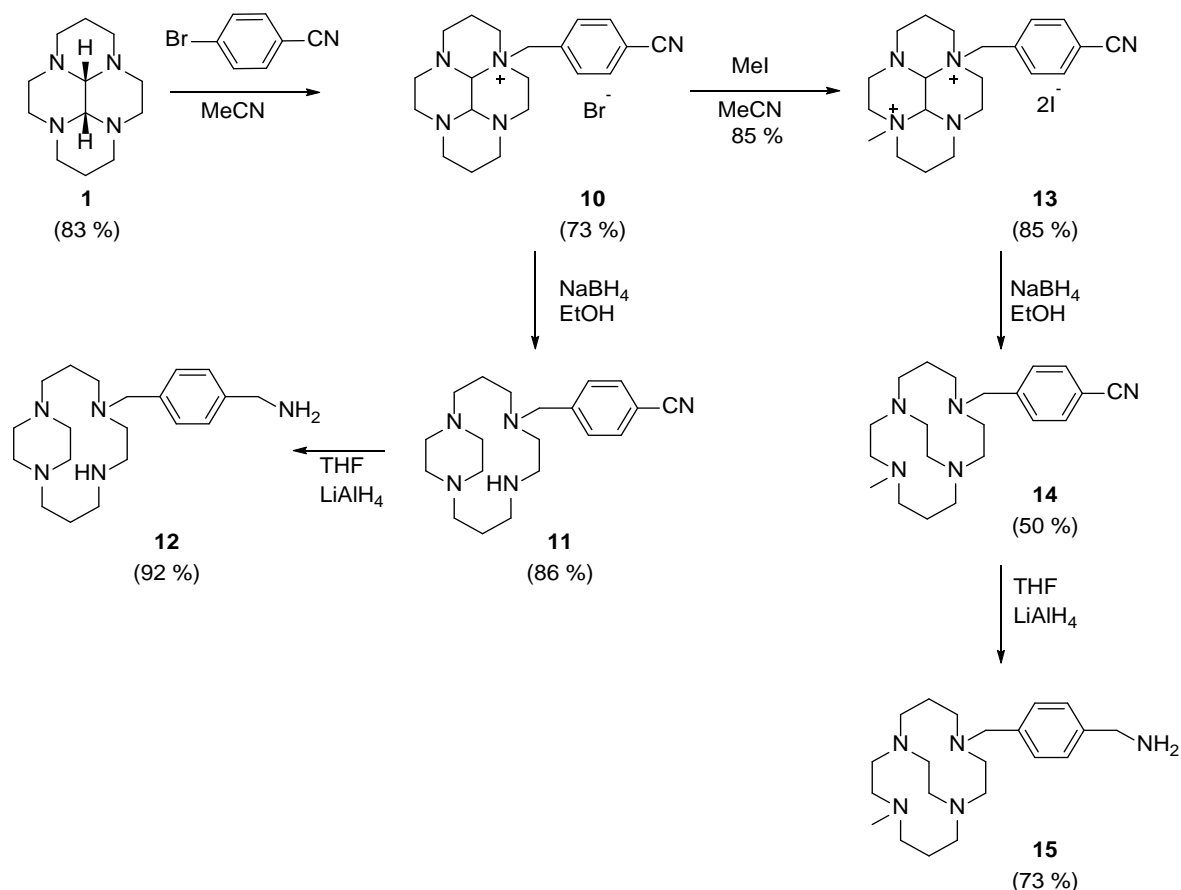
Furthermore, the RCY did not increase significantly with an increase in reaction time. After 2 hours, 18 mM of [Cu25] gave a maximum labelling yield of 11%. These results prove that the second approach (green arrows) depicted in Figure 55 is not viable, therefore the first approach (red arrow) must be used in the design of the radiotracers.

3.5 Synthesis of tetraazamacrocycles conjugated to a BFC

3.5.1 Synthesis of the mono-macrocycle gallium compounds

3.5.1.1 Synthesis of the mono-macrocycle precursors

The mono-cyclam configurationally restricted macrocycles were synthesised due to the relative ease of synthesis (compared to the bis-macrocycles) and their potential for use as model compounds in radiolabelling procedures. Bridged cyclam was synthesised and converted to the side bridged and cross bridged cyclam derivatives following established literature preparations.^{219, 255, 256}



Scheme 6: Synthetic route for the synthesis of the mono-macrocycles **1** (side bridge) and **2** (cross bridge).

All compounds shown in Scheme 6 were produced in good yield and fully characterised. Previous group members reported the use of the reduction of the cyclam/cyclen glyoxal bridge using a large excess (70 *eq.*) of sodium borohydride and leaving the reaction to stir at room temperature for a fortnight.²⁵⁷ However, as well as being slow, this method was shown to introduce an impurity (< 10%). An alternative microwave method was developed, as discussed in chapter 2, and applied to the synthesis of both side bridged and cross bridged compounds. Sodium borohydride (5 *eq.*) was added to **10** or **13** and heated in the microwave (100°C, 300 W) for either 30 min (SB) or 4 hr (CB). NMR spectra and CHN analysis confirmed that a higher purity product was isolated using this method.

The compounds **12** and **15** were synthesised by a lithium aluminium hydride reduction. Rachel Smith, a previous member of the group had tried several different methods for this reduction including the use of borane-tetrahydrofuran complex and Raney nickel, however both proved ineffective.²⁵⁷ The method used was modified from a procedure reported by Hackling *et al.* with the excess LiAlH₄ reacted with water and sodium hydroxide for facile separation at the end of the reaction.²⁵⁸ Both **12** and **15** were produced in high yield (92 and 73%, respectively) and high purity.

As previously stated, the inclusion of a metal ion in the cyclam ring enhances binding to the CXCR4 receptor. Hence metal complexes of **12** and **15** were formed with copper(II), zinc(II) and nickel(II) to give a library of structures (see Figure 58). The inclusion of a metal ion into the CB cavity is more challenging than the SB equivalent due to the increase in structural rigidity of the cyclam. In addition, nickel(II) and zinc(II) CB complexes are more difficult to synthesise because protons abstracted from water/solvent molecules must be displaced from the cavity by the metal ions. The same issue does not occur with copper(II), as copper(II) ions compete more effectively with the protons. As a result the SB metal complexes were formed by stirring at RT for 4-8 hours with the metal acetate salt. The CB cyclam derivatives required an overnight reflux to form the desired metal complexes.

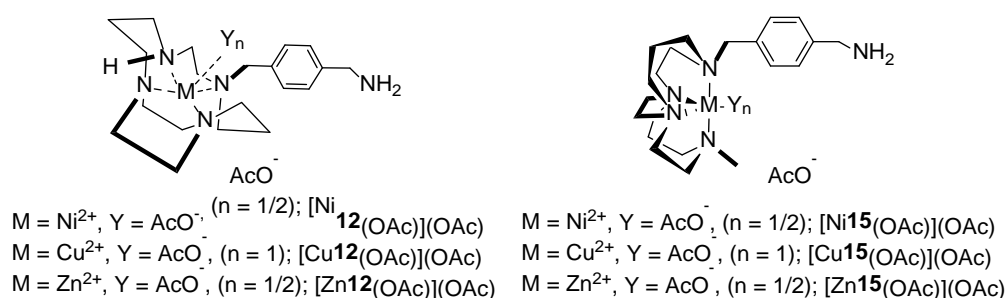


Figure 58: Library of metal complexes formed with zinc(II), copper(II) and nickel(II)

As stated in chapter two, the analysis of all of the fractions from the size exclusion chromatography purification by MS meant that fewer fractions were selected to be combined, giving a higher purity product but lowering the yields compared to those previously reported.²⁵⁷

The metal complexes ($[\text{Ni}26(\text{OAc})](\text{OAc})$, $[\text{Cu}26(\text{OAc})](\text{OAc})$, $[\text{Zn}26(\text{OAc})](\text{OAc})$, $[\text{Cu}27(\text{OAc})](\text{OAc})$ and $[\text{Zn}27(\text{OAc})](\text{OAc})$) were also synthesised and purified. Formic acid was added to switch the counter anions away from a mixture of anions including TFA to allow clearer identification of the peak in the mass spectrum. This approach was successful and allowed assignment of the spectra.

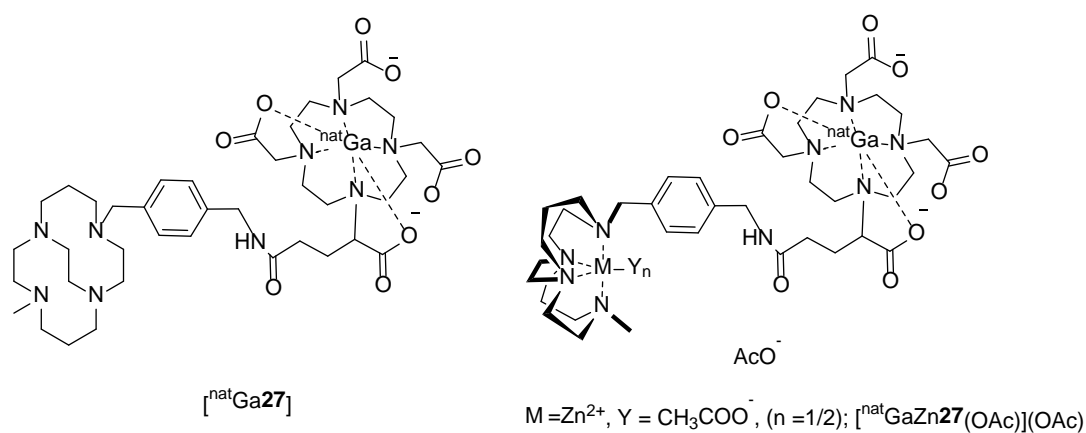


Figure 60: Non-radioactive analogues of compounds **27** and $[\text{Zn}27(\text{OAc})](\text{OAc})$ with gallium(III) nitrate.

Non-radioactive gallium(III) complexes of **27** and $[\text{Zn}27(\text{OAc})](\text{OAc})$ were synthesised to allow the development of HPLC conditions for radiolabelling and to allow *in vitro* bioassay data to be collected (see Figure 60). The gallium complexes were obtained using a procedure reported by Poschenrieder *et al.* (the same procedure that was used in section 2.3.4 to form the gallium complexed **P4** antagonist).¹⁷³

3.6 *In vitro* testing of the mono-tetraazamacrocyclic compounds

Calcium signalling assays were carried out for the mono-tetraazamacrocyclic compounds to determine the affinity for the CXCR4 receptor (see Table 15). Some assays have not yet been returned for the same compound batch, however, past work carried out by the Archibald group on the precursor compounds offers some data for comparison.^{257, 262} All assays were carried out by the research group of Prof Dominique Schols at the Rega Institute (KU Leuven) and AMD3100 was included as a reference compound.

Table 15: Summary of biological assay data generated for CXCR4 antagonist determined by antibody displacement in Jurkat cells and calcium signalling in U87-CXCR4 cells. ^a represents data taken from past work carried out by the Archibald group.

Antagonist	Calcium Signalling IC ₅₀ ^a /nM U87- CXCR4
12	>5000 ^a
[Ni 12 (OAc)](OAc)	>5000 ^a
[Cu 12 (OAc)](OAc)	2200 ^a
[Zn 12 (OAc)](OAc)	34 ^a
15	>5000 ^a
[Ni 15 (OAc)](OAc)	>5000 ^a
[Cu 15 (OAc)](OAc)	222 ^a
[Zn 15 (OAc)](OAc)	273 ^a
26	>5000
[Ni 26 (OAc)](OAc)	>5000
[Cu 26 (OAc)](OAc)	>5000
[Zn 26 (OAc)](OAc)	>5000
27	3737
[Cu 27 (OAc)](OAc)	>5000
[Zn 27 (OAc)](OAc)	2366
[^{nat} GaZn 27 (OAc)](OAc)	>5000
AMD3100	175

The copper(II) and zinc(II) complexes of the CB configurationally restricted macrocycles **15** and **27** were shown to have some activity in the assay, although this is still at a low level compared to bis-tetraazamacrocyclic compounds. The activity of CB compounds can be attributed to the *cis*-V configuration of the CB macrocycles allowing for a more favourable bonding interaction with the aspartate residues on the surface of the CXCR4 receptor.²⁶³

The zinc(II) containing mono-cyclam compounds have higher affinity for the receptor than the nickel(II) and copper(II) analogues. A possible explanation for this is the geometric flexibility of the d^{10} zinc(II) ion compared to d^9 copper(II) and d^8 nickel(II).

The inclusion of the DOTAGA moiety in both antagonists **26** and **27** appears to reduce affinity for the receptor. This is not unexpected as the negative charge present on the DOTAGA is likely to interact unfavourably with negatively charged aspartate residues on the receptor surface. Alternatively, it could be possible that one of the free carboxylates on the DOTAGA could be intructing with the transitional metal inhibiting the necessary metal-aspartate interaction needed to bind to the CXCR4 receptor.

This effect has also been observed by Varasteh *et al.* with a different biological target. In 2015, they investigated the effect that four different chelators (NOTA, NODA-GA, DOTA and DOTAGA) had on the affinity of a gastrin releasing peptide receptor antagonist.²⁶⁴ Although DOTA and DOTAGA differ in size, more importantly they differ in the number of carboxylate groups available for coordination to gallium-68. The overall charges on the complex when DOTA and DOTAGA are chelated with gallium(III) are 0 and -1, respectively. The group reported that the neutral DOTA derivative [^{nat}Ga][Ga-BFC-PEG2-RM26] peptide had a higher affinity for the receptor than the negatively charged DOTAGA derivative.²⁶⁴

None of the molecules shown in Table 15 are sufficiently potent to be considered for *in vivo* characterisation. However, they are useful for optimisation of radiolabelling conditions. This was carried out to develop protocols for use with higher affinity antagonists that may only be available in smaller amounts.

3.7 Development of radiolabelling conditions for mono-cyclam DOTAGA compounds

In order to develop gallium-68 radiolabelling conditions for the mono-cyclam DOTAGA compounds (**26** and **27**) and the metal complexes, the extensive literature for labelling DOTA with gallium-68 was consulted (see a summary of conditions used in Table 6 (section 1.4.4.1)). Based on this data gallium-68 radiolabelling reactions were carried out in sodium acetate buffer (0.2 M, pH 4.6) and heated at 95°C for 20 min. These conditions are quite harsh but the molecules used should be sufficiently robust to tolerate the elevated temperature.^{14, 265} Radio-TLC was used to monitor the progress of labelling reactions, using 0.1 M citrate buffer as eluent as reported by Berry *et al.*¹⁰³ The radiolabelled ligand was shown to remain at the baseline, while the “free” gallium travelled with the solvent front (Figure 61, A and B).

The effect of temperature (25°C, 40°C, 60°C and 90°C) was investigated with a high concentration (0.5 mM) of antagonist **27**. The results shown in Figure 61 C, indicate the expected result, that high temperatures are required to achieve complex formation. Although, 100% conversion could be achieved at 60°C, the reaction time required was 45-60 minutes.

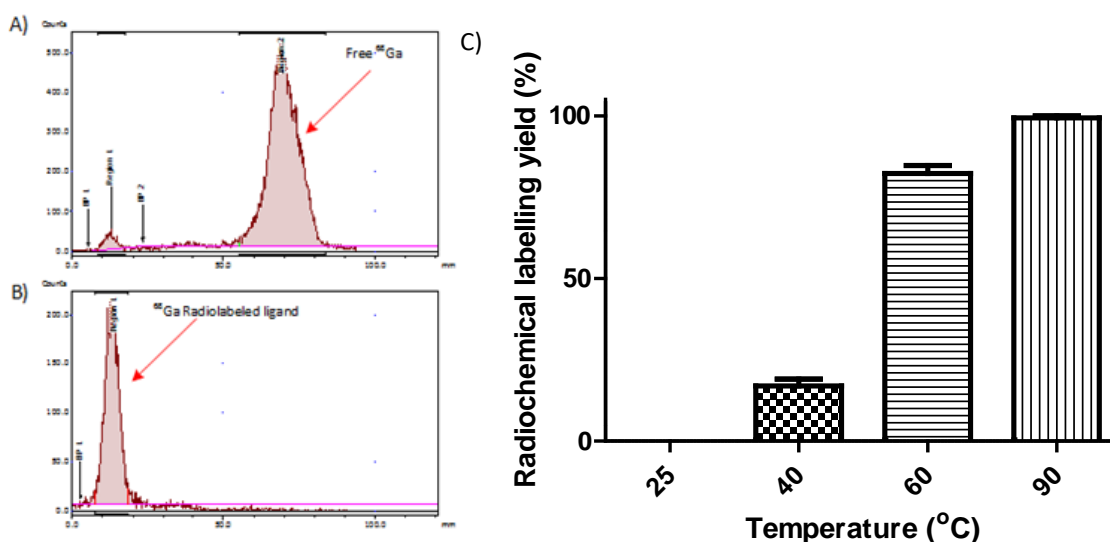


Figure 61: A) Radio-TLC illustrating free ⁶⁸Ga, in 0.1 M citric acid/trisodium citrate 1:1 buffer; B) Radio-TLC illustrating 100% labelling of ⁶⁸Ga[4], in 0.1 M citric acid/trisodium citrate 1:1 buffer; C) Graph showing effect of temperature on radiolabelling yield of ligand **27**, (n=3).

The next parameter to be optimised was the concentration of precursor used in the reaction, **27** was radiolabelled using 5-20 MBq of gallium-68 and heated at 95°C for 20 minutes with the RCY monitored by radio-TLC as before.

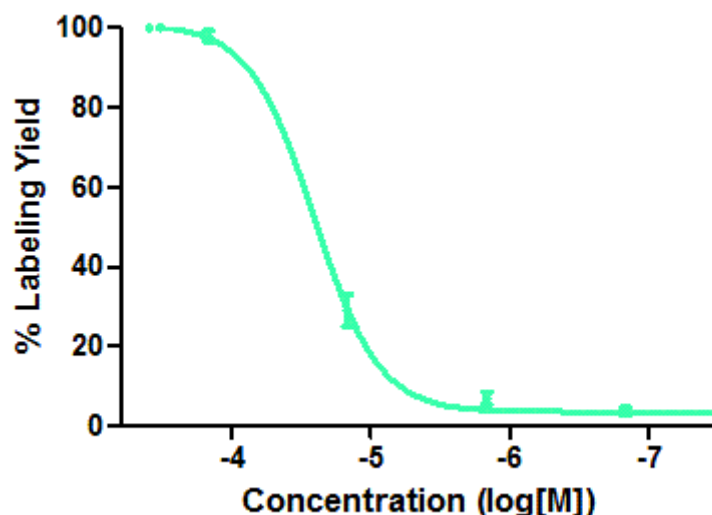


Figure 62: Graph showing effect of concentration on labelling yield with $[^{68}\text{Ga}][\text{Ga}27]$.

As Figure 62 shows, > 95% radiolabelling of antagonist **27** was achieved with *ca.* 100 μM (100 μL ; corresponding to *ca.* 10 nmol). This was slightly higher than the minimum concentration of DOTA required for labelling reported in the literature.²⁶⁶ This may be due to slight inaccuracies in determination of the concentration of the compound due to the presence of salts from HPLC purification.

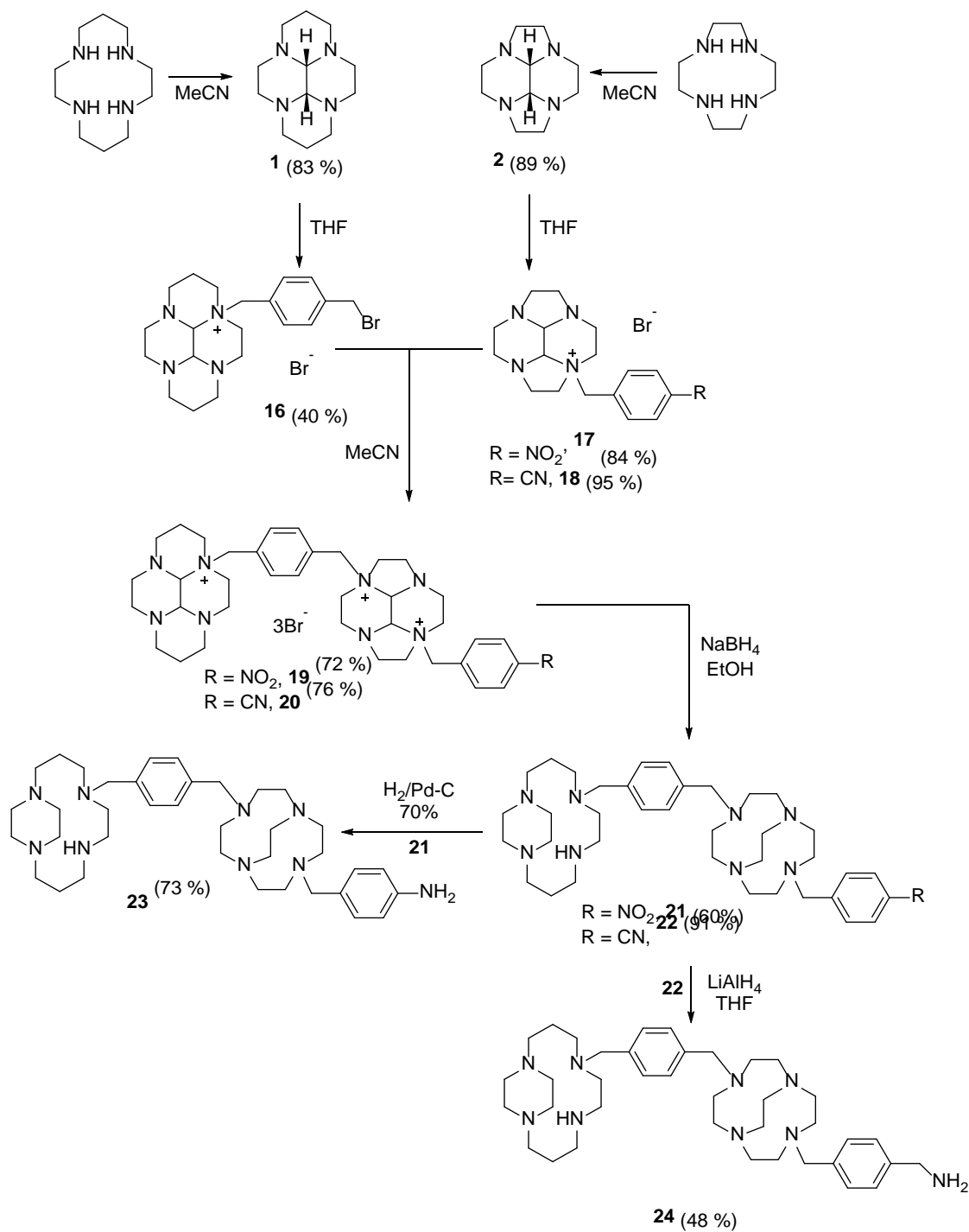
Using these conditions $[^{68}\text{Ga}][\text{Ga}27]$ was obtained with a $32.2 \pm 14.1\%$ decay corrected RCY, whilst $[^{68}\text{Ga}][\text{GaCu}27(\text{OAc})](\text{OAc})$ gave more consistent results with decay corrected RCY of $41.7 \pm 5.6\%$. The partition coefficient (logP) of $[^{68}\text{Ga}][\text{Ga}27]$ was determined to be -2.66 ± 0.12 , confirming the predicted hydrophilic properties of the compound. Column recoveries were also performed to rule out the possibility that the low labeling percentages were due to activity remaining on the column.

Buffer stability of $[^{68}\text{Ga}][\text{Ga}27]$ was measured and showed that the compound was 100% stable after 3 hours at 37.5°C in PBS solution. In addition, stability studies were also conducted with apo-transferrin (as gallium-68 has a similar atomic radius to iron(II), iron scavenging pathways form the primary mechanism for gallium(III) bioprocessing *in vivo*).²⁶⁷ A modified procedure based on that reported by Ma *et al.* was used in which an excess of apo-transferrin (0.6 mg) was incubated with the tracer at 37°C.²⁶⁸ TLC analysis showed that after 3 hours 100% of gallium-68 remained chelated. Similar stability and logP values were also observed for $[^{68}\text{Ga}][\text{Ga}26]$ (logP = -2.63 ± 0.2) and $[^{68}\text{Ga}][\text{GaCu}27(\text{OAc})](\text{OAc})$ (logP = -2.59 ± 0.2).

3.8 Synthesis of the bis-cyclam/cyclen BFC conjugates and gallium radiolabelling

The chemistry and radiochemistry had been trialed using the more readily synthesised mono-cyclam compounds, the strategy developed was applied to the higher affinity bis-cyclam/cyclen compounds.

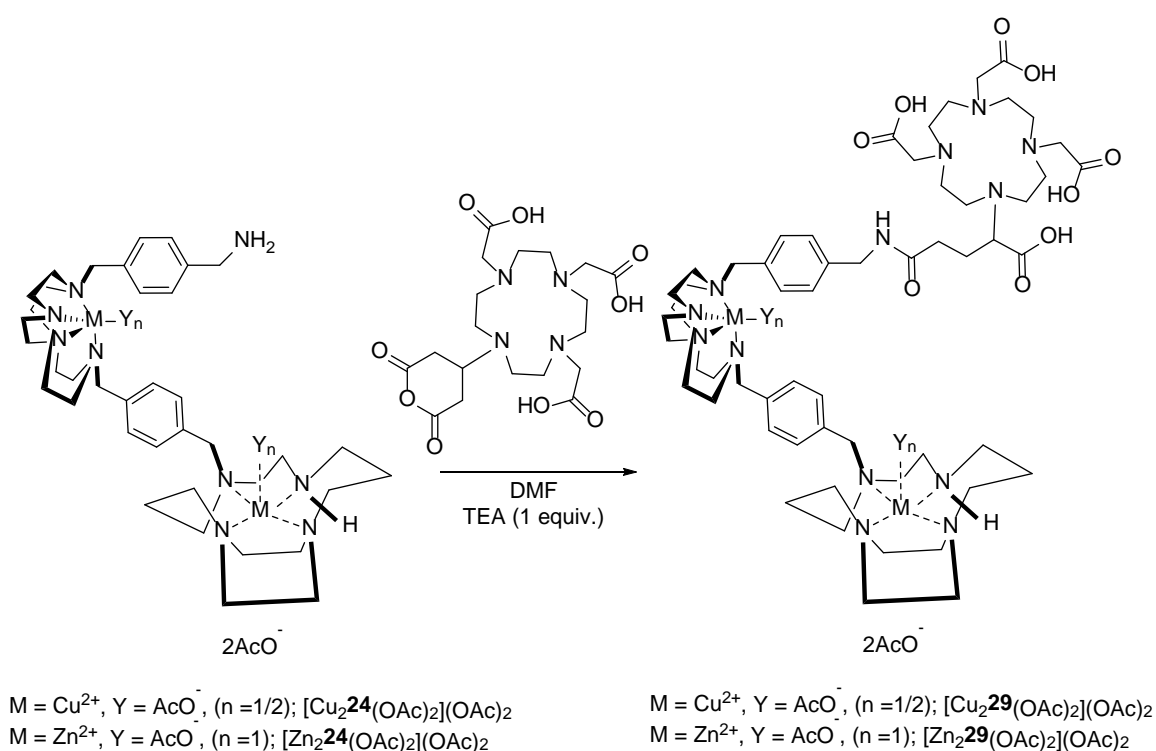
3.8.1 Synthesis of the first and second generation of bis-cyclam/cyclen compounds



Scheme 7: Synthetic route for the synthesis of the bis-macrocycle **23** and **24**.

Initially the bis-cyclam/cyclen aniline compound, **23** (Scheme 7), and the metal complexes were synthesised and attempts were made to react these compounds with DOTAGA anhydride (**28**, $[\text{Cu}_2\mathbf{28}(\text{OAc})_2](\text{OAc})_2$ and $[\text{Zn}_2\mathbf{28}(\text{OAc})_2](\text{OAc})_2$). However, the reaction was very low yielding, due to the delocalisation of the lone pair of electrons on the nitrogen into the phenyl ring. Therefore, these compounds were not developed further and the benzyl amine equivalent compound was synthesised (**24**, Scheme 7).

Using the conditions developed for the mono-cyclam compounds, **24** and its metal complexes were reacted with DOTAGA anhydride to form **29**, $[\text{Cu}_2\mathbf{29}(\text{OAc})_2](\text{OAc})_2$ and $[\text{Zn}_2\mathbf{29}(\text{OAc})_2](\text{OAc})_2$ (see Scheme 8). Each compound was purified by semi-preparative HPLC to remove any unreacted DOTAGA anhydride. As reported previously with the mono-cyclam compounds, the mass spectra and elemental analysis were complicated by the presence of cations and variations in bound counter anions. The mass spectra were simplified by the addition of formic acid.



Scheme 8: Scheme showing the synthesis of tracers $[\text{Cu}_2\mathbf{29}(\text{OAc})_2](\text{OAc})_2$ and $[\text{Zn}_2\mathbf{29}(\text{OAc})_2](\text{OAc})_2$.

Non-radioactive analogues of the tracers were also synthesised to give $[\text{natGa}\mathbf{29}]$, $[\text{natGaCu}_2\mathbf{29}(\text{OAc})_2](\text{OAc})_2$ and $[\text{natGaZn}_2\mathbf{29}(\text{OAc})_2](\text{OAc})_2$. This allowed HPLC conditions to be determined and the compounds to be analysed in biological assays.

3.8.2 Developing radiolabelling conditions for bis-cyclam/cylen DOTAGA compounds

The conditions used for labelling the mono-cyclam compounds were used as a starting point for this work. Initially a concentration of 0.1 mM of each precursor (**29**, $[\text{Cu}_2\mathbf{29}(\text{OAc})_2](\text{OAc})_2$ and $[\text{Zn}_2\mathbf{29OAc})_2](\text{OAc})_2$) was labelled in 0.2 M sodium acetate buffer (0.2 M, pH 4.6, 20 mins at 95°C) in which gave high radiolabelling yields.

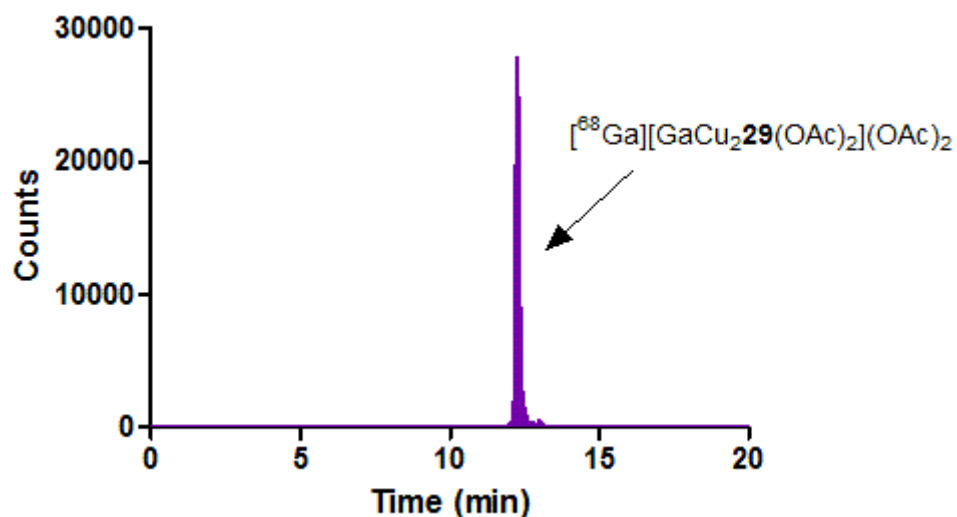


Figure 63: Radio-HPLC chromatograph of $[\text{}^{68}\text{Ga}][\text{GaCu}_2\mathbf{29}(\text{OAc})_2](\text{OAc})_2$.

The radio-HPLC trace of $[\text{}^{68}\text{Ga}][\text{GaCu}_2\mathbf{29}(\text{OAc})_2](\text{OAc})_2$ is shown in Figure 63. This matches the elution time of the non-radioactive analogue ($[\text{}^{\text{nat}}\text{GaCu}_2\mathbf{29}(\text{OAc})_2](\text{OAc})_2$) with the tracer eluting *ca.* 12 min 30 sec. The unlabelled compound $[\text{Cu}_2\mathbf{29}(\text{OAc})_2](\text{OAc})_2$ eluted earlier than the radiotracer. Similar HPLC chromatographs were obtained for $[\text{}^{68}\text{Ga}][\text{Ga}\mathbf{29}]$ and $[\text{}^{68}\text{Ga}][\text{GaZn}_2\mathbf{29}(\text{OAc})_2](\text{OAc})_2$.

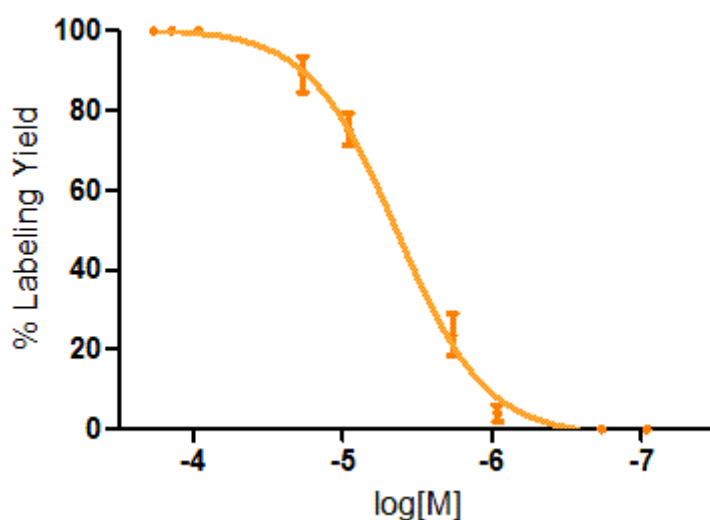


Figure 64: Effect of varying the concentration of **29** on the labelling yield with gallium-68, ($n=3$).

Variation of the concentration of **29** was investigated to determine the optimal concentration for radiolabelling. Figure 64 shows the results obtained for the formation of $[^{68}\text{Ga}][\text{Ga}\mathbf{29}]$ which gave an EC_{95} value of *ca.* 22 μM . This is consistent with a concentration graph reported by Berry *et al.*, who showed that a >95% gallium-68 radiolabelling yield was achieved with a concentration of 10 μM of DOTA.^{265, 269} Similar results were seen for $[^{68}\text{Ga}][\text{GaCu}_2\mathbf{29}(\text{OAc})_2](\text{OAc})_2$ and $[^{68}\text{Ga}][\text{GaZn}_2\mathbf{29}(\text{OAc})_2](\text{OAc})_2$ which gave an EC_{95} value of *ca.* 30-46 μM . This is in same range as concentrations reported for related chelators in the literature.²⁶⁶

Table 16: Radiochemical properties of tracers $[^{68}\text{Ga}][\text{Ga}\mathbf{29}]$, $[^{68}\text{Ga}][\text{GaCu}_2\mathbf{29}(\text{OAc})_2](\text{OAc})_2$ and $[^{68}\text{Ga}][\text{GaZn}_2\mathbf{29}(\text{OAc})_2](\text{OAc})_2$.

Tracer	Partition Coefficient	Decay corrected RCY%	Stability in bovine serum after 3 hours	Stability in apo-transferrin after 3 hours
$[^{68}\text{Ga}][\text{Ga}\mathbf{29}]$	- 2.29 ± 0.18	25.0 ± 9.0	100%	100%
$[^{68}\text{Ga}][\text{GaCu}_2\mathbf{29}(\text{OAc})_2](\text{OAc})_2$	- 2.55 ± 0.19	14.2 ± 4.1	100%	100%
$[^{68}\text{Ga}][\text{GaZn}_2\mathbf{29}(\text{OAc})_2](\text{OAc})_2$	- 2.60 ± 0.17	21.3 ± 7.0	100%	100%

Table 16 shows some of the radiochemical properties of the three tracers. Column recoveries were performed on all three tracers which confirmed that less than 5% of the activity remained on the column after the purification. All tracers were shown to be 100% stable in serum and stable when competing with apo-transferrin. The partition coefficient of $[^{68}\text{Ga}][\text{Ga}\mathbf{29}]$ was slightly less hydrophilic than the metal complexes, as would be expected.

3.9 *In vitro* CXCR4 binding assays of tetraazamacrocycles

3.9.1 Calcium signalling assay

As with the mono-cyclam compounds in Section 3.6.1.2 a calcium signalling assay (using a CXCR4 transfected U87 cell line with CXCL12) was carried out on the library of bis-cyclam compounds produced. The data was collected by the research group of Prof Dominique Schols at the Rega Institute (KU Leuven).

Table 17: Summary of biological assay data generated for CXCR4 antagonist determined by antibody displacement in Jurkat cells and calcium signalling in U87-CXCR4 cells. ^a indicates data taken from past work carried out by the Archibald group.

Antagonist	Calcium Signalling IC ₅₀ ^a /nM U87-CXCR4
[^{nat} GaP4]	102
20	>5000
24	>5000
[Cu ₂ 24 (OAc) ₂](OAc) ₂	100
[Zn ₂ 24 (OAc) ₂](OAc) ₂	1
29	>5000
[Cu ₂ 29 (OAc) ₂](OAc) ₂	142
[Zn ₂ 29 (OAc) ₂](OAc) ₂	>5000
[^{nat} Ga 29]	>5000
[^{nat} GaZn ₂ 29 (OAc) ₂](OAc) ₂	>5000

As seen previously with the mono-cyclam compounds, the inclusion of metal ions into the cyclam/cyclen rings increases binding affinity. **24** (IC₅₀ = >5000 nM) forms the highest affinity antagonist, [Zn₂**24**(OAc)₂](OAc)₂ when the zinc(II) complex is formed (IC₅₀ = 1 nM). The trends between the copper(II) and zinc(II) complexes of **24** are as expected with a higher affinity for the zinc(II) complex, however the lack of affinity for the zinc(II) complex of **29** and the gallium(III) complex is unexpected but may be due to the proximity of the DOTAGA chelator to the binding group. Further study is needed with these compounds and the synthesis of the gallium(III) complex of the copper(II) **29** compound is required. Whilst it would be expected that the addition of the DOTAGA chelator would disrupt binding, the loss of affinity of the zinc(II) complex to this degree was not predicted. The results for the copper(II) complex of **29** shows a 50 nM reduction in affinity, which is minimal but not in line with the results observed for the [Zn₂**29**(OAc)₂](OAc)₂ compound. Further investigation and repeat syntheses are required as these results do not give a consistent set of data.

3.9.2 CXCR4 expressing cell binding assay with radiotracers

To investigate the binding of these bis-cyclam/cyclen gallium-68 tracers to the CXCR4 receptor a cell binding assay was carried out with $[^{68}\text{Ga}][\text{GaZn}_2\mathbf{29}(\text{OAc})_2](\text{OAc})_2$ and $[^{68}\text{Ga}][\text{GaCu}_2\mathbf{29}(\text{OAc})_2](\text{OAc})_2$. Interaction with the CXCR4 receptor was determined by cell binding in U87, U87-CXCR4 and Jurkat cells. To show CXCR4 specificity a blocking study was carried out, where U87-CXCR4 and Jurkat cells were blocked with $20\ \mu\text{M}\ [\text{Cu}_2\mathbf{5}(\text{OAc})_2](\text{OAc})_2$. Cells were then incubated with 28 kBq of tracer for 60 minutes on ice to avoid receptor internalisation.

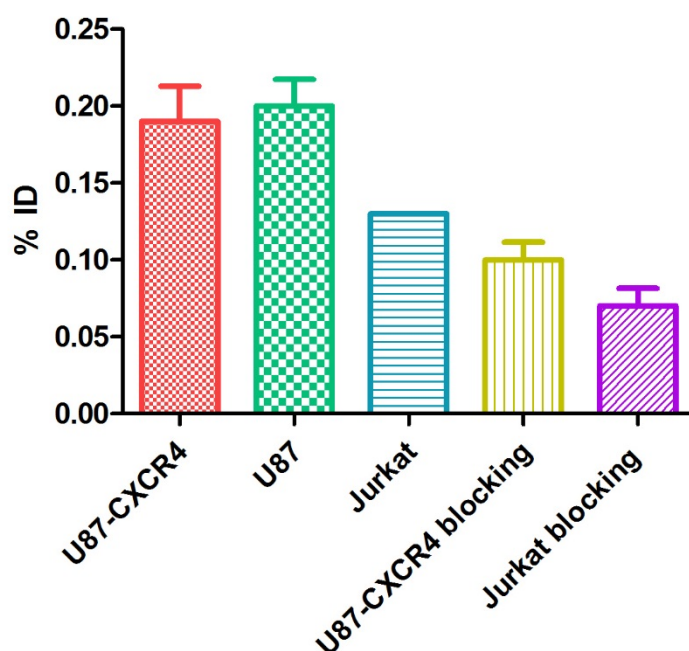


Figure 65: Cell binding of $[^{68}\text{Ga}][\text{GaZn}_2\mathbf{29}(\text{OAc})_2](\text{OAc})_2$ in U87, U87-CXCR4 and Jurkat cells, data is represented as percentage of incubated dose. Data presented as mean \pm standard deviation. % ID = percentage incubated dose. ($n=3$) (data collected by Ms. Cecília Miranda).

Figure 65 shows the percentage of incubated tracer bound (in this case $[^{68}\text{Ga}][\text{GaZn}_2\mathbf{29}(\text{OAc})_2](\text{OAc})_2$) in the three cell lines. The results revealed low uptake ($<0.2\%$), with no significant difference of tracer accumulation between CXCR4-expressing cells U87-CXCR4 and the negative control (U87 cells), suggesting it was not specific binding to CXCR4. Blocking experiments showed a slight reduction in binding to U87-CXCR4 and Jurkat cells. $[^{68}\text{Ga}][\text{GaCu}_2\mathbf{29}(\text{OAc})_2](\text{OAc})_2$ also showed similar results when tested in Jurkat cells with an average percentage of the incubate dose binding of 0.18% .

To validate the assay, the same experiment was carried out with $[^{68}\text{Ga}][\text{GaP}\mathbf{4}]$ in MM.1S, U87-CXCR4 and U87 cells. As shown in Figure 66; $[^{68}\text{Ga}][\text{GaP}\mathbf{4}]$ had approximately 20 times higher uptake in U87-CXCR4 compared to U87 cells (3.9% and 0.2% respectively). This shows, as expected, that $[^{68}\text{Ga}][\text{GaP}\mathbf{4}]$ is binding to the CXCR4 receptor.

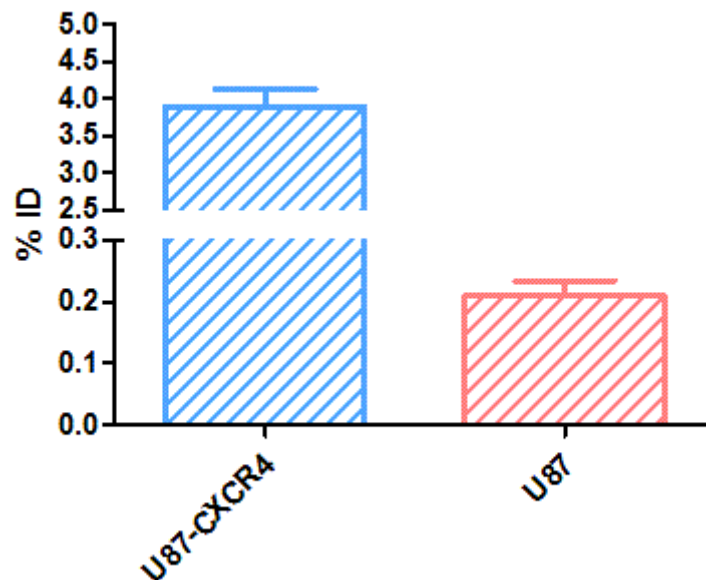


Figure 66: Cell binding of $[^{68}\text{Ga}][\text{GaP4}]$ in U87-CXCR4 and U87, data is represented as percentage of incubated dose. % ID = percentage incubated dose. ($n=3$) (data collected by Ms. Cecília Miranda).

Comparing the binding of $[^{68}\text{Ga}][\text{GaZn}_2\mathbf{29}(\text{OAc})_2](\text{OAc})_2$ to $[^{68}\text{Ga}][\text{GaP4}]$ (*ca.* 0.2% to 3.9%; respectively) in U87-CXCR4 cells, it is unlikely that $[^{68}\text{Ga}][\text{GaZn}_2\mathbf{29}(\text{OAc})_2](\text{OAc})_2$ is binding effectively to the CXCR4 receptor. These results are in agreement with the calcium signalling assay results shown in Table 17 as well as FACS data (data not shown).

3.10 *In vivo* comparison of $[^{68}\text{Ga}][\text{GaZn}_2\mathbf{29}(\text{OAc})_2](\text{OAc})_2$

Mice bearing CXCR4 expressing tumours were available prior to the full set of calcium signalling data and so $[^{68}\text{Ga}][\text{GaZn}_2\mathbf{29}(\text{OAc})_2](\text{OAc})_2$ was taken *in vivo* as the results on the precursor compound showed high affinity ($[\text{Zn}_2\mathbf{29}(\text{OAc})_2](\text{OAc})_2$ $\text{IC}_{50} = 1$ nM).

CD-1 nude mice were subcutaneously inoculated into the right flank with 5×10^6 MM.1S cells (expression shown in Figure 46), tumours were allowed to grow until the tumour size reached 100-300 mm³. Dynamic PET images were obtained upon injection of ca. 2.4 MBq of $[^{68}\text{Ga}][\text{GaZn}_2\mathbf{29}(\text{OAc})_2](\text{OAc})_2$ via the tail vein. As shown in Figure 67, the *in vivo* pharmacokinetics of $[^{68}\text{Ga}][\text{GaZn}_2\mathbf{29}(\text{OAc})_2](\text{OAc})_2$ is characterised by a high accumulation in liver and the kidneys and bladder due to clearance of tracer. No significant accumulation was observed in CXCR4 expressing organs such as spleen, bone marrow and bony growth plates, or the CXCR4 expressing tumour.

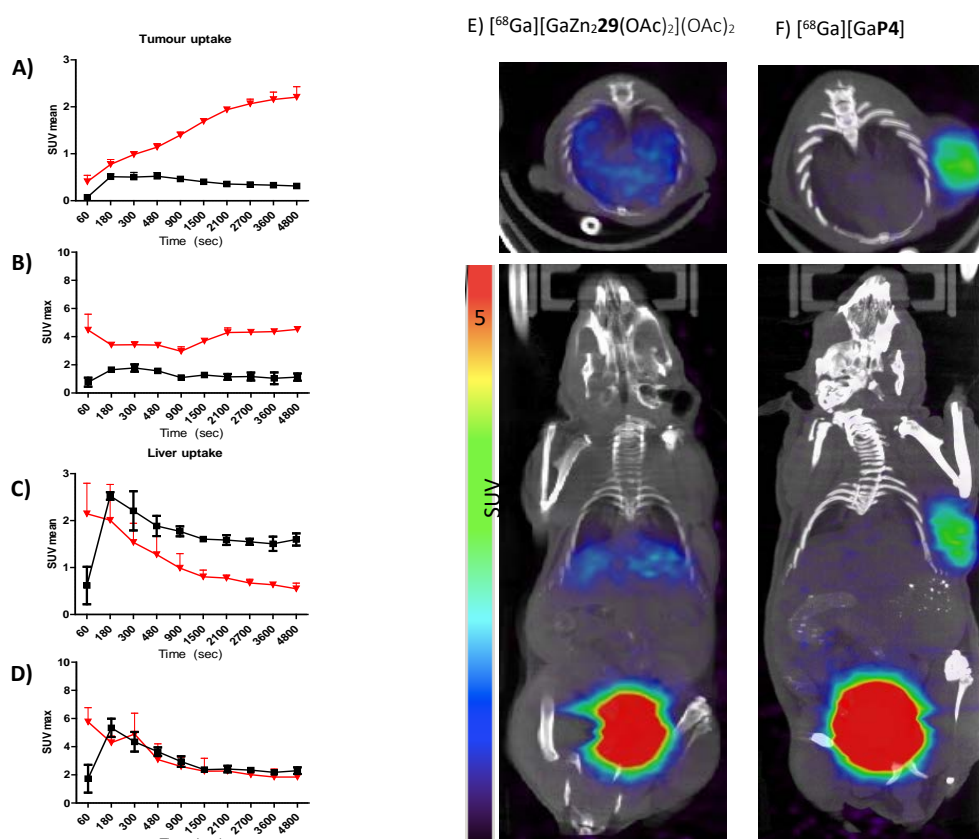


Figure 67: Comparison of $[^{68}\text{Ga}][\text{GaZn}_2\mathbf{29}(\text{OAc})_2](\text{OAc})_2$ (black) and $[^{68}\text{Ga}][\text{GaP4}]$ (orange) uptake in MM1.s tumours expressing low levels of CXCR4. A, B: Time activity curves showing tumour uptake of $[^{68}\text{Ga}][\text{GaZn}_2\mathbf{29}(\text{OAc})_2](\text{OAc})_2$ and $[^{68}\text{Ga}][\text{GaP4}]$. C, D) Time activity curves showing liver uptake of $[^{68}\text{Ga}][\text{GaZn}_2\mathbf{29}(\text{OAc})_2](\text{OAc})_2$ and $[^{68}\text{Ga}][\text{GaP4}]$ ($n=3$). E) and F): Representative coronal PET/CT image of $[^{68}\text{Ga}][\text{GaZn}_2\mathbf{29}(\text{OAc})_2](\text{OAc})_2$ and $[^{68}\text{Ga}][\text{GaP4}]$ uptake in MM.1S tumour-bearing CD-1 nude mice (90 minutes post injection). (Data collected by Ms. Cecilia Miranda).

In order to validate the *in vivo* model and show CXCR4 expression in MM1.S tumours $[^{68}\text{Ga}][\text{GaP4}]$ was used as a control CXCR4 antagonist (although it only binds to human CXCR4 and so

only tumour binding should be observed). As shown in Figure 67, the *in-vivo* pharmacokinetics of [⁶⁸Ga][GaP4] are characterised by a high accumulation in kidneys and bladder due to clearance of tracer, as well as significant uptake in the MM1.S tumour was observed, and is consistent with the work of Philipp-Abbrederis *et al.*²⁷⁰

The *in vivo* 90 minute scan of tracer [⁶⁸Ga][GaZn₂29(OAc)₂](OAc)₂ showed insignificant uptake in the MM1.S tumour. This agrees with *in vitro* data that [⁶⁸Ga][GaZn₂29(OAc)₂](OAc)₂ has low affinity toward the CXCR4 receptor. [⁶⁸Ga][GaZn₂29(OAc)₂](OAc)₂ was shown to be excreted renally.

Although some low levels of uptake of [⁶⁸Ga][GaZn₂29(OAc)₂](OAc)₂ is seen in the liver (which naturally expresses murine CXCR4), on comparison to scans with [⁶⁸Ga]gallium citrate (see Figure 68) in wild-type mice, the liver uptake was not significant. However, more scans are needed with [⁶⁸Ga]gallium citrate as it is known to be variable between models, with the time of day and fasted/non-fasted and food known to effect the biodistribution.²⁷¹

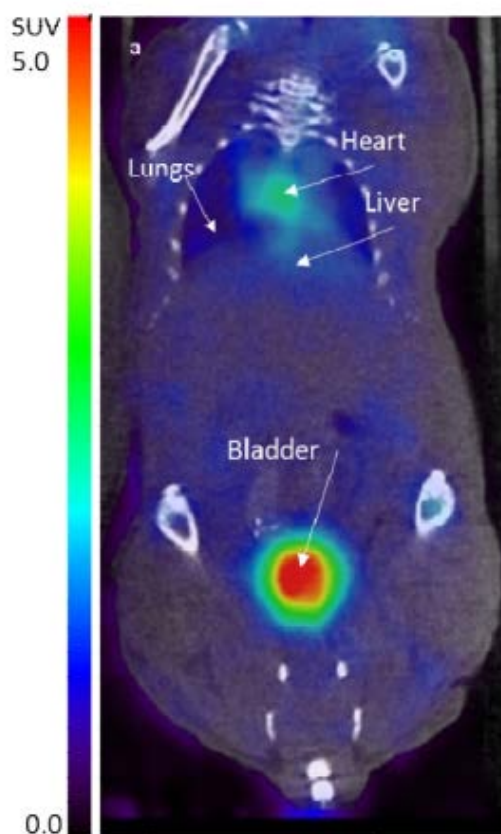


Figure 68: Representative coronal PET/CT image of [⁶⁸Ga]gallium citrate scan in wild type nude mice (10 MBq, 90 minutes post injection).

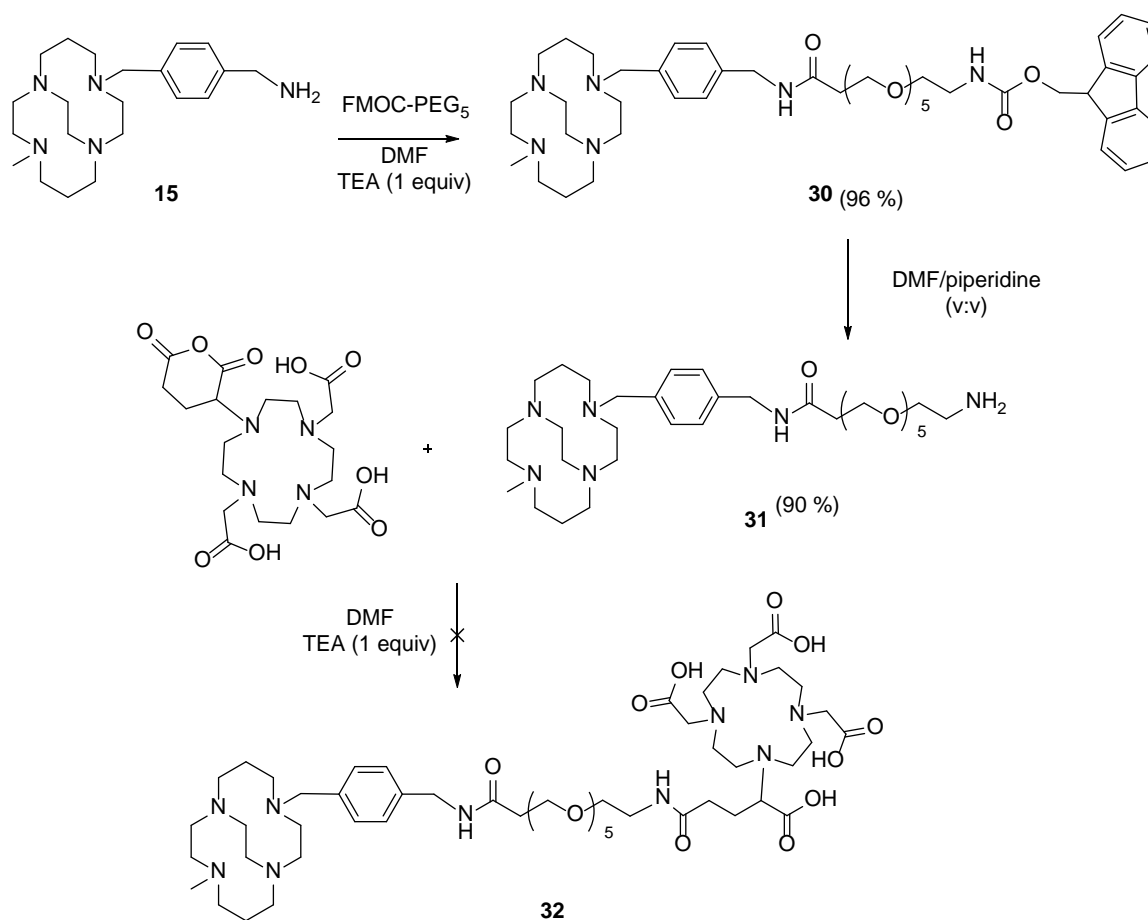
3.11 Second generation of DOTAGA conjugated macrocyclic compounds

Due to the low CXCR4 affinity observed for the metal complexes of **29**, alternative approaches were investigated to prevent any steric or charge repulsion interaction between the DOTAGA BFC and the CXCR4 receptor. The first approach attempted used a PEG linker to increase the distance between the BFC and the CXCR4 binding component. Secondly, a pre-targeted approach using bioorthogonal click chemistry for *in vivo* reaction was investigated as this would allow the high affinity antagonist to bind prior to administration of the reactive radiolabelled component. The third approach was the use of an alternative BFC that is compatible with kit-like labelling with gallium-68 was considered and tested with the CXCR4.2 peptide (to give an analogue of Pentixafor).

3.11.1 Incorporation of PEG linker between the CXCR4 binding component and the BFC

3.11.1.1 Synthetic strategy for PEG linker compound

Scheme 9 shows the trial reaction scheme that was carried out to form mono-cyclam compound **32** which includes a PEG linker. The coupling of the mono-macrocycle compound **15**, with the Fmoc protected PEG₅ was carried out in anhydrous conditions to give the pure product in good yield.



Scheme 9: Attempted scheme for the synthesis of the extended pegylated antagonist **32**.

31 was produced by a standard Fmoc deprotection with piperidine and was purified via semi-preparative HPLC.²⁷² However, the conjugation of **31** with DOTAGA anhydride was unsuccessful. It is possible that the DOTAGA anhydride had hydrolysed to form the less reactive ring open derivative, however, anhydrous conditions and inert atmosphere were employed throughout the synthesis. It could have also been possible that reactive amine of antagonist **15** could have reacted twice with DOTAGA anhydride, hence the expected product was not found.

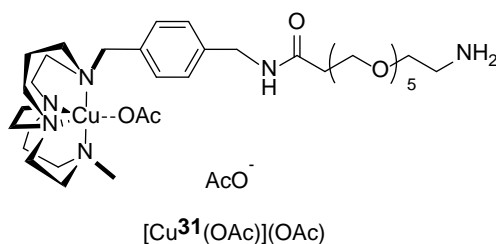
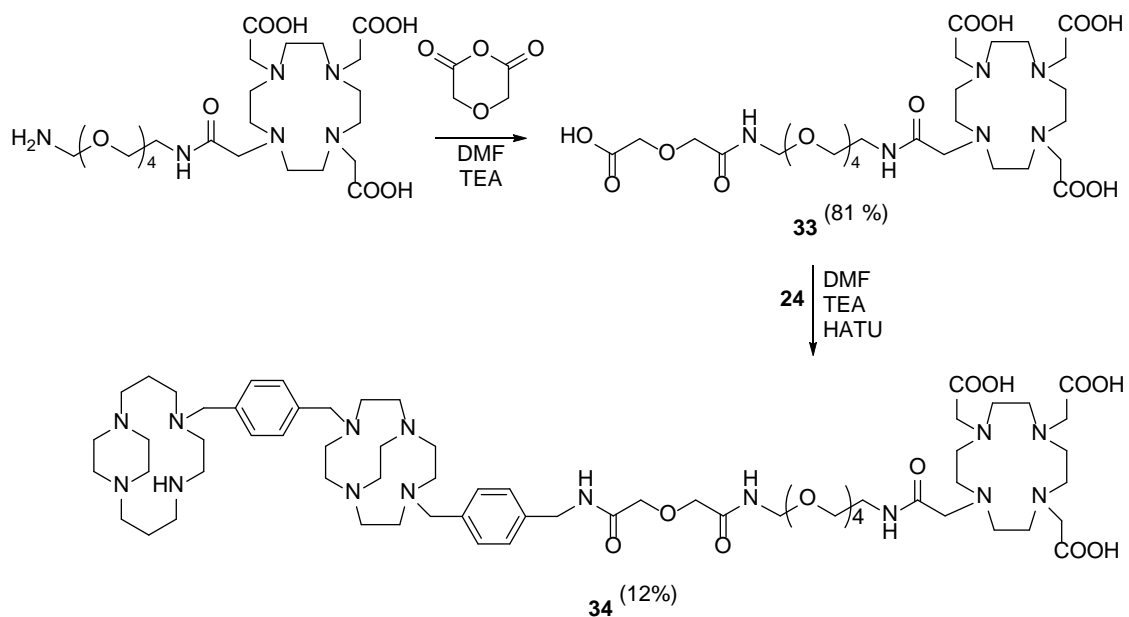


Figure 69: Structure of extended mono- copper antagonist; $[\text{Cu}^{\mathbf{31}}(\text{OAc})](\text{OAc})$

The same procedure was attempted with the copper(II) complex of **31**, with the initial formation of the PEG derivative, $[\text{Cu}^{\mathbf{31}}(\text{OAc})](\text{OAc})$ giving the desired product in a high yield, see Figure 69. However, as before, the conjugation to DOTAGA anhydride did not give the desired product. Due to the problems encountered with this synthetic strategy an alternative procedure using $\text{NH}_2\text{-PEG}_4\text{-DOTA}$ was investigated. This BFC also had the benefit that it has one less carboxylic acid group than DOTAGA, hence, would give a neutral complex with gallium(III).

Scheme 10, shows the reaction scheme used to produce **33**. $\text{NH}_2\text{-PEG}_4\text{-DO3A}$ was reacted with diglycolic anhydride via a ring-opening reaction to give an acid group which could be activated to allow conjugation to the primary amine on the tetraazamacrocyclic antagonist. **33** formed in a high yield and purity with the expected number of carbonyl peaks clearly observed in the ^1H and ^{13}C NMR spectrum.



Scheme 10: Synthesis of PEG containing compound **34**.

The coupling of **33** with the bis-tetraazamacrocycle **24** was carried out in anhydrous amine-free DMF with one equivalent of base and coupling agent (HATU). The reaction was shaken at RT for 24 hours, and MS was used to monitor the reaction via the disappearance of the starting material. Semi-preparative HPLC was used to isolate the **34** in a yield of 12%. The low yield may be due to insufficient activation of the carboxylic acid group **24**. In the future, the reaction could be carried out with 5 equivalents of HATU and base due to the other carboxylic acid groups present on **33**. However, as sufficient product was collected for radiolabelling, no further optimisation was carried out for this reaction.

The synthesis of the copper and zinc complexes of **34**; $[(\text{Cu}_2\mathbf{34}(\text{OAc})_2)(\text{OAc})_2]$ and $[\text{Zn}_2\mathbf{34}(\text{OAc})_2](\text{OAc})_2$ was attempted, see Figure 70. However, even with the higher ratio of activating agent and base, the desired product was not isolated. The reaction was followed via analytical HPLC which showed the disappearance of the starting material, however several new peaks formed on reaction, and analysis by MS did not give any identifiable peaks for the product. It is likely that, as has been observed previously, exchange of bound counter anions has made identification of the product challenging. Alternatively, the activation of one or more of the other carboxylic acid groups of the DO3A compound could lead to formation of by-products.

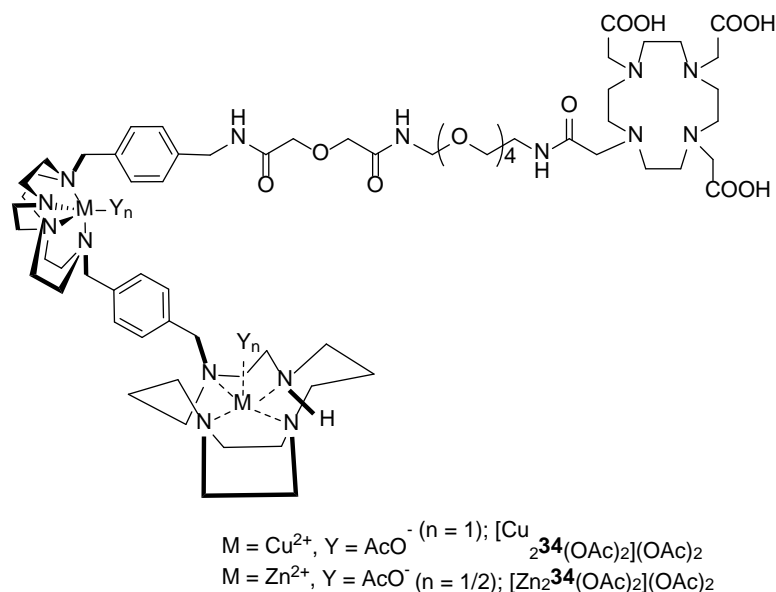


Figure 70: Structures of metal complexes $[\text{Cu}_2\mathbf{34}(\text{OAc})_2](\text{OAc})_2$ and $[\text{Zn}_2\mathbf{34}(\text{OAc})_2](\text{OAc})_2$.

More work is needed to develop reaction conditions for the formation of $[\text{Cu}_2\mathbf{34}(\text{OAc})_2](\text{OAc})_2$ and $[\text{Zn}_2\mathbf{34}(\text{OAc})_2](\text{OAc})_2$. An alternative synthetic approach using protected DOTA/ DO3A derivatives may be needed if by-products are being formed.

3.11.1.2 Radiolabelling of **34**

Although the synthesis of $[\text{Cu}_2\mathbf{34}(\text{OAc})_2](\text{OAc})_2$ and $[\text{Zn}_2\mathbf{34}(\text{OAc})_2](\text{OAc})_2$ were not successful. The metal-free precursor was synthesised in high purity and so gallium-68 radiolabelling experiments were carried out using this compound.

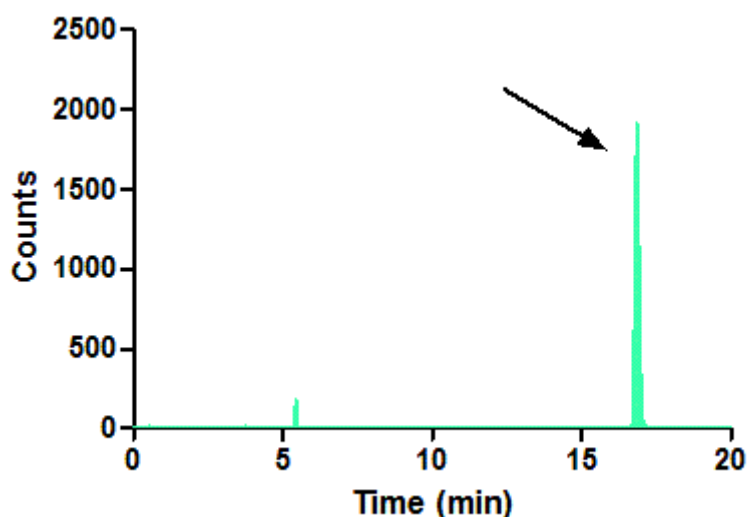


Figure 71: Radio HPLC trace of $[\text{68Ga}][\text{Ga}\mathbf{34}]$, run in acidic conditions after 3 hr.

Radiolabelling was achieved using the same conditions as in section 3.7; 0.2 M sodium acetate buffer (pH 4.6) reacting for 20 mins at 95°C. Figure 71 shows the radio-HPLC trace taken

after 3 hrs in acidic conditions of [⁶⁸Ga][Ga**34**]. The labelled compound was >95% stable in acidic conditions and PBS at 37.5°C for up to 3 hours. As the study was a single data point (n = 1) more comprehensive stability analysis should be carried out. **34** was radiolabelled in a 42.9% decay corrected yield, similar to the yields obtained with other DOTA/DO3A containing tracers, such as **P4**. Column recovery was used to determine minimal activity was retained on the HPLC column.

3.11.1.3 *In vitro* CXCR4 binding assay for **34** and complex

Calcium signalling studies were again carried out on **34** and the crude reaction mixture from the reaction to form [Zn₂**34**(OAc)₂](OAc)₂ to determine whether the inclusion of the PEG group enhanced the affinity of the antagonist towards the CXCR4 receptor, see Table 18 (as previously assays were completed by the research group of Prof Dominique Schols at the Rega Institute (KU Leuven)).

Table 18: Summary of biological assay data generated for CXCR4 antagonist determined by antibody displacement in Jurkat cells and calcium signalling in U87-CXCRR cells (* indicates crude sample mixture, not purified by HPLC).

Antagonist	Calcium Signalling IC ₅₀ /nM U87-CXCR4
34	>5000
[Zn ₂ 34 (OAc) ₂](OAc) ₂ *	>5000

Inclusion of the PEG group did not appear have the desired result of increasing the CXCR4 affinity for the zinc(II) complex of **34**, although only the crude reaction mixture was analysed and the compound has not been fully characterised. The positioning of the PEG chain could be causing steric interactions but this was not expected. Until the pure metal complexes are isolated and analysed no firm conclusions can be drawn on the affinity of these compounds. Further work and development of alternative synthetic procedures are required to produce pure samples of [Cu₂**34**(OAc)₂](OAc)₂ and [Zn₂**34**(OAc)₂](OAc)₂.

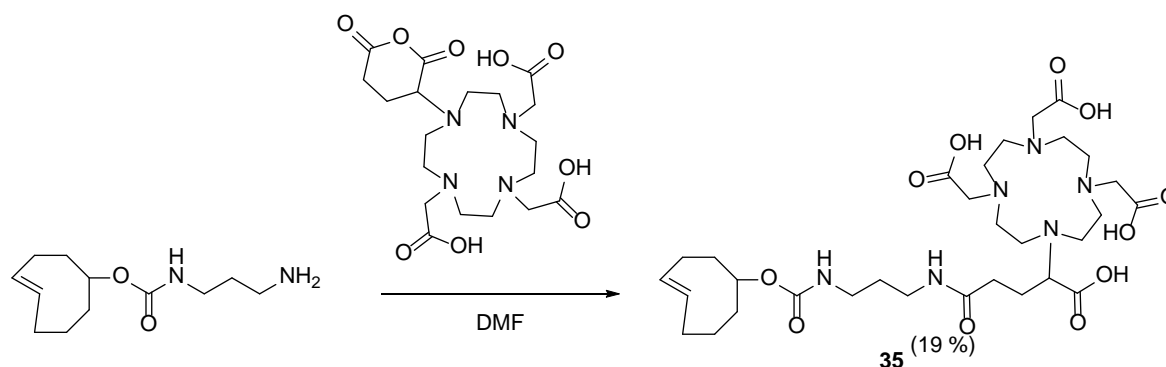
3.11.2 Pretargeted *in vivo* click chemistry CXCR4 antagonists

As introduced in section 3.2 the pretargeted approach offers several advantages over direct tracer imaging. There are many reports in the literature of the pretargeted approach improving the performance of immuno-PET and allowing for the use of shorter half-life positron-emitting radionuclides such as gallium-68 or fluorine-18 rather than long-lived radioisotopes with mAbs to improve patient dosimetry.²⁷³⁻²⁷⁶ However, for this work the main advantage may be that the antagonist moiety binds to the receptor first and so any problematic steric or charge based interactions with the BFC-radiometal component on binding may be avoided.

3.11.2.1 Synthetic strategy to produce click chemistry precursors

The *trans*-TCO and tetrazine compounds that were available in the laboratory had the opposite functional groups to the preferred approach for this work. The usual approach is to have the thermally unstable *trans*-TCO moiety conjugated to the targeting group/antagonist and the more thermally stable tetrazine moiety conjugated to the BFC, which encounters the high temperatures needed for radiolabelling. Although strategies of reversing the reactive moieties in the available (eg. diglycolic anhydride) were considered; it was decided that the additional synthetic steps and loss in yield could be avoided by labelling the *trans*-TCO moiety at a lower temperature for a longer time. Alternate *trans*-TCO and tetrazine precursors could be purchased if the approach was validated.

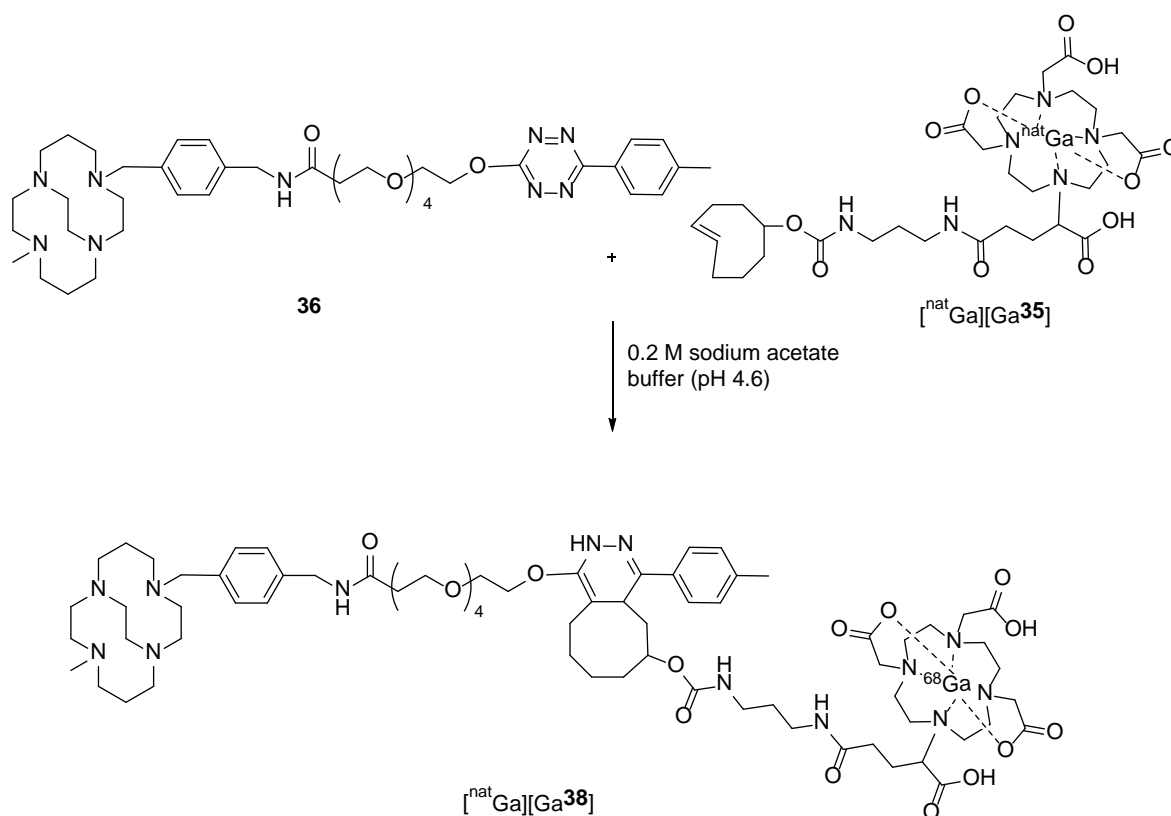
Scheme 11 shows the synthesis of the *trans*-TCO DOTAGA moiety, **35**. Synthesis of **35** was carried out in anhydrous amine-free DMF shaken at room temperature for 48 hours. The reaction was monitored by MS with the disappearance of starting material and the appearance of the $[M+H]^+$ product peak. ¹H NMR revealed that further purification was required and semi-preparative HPLC was carried out with **35** eluting at 14 min 35 sec to give a 19% yield.



Scheme 11: The synthesis of *trans*-cyclooctene compound **35**.

3.11.2.2 Bioorthogonal reaction between tetrazine and *trans*-TCO components

The bioorthogonal reaction between tetrazine and *trans*-TCO has been reported in the literature to progress rapidly and under physiological condition.^{244, 247, 274, 277-279} Attempts were made to react **36** and [^{nat}Ga][Ga**35**] (Scheme 12) with a molar equivalent ratio in 0.2 M sodium acetate buffer (pH 4.6) and shaken (550 RPM) at RT for an hour. The literature reports indicated that these reaction conditions would be appropriate.^{247, 280-282}



Scheme 12: The attempted reaction to produce [^{nat}Ga][Ga**38**].

MS showed the disappearance of starting material and the appearance of high molecular mass (> 1200 gmol⁻¹) peaks. However, the masses could not be assigned to the expected product and HPLC analysis showed a number of new peaks had formed. Collection of these peaks showed that they had the same high molecular mass values. A possible explanation is that the *trans*-TCO was stored for *ca.* three years and could have degraded. The ¹H NMR spectrum of the *trans*-TCO starting material showed the presence of a broad peak at 5.53-5.69 ppm corresponding to the *trans*-TCO protons. However, a *ca.* 15% non-reactive impurity was also present.

3.11.2.3 Radiolabelling of **35** with gallium-68

An attempt was made to radiolabel **35** with gallium-68 at room temperature, to minimise the effect on the strained cyclooctene ring. However, even with a high precursor concentration (0.5 mM) in 0.2 M sodium acetate buffer (pH 4.6) only a *ca.* 20% radiolabelling yield was observed. The temperature was increased to 60°C, and after 40 mins *ca.* 70% radiolabelling was achieved. Analytical HPLC showed a single peak at 14 min and 54 sec corresponding to [⁶⁸Ga][Ga**35**] with free gallium (at the solvent front). The product was purified by semi-preparative HPLC to give [⁶⁸Ga][Ga**35**] in a 21.7% decay corrected yield.

In a test reaction, the radiolabelled moiety [⁶⁸Ga][Ga**35**] (before semi-preparative HPLC purification) was combined with **36** at a (1:1 ratio) and incubated in PBS solution at 37°C for 5 mins, to represent *in vivo* conditions. The reaction solution was analysed by radio-HPLC (see Figure 73).

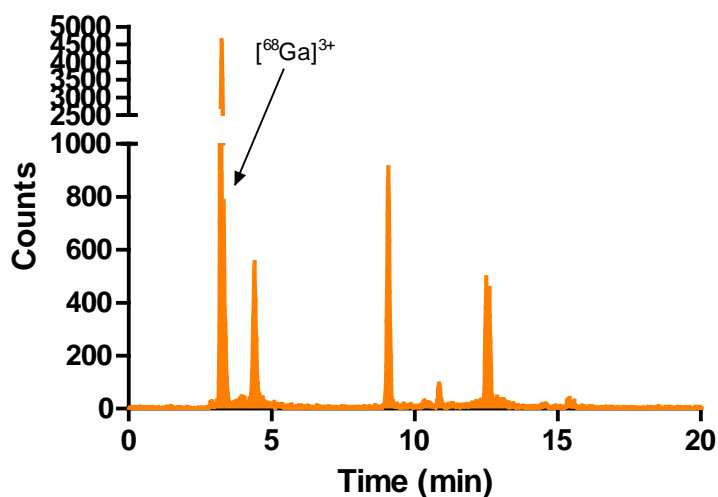


Figure 73: Radio-HPLC trace for the attempted radiolabelling of [⁶⁸Ga][Ga**38**].

The radio-HPLC trace shows a number of peaks, and is similar to the HPLC trace obtained in the attempt to synthesise [^{nat}Ga][Ga**38**]. As it was unknown whether these peaks corresponded to various protonation states of [⁶⁸Ga][Ga**38**] or were by-products no further development was attempted.

3.11.2.4 Alternate CXCR4 click chemistry precursors

Initial synthesis of the pretargeted components shown in Scheme 12 took advantage of stocks of *trans*-TCO and tetrazine compounds that were available in the laboratory. The components however, were functionalised the opposite way around to the expected reaction components with the *trans*-TCO component being radiolabelled at low temperature to give low yields to maintain stability of this component.

However, after the initial chemistry had been tested the alternate precursors were purchased and the compounds synthesised. Figure 74 shows the structure of **39** and **40**, which were synthesised by similar routes to those described in section 3.11.2.1.

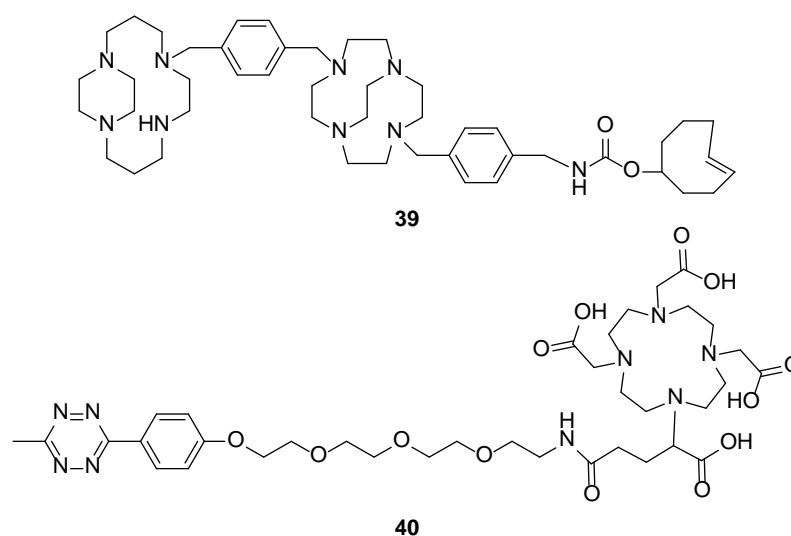


Figure 74: Structures of the alternative TCO and tetrazine click components **39** and **40**.

The *trans*-TCO containing CXCR4 binding component **39** was synthesised in anhydrous DMF, with one equivalent of base and shaken at RT, the reaction progress was monitored by analytical HPLC which showed a reduction in starting material after 48 hours. The product was purified by reverse phase semi-preparative HPLC to give a 42% yield. **40** was synthesised with DOTAGA anhydride in excess (0.9:1) to ensure full reaction of the methyltetrazine-PEG₄-amine. The reaction was carried out in anhydrous DMF with one equivalent of base and shaken at RT for 24 hours. Spillage resulted in a lower than expected yield of 38% but the product was shown to be >80% pure by ¹H NMR. Further purification is required to remove unreacted DOTAGA before this compound can be radiolabelled.

Due to time constraints the reactions of the pretargeted components **39** and **40** could not be fully investigated. However, this approach is of high interest and may be investigated further in the research group in the future. The inclusion of the *trans*-TCO on the targeting component, should allow for high radiochemical yields of the gallium-68 labelled precursor to be achieved.

3.12 Tripodal tris(hydroxypyridinone) chelator conjugated CXCR4 binding peptide

The tripodal chelator tris(hydroxypyridinone) (THP, discussed previously in section 1.4.4.6) has been shown to rapidly form a complex with gallium-68 at room temperature and neutral pH in high yield and purity. The chelator has previously been conjugated to peptides and proteins without disruption of their *in vivo* targeting properties.^{104, 283-286}

The use of THP could also have the added advantage for conjugation to the configurationally restricted tetraazamacrocycles (**24**, [Cu₂**24**(OAc)₂](OAc)₂ and [Zn₂**24**OAc)₂](OAc)₂) of forming a neutral complex with gallium(III) in contrast to DOTAGA, which forms a negatively charged complex with gallium(III). As the surface of the CXCR4 protein is negatively charged electrostatic repulsion may disrupt binding.

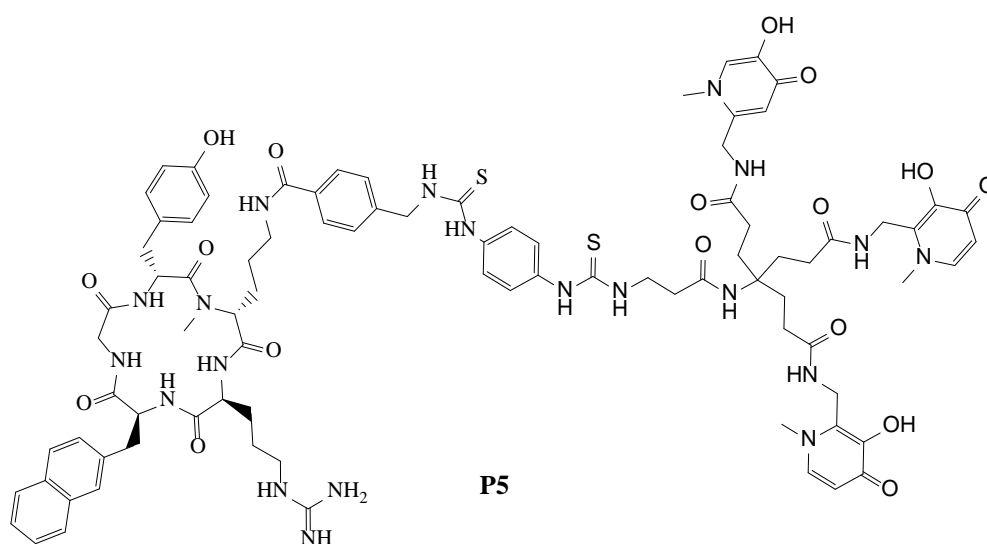


Figure 75: Structure of THP conjugated CPCr4.2 **P2** peptide (a Pentixafor analogue)

As an initial investigation of the use of THP as a gallium-68 chelator in CXCR4 targeting, it was conjugated to the previously synthesised peptide, **P2** (discussed in chapter 2). Figure 75 shows the structure of the peptide THP conjugate, **P5**.

3.12.1 Synthetic of a THP Pentixafor analogue

The synthesis of **P2** has previously been discussed. The protected THP-PhNCS was provided with the phenol groups protected as benzyl ethers (by Dr Michelle Ma, Kings College London). Deprotection of THP was achieved using the procedure reported by Ma *et al.* in 2016.²⁸⁶ The compound was stirred for an hour at room temperature in boron trichloride dichloromethane solution (1 M) under an inert atmosphere with the addition of methanol.²⁸⁷ An overall yield of 43% was achieved which is slightly lower than that reported by Ma *et al.* (compound **41**, 58%).

For the conjugation of peptide **P3** with **41** (THP-PhNCS) a similar approach to that reported by Ma *et al.* was attempted.²⁸⁶ The peptide was dissolved in dimethyl sulfoxide with one equivalent of THP-PhNCS and diisopropylethylamine (5 equiv.) was added. The reaction was heated in a microwave (120°C, 300 W, 30 min) similar to the successful conjugation of cyclic peptide cyclic-(RGDFK) with THP-PhNCS.

Unfortunately, the HPLC analysis showed several (15+) different peaks. LC-MS did not show the expected product mass for these peaks or the presence of the starting material, indicating that the peptide was unstable under these conditions. To confirm this, a small amount of **P2** was placed under the same reaction conditions without the THP-NCS in the microwave (120°C, 300 W, 30 min) and a similar HPLC trace was produced.

An alternative conjugation approach was attempted. The peptide and the THP-NCS were combined in anhydrous DMF with triethylamine added dropwise. The reaction was left stirring at room temperature for 16 hours, with reaction progress monitored by MS. The desired compound was then isolated and purified by semi-preparative HPLC and confirmed by NMR and MS.

3.12.2 Radiolabelling of the THP-Pentixafor analogue with gallium-68

Ma *et al.* reported the radiolabelling of $\alpha_v\beta_3$ integrin-targeting pentapeptides using gallium-68 produced either directly from the generator or eluate that was processed.²⁸⁸ The reaction proceeded in ammonium acetate (2 M, pH ~ 6.5), with complex formation achieved within 2-5 mins.²⁸⁶ Demonstrating the rapid labelling achievable with THP over other BFCs such as DOTA.

An adaptation of these conditions and those previously used for labelling of Pentixafor gave 100% radiolabelling after 5 min at a neutral pH. The labelled product was then purified by reverse phase semi-preparative HPLC (radio-HPLC trace shown in Figure 76).

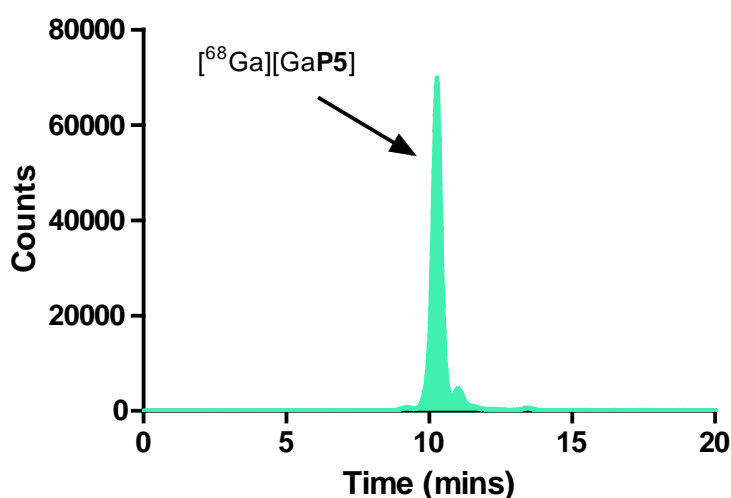


Figure 76: Radio HPLC trace of $[^{68}\text{Ga}][\text{GaP5}]$

A decay corrected radiochemical yield of 76.8% was achieved; this is significantly higher than that achieved with the standard Pentixafor **P4** ($22.4 \pm 19.5\%$).

3.12.3 *In vivo* validation of P5

An *in vivo* comparative study was designed between **P5** and Pentixafor (**P4**), to allow a direct evaluation of the effect of the BFC. CD-1 nude mice were subcutaneously inoculated into the left flank with 5×10^6 MM.1S cells (expression shown in in Figure 46), tumours were allowed to grow until the tumour size reached 100-300 mm³.

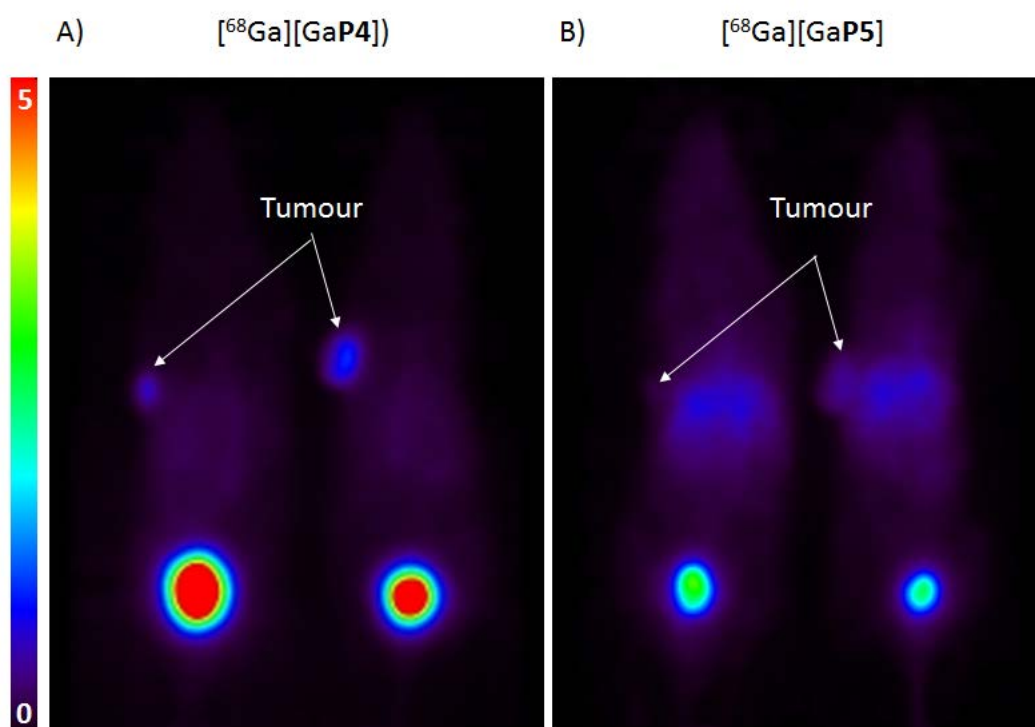


Figure 77: PET scan of $[^{68}\text{Ga}][\text{GaP4}]$ (A -left) and $[^{68}\text{Ga}][\text{GaP5}]$ (B - right) uptake in MM.1S tumour-bearing CD-1 nude mice (coronal maximum intensity projections at 46-66 minutes). (Data collected by Dr. C. Cawthorne).

Figure 77 shows the PET scans obtained for tracers $[^{68}\text{Ga}][\text{GaP4}]$ (left) and $[^{68}\text{Ga}][\text{GaP5}]$ (right). The images show that $[^{68}\text{Ga}][\text{GaP4}]$ (left) demonstrated higher uptake in the CXCR4 positive tumour (SUV_{max} ca. 3.2% ID/g) compared to $[^{68}\text{Ga}][\text{GaP5}]$ (SUV_{max} ca. 1.9% ID/g). Both tracers showed renal clearance via the kidneys and bladder, however $[^{68}\text{Ga}][\text{GaP5}]$ showed a higher uptake and retention in the liver than $[^{68}\text{Ga}][\text{GaP4}]$.

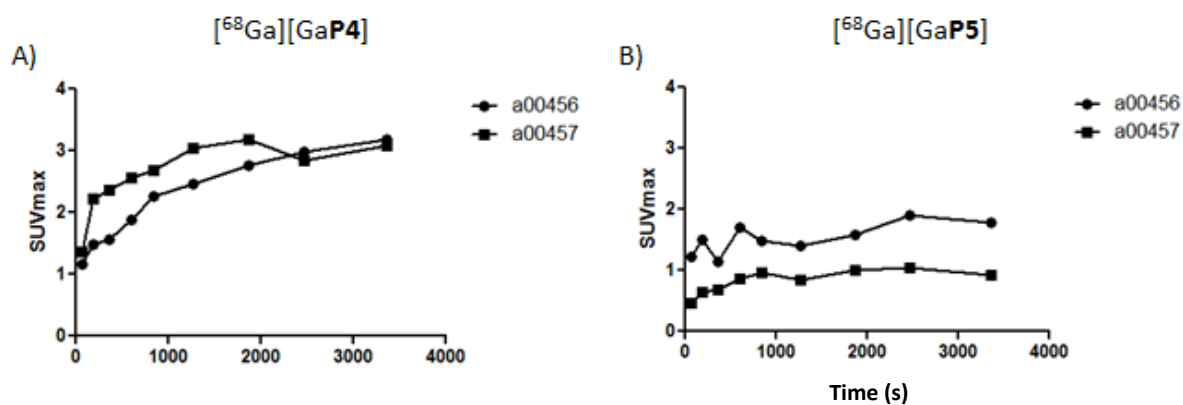


Figure 78: Dynamic tumour time activity curves acquired during 90 mins in mice (SUV_{max}). A) (left) injected with [68Ga][GaP4]; B) (right) injected with [68Ga][GaP5]. Experiments carried out in two mice (a00456 and a00457).

The explanation for the variation between the two tracers could possibly be due to the increased lipophilicity of the THP moiety in [68Ga][GaP5]. It appears the increase in lipophilicity is detrimental to the biodistribution of the tracer. Further *in vitro* assay analysis are necessary to verify these preliminary findings. However, the use of the BFC THP has shown effective radiolabelling can be achieved at natural pH and short reaction durations. The lipophilicity could be modified in future by inclusion of a PEG spacer.

3.13 Conclusion

Various approaches have been investigated for the development of a gallium-68 labelled CXCR4 imaging tracer. DOTAGA containing mono and bis-tetraazamacrocycle compounds were successfully synthesised, purified and radiolabelled in high yields. However *in vitro* and *in vivo* validation of these tracers, revealed that the carboxylic acid pendant from the DOTAGA appeared to have a disruptive effect on the binding of these compounds to the CXCR4 receptor.

Strategies to combat this were investigated, with the inclusion of a PEG spacer to separate the binding moiety and the BFC. **34** was successfully synthesised and radiolabelled with gallium-68 in high radiochemical purity. However, the corresponding metal complexes of **34** ($[\text{Cu}_2\mathbf{34}(\text{OAc})_2](\text{OAc})_2$ and $[\text{Zn}_2\mathbf{34}(\text{OAc})_2](\text{OAc})_2$) were not successfully synthesised with MS analysis inconclusive.

A pretargeted approach utilising an IDDA reaction between *trans*-TCO and tetrazine was investigated. Partial success was achieved with the synthesis of click precursors **35** and **36**. However, radiolabelling of **35** and combination with antagonist **36** gave a mixture of compounds in the HPLC and the desired product was not identified. Further development of the pretargeted approach was carried out with the successful synthesis of **39** and **40** (alternate click precursors with the functionality reversed to allow elevated temperatures for radiolabelling).

The novel THP conjugated peptide analogue of Pentixafor, **P5** was synthesised and radiolabelled with gallium-68. The inclusion of THP enabled radiolabelling at physiological pH within 5 minutes in high RCY, however, the inclusion of the THP BFC had a detrimental effect on tumour uptake *in vivo* when compared to the standard Pentixafor tracer (**P4**).

3.14 Future work

The second generation of PEG linker antagonist compounds showed promise with the radiolabelling of **34**. However, in order for these compounds to have high affinity towards the CXCR4 receptor the metal complexes need to be synthesised in high purity. Further research is required to investigate conjugation conditions to produce $[\text{Cu}_2\mathbf{34}(\text{OAc})_2](\text{OAc})_2$ and $[\text{Zn}_2\mathbf{34}(\text{OAc})_2](\text{OAc})_2$.

Although initial work using the pretargeted approach with compounds **39** and **40** was conducted, further work is needed to fully characterise these compounds. The click reaction could also be investigated under physiological conditions and monitored by HPLC to ensure that the bioorthogonal reaction occurs. Radiolabelling of **40**, is likely to be similar to related compounds but the HPLC conditions for separation needed to be investigated. In addition, *in vitro* assays should be completed on **39**, **40** and **L36** (see Figure 79), to verify whether the bioorthogonal reaction and the presence of the BFC affects the compound affinity for the CXCR4 chemokine receptor. Transition metal complexes (copper(II) and zinc(II)) can be formed with **39** to form a higher affinity CXCR4 antagonist.

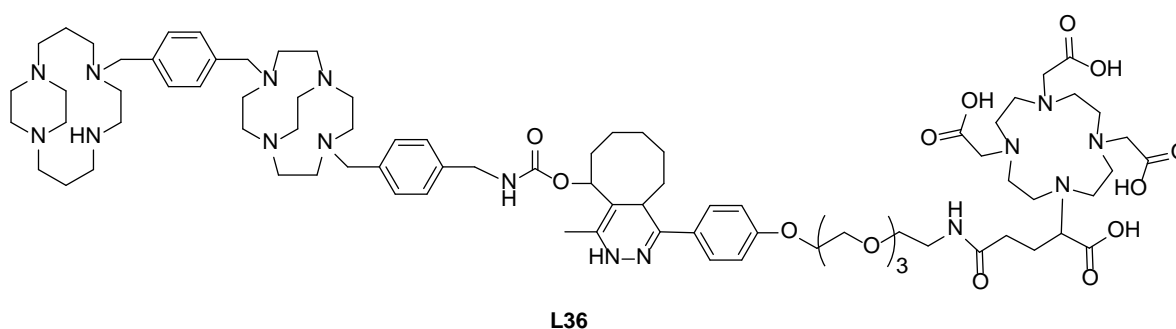


Figure 79: Future structure of antagonist **L36**, formed from the IDDA reaction between **39** and **40**.

In vivo click experiments can be planned, to investigate the optimal time needed to allow circulation, binding and clearance of antagonists based on **39** prior to the addition of the radiolabelled click component $^{68}\text{Ga}[\text{Ga}\mathbf{40}]$.

Further *in vitro* validation should be completed on the THP containing peptide, **P5**, including calcium signalling assays on peptide **P5** to allow binding comparison (IC_{50} values) and determine the influence of the different BFCs. In addition, the partition coefficient of **P4** and **P5** should be determined to investigate the difference in lipophilicity of the two tracers.

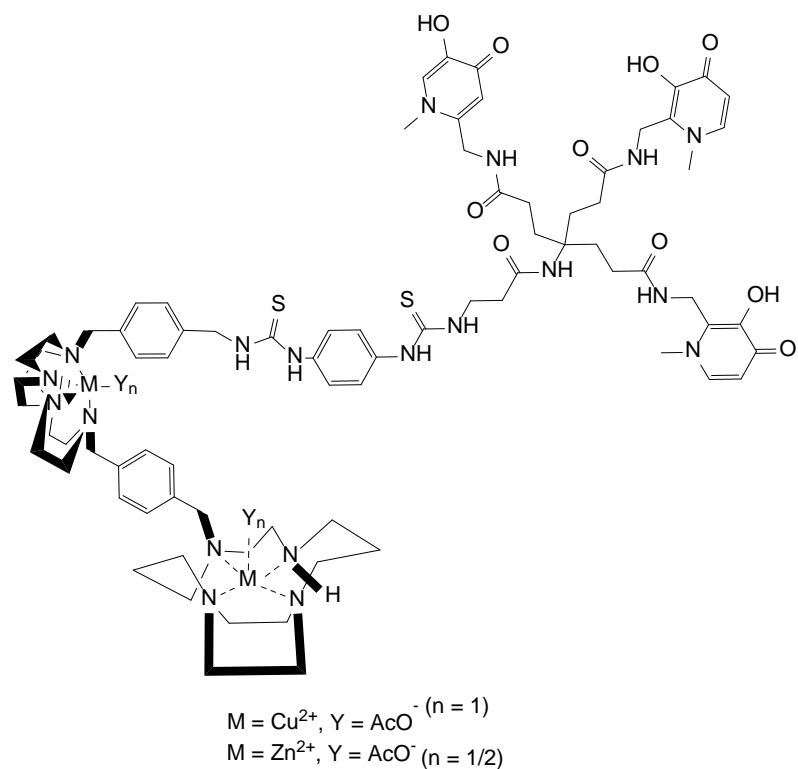


Figure 80: Proposed structure for gallium-68 bis-macrocylic antagonists.

The attachment of THP to the metal complexes of the bis-tetraazamacrocycles should be investigated (see Figure 80). The lack of charge on the neutral gallium(III) complex with THP could be a good match to avoid disruption of the binding interaction with the CXCR4 receptor.

Chapter 4

Development of imaging
probes for the CXCR4
chemokine receptor labelled
with fluorine-18

4.1 Previously developed strategies and current state-of-the-art

Due to its nuclear properties and facile preparation by proton bombardment of [^{18}O]-water, fluorine-18 has become one of the most widely used radionuclides in PET research (discussed in more detail in section 1.3.3). Historically, radiolabelling with fluorine-18 has relied on the formation of a covalent C- ^{18}F bond, see Figure 81. However, recently there have been several techniques developed that allow labelling with fluorine-18 via formation of bonds to inorganic elements.^{47, 289-292}

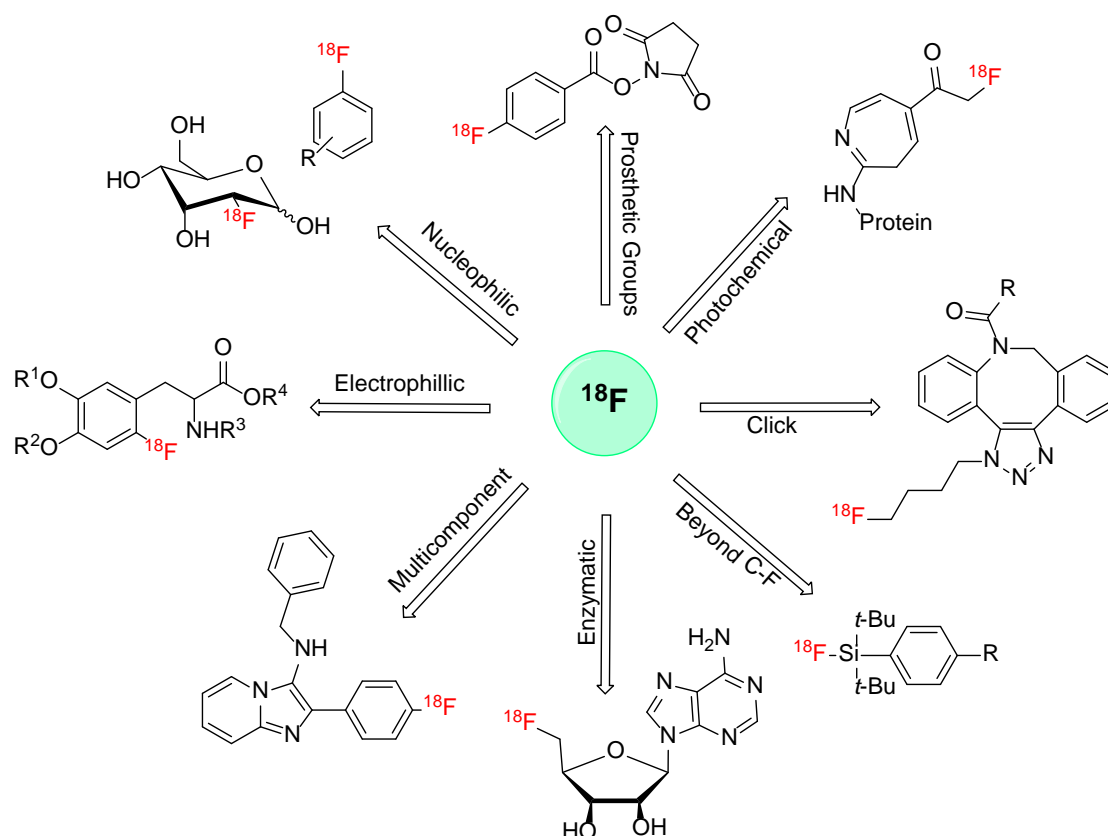


Figure 81: Various techniques used for radiolabelling radiopharmaceuticals with fluorine-18 (image adapted from that reported by Cole *et al.*).²⁸⁹

The focus of the work described herein is on the use of inorganic radiofluorination techniques rather than C-F bond formation. Several of the inorganic elements used for radiofluorination have favourable characteristics over carbon labelling. For example, they form stronger bonds (i.e. higher bond enthalpy) with fluorine, Table 5 in section 1.3.3.1, and can be achieved in simple one step reactions.²⁹²

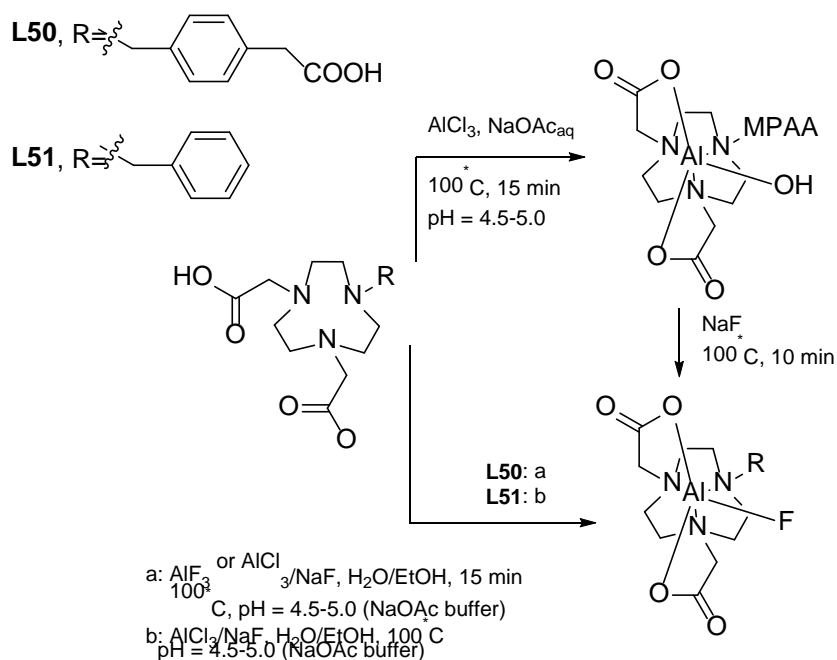
4.1.1 Aluminium radiofluorination

As reported in Table 5 (section 1.3.3.1) which summarises the average bond energies of fluorine and inorganic atoms; aluminium is the most fluorophilic element of the series (bond enthalpy 675 kJ mol^{-1}).²⁹³ The aluminium(III)-fluoride coordination bond is able to form selectively at dilute fluoride concentrations without the need of azeotropic drying.^{294, 295}

McBride *et al.* were the pioneers in this field of research. In 2009 they hypothesised that fluorine-18 would form a stable $[\text{}^{18}\text{F}]\text{AlF}$ complex.^{294, 295} The group initially reported chelation of the $[\text{}^{18}\text{F}]\text{AlF}$ complex with DTPA conjugated to a pre-targeting peptide (IMP272). However, the radiolabelled DTPA-peptide was unstable in water at room temperature; with radioisotope release of 17% over a 40 minute period. As a result, other chelators were investigated, such as NOTA, NODA, C-NETA and TACN.^{289, 290, 295} McBride *et al.* found that of these chelators NOTA had the best properties; with high complex stability in serum reported.²⁹⁵ The group also reported the X-ray crystal structure showing that NOTA binds to the $[\text{}^{18}\text{F}]\text{AlF}$ moiety as pentadentate chelator using the three nitrogens and two of the carboxylates with the sixth site of the aluminium(III) filled with a fluoride ion.²⁹⁶

McBride *et al.* went on to label a pretargeted hapten peptide (IMP449) conjugated to NOTA.²⁹⁵ Initially radiolabelling yields of only 5% were achieved but this was later improved up to 20% with the addition of an organic co-solvent.²⁹⁵ *In vivo* biodistribution studies were carried out with the peptide as well as a comparative study with $[\text{}^{18}\text{F}]\text{FDG}$. Although scans revealed that tumour uptake was higher for $[\text{}^{18}\text{F}]\text{FDG}$, the pretargeted $[\text{}^{18}\text{F}]\text{AlF}$ peptide gave more favourable tumour-to-blood ratios with less residual activity in non-target organs. Importantly no bone uptake was observed indicating that the $[\text{}^{18}\text{F}]\text{AlF}$ complex is stable enough to obtain images when chelated with NOTA.²⁹⁵

In 2011, two papers appeared simultaneously both reporting on the coordination chemistry of the $[\text{}^{18}\text{F}]\text{AlF}$ complex with various chelators.^{297, 298} D'Souza *et al.* reported the X-ray structure and labelling of NODA-MPAA (MPAA = methylphenylacetic acid, compounds **L50**, Scheme 13) as an improvement on NOTA.²⁹⁷ The absence of the carboxylic acid that could compete for coordination enhances labelling yields as aluminium(III) can no longer form a hexadentate complex with the BFC, and therefore the sixth site is available to bind to a fluoride ion.²⁹⁷ Shetty *et al.* also reported the X-ray structure of a pentadentate ligand NODA-Bn with AlCl_3/NaF (Scheme 13).²⁹⁸ The group again reported an enhanced labelling yield achieved with **L52** over NOTA, confirming the presence of the third acetic acid group in NOTA has a negative impact on the coordination of fluoride to aluminium(III).²⁹⁸



Scheme 13: Synthesis of ^{18}F AlF NODA complexes **L50** and **L51**.^{297, 298}

Both papers also confirmed the findings of McBride *et al.* showing that radiolabelling of compounds **L50** and **L51** could be improved by the addition of an organic co-solvent (eg. ethanol); however, there was no explanation as to why this was the case.

In 2012, McBride demonstrated the flexibility of this technique by labelling heat sensitive proteins.²⁹⁹ The NODA conjugated Fab fragments were labelled in high yields with the ^{18}F AlF complex at room temperature after 10-15 mins. The proteins were shown to be stable and maintained their biological affinity when tested *in vivo* with selective localisation in tumour models.

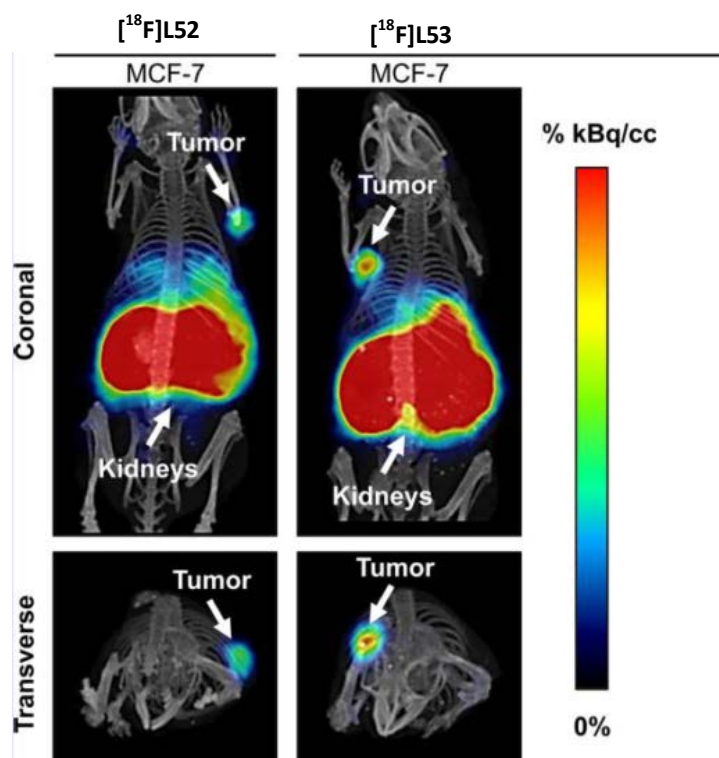


Figure 82: PET/CT images of MCF-7 tumour-bearing mice using [^{18}F][AIFL52] and [^{18}F][AIFL53]; scans taken after 60 mins in mice bearing MCF-7 tumours. (Reproduced from Da Pieve *et al.*)³⁰⁰

Da Pieve *et al.* investigated two separate approaches (direct and pretargeted) for imaging the overexpression of HER3 receptors in tumours.³⁰⁰ The direct approach used NOTA conjugated to the HER3 affibody (**L53**), whereas the pretargeted approach used the IEDDA reaction, see section 3.2, between a tetraazine functionalized NODA chelator and the TCO functionalised affibody. Both approaches utilised the ‘one-pot’ labelling of NOTA (**L52**) and NODA (**L53**) with the [^{18}F]AIF complex. Labelling and purification of the antagonist **L53** was reported to be higher yielding (34-54%) than that of **L52** (12-43%).³⁰⁰ This supports the reports by D’Souza *et al.* and Shetty *et al.* that the NODA BFC gives higher yields than NOTA, due to the pentadentate nature of the chelator.^{297, 298}

In vivo studies to evaluate both tracers were carried out in HER3-expressing MCF-7 tumour-bearing mice (Figure 82). The biodistribution data of each tracer 60 mins after injections revealed that the direct NOTA approach gave higher tumour uptake (**L52**, 4.96 ID/g), than the pretargeted NODA approach (**L53**, 4.36 ID/g)³⁰⁰. The NODA derivative also showed higher accumulation in the intestine and scans indicating tracer clearance via hepatobiliary excretion. This was attributed to the increase in lipophilicity of NODA compared to NOTA. Nonetheless, the application of both tracers is limited due to large amount of kidney uptake seen in both cases, seen in Figure 82.³⁰⁰

Since the initial report of the [^{18}F]AIF technique there have been many publications on the use of this methodology in labelling peptides, small molecules, and proteins.^{275, 301-310} The first clinical

trial involving labelling of RGD peptide using a lyophilised kit with [¹⁸F]AIF has been carried out.³¹¹ Nine patients with primary lung cancer were scanned with [¹⁸F]AIF-NOTA-RDG, known as [¹⁸F]Alfatide; and [¹⁸F]FDG in a comparative study. [¹⁸F]Alfatide was reported to identify all the primary tumours, with tumour uptake of 2.9 ± 0.10 ID/g reported.³¹¹

4.1.2 Fluorine-18 labelled probes for imaging the CXCR4 chemokine receptor

Despite the significant number of labelling techniques and availability of fluorine-18 only a few attempts have so far been attempted to develop a fluorine-18 labelled CXCR4 specific tracer. In section 1.6.11 peptide derivatives of T140 are discussed that have been adapted for radiolabelling with fluorine-18.^{159, 161}

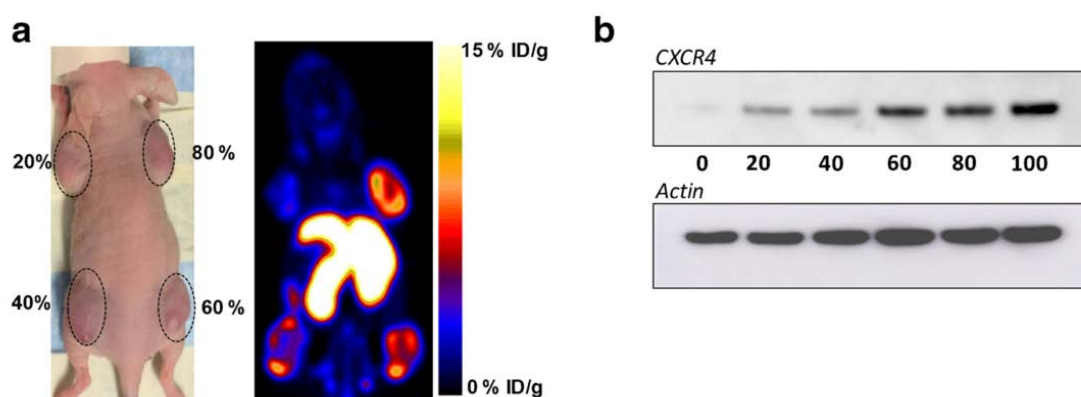


Figure 83: a) Representative photograph (left) and PET image (right) of a mouse bearing tumours with different amounts of CHO-CXCR4 cells (20, 40, 60 and 80%) at 1 hr post-injection of [¹⁸F][AIFNOTA-T140]. B) Western blot of CXCR4 expression by tumours generated by increasing proportion of CHO-CXCR4 cells. (Reproduced from Yan *et al.*)³¹²

Recently Yan *et al.* reported the labelling of the CXCR4 binding peptide T140 using [¹⁸F][AIFNOTA]. PET scans were carried out using mice with CHO-CXCR4 and CHO-negative tumours. The results showed high uptake ($8.63 \pm 1.08\%$ ID/g) at 2 h post-injection in the CXCR4 positive tumours, which was 26-fold greater than the uptake in the negative tumours ($0.34 \pm 0.01\%$ ID/g) at 2 h post-injection.³¹² The specificity of the tracer was shown using tumour xenografts with different ratios of CXCR4-negative and CXCR4-positive cells; see Figure 83. A correlation was made between uptake and levels of CXCR4 protein present, however, the paper does not comment on the non-homogenous nature of the tumours. HTC staining is not presented and so it is unknown whether either poor tumour penetration of the tracer or unusual tumour model growth explains the observed results. Further work is required to validate the binding and targeting behaviour of this tracer.

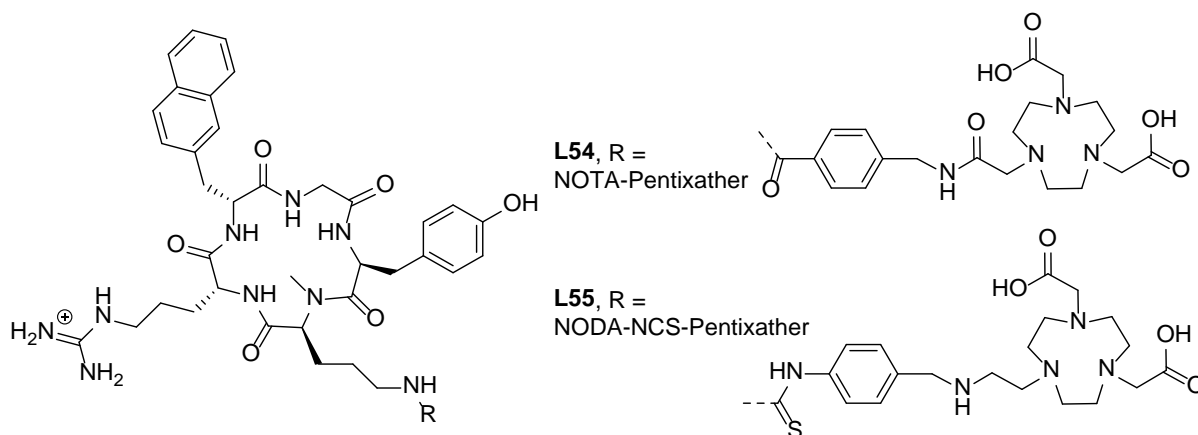


Figure 84: Structures of adapted Pentixafor peptide of Al^[18F] labelling ; **L54**, NODA-Pentixafor and **L55**, NODA-NCS-Pentixafor.

In 2016, Poschenrieder *et al.* reported the first fluorine-18 radiolabelled Pentixafor derived CXCR4 targeting construct.³¹³ The group synthesised two derivatives of Pentixafor; **L54** (NODA) and **L55** (NCS-NODA) shown in Figure 84. IC₅₀ affinities were used to select **L54** as the lead candidate as [AlFL**54**] gave an IC₅₀ value of 17.9 nM, while [AlFL**55**] gave a value of 302 nM in the assay carried out. In fact AlFL**54** gave a lower IC₅₀ value than that of [^{nat}Ga]Pentixafor (24.8 nM) in the same assay.³¹³ This was further confirmed by internalisation and efflux studies that revealed [¹⁸F][AlFL**54**] showed a 3-fold increase in the total cellular uptake after 60 minutes compared to [⁶⁸Ga]Pentixafor.³¹³ Biodistribution data carried out in Daudi lymphoma-bearing SCID mice showed an uptake of [¹⁸F][AlFL**54**] 13.9% ID/g in CXCR4 bearing tumours an hour after injection. Blocking studies were also carried out using AMD3100 to prove the specificity of [¹⁸F][AlFL**54**].³¹³

However, the *in vitro* results were not matched by the *in vivo* data. It was concluded the enhanced lipophilicity of [¹⁸F][AlFL**54**] had a problematic effect on tracer biodistribution. [¹⁸F][AlFL**54**] showed higher plasma protein binding than previously seen with [⁶⁸Ga]Pentixafor; as a result delayed blood clearance was observed resulting in a higher background signal. The biodistribution data also showed high uptake in non-targeted organs at 60 mins indicating hepatobiliary excretion. Of greater concern was the high level of activity seen in the bones (2.7% ID/g) indicating *in vivo* defluorination was occurring.³¹³

4.2 Proposed strategy

The development of a fluorine-18 based CXCR4 imaging tracer would be clinically desirable. The preferred nuclear properties combined with the fact many hospitals currently have access to a regular supply of fluorine-18 tracers (on-site or externally produced with transportation possible). The work in this chapter aims to develop a high affinity tetraazamacrocyclic antagonist that contain a BFC to allow for the labelling with [^{18}F]AlF complex. The advantages of small molecule tracers over the previously reported peptide approaches include the enhanced shelf-life, higher metabolic stability and stability to higher radiolabelling temperatures, which small ligands intrinsically have over peptides. The design, synthesis and radiolabelling optimisation of novel tetraazamacrocyclic fluorine radiolabelled CXCR4 antagonists are reported herein. The structures of the target molecules are shown in Figure 85.

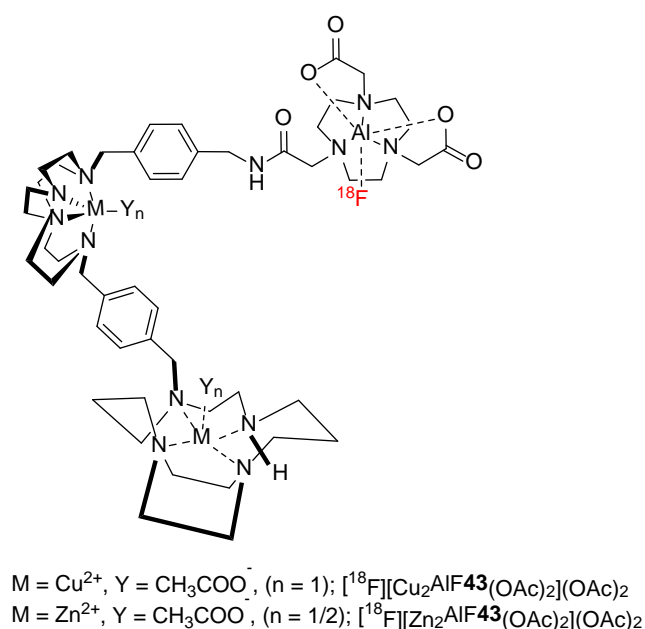


Figure 85: Structure of target molecule radiolabelled via aluminium radiofluorination.

As described in previous chapters, the design of the tetraazamacrocyclic ligands are based on knowledge the Archibald group has developed over the past decade for high affinity CXCR4 antagonists. The bis-tetraazamacrocycles coordinated to metal ions in the cyclam and cyclen rings enhance affinity for and residence time at the CXCR4 receptor.¹⁹⁹

As reported in section 4.1.1, pentadentate BFC NODA has been reported to have a higher radiolabelling yields and stability. Therefore, as shown in Figure 85, the NODA BFC moiety was incorporated into the design of these CXCR4 antagonists. The NODA moiety would also allow for antagonists to be radiolabelled with other radiometals such as copper-64, gallium-68, and indium-111.²⁴

Radiofluorination was initially optimised using a model compound, a NODA-amide containing derivative, before attempting to label the bis-tetraazamacrocyclic derivatives due to improved availability of the precursor. Optimised temperatures, concentrations, and solvent were determined with the model compound. The conditions were then applied to label the high affinity CXCR4 antagonists, although access to fluorine-18 and time constraints prevented completion of the part of the work.

4.2.1 Synthesis of a test compound

The aims of this research are the development of a conjugated NODA-amide antagonist followed by optimisation of radiofluorination conditions. The inclusion of an aromatic group in the prosthetic group allows convenient detection of this component using a UV detector on the HPLC. Figure 86 shows the structure of **42** which was readily formed from the reaction of N-hydroxysuccinimide ester NODA (NODA-NHS) and benzyl amine.

The procedure for the reaction was adapted from that reported by Jacobson *et al.* and Yan *et al.* who conjugated NODA-NHS ester to derivatives of the T140 peptide to allow for radiolabelling via various methods.^{162, 312} In both cases the peptide and NODA-NHS were combined in DMF with five equivalents of base (DIPEA), and shaken at 4°C overnight. Similar procedures have been used to conjugate a variety of peptides to NODA-NHS.^{307, 308, 314}

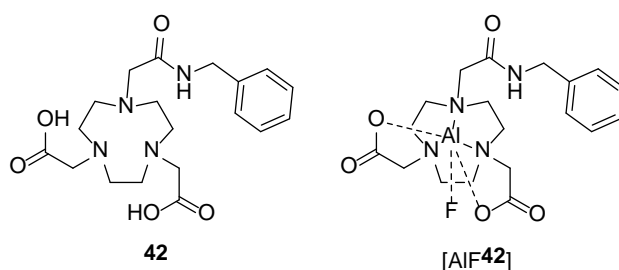


Figure 86: Structure of compound **42** and the non-radioactive standard $[AlF42]$.

Benzylamine was combined with one equivalent of NODA-NHS in amine-free DMF, with three equivalents of base. The reaction was stirred at room temperature overnight before being purified by semi preparative HPLC. **42** was formed in high yield (*ca.* 80%).

The non-radioactive analogue of **42** was required for HPLC method development. Cleeren *et al.* reported the synthesis of AlF reference compounds in a paper looking at developing new chelators for aluminium based radiofluorination.³¹⁵ Initially sodium fluoride was combined with an aqueous solution of $AlCl_3$, where the pH was adjusted to 4. The reaction was stirred for 10 mins before the chelate was added and then the mixture was heated at 40°C for an hour.³¹⁵ The paper does not report the yield of the aluminium(III) compound but reports MS characterisation. Similarly Poschenrieder *et al.* reported the chelation of AlF by NODA using a mixture of sodium fluoride, $AlCl_3$

in 0.5 M sodium acetate buffer pH 4 and ethanol (50%, volume/volume) heated at 120°C for 20 min (20-50% HPLC yield).¹⁷³

This approach was attempted with the reaction being carried out with 1.2 equivalents AlCl_3 and NaF in 0.5 M sodium acetate buffer and ethanol (50%, v/v) at 90°C. After an hour the reaction mixture was analysed by HPLC which showed the appearance of a new peak, which was confirmed to be the desired product by MS. The HPLC yield was ca. 40-50%; similar to that reported by Poschenrieder *et al.*, therefore no further attempts were made to optimise these conditions.

4.3 Optimisation of radiofluorination conditions using the test compound

Initially McBride *et al.* reported ^{18}F AlF labelling as a 'two pot' synthesis.²⁹⁵ Firstly the ^{18}F [AlFCl₂] moiety was formed from the addition of the ^{18}F fluoride ion to AlCl_3 , typically heated for 10-20 mins. This was followed by the addition of the BFC containing ligand and heated for a further 10-20 mins to give the labelled tracer. Alternatively; Liu *et al.* showed several years later that efficient radiolabelling could also be achieved if these two stages were combined in a 'one-pot' radiolabelling procedure; the results offered shorter reaction times while still maintaining consistent radiolabelling yields.³¹⁶ The 'one pot' procedure was used in this work.

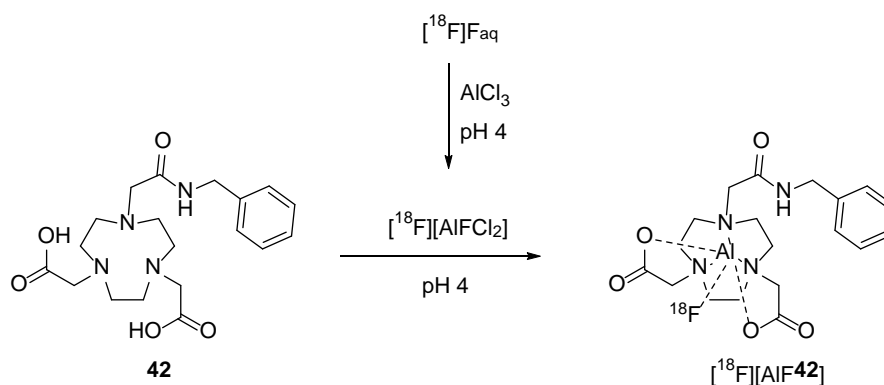


Figure 87: Trial reaction using benzyl-NODA, **42**, to optimise radiolabelling conditions with ^{18}F AlF complex.

Figure 87 shows the trial reaction for labelling benzyl-NODA-amide, compound **42**, used to optimise radiolabelling conditions in this work. Several factors influence both the labelling of the NODA-amide containing antagonist and the formation of the ^{18}F [AlFCl₂] intermediate. The literature has many differing reports on the concentration/amounts of reagents, temperature and co-solvents used to achieve the highest specific activity. Therefore, each factor was investigated separately to identify the key influences.

4.3.1 Reaction pH and buffer

Throughout the literature on [^{18}F]AlF radiofluorination; the most consistently reproduced factor in radiolabelling procedures is pH. It is well-established that the reaction must take place in acidic conditions (pH 4-4.5) to prevent the hydrolysis of aluminium fluoride in solution.³¹⁷ At pH 4, the carboxylic acid groups of NODA (pK_a 3-4) are partially deprotonated and are available to form an ionic bond with the aluminium ion. However, if a slightly higher pH (>4.5) is used for labelling they become fully protonated and therefore a reduction in labelling yield is observed.

In 2016, Cleeren *et al.* reported the labelling of new chelators with [^{18}F]AlF, which consisted of acyclic phenols and carboxylic acid groups.³¹⁵ Radiolabelling was attempted using an adapted procedure by McBride *et al.* (0.1 M sodium acetate, pH 4), however the new chelators were reported to have low radiochemical yield of *ca.* 8% even at the high temperature of 110°C.³¹⁵ The low yield observed could be attributed to the fact that phenol has a higher pK_a value (9-10), therefore, at pH 4 more of the phenols are protonated and thus unable to chelate to the [^{18}F]AlF intermediate as effectively.³¹⁵

Laverman *et al.* investigated the effect of different buffers on the labelling of a NOTA conjugate.³¹⁸ The group investigated sodium citrate and sodium acetate buffer, as well as other buffers, all at 1 M and pH *ca.* 4.1. The group found that no radiolabelling was achieved in sodium citrate buffer, likely because of the high affinity of citric acid for aluminium(III) ions, as described by Rajan *et al.*³¹⁹ Therefore as a result of this study; radiofluorination of **42** was carried out in the commonly reported 0.1 M sodium acetate buffer (pH 4.0).^{275, 290, 300, 304, 305, 312}

4.3.2 Effect of the addition of co-solvents

D'Souza *et al.* reported that the radiochemical yield can be increased by up to 50% with the addition of a co-solvent (>50% v/v).²⁹⁷ Ethanol is an ideal choice due to its higher compatibility with biological systems than other solvents. Although D'souza *et al.* reported that many solvents such as acetonitrile, *n*-propanol, isopropanol, *tert*-butyl alcohol, acetone, dioxane, tetrahydrofuran, dimethylsulfoxide, and dimethyl formamide all had a positive effect on radiolabelling yield.²⁹⁷ As stated in section 4.1.2 no explanation was given as to how these co-solvents increase the yield. One possible explanation for this observation could be that the addition of the co-solvent is enhancing the solubility of the [^{18}F]AlF complex/antagonist; or alternatively it forms an intermediate with the aluminium(III) ion aiding radiofluorination.

The same group reported that labelling was still enhanced with sterically hindered organic co-solvents like *tert*-butyl alcohol. If the co-solvent is involved in formation of an intermediate coordination sphere the additional steric bulk would be expected to have a negative effect on

radiolabelling yield. This effect is of interest and worthy of further investigation. As radiolabelling yields for each solvent were not reported in the literature this effect was investigated with co-solvents that have varying levels of steric bulk, heteroatoms and rigidity (ethanol, acetonitrile, 2-propanol, 1,4-dioxane, *tert*-butyl alcohol, tetrahydrofuran and methyl *tert*-butyl ether). A related study by Laverman *et al.* also looked at the effect of different co-solvents in labelling NOTA conjugates with the [¹⁸F]AlF complex. The group also investigated the effect of the amount (v/v) of co-solvent on the increase in labelling. They reported that the highest labelling efficient was obtained at 80% (v/v) ratio with ethanol.³¹⁸

In this work, the modified radiolabelling procedure reported by Da Pieve *et al.* was used as a starting point.³⁰⁰ Each reaction consisted of [¹⁸F]fluoride (aqueous, pH 4.0, *ca.* 100-200 MBq), 3 μ L of a 2 mM stock solution of AlCl₃, combined with compound **42** (0.1 mM, in 0.1 M acetate buffer, pH 4.0) with 50% (v/v) an organic co-solvent or buffer added. The solution was heated at 100°C and stirred at 350 RPM for 20 minutes. The reaction was monitored by radio-TLC using silica plates with acidified methanol as eluent ($R_f = 0.22$).

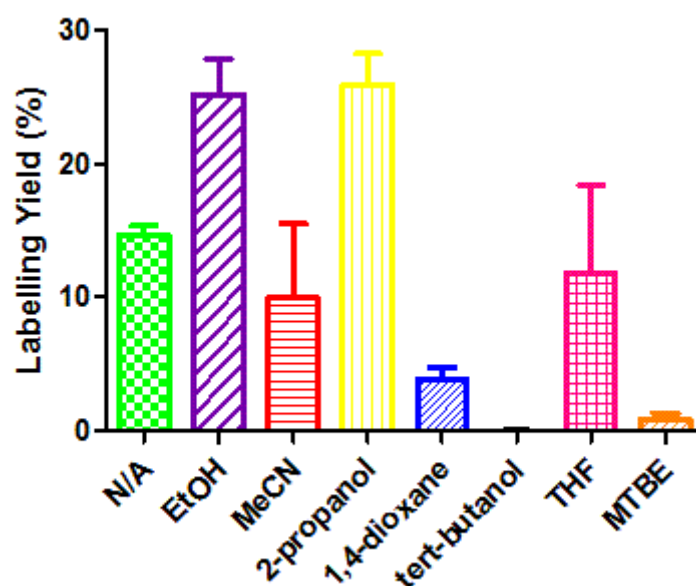


Figure 88: Comparative study of labelling compound **42** with [¹⁸F]AlF with and without the presence of ethanol (n = 4).

Figure 88 shows the results of the effect different organic co-solvents had on labelling yield of **42**. Labelling in the presence of ethanol saw a similar increase to that reported by D'souza *et al.*²⁹⁷ However, acetonitrile and tetrahydrofuran had no effect on the labelling yield. Additionally, the sterically hindered solvents *tert*-butyl alcohol and methyl *tert*-butyl ether showed a decrease in

labelling yield. This was unexpected as D'souza *et al.* reported an increase in yield when using *tert*-butyl alcohol.²⁹⁷

As these changes are unlikely to affect the solubility of **42**, it is thought that the co-solvents interact with the aluminium ion to influence the formation of the [¹⁸F]AlF complex. Solvents containing an alcohol group enhanced the formation and therefore, ethanol was used in radiolabelling reactions in this work. The larger sterically hindered co-solvents appeared to have a detrimental effect on the radiolabelling, this may be because they limit the accessibility of the aluminium ion to the fluoride ion for coordinate bond formation.

4.3.3 Optimisation of the concentration of the AlCl₃ stock

Specific activity is a concern when developing radiotracers, however, this is particularly true when radiolabelling with [¹⁸F]AlF complex. The [¹⁸F]AlF complex is formed when the fluoride ion encounters AlCl₃, and is heated at high temperatures for several minutes. However AlCl₃ is equally likely to complex with the NODA-amide chelator, and the AlCl and [¹⁸F]AlF tracer complexes cannot be separated easily by HPLC. Therefore, the amount of AlCl₃ must be closely controlled; too much lowers specific activity and not enough reduces radiochemical yield.

The amount of the AlCl₃ 2 mM stock solution added in this work to form the [¹⁸F]AlF complex was also investigated as the literature has several contrasting reports. Meyer *et al.* report using 25 µL (*ca.* 1:40 substrate to AlCl₃ ratio) of a 2 mM stock of AlCl₃ and achieve the highest radiochemical yields reported in the literature (54–65%, decay-corrected to the start of synthesis).²⁷⁵ However, other researchers report the addition of between 3-22 microliters of a 2 mM stock of AlCl₃, in most cases a 1:1 ratio or slightly lower is used.^{290, 300, 304, 305, 312, 320}

Therefore trial reactions using the same concentration of compound **42** while varying the volume of AlCl₃ 2 mM stock solution added (1, 2, 3, 5, 10, 15, 20 and 25 µL) were conducted. Each reaction was made up to a total volume of 100 µL (50% ethanol: 50% 0.1 M acetate buffer, pH4, v/v). The reaction was monitored by analytical radio-HPLC with a typical HPLC trace of shown in Figure 89.

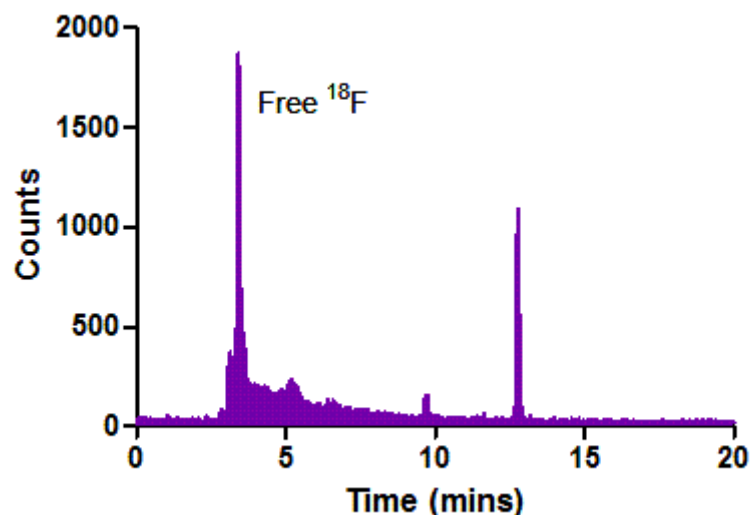


Figure 89: Radio-HPLC trace of compound $[^{18}\text{F}][\text{AlF}_4]^-$.

Figure 90 shows the radiolabelling yields observed upon varying the initial volume of AlCl_3 used for labelling. The highest radiochemical yield of *ca.* 27% was achieved using 20 μL of the 2 mM stock solution of AlCl_3 (*ca.* 1:6 substrate to AlCl_3 ratio). The addition of 5 μL of the 2 mM stock solution of AlCl_3 represented *ca.* 1:1 molar ratio giving a 4% radiolabelling yield; and 3 μL represented *ca.* 1:0.9 molar ratio giving a 3.5% radiolabelling yield. The results for the addition of 1, 2 and 3 μL all give similar results for the percentage radiolabelled; although pipetting errors may contribute at these very low concentrations.

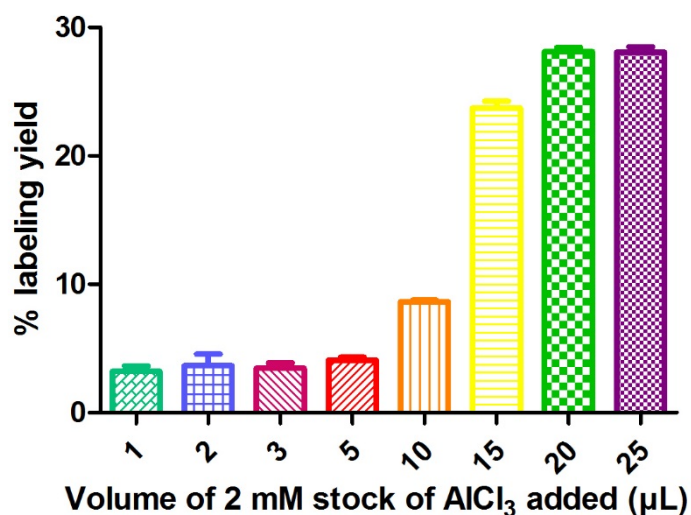


Figure 90: Effect on radiolabelling yield by varying the volume of AlCl_3 stock added to each reaction, ($n = 3$).

As a result of the experiments carried out, a ratio of 1:0.9 substrate to AlCl_3 was selected as the optimised ratio for preparation of the ^{18}F AlF complex. Although higher radiolabelling yields can be achieved with larger volumes of 2 mM stock solution of AlCl_3 a trade-off is needed to ensure specific activity is suitable for imaging purposes.

4.3.4 Optimisation of the concentration of the chelator

The concentration of the chelator was also investigated as this also plays a key role in the specific activity of the tracer. Contrary to what is reported in other parts of this work where nearly 100% radiolabelling yields are observed, labelling yields with ^{18}F AlF complexes are lower. Therefore, as with the concentration of AlCl_3 stock used, a compromise is required.

As described previously 3 μL of a 2 mM stock solution of AlCl_3 was used to form the ^{18}F AlF complex. Each reaction of varying concentration was made up to 100 μL (50% ethanol: 50% 0.1 M acetate buffer, pH4, v/v). The reaction was monitored by radio-TLC using silica plates with acidified methanol as eluent ($R_f = 0.22$).

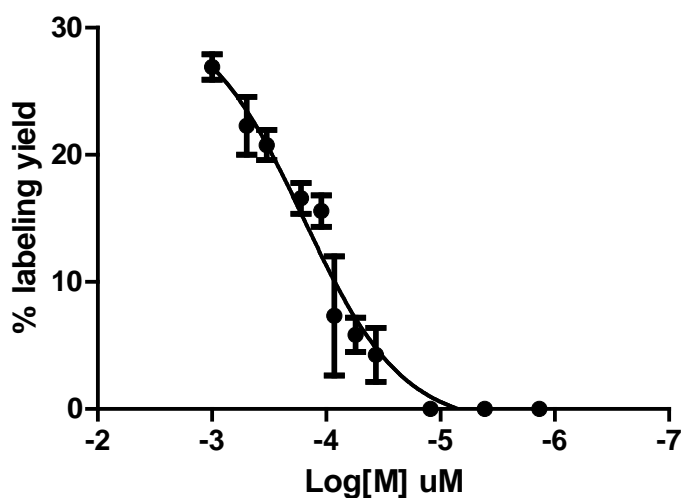


Figure 91: Graph showing the effect of varying the concentration of benzyl-NODA-amide, **42** on radiolabelling yield, ($n = 3$).

Figure 91 shows the effect of varying the ligand concentration on radiolabelling yield. The highest yield of 27% was seen at the highest concentration, 1 mM of **42**. Da Pieve *et al.* reported the radiolabelling of NOTA-peptide with a concentration of *ca.* 30 μM , however, this resulted in a very low labelling yields for **42**. Therefore, a concentration of 100 μM of **42** was selected as a radiolabelling yield of 16% was achieved, and the UV-HPLC trace showed very low absorbance indicating that specific activity is likely to be acceptable.

4.3.5 Optimisation of temperature

Temperature has also been shown to effect radiolabelling in these systems. In the vast majority of examples in the literature NODA and NOTA derivatives were radiolabelled at a temperatures from 90-110°C.^{275, 290, 300, 304, 305, 312} This is typical for macrocyclic chelators which require a high temperatures to rearrange the ligand structure in order to accommodate the [¹⁸F]AlF complex.⁶ Cleeren *et al.* designed linear chelators to decrease the rigidity of chelators and allow faster kinetics for labelling.³¹⁵

The selected concentration of **42**, was combined with 3 µL of a 2 mM stock solution of AlCl₃ in sodium acetate buffer (pH 4, 0.5 M), [¹⁸F]fluoride (5-25 MBq,) and co-solvent (ethanol; 50:50 v/v) and heated at the given temperature for 20 mins. Each reaction was monitored via radio-TLC (acidified methanol as eluent).

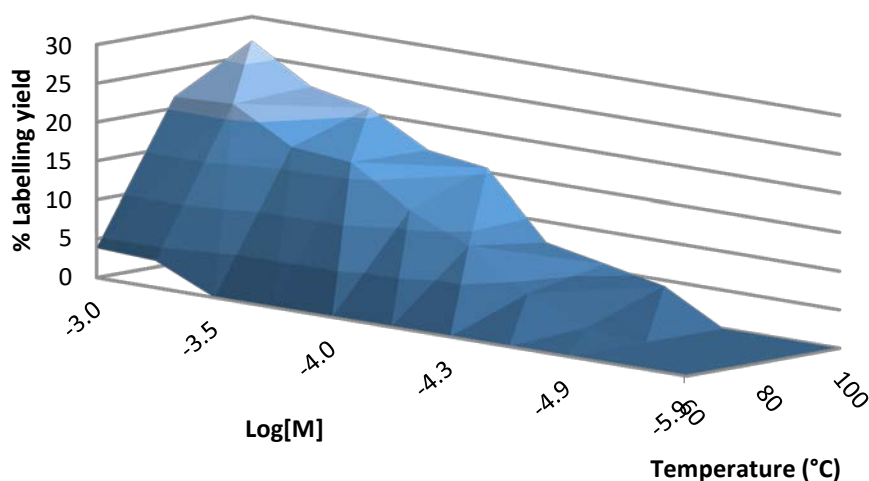


Figure 92: Graph showing the effect of temperature and concentration on radiolabelling yields of compound **42**, ($n = 3$).

Figure 92 shows the effect that temperature as well as concentration has on the radiolabelling yield. The highest concentration (1 mM) gave the highest labelling yield at 100°C, with a significant reduction at 80°C, and a further decrease at 60°C. This is in line with the report by Laverman *et al.* who completed a similar study investigating the effect of temperature of labelling NOTA conjugated peptide (IMP466).³¹⁸ As a result of this study the optimal temperature selected for [¹⁸F]AlF labelling is 100°C.

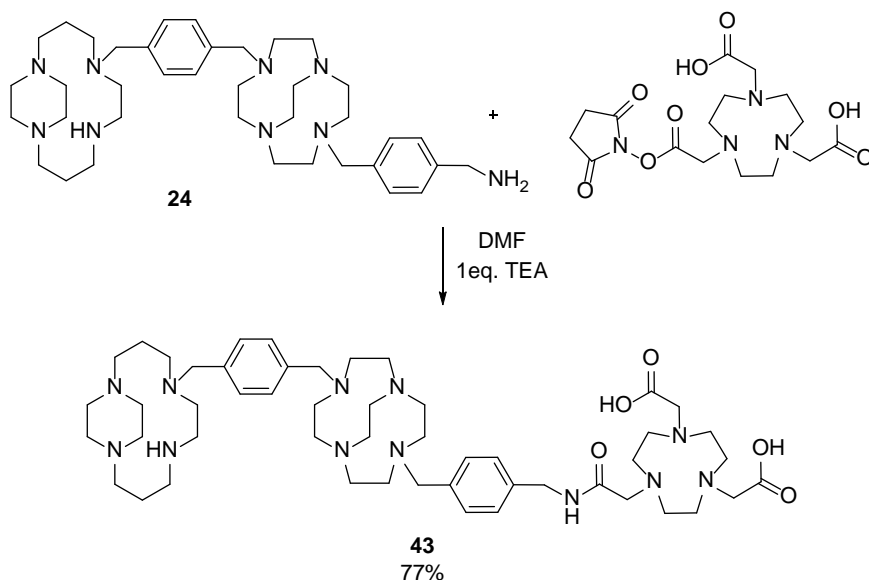
4.3.6 Overall optimised conditions and stability

Radiolabelling of **42** was carried out using a 'one-pot' synthesis and the highest radiolabelling and specific activity were achieved by reacting 1:0.9 molar amounts of AlCl_3 with **42** (100 μM) in the presence of 0.1 M sodium acetate (pH 4) and 50% ethanol (v/v) at 100°C for 20 min to give $^{18}\text{F}[\text{AlF42}]$ (16-22% RCY). These optimised conditions were then ready to be applied to the labelling of the CXCR4 antagonists **43**, $[\text{Cu}_2\text{43}(\text{OAc})_2](\text{OAc})_2$ and $[\text{Zn}_2\text{43}(\text{OAc})_2](\text{OAc})_2$.

Stability of $^{18}\text{F}[\text{AlF42}]$ was monitored by analytical HPLC after being passed through a preconditioned C18 cartridge and $^{18}\text{F}[\text{AlF42}]$ was shown to be stable up to 3 hours in PBS solution at 37°C. This is in agreement with what has been reported in the literature for the stability of $^{18}\text{F}[\text{AlF-NODA}]$ complexes.^{295, 297, 315}

4.4 Synthesis of high affinity CXCR4 antagonists for fluorine-18 labelling

4.4.1 Synthesis of bis-tetraazamacrocycle NODA-amide and metal containing derivatives



Scheme 14: Synthetic pathway for the formation of compound **43**.

Using the same conditions reported for the conjugation of **42**, the bis-tetraazamacrocyclic CXCR4 antagonist, **43**, shown in Scheme 14 was synthesised. HPLC purification was needed as starting material was still present after reaction. The peak that eluted at *ca.* 12-13 min was shown to be the desired product (MS and NMR).

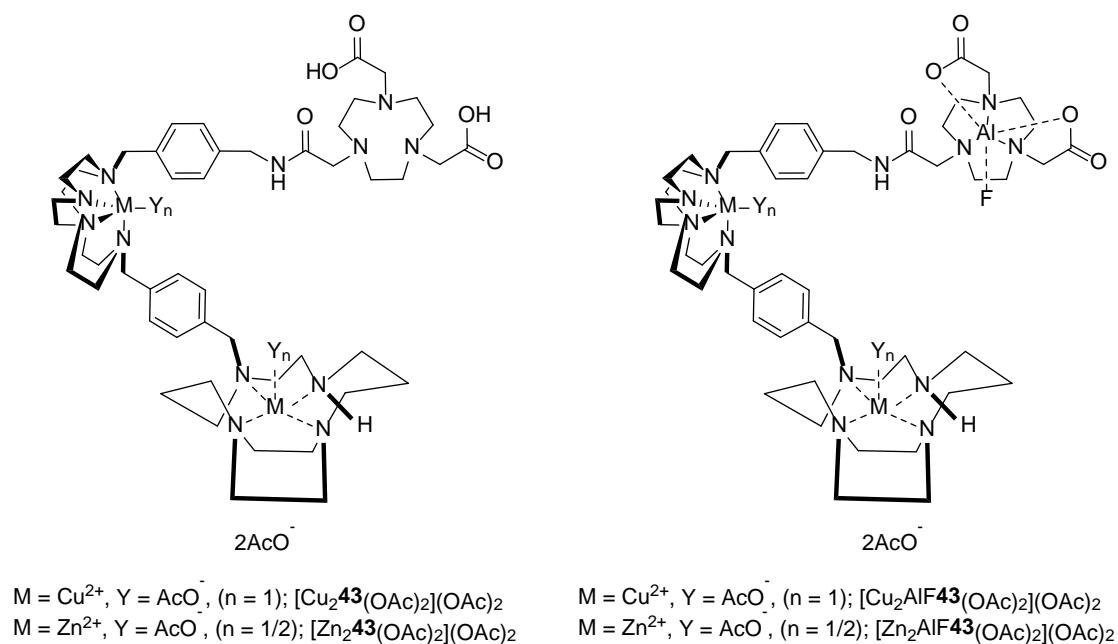


Figure 93: Structure of compound **43** metal derivatives.

Similar reactions to that shown in Scheme 14 were carried out using the metal complexes $[\text{Cu}_2\mathbf{24}(\text{OAc})_2](\text{OAc})_2$ and $[\text{Zn}_2\mathbf{24}(\text{OAc})_2](\text{OAc})_2$ to form compounds $[\text{Cu}_2\mathbf{43}(\text{OAc})_2](\text{OAc})_2$ and $[\text{Zn}_2\mathbf{43}(\text{OAc})_2](\text{OAc})_2$; shown in Figure 93. Compounds **43**, $[\text{Cu}_2\mathbf{43}(\text{OAc})_2](\text{OAc})_2$ and $[\text{Zn}_2\mathbf{43}(\text{OAc})_2](\text{OAc})_2$ were purified by semi-preparative HPLC and analysed by MS. As discussed previously in chapter 3 (section 3.4) it is essential that the metal complex formation is carried out before the conjugation reaction to prevent coordination of a metal ion into the NODA-amide component, which would block coordination of the aluminium(III) ion. This is also why high grade metal free reagents were used throughout the synthetic process.

$[\text{Cu}_2\mathbf{43}(\text{OAc})_2](\text{OAc})_2$ was isolated in high yields (>70%), however due to equipment failure during the purification process $[\text{Zn}_2\mathbf{43}(\text{OAc})_2](\text{OAc})_2$ was isolated in a lower yield but it is expected that similar yields could be achieved if no problems were encountered.

$[\text{AlF}\mathbf{42}(\text{OAc})_2](\text{OAc})_2$ and $[\text{Cu}_2\text{AlF}\mathbf{43}(\text{OAc})_2](\text{OAc})_2$ were formed following the procedure previously described; the compounds were purified by semi-preparative HPLC. However, although several new peaks were seen for $[\text{Zn}_2\text{AlF}\mathbf{43}(\text{OAc})_2](\text{OAc})_2$ in the HPLC, the mass spectra could not be assigned to the expected products. This may be due to the presence of unexpected counter-anions and so further investigation is required.

4.4.2 Attempted radiolabelling of bis-tetraazamacrocycle antagonists

Using the previously optimised conditions developed in Section 4.3.6 attempts were made to radiolabel **43** and $[\text{Cu}_2\mathbf{43}(\text{OAc})_2](\text{OAc})_2$. Initially (as detailed in Table 19), $[\text{Cu}_2\mathbf{43}(\text{OAc})_2](\text{OAc})_2$ (100 μM) was reacted with $^{18}\text{F}]\text{AlF}$ using a 1:0.9 volume ratio of 2 mM AlCl_3 solution to 50:50 v/v of ethanol/0.1 M sodium acetate (pH 4), heated at 100°C for 20 min.

Table 19: Reaction conditions trailed for the labelling of antagonists $[\text{Cu}_2\mathbf{43}(\text{OAc})_2](\text{OAc})_2$ and **43** with aluminium fluorine-18.

Antagonist	Concentration (μM)	Ratio of AlCl_3 added	Duration (min)	% labelling yield via TLC
$[\text{Cu}_2\mathbf{43}(\text{OAc})_2](\text{OAc})_2$	100	1:0.9	20	0
	500	1:0.9	20	0
	500	1:2	40	2
43	500	1:0.9	20	2 \pm 0.5

However, upon analysis by radio-TLC the desired radiolabelled product was not formed. Therefore the initial concentration of $[\text{Cu}_2\mathbf{43}(\text{OAc})_2](\text{OAc})_2$ was increased from 100 μM to 500 μM ; this however also did not lead to the formation of the radiolabelled product. Previously increasing the concentration of 2 mM AlCl_3 (section 4.3.3, Figure 90) saw an increase in percentage radiolabelling, therefore the concentration of AlCl_3 used for labelling $[\text{Cu}_2\mathbf{43}(\text{OAc})_2](\text{OAc})_2$ was also doubled along with the reaction duration. Table 19 and Figure 94 show that the radio-TLC for the attempted labelling of $^{18}\text{F}][\text{Cu}_2\text{AlF}\mathbf{43}(\text{OAc})_2](\text{OAc})_2$ showing *ca.* 2% yield was achieved. HPLC was used to confirm that the activity which remained on the base line was free $^{18}\text{F}^-$ and although the desired product is the most likely labeled compound, HPLC identification with the cold standard is required to confirm the presence of $^{18}\text{F}][\text{Cu}_2\text{AlF}\mathbf{43}(\text{OAc})_2](\text{OAc})_2$.

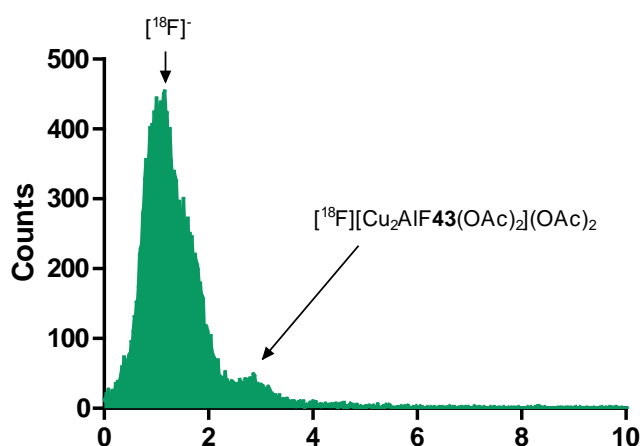


Figure 94: Radio-TLC trace of $^{18}\text{F}][\text{Cu}_2\text{AlF}\mathbf{43}(\text{OAc})_2](\text{OAc})_2$ showing *ca.* 2% radiolabelling yield.

The result of such a low yield for this complex may be due to other ions such as sodium already being present in the NODA BFC prior to radiolabelling. The competition with these ions to form the $[^{18}\text{F}]\text{AlF}$ complex could be responsible for the low yield. The metal complex antagonists have a higher probability of existing in these salt formations due to the charged metal ions they process. Therefore, attempts were also made to radiolabel the metal-free compound **43**. Using the conditions outlined in Table 19; a similar radiolabelling yield of 2% was achieved for the formation of $[^{18}\text{F}][\text{AlF}\mathbf{43}]$.

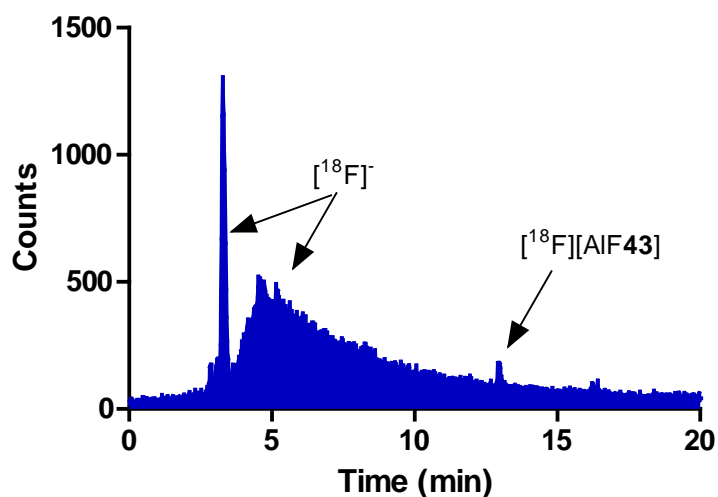


Figure 95: Radio-HPLC trace of $[^{18}\text{F}][\text{AlF}\mathbf{43}]$.

Figure 95 shows the radio-HPLC trace collected of $[^{18}\text{F}][\text{AlF}\mathbf{43}]$, as the radiolabelling yield was so low the product could not be isolated and separated from the free fluorine. Due to time constraints caused by cyclotron downtime when the work was being completed for this project, the conditions for radiolabelling the bis-tetraazamacrocycles could not be further investigated. **42** and the bis-macrocycles (**43** and $[\text{Cu}_2\mathbf{43}(\text{OAc})_2](\text{OAc})_2$) may be influencing the pH of the reaction mixture and this should be investigated in the future.

4.5 *In vitro* CXCR4 binding assays

In vitro validation was completed on the library of CXCR4 antagonists described in this chapter. Due to the delay in running of the assays this was carried out after radiolabelling experiments. To investigate the affinity towards the CXCR4 receptor calcium signalling assays were carried out to determine IC₅₀ values of the compounds. Known antagonist AMD3100 was also included in these assays as a standard.

Table 20: Table showing the IC₅₀ values determined in the calcium signalling assay for macrocyclic compounds. ^a Concentration required to reduce the level of Ca²⁺ ions observed during a 'normal' signalling process by 50% (IC₅₀) in U87-CXCR4 cells.

Antagonist	Calcium Signalling IC ₅₀ ^a /nM U87-CXCR4
24	>5000
[Cu ₂ 24 (OAc) ₂](OAc) ₂	100
[Zn ₂ 24 (OAc) ₂](OAc) ₂	1
43	>5000
[Cu ₂ 43 (OAc) ₂](OAc) ₂	210
[Zn ₂ 43 (OAc) ₂](OAc) ₂	4
[AlF 43]	2484
[Cu ₂ AlF 43 (OAc) ₂](OAc) ₂	>5000
[Zn ₂ AlF 43 (OAc) ₂](OAc) ₂	95
AMD3100	175

Table 20 shows that the inclusion of the NODA BFC moiety did not have a significant affect on the affinity of the antagonist towards the CXCR4 receptor; with all IC₅₀ values of **43**, [Cu₂**43**(OAc)₂](OAc)₂ and [Zn₂**43**(OAc)₂](OAc)₂ remaining similar to the unmodified compounds (**24**, [Zn₂**24**(OAc)₂](OAc)₂, [Zn₂**24**(OAc)₂](OAc)₂).

The antagonists [Zn₂**43**(OAc)₂](OAc)₂ and [Cu₂**43**(OAc)₂](OAc)₂ gave high potency IC₅₀ values of 4 nM and 210 nM for the inhibition of CXCL12 induced signalling in Jurkat cells. These IC₅₀ values show high affinity towards the CXCR4 receptor matching that shown by AMD3100. Therefore, both these antagonist show potential for further development and labelling as CXCR4 PET imaging agents. To determine the effect of radiolabelling to form the [¹⁸F]AlF complex, the non-radioactive AlF complexes were synthesised and affinity also tested.

The inclusion of the AlF complex saw an increase in CXCR4 affinity with regards to antagonist **43**, although at micromolar levels this may not have high relevance. However, for both [Cu₂AlF**43**(OAc)₂](OAc)₂ and [Zn₂AlF**43**(OAc)₂](OAc)₂ AlF complexation had a negative effect on

CXCR4 affinity (>5000 and 95 nM, respectively). The value obtained for antagonist $[\text{Cu}_2\text{AlF43}(\text{OAc})_2](\text{OAc})_2$ although expected to be lower affinity than that of $[\text{Zn}_2\text{AlF43}(\text{OAc})_2](\text{OAc})_2$ was still surprising. Further repeats need to be carried out to determine if this result is correct and that steric effects are having a detrimental effect on the binding of the antagonist towards the CXCR4 receptor. The copper(II) complex for these chelators is not presenting the optimum geometry of the metal ion for binding to aspartate residues and so would be expected to be lower based on the previous data.

Although the IC_{50} value of antagonist $[\text{Zn}_2\text{AlF43}(\text{OAc})_2](\text{OAc})_2$ significantly decreased upon aluminium(III) complex formation, it is still of suitable affinity towards the CXCR4 receptor for further development as an *in vivo* tracer.

4.6 Conclusion

In conclusion, novel NODA conjugated bis-tetraazamacrocyclic antagonists (**43**, $[\text{Cu}_2\mathbf{43}(\text{OAc})_2](\text{OAc})_2$ and $[\text{Zn}_2\mathbf{43}(\text{OAc})_2](\text{OAc})_2$) were synthesised to allow labelling via the $^{18}\text{F}]\text{AlF}$ complex for the development of a fluorine based CXCR4 receptor binding tracer.

Radiolabelling procedures using the ABT cyclotron produced fluorine-18 fluoride were investigated for a NODA-amide containing derivative, **42**. The molar ratios of AlCl_3 and as the concentration of ligand were varied to optimise radiolabelling yields while maintaining specific activity, resulting in the following conditions, 1: 0.9 molar ratio of AlCl_3 with the tracer precursor **42**, of which 100 μM is used.

The radiolabelling yield was also shown to improve considerably when performing the reaction with an organic co-solvent such as ethanol or 2-propanol. This is in agreement with what has been reported in the literature. However, while D'Souza *et al.* reported that other sterically bulky co-solvents such as *tert*-butanol also had an enhancing effect on radiochemical yields, this was not found in this work for **42**.²⁹⁷ Discussion in the literature has indicated that hydrophilic organic solvents might better solubilise the $^{18}\text{F}]\text{AlF}$ moiety, however no evidence or detailed results have been provided in support of this. The theory supported by the data reported in this chapter is that the co-solvent (ethanol or 2-propanol) may coordinate to the aluminium(III) ion and then be easily displaced to form the desired complex. The sterically bulky co-solvent appears to hamper this process, as evidenced by the decrease in yield. Ethanol was used in preference to 2-propanol in subsequent experiments due to the ease of evaporation and the increased compatibility with *in vivo* studies.

The optimised conditions were determined to be 1:0.9 molar amounts of AlCl_3 and **42** (100 μM) at 100°C for 20 mins yielding $^{18}\text{F}][\text{AlF}\mathbf{42}]$ (16-22% RCY) with a retention time of 12 min 45 sec on the HPLC, and the compound was shown to be stable for up to 3 hours in PBS solution at 37°C. However these optimised conditions were shown to be ineffective at labelling antagonists $[\text{Cu}_2\mathbf{43}(\text{OAc})_2](\text{OAc})_2$ and **43**.

In vitro assays were carried out on all the antagonists discussed in this chapter with $[\text{Zn}_2\text{AlF}\mathbf{43}(\text{OAc})_2](\text{OAc})_2$ proving to have the highest affinity of all the molecules tested; $\text{IC}_{50} = 95 \text{ nM}$ in the calcium signalling assay. The potency of $[\text{Zn}_2\text{AlF}\mathbf{43}(\text{OAc})_2](\text{OAc})_2$ is higher than that of AMD3100, indicating the possibility of further development to form a CXCR4 imaging probe.

4.7 Future work

Further work is needed to develop conditions that produce high radiolabelling yields and high specific activity tracers of antagonists $[\text{M}_2\mathbf{43}(\text{OAc})_2](\text{OAc})_2$ and **43**. Two possible explanations as to why the optimised radiolabelling conditions seen with compound **42** did not translate to the bis-tetraazamacrocycles could be the presence of other metal ions in the NODA BFC introduced throughout the synthesis or purification method competing with the formation of the $^{18}\text{F}]\text{AlF}$ complex. Alternately; pH is very important for $^{18}\text{F}]\text{AlF}$ radiolabelling, with the exact pH of 4 (Section 4.3.1) being necessary. It could be possible that the bis-tetraazamacrocycles could be influencing the reaction pH, therefore, reducing the labelling yield. Due to time constraints these parameters could not be investigated further. Therefore, it is necessary to investigate strengths of buffers and salt formation to increase radiolabelling yield before this work can be taken further.

Further *in vitro* repeats are necessary for antagonist $[\text{Cu}_2\text{AlF}\mathbf{43}(\text{OAc})_2](\text{OAc})_2$ and $[\text{Zn}_2\text{AlF}\mathbf{43}(\text{OAc})_2](\text{OAc})_2$ to confirm the IC_{50} values that are shown in Table 20. $[\text{Cu}_2\text{AlF}\mathbf{43}(\text{OAc})_2](\text{OAc})_2$ has a low potency IC_{50} value which is unexpected and so to confirm this, resynthesise and further *in vitro* validation would be carried out.

Once the radiochemistry is optimised, biodistribution studies could be carried out *in vivo* to evaluate the circulation and clearance of the zinc(II) NODA antagonist, which is the lead compound. Da Pieve *et al.* and Poschenrieder *et al.* did report hepatobiliary excretion and slow blood clearance with their $^{18}\text{F}]\text{AlF}$ -NOTA peptide conjugates, however, these are much larger molecules than the antagonists reported in this chapter with the peptide potentially influencing the properties to a greater extent.^{300, 313}

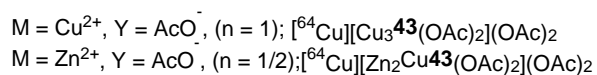
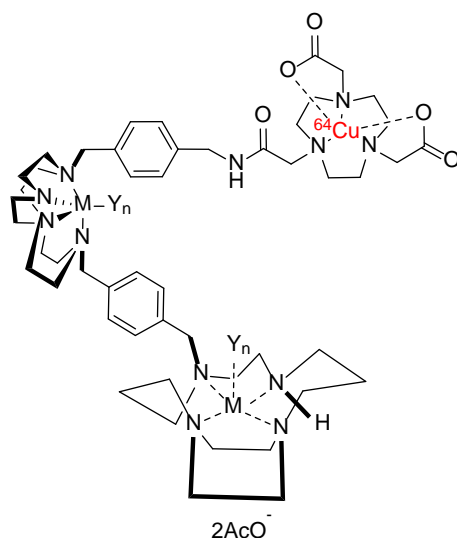


Figure 96: Potential alternative radiotracers that can be formed for compound **43**, $[\text{Cu}_2\mathbf{43}(\text{OAc})_2](\text{OAc})_2$ and $[\text{Zn}_2\mathbf{43}(\text{OAc})_2](\text{OAc})_2$ with copper-64 for high affinity antagonists of the CXCR4 receptor.

A potential alternative use for the complexes with a NODA-amide arm synthesised in this chapter is depicted in Figure 96; where compounds **43**, $[\text{Cu}_2\mathbf{43}(\text{OAc})_2](\text{OAc})_2$ and $[\text{Zn}_2\mathbf{43}(\text{OAc})_2](\text{OAc})_2$ could be radiolabelled with copper-64, with $[^{64}\text{Cu}][\text{Zn}_2\text{Cu}\mathbf{43}(\text{OAc})_2](\text{OAc})_2$ for a particularly interesting compound comparison with the radiolabelled compounds in this chapter and also the bis-tetraazamacrocycle complexes discussed in Chapter 2.

Chapter Five

Synthesis and radiolabelling of CXCR4 antagonists with technetium-99m for SPECT imaging

5.1 Previously developed strategies and current state-of-the-art

The interest in CXCR4 chemokine receptor as an imaging target has mainly resulted in the development of PET imaging agents with the only clinically translated agent utilising the gallium-68 isotope. However, due to the widespread availability of clinical SPECT facilities, there is potential demand for SPECT tracers that could routinely be prepared in standard SPECT radiopharmacies and used for CXCR4 imaging.

The basic principles of SPECT imaging and the key radioisotopes utilised were introduced in Chapter 1 (section 1.1.2). One of the advantages of SPECT over PET is the achievable spatial resolution due to detection of the directly released gamma photon. The radioisotopes routinely used for SPECT are also widely available as many have longer half-lives or can be produced via a generator rather than a cyclotron. Furthermore, γ -rays of different energies are produced by the different SPECT isotopes which can be employed in concurrent imaging of various functions and metabolic processes with the use multiple isotopes simultaneously (see Table 21).^{321, 322}

Table 21: Radioisotopes used for different clinical studies by SPECT imaging and their properties.

Study	Radioisotope	Emission energy (keV)	Half-life	Radiopharmaceutical	Ref
Bone Scan	technetium-99m	140	6 hours	Phosphonates/ Bisphosphonates	320
Myocardial perfusion scan	technetium-99m & thallium-201	140 & 135	6 hours & 73 hours	Tetrofosmin; Sestamibi	323
Brain scan	technetium-99m	140	6 hours	hexamethylpropylene amine oxime; ethyl cysteinate dimer	324
Tumour scan	iodine-123	159	13 hours	Iobenguane	325
White cell scan	indium-111 & technetium-99m	171 & 245	67 & 6 hours	<i>In vitro</i> labelled leucocytes	326

The SPECT isotopes indium-111 and iodine-125, which have relatively long half-lives have been used for labelling CXCR4 specific peptides and antibodies.^{158, 327-330} Whilst lower molecular weight (small molecule) antagonists have been radiolabelled with the shorter lived isotopes gallium-67 and technetium-99m.^{331, 332}

5.1.1 Technetium and rhenium isotopes

Over the last decade technetium and rhenium have become increasingly used, respectively, as diagnostic and therapeutic radiopharmaceuticals. As technetium has no stable isotopes, rhenium

analogue complexes have provided an essential model system to evaluate the potential physicochemical properties of technetium-99m tracers by analogy.^{333, 334} As rhenium is located in the same group as technetium in the transition series (it is the third row congener), the two elements share many isostructural complexes. However, there are a some differences between the two elements that need to be taken into account when making a comparison.³³⁵ Rhenium complexes are harder to reduce but easier to oxidise; as a result the perrhenate anion is more stable to reduction than pertechnetate. Rhenium complexes are also more kinetically inert than their technetium-99m counterparts, meaning that labelling at higher temperatures is often necessary.³³⁵

In addition to the use of rhenium to form non-radioactive analogues of technetium-99m tracers, a large and rapidly developing area of interest is the use of β -emitting rhenium-186 and rhenium-188 radioisotopes as therapeutic agents. Clinically, rhenium-186 and rhenium-188 have found the most widespread application for bone pain relief in outpatients with skeletal metastases.³³⁶⁻³³⁸ Rhenium-188 forms a complex with hydroxyethylene diamine phosphonate (HEDP) and has the advantage of being relatively low cost and readily available (via an on-site commercially available generator) leading to high interest in further developing these applications.^{339, 340}

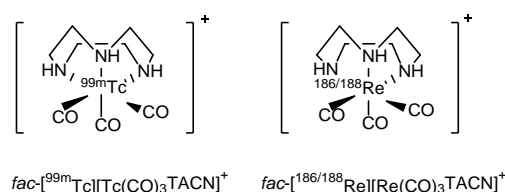


Figure 97: Structures of imaging moieties $fac-[^{99m}\text{Tc}][(\text{CO})_3\text{TACN}]^+$, $fac-[^{186/188}\text{Re}][\text{Re}(\text{CO})_3\text{TACN}]^+$.

In general for the preparation of technetium or rhenium radiopharmaceuticals the pertechnetate/perrhenate ions must be reduced by an appropriate reducing agent and coordinated with a chelator. In order to be effective the chelator must stabilise the lower oxidation states, as well as influencing the biological distribution pathway. Currently, several reliable techniques for high yielding syntheses are reported in the literature that offer robust methods for labelling with technetium and rhenium.³³⁵ In recent years, there has been a trend for the use of tricarbonyl rhenium(I) and technetium(I) complexes for labelling to form radiopharmaceuticals; see Figure 97.³⁴¹⁻³⁴³

There have been many mono-, bi- and tridentate BFCs reported for complex formation with the $fac-[^{99m}\text{Tc}(\text{CO})_3]^+$ core using a variety of donor atoms to complete the octahedral coordination sphere.³⁴⁴ Egli *et al.* made the important discovery that the $fac-[^{99m}\text{Tc}(\text{CO})_3]^+$ core reacts with certain amino acids and amino acid fragments. Of particular importance is the high affinity the $fac-[^{99m}\text{Tc}(\text{CO})_3]^+$ core has for histidine at low concentrations (10^{-6} M).³⁴⁵ Alberto *et al.* exploited this

discovery designing bifunctional analogues of histidine to complex with the technetium(I) tricarbonyl core.³⁴⁶

The use of a bidentate BFC for binding the $fac-[^{99m}Tc(CO)_3]^+$ core can give complexes that suffer from significant retention in the blood pool *in vivo* and also in the organs of excretion (liver and kidneys). This is likely due to the remaining H₂O ligand being exchanged with other coordinating functional groups *in vivo*, causing the ^{99m}Tc to be retained in tissues.^{347, 348} Stability to ligand exchange has been shown to increase with a tridentate ligand.

Conditions for radiolabelling with $fac-[^{99m}Tc(CO)_3]^+$ have utilised various pH's, solvents and temperatures. In 2016, Imstepf *et al.* reported the synthesis and labelling of a doxorubicin-metalloconjugate with tricarbonyl technetium-99m.³⁴⁹ The three labile water ligands of the $fac-[^{99m}Tc(CO)_3]^+$ core were readily displaced by the 2,2'-dipicolylamine (DPA) group with high radiolabelling efficiency (95%). However, it was stated that radiolabelling conditions needed to be mild and carefully controlled. Optimisation studies revealed that there was a trade off with lower pHs (4-5) which keep the doxorubicin chelators in solution, however, this had a negative impact on the labelling yield. Alternatively, if too low a pH was used, although there was an enhanced labelling efficiency, the hydrophobic nature of the protonated chelator would cause it to precipitate out of solution. Therefore, efficient aqueous labelling was achieved at 55-60°C for 30 mins with the pH carefully adjusted to between 6-7.³⁴⁹

Kasten *et al.* reported the successful labelling of a novel isothiocyanate-functionalized bifunctional chelator based on DPA at neutral pH in 10 mM neutral sodium phosphate buffer with heating at 70°C for 30-60 mins. This neutral pH and lower temperature making these conditions ideal for sensitive biological targeting groups, with the trade-off in the reaction time necessary to achieve high radiolabelling yields.³⁵⁰

Triazacyclononane (TACN) has been reported in the literature to form stable complexes with technetium and rhenium ions of various oxidation states.³⁵¹⁻³⁵⁷ In 1992, Alberto *et al.* reported the effective, facile rapid labelling of TACN with the tricarbonyl technetium-99m core.³⁵⁸ In 2008, Suzuki *et al.* radiolabelled two macrocyclic triamine compounds of varying ring sizes with $fac-[^{99m}Tc(CO)_3]^+$.⁹⁷ Labelling was performed in a neutral pH buffer with heating at 100°C for 30 mins to achieve high radiochemical yields. The group characterised the stability and *in vivo* biodistribution of the two labelled macrocyclic complexes, finding the smaller, TACN, macrocycle to have greater stability and a rapid excretion pathway. Therefore, it was concluded that TACN is a useful synthon as a basic chelating molecule for not only technetium-99m radiopharmaceuticals but also for rhenium-188/186 therapeutic radiopharmaceuticals.

Vanbilloen *et al.* reported a comparison study of the labelling of various cyclic polyamines (cyclam, cyclen and TACN) with $fac-[^{99m}Tc(CO)_3]^+$.³⁵⁷ The group reported that, out of the three cyclic polyamines studied, TACN has the most useful biodistribution profile, showing rapid clearance from the blood (mainly via the kidneys) with no significant uptake seen in the intestines.³⁵⁷

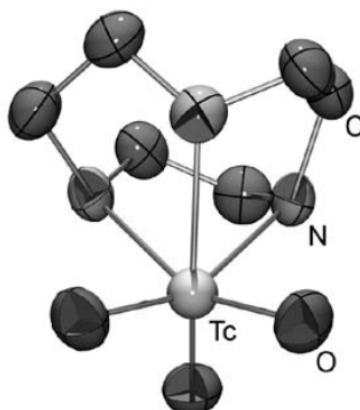


Figure 98: Crystal structure of $fac-[^{99m}Tc][Tc(O)_3TACN]^+$. Hydrogen atoms omitted for clarity. (Reproduced from Braband *et al.*).³⁵⁹

In 2012, Braband *et al.* reported the radiolabelling of TACN with a $fac-[Tc(O)_3]^+$ core (see Figure 98), which is significantly smaller than the $fac-[^{99m}Tc(CO)_3]^+$ core.³⁶⁰ These complexes are stable in water at neutral and basic pH, but do decompose slowly under acidic conditions. Braband *et al.* went on to demonstrate the potential of $fac-[^{99m}Tc(O)_3]^+$ labelled TACN as a precursor to labelling pharmacophores, amino acids and carbohydrates.³⁶¹ The group developed a protocol for the synthesis of $fac-[^{99m}Tc(O)_3]^+$ labelled TACN that is clinically translatable using ion exchange resin and hydrophilic interaction liquid chromatography (HILIC) for purification. The group reported that $fac-[^{99m}Tc(O)_3]^+$ labelled TACN had favourable biodistribution, having rapid clearance via the kidneys. This differs to $fac-[^{99m}Tc(CO)_3]^3$ which has been shown to bind to blood proteins preventing such rapid clearance.³⁴⁵ The $[^{99m}Tc(O)_3(TACN)]^+$ moiety was shown to be reactive towards alkenes, allowing its use in [3+2]cycloaddition reactions. The group also successfully labelled a hypoxia targeting pharmacophore, an amino acid analogue and a glucose derivative, showing the versatility of the $[^{99m}TcO_3(TACN)]^+$ moiety.^{361, 362}

5.1.2 SPECT tracers to target the CXCR4 receptor

One of the first examples of a SPECT tracer targeting the CXCR4 chemokine receptor was reported by Hanaoka *et al.* who radiolabelled the known peptide antagonist Ac-TZ14011 with indium-111.¹⁵⁸ Biodistribution data collected in mice bearing the CXCR4-expressing pancreatic carcinoma AsPC-1 showed low levels of accumulation of indium-111 peptide in the CXCR4 expressing tumour after an hour (0.51%ID/g).¹⁵⁸ Blocking studies involving the simultaneous co-injection of the unlabelled Ac-TZ14011, as well as, $[^{111}In]$ -DTPA-Ac-TZ14011 did show a drop in the tumour-to-muscle

ratio indicating the specificity of the tracer for CXCR4. However, the low levels of tumour uptake coupled with the high levels of non-specific uptake in the kidneys and liver limited further development of the tracer.

In 2008, technetium-99m radiolabelled CXCL12 (the natural ligand of CXCR4) was developed for use as a SPECT tracer for imaging the increased levels of CXCR4 expression as a result of myocardial infarctions.³⁶³ However, accumulation in the infarcted tissue was low, at 0.57%ID/g at 2 hours post-injection. There was a 5-fold increase compared to non-infarcted tissue, nonetheless, the uptake in non-targeted organs was too high to consider this tracer suitable for further development.

In 2016, Fu *et al.* reported the labelling of small-interference RNA (siRNA) with technetium-99m for the imaging of CXCR4 receptor expression levels.³⁶⁴ The CXCR4 siRNA was labelled using the BFC hydrazinonicotinamide (HYNIC) approach. Biodistribution studies were completed using mice bearing MDA-MB-231 tumours, analysis revealed that, after one hour post injection, accumulation of the tracer in the tumour was 4.45% ID/g, however much higher accumulation was seen in the liver and kidneys (15.68% ID/g and 13.88% ID/g respectively).³⁶⁴ As a control, a non-specific technetium-99m labelled siRNA was also investigated which showed a similar biodistribution, with the notable exception being in the CXCR4 positive tumour; showing specificity of the CXCR4 siRNA tracer. However, the high accumulation and long retention time in the excretion organs indicated poor dosimetry for the tracer.

Technetium-99m has also been utilised to radiolabel the cyclam ring in AMD3100 reported by Zhang *et al.* in 2010.³⁶⁵ The complexation of technetium-99m with macrocycles such as cyclam has been known since the 1980s.^{366, 367} An *in vivo* study with the radiolabelled [^{99m}Tc][TcAMD3100] was conducted in a liver tumour animal model, resulting in poor quality SPECT scans showing limited accumulation in the tumours. This is not a convincing study with precise values (such as %ID/g and tumour-to-muscle ratios) not reported in the paper, perhaps indicating the limitations of this compound.

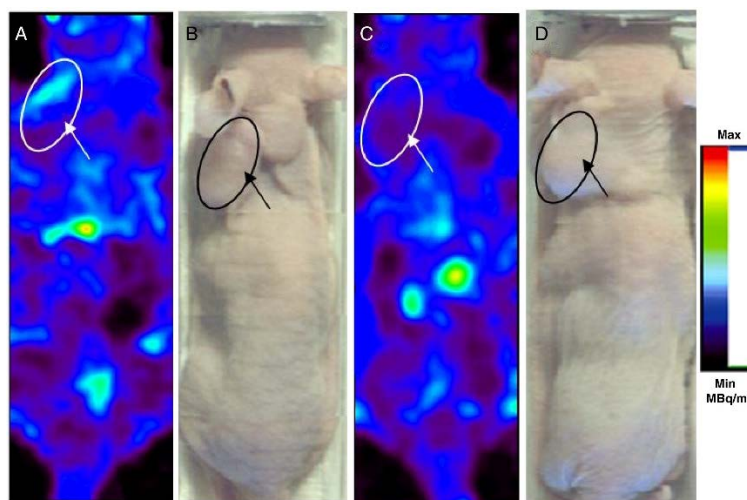


Figure 99: CXCR4 imaging in PC-3 tumour xenografts bearing mice with [^{99m}Tc][TcAMD3100]. A) SPECT image of [^{99m}Tc][TcAMD3100] and B) digital image of control animal. C) SPECT image after administration of a blocking dose of AMD3100 (20 mg/kg). D) Digital image of the blocked mice. Arrow indicates the tumour. (Reproduced from Hartimath *et al.*).³³²

A more in-depth technetium-99m labelling study of AMD3100 was carried out by Hartimath *et al.* three years later.³³² The *in vivo* imaging model utilised PC-3 prostate cancer tumours and showed a maximum tumour uptake of [^{99m}Tc][TcAMD3100] at $\sim 1.7\%$ ID/g, see Figure 99. Hartimath *et al.* included a blocking dose scan (20 mg/kg AMD3100), in which tumour uptake was reduced, indicating a level of specificity of this tracer. However, it is important to note that peak uptake occurred within the first 5 minutes following initial injection, followed by wash out over the duration of the 60 minute scan. The poor pharmacokinetics of the tracer limit its potential for clinical use. Hartimath *et al.* reported uptake at 60 minutes in a number of non-target tissues, such as the liver, lungs, thymus, intestine, spleen and bone, however the authors justified this uptake pattern as being in endogenous high expressing CXCR4 tissues and indicated that a reduction in uptake was observed when a blocking dose of AMD3100 was administered.³³² Overall this work is unconvincing and there is insufficient characterisation of the binding profile of the radiolabelled derivative.

Labelling of AMD3100 with technetium-99m is an inherently flawed strategy to develop a SPECT tracer. In 1981 Zuckman *et al.* reported the X-ray structures of technetium(V) complexes with cyclam.³⁶⁸ Unlike other technetium(V) complexes with chelators that contain strong π -donors that form an overall neutral square pyramid complex, cyclam forms a stable trans-dioxo- TcO_2^+ complex with an approximately octahedral geometry.^{369, 370} An element of strain is introduced due to the metal-N donor atom distance (2.125 Å) of the complex being longer than the optimal M-N distance of about 2.07 Å in the case of cyclam.³⁷¹ The dioxo- TcO_2^+ complex changes the shape of the complex with the protruding oxo-groups which will not exchange with amino acid side chain donor atoms (e.g. aspartate) and this is likely to have a detrimental effect on binding interactions with the CXCR4 receptor.

5.2 Synthetic strategy for next generation ^{99m}Tc tracers

Previous strategies to image the CXCR4 receptor using technetium-99m with small molecule antagonists like AMD3100 have resulted in poor affinity and low quality images. Labelling the cyclam ring directly with technetium(V)-99m was shown to be prone to transchelation due to the metal ion being unable to form a stable coordination geometry and disruption of receptor binding.³⁷²

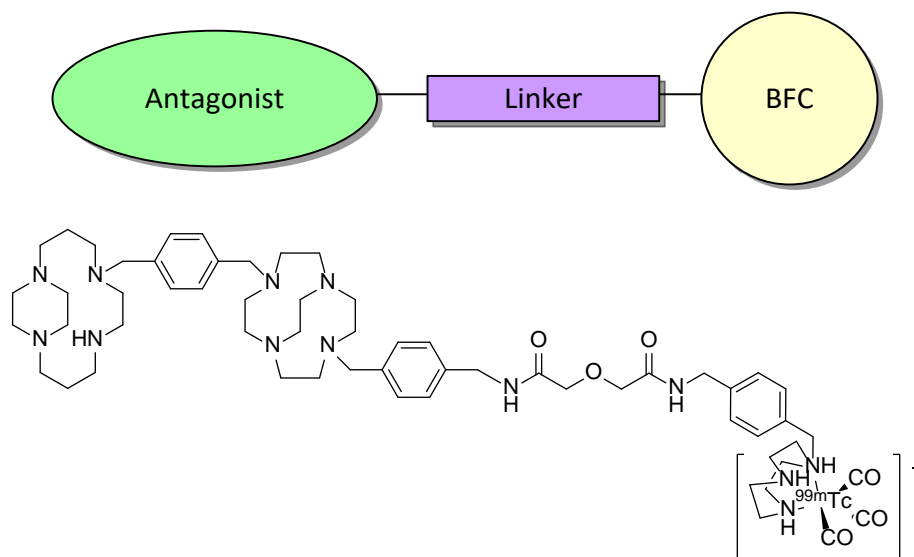


Figure 100: Schematic representations for the design of CXCR4 specific SPECT tracers and example of structure of target molecule.

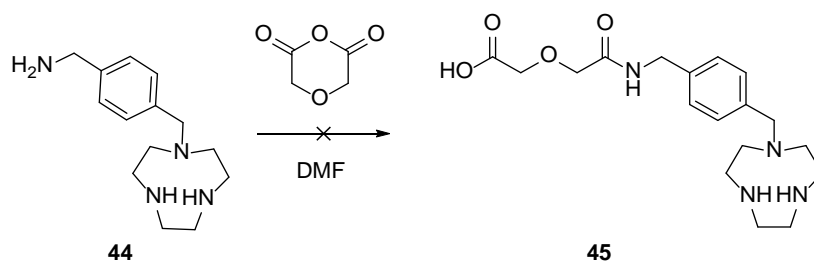
The structure of the SPECT antagonist proposed in this chapter is composed of two components; a binding moiety and a labelling moiety; see Figure 100. The binding moiety is based on knowledge the Archibald group has gained on high affinity CXCR4 antagonist design. As discussed in detail in section 2.1.2, with the use of structurally restricted azamacrocycles chelated to transition metals to enhance binding to the CXCR4 receptor.^{82, 199} An extended linker/spacer moiety allows for conjugation to a BFC that could be labelled with technetium(I)-99m. The aim is to produce a high affinity antagonist where the inclusion of the BFC does not have a negative impact on affinity.

The molecules discussed in this chapter have been designed to exploit the coordination chemistry of the technetium(I)-99m tricarbonyl intermediate.^{97, 373-375} TACN was chosen as the BFC for the incorporation of $fac-[^{99m}\text{Tc}(\text{OH}_2)_3(\text{CO})_3]^+$; it is a tridentate chelator and allows for rapid complex formation.

Trial reactions were initially carried out using a (relatively) low affinity mono-macrocyclic antagonist to determine the most effective synthetic route. The CB copper chelated mono-macrocyclic antagonist is an accessible synthetic target to allow the radiochemistry to be optimised for the BFC TACN, before transferring the conditions to the higher affinity bis-azamacrocyclic compound.

5.2.1 Mono-macrocycle CXCR4 antagonists conjugated to TACN

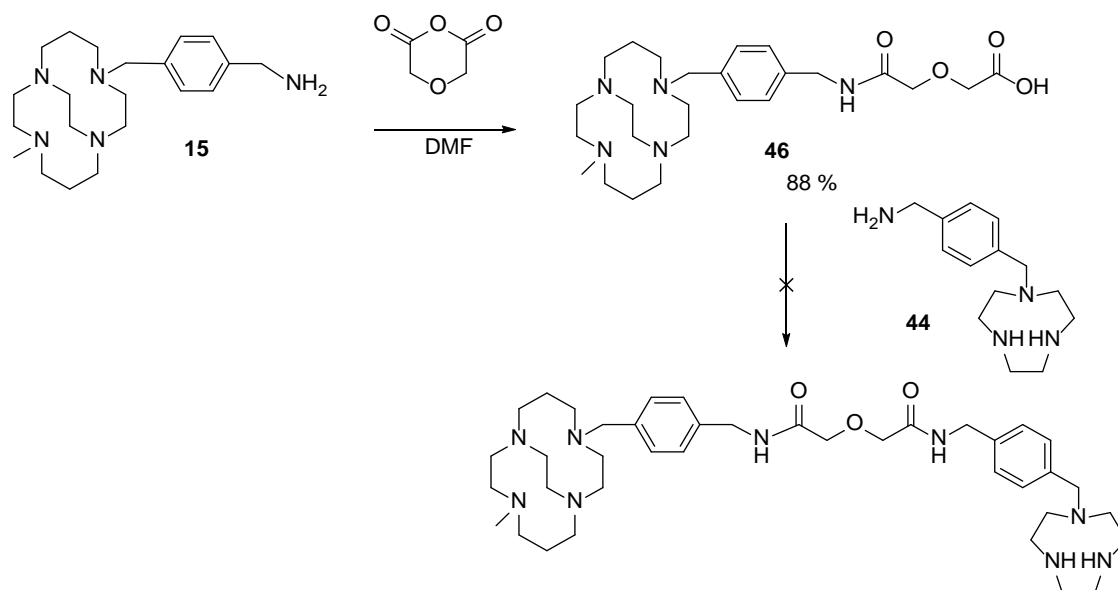
The BFC benzyl amine TACN, **44**, was prepared by a member of the Archibald group and supplied for us in this project (Ms. Zainab Al-Ali). Diglycolic anhydride was reacted with TACN to introduce a carboxylic acid terminating group and allow further modification. Diglycolic anhydride reacts via a ring opening mechanism rapidly at room temperature, and will predominantly give only one product due to the sterics of the ring opening. As shown in Scheme 15, diglycolic anhydride was added slowly dropwise to a solution of benzyl amine TACN, **44**, in a 1:1 ratio in dry DMF. Mass spectrometry analysis showed the formation of the mono-, bis- and tris- substituted product, due to the secondary amines on the TACN also reacting with diglycolic anhydride. This reaction was not useful under these conditions with the wide range of products formed and so no purification attempts were made.



Scheme 15: Attempted ring-opening of diglycolic anhydride and benzyl amine TACN derivative.

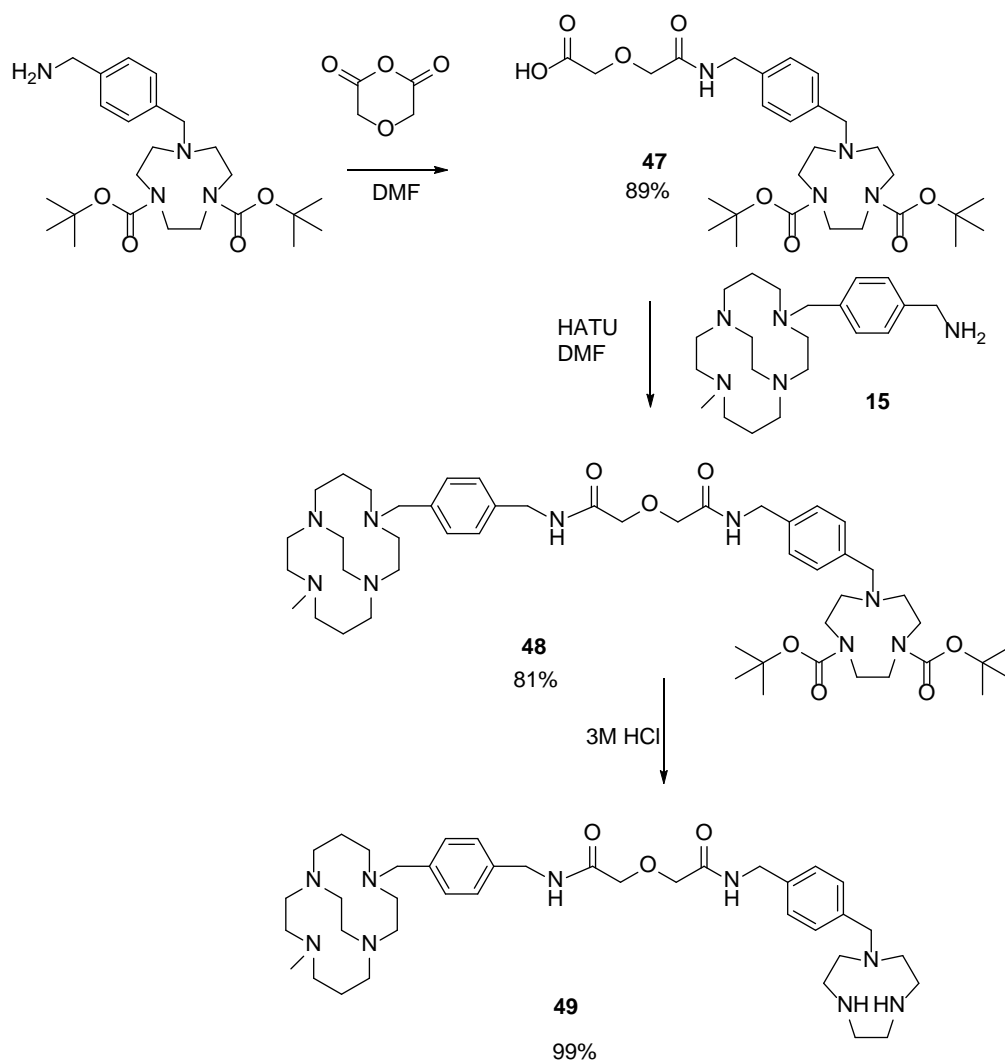
To avoid issues with the presence of reactive secondary amines on compound **44**, an alternate approach was carried out which reacted the diglycolic anhydride with the mono-cross bridge azamacrocycle antagonist component prior to reaction with the TACN derivative, see Scheme 16. There are no secondary amine groups on compound **15**, as all nitrogen positions are alkylated in the cross bridged cyclam derivative. Compound **46**, was formed in high yield after 16 hours of shaking at room temperature in amine-free dry DMF. The diglycolic ring opening reaction with primary amines has been shown in the past not only to be reproducible but to go to completion even with a 1:1 ratio.²⁵⁷ Characterisation of the product indicated that no further purification was necessary.

Compound **46** was then reacted with benzyl amine TACN, **44**, in the presence of HATU and 10 equivalents of base (TEA) in an attempt to activate the carboxylic acid, see Scheme 16. The reaction was monitored *in situ* by mass spectrometry and, after three days, formation of the desired product was still not observed. There may again be issues with the unwanted reaction of the secondary amines on the TACN component.



Scheme 16: Attempted synthesis of antagonist with benzyl amine TACN chelated group.

To overcome any reaction of the secondary amines, the BOC protected analogue of the benzyl amine TACN compound, see Scheme 17, was used instead. Mass spectrometry and NMR analysis show that the reaction of protected TACN and diglycolic anhydride was successful and a pure product was obtained. Compound **47** was then conjugated to the antagonist **15** in the presence of 10 equivalents of base (TEA) and 1 equivalent of HATU. The reaction was carried out in dry amine free DMF at room temperature. Purification was carried out using semi-preparative RP-HPLC to give the desired product as an analytically pure compound **48**.



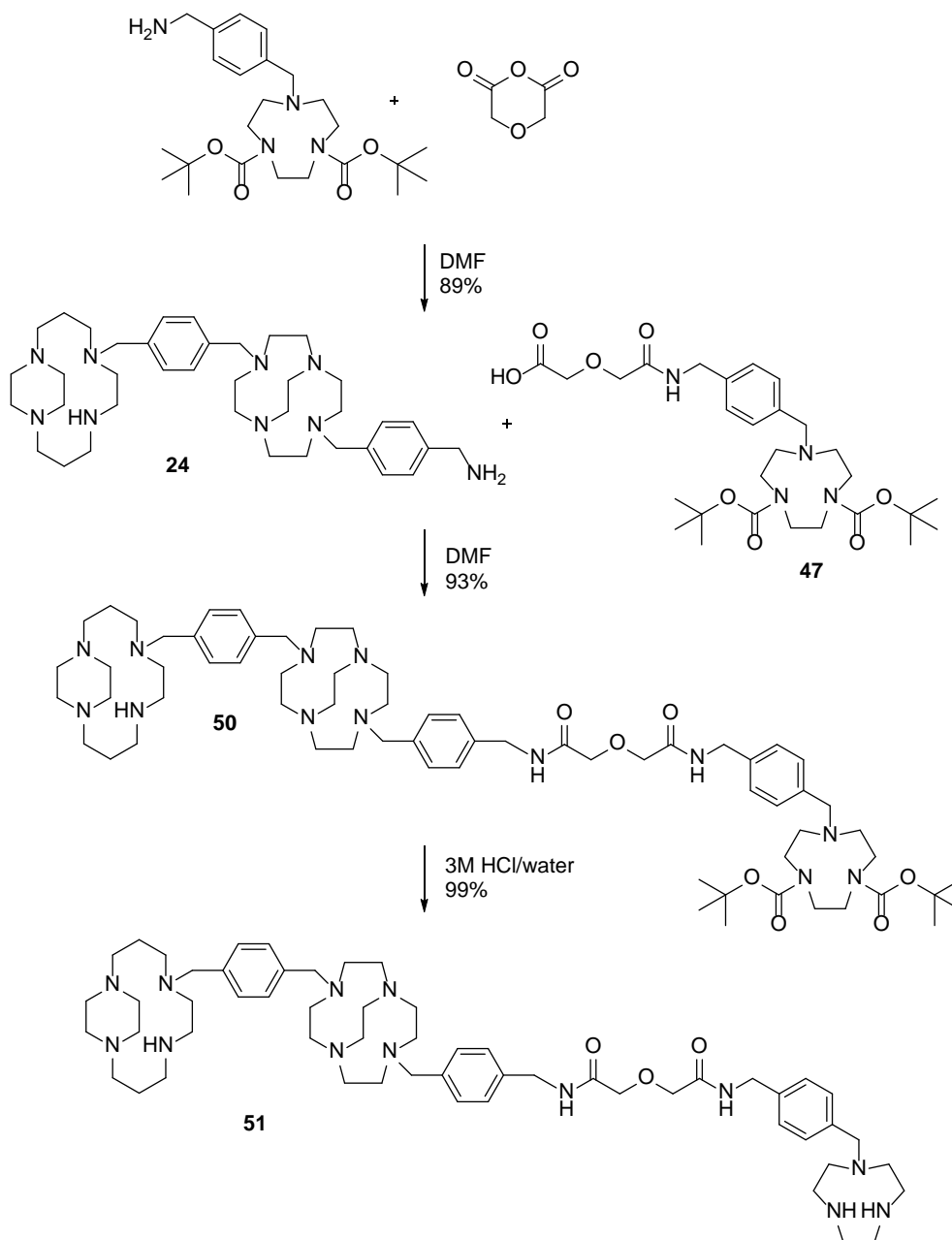
Scheme 17: Pathway used for the successful synthesis of compound **49**.

Cleavage of the Boc protecting groups of TACN has been reported in the literature using various high yielding methods; including conc. HCl^{376, 377}, conc. nitric acid and 10% TFA in dichloromethane.²⁷² Antagonist **48** was de-protected using a modified version of the procedure reported by Graham *et al*; with 3 M HCl used to cleave the BOC protecting group to form **49**.³⁷⁸ The reaction was stirred at room temperature for 16 hours, and then evaporated under reduced pressure. The removal of the *t*-butyl groups was confirmed by ¹H NMR.

5.2.2 Bis-macrocycle TACN conjugated CXCR4 receptor antagonists

Following the synthesis of the mono-macrocycle antagonist compound for technetium-99m labelling (compound **49**); the optimised procedure was used to synthesise the bis-macrocylic antagonist TACN derivatives. As stated in Chapter 2, section 2.2, the bis-azamacrocyclic compounds have a higher affinity for the CXCR4 receptor. The additional cyclam ring allows for binding to two aspartate side chains on the surface of the CXCR4 receptor. The synthesis is outlined in Scheme 18, using compound **24** as an example.

Compound **50** was synthesised using a similar method to compound **48**, in amine-free dry DMF with 10 equivalents of base (TEA) and one equivalent of HATU to activate the carboxylic group on compound **6**. Mass spectrometry confirmed the formation of compound **49**, however, impurities were also present (observed in the HPLC trace as well as in the NMR spectrum). The compound was not purified by semi-preparative HPLC at this stage as the presence of TFA in the HPLC mobile phase could lead to the deprotection of the secondary amine groups and reduce yield.



Scheme 18: Route for the synthesis of the TACN conjugated bis-macrocycle antagonist, **51**.

Antagonist **50** was deprotected using 3M HCl shaken overnight at room temperature. The reaction mixture was concentrated in *vacuo* before being purified by semi-preparative HPLC. Mass spectrometry showed formation of the desired product. Proton NMR also confirmed the TACN moiety had been fully deprotected with the disappearance of the t-butyl group previously observed for **51** at 1.42-1.48 ppm.

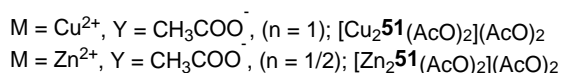
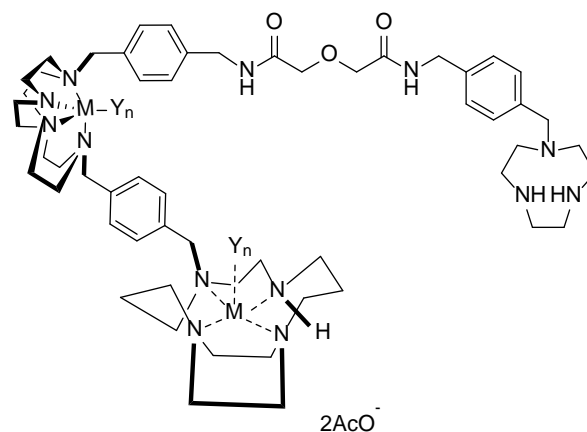


Figure 101: Structures of metal complexation of compound **51** copper(II) and zinc(II); $[\text{Cu}_2\mathbf{51}(\text{OAc})_2](\text{OAc})_2$, and $[\text{Zn}_2\mathbf{51}(\text{OAc})_2](\text{OAc})_2$, respectively.

$[\text{Zn}_2\mathbf{51}(\text{OAc})_2](\text{OAc})_2$ (see Figure 101) was synthesised, by reacting the preformed metal complex under the same conditions as the bis-macrocyclic chelator. The zinc(II) ions did not inhibit the amide bond formation reaction.

The formation of $[\text{Cu}_2\mathbf{51}(\text{OAc})_2](\text{OAc})_2$ proved to be more challenging. The first attempts at coupling compound **47** with $[\text{Cu}_2\mathbf{24}(\text{OAc})_2](\text{OAc})_2$ resulted in a green solid, which, when analysed, revealed the transchelation of one of the copper(II) ions. The instability of the complex could be due to the presence of the TEA in the solution. The reaction was carried out again without any base, and monitored by HPLC. The reaction proceeded much more slowly (shake at room temperature for 4 days) after which the reaction was purified by semi-preparative HPLC. $[\text{Cu}_2\mathbf{51}(\text{OAc})_2](\text{OAc})_2$ eluted at 10min 17 sec. The formation of a transchelated monometallic side-product and the slow reaction results in a low 41% yield.

5.2.3 Preparation of rhenium cold standard CXCR4 receptor antagonist

As technetium has no stable isotopes, $fac-[Re(CO)_3L]^n$ is used as an analogue to investigate complex formation.^{333, 334} Alberto *et al.* reported the synthesis of a water soluble rhenium compound, $fac-[NEt_4]_2[ReBr_3(CO)_3]$.³⁷⁹ This compound was synthesised and provided by a member of the Archibald group (Ms. Rebecca Hargreaves), using the procedure outlined by Alberto *et al.*³⁷⁹

Bullok *et al.* reported the coordination of a TACN labelled peptide with $fac-[NEt_4]_2[ReBr_3(CO)_3]$ by stirring in water heated to 85-90°C for 30 min, HPLC analysis revealed a complex spectra, due to structural isomers arising from multiple coordination combinations.³⁸⁰ These conditions were used in a reaction with **49**, but did not result in the desired product. Complex formation from $fac-[NEt_4]_2[ReBr_3(CO)_3]$ with **49**, was achieved by overnight stirring at room temperature in dry DMF with 1:1 equivalents of the metal complex precursor. This is a similar method to that used to form gallium DOTA complexes as stable isotope analogues, described in section 3.5.1.2.

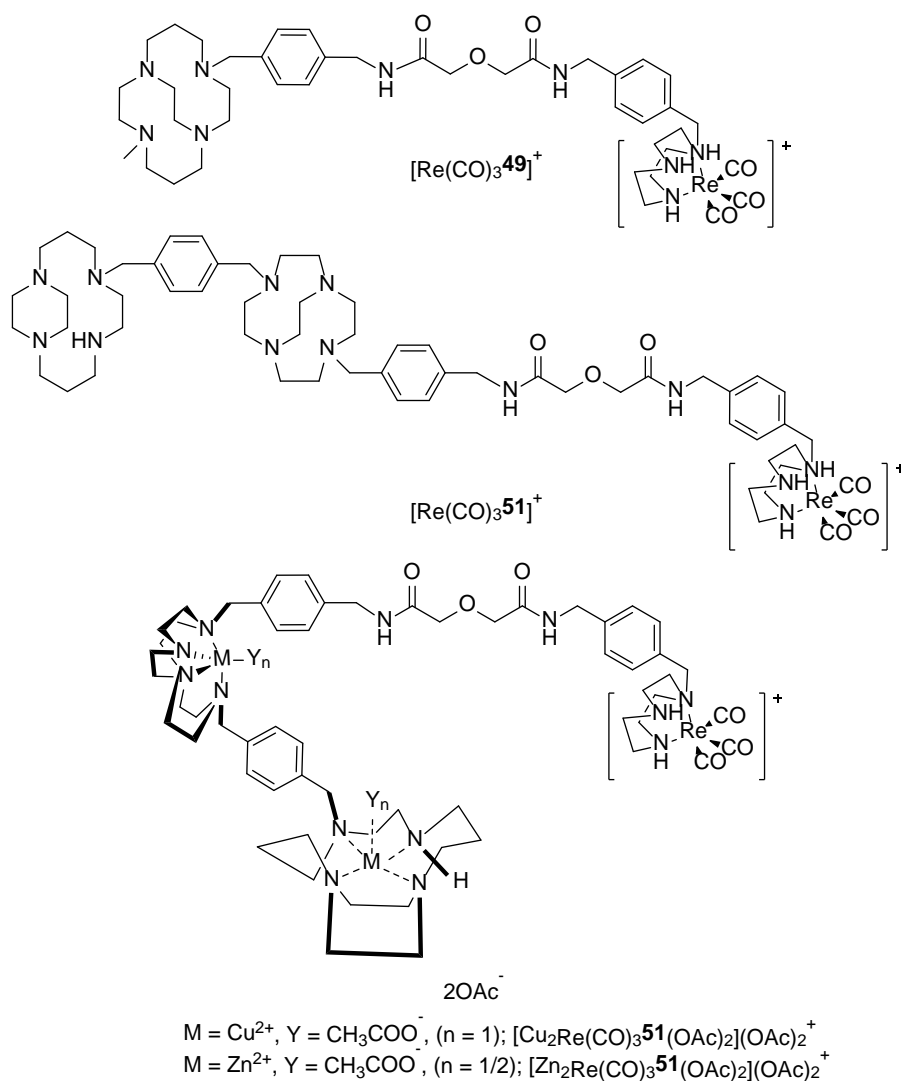


Figure 102: Structure of rhenium cold standards of compound **49**, and of the metal complex of compound **51**.

Mass spectrometry showed a peak for the $[M-CO]^+$ ion. Analytical HPLC analysis of compound $[Re(CO)_3\mathbf{49}]OAc$ also showed the appearance of a new peak with a retention time of *ca.* 7 min.

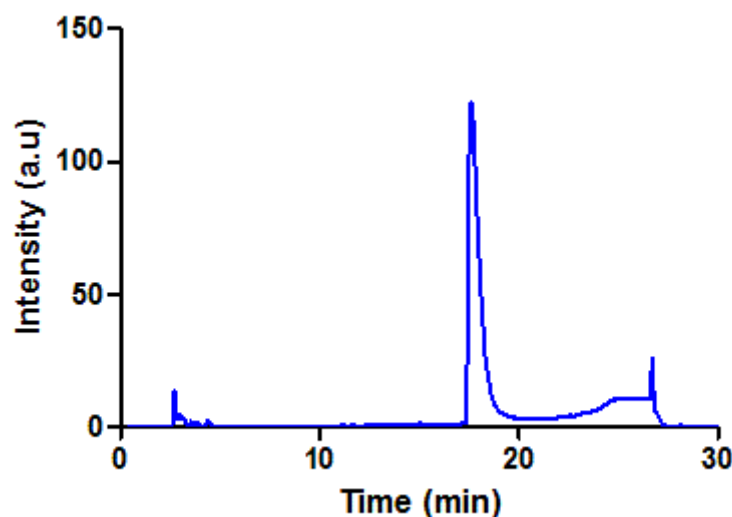


Figure 103: Graph showing the UV HPLC trace of compound $[Re(CO)_3\mathbf{51}]^+$ eluting at 10 min 20 sec.

Compounds $[Re\mathbf{51}]^+$, $[Cu_2Re\mathbf{51}(AcO)_2](AcO)_2^+$ and $[Zn_2Re(CO)_3\mathbf{51}(AcO)_2](AcO)_2^+$ (shown in Figure 102) were synthesised in the same way as $[Re\mathbf{49}]$. $[Re\mathbf{51}]$ gave a new broad peak in the range 17-19 min when analysed by HPLC, see Figure 103. It was challenging to assign the peaks for $[Cu_2Re(CO)_3\mathbf{51}(AcO)_2](AcO)_2^+$ and $[Zn_2Re(CO)_3\mathbf{51}(AcO)_2](AcO)_2^+$ due to number of metal ions and splitting patterns, however, the shift in the HPLC peaks indicated complex formation had occurred, although further analysis is required to fully characterise these compounds.

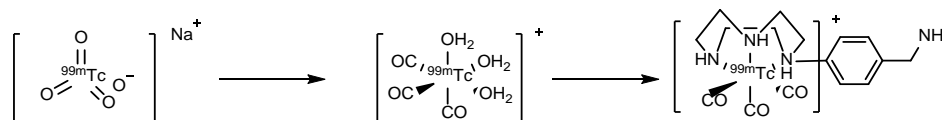
5.3 Radiolabelling with technetium-99m

5.3.1 Introduction and past strategies

As discussed in section 5.2, the technetium-99m tricarbonyl chemistry developed by Alberto *et al.* is one of the most promising and well developed organometallic cores for the formation of technetium tracers, and hence was chosen for labelling of the antagonists in this work.^{342, 343, 358, 379} The precursor is directly accessible from sodium pertechnetate.³⁴⁰ Kits are commercially available (Mallinckrodt-Tyco Med, Isolink) to form the tricarbonyl precursor, however it can also be synthesised in quantitative yields by adding generator eluate to a vial containing the appropriate reducing agents that is assembled in house.³⁸¹

5.3.2 Preparation of technetium-99m tricarbonyl

The synthesis of the *fac*-[^{99m}Tc(CO)₃]⁺ core (Scheme 19) was prepared fresh daily using the procedure reported by Alberto *et al.*³⁸¹ The eluted ^{99m}TcO₄⁻ saline solution (0.7 - 2.5 GBq) was combined to a mixture of sodium tetraborate decahydrate, sodium carbonate, potassium sodium tartrate tetrahydrate and disodium boranocarbonate. An incubation time of 20 min at 90°C was routinely used, and the progress on the reduction monitored via TLC as shown in Figure 104 B (eluent: saline solution, technetium(I) stays on baseline and technetium(VII) has an RF = 0.55).



Scheme 19: Scheme showing the synthesis of [^{99m}Tc(OH₂)₃(CO)₃]⁺ from Na^{99m}TcO₄, followed by labelling with TACN-benzyl amine

HPLC conditions were developed to allow analysis of the two different oxidation state species of technetium. Semi-preparative HPLC showed technetium(VII) (TcO₄⁻) eluted with a retention time of 3 min 50 sec in mainly aqueous conditions, whereas the technetium(I) ([^{99m}Tc(H₂O)₃(CO)₃]⁺) species eluted with a higher proportion of acetonitrile to give a broad peak at 25-28 min, see Figure 104.

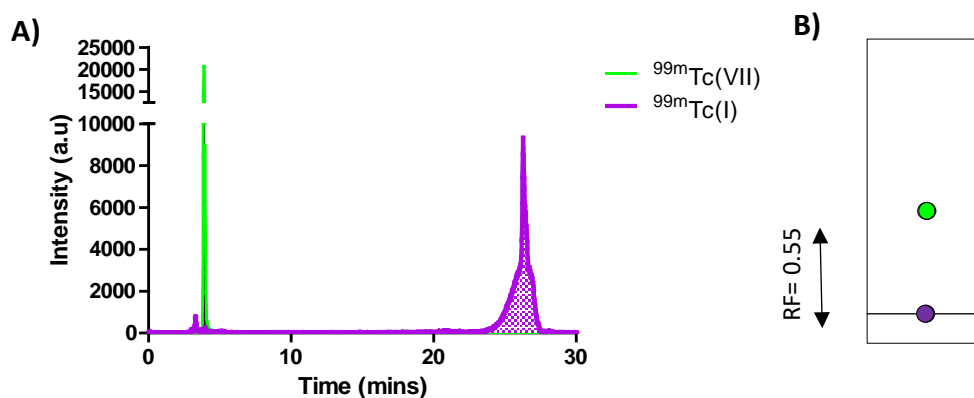


Figure 104: A) Graph showing the overlay HPLC chromatographs of ^{99m}Tc(VII) (green), ^{99m}Tc(I) (purple) species. B) Schematic representation of the radio-TLC of the separation of the of ^{99m}Tc(VII) (green), ^{99m}Tc(I) (purple) species, carried out in saline solution.

Overall reduction yields (integration of TLC) showed a yield of between *ca.* 65-90% achieved with each elution. This yield is lower than has been reported for reduction of technetium(VII) with the same reagents. Sogbein *et al.* reported a \geq 95% determined by HPLC when the reducing agents were purged with nitrogen for 10 mins before being heated at 70° C for 30 mins.³⁸² The lower yield is most likely due the vial used and how well it retains the inert atmosphere. Sogbein *et al.* carried

out reductions in a penicillin vial, whereas HPLC vials were used in this work (purged with argon for 10 mins).

5.3.3 Optimisation of radiolabelling conditions for **44**

To determine the optimum conditions for labelling of the CXCR4 antagonists, experiments were conducted using the TACN component **44**, as this was available in larger amounts for repeat reactions. It was not expected that attachment to the antagonist would significantly affect labelling procedure.

Initially, different buffers at varying pHs were investigated, each time using approximately 5-25 MBq of $fac-[^{99m}Tc(OH_2)_3(CO)_3]^+$ in 200 μ L of the de-gassed buffer. Reaction conditions consisted of 2 mM concentration of **44**, heated at 90°C and shaken at 500 RPM for 30 min. The procedure was a modified version of that reported by Lipowska *et al.*, in which a tracer derived from aspartic-*N*-monoacetic acid was radiolabelled with $fac-[^{99m}Tc(OH_2)_3(CO)_3]^+$ at 90°C for 30 min in high radiolabelling yields.³⁸³

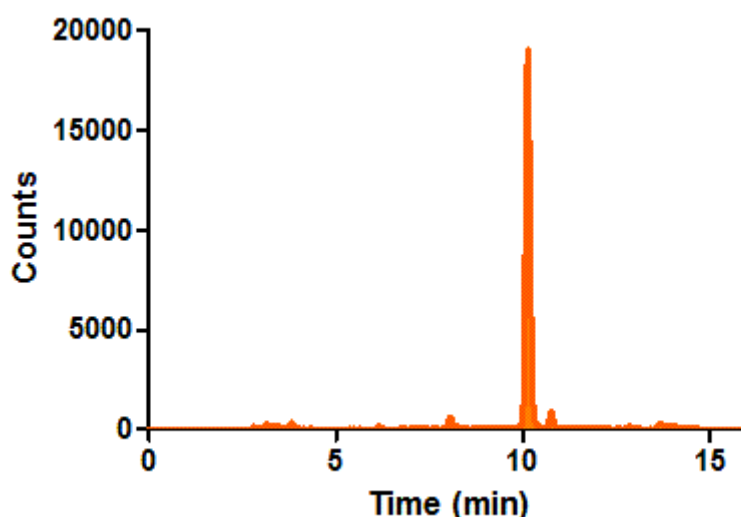


Figure 105: Radio-HPLC chromatograph of compound $[^{99m}Tc][Tc(CO)_3\mathbf{44}]^+$ eluting at 10 min and 20 sec.

The reactions were monitored by HPLC, as shown in Figure 105 $[^{99m}Tc][Tc(CO)_3\mathbf{44}]^+$ elutes at *ca.* 10 min 20 sec, and integration of the peak area showed >95% radiolabelling yield. This yield was validated by the performance of a column recovery ensuring radiation was not being retained.

Table 22: Table showing the variations in yield using different buffers and pH values (n=1).

Solvent	pH	Temperature (°C)	Percentage Radiolabelled
Aqueous	11	90	81
	7		46
0.1 M Phosphate	11	90	88
	7		89
0.1 M sodium acetate	11	90	94
	6		27
0.1 M HEPES	11	90	88
	6		27
0.1 M PBS/30% MeOH	11	90	92
	7		57

Table 22 lists the yields achieved under different reaction conditions. The buffers selected have all been reported in the literature for labelling TACN with technetium-99m.^{342, 350, 364, 384, 385} A range of pH values were investigated, from neutral (pH 6-7) to basic (pH 11), to determine the optimum buffer salt and pH for labelling.

As shown in Table 22, the highest yield was achieved using sodium acetate as the buffer at pH 11; however as these reactions were the result of a single measurement it is likely that all of the results between 81-94% are within experimental error of the TLC measurement. Therefore, all of the aqueous solvent systems at basic pH showed high labelling yields. These results agree with the literature reports, where basic pH values show higher labelling yields, due to the deprotonation of the nitrogen donors of TACN, which will be quaternised at neutral pH.³⁴⁹

Most of the aqueous buffers at neutral pH showed a low labelling yield (27-57%) except sodium phosphate buffer (pH 7, 88%, see Table 22). This is in agreement with the labelling yields reported by Kasten *et al.* who radiolabelled biomolecules conjugated to 2,2'-dipicolylamine (DPA) with *fac*-[^{99m}Tc(OH₂)₃(CO)₃]⁺ in sodium phosphate buffer (pH 7.4).³⁵⁰ Suzuki *et al.* also reported high radiolabelling yields of TACN with phosphate buffer (pH 7.4).⁹⁷

Therefore, sodium phosphate buffer (pH 7) is effective for achieving high labelling yield with pH sensitive tracers such as peptides, antibodies and viruses, however as the tetraazamacrocyclic CXCR4 antagonists are stable at both high and low pH further optimisation of radiolabelling conditions was carried out at pH 11.

Labelling was shown to occur at high temperatures, but there are literature reports of efficient labelling at room and physiological temperatures. The reactions were carried out as before with **44** in 200 μL of aqueous (pH 11) solution while being heated at either 25°C, 37°C or 90°C. After 30 mins at room temperature none of the TACN-benzyl amine had labelled, with only a small increase seen at the elevated temperature of 37°C. This is in line with what has been seen with labelling of cyclam with the $\text{fac-}[^{99\text{m}}\text{Tc}(\text{CO})_3]^{3+}$ moiety in the past. Vanbilloen *et al.* reported poor labelling at temperatures below 70°C, with a >90% achieved at 100°C.³⁵⁷

The reports of radiolabelling biomolecules with $\text{fac-}[^{99\text{m}}\text{Tc}(\text{OH}_2)_3(\text{CO})_3]^+$ at 37°C all require a longer reaction time to achieve effective labelling yields. In 2012, Mees *et al.* reported labelling of a His-tagged protein with $\text{fac-}[^{99\text{m}}\text{Tc}(\text{OH}_2)_3(\text{CO})_3]^+$ at 37°C but this required an incubation time of 1-1.5 hours.³⁸⁴ Similarly Badar *et al.* reported the radiolabelling of another His-tagged protein with $\text{fac-}[^{99\text{m}}\text{Tc}(\text{OH}_2)_3(\text{CO})_3]^+$ at 37°C which required over 2 hours.³⁸⁶

Although increasing reaction time for labelling **44** at 37°C is likely to increase labelling yield, as higher temperatures do not degrade the azamacrocyclic compounds, the more convenient short reaction time of 30 mins at 90°C was selected.

The lowest concentration to achieve *ca.* 100% radiolabelling was determined. Concentrations of **44** ranging from 0.1 μM to 12 mM (each 150 μL corresponding to amounts of 15 pmol–100 μmol) were tested and the percentage radiolabelling yield was determined by HPLC.

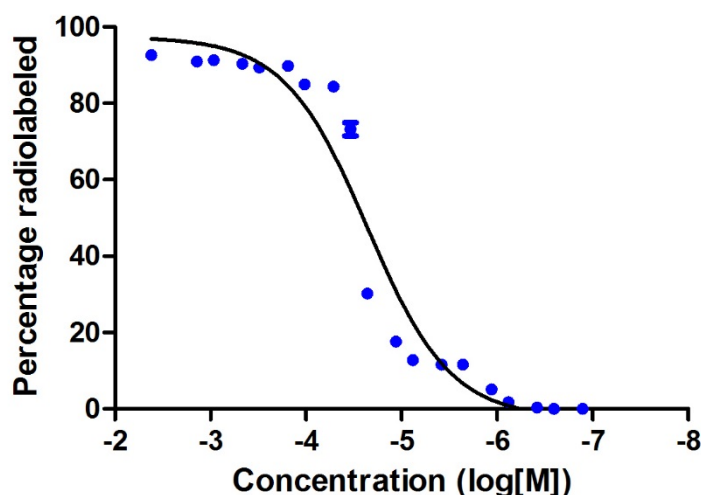


Figure 106: The effect of varying the concentration (M) of compound **44** on radiolabelling efficiency ($n = 3$).

Figure 106 shows the different concentrations that were tested ($n = 3$). Figure 106 gives an EC_{95} value of *ca.* 0.5 μM . Therefore, the developed conditions for labelling compounds **49** and **51** used 0.5 μM (75 pmol) of antagonist in aqueous solution (pH 11), heated and shaken at 90°C (500 RPM for 30 mins).

5.3.4 Radiolabelling of **49**

$[^{99m}\text{Tc}][\text{Tc}\mathbf{49}]^+$ was successfully radiolabelled using the conditions optimised for **44**. $[^{99m}\text{Tc}][\text{Tc}\mathbf{49}]$ was purified by semi-preparative HPLC with the peak of interest eluting (identified using the cold standard, $[\text{Re}\mathbf{49}]$) at 7 min 15 sec. The fraction was then dried using the addition of ethanol (*ca.* 2.5 mL) before being reconstituted in PBS to give $[^{99m}\text{Tc}][\text{Tc}(\text{CO})_3\mathbf{49}]^+$ in a decay corrected radiochemical yield of $39.8 \pm 2.8\%$ ($n = 2$).

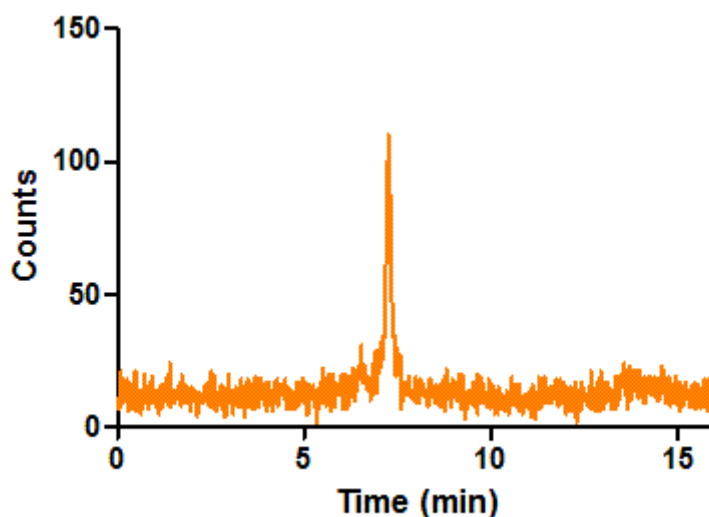


Figure 107: Radio-HPLC of compound $[^{99m}\text{Tc}][\text{Tc}(\text{CO})_3\mathbf{49}]^+$ taken after 3 hours stability in PBS solution at 37°C.

$[^{99m}\text{Tc}][\text{Tc}\mathbf{49}]^+$ was evaluated for stability in PBS solution at 37°C with samples analysed by radio-HPLC every 30 mins up to three hours. Figure 107 shows the HPLC trace taken after three hours in PBS solution, showing 100% stability.

The partition coefficient of $[^{99m}\text{Tc}][\text{Tc}(\text{CO})_3\mathbf{49}]^+$ was determined, -1.48 ± 0.04 ($n = 3$). This is higher than the partition coefficient values determined for the gallium-68 labelled antagonist described in Chapter 3. The decrease in hydrophilicity of the TACN BFC compounds (compared to DOTA) would be expected due to the inclusion of the more lipophilic $\text{Tc}(\text{CO})_3^+$ moiety.

5.3.5 Radiolabelling of **51** and its derivatives

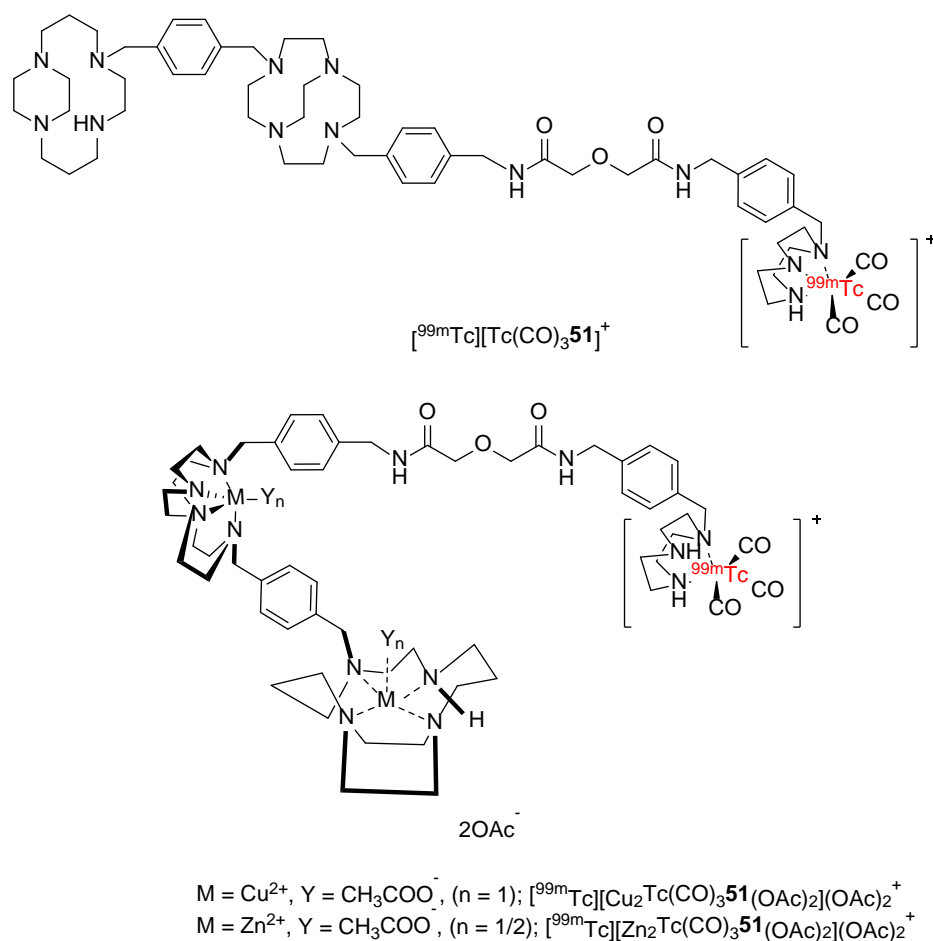


Figure 108: Structure of technetium-99m radiolabelled compound **51** and bis-copper derivative.

The multi-macroyclic compound $[\text{}^{99\text{m}}\text{Tc}][\text{Tc}(\text{CO})_3\mathbf{51}]^+$ (shown in Figure 108) was radiolabelled using the conditions previously discussed in section 5.3.1. 75 pmol of **51** was made up in aqueous solution (pH 11) and combined with 47-331 MBq of *fac*- $[\text{}^{99\text{m}}\text{Tc}(\text{CO})_3]^+$ to give an overall reaction volume of 200 μL . The reaction was heated at 90°C and shaken (500 RPM), before purification by semi-preparative HPLC, with the broad peak at *ca.* 12 min identified as the product by the use of non-radioactive rhenium compound ($[\text{Re}(\text{CO})_3\mathbf{51}]^+$) to give the product in a decay corrected radiochemical yield of $43.3 \pm 7.1\%$ ($n = 5$).

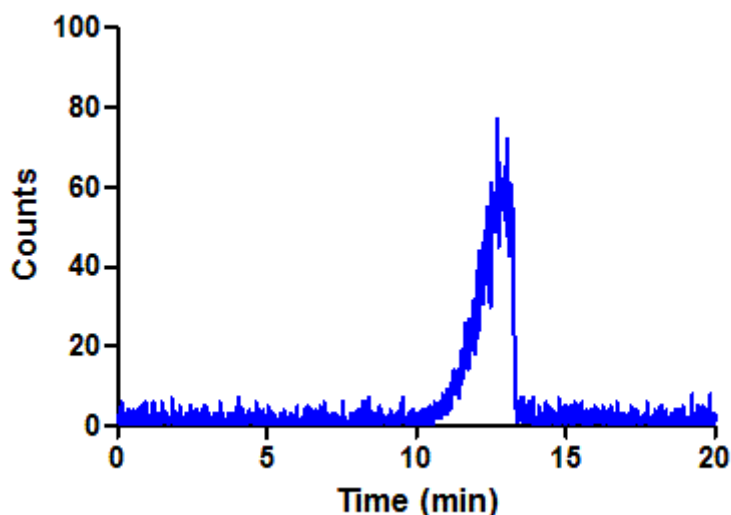


Figure 109: Radio-HPLC trace of compound $[^{99m}\text{Tc}][\text{Tc}(\text{CO})_3\mathbf{51}]^+$ taken after 3 hours in PBS solution at 37°C.

Figure 109 shows the radio-HPLC trace obtained after three hours incubation at 37°C in PBS solution for $[^{99m}\text{Tc}][\text{Tc}\mathbf{51}]$ demonstrating the stability of the compound with no sign of transchelation or degradation. The stability of $[^{99m}\text{Tc}][\text{Tc}(\text{CO})_3\mathbf{51}]^+$ was also assessed under acidic conditions; after the semi-prep run, the solution is at pH 3.5 due to the presence of TFA in the mobile phase. This solution was heated at 37°C and analysed by HPLC at 30 min intervals. As with the PBS solution, the $[^{99m}\text{Tc}][\text{Tc}(\text{CO})_3\mathbf{51}]$ complex proved to be stable over the three hour period.

Stability tests using bovine serum were also carried out using *ca.* 4 MBq of $[^{99m}\text{Tc}][\text{Tc}(\text{CO})_3\mathbf{51}]^+$. The mixture was heated at 37°C, and an aliquot of the solution was taken at 30 min intervals and denatured with methanol. The samples were centrifuged and the supernatant analysed using HPLC. However, the radioactivity was retained within the protein pellet. It is unlikely that the technetium-99m has completely transchelated, as it has been proven to be stable in PBS and acidic solution. Therefore, $[^{99m}\text{Tc}][\text{Tc}(\text{CO})_3\mathbf{51}]^+$ appears to bind to proteins within the bovine serum.

The interaction with serum proteins does correspond with reports in the literature.³⁴⁵ It was concluded that the non-specific binding seen could be due to the *fac*- $[^{99m}\text{Tc}(\text{CO})_3]^+$ moiety undergoing a ligand exchange with proteins present in the bovine serum. Bovine serum mainly consists of albumin, which contains six accessible histidine residues on the surface (with sixteen in total).³⁸⁷ The *fac*- $[^{99m}\text{Tc}(\text{CO})_3]^+$ moiety could possibly be forming one or more coordination bonds to these histidine residues via ligand exchange of a carbonyl or one of the TACN nitrogens. Whether this is binding $[^{99m}\text{Tc}][\text{Tc}(\text{CO})_3\mathbf{51}]^+$ intact to the protein or transchelating is unknown and needs further investigation.

The partition coefficient of $[^{99m}\text{Tc}][\text{Tc}(\text{CO})_3\mathbf{51}]^+$ was determined giving a $\log P$ value of -1.50 ± 0.04 ($n = 3$), similar to that of $[^{99m}\text{Tc}][\text{Tc}(\text{CO})_3\mathbf{49}]^+$.

$[^{99m}\text{Tc}][\text{Cu}_2\text{Tc}(\text{CO})_3\mathbf{51}(\text{OAc})_2](\text{OAc})_2$ (structure shown in Figure 108) was also successfully radiolabelled using the optimised conditions. Purification was carried out using semi-preparative HPLC, with the radiolabelled complex, $[^{99m}\text{Tc}][\text{Cu}_2\text{Tc}(\text{CO})_3\mathbf{51}(\text{OAc})_2](\text{OAc})_2^+$ eluting earlier than the metal free derivative, $[^{99m}\text{Tc}][\text{Tc}(\text{CO})_3\mathbf{51}]^+$, matching with the elution order observed for the rhenium cold standards (see Section 5.2.3). A radiochemical decay corrected yield of 46.0% ($n = 1$) was achieved after semi-preparative HPLC purification and transfer to PBS.

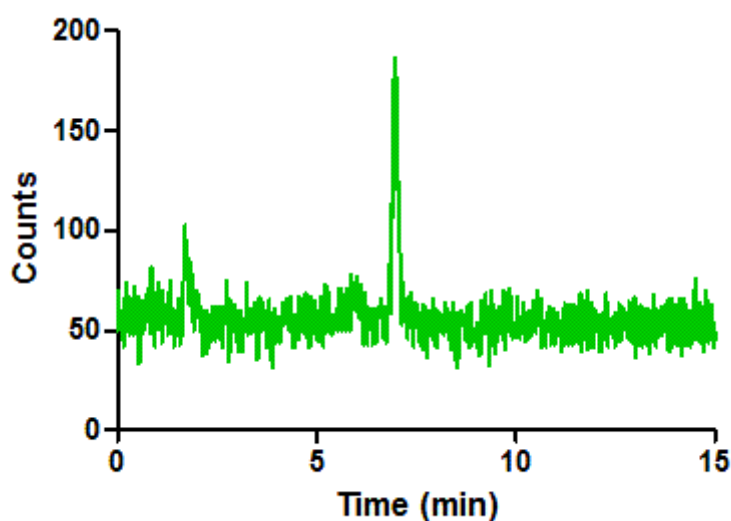


Figure 110: Radio-HPLC of compound $[^{99m}\text{Tc}][\text{Cu}_2\text{Tc}(\text{CO})_3\mathbf{51}(\text{OAc})_2](\text{OAc})_2^+$ taken after three hours stability in acidic (0.1% TFA) solution at 37°C.

Stability studies were again carried out in PBS and acidic solution over a period of three hours at 37°C. Figure 110 shows the radio-HPLC traces collected after three hours in acidic conditions, at this time point the small peak due to the 'free' technetium(I) species can be seen at 2 min 20 sec. Bovine serum stability was also investigated for compound $[^{99m}\text{Tc}][\text{Cu}_2\text{Tc}(\text{CO})_3\mathbf{51}(\text{OAc})_2](\text{OAc})_2^+$; however, as was observed for $[^{99m}\text{Tc}][\text{Tc}\mathbf{51}]^+$, the radioactive material was bound to the protein pellet and could not be extracted for HPLC analysis.

The $\log P$ value obtained for $[^{99m}\text{Tc}][\text{Cu}_2\text{Tc}(\text{CO})_3\mathbf{51}(\text{OAc})_2](\text{OAc})_2^+$ is 0.59 ± 0.22 ($n = 3$). The decrease in hydrophilicity can be attributed to nitrogen atoms on the cyclam and cyclen rings no longer being able to form H-bonds due to the formation of the copper(II) complex.

5.4 *In vitro* CXCR4 receptor binding studies

To determine the affinity of the technetium-99m probes discussed in this chapter an *in vitro* assay was carried out to determine how efficiently the molecules could block the CXCL12 initiated signalling process. The calcium signalling assay has been used frequently as it is the most reliable measure of the antagonist properties of molecules binding to CXCR4. It can be complex to set up to give reproducible results, hence all of the compounds were analysed by the research group of Prof Dominique Schols at the Rega Institute (KU Leuven) where the assay was originally developed. The results can be used to identify which antagonists could be investigated as CXCR4 SPECT imaging probes.

Table 23: Table showing the IC₅₀ values determined by for bis-macrocyclic compounds. Concentration required to reduce the level of Ca²⁺ ions observed during a 'normal' signalling process by 50% (IC₅₀) in U87-CXCR4 cells.

Antagonist	Calcium Signalling IC ₅₀ ^a /nM U87-CXCR4
44	>5000
49	>5000
[Cu 49 (OAc)](OAc)	>5000
[Re(CO) ₃ 49] ⁺	>5000
51	2022
[Re(CO) ₃ 51] ⁺	1883
[Cu ₂ 51 (OAc) ₂](OAc) ₂	79
[Zn ₂ 51 (OAc) ₂](OAc) ₂	2894
[Cu ₂ Re(CO) ₃ 51 (OAc) ₂](OAc) ₂ ⁺	136
[Zn ₂ (CO) ₃ Re 51 (OAc) ₂](OAc) ₂ ⁺	>5000
AMD3100	175

As expected **44** and **49** and the metal complexes of **49** (the mono-tetraazamacrocycle derivative) showed low affinity towards the CXCR4 receptor with no measurable activity in the range investigated (up to 5 μM). The bis-tetraazamacrocyclic compound **51** and its non-radioactive rhenium analogue ([Re(CO)₃**51**]⁺) both showed μM level activity, however previous characterisation using this assay has indicated that values around (or below) 100 nM are needed to give sufficient binding capability for *in vivo* imaging to be effective.

Addition of copper(II) ions to the tetraazamacrocycle components to give [Cu₂**51**(OAc)₂](OAc)₂ and [Cu₂Re(CO)₃**51**(OAc)₂](OAc)₂⁺ resulted in the most potent compounds, see Table 23, with IC₅₀; 79 and 136 nM. Both antagonists have a lower IC₅₀ value than AMD3100 which was included as a control. These values are consistent with the expectation that inclusion of

transition metals into the cyclam/cyclen rings increases binding affinity for the CXCR4 receptor. It was an unexpected result that the zinc(II) complexes had low affinity for the receptor, it would be predicted for this structural type that the zinc(II) complexes would be at least as active as the copper(II) complexes due to the flexibility in coordination sphere and geometry. This is an anomalous result for this class of compounds in the wider context of other work carried out in the Archibald group (with over 1000 compounds analysed). $[\text{Zn}_2\text{Re}(\text{CO})_3\mathbf{51}(\text{OAc})_2](\text{OAc})_2^+$ was synthesised from the analysed batch of $[\text{Zn}_2\mathbf{51}(\text{OAc})_2](\text{OAc})_2$, therefore if there was an impurity or other problem with the first compound this would be carried forward to the second compound. Ideally the zinc(II) complexes would be resynthesised as a fresh batch and the assay re-run. It seems unlikely that the assay result is correct but it is not immediately obvious where the issue lies as the complex was analysed and purified. Further research work is required to confirm or refute these results and other assays could be used to assess the compounds.

5.5 Conclusion

This chapter outlines the synthesis of mono- and bis-tetraazamacrocyclic compounds that have been adapted to include a BFC that allows for labelling with technetium-99m, as the technetium(I) tricarbonyl species. Metal ion complexes of **49** and **51** were formed and purified and a “cold standard” (rhenium compound) was prepared and characterised for each compound. HPLC/TLC conditions were developed for identification of the different oxidation state technetium-99m species. Optimisation of radiolabelling conditions was carried out using the TACN precursor and found to give the highest yield under the following conditions: basic aqueous solution, 0.5 μM (75 pmol) and heated at 90°C for 30 min.

An *in vitro* CXCL12 stimulated calcium signalling assay was carried out on the library of compounds produced. Antagonist $[\text{Cu}_2\text{Re}(\text{CO})_3\mathbf{51}(\text{OAc})_2](\text{OAc})_2^+$ was shown to be a more potent antagonist than AMD3100. Hence the technetium analogue of this compound was the most promising candidate to select for further investigation as a CXCR4 targeting SPECT imaging probe.

49, **51** and $[\text{Cu}_2\mathbf{51}(\text{OAc})_2](\text{OAc})_2$ were successfully labelled with technetium-99m tricarbonyl and stability/logP determined. Stability in acidic solutions and PBS solution showed a stability of >95% after 3 hours. However, studies carried out in bovine serum showed complete binding to the proteins present. It is unlikely that transchelation of the technetium-99m radioisotope is occurring due the stability in the other media. The *fac*- $[\text{}^{99\text{m}}\text{Tc}(\text{CO})_3]^+$ moiety has previously been reported to suffer from high retention to blood proteins in the literature.^{347, 348} This has been attributed to ligand exchange of carbonyl groups on the *fac*- $[\text{}^{99\text{m}}\text{Tc}(\text{CO})_3]^+$.

The serum protein interaction seen with the tracers could be problematic. However, further studies are needed to assess the potential of these tracers as *in vivo* CXCR4 imaging agents. In the best case scenario, the protein binding could be beneficial as it could increase circulation time in the bloodstream, possibly leading to higher CXCR4 binding in the tumour. Further work is needed to investigate this and, dependent on the results, modification of the structure to reduce protein binding.

5.6 Future work

Further work to investigate and understand the protein binding mechanism in bovine serum would be of interest. Several proteins can be tested, with albumin and beta/ gamma globulins forming the major protein components of bovine serum they would be the obvious initial targets for testing.³⁸⁸ Biodistribution data *in vivo* would also be useful to assess to what degree the protein binding effects the circulation and retention of these tracers. A competition reaction with histidine could also be carried out, as a competing ligand for the $fac-[^{99m}Tc(CO)_3]^+$ moiety (ideally complexed with the TACN) would reveal if exchange of the carbonyl groups occurs. A series of reactions varying concentrations of histidine (10-100 nmol/mL) mixed with the labelled compound and sampled to monitor the reaction by HPLC at various time points would be a useful approach. A similar study was conducted by Suzuki *et al.* to determine the stability of a series of $fac-[^{99m}Tc(CO)_3]^+$, they were able to determine which structure were the least liable for further *in vivo* validation.⁹⁷

Braband *et al.* by-passed the protein binding issue seen for the $fac-[^{99m}Tc(CO)_3]^+$ moiety by instead using $fac-[^{99m}Tc(O)_3]$ to label the TACN BFC.^{360, 361} The group reports that the $fac-[^{99m}Tc(O)_3(TACN)]^+$ complex demonstrated high *in vivo* stability and had rapid excretion, in contrast to the pharmacokinetic profile observed for $fac-[^{99m}Tc(CO)_3]^+$ complexes. Therefore, labelling of the CXCR4 antagonist could be carried out using the $fac-[^{99m}Tc(O)_3]^+$ moiety instead. Optimisation of the properties could give a promising tracer for SPECT imaging of CXCR4 expressing tumours *in vivo*.

As discussed in Section 5.4 further work is needed to resynthesise and test the zinc(II) bis-tetraazamacrocyclic compounds $[Zn_2\mathbf{51}(OAc)_2](OAc)_2$ and $[Zn_2Re(CO)_3\mathbf{51}(OAc)_2](OAc)_2^+$ which gave surprisingly low potency IC_{50} values in the *in vitro* CXCR4 binding assays.

Chapter Six

Synthesis of fluorescent dye labelled CXCR4 imaging probes

6. Strategy for optical probe design and current state-of-the-art in CXCR4 optical imaging

6.1 Introduction to optical imaging

Optical Imaging (OI) relies on the use of visible, ultraviolet or infrared light to give high resolution images to a sub-cellular level. The key advantages are the resolution and the non-ionising radiation with the disadvantage of poor tissue penetration due to absorption and scattering. Multimodality imaging allows for the advantages of OI to be paired with other imaging techniques to provide superior imaging quality.³⁸⁹

In clinical settings, fluorescent probes can be used to detect tumours close to the skin surface such as in breast cancer, together with use of an endoscopy cameras to allow imaging of tumours in the oesophagus or colon. Recently there has been a great deal of interest in fluorescent probes to allow intra-operative visualization for guidance to assist surgeons in the dissection of diseased tissue. Fluorophores in the UV and visible region suffer from light scattering and absorbed abundantly by tissue chromophores, in particular by haemoglobin and water, leading to considerable signal attenuation making them unsuitable for imaging tumours a few millimetres below the skin surface.³⁹⁰ Fluorophores which emit in the near-infrared (NIR) region in the range of 650-900 nm can penetrate more deeply (several centimetres) making them more practical for *in vivo* applications.³⁹¹

6.2 Overview of optical imaging probes for the the CXCR4 receptor

Radiolabelled [¹²⁵I]CXCL12 was initially utilised as a competitor in assays to evaluate the CXCR4-binding of synthetic compounds such as AMD3100^{121, 181}, AMD3465³⁹², and T140¹⁵⁴ and its derivatives.³⁹³ Methods using radioisotopes offer highly sensitive assays, however, they are expensive and not always feasible.³⁹⁴ Therefore, there was early interest in optical probes based on CXCR4 and the development of other CXCR4 specific fluorescent probes.

6.2.1 Optical imaging probes to target CXCR4 derived from CXCL12

In an early study in 2005 carried out by Dar *et al.*, CXCL12 was fluorescently tagged for the visualisation of the CXCR4-dependent internalisation of CXCL12 by stromal bone marrow cells.³⁹⁵ Dar *et al.* were the first to utilise fluorescein isothiocyanate FITC-CXCL12 as an imaging probe, this was followed by a study reported in 2006 by Kollet *et al.* to show the role of bone resorbing osteoclasts in homeostasis and stress induced mobilisation of progenitor cells.³⁹⁶

In 2011, Meincke *et al.* reported the conjugation of CXCL12 with a NIR fluorescent dye; IRDye®800CW-*N*-Hydroxy-succinimide ester ($E_{\text{max}}/E_{\text{mmax}} = 778/779 \text{ nm}$).³⁹⁷ The group were interested in both the sensitivity and selectivity of the probe binding to CXCR4 and also CXCR7; so consequently designed *in vitro* experiments using transfected MCF-7 cells which have high levels of

expression of CXCR4 and CXCR7 alongside glioma cells (A764) which only express CXCR7.³⁹⁸ The group carried out a series of *in vivo* studies in immunodeficient mice that were inoculated subcutaneously with MCF-7 and A764 cells, shown in Figure 111. Both tumours were visualised with the CXCL12 conjugate dye. Uptake of the conjugated dye can also be seen in the liver and bone marrow of the hind legs which are known to naturally express CXCR4.

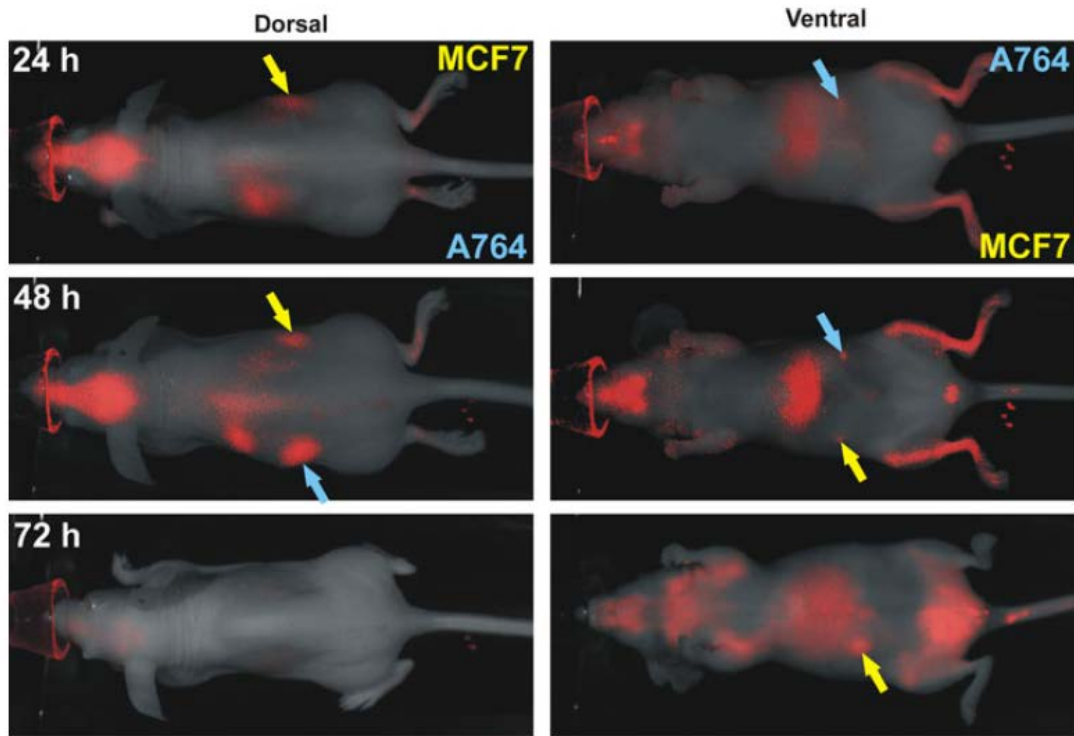


Figure 111: Visualisation of subcutaneous tumours in mice with CXCL12-IRDye800. MCF-7 breast tumour (yellow arrow) and A764 glioma cells (blue arrow) were implanted subcutaneously into the right and left flank respectively. (Reproduced from Meincke *et al.*)³⁹⁷

6.2.2 Optical imaging probes to target CXCR4 derived from peptides

In 2008, Oishi *et al.* built upon previously reported work on T140-based peptide derivatives as CXCR4 antagonists, to develop a series of fluorescently tagged peptides for imaging of the CXCR4 receptor.³⁹⁹ The peptide was successfully conjugated to fluorescein ($Ex_{max}/Em_{max} = 492/520$ nm) and Alexa Fluor® 488 ($Ex_{max}/Em_{max} = 495/519$ nm) by acylation to the α -amino group of the N-terminal Arg1 residue or on the D-lys8 residue via the ϵ -amino group shown in Figure 112, to synthesise a series of T140 derivatives; **L56-L65** (structures detailed in Table 24).

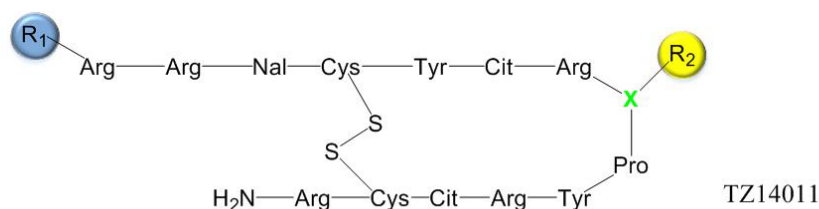


Figure 112: A schematic diagram of the fluorescently coupled peptide-conjugates derived for Ac-TZ14011 that have been investigated as optical probes for CXCR4. R1 and R2 indicate the sites of modification outlined in table 24.³⁹⁹⁻⁴⁰¹

Oishi *et al.* evaluated the library of peptides, **L56-L65**, for CXCR4-antagonist activity by measuring the inhibition of [¹²⁵I]CXCL12 binding to transfected CXCR4 Chinese hamster ovary (CHO) cells.³⁹⁹ The replacement of D-Lys8 in the parent peptide; **L56**, with D-glutamic acid; **L57**, showed no significant change on inhibition (IC_{50} **L56** =5.2 nM; IC_{50} **L57** =6.7 nM; Table 24). However, inclusion of fluorescein at the N-terminus (R₁; Figure 112) in derivatives of **L56** and **L57** led to a 5 fold decrease in binding affinity of the D-lys8 peptide **L58** (IC_{50} **L58** =24 nM; Table 24) and a 30 fold decrease for the D-Glu peptide **L59** (IC_{50} **L59** =199 nM; Table 24). This was also seen when the N- terminus was labelled with Alexa Fluor® 488 to give peptide **L60**, which caused a significant decrease in inhibitory activity (IC_{50} **L60** = 5700 nM; Table 24) compared to **L56**.³⁹⁹ Thus the presence of a fluorophore at the N-terminus was shown to disrupt binding to the CXCR4 receptor.

Alternatively, labelling at the ϵ -amino group of the D-lys8 (R₂; Figure 112) residue caused only a minor reduction in potency when labelled with fluorescein (IC_{50} **L61** =16 nM; IC_{50} **L62** =26 nM; Table 24). The inclusion of anaminocaproic acid residue (Acp) spacer was also employed in an effort to improve affinity and efficient coupling. The biotin-Acp-labelled peptide **L63** was revealed to be a potent inhibitor (IC_{50} **L63** =11 nM; Table 24). This would indicate that the D-lys8 position is less important in the direct docking of the peptide to the CXCR4 receptor making it a more appropriate position for labelling with a fluorophore. The Alexa Fluor® 488 labelled peptide **L64** without a Acp spacer showed nearly equipotent inhibitory activity to that of the parent peptide **L56** (IC_{50} **L64** =8.1 nM; Table 24). However, the use of the Acp spacer with the dye appeared to cause some unfavourable interaction with the receptor as potency decreases.

Table 24: Biological activity of fluorescently labelled T140 analogues. ^aIC₅₀ values obtained with [¹²⁵I]CXCL12 on CHO cells unless otherwise stated; ^bIC₅₀ values obtained with [¹²⁵I]CXCL12 on HeLa-CD4-CCR5 cells.^{399, 401}

Peptide derivative	IC ₅₀ value ^a (nM)	Reference
L56: R ₁ =acetyl; R ₂ = H; X=D-Lys	5.2	399
L57: R ₁ =acetyl; R ₂ = H; X=D-Glu	6.7	399
L58: R ₁ =fluorescein; R ₂ = H; X=D-Lys	24	399
L59: R ₁ =fluorescein; R ₂ = H; X=D-Glu	199	399
L60: R ₁ = Alexa Fluor [®] 488; no R ₂ ; X=D-Glu	5700	399
L61: R ₁ =acetyl; R ₂ =fluorescein; X=D-Lys	16	399
L62: R ₁ =acetyl; R ₂ =fluorescein- Acp; X=D-Lys	26	399
L63: R ₁ =acetyl; R ₂ =biotin-Acp; X=D-Lys	11	399
L64: R ₁ =acetyl; R ₂ =Alexa [®] Fluor 488; X=D-Lys	8.1	399
L65: R ₁ =acetyl; R ₂ =Alexa [®] Fluor 488-Acp; X=D-Lys	267	399
L66: R ₁ =acetyl; R ₂ =TAMRA-hexamethylene; X=D-Lys	14 ^b	401
L67: R ₁ =acetyl; R ₂ =Fluorescein-hexamethylene; X=D-Lys	11 ^b	401

The two most potent peptides **L61** and **L64** that had been modified with fluorescein and Alexa Fluor[®] 448 at the D-lys8 residue were studied *in vitro*. Confocal microscopy studies were carried out on transfected CXCR4-expressing HEK293 cells, CXCR7-expressing HEK293 cells and CXCR4-negative cell line. The cell surface of the CXCR4-expressing cells were visibly stained with both peptides **L61** and **L64**, with no non-specific uptake in the cytoplasm observed. Furthermore, the lack of fluorescence in the control and importantly the CXCR7-expressing cell-line showed the selectivity of these T140 derivatives for CXCR4.

In a follow up study Nomura *et al.* synthesised a T140 derivative which incorporated a hexamethylene spacer between the fluorescent probe and the peptide.⁴⁰¹ Covalent attachment of 5-carboxytetramethylrhodamine, (TAMRA, structure shown in Figure 112, Ex_{max}/Em_{max} = 555/576 nm) forming peptide **L66**, and attachment of fluorescein to give peptide **L67**. The inclusion of the hexamethylene spacer was designed to increase the distance between the bulky fluorescent probe and the interacting residues (Arg2, Nal3, Tyr5 and Arg14) on the T14011; which are key to CXCR4 binding activity.

Peptides **L66** and **L67** were both shown to be a potent antagonists (IC₅₀ **L66** =14 nM; IC₅₀ **L67** =11 nM; Table 24) and specific to CXCR4. Nomura *et al.* went on to demonstrate the potential use of peptide **L67** as an alternative in binding inhibition assays for use in high throughput screening of potential pharmacophores by comparing IC₅₀ values determined with [¹²⁵I]CXCL12 of twenty-four

cyclic pentapeptide derivatives of FC131. Correlation between the two sets of data demonstrating that fluorescent probes could be used to determine binding affinities of CXCR4 targeting agents.

Other research groups have also developed alternative Ac-TZ14011 derivatives and other short fluorophore labelled peptides in an attempt to form a CXCR4 specific optical imaging probe.^{327, 400, 402, 403} However, most had disadvantages compared with those already discussed.^{400 404} Van de Berg *et al.* also adapted the structure of Ac-TZ14011. The group incorporated fluorescein isothiocyanate (FITC) ($E_{x_{max}}$ 494 nm/ $E_{m_{max}}$ 520 nm) at the D-lys8 position of Ac-TZ14011.⁴⁰⁰ IC_{50} values were not reported and confocal studies showed non-specific cellular uptake (see Figure 113).

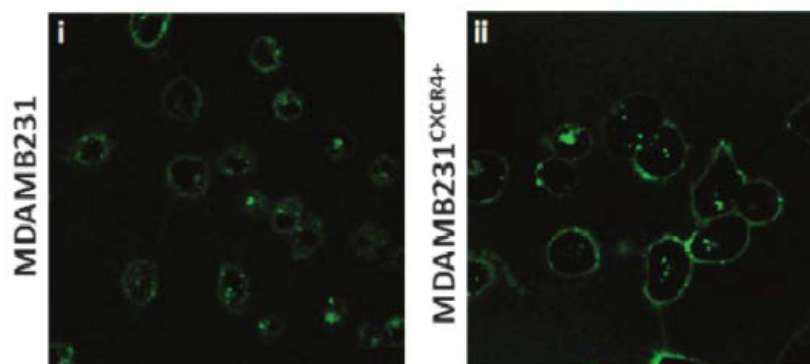


Figure 113: Confocal images of 0.1 μ M of Ac-TZ14011-FITC distribution in live MDAMB231 and MDAMB231^{CXCR4+} tumour cells. (Reproduced from Van de Berg *et al.*).⁴⁰⁰

There have been several reports of derivatives of FC131, [cyclo(-D-Tyr-Arg-Arg-Nal-D-cys-), being fluorescent labelled for imaging the CXCR4 receptor. Tanaka *et al.* reported the synthesis of a series of bivalent FC131 compounds (**L68-L70**) containing poly-L-proline and PEGylated poly-L-proline- type linkers.⁴⁰⁵ Of the compounds synthesised, **L68** and **L69** (structures shown in Figure 114), showed promising IC_{50} values of 9.9 and 13.9 nM respectively, greater than FC131 (31.5 nM). Tanaka *et al.* suggest that the increase in binding is due the bivalent FC131 ligand interacting with CXCR4 dimers formed in the cell membrane.⁴⁰⁶ The group carried out a series of confocal experiments with high and low expressing CXCR4 cell lines and were able to show affinity for the CXCR4 receptor.

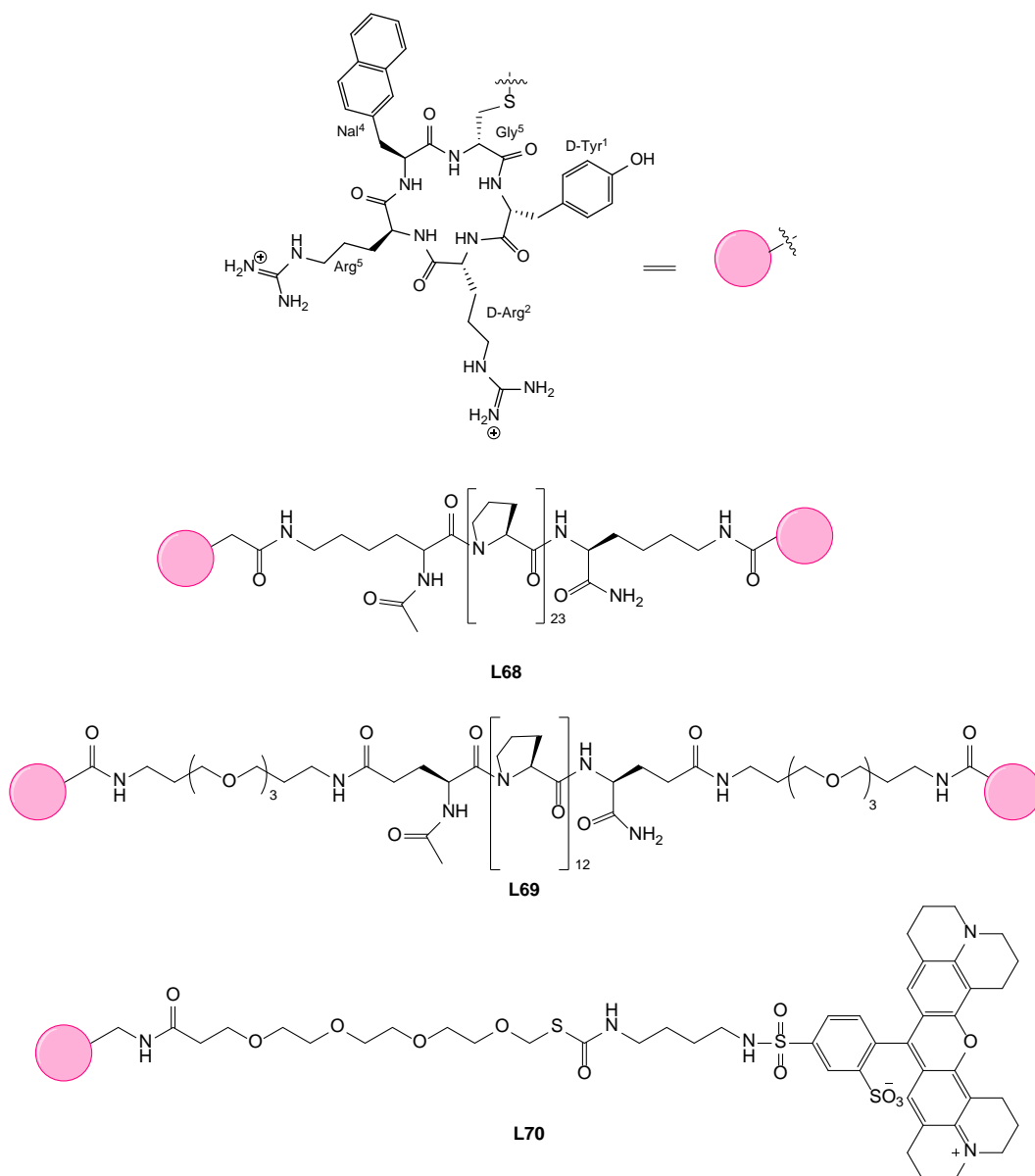


Figure 114: Structures of FC131 and bivalent derivatives.^{405, 407}

More recently, Nomura *et al.* explored the use of including a NIR cyanine dye with the poly-L-proline linkers again producing bivalent probes.⁴⁰⁸ There was a marked decrease in binding compared to the unlabelled bivalent ligand and monomer FC131 which were attributed to steric interactions with the cyanine dye. A similar strategy of labelling FC131 derivatives has also been reported by Tietz *et al.*, who conjugated the peptides and Texas Red bromoacetamide fluorescent dye ($E_{x_{max}}$ 589 nm/ $E_{m_{max}}$ 615 nm) on the surface of dextran coated iron oxide nanoparticles to produce multimodal PET/MRI imaging agents.⁴⁰⁷ Fluorescence microscopy studies with MDAMB-231 cells revealed rapid saturation and a uniform level of fluorescence, however, uptake in the cytoplasm revealed high levels of internalisation of the probe reducing the utility of this system (see Figure 115).

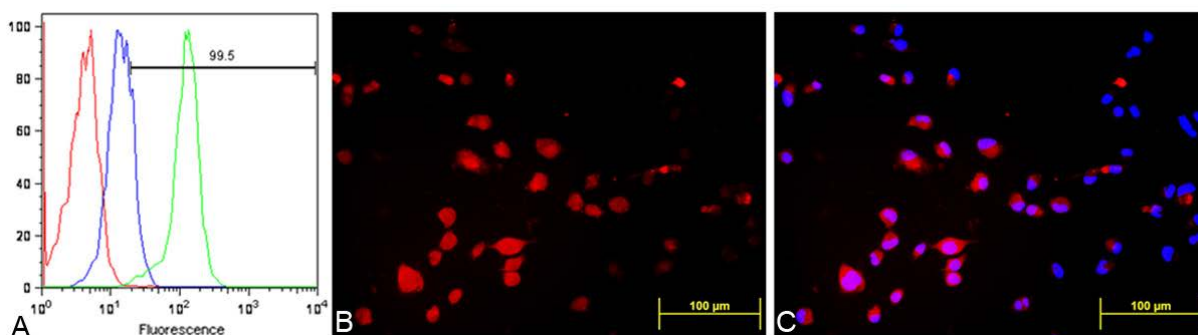


Figure 115: FACS analysis of MDA-MB-231 cells alone (red), incubated with a 100 nM (blue) and 1000 nM (green) dose of FC131-1-1-Red for 60 min at 37°C (A), fluorescence microscopy images of MDA-MB-231 cells after incubation with FC131-1-1-Red (B), co-localization with DAPI (C) (Reproduced from Nomura *et al.*).⁴⁰⁷

Santagata *et al.* reported the functionalisation of their previously developed CXCR4 targeting peptide (Arg-Ala-[Cys-Arg-Phe-Phe-Cys]) with the commercially available NIR Vivo Tag-S 750 dye.⁴⁰⁹ Figure 116 shows the confocal images collected for PepR-NIR750 probe in B16-CXCR4 cancer cells. The probe was shown to be specific for CXCR4 and *in vivo* validation of showed uptake in CXCR4 positive tumours and lung metastases.

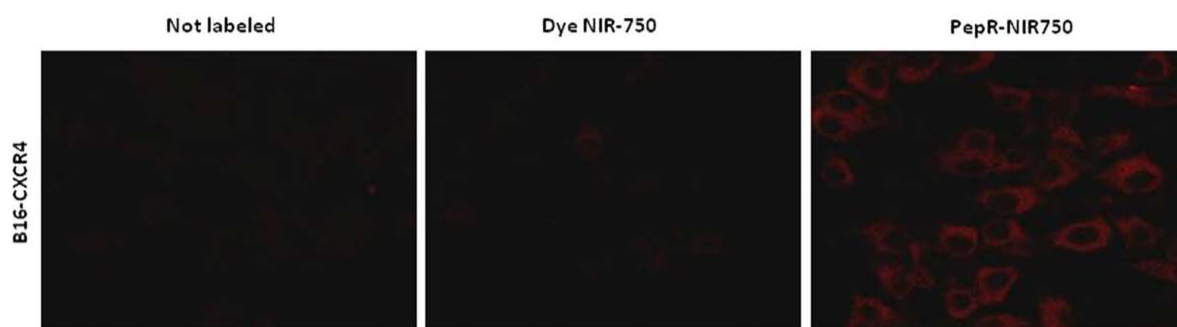


Figure 116: Confocal images for PepR-NIR750 and dye alone (NIR-750) showing binding to B16-CXCR4 tumour cells (Reproduced from Santagata *et al.*).⁴⁰⁹

6.2.3 Optical imaging probes derived from small molecule antagonists of CXCR4

Compared to the peptide-based probes, these small molecule probes have the advantage of greater stability, solubility and, in many cases, improved biodistribution.⁴¹¹⁻⁴¹³ However, the properties of small molecule antagonists are influenced to a greater extent by conjugation of the fluorophore which is likely to be of a similar size to the antagonist molecule itself.

In 2007, the Archibald group reported a low molecular weight CXCR4 antagonist consisting of a side-bridged cyclam macrocycle bound to a rhodamine isothiocyanate (RITC) moiety (**L71**, structure shown in Figure 117).⁴¹⁴ The inclusion of a paramagnetic metal ion such as copper(II), **L72**, had a significant quenching (*ca.* 75%) on the fluorescence signal of rhodamine. *In vitro* studies were carried out using Jurkat cells revealed that the copper(II) complex had a higher affinity than the free chelator. Metal complexed **L72** was able to effectively inhibit the binding of CXCR4-specific

antibodies, however, non-specific cellular uptake was observed in the confocal microscopy experiments possibly due to active transport processes.

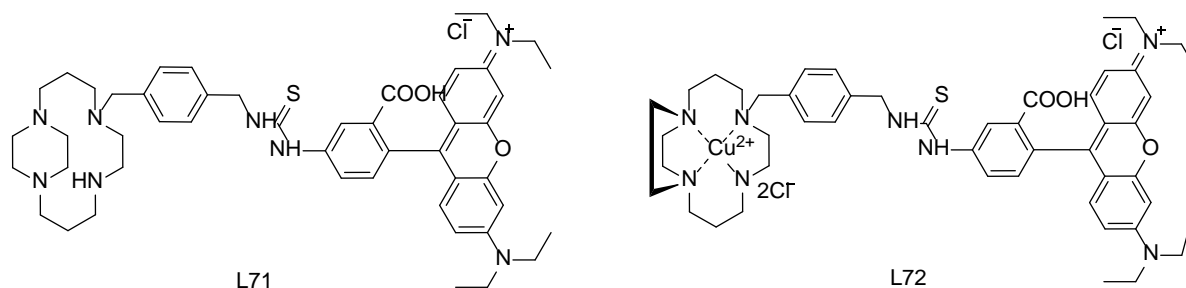


Figure 117: Structures of side-bridge cyclam RITC containing CXCR4 antagonists synthesised by Khan *et al.*⁴¹⁵

Another fluorescent small molecule derived from AMD3100 was reported by Knight *et al.* and incorporated an anthracene linker group, **L73**; as well as metal complexation with several transition metals, **L74-76** (structures shown in Figure 118).⁴¹⁶ Competition binding assays were conducted to determine the binding affinity of the free ligand, **L73**, and metal complexes, $[\text{Ni}_2\text{L73}]$, $[\text{Zn}_2\text{L73}]$ and $[\text{Cu}_2\text{L73}]$, the results revealing a significant loss in affinity when compared to AMD3100 (reduced from 0.6 to 3.4 μM).⁴¹⁶ The anthracene containing compounds showed non-specific binding via transport across the plasma membrane that was attributed to the increase in lipophilicity on addition of the anthracene group.

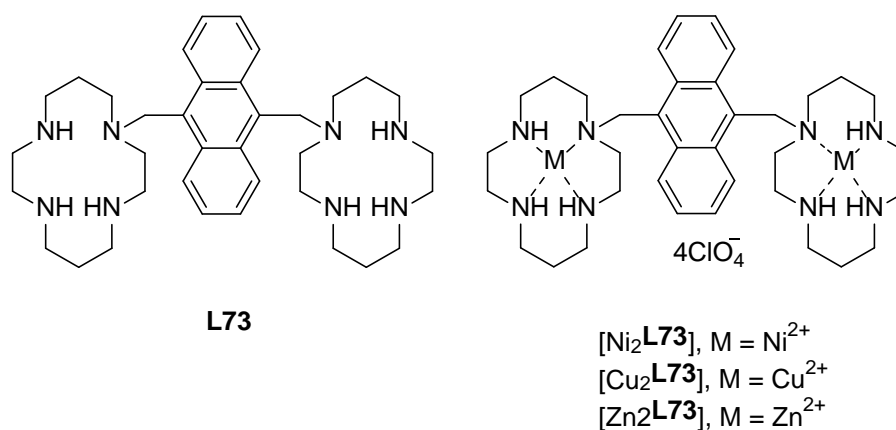


Figure 118: Structures of anthracenyl derivatives of AMD3100 and its metal complexes synthesised by Knight *et al.*⁴¹⁶

In 2011, Oltmanns *et al.* published a library of fluorescent cyclen macrocycle zinc(II) complexes with similar structural motif to that of AMD3100.⁴¹⁴ They evaluated their ability as apoptosis/necrosis imaging agents (**L74-L79**, Figure 119) and showed that the incorporation of zinc(II) cyclen groups affected the intensity of fluorescence. The group went on to radiolabel these complexes with fluorine-18 and reported PET scans that showed clearly a significant uptake in an irradiated tumour. It is stated in the paper that the compounds do not bind to CXCR4 however

subsequent work in the Archibald group has shown that this class of compounds have high affinity for the CXCR4 receptor.

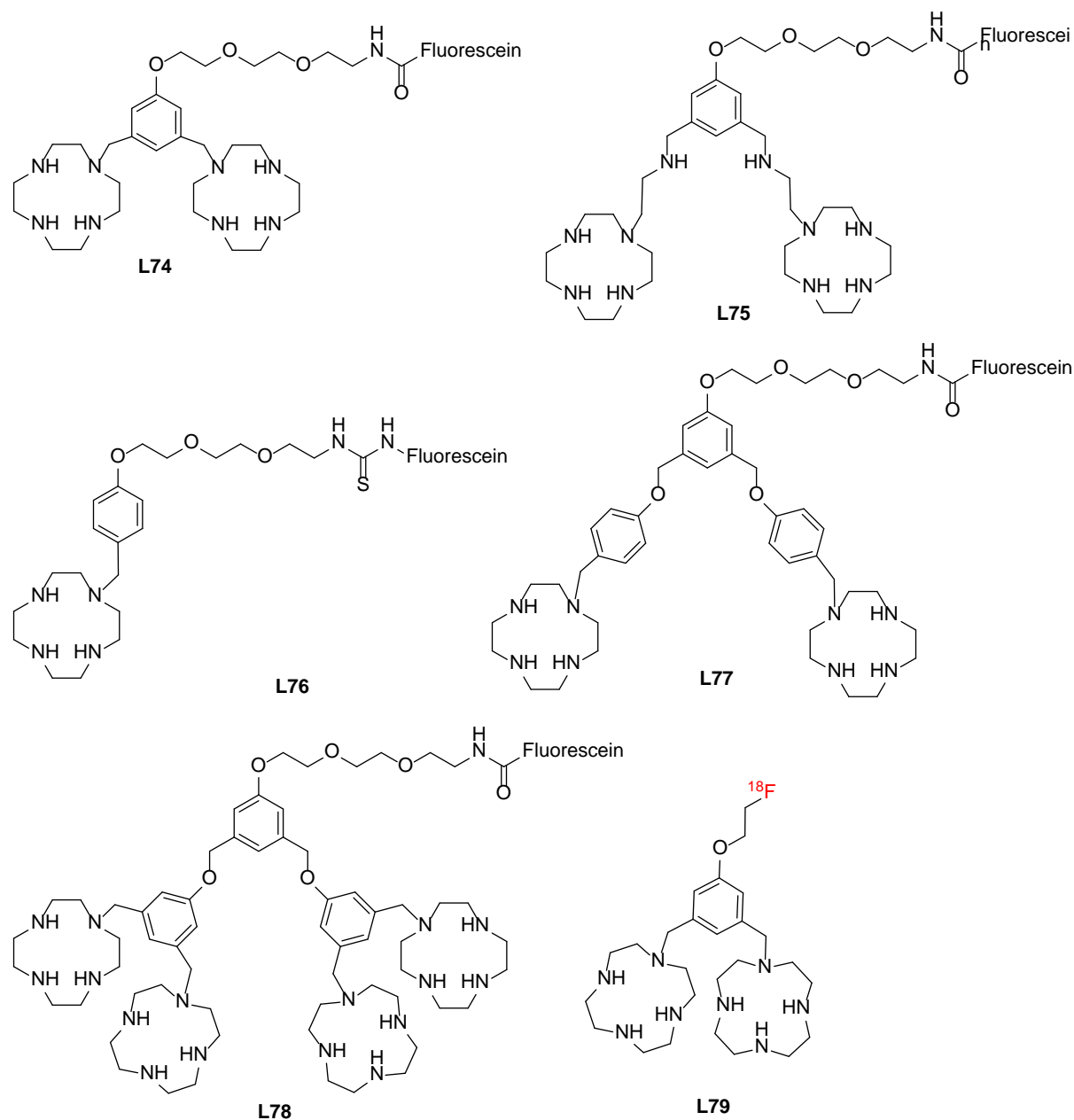
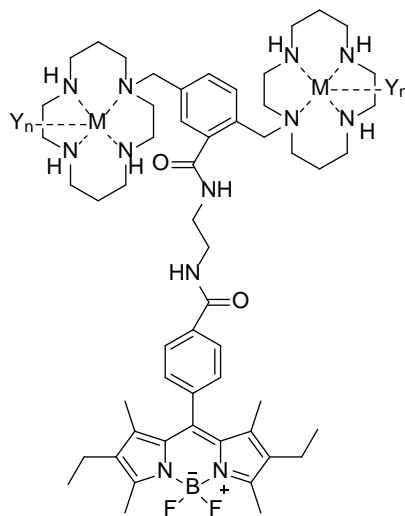


Figure 119: Structures of the fluorescent macrocycles synthesised by Oltmanns *et al.*⁴¹⁴

In 2015, Poty *et al.* reported the synthesis of BODIPY conjugated AMD3100 metal complex derivatives (structure shown in Figure 120, $E_{x_{max}}/E_{m_{max}} = 524/540$ nm).⁵³ The probes were complexes with nickel(II) ($[Ni_2L80]$) and zinc(II) ($[Zn_2L80]$) to enhance the affinity toward the CXCR4 receptor.⁵³ Poty *et al.* functionalised the phenyl moiety of the AMD3100 structure by the inclusion on an ester or an ethylenediamine moiety. However, IC_{50} values revealed that these modifications to

the phenyl moiety had a negative effect on CXCR4 affinity indicating that the phenyl moiety has an important role for the binding to the receptor.



M = N/A, Y = N/A; **L80**
M = Ni²⁺, Y = CH₃CO₂⁻, (n = 1/2); [Ni₂**L80**]
M = Zn²⁺, Y = CH₃CO₂⁻, (n = 1/2); [Cu₂**L80**]

Figure 120: Structure of AMD3100 BODIPY containing metal complex derivatives.⁵³

6.3 Proposed strategy to synthesise azamacrocyclic CXCR4 binding compounds conjugated to fluorescent dyes

Building upon the work previously done in the Archibald group (discussed in section 6.3.3), the library of configurational restricted macrocycles was extended with both the mono- and bis-tetraazamacrocycles being adapted to allow the conjugation with the fluorescent dyes rhodamine-B isothiocyanate and 5/6-carboxy fluorescein succinimidyl ester (example shown in Figure 121).⁴¹⁵ These dyes were selected as inexpensive starting points to probe the effects of the conjugation on affinity. The plan was to then extend this work to NIR fluorophores. Formation of metal complexes and *in vitro* assays would be carried out to gain a full understanding of the design parameters.¹⁹⁹

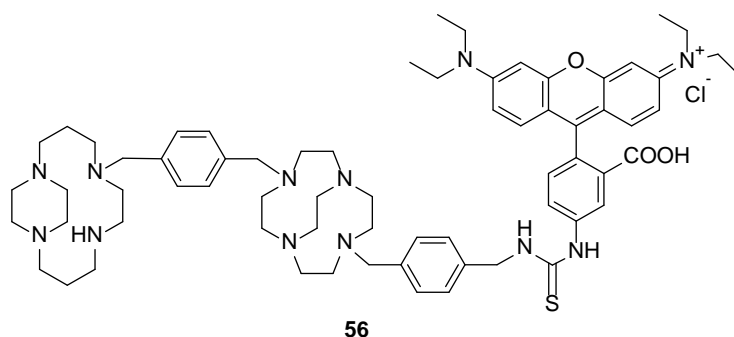


Figure 121: Structures of target molecules to be developed for OI of the CXCR4 receptor.

6.4 Synthesis of library of fluorophore macrocyclic compounds

6.4.1 Mono-macrocyle fluorescent compounds

Initially the mono tetraazamacrocycles **12** and **15** and their metal complexes were used to optimise the reaction conditions before moving to the bis tetraazamacrocyclic compounds. In the procedure outlined by Khan, the amino macrocycle and the isothiocyanate functionalised fluorescent dye were stirred together in methanol with one equivalent of trimethylamine for 16 hours. The reaction mixture was evaporated and purified by size exclusion chromatography.⁴¹⁵ As discussed previously, the procedure was modified to include the direct analysis of each fraction from the column by mass spectrometry. Using this procedure the library of compounds shown in Figure 122 were synthesised. The rhodamine compounds (**52**, **54** and the metal complexes derivatives) were on average higher yielding than the fluorescein compounds (**53**, **55** and the metal complexes derivatives).

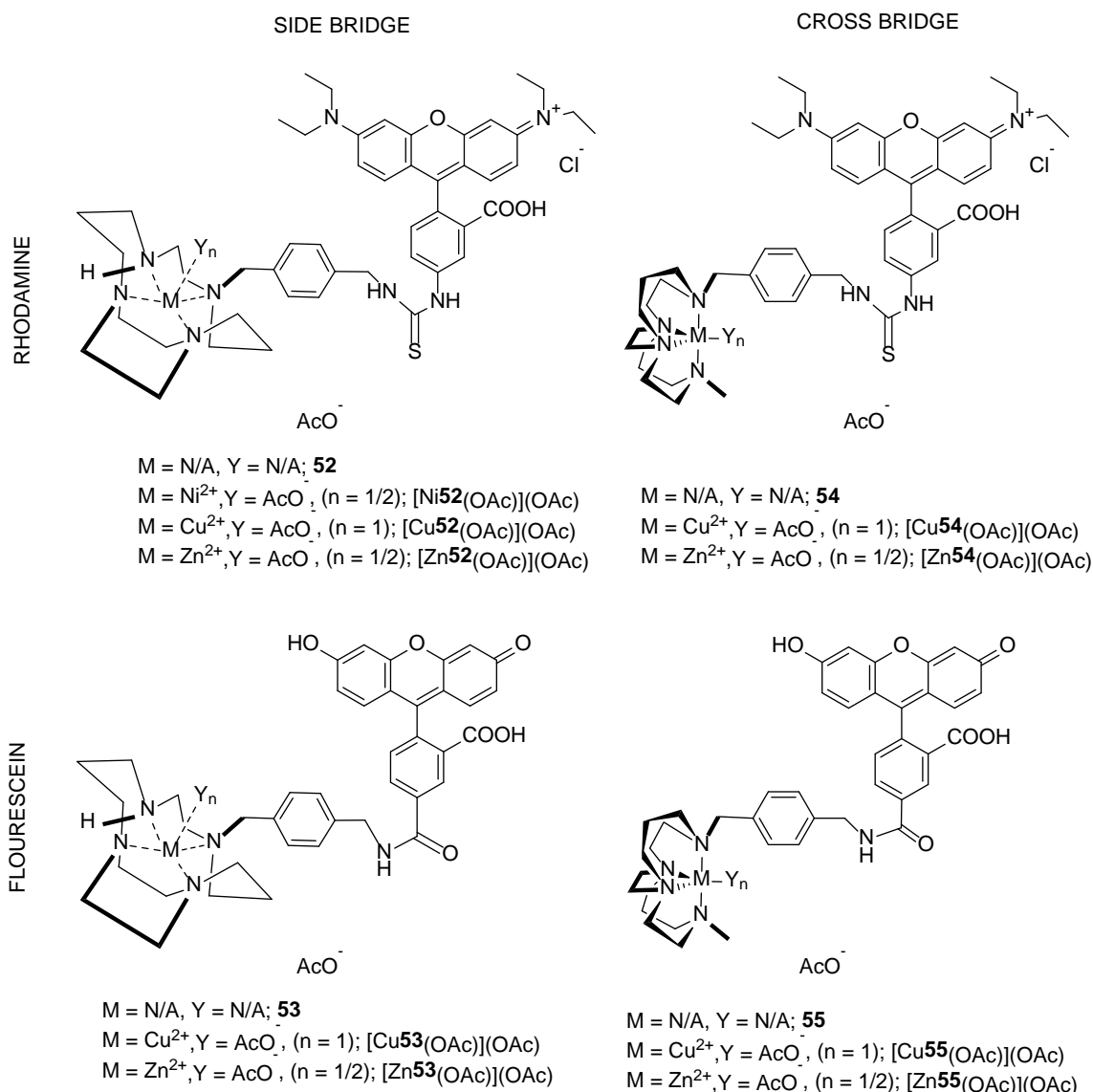


Figure 122: Library of configurational restricted fluorescent mono-macrocycles conjugated to rhodamine or fluorescein.

Mass spectrometry analysis of some of the complexes, especially the metal complexed rhodamine fluorophores ([Ni**52**(OAc)](OAc), [Cu**52**(OAc)](OAc), [Zn**52**(OAc)](OAc), [Cu**54**(OAc)](OAc), and [Zn**54**(OAc)](OAc)) was challenging due to the range of counter anions that could be carried with the molecule. Fluorescein derivatives exhibit multiple, pH dependent ionic equilibria.^{417, 418} Both the phenol and carboxylic acid functional groups can be ionised in aqueous solutions above pH 9; while acidification of the fluorescein dianion first protonates the phenol (pKa ~6.4) to yield the fluorescein monoanion, then the carboxylic acid (pKa <5).⁴¹⁹ Only the monoanion and dianion of fluorescein are fluorescent, with quantum yields of 0.37 and 0.93, respectively.⁴¹⁹ Hence, fluorescence intensity is reduced at acidic pH.

Table 25: Emission and excitation wavelengths of the fluorescent macrocyclic compounds

Compound	λ_{abs} (nm)	λ_{em} (nm)
52	555	580
[Ni 52 (OAc)](OAc)	555	580
[Cu 52 (OAc)](OAc)	555	580
[Zn 52 (OAc)](OAc)	555	580
53	485	519
[Cu 53 (OAc)](OAc)	485	520
[Zn 53 (OAc)](OAc)	485	519
54	555	580
[Ni 54 (OAc)](OAc)	555	580
[Cu 54 (OAc)](OAc)	555	580
[Zn 54 (OAc)](OAc)	555	580
55	460	490
[Cu 55 (OAc)](OAc)	455	470
[Zn 55 (OAc)](OAc)	455	470
56	545	559
[Cu ₂ 56 (OAc) ₂](OAc) ₂	545	570
[Zn ₂ 56 (OAc) ₂](OAc) ₂	545	570
57	495	525
[Cu ₂ 57 (OAc) ₂](OAc) ₂	495	525
[Zn ₂ 57 (OAc) ₂](OAc) ₂	495	525

It is expected that the bis-tetraazamacrocyclic compounds will be more potent antagonists than the mono-tetraazamacrocyclic compounds. The compounds are in the process of being analysed for CXCR4 binding potency, which is complicated by the use of fluorescent dyes in both the calcium signalling assay and CXCL12 competition binding assay.

Preliminary confocal microscopy experiments were carried out with **52** and [Cu₂**57**(OAc)₂](OAc)₂ in U87-CXCR4 cells. Both compounds showed high levels of non-specific uptake into the cells (likely due to the dye components) and so further data is required before this work can be pursued. If high affinity dye conjugated antagonists are identified in the binding assays then modification with alternate dyes to prevent non-specific uptake can be carried out.

6.5 Strategy to synthesise CXCR4 binding peptides conjugated to a near-IR emitting dye

Two of the first FDA approved non-targeted fluorescent dyes used in surgery are Indocyanine Green (ICG) and Methylene Blue (MB).⁴²⁰ Both ICG and MB are blood pool agents that are not inherently specific for any tumour. NIR dyes ($Em_{min}/Em_{max} = 650/900$ nm) that allow deeper imaging (few cm) are likely to form the next generation of dyes for fluorescent guided surgeries. As already discussed, due to high expression levels in many cancers, the development of a NIR CXCR4 antagonist is desirable. Of the peptidic agents used in imaging, the gallium-68 tracer Pentixafor based on the FC131 peptide has seen the most successful clinical translation.⁴²¹⁻⁴²⁴ Therefore, a NIR dye conjugated FC131 (Pentixafor) derivative is reported in this thesis.

The key NIR dye properties are for *in vivo* application are excitation/emission range, extinction coefficient, quantum yield, solubility and photostability.⁴²⁵ The extinction coefficient must be relatively high, with the extinction coefficients of the current clinically used dyes, ICG and MB, 121,000 and 71,200 $M^{-1}cm^{-1}$, respectively.⁴²⁶ In this work, azaborodipyrromethane (4,4-difluoro-4-borata-3a-azonia-4a-aza-s-indacene, aza-BODIPY) dyes were selected through a collaboration with the group of Professor Ross Boyle at the University of Hull.⁴²⁷⁻⁴²⁹

6.5.1 Proposed strategy to produce CXCR4.2 conjugates with aza-BODIPY

The reported examples of NIR CXCR4 fluorescent probes in the literature have used commercially available NIR dyes.^{397, 408, 409, 430} Figure 124 shows the proposed structures of two CXCR4 binding NIR dye peptide. The targeting moiety is derived for FC131 peptide (discussed fully in chapter 2) either azide or amine functionalised. The NIR fluorophore is a novel aza-BODIPY compound and was synthesised by Ms. Miffy Cheng. Aza-BODIPY compounds have previously been shown to have desirable photophysical properties however the appropriately functionalised derivatives are not widely available for conjugation and they have poor solubility in biological media.^{429, 431, 432} The novel aza-BODIPY dye contains an alkyne or acid group for conjugation and a sulfonate group to improve aqueous solubility.

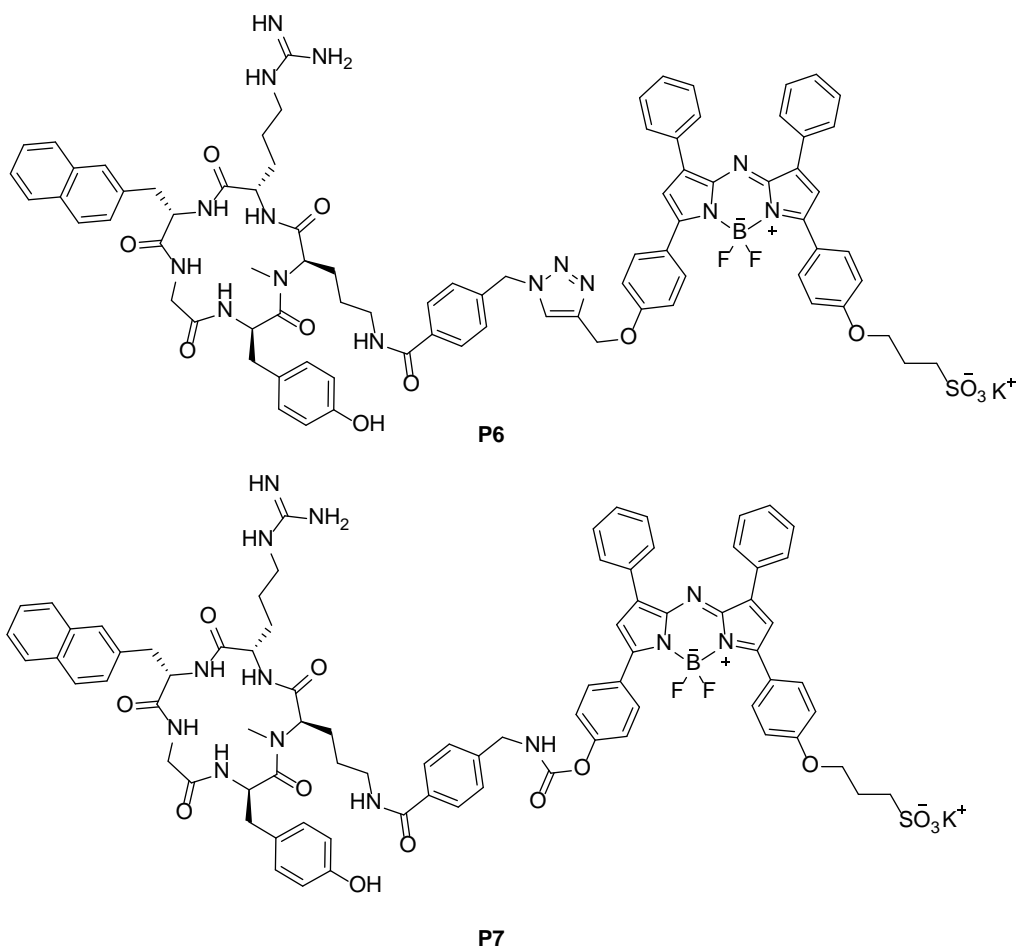


Figure 124: Structures of BODIPY-CPCR4.2 conjugates **P6** and **P7**.

6.5.2 Synthesis of the aza-BODIPY conjugated peptide

Initially the synthesis of peptide **P6** was attempted using aza-BODIPY-alkyne (prepared by Ms. Miffy Cheng) and the azide functionalised **P3**. Standard copper mediated click reaction conditions were used with the reaction mixture stirred in DMF overnight at room temperature in the presence of sodium ascorbate.⁴³³ However, the desired product was not isolated or observed in the MS and so an alternative route was investigated.

For the synthesis of peptide **P7**, an amide bond formation reaction was attempted using the aza-BODIPY functionalised with an acid group. The conjugation proceeded as expected and after 16 hours the product peak could be seen in analytical HPLC and MS. Initially the product was purified using reverse phase C18 semi-preparative HPLC, however, an alternative approach using a C18 cartridge was later employed to remove the highly water-soluble unreacted peptide (**P2**) and coupling reagents. The product was isolated in >95% purity (determined by analytical RP-HPLC).

6.5.3 Determination of photophysical properties of the aza-BODIPY peptide conjugate

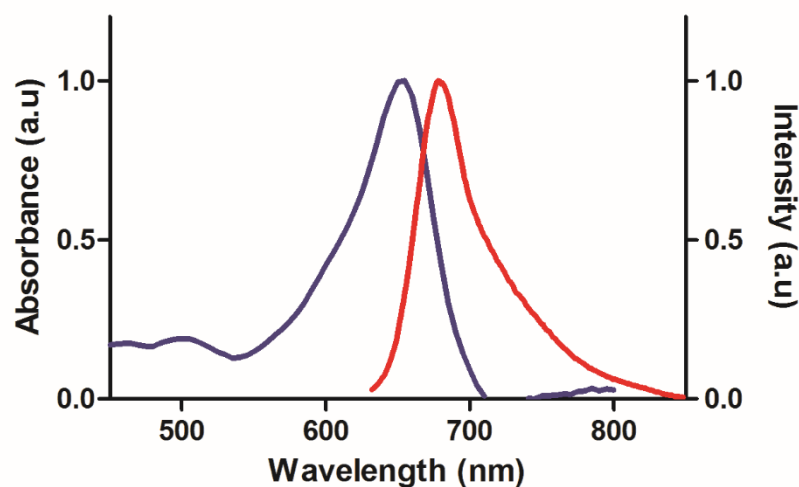


Figure 125: Absorption (blue line) and emission (red line) spectra of **P7**. (Date collected by Ms. Miffy Cheng).

Figure 125 shows the absorption and emission spectra of peptide **P7** (data collected by Ms. Miffy Cheng). Maximum absorbance was seen at 655 nm, and maximum emission seen at 681 nm. Photophysical properties of peptide **P7** and the aza-BODIPY starting material were studied in acetonitrile at room temperature; shown in Table 26. The extinction coefficient of **P7** (*ca.* 35,400 M⁻¹cm⁻¹) shows efficient fluorescence, although it is lower than ICG and MB FDA approved dyes; 121,000 and 71,200 M⁻¹cm⁻¹, respectively.⁴²⁶ The value is in the same range as that reported by Poty *et al.* with AMD3100 for their conjugated BODIPY fluorophore, **L80** (ranging from 30200 to 53900 M⁻¹cm⁻¹).⁵³

Table 26: Photophysical properties of the BODIPY starting material and peptide **P7** in PBS at 298K.

Compound	Solvent	$\lambda_{\text{abs}}(\text{nm})$	$\lambda_{\text{em}}(\text{nm})$	$\epsilon (\text{M}^{-1}\text{cm}^{-1})$	Φ_{f}	Brightness ^b (M ⁻¹ cm ¹)
Aza-BODIPY	MeCN	660	710	37102	0.23	8534
P7	MeCN	655	681	35380	0.60	21228

The Φ_{F} value of **P7** was determined to be 0.60 which is significantly higher than the starting material. The phenomenon of a hypochromic shift and significant increase in fluorescence quantum yield is suspected to be due to the conjugation to a hydrophilic sterically hindered group, reducing the aggregation of the dye in polar solvent or enhanced π - π interaction.⁶

On comparison to the CXCR4 tetraazamacrocyclic BODIPY antagonists developed by Poty *et al.* higher quantum yields and brightness were achieved with **P7**. Poty *et al.* achieved between 0.05-0.27 with the inclusion of the metal into the AMD3100 analogue having a marked increase on

quantum yield.⁵³ **P7** is *ca.* 2.5 times brighter than the unconjugated aza-BODIPY fluorophore and the best fluorophore reported by Poty *et al.*⁵³

6.5.3 *In vitro* CXCR4 binding assays for the aza-BODIPY peptide conjugate

Peptide **P7** and the related compounds were evaluated for blocking of the CXCL12 induced calcium flux in transfected U87 cells. 65

Table 27: IC₅₀ values of Pentixafor peptide and aza-BODIPY derivatives. Concentration required to reduce the level of Ca²⁺ ions observed during a 'normal' signalling process by 50% (IC₅₀) in U87-CXCR4 cells.

Compound	Calcium Signalling IC ₅₀ /nM
P4	4
P7	42

Table 27 shows the IC₅₀ values obtained from the calcium signalling assay. The aza-BODIPY containing peptide, **P7** has a slightly lower affinity towards the CXCR4 receptor when compared to the parent amino peptide **P4** but is still in the range for a useful probe. The aza-BODIPY dye, despite considerable steric bulk and the presence of the sulfonate group, does not have a detrimental effect on CXCR4 binding warranting further investigation of this construct as a NIR imaging probe.

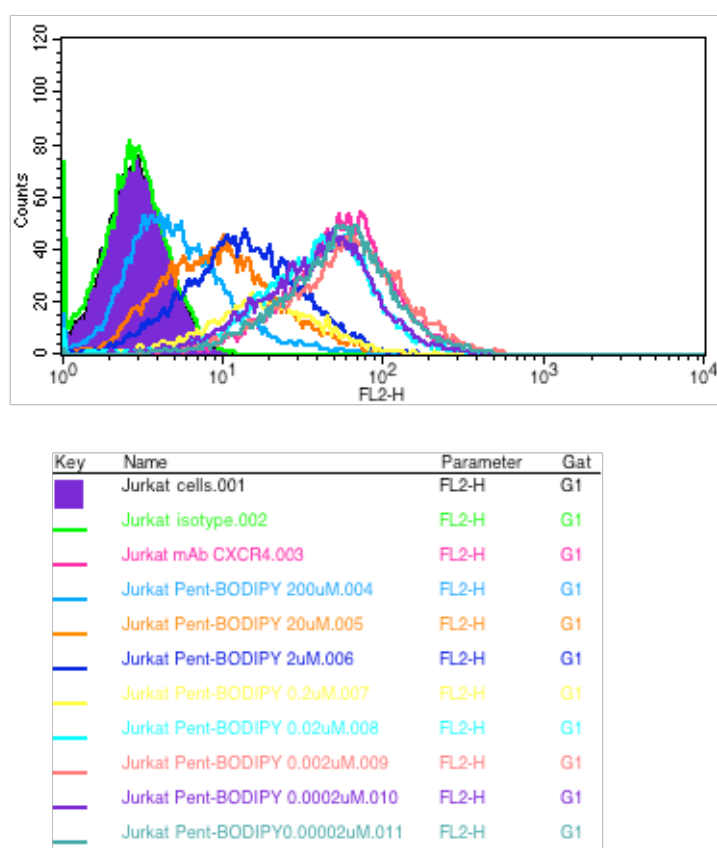


Figure 126: Flow cytometric histogram plots for binding of 12G5 mAb in competition with peptide **P7** at varying concentrations in Jurkat cells.

To investigate affinity by competition for binding with CXCR4 antibodies, cells were exposed to varying concentrations of peptide **P7** and binding inhibition determined by flow cytometry (Figure 126). The fluorescence of the **P7** antagonist could not be directly measured due to excitation and emission wavelengths, therefore the fluorescence of the PE-antibody conjugate (12G5) was detected.

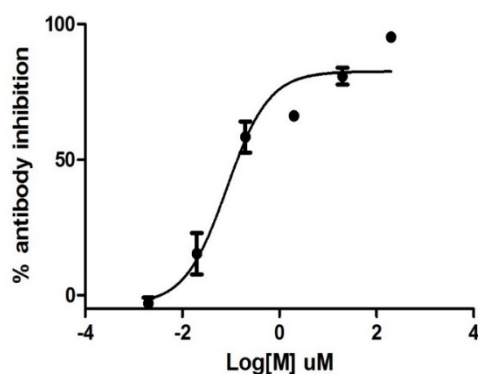


Figure 127: Antibody (IgG2A) displacement concentration curve obtained for P7 in Jurkat cells, $n = 3$.

The IC_{50} value of 82.7 nM was determined in this assay. This showed a 3.5 fold reduction in affinity on comparison with gallium Pentixafor ([Ga**P4**]) which was determined in the same assay (IC_{50} 22.9 nM, $n = 1$, data collected by Ms. Cecilia Miranda). These results are in a similar range to those reported in Table 27 for the calcium signalling assays but give a different CXCR4 dependent biological readout.

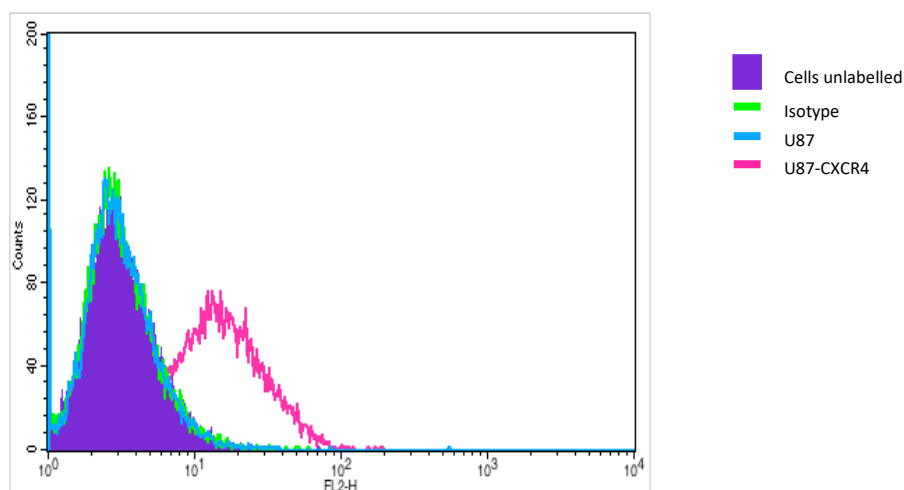


Figure 128: CXCR4 expression in U87-CXCR4 vs U87 cells as determined by flow cytometry.

To further investigate the properties of **P7**, confocal microscopy experiments in cell lines of varying CXCR4 expression were carried out. Due to the problem of non-specific uptake seen using formalin fixed cells reported by Van de Berg *et al.* confocal imaging experiment were performed using live cells.⁴⁰⁰ The expression levels of CXCR4 receptors in U87 and U87-CXCR4 cell lines were determined via flow cytometry (see Figure 128).

Various concentrations of **P7** were investigated for confocal imaging in U87-CXCR4 cells, with other experimental parameters remaining unchanged. Tietz *et al.* reported an incubation time effect on fluorescence when using a T140 dye conjugate in CXCR4 expressing cells.⁴⁰⁷ An increase in fluorescence was noted from 5 to 30 min with little further increase after 60 min. Similar experiments were carried out with the cells incubated at 4°C rather than 37°C as this is known to cause internalisation of the CXCR4 receptor.

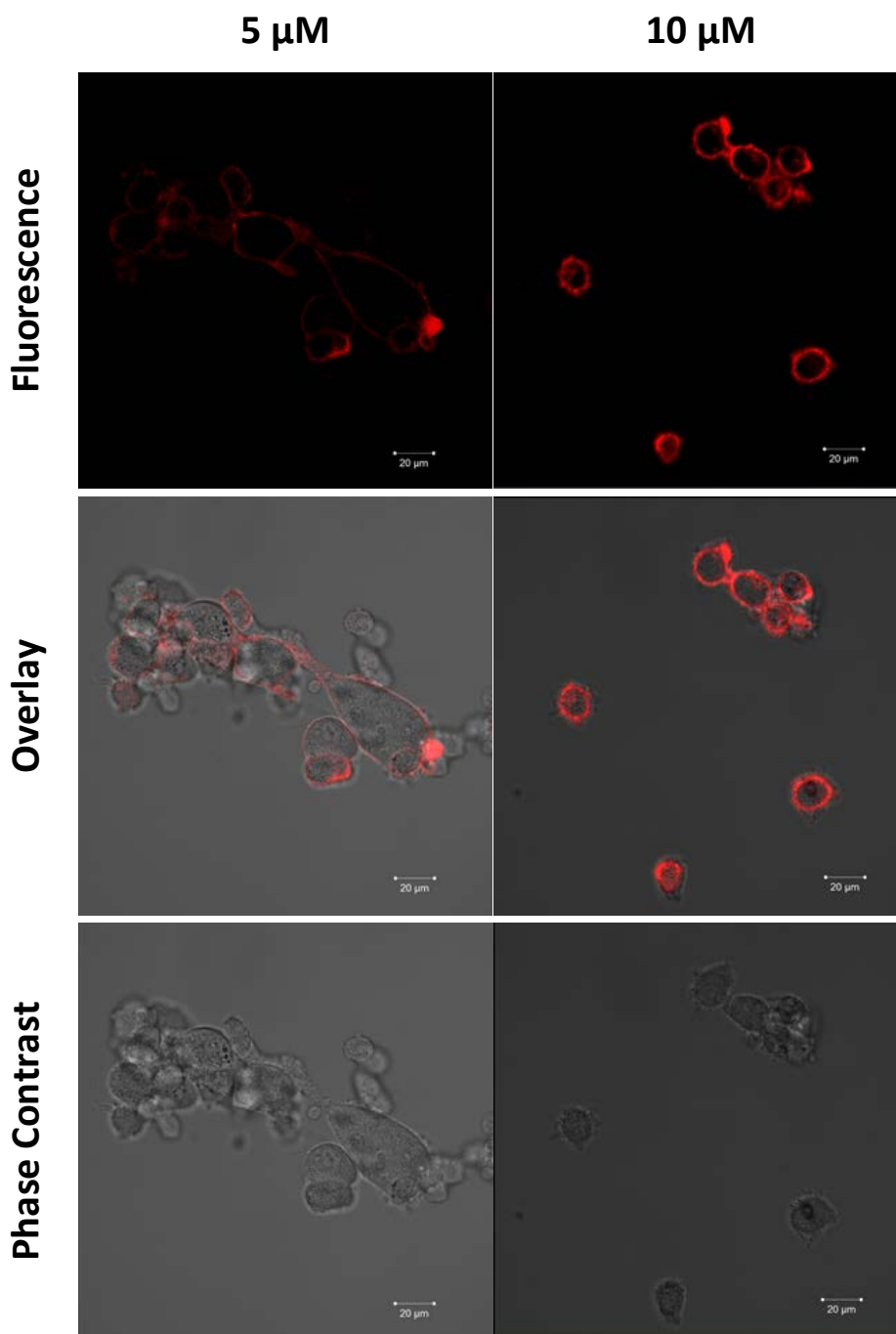


Figure 129: Confocal microscopy images of peptide **P7** in U87-CXCR4 cells at 5 and 10 μ M.

Figure 129 shows the results using a concentration of 5 and 10 μM of **P7** incubated with *ca.* 4000 cells. All concentrations showed binding to CXCR4 on the membrane of the U87-CXCR4 cells with the higher concentrations providing the highest fluorescent signal. Imaging of **P7** using confocal microscopy showed no degradation or bleaching when exposed to sustained laser irradiation (10-20 min). Further work could lower the concentration to 0.1 μM to give a direct comparison with the concentration used for NIR probes reported by Santagata *et al.* and Meincke *et al.*^{397, 409}

Z-stacking experiments were conducted to illustrate that the peptide **P7** was binding in the membrane of the cell rather than being internalised (see section 10.1). To determine the specificity of the **P7** towards CXCR4, confocal images were also collected on the low/non-expressing U87 cell line (shown using FACS, Figure 128). Again each experiment was conducted with 5 μM of **P7** incubated for 30 min at 4°C, however, inconsistent results were observed and these experiments need to be repeated.

CXCR4 competition/blocking experiments were attempted using the confocal. The experiments were carried out using a small molecule antagonist $[\text{Cu}_2\mathbf{5}(\text{OAc})_2](\text{OAc})_2$ and CXCR4 specific antibody 12G5. However, incomplete blocking was observed due to problems either with the concentration or procedure. (Results shown in the appendix, Section 10).

These preliminary *in vitro* results show the potential of **P7** as a NIR CXCR4 imaging probe. Further work is needed to fully validate the compound performance with repeats and optimisation of some of the microscopy protocols.

6.6 Conclusion

A library of small macrocyclic antagonists conjugated to rhodamine or fluorescein were synthesised but have not yet been fully analysed. When *in vitro* assay results are obtained, structure activity relationships can be determined. It is expected that non-specific cellular uptake will be observed with the dyes used and preliminary confocal microscopy data supported this. If sufficient receptor affinity is demonstrated, then a second generation of compounds with alternate dye components can be investigated.

A novel aza-BODIPY conjugate FC131 peptide, **P7** was synthesised and purified to give a potential NIR CXCR4 imaging probe. The FC131 peptide has shown to be of clinical relevance when labelled with gallium-68 (Pentixafor), this work has produced a novel NIR analogue of Pentixafor used for fluorescence imaging. The conjugate maintained the excellent photophysical properties of the aza-BODIPY fluorophore and had high affinity for the CXCR4 receptor (**P7**; $IC_{50} = 42$ nM). This was confirmed through *in vitro* CXCL12 stimulated calcium flux assays, mAb competition binding and confocal experiments.

6.7 Future work

The small macrocyclic antagonists can be developed with alternative fluorophores that possess better photophysical properties and do not have the impact on the non-specific uptake of the conjugate. Cyanine dyes or BODIPY derivatives could be used and this is still worthwhile for further investigation. These compounds could have the advantages of high affinities and long receptor residence times coupled with increased metabolic stability offer some significant advantages over the peptides.

The NIR dye peptide conjugate **P7** CXCR4 can be further studied to determine photophysical properties (e.g. extinction coefficient and quantum yield) in biologically relevant media to mimic the *in vivo* environment. Further *in vitro* validation on the NIR conjugated peptide **P7** is also suggested. Along with repeats of the confocal experiments carried out with blocking compounds, the studies could be extended to include a wider range of CXCR4 binding molecules and proteins (e.g. AMD3100, unlabelled peptide and CXCL12). Further studies using FACS could be carried out to assess the affinity and specificity of the **P7** probe. A flow cytometer with the capability to measure fluorescence in the NIR region would allow for the direct detection of the **P7** antagonist. Competition binding experiments could then be conducted in the positive and negative cell lines allowing for quantitative validation of the uptake/binding of the tracer. This technique will not differentiate between internalised and membrane bound probe but that distinction can be made with complementary confocal microscopy experiments.

There is also potential for *ex vivo* and *in vivo* studies to be carried out with the **P7** antagonist. *In vivo* biodistribution data would be interesting to evaluate whether the hydrophobic nature of the fluorophore affects circulation time as well as excretion pathways, compared to the radiolabelled Pentixafor derivative. Structural changes may be required to introduce a pharmacokinetic behaviour modifying linker, such as a PEG chain.

There has been a lot of recent interest in multi-modal imaging probes. BODIPY dyes have been shown to allow for the inclusion of the positron emitting radioisotope fluorine-18 to give multimodal positron emission tomography (PET)/optical imaging agents.⁴³⁴⁻⁴³⁷ Formation of BODIPY based PET/optical multimodal imaging can be achieved via B–F bond formation or modification of the structural backbone to incorporate the radiolabel.²⁹²

Chapter Seven

Conclusion

7. Conclusion

7.1 Overview

This work highlights the synthesis of novel peptide and highly stability metal macrocyclic complexes for potential use as CXCR4 receptor targeted cancer diagnosis agents. Figure 130 depicts several of the key antagonists and the imaging modality which is being used for each construct.

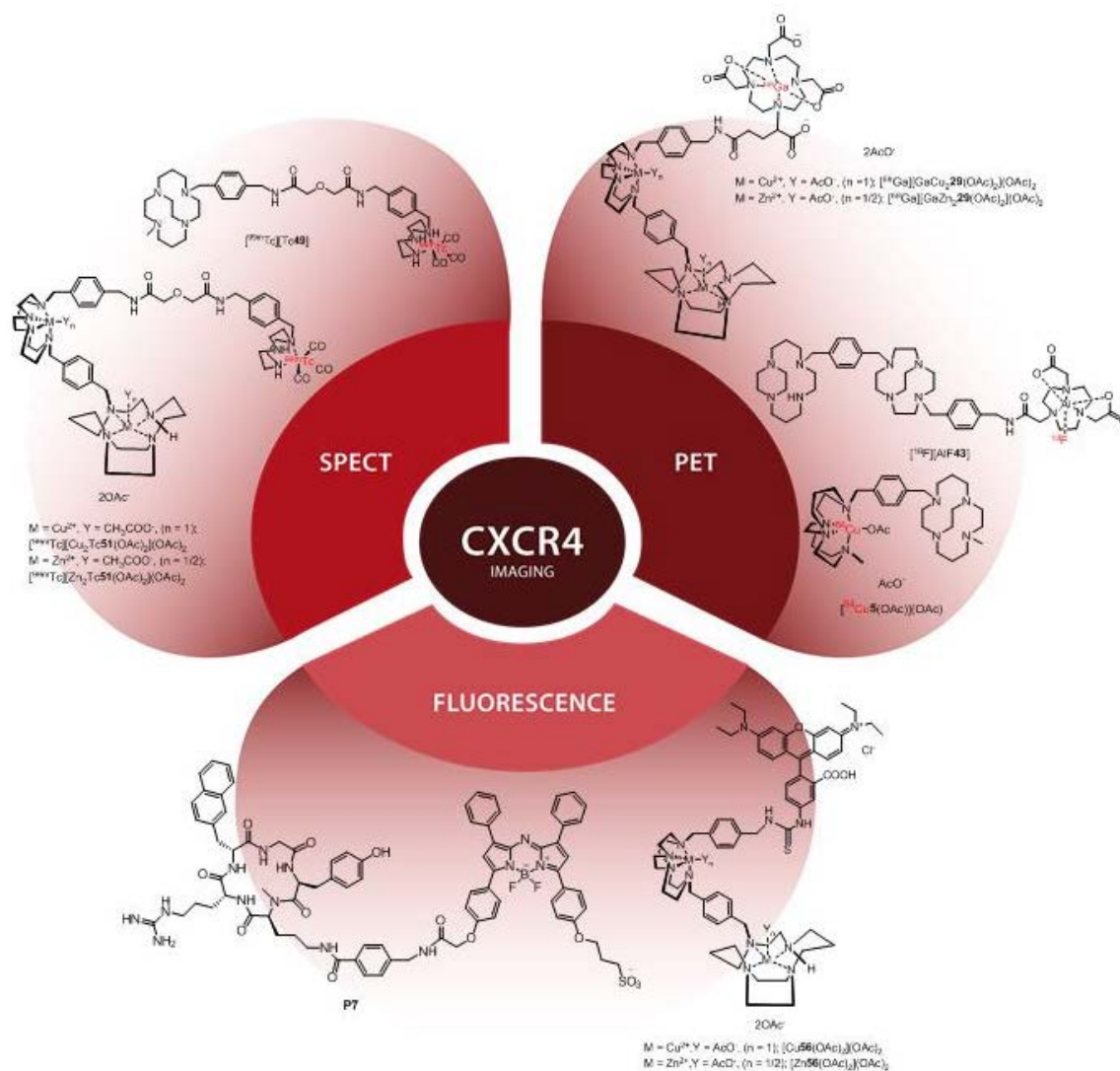


Figure 130: Summary of different modalities for imaging the CXCR4 receptor and examples of antagonists investigated.

The development of new therapeutic and diagnostic agents is a growing area of research. The most common cause of cancer related deaths is not from the primary tumour but from metastatic tumours, therefore the CXCR4 chemokine receptor which is overexpressed in over 23 different cancers and plays a key role in the metastatic process is a key target.

The inclusion of configurationally restricted cyclam/cyclen macrocycles in the compounds reported in this work is designed to overcome stability limitations and optimise coordination interactions with the residues on the receptor, to provide stable and high affinity CXCR4 antagonists.

The work previously carried out by the Archibald group to design high affinity CXCR4 antagonists has been advanced by the inclusion of radioisotopes and fluorophores for the development of PET, SPECT and optical imaging. For the development of a CXCR4 targeted PET imaging agent, the radioisotopes copper-64, gallium-68 and fluorine-18 were all investigated.

AMD3100 and AMD3465 have been labelled with copper-64 in studies previously reported in the literature. However, due to the flexibility of the cyclam ring, transchelation of the copper-64 was observed with high liver uptake, limiting further development of these tracers to clinical application. Although the gallium-68 peptide, Pentixafor has undergone clinical translation, other small molecule CXCR4 antagonists have not made the same leap out of the researching laboratories. Other isotopes of interest are fluorine-18 (PET) and technetium-99m (SPECT) due to half-life and availability. Targeted optical imaging is also of high interest, particularly with regard to the development of fluorescence guided surgery.

7.2 Main achievements in this work

The synthesis of a series of novel configurationally restricted mono- and bis tetraazamacrocyclic compounds attached to BFCs or fluorophores with potential for imaging the CXCR4 receptor have been reported in this work.

An improved synthetic procedure for the CB bis-tetraazamacrocyclic compound **5**, was designed to give increased yield and higher purity. Compound **5** was radiolabelled with copper-64 [⁶⁴Cu][Cu**5**(OAc)](OAc) with a 41.6 ± 4.6% RCY. Non-radioactive derivatives; [Cu**5**(OAc)](OAc) and [Cu₂**5**(OAc)₂](OAc)₂ were shown to be high affinity CXCR4 antagonists (IC₅₀ = 60 nM and 4 nM, respectively).

In vivo dynamic PET/CT scans showed that [⁶⁴Cu][Cu**5**(OAc)](OAc) had specific binding to CXCR4, with uptake in the CXCR4 positive tumour being 8 fold higher than that in the CXCR4 negative tumour (U87-CXCR4, 20.21 ± 5.78%; U87, 3.0 ± 0.5). Blocking experiments of tracer [⁶⁴Cu][Cu**5**(OAc)](OAc) using [Cu₂**5**(OAc)₂](OAc)₂ showed reduction of tumour and liver uptake by more than 90%. The study demonstrates that the copper-64 chelated complex is stable and no transchelation is observed, which has previously hampered the further development of copper-64 labelled AMD3100 and AMD3465 tracers.

The CXCR4 receptor binding PET tracer Pentixafor was synthesised to use in comparator studies and some novel derivatives were also synthesised including an azide functionalised compound **P3**. The inclusion of the azide allows for click chemistry reactions with appropriate BFCs for other radioisotopes or fluorophores.

Work was carried out to develop gallium-68 BFC functionalised tetraazamacrocyclic compounds. The inclusion of DOTAGA had a negative impact on the affinity of the antagonists. For example, the non-conjugated antagonists $[\text{Cu}_2\mathbf{24}(\text{OAc})_2](\text{OAc})_2$ and $[\text{Zn}_2\mathbf{24}(\text{OAc})_2](\text{OAc})_2$ showed high CXCR4 affinities (IC_{50}) of 100 nM and 1 nM respectively; however, upon conjugation the potency decreased to >5000 nM for both $[\text{Cu}_2\mathbf{29}(\text{OAc})_2](\text{OAc})_2$ and $[\text{Zn}_2\mathbf{29}(\text{OAc})_2](\text{OAc})_2$. This decrease in affinity was attributed to the close proximity of the negatively charged glutamate of the DOTAGA. Additional *in vitro* and *in vivo* studies, confirmed that these compound were not suitable for targeted imaging of the CXCR4 receptor. Alternative designs were investigated with PEG chain linkers, a pretargeted approach and alternative BFCs all explored but high affinity CXCR4 targeting gallium-68 tracers were not produced in this work.

The novel CXCR4 binding THP conjugated peptide, **P5**, was synthesised and radiolabelled at physiological pH within 5 mins. This is advantageous over the widely used Pentixafor DO3A containing peptide, which requires acidic pH and a longer reaction time to label. *In vivo* studies with $^{68}\text{Ga}[\text{GaP5}]$ gave an SUV_{max} ca. 1.9% ID/g, which was lower than that achieved by Pentixafor, $^{68}\text{Ga}[\text{GaP4}]$. The reduction in tumour accumulation and higher liver uptake is likely due to the increased lipophilicity of the THP BFC of **P5**. Optimisation of this property with PK modifying linkers would be a possible route to improve the tracer and to exploit the excellent labelling properties.

In the development of a fluorine-18 antagonist, novel NODA conjugated bis-tetraazamacrocyclic compounds (**43**, $[\text{Cu}_2\mathbf{43}(\text{OAc})_2](\text{OAc})_2$ and $[\text{Zn}_2\mathbf{43}(\text{OAc})_2](\text{OAc})_2$) were synthesised and radiofluorination attempted using the inorganic $^{18}\text{F}[\text{AlF}]$ complex. Calcium signalling assays determined the antagonist $[\text{Zn}_2\text{AlF}\mathbf{43}(\text{OAc})_2](\text{OAc})_2$ to be the most potent of the molecules tested ($\text{IC}_{50} = 95$ nM). These antagonists also offer the potential for labelling with other radioisotopes.

The literature contains very few reports on the development of CXCR4 targeted SPECT imaging agents. Therefore, the design and radiolabelling of novel CXCR4 SPECT tracers such as $^{99\text{m}}\text{Tc}[\text{Cu}_2\text{Tc}\mathbf{51}(\text{OAc})_2](\text{OAc})_2$ was investigated. *In vitro* assays carried out on the non-radioactive rhenium, analogues revealed that antagonist $[\text{Cu}_2\text{Re}\mathbf{51}(\text{OAc})_2](\text{OAc})_2$ had a IC_{50} inhibition value similar to that of AMD3100, and thus warranted further development. $^{99\text{m}}\text{Tc}[\text{Cu}_2\text{Tc}\mathbf{51}(\text{OAc})_2](\text{OAc})_2$ was successfully radiolabelled in a 46% decay-corrected RCY. The tracers were shown to be stable in PBS up to 3 hours, however, high protein binding was seen in serum, which needs further investigation to determine if it is problematic for application of the tracer.

A library of configurationally restricted tetraazamacrocycles was conjugated to fluorophores and is ready for *in vitro* evaluation, although it is expected that these compounds will have non-

specific cellular uptake due to the dyes used. A NIR azo-BODIPY dye conjugated peptide, **P7**, was also developed showing high affinity for the CXCR4 receptor ($IC_{50} = 42$ nM) with preliminary confocal microscopy experiments indicating the potential of this NIR probe.

7.3 Wider context and applicability of some aspects of the research

An effective and reproducible synthetic route for the synthesis of configurationally restricted bis-tetraazamacrocycles using microwave reduction has been outlined in this work. The new procedure dramatically reduces synthesis time, and minimises the quantity of reducing agent used, as well as increasing purity of the product. This work also outlines alternative purification methods for the metal complexes of bis-tetraazamacrocyclic compounds using HPLC and fraction analysis via MS in conjunction with size exclusion chromatography which increases the purity of the isolated compound. Significant time was spent on the development of semi-preparative HPLC purification methods for these highly challenging multi-charge/protonation state molecules. The greatest success was seen with the addition of a controlled amount of trifluoroacetic acid to the mobile phase, allowing species to elute fully protonated with narrow peaks.

In vivo studies conducted with $[^{64}\text{Cu}][\text{Cu5}(\text{OAc})](\text{OAc})$ demonstrated high affinity and specificity toward the CXCR4 chemokine receptor. Importantly, unlike the copper-64 CXCR4 antagonists reported previously (AMD3100 and AMD3465 derivative) no transchelation was observed. This validates the theory that configurational restricting these tetraazamacrocyclic compound increases metal ion complexation stability.

The peptide synthesis procedures outlined in this work improved upon those reported in the literature, using alternate deprotection strategies. This improved procedure was utilised to form the novel and versatile CXCR4 targeting peptide derivative, **P3**.

Chapter Eight

Future Work

8. Future work

8.1 Short-term goals

A more detailed biological evaluation of mono- and bis-tetraazamacrocyclic metal complexes discussed throughout is necessary to establish how they are acting as high affinity antagonists. This could be achieved through site directed mutagenesis experiments with selected residues on the CXCR4 receptor changed to determine impact on binding.^{180, 186} It would also be beneficial to determine the crystal structures of these novel BFC/fluorophore containing macrocycles; to confirm their structures match those previously characterised. While the majority of the metal containing tracers reported include either zinc(II) or copper(II) ions, nickel(II) has also proven to be effective and so investigation of the nickel(II) may be of interest.¹⁹⁹

Whilst partial success was seen with the synthesis of the gallium-68 pretargeted compounds **39** and **40**; further validation is needed with respect to the bioorthogonal IDDA reaction between the two components. Biological testing and radiolabelling would also need investigating before any *in vivo* experimental design can be considered.

As stated in Section 3.12 the lipophilicity of peptide **P5** with the inclusion of the THP BFC was shown to be detrimental to tumour uptake *in vivo*. This could be modified as discussed previously and lipophilicity measurements correlated with biodistribution results to clearly determine the impact of this parameter.

It is worth re-investigating the synthesis of gallium-68 labelled $[\text{Cu}_2\mathbf{34}(\text{OAc})_2](\text{OAc})_2$ and $[\text{Zn}_2\mathbf{34}(\text{OAc})_2](\text{OAc})_2$. These PEG chain linker compounds not only have an increased distance between the binding moiety and the BFC, but also have one less carboxylic acid present compared to DOTAGA. This is likely to improve the affinity of the antagonist, reducing the repulsion. Further investigation of these compounds would be useful to understand the impact of the linkers

The radiolabelling of the Al-F compounds of $[\text{Cu}_2\mathbf{43}(\text{OAc})_2](\text{OAc})_2$ and **43** showed a poor overall yield of *ca.* 2%. Optimised radiofluorination conditions need to be developed to deliver a high specific activity tracer in good yield. Alternatively; as illustrated in Figure 96, antagonists $[\text{Cu}_2\mathbf{43}(\text{OAc})_2](\text{OAc})_2$ and **43** could also be radiolabelled with copper-64 or gallium-68.

For development of technetium-99m tracers, an alternative to the $\text{fac}-[{}^{99\text{m}}\text{Tc}(\text{CO})_3]^+$ moiety could be investigated using the same antagonists (**49**, **51** and $[\text{Cu}_2\mathbf{51}(\text{OAc})_2](\text{OAc})_2$). As mention in section 5.1.2, Braband *et al.* used a $\text{fac}-[{}^{99\text{m}}\text{Tc}(\text{O})_3]$ to label the TACN BFC.^{360, 361} The group reports that the $\text{fac}-[{}^{99\text{m}}\text{Tc}(\text{O})_3(\text{TACN})]^+$ complex demonstrated superior *in vivo* stability and excretion, compared to tracers formed with the tri-carbonyl $\text{fac}-[{}^{99\text{m}}\text{Tc}(\text{CO})_3]^+$ complexes. Therefore, it would

be interesting to radiolabel the CXCR4 antagonists with the *fac*-[^{99m}Tc(O)₃] moiety, to determine whether stability or *in vivo* biodistribution could be enhanced.

8.2 Long-term goals

8.2.1 Synthesis

Throughout the work presented, the configurationally restricted bis-tetraazamacrocycle **24** and its metal complexes derivatives were selected as the base structure to modify. Antagonist **24** was selected due to its relative ease of synthesis and high affinity towards CXCR4. The Archibald research group along with collaborators have synthesised a large library of configurationally restricted bis-tetraazamacrocycles structures (>1000). Figure 131 depicts examples of other high affinity configurationally restricted bis-tetraazamacrocycles that have been synthesised and characterised. These structures are either aryl- (**L77-78**) or C-functionalised (**L79-80**), allowing further modifications to be made.

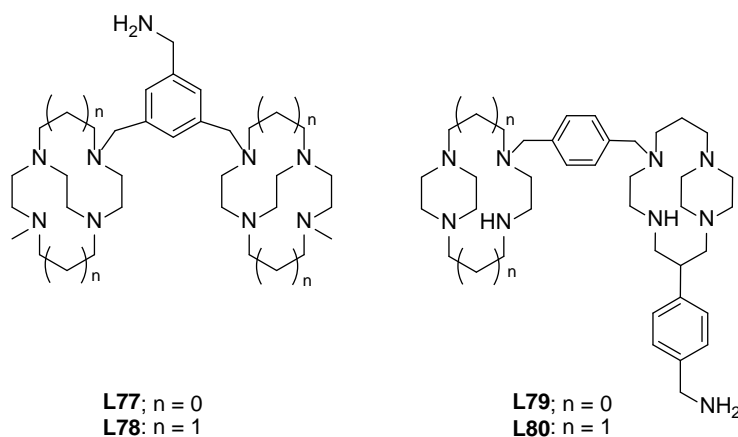


Figure 131: Structures of some of the other library of configurationally restricted bis-tetraazamacrocycles CXCR4 antagonists synthesised by the Archibald research group.^{257, 438}

The azide derivative, **P3**, forms a useful precursor for facile modification to generate peptidic CXCR4 binding compounds. The formation of alkyne derived NOTA BFC would allow facile labelling with a wide range of radioisotopes for both imaging and therapeutic applications as an alternative to Pentixafor/Pentixather (structures shown in Figure 132). The click reaction between **P3** and the alkyne aza-BODIPY NIR dye was unsuccessful (**P6**), and so further work needs to be carried out to develop this. Other commercially available alkyne containing NIR dyes could also be tested such as Sulfo-Cyanine7.5 alkyne (Lumiprobe) which have high quantum yields and emission spectra ideal for *in vivo* applications.

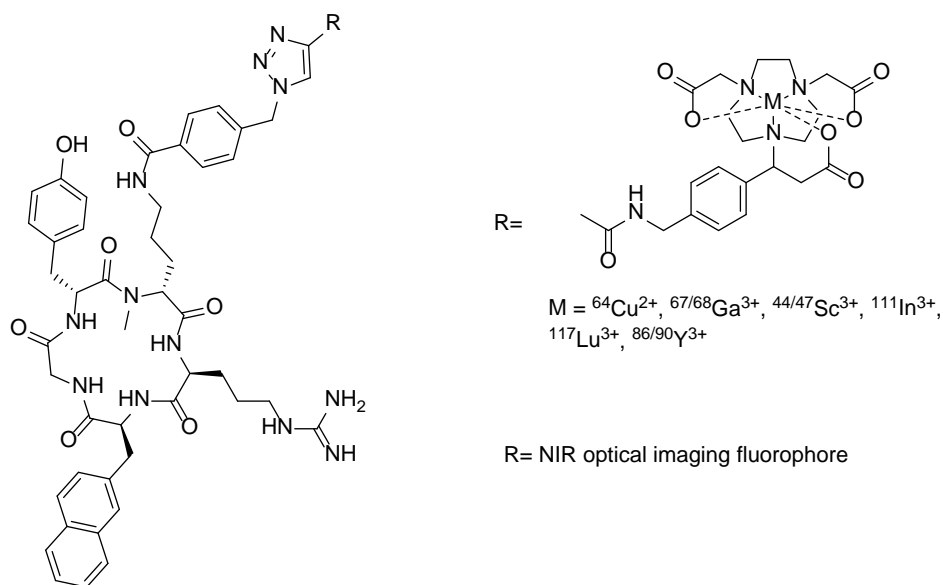
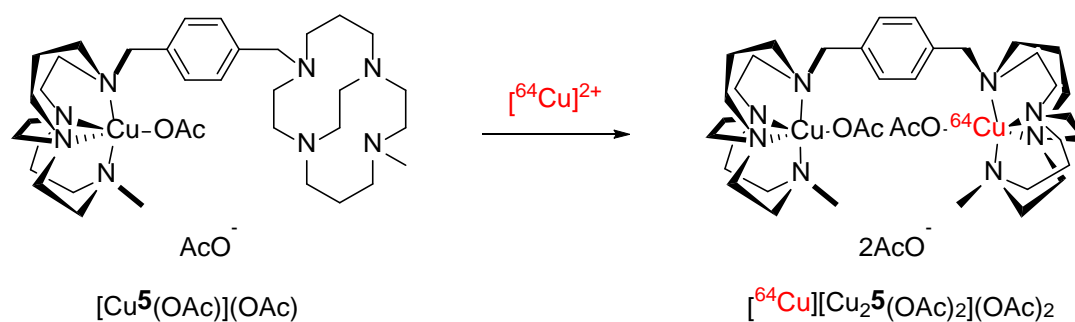


Figure 132: Proposed therapeutic and imaging agents that could be synthesised with the azide CXCR4 peptide **P3**.

It would be interesting to investigate the conjugation of the metal complex bis-tetraazamacrocycles ($[\text{Cu}_2\mathbf{24}(\text{OAc})_2](\text{OAc})_2$ and $[\text{Zn}_2\mathbf{24}(\text{OAc})_2](\text{OAc})_2$) to the BFC THP, (structures shown in Figure 80). The use of THP allows for rapid radiolabelling to be achieved at neutral pHs in a kit like formulation which is attractive to radiopharmacies.

8.2.2 Radiolabelling and Biological validation



Scheme 20: Alternative radiolabelling procedure for $[\text{Cu}_5(\text{OAc})](\text{OAc})$ with copper-64 to form $[^{64}\text{Cu}][\text{Cu}_2\mathbf{5}(\text{OAc})_2](\text{OAc})_2$.

Alternative radiolabelling conditions for the formation of $[^{64}\text{Cu}][\text{Cu}_2\mathbf{5}(\text{OAc})_2](\text{OAc})_2$ could be investigated using high purity $[\text{Cu}_5(\text{OAc})](\text{OAc})$ which can be combined with copper-64, as shown in Scheme 20. Specific activity would need to be fully investigated using both the alternative radiolabelling technique and HPLC purification conditions optimised before *in vitro* and *in vivo* experiments could be carried out.

In vitro and *in vivo* evaluation should be completed with the NIR fluorescent aza-BODIPY peptide **P7**. Initially results via FACS have shown the affinity for the CXCR4 receptor is maintained in the dye conjugated peptide, further FACS/confocal studies can be used to assess the specificity of the imaging probe. This can be completed using direct detection of the probe in U87 vs U87-CXCR4 cell lines via FACS, or blocking studies undertaken with confocal microscopy. *In vivo* experiments investigating the biodistribution and uptake of **P7** in CXCR4 expressing tumour bearing mice could then be conducted.

Chapter Nine

Experimental

9.1. General Method

9.1.1 General notes

Bulk solvent was removed by rotary evaporation on a Büchi RE 111 evaporator equipped with a diaphragm vacuum pump, trace solvent was removed in a vacuum oven. Reactions were performed at room temperature (RT) unless otherwise stated. All metal containing compounds were purified via size exclusion chromatography using Sephadex LH20, which was pre-soaked in methanol overnight.

9.1.2 NMR spectroscopy

All NMR data was collected on a JEOL JNM-LA400 spectrometer at 400 and 100 MHz for ^1H and ^{13}C respectively, using the indicated solvents. Chemical shifts are reported in parts per million, ppm, for ^1H NMR and ^{13}C NMR spectra and coupling constants, J, reported in Hertz, Hz. Splitting patterns are assigned as s: singlet, d: doublet, dt: double triplet, t: triplet, q: quartet, m: multiplet, td: triple doublet and br: broad signal.

9.1.3 Mass Spectrometry

Electrospray MS was performed at the University of Hull using either a ADVION MS SOP or Finnegan MAT 900 XLT system. Accurate mass spectrometry measurements (HRMS) were recorded at the EPSRC National Mass Spectrometry Service Centre at the University of Swansea using a LQT Orbitrap XL.

9.1.4 Elementary analysis

CHN analysis was performed using a CHN analyser EA1108 (Carlo Erba). Most compounds were within the limit of 0.4% of the expected ratios, however some were within 0.5%. This higher limit is due to products being viscous oils which make elemental analysis challenging. For other products, higher solvent association or salt impurities are likely to cause the larger deviation from the predicted element values.

9.1.5 Radio-Thin layer chromatography (Radio-TLC)

Radio-TLC was performed using Scan-RAM Radio TLC detector.

9.1.6 UV-visible Spectroscopy

A Varian Cary 50 Bio UV-vis spectrometer was used measuring absorption spectra from 250 nm to 800 nm.

9.1.7 Fluorescence Spectroscopy

A Varian Cary Eclipse Fluorescence spectrometer was used measuring excitation and emission from 400 nm to 800 nm.

9.1.8 Materials

Reagents for chemical reactions were purchased from Sigma-Aldrich, Fisher, CheMatech, Acros, and Click-Chemistry Tools. Chemicals were used as received without further purification. Solvents used were of general purpose grade and used as received. Acetonitrile (MeCN), dichloromethane (DCM), tetrahydrofuran (THF), and methanol (MeOH) were dried over molecular sieves, following activation at 300 °C for 18 h.

9.2 HPLC purification

9.2.1 Analytical

9.2.1.1 System A

Analytical RP-HPLC (ACE 5, C18 column, 4.6 × 250 mm 100) with (ethanol) and (20 mM sodium acetate, pH 5) as eluents, an isocratic gradient of 5% (5 min) of (20 mM sodium acetate, pH 5), then a linear gradient from 5 to 80% (35 min) at a flow rate of 1.0 mL.min⁻¹. UV-Vis detection with an Agilent Technologies 1200 series diode array detector at 214, 254, 280, 300 nm. Radio-count detected with a Flow-RAM, NaI radio-HPLC detector (PMT1-310437).

9.2.1.2 System B

Analytical RP-HPLC (ACE 5, C18 column, 4.6 × 250 mm 100) with (ethanol) and (20 mM sodium acetate, pH 3) as eluents, an isocratic gradient of 5% (5 min) of (20 mM sodium acetate, pH 3), then a linear gradient from 5 to 80% (35 min) at a flow rate of 1.0 mL.min⁻¹. UV-Vis detection with an Agilent Technologies 1200 series diode array detector at 214, 254, 280, 300 nm. Radio-count detected with a Flow-RAM, NaI radio-HPLC detector (PMT1-310437).

9.2.1.3 System C

Analytical RP-HPLC (ACE 5, C18 column, 10.0 × 250 mm) with (acetonitrile/0.1% TFA) and (H₂O/0.1% TFA) as eluents, initially isocratic gradient of 2% (5 mins) (acetonitrile/0.1% TFA) before increasing to 30% (18 min) (acetonitrile/0.1% TFA), at a flow rate of 1.0 mL.min⁻¹. UV-Vis detection with an Agilent Technologies 1200 series diode array detector at 214, 254, 280, 300 nm.

9.2.1.4 System D

Analytical RP-HPLC (ACE 5, C18 column, 10.0 × 250 mm) with (acetonitrile/0.1% TFA) and (H₂O/0.1% TFA) as eluents, initially isocratic gradient of 40% (5 mins) (acetonitrile/0.1% TFA) before increasing to 90% (20 min) (acetonitrile/0.1% TFA), before increasing further to 90% (0.5 min) (acetonitrile/0.1% TFA) becoming isocratic at 90% (5 min) at a flow rate of 1.0 mL.min⁻¹. UV-Vis detection with an Agilent Technologies 1200 series diode array detector at 214, 254, 280, 300 nm.

9.2.1.5 System E

Analytical RP-HPLC (ACE 5, C18 column, 10.0 × 250 mm) with (acetonitrile/0.1% TFA) and (H₂O/0.1% TFA) as eluents, initially isocratic gradient of 5% (5 mins) (acetonitrile/0.1% TFA) before increasing to 65% (15 min) (acetonitrile/0.1% TFA), at a flow rate of 1.0 mL.min⁻¹. UV-Vis detection with an Agilent Technologies 1200 series diode array detector at 214, 254, 280, 300 nm.

9.2.1.6 System F

Analytical RP-HPLC (ACE 5, C18 column, 10.0 x 250 mm) with (acetonitrile/0.1% TFA) and (H₂O/0.1% TFA) as eluents, initially isocratic gradient of 10% (5 mins) (acetonitrile/0.1% TFA) before increasing to 90% (20 min) (acetonitrile/0.1% TFA), at a flow rate of 1.0 mL.min⁻¹. UV-Vis detection with an Agilent Technologies 1200 series diode array detector at 214, 254, 280, 300 nm. Radio-count detected with a Flow-RAM, NaI radio-HPLC detector (PMT1-310437).

9.2.1.6 System G

Analytical RP-HPLC (ACE 5, C18 column, 10.0 x 250 mm) with (acetonitrile/0.1% TFA) and (H₂O/0.1% TFA) as eluents, initially isocratic gradient of 2% (5 mins) (acetonitrile/0.1% TFA) before increasing to 70% (15 min) (acetonitrile/0.1% TFA), at a flow rate of 1.0 mL.min⁻¹. UV-Vis detection with an Agilent Technologies 1200 series diode array detector at 214, 254, 280, 300 nm. Radio-count detected with a Flow-RAM, NaI radio-HPLC detector (PMT1-310437).

9.2.1.7 System H

Analytical radio-HPLC (ACE Excel, C18 column, 4.6 x 250 mm) with (CH₃CN/0.1% TFA) and (H₂O/0.1% TFA) as eluents, initially isocratic at 2% (CH₃CN/0.1% TFA) (5 mins), linear gradient from 2 to 70% (20 min) of (CH₃CN/0.1% TFA) at a flow rate of 1.0 mL.min⁻¹. UV-Vis detection with an Agilent Technologies 1200 series diode array detector at 214, 254, 280, 300 nm. Radio-count detected with a Flow-RAM, NaI radio-HPLC detector (PMT1-310437).

9.2.1.8 System I

Analytical RP-HPLC (ACE Excel, C18 column, 4.6 x 250 mm) with (CH₃CN/0.1% TFA) and (H₂O/0.1% TFA) as eluents, initially isocratic at 5% (CH₃CN/0.1% TFA) (5 mins), linear gradient from 2 to 65% (20 min) of (CH₃CN/0.1% TFA) at a flow rate of 1.0 mL.min⁻¹. UV-Vis detection with an Agilent Technologies 1200 series diode array detector at 214, 254, 280, 300 nm.

9.2.1.9 System J

Analytical RP-HPLC (ACE Excel, C18 column, 4.6 x 250 mm) with (CH₃CN/0.1% TFA) and (H₂O/0.1% TFA) as eluents, initially isocratic at 12% (CH₃CN/0.1% TFA) (5 mins), linear gradient from 12 to 55% (20 min) of (CH₃CN/0.1% TFA) at a flow rate of 1.0 mL.min⁻¹. UV-Vis detection with an Agilent Technologies 1200 series diode array detector at 214, 254, 280, 300 nm.

9.2.1.10 System K

Analytical RP-HPLC (ACE Excel, C18 column, 4.6 x 250 mm) with (CH₃CN/0.1% TFA) and (H₂O/0.1% TFA) as eluents, initially isocratic at 2% (CH₃CN/0.1% TFA) (5 mins), linear gradient from 2 to 55% (20 min) of (CH₃CN/0.1% TFA) at a flow rate of 1.0 mL.min⁻¹. UV-Vis detection with an Agilent Technologies 1200 series diode array detector at 214, 254, 280, 300 nm.

9.2.1.11 System L

Analytical RP-HPLC (ACE Excel, C18 column, 4.6 x 250 mm) with (CH₃CN/0.1% TFA) and (H₂O/0.1% TFA) as eluents, initially isocratic at 2% (CH₃CN/0.1% TFA) (5 mins), linear gradient from 2 to 50% (20 min) of (CH₃CN/0.1% TFA), linear gradient to 80% (5 min) at a flow rate of 1.0 mL.min⁻¹. UV-Vis detection with an Agilent Technologies 1200 series diode array detector at 214, 254, 280, 300 nm.

9.2.1.12 System M

Analytical RP-HPLC (ACE 5, C18 column, 4.6 × 250 mm 100) with (methanol) and (0.2 M ammonium formate buffer, pH 6.5) as eluents, a linear gradient from 49 to 60% (20 min) of (methanol) at a flow rate of 1.0 mL/min⁻¹. UV-Vis detection with an Agilent Technologies 1200 series diode array detector at 214, 254, 280, 300 nm.

9.2.1.13 System N

Analytical RP-HPLC (ACE 5, C18 column, 4.6 × 250 mm 100) with (CH₃CN/0.1% TFA) and (0 H₂O/0.1% TFA) as eluents, initially a linear gradient from 20 to 95% (20 min) of (CH₃CN/0.1% TFA), isocratic at 95% (5 min) at a flow rate of 1.0 mL/min⁻¹. UV-Vis detection with an Agilent Technologies 1200 series diode array detector at 214, 254, 280, 300 nm.

9.2.1.14 System O

Analytical radio-HPLC (ACE Excel, C18 column, 4.6 x 250 mm) with (CH₃CN/0.1% TFA) and (H₂O/0.1% TFA) as eluents, initially isocratic at 2% (CH₃CN/0.1% TFA) (5 mins), linear gradient from 2 to 30% (10 min) of (CH₃CN/0.1% TFA) at a flow rate of 1.0 mL.min⁻¹. UV-Vis detection with an Agilent Technologies 1200 series diode array detector at 214, 254, 280, 300 nm. Radio-count detected with a Flow-RAM, NaI radio-HPLC detector (PMT1-310437).

9.2.2 Semi-preparative

9.2.2.1 System 1

Semi-preparative RP-HPLC (ACE Excel, C18 column, 10.0 x 250 mm) with (ethanol) and (20 mM sodium acetate, pH 6.8) as eluents, initially linear gradient from 5% (10 min) of (ethanol), followed by a linear gradient to 50% (0.5 min) of (ethanol) where the gradient stayed isocratic at 50% (10 min). Then a return to initial condition by linear gradient from 50 to 5% (0.5 min), before remaining isocratic from 5% (10 min) of (ethanol) at a flow rate of 5.0 mL.min⁻¹. UV-Vis detection with an Agilent Technologies 1200 series diode array detector at 254 nm. Radio-count detected with a Flow-RAM, NaI radio-HPLC detector (PMT1-310437).

9.2.2.2 System 2

Semi-preparative RP-HPLC (ACE 5, C18 column, 10.0 x 250 mm) with (methanol/0.1% TFA) and (H₂O/0.1% TFA) as eluents, isocratic gradient of 89% (30 mins) (H₂O/0.1% TFA) at a flow rate of 5.0 mL.min⁻¹. UV-Vis detection with an Agilent Technologies 1200 series diode array detector at 254 nm. Radio-count detected with a Flow-RAM, NaI radio-HPLC detector (PMT1-310437).

9.2.2.3 System 3

Semi-preparative RP-HPLC (ACE 5, C18 column, 10.0 x 250 mm) with (methanol/0.1% TFA) and (H₂O/0.1% TFA) as eluents, isocratic gradient of 85% (30 mins) (H₂O/0.1% TFA) at a flow rate of 5.0 mL.min⁻¹. UV-Vis detection with an Agilent Technologies 1200 series diode array detector at 254 nm. Radio-count detected with a Flow-RAM, NaI radio-HPLC detector (PMT1-310437).

9.2.2.4 System 4

Semi-preparative RP-HPLC (ACE 5, C18 column, 10.0 x 250 mm) with (acetonitrile/0.1% TFA) and (H₂O/0.1% TFA) as eluents, initially isocratic gradient of 5% (5 mins) (acetonitrile/0.1% TFA) before increasing to 40% (10 min) (acetonitrile/0.1% TFA) at a flow rate of 5.0 mL.min⁻¹. UV-Vis detection with an Agilent Technologies 1200 series diode array detector at 254 nm.

9.2.2.5 System 5

Semi-preparative RP-HPLC (ACE 5, C18 column, 10.0 x 250 mm) with (acetonitrile/0.1% TFA) and (H₂O/0.1% TFA) as eluents, initially isocratic gradient of 2% (5 mins) (acetonitrile/0.1% TFA) before increasing to 30% (20 min) (acetonitrile/0.1% TFA) at a flow rate of 5.0 mL.min⁻¹. UV-Vis detection with an Agilent Technologies 1200 series diode array detector at 254 nm.

9.2.2.6 System 6

Semi-preparative RP-HPLC (ACE 5, C18 column, 10.0 x 250 mm) with (acetonitrile/0.1% TFA) and (H₂O/0.1% TFA) as eluents, initially isocratic gradient of 5% (5 mins) (acetonitrile/0.1% TFA) before

increasing to 65% (15 min) (acetonitrile/0.1% TFA) at a flow rate of 5.0 mL.min⁻¹. UV-Vis detection with an Agilent Technologies 1200 series diode array detector at 254 nm.

9.2.2.7 System 7

Semi-preparative RP-HPLC (ACE 5, C18 column, 10.0 x 250 mm) with (acetonitrile/0.1% TFA) and (H₂O/0.1% TFA) as eluents, initially isocratic gradient of 5% (5 mins) (acetonitrile/0.1% TFA) before increasing to 95% (20 min) (acetonitrile/0.1% TFA) at a flow rate of 5.0 mL.min⁻¹. UV-Vis detection with an Agilent Technologies 1200 series diode array detector at 254 nm.

9.2.2.8 System 8

Semi-preparative RP-HPLC (ACE 5, C18 column, 10.0 x 250 mm) with (acetonitrile/0.1% TFA) and (H₂O/0.1% TFA) as eluents, initially isocratic gradient of 5% (5 mins) (acetonitrile/0.1% TFA) before increasing to 20% (15 min) (acetonitrile/0.1% TFA) at a flow rate of 5.0 mL.min⁻¹. UV-Vis detection with an Agilent Technologies 1200 series diode array detector at 254 nm.

9.2.2.9 System 9

Semi-preparative RP-HPLC (ACE Excel, C18 column, 10.0 x 250 mm) with (CH₃CN/0.1% TFA) and (H₂O/0.1% TFA) as eluents, initially linear gradient from 2 to 70% (20 min) of (CH₃CN/0.1% TFA) at a flow rate of 5.0 mL.min⁻¹. UV-Vis detection with an Agilent Technologies 1200 series diode array detector at 254 nm. Radio-count detected with a Flow-RAM, NaI radio-HPLC detector (PMT1-310437).

9.2.2.10 System 10

Semi-preparative RP-HPLC (ACE Excel, C18 column, 10.0 x 250 mm) with (CH₃CN/0.1% TFA) and (H₂O/0.1% TFA) as eluents, initially isocratic at 2% (CH₃CN/0.1% TFA) (5 mins), linear gradient from 2 to 55% (20 min) at a flow rate of 5.0 mL.min⁻¹. UV-Vis detection with an Agilent Technologies 1200 series diode array detector at 254 nm.

9.2.2.11 System 11

Semi-preparative RP-HPLC (ACE Excel, C18 column, 10.0 x 250 mm) with (CH₃CN/0.1% TFA) and (H₂O/0.1% TFA) as eluents, initially linear gradient from 15 to 30% (20 min) of (CH₃CN/0.1% TFA) at a flow rate of 5.0 mL.min⁻¹. UV-Vis detection with an Agilent Technologies 1200 series diode array detector at 254 nm. Radio-count detected with a Flow-RAM, NaI radio-HPLC detector (PMT1-310437)

9.2.2.12 System 12

Semi-preparative RP-HPLC (ACE Excel, C18 column, 10.0 x 250 mm) with (CH₃CN/0.1% TFA) and (H₂O/0.1% TFA) as eluents, initially isocratic at 2% (CH₃CN/0.1% TFA) (5 mins), linear gradient from 2 to 50% (20 min) of (CH₃CN/0.1% TFA) at a flow rate of 5.0 mL.min⁻¹. UV-Vis detection with an Agilent Technologies 1200 series diode array detector at 254 nm.

9.2.2.13 System 13

Semi-preparative RP-HPLC (ACE Excel, C18 column, 10.0 x 250 mm) with (CH₃CN/0.1% TFA) and (H₂O/0.1% TFA) as eluents, initially isocratic at 2% (CH₃CN/0.1% TFA) (5 mins), linear gradient from 2 to 50% (20 min) of (CH₃CN/0.1% TFA), linear gradient to 80% (5 min) of (CH₃CN/0.1% TFA) at a flow rate of 5.0 mL·min⁻¹. UV-Vis detection with an Agilent Technologies 1200 series diode array detector at 254 nm.

9.2.2.14 System 14

Semi-preparative RP-HPLC (ACE Excel, C18 column, 10.0 x 250 mm) with (CH₃CN/0.1% TFA) and (H₂O /0.1% TFA) as eluents, initially linear gradient from 10 to 70% (20 min) of (CH₃CN/0.1% TFA) at a flow rate of 5.0 mL·min⁻¹. UV-Vis detection with an Agilent Technologies 1200 series diode array detector at 254 nm. Radio-count detected with a Flow-RAM, NaI radio-HPLC detector (PMT1-310437).

9.2.2.15 System 15

Semi-preparative RP-HPLC (ACE Excel, C18 column, 10.0 x 250 mm) with (CH₃CN/0.1% TFA) and (H₂O/0.1% TFA) as eluents, initially linear gradient from 15 to 35% (20 min) of (CH₃CN/0.1% TFA) at a flow rate of 5.0 mL/min⁻¹. UV-Vis detection with an Agilent Technologies 1200 series diode array detector at 254 nm.

9.2.2.16 System 16

Semi-preparative RP-HPLC (ACE Excel, C18 column, 10.0 x 250 mm) with (methanol) and (0.2 M ammonium formate buffer, pH 6.5) as eluents, a linear gradient from 49 to 60% (20 min) of (methanol) at a flow rate of 5.0 mL/min⁻¹. UV-Vis detection with an Agilent Technologies 1200 series diode array detector at 254 nm.

9.2.2.17 System 17

Semi-preparative RP-HPLC (ACE Excel, C18 column, 10.0 x 250 mm) with (CH₃CN/0.1% TFA) and (H₂O/0.1% TFA) as eluents, initially linear gradient from 20 to 40% (20 min) of (CH₃CN/0.1% TFA) at a flow rate of 5.0 mL/min⁻¹. UV-Vis detection with an Agilent Technologies 1200 series diode array detector at 254 nm.

9.2.2.18 System 18

Semi-preparative RP-HPLC (ACE Excel, C18 column, 10.0 x 250 mm) with (methanol) and (0.2 M ammonium formate buffer, pH 6.5) as eluents, initially linear gradient from 40 to 55% (20 min) of (methanol), at a flow rate of 5.0 mL/min⁻¹. UV-Vis detection with an Agilent Technologies 1200 series diode array detector at 254 nm. Radio-count detected with a Flow-RAM, NaI radio-HPLC detector (PMT1-310437).

9.2.2.19 System 19

Semi-preparative RP-HPLC (ACE Excel, C18 column, 10.0 x 250 mm) with (CH₃CN/0.1% TFA) and (H₂O /0.1% TFA) as eluents, initially isocratic conditions at 2% (5 min) of (CH₃CN/0.1% TFA), followed by a linear gradient from 2 to 60% (10 min) of (CH₃CN/0.1% TFA) at a flow rate of 5.0 mL.min⁻¹. UV-Vis detection with an Agilent Technologies 1200 series diode array detector at 254 nm. Radio-count detected with a Flow-RAM, NaI radio-HPLC detector (PMT1-310437).

9.2.2.20 System 20

Semi-preparative RP-HPLC (ACE Excel, C18 column, 10.0 x 250 mm) with (CH₃CN/0.1% TFA) and (H₂O /0.1% TFA) as eluents, initially isocratic conditions at 2% (5 min) of (CH₃CN/0.1% TFA), followed by a linear gradient from 2 to 30% (20 min) of (CH₃CN/0.1% TFA) at a flow rate of 5.0 mL.min⁻¹. UV-Vis detection with an Agilent Technologies 1200 series diode array detector at 254 nm. Radio-count detected with a Flow-RAM, NaI radio-HPLC detector (PMT1-310437).

9.2.2.21 System 21

Semi-preparative RP-HPLC (ACE Excel, C18 column, 10.0 x 250 mm) with (CH₃CN/0.1% TFA) and (H₂O /0.1% TFA) as eluents, initially isocratic conditions at 2% (5 min) of (CH₃CN/0.1% TFA), followed by a linear gradient from 2 to 80% (15 min) of (CH₃CN/0.1% TFA) at a flow rate of 5.0 mL.min⁻¹. UV-Vis detection with an Agilent Technologies 1200 series diode array detector at 254 nm. Radio-count detected with a Flow-RAM, NaI radio-HPLC detector (PMT1-310437).

9.2.2.22 System 22

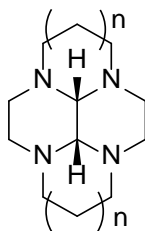
Semi-preparative RP-HPLC (ACE Excel, C18 column, 10.0 x 250 mm) with (methanol) and (0.2 M ammonium formate buffer, pH 6.5) as eluents, initially a linear gradient from 50 to 0% (20 min) of (0.2 M ammonium formate buffer, pH 6.5) at a flow rate of 5.0 mL.min⁻¹. UV-Vis detection with an Agilent Technologies 1200 series diode array detector at 254 nm. Radio-count detected with a Flow-RAM, NaI radio-HPLC detector (PMT1-310437).

9.2.2.23 System 23

Semi-preparative RP-HPLC (ACE Excel, C18 column, 10.0 x 250 mm) with (methanol) and (0.2 M ammonium formate buffer, pH 6.5) as eluents, initially a linear gradient from 50 to 20% (20 min) of (0.2 M ammonium formate buffer, pH 6.5) at a flow rate of 5.0 mL.min⁻¹. UV-Vis detection with an Agilent Technologies 1200 series diode array detector at 254 nm. Radio-count detected with a Flow-RAM, NaI radio-HPLC detector (PMT1-310437).

9.3 Compound Synthesis

9.3.1 Synthesis of *cis*-3,5,8,10-tetraazaperhydropyrene (**1**) and *cis*-13-1,4,7,10-tetraazatetracyclo[5.5.1.0^{4,14}.0^{10,13}]tetradecane (**2**)



$$n \equiv \begin{matrix} 1 \\ 0 \\ 1 \\ 2 \end{matrix}$$

General procedure A

The macrocycle was dissolved in methanol and cooled to -10°C using a dry ice acetone bath. A cold (0°C) aqueous solution of glyoxal was added dropwise over 90 min. The clear solution was stirred at -10°C for 30 min then at RT for 3 hours. The solvent was removed *in vacuo* and the crude solid was redissolved in diethyl ether. The filtrate was dried (magnesium sulphate), filtered and solvent removed *in vacuo*.

Cis-3,5,8,10-tetraazaperhydropyrene (**1**)

Amounts: 1,4,8,11-tetraazacyclotetradodecane (4.0 g, 20.0 mmol), methanol (400 mL), glyoxal (40%, 2.93 g, 50.5 mmol), diethyl ether (100 mL). To yield a white solid, *cis*-3,5,8,10-tetraazaperhydropyrene (**1**), (3.67 g, 16.5 mmol, 82.7% yield).

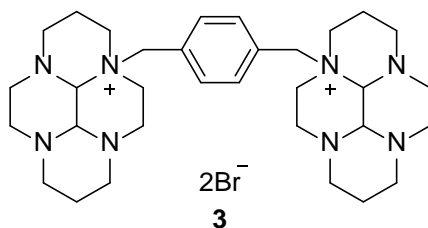
^1H NMR (400 MHz, CDCl_3 , δ): 1.21 (m, N- β - CH_2 , 2H), 2.09-2.41 (m, N- α - CH_2 , 8H), 2.75 (d, $J = 12.0$ Hz, N- β - CH_2 , 2H), 2.91-2.95 (m, N- α - CH_2 , 6H), 3.06 (s, H_{aminal} , 2H), 3.55 (t, $J = 8.0$ Hz, N- α - CH_2 , 2H). ^{13}C NMR (100 MHz, CDCl_3 , δ): 19.70 (N- β - CH_2), 44.87 (N- α - CH_2), 52.59 (N- α - CH_2), 54.46 (N- α - CH_2), 56.15 (CH). MS (ES-MS): m/z 222.9 (M^+). Anal. calcd for $\text{C}_{12}\text{H}_{22}\text{N}_4^+$: C, 64.83; H, 9.97; N, 25.20. Found, : C, 64.67; H, 10.03; N, 24.98.

***Cis*-13-1,4,7,10-tetraazatetracyclo[5.5.1.0^{4,14}.0^{10,13}]tetradecane (2)**

Amounts: 1,4,7,10-Tetraazacyclododecane (4.18 g, 24.3 mmol), methanol (400 mL), glyoxal (40%, 2.50 g, 60.7 mmol), diethyl ether (100 mL). To yield a white solid, *cis*-13-1,4,7,10-tetraazatetracyclo[5.5.1.0^{4,14}.0^{10,13}]tetradecane (**2**), (4.19 g, 18.9 mmol, 88.9% yield).

¹H NMR (400 MHz, CDCl₃, δ): 2.49-2.61 (m, N-α-CH₂, 4H), 2.72-2.78 (m, N-α-CH₂, 4H), 2.89-3.02 (m, N-α-CH₂, 8H), 3.13 (s, H_{aminal}, 2H). ¹³C NMR (100 MHz, CDCl₃, δ): 44.88 (N-α-CH₂), 50.02 (N-α-CH₂), 52.61 (N-α-CH₂), 54.49 (N-α-CH₂), 56.17 (C_{aminal}). MS (ES-MS): *m/z* 194.9 (M⁺). Anal. Calcd for C₁₀H₁₉N₄: C, 61.82; H, 9.34; N, 28.84. Found, : C, 61.67; H, 9.29; N, 28.16.

9.3.2 Synthesis of *cis*-3,3'-(1,4-phenylenebis(methylene)-bis(decahydro-3,5,8,10-tetraazapyrenim) dibromide (**3**)



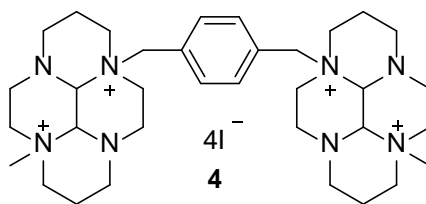
General procedure B

Macrocycle was added to dry acetonitrile, to this pendent arm was added and the solution stirred under argon for 3 d at RT. Following this the resulting precipitate was filtered and washed with acetonitrile and diethyl ether. Dried under vacuum on a Schlenk line.

Amounts: *Cis*-3,5,8,10-tetraazaperhydropyrene (**1**) (5.20 g, 23.4 mmol), 1,4-bis-bromomethylbenzene (3.09 g, 11.7 mmol), dry acetonitrile (120 mL), dry acetonitrile (2 x 10 mL) and diethyl ether (2 x 10 mL). To yield a white powder, *cis*-3,3'-(1,4-phenylenebis(methylene)-bis(decahydro-3,5,8,10-tetraazapyrenim) dibromide (**3**), (3.17 g, 11.6 mmol, 48.4%).

^1H NMR (400 MHz, D_2O , δ): 1.43 (d, $J = 12.0$ Hz, N- β - CH_2 , 2H), 1.76 (d, $J = 12.0$ Hz, N- β - CH_2 , 2H), 2.10-2.31 (m, N- α - CH_2 , 6H), 2.45-2.48 (m, N- β - CH_2 , 4H), 2.60 (t, $J = 8.0$ Hz, N- α - CH_2 , 2H), 2.97-3.13 (m, N- α - CH_2 , 16H), 3.23 (t, $J = 8.0$ Hz, N- α - CH_2 , 2H), 3.32-3.34 (m, N- α - CH_2 , 2H), 3.43-3.61 (m, N- α - CH_2 , 4H), 3.67 (s, H_{aminal} , 2H), 4.20 (t, $J = 8.0$ Hz, CH_2 -Ar, 2H), 4.12 (s, H_{aminal} , 2H), 5.13 (d, $J = 12.0$ Hz, CH_2 -Ar, 2H), 7.63 (s, Ar H, 4H). ^{13}C NMR: (100 MHz, D_2O , δ): 18.11 (N- β - CH_2), 18.45 (N- β - CH_2), 41.94 (N- α - CH_2), 46.69 (N- α - CH_2), 48.33 (N- α - CH_2), 51.47 (N- α - CH_2), 52.04 (N- α - CH_2), 53.42 (N- α - CH_2), 54.09 (N- α - CH_2), 60.25 (N- α - CH_2), 61.75 ($\underline{\text{C}}\text{H}_2$ -Ar), 69.69 (C_{aminal}), 82.40 (C_{aminal}), 128.65 (C-Ar), 134.05 (Ar-H). MS (ES-MS): m/z 274.2 (M-2Br, 159.8). Anal. Calcd for $\text{C}_{32}\text{H}_{52}\text{N}_8\text{Br}_2 \cdot \text{H}_2\text{O}$: C, 52.89; H, 7.49; N, 21.99. Found: C, 53.02; H, 7.52; N, 21.82.

9.3.3 Synthesis of 3-(4(8-methyl-*cis*-decahydro-(5,10-diaza-bicyclo[6.6.2]hexadeco-11-ylmethyl)-benzyl)-1,4,8,11-tetraaza-bicyclo[6.6.2]-hexadecane (**4**)



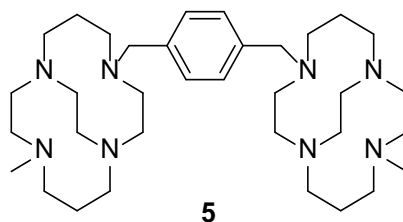
General procedure C

The macrocycle was suspended in anhydrous MeCN under argon. Iodomethane was added dropwise. The white suspension was left to stir for 10 days. A second portion of iodomethane was added after 5 days. Excess iodomethane was removed by flowing nitrogen through the suspension for 30 min. The solid was collected by filtration, washed with ether and dried under vacuum on a Schlenk line.

Amounts: *Cis*-3,3'-(1,4-phenylenebis(methylene))-bis(decahydro-3,5,8,10-tetraazapyrenim) dibromide **3** (2.00 g, 2.83 mmol), acetonitrile (100 mL), iodomethane (1.60 g, 14.1 mol then 0.8 g, 7.05 mmol) diethyl ether (2 x 50 mL). To yield a white solid 3-(4(8-methyl-*cis*-decahydro-(5,10-diaza-bicyclo[6.6.2]hexadeco-11-ylmethyl)-benzyl)-1,4,8,11-tetraaza-bicyclo[6.6.2]-hexadecane (**4**), (1.74 g, 2.60 mmol, 92.1%).

¹H NMR (400 MHz, DMSO-d₆, δ): 1.78 (δ, *J* = 16 Hz, N-β-CH₂, 2H), 1.88 (d, *J* = 12 Hz, N-β-CH₂, 2H), 2.08 (s, CH₃, 3H), 2.33-2.40 (m, CH₃, 3H), 2.43-2.48 (m, N-β-CH₂, 4H) 2.76-3.25 (m, N-α-CH₂, 16H), 3.37-3.50 (m, N-α-CH₂, 8H), 3.56-3.69 (m, N-α-CH₂, 4H), 3.75-3.85 (m, H_{aminal}, 2H), 4.25-4.36 (m, N-α-CH₂, 4H), 4.82-4.94 (m, H_{aminal}, 2H), 5.15-5.49 (m, CH₂-Ar, 4H), 7.72-7.78 (m, Ar H, 4H). ¹³C NMR (100 MHz, DMSO-d₆, δ): 18.14 (N-β-CH₂), 18.45 (N-β-CH₂), 37.87 (N-α-CH₂), 38.09 (N-α-CH₂), 38.31 (N-α-CH₂), 46.54 (N-α-CH₂), 46.67 (N-α-CH₂), 48.38 (N-α-CH₃), 51.14 (N-α-CH₂), 61.01 (N-α-CH₂), 61.48 (N-α-CH₂), 65.54 (CH₂-Ar), 77.05 (C_{aminal}), 77.25 (C_{aminal}), 128.50 (C-Ar), 135.22 (Ar-H). MS (ES-MS): *m/z* 416.66 (M-2I, 253.8). Anal. Calcd for C₃₄H₅₈I₄N₈·H₂O·Cl: C, 53.79; H, 5.39; N, 9.82. Found.: C, 35.48; H, 5.50; N, 9.90.

9.3.4 Synthesis of 1,4-bis((11-methyl-1,4,8,11-tetraazabicyclo[6.6.2]hexadecan-4-yl)methyl)benzene (**5**)



General procedure D

The macrocycle was dissolved in ethanol and sodium borohydride was added in small portions. The mixture was stirred for 14 days at RT. Water was added to decompose excess sodium borohydride and the solvents were removed *in vacuo*. The residue was taken up into water and made strongly basic (pH 14, KOH). The basic solution was extracted with dichloromethane, the combined organic extracts were dried (Na_2SO_4), filtered and solvent removed *in vacuo* and dried under vacuum on a Schlenk line.

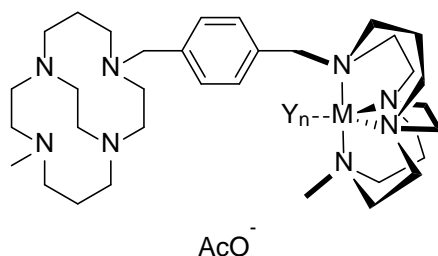
Amounts: 3-(4(8-Methyl-*cis*-decahydro-(5,10-diaza-bicyclo[6.6.2]hexadeco-11-ylmethyl)-benzyl)-1,4,8,11-tetraaza-bicyclo[6.6.2]-hexadecane (**4**) (7.3 g, 6.73 mmol), sodium borohydride (14.6 g, 386 mmol), ethanol (400 mL), water (100mL, 150 mL), dichloromethane (5 x 50 mL). To yield a clear oil, 1,4-bis((11-methyl-1,4,8,11-tetraazabicyclo[6.6.2]hexadecan-4-yl)methyl)benzene (**5**) (1.42 g, 2.44 mmol, 36.2% yield).

Analytical RP-HPLC analysis carried out with System A; 9.2.1.1 (multiple broad peak; $t_r = 10\text{-}14$ min). $^1\text{H-NMR}$ (400 MHz, D_2O , δ): 1.52-1.98 (M, N- β - CH_2 , 8H), 2.20 (s, CH_3 , 6H), 2.85-3.12 (m, N- α - CH_2 , 16H), 3.21-3.75 (m, N- α - CH_2 , 24H), 4.83 (s, CH_2 -Ar, 4H), 7.26 (dd, $J = 11.0$ Hz, Ar, 4H). $^{13}\text{C NMR}$ (100 MHz, CDCl_3 , δ): 26.97 (N- β - CH_2), 27.88 (N- β - CH_2), 29.79 (N- β - CH_2), 43.09 (CH_3), 52.12 (N- α - CH_2), 52.37 (N- α - CH_2), 54.10 (N- α - CH_2), 54.98 (N- α - CH_2), 56.07 (N- α - CH_2), 56.34 (N- α - CH_2), 56.76 (N- α - CH_2), 58.02 (N- α - CH_2), 59.31 (N- α - CH_2), 59.82 (CH_2 -Ar), 128.72 (C-Ar). MS (HRMS): m/z (M^{2+}) calcd for $\text{C}_{34}\text{H}_{64}\text{N}_8^{2+}$, 292.2621 found, 292.2614. Anal. Calcd for $\text{C}_{34}\text{H}_{64}\text{N}_8 \cdot 3.5\text{H}_2\text{O} \cdot 1.1\text{EtOH} \cdot 2.3\text{HCl}$: C, 55.71; H, 10.06; N, 14.36. Found: C, 55.79; H, 10.12; N, 14.55.

9.3.5 Synthesis of mono metal complexes of ligand 1,4-bis((11-methyl-1,4,8,11-tetraazabicyclo[6.6.2]hexadecan-4-yl)methyl)benzene ([Ni5(OAc)](OAc), [Cu5(OAc)](OAc),

and

[Zn5(OAc)](OAc))



M = Ni²⁺, Y = AcO⁻, (n = 1/2), [Ni⁵(OAc)](OAc)

M = Cu²⁺, Y = AcO⁻, (n = 1), [Cu⁵(OAc)](OAc)

M = Zn²⁺, Y = CH₃CO₂⁻, (n = 1/2), [Zn⁵(OAc)](OAc)

General Procedure E

Macrocycle was dissolved in dry degassed methanol to this a dry methanolic solution of metal salt was added dropwise. For non-configurational restricted macrocycles and side bridge the reaction is stirred at RT for 8 hours. For cross bridge macrocycles the solution was heated at reflux overnight after which the solvent was reduced *in vacuo* ~5 mL and purified via size exclusion chromatography using a LH20 Sephadex column (methanol). Mass spectrometry was used to identify the correct fractions which were recombined and reduced *in vacuo*.

1,4-Bis((11-methyl-1,4,8,11-tetraazabicyclo[6.6.2]hexadecan-4-yl)methyl)benzene nickel(II) acetate [Ni⁵(OAc)](OAc)

Amounts: 1,4-Bis((11-methyl-1,4,8,11-tetraazabicyclo[6.6.2]hexadecan-4-yl)methyl)benzene (5) (40.0 mg, 69.0 μmol), dry methanol (10 mL), nickel(II) acetate (15.0 mg, 69.0 μmol). To yield a light green solid, 4-methyl-11-(4-(4-methyl-1,4,8,11-tetraaza-bicyclo[6.6.2]hexadecylmethyl)-benzyl)-1,2,8,11-tetraaza-bicyclo[6.6.2]-hexadecane nickel(II) acetate ([Ni⁵(OAc)](OAc)), (33.2 mg, 51.0 μmol, 73.8%).

MS (ES-MS): *m/z* 350.1 (M-CH₃CO₂⁻, 34). Anal. calcd for C₃₈H₆₈NiN₈O₄·0.7MeOH·2.1H₂O: expected: C, 56.69; H, 9.22; N, 13.67. Found: C, 56.71; H, 9.18; N, 13.82.

1,4-Bis((11-methyl-1,4,8,11-tetraazabicyclo[6.6.2]hexadecan-4-yl)methyl)benzene copper(II) acetate [Cu₅(OAc)](OAc)

Amounts: 1,4-Bis((11-methyl-1,4,8,11-tetraazabicyclo[6.6.2]hexadecan-4-yl)methyl)benzene (5) (200.0 mg, 0.34 mmol), dry methanol (50 mL), copper(II) acetate (60.8 mg, 0.34 mmol). To yield a blue solid, 1,4-bis((11-methyl-1,4,8,11-tetraazabicyclo[6.6.2]hexadecan-4-yl)methyl)benzene copper(II) acetate ([Cu₅(OAc)](OAc)), (212.0 mg, 0.32 mmol, 95.0%).

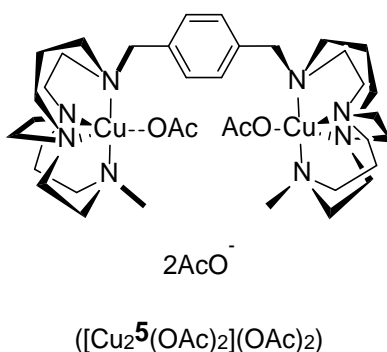
Analytical RP-HPLC analysis carried out with System A (Section 9.2.1.1) (multiple broad peak; t_r = 17-18 min) and System B (Section 9.2.1.2) (multiple broad peak; t_r = 9.30-12 min). MS (HRMS): m/z calcd for C₃₆H₆₆N₈CuO₂²⁺, 352.7297; found, 352.7285. Anal. calcd for C₃₈H₆₈CuN₈O₄·2.5Na·3H₂O: expected: C, 52.10; H, 8.51; N, 12.79. Found,: C, 52.26; H, 8.46; N, 12.50.

1,4-Bis((11-methyl-1,4,8,11-tetraazabicyclo[6.6.2]hexadecan-4-yl)methyl)benzene zinc(II) acetate [Zn₅(OAc)](OAc)

Amounts: 1,4-Bis((11-methyl-1,4,8,11-tetraazabicyclo[6.6.2]hexadecan-4-yl)methyl)benzene (5) (40.0 mg, 68.6 μmol), dry methanol (10 mL), zinc(II) acetate (15.1 mg, 68.6 μmol). To yield off-white solid 1,4-bis((11-methyl-1,4,8,11-tetraazabicyclo[6.6.2]hexadecan-4-yl)methyl)benzene zinc(II) acetate ([Zn₅(OAc)](OAc)), (47.7 mg, 62.4 μmol, 91.0%).

MS (ES-MS): m/z 353.0 (M-CH₃CO₂, 34). Anal. calcd for C₃₈H₆₈ZnN₈O₄·1.2MeOH: expected: C, 59.55; H, 8.94; N, 14.62. Found,: C, 59.32; H, 9.02; N, 14.55.

7.3.6 Synthesis of bis copper complexes of ligand 1,4-bis((11-methyl-1,4,8,11-tetraazabicyclo[6.6.2]hexadecan-4-yl)methyl)benzene ($[\text{Cu}_2\mathbf{5}(\text{OAc})_2](\text{OAc})_2$)

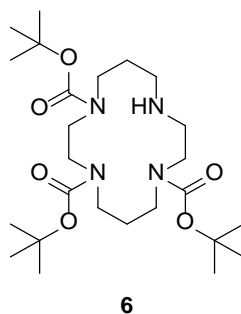


General procedure E was followed.

Amounts: 1,4-Bis((11-methyl-1,4,8,11-tetraazabicyclo[6.6.2]hexadecan-4-yl)methyl)benzene (**5**) (200.0 mg, 0.343 mmol), dry methanol (50 mL), copper(II) acetate (121.6 mg, 0.670 mmol). To yield a blue solid, 1,4-bis((11-methyl-1,4,8,11-tetraazabicyclo[6.6.2]hexadecan-4-yl)methyl)benzene bis-copper(II) acetate ($[\text{Cu}_2\mathbf{5}(\text{OAc})_2](\text{OAc})_2$), (87.6%, 198.0 mg, 0.271 mmol).

Analytical RP-HPLC analysis carried out with System B (Section 9.2.1.2) (multiple broad peak; $t_r = 16-19$ min). Purified using RP semi-preparative HPLC System 1 (Section 9.2.2.1) (multiple peaks, $t_r = 04:50-07:15$). MS (ES-MS, run in formic acid): m/z 400.07 ($\text{M}-4\text{CH}_3\text{CO}_2+\text{HCO}_2+\text{H}$). Anal. calcd for $\text{C}_{42}\text{H}_{76}\text{Cu}_2\text{N}_8\text{O}_8$: expected: C, 53.20; H, 8.08; N, 11.82. Found: C, 53.29; H, 8.09; N, 11.62.

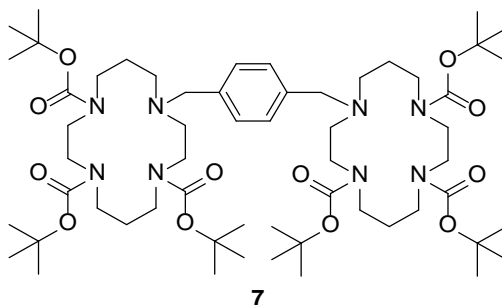
9.3.7 Synthesis of 1,4,8-tris(*tert*-butoxycarbonyl)-1,4,8,11-tetraazacyclotetradecane (**6**)



1,4,8,11-Tetraazacyclotetradecane (1.0 g, 4.99 mmol) was dissolved in dichloromethane (300 mL) and made basic by the addition of triethylamine (3.47 mL, 24.96 mmol). Di-*tert*-butyl dicarbonate (3.44 mL, 14.98 mmol) was then added dropwise over a period of 2 hours. The reaction was stirred overnight, then concentrated *in vacuo*. The crude product was then purified via silica gel flash column chromatography. Eluting with ethyl acetate/methanol (95:5) to yield a white solid, 1,4,8-tris(*tert*-butoxycarbonyl)-1,4,8,11-tetraazacyclotetradecane (**6**) (1.5 g, 3.10 mmol, 62.0% yield).

^1H NMR (400 MHz, CD_3Cl , δ): 1.32 (s, CH_3 , 27H), 1.66-1.82 (m, N- β - CH_2 , 4H), 2.52-2.59 (m, N- α - CH_2 , 4H), 2.76-2.79 (m, N- α - CH_2 , 2H), 3.03-3.09 (m, N- α - CH_2 , 4H), 3.28-3.30 (m, N- α - CH_2 , 4H). ^{13}C NMR (100 MHz, CD_3Cl , δ): 22.6 (N- β - CH_2), 24.9 (N- β - CH_2), 29.2 (N- α - CH_2), 41.0 (N- α - CH_2), 41.2 (CH_3), 46.5 (N- α - CH_2), 52.1 (N- α - CH_2), 54.5 (N- α - CH_2), 82.3 ($\underline{\text{C}}\text{-CH}_3$), 140.8 (C=O). MS (HRMS): m/z (M^+) calcd for $\text{C}_{25}\text{H}_{49}\text{N}_4\text{O}_6^+$, 501.3647; found, 501.3646. Anal. calcd for $\text{C}_{25}\text{H}_{48}\text{N}_4\text{O}_6 \cdot \text{C}_4\text{H}_8\text{O}_2$: expected: C, 61.16; H, 9.59; N, 9.52. Found: C, 61.55; H, 9.84; N, 9.64.

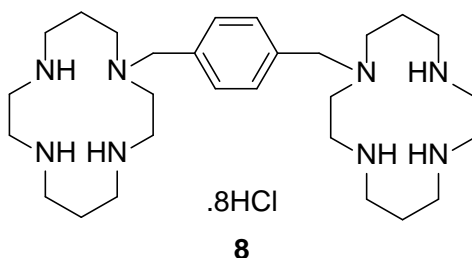
9.3.8 Synthesis of hexa-*tert*-butyl-11,11'-(1,4-phenylenebis(methylene))bis(1,4,8,11-tetraazacyclotetradecane-1,4,8-tricarboxylate (**7**))



To a solution of α,α' -dibromo-*p*-xylene (0.13 g, 0.50 mmol) in dry acetonitrile (150 mL), potassium carbonate (0.41 g, 3.00 mmol) and 1,4,8-tris(*tert*-butoxycarbonyl)-1,4,8,11-tetraazacyclotetradecane (**6**) (0.50 g, 1.00 mmol) was added. The solution was refluxed for 18 hours, before being reduced *in vacuo*. The reaction was taken in up in water (50 mL) and aqueous layer extracted with dichloromethane (3 x 50 mL). The combined organic phase was dried (MgSO_4), and evaporated, and the residue purified by column chromatography on silical gel (ethyl acetate/hexane) to yield a pale yellow solid, hexa-*tert*-butyl-11,11'-(1,4-phenylenebis(methylene))bis(1,4,8,11-tetraazacyclotetradecane-1,4,8-tricarboxylate (**7**)), (0.67 g, 0.607 mmol, 60.8% yield).

^1H NMR (400 MHz, CD_3Cl , δ): 1.32 (s, CH_3 , 54H), 1.52-1.58 (m, N- β - CH_2 , 4H), 1.66-1.69 (m, N- β - CH_2 , 4H), 2.36-2.47 (m, N- α - CH_2 , 8H), 2.82-3.14 (m, N- β - CH_2 , 20H), 3.24-3.29 (m, N- β - CH_2 , 4H), 4.12 (s, CH_2 -Ar, 4H), 7.26 (dd, $J = 11.0$ Hz, Ar-H, 4H). ^{13}C NMR (100 MHz, CD_3Cl , δ): 22.4 (N- β - CH_2), 23.9 (N- β - CH_2), 26.5 (C- CH_3), 48.2 (N- α - CH_2), 49.1 (N- α - CH_2), 50.6 (N- α - CH_2), 51.1 (N- α - CH_2), 54.7 (N- α - CH_2), 56.9 (N- α - CH_2), 67.2 (CH_2 -Ar), 85.4 (C- CH_3), 129.5 (C-Ar), 131.9 (C-Ar), 148.3 (C=O). MS (HRMS): m/z (M+Na, 23) calcd for $\text{C}_{58}\text{H}_{102}\text{N}_8\text{O}_{12}\text{Na}^+$, 1125.7509; found, 1125.7492. Anal. calcd for $\text{C}_{58}\text{H}_{102}\text{N}_8\text{O}_6 \cdot 1.2\text{H}_2\text{O}$: expected: C, 61.92; H, 9.35; N, 9.96. Found.: C, 62.03; H, 9.21; N, 10.04.

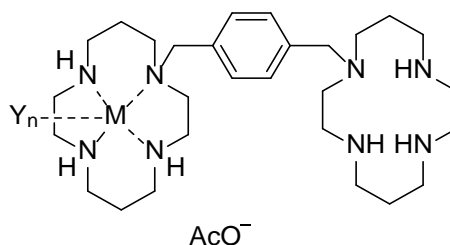
9.3.9 Synthesis of 1,1'-(1,4-phenylenebis(methylene))bis-1,4,8,11-tetraazacyclotetradecane octahydrochloride (**8**)



Hexa-*tert*-butyl 11,11'-(1,4-phenylenebis(methylene))bis(1,4,8,11-tetraazacyclotetradecane-1,4,8-tricarboxylate (**7**) (0.65 g, 590.0 μ mol) was dissolved in 5 mL of hydrochloric acid (3 M). The reaction was stirred under argon for 16 hours, upon which the reaction was reduced *in vacuo* to yield the off-white precipitate, 1,1'-(1,4-Phenylenebis(methylene))bis-1,4,8,11-tetraazacyclotetradecane octahydrochloride (**8**), (0.42 g, 0.53 mmol, 90.4% yield).

^1H NMR (400 MHz, CD_3Cl , δ): 1.86-1.94 (m, N- β - CH_2 , 4H), 1.97-2.08 (m, NH, 6H), 2.96 (m, N- α - CH_2 , 4H), 3.09-3.33 (m, N- α - CH_2 , 28H), 4.04 (s, CH_2 -Ar, 4H), 7.38 (s, Ar-H, 4H). ^{13}C NMR (500 MHz, D_2O , δ): 18.19 (N- β - CH_2), 18.66 (N- β - CH_2), 30.18 (N- α - CH_2), 37.23 (N- α - CH_2), 37.45 (N- α - CH_2), 41.08 (N- α - CH_2), 41.68 (N- α - CH_2), 44.64 (N- α - CH_2), 47.62 (N- α - CH_2), 58.52 ($\underline{\text{C}}\text{H}_2$ -Ar), 131.06 (C-Ar), 131.92 (C-Ar). MS (HRMS): m/z (M^+) calcd for $\text{C}_{28}\text{H}_{63}\text{N}_8\text{Cl}_8^+$, 791.3997; found, 791.2678. Anal. calcd for $\text{C}_{28}\text{H}_{54}\text{N}_8 \cdot 8\text{HCl} \cdot 2.2\text{H}_2\text{O}$: expected: C, 40.32; H, 8.02; N, 13.43. Found,: C, 40.75; H, 8.08; N, 13.23.

9.3.10 Synthesis of mono metal complexes of 1,1'-(1,4-phenylenebis(methylene))bis(1,4,8,11-tetraazacyclotetradecane) ([Ni8(OAc)](OAc), [Cu8(OAc)](OAc) and [Zn8(OAc)](OAc))



M = Ni²⁺, Y = AcO⁻, (n = 1/2), [Ni8(OAc)](OAc)
M = Cu²⁺, Y = AcO⁻, (n = 1), [Cu8(OAc)](OAc)
M = Zn²⁺, Y = AcO⁻, (n = 1/2), [Zn8(OAc)](OAc)

General procedure E was followed.

1,1-(1,4-Phenylenebis(methylene))bis(1,4,8,11-tetraazacyclotetradecane) nickel(II) acetate [Ni8(OAc)](OAc)

Amounts: 1,1'-(1,4-Phenylenebis(methylene))bis-1,4,8,11-tetraazacyclotetradecane octahydrochloride (**8**) (50.0 mg, 60.2 μmol), dry methanol (10 mL), nickel(II) acetate (14.9 mg, 60.2 μmol). To yield a light green solid, 1,1'-(1,4-Phenylenebis(methylene))bis(1,4,8,11-tetraazacyclotetradecane) nickel(II) acetate ([Ni8(OAc)](OAc)), (50.9 mg, 52.4 μmol, 87.0%).

MS (ES-MS): *m/z* 311.2 (M-CH₃CO₂+H, 33). Anal. calcd for C₃₂H₆₀N₈NiO₄·4.2HCl·1.1H₂O·0.2MeOH: expected: C, 44.55; H, 8.18; N, 12.23. Found: C, 44.32; H, 8.05; N, 12.10.

1,1'-(1,4-Phenylenebis(methylene))bis(1,4,8,11-tetraazacyclotetradecane) copper(II) acetate [Cu8(OAc)](OAc)

Amounts: 1,1'-(1,4-Phenylenebis(methylene))bis-1,4,8,11-tetraazacyclotetradecane octahydrochloride (**8**) (50.0 mg, 60.2 μmol), dry methanol (5 and 10 mL), copper(II) acetate (10.9 mg, 060.2 μmol). To yield a blue solid, 1,1'-(1,4-Phenylenebis(methylene))bis(1,4,8,11-tetraazacyclotetradecane) copper(II) acetate ([Cu8(OAc)](OAc)), (48.0 mg, 50.6 μmol, 84.0%).

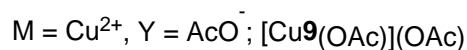
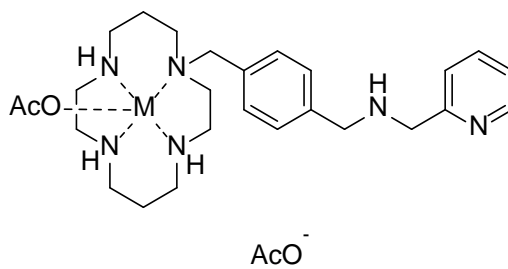
Purified using RP semi-preparative HPLC System 2 (Section 9.2.2.2) (multiple peaks, t_r = 19-20 min). MS (ES-MS): m/z 312.5 (M-CH₃CO₂+H, 33). Anal. calcd for C₃₂H₆₀CuN₈O₄·4HCl·1H₂O: expected: C, 45.31; H, 7.84; N, 13.21. Found, : C, 45.72; H, 7.99; N, 13.10.

**1,1'-(1,4-Phenylenebis(methylene))bis(1,4,8,11-tetraazacyclotetradecane) zinc(II) acetate
[Zn8(OAc)](OAc)**

Amounts: 1,1'-(1,4-Phenylenebis(methylene))bis(1,4,8,11-tetraazacyclotetradecane) (**8**) (50.0 mg, 60.2 μmol), dry methanol (10 mL), zinc(II) acetate (11.0 mg, 60.2 μmol). To yield an off-white solid, 1,1'-(1,4-Phenylenebis(methylene))bis(1,4,8,11-tetraazacyclotetradecane) zinc(II) acetate ([Zn8OAc)](OAc), (48 mg, 49.1 μmol, 81.0%).

MS (ES-MS): m/z 313.6 (M-CH₃CO₂+H, 33). Anal. calcd for C₃₂H₆₀ZnN₈O₄·4HCl·3.5H₂O: expected: C, 42.94; H, 8.00; N, 12.52. Found, : C, 43.04; H, 8.15; N, 12.43.

9.3.11 Synthesis of copper complexed AMD3465 hexahydrobromide ([Cu9(OAc)](OAc))

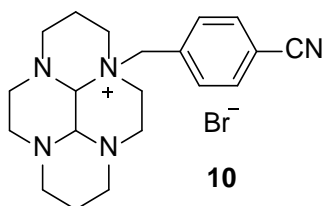


General Procedure E was followed.

Amounts: AMD3465 hexahydrobromide (Abcam, 10.0 mg, 0.010 mmol), copper(II) acetate (2.12 mg, 0.010 mmol), dry methanol (50 mL). To yield a blue solid, AMD3465 copper(II) acetate ([Cu9(OAc)](OAc)) (2.25 mg, 5.0 μmol , 44.7% yield).

Purification using RP semi-preparative HPLC System 3 (Section 9.2.2.3) (multiple peaks, $t_r = 18\text{-}20$ min). MS (ES-MS): m/z 586.2 (M-2CH₃CO₂+TFA). Anal. calcd for C₃₂H₄₄CuNO₄.2HBr.H₂O: expected: C, 43.56; H, 6.27; N, 10.89. Found,: C, 43.08; H, 6.26; N, 11.32.

9.3.12 Synthesis of 3a-(4-(bromomethyl)benzyl)-decahydro-3a,5a,8a,10a-tetraaza-pyrenium bromide (**10**)

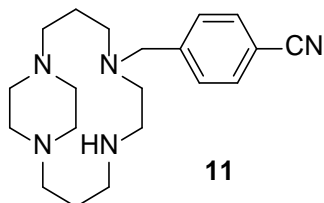


General procedure B was followed.

Amounts: *Cis*-3a,5a,8a,10a-Tetraazaperhydropyrene (**1**) (3.67 g, 16.5 mmol), dry acetonitrile (150 mL), 4-(bromomethyl)benzonitrile (8.01 g, 41.3 mmol), diethyl ether (2 x 25 mL). To yield a white solid, 3a-(4-(bromomethyl)benzyl)-decahydro-3a,5a,8a,10a-tetraaza-pyrenium bromide (**10**), (5.49 g, 13.2 mmol, 72.9%).

^1H NMR (400 MHz, D_2O , δ): 1.42 (d, $J = 13.4$ Hz, N- β - CH_2 , 1H), 1.74 (d, $J = 8.0$ Hz, N- β - CH_2 , 1H), 2.07-2.30-2.34 (m, N- α - CH_2 , 2H), 2.42-2.48 (m, N- β - CH_2 , 2H), 2.96-3.11 (m, N- α - CH_2 , 8H), 3.18-3.32 (m, N- α - CH_2 , 2H), 3.42-3.57 (m, N- α - CH_2 , 2H), 3.67 (s, H_{aminal} , 1H), 4.19 (t, $J = 12$ Hz, CH_2 -Ar, 1H), 4.30 (s, H_{aminal} , 1H), 5.18 (d, $J = 12.0$ Hz, CH_2 -Ar, 1H), 7.67 (dd, $J = 8.0$ Hz, Ar H, 2H), 7.88 (dd, $J = 8.0$ Hz, Ar H, 2H). ^{13}C NMR (100 MHz, D_2O , δ): 18.10 (N- β - CH_2), 18.50 (N- β - CH_2), 42.06 (N- α - CH_2), 46.68 (N- α - CH_2), 48.74 (N- α - CH_2), 51.46 (N- α - CH_2), 52.04 (N- α - CH_2), 53.43 (N- α - CH_2), 54.07 (N- α - CH_2), 60.34 (N- α - CH_2), 61.66 (CH_2 -Ar), 69.67 (C_{aminal}), 82.68 (C_{aminal}), 113.98 (C-Ar), 118.72 (CN), 131.17 (Ar-H), 133.32 (Ar-H), 134.02 (C-Ar). MS (ES-MS): m/z 338.6 (M-Br, 79.9). Anal. calcd for $\text{C}_{20}\text{H}_{28}\text{BrN}_5$: C, 57.42; H, 6.75; N, 16.74. Found: C, 57.60; H, 6.80; N, 16.80.

9.2.13 Synthesis of 1-(4-cyanobenzyl)-1,4,8,11 tetraazabicyclo[10.2.2]-hexadecane (**11**)



Attempted method 1:

3a-(4-(Bromomethyl)benzyl)-decahydro-3a,5a,8a,10a-tetraaza-pyrenium bromide (**10**) (5.5 g, 13.1 mmol) was dissolved in ethanol (250 mL) and sodium borohydride (12.42 g, 328.4 mmol) was added in small portions. The mixture was stirred for 30 min at RT, then heated to reflux for 2 hours. Water was added to decompose excess sodium borohydride and the solvents were removed *in vacuo*. The residue was taken up into water (100 mL) made strongly basic (pH 14, KOH). The basic solution was extracted with dichloromethane (5 x 50 mL), the combined organic extracts were dried (Na₂SO₄), filtered and solvent removed *in vacuo* to yield a white solid. Analytical data indicated that the desired product was not obtained in sufficient purity.

Preferred Method 2:

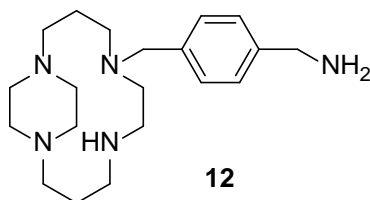
General procedure F:

The macrocycle was dissolved in ethanol and sodium borohydride was added in small portions, and sonicated for a period of time. The solution was heated at 100°C for 30 min in the microwave in the microwave and the solvent removed *in vacuo*. Water was added to decompose excess sodium borohydride and the solvents were removed *in vacuo*. The residue was taken up into water and made strongly basic (pH 14, KOH). The basic solution was extracted with dichloromethane, the combined organic extracts were dried (Na₂SO₄), filtered and solvent removed *in vacuo*.

Amounts: 3a-(4-(Bromomethyl)benzyl)-decahydro-3a,5a,8a,10a-tetraaza-pyrenium bromide (**10**) (0.50 g, 1.20 mmol), ethanol (10 mL), sodium borohydride (0.23 g, 5.98 mmol), microwaved (100°C, 300 W, 30 min), water (100mL, 150 mL), dichloromethane (5 x 50 mL). To yield a clear oil, 4-(1,5,8,12-tetraazabicyclo[10.2.2]hexadecan-8-ylmethyl)benzonitrile (**11**), (0.35 g, 1.02 mmol, 85.8% yield).

^1H NMR (400 MHz, CDCl_3 , δ): 1.61-1.76 (m, N- β - CH_2 , 4H), 2.18-2.24 (m, N- α - CH_2 , 2H), 2.48-2.64 (m, N- α - CH_2 , 12H), 2.85 (t, $J = 8$ Hz, N- α - CH_2 , 2H), 2.94-2.99 (m, N- α - CH_2 , 2H), 3.11-3.18 (m, N- α - CH_2 , 2H), 3.63 (s, CH_2 -Ar + NH, 3H), 7.37 (dd, $J = 8.0$, Hz, Ar-H, 2H), 7.57 (dd, $J = 8.1$ Hz, Ar-H, 2H). ^{13}C NMR (100 MHz, CDCl_3 , δ): 23.66 (N- β - CH_2), 26.14 (N- β - CH_2), 48.25 (N- α - CH_2), 48.42 (N- α - CH_2), 50.26 (N- α - CH_2), 51.38 (N- α - CH_2), 54.75 (N- α - CH_2), 54.98 (N- α - CH_2), 55.51 (N- α - CH_2), 57.00 (N- α - CH_2), 57.70 ($\underline{\text{C}}\text{H}_2$ -Ar), 110.82 (C-Ar), 118.85 (CN), 129.88 (Ar-H), 131.96 (Ar-H), 144.61 (C-Ar). MS (HRMS): m/z calcd for $\text{C}_{20}\text{H}_{31}\text{N}_5^+$, 342.2658; found, 342.2652. Anal. calcd for $\text{C}_{20}\text{H}_{31}\text{N}_5 \cdot 0.9\text{H}_2\text{O} \cdot 0.5\text{EtOH}$: C, 65.62; H, 9.49; N, 18.22. Found.: C, 65.47; H, 9.48; N, 18.54.

9.3.14 Synthesis of 1-(4-aminomethylbenzyl)-1,4,8,11-tetraazabicyclo[10.2.2]-hexadecane (12)



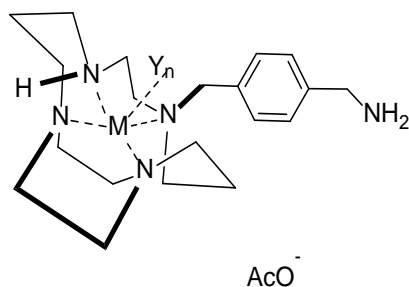
General procedure G

LiAlH₄ was dissolved in anhydrous THF. The macrocycle in anhydrous THF was added dropwise under ice-cooling. After complete addition the mixture was stirred for 30 min and then heated to reflux for 3 hours. The reaction was cooled in an ice-bath, water was added dropwise followed by 15% sodium hydroxide solution followed by a second portion of water. The resulting white precipitate was filtered and washed with THF then water. The aqueous layer was made strongly basic (pH > 12, KOH) and extracted with THF. The organic phases were dried (Na₂SO₄), filtered and solvents removed *in vacuo*.

Amounts: 1-(4-Cyanobenzyl)-1,4,8,11-tetraazabicyclo[10.2.2]-hexadecane (**11**) (4.67 g, 13.16 mmol), Lithium aluminium hydride (2.07 g, 4.14 mmol), anhydrous THF (80 mL), water (1 mL), 15% sodium hydroxide solution (1 mL), THF (2 x 20), water (2 x 10 mL), THF (5 x 25 mL). To yield a pale yellow oil, 1-(4-aminomethylbenzyl)-1,4,8,11-tetraazabicyclo[10.2.2]-hexadecane (**12**), (4.21 g, 12.2 mmol, 92.0%).

¹H NMR (400 MHz, CDCl₃, δ): 1.70-1.81 (m, N-β-CH₂, 4H), 2.91-2.03 (m, N-α-CH₂, 2H), 2.45-2.66 (m, N-α-CH₂, 10H), 2.67-2.83 (m, NH₂, 2H), 3.14 (br s, NH, 1H), 3.22-3.31 (m, N-α-CH₂, 6H), 3.42-3.58 (m, N-α-CH₂, 2H), 3.67 (s, CH₂-Ar, 2H), 3.82 (s, CH₂-Ar, 2H), 7.11-7.26, (br ov, Ar H, 4H). ¹³C NMR (100 MHz, CDCl₃, δ): 24.34 (N-β-CH₂), 26.97 (N-β-CH₂), 48.07 (N-α-CH₂), 52.38 (N-α-CH₂), 54.11 (N-α-CH₂), 54.97 (N-α-CH₂), 55.84 (N-α-CH₂), 56.35 (N-α-CH₂), 56.58 (N-α-CH₂), 56.81 (N-α-CH₂), 57.72 (N-α-CH₂), 59.03 (N-α-CH₂), 59.42 (CH₂-Ar), 62.90 (CH₂-NH₂), 125.35 (C-Ar), 126.87 (Ar-H), 137.65 (Ar-H), 139.07 (C-Ar). MS (ES-MS): *m/z* 346.5 (M⁺). Anal. calcd for C₂₀H₃₅N₅·1.3H₂O·1.3THF: C, 65.60; H, 10.20; N, 15.18. Found, : C, 65.65; H, 9.76; N, 15.12.

9.3.15 Synthesis of metal complexes of ligands 1-(4-aminomethylbenzyl)-1,4,8,11-tetraazabicyclo[10.2.2]-hexadecane ([Ni**12**(OAc)](OAc), [Cu**12**(OAc)](OAc) and [Zn**12**(OAc)](OAc)



M = Ni²⁺, Y = AcO⁻, (n = 1/2); [Ni**12**(OAc)](OAc)
M = Cu²⁺, Y = AcO⁻, (n = 1); [Cu**12**(OAc)](OAc)
M = Zn²⁺, Y = AcO⁻, (n = 1/2); [Zn**12**(OAc)](OAc)

General procedure E was followed.

1-(4-aminomethylbenzyl)-1,4,8,11-tetraazabicyclo[10.2.2]-hexadecane nickel(II) acetate
[Ni12**(OAc)](OAc)**

Amounts: 1-(4-Aminomethylbenzyl)-1,4,8,11-tetraazabicyclo[10.2.2]-hexadecane (**12**) (96.4 mg, 250.0 μmol), methanol (5 mL and 20 mL), nickel(II) acetate tetra-hydrate (122.1 mg, 490.0 μmol). To yield a light green solid, 1-(4-aminomethylbenzyl)-1,4,8,11-tetraazabicyclo[10.2.2]-hexadecane mono nickel(II) acetate ([Ni**12**(OAc)](OAc), (52.0 mg, 101.8 μmol, 40.7% yield).

MS (ES-MS): *m/z* 462.1 (M-CH₃CO₂, 34). Anal. calcd for C₂₄H₄₁ZnN₅O₄·0.8MeOH·0.5H₂O: expected: C, 53.48; H, 8.18; N, 12.57. Found: C, 53.32; H, 8.11; N, 12.67.

**1-(4-aminomethylbenzyl)-1,4,8,11-tetraazabicyclo[10.2.2]-hexadecane copper(II) acetate
[Cu₁₂(OAc)](OAc)**

Amounts: 1-(4-Aminomethylbenzyl)-1,4,8,11-tetraazabicyclo[10.2.2]-hexadecane (**12**) (25.9 mg, 70.0 μ mol), dry methanol (5 mL, 10 mL), copper(II) acetate monohydrate (33.0 mg, 170.0 μ mol). To yield a blue solid, 1-(4-aminomethylbenzyl)-1,4,8,11-tetraazabicyclo[10.2.2]-hexadecane mono copper(II) acetate ([Ni**12**(OAc)](OAc)), (21.0 mg, 36.0 μ mol, 55.2% yield).

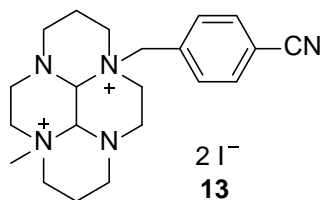
MS (ES-MS): *m/z* 467.1 (M-CH₃CO₂, 34). Anal. calcd for C₂₄H₄₁CuN₅O₄·1.8H₂O: expected: C, 53.22; H, 7.93; N, 12.95. Found,: C, 53.28; H, 7.90; N, 13.11.

**1-(4-aminomethylbenzyl)-1,4,8,11-tetraazabicyclo[10.2.2]-hexadecane mono zinc(II) acetate
[Zn₁₂(OAc)](OAc)**

Amounts: 1-(4-Aminomethylbenzyl)-1,4,8,11-tetraazabicyclo[10.2.2]-hexadecane (**12**) (95.1 mg, 0.240 mmol), methanol (5 mL, 20 mL), zinc(II) acetate (111.0 mg, 0.600 mmol). To yield a white solid, 1-(4-aminomethylbenzyl)-1,4,8,11-tetraazabicyclo[10.2.2]-hexadecane mono zinc(II) acetate ([Zn**12**(OAc)](OAc)), (107 mg, 0.203 mmol, 83.9% yield).

MS (ES-MS): *m/z* 468.1 (M-CH₃CO₂, 34). Anal. calcd for C₂₄H₄₁ZnN₅O₄·0.6MeOH: expected: C, 53.90; H, 7.98; N, 12.77. Found,: C, 53.87; H, 8.00; N, 12.71.

9.3.16 Synthesis of 3a-(4-cyanobenzyl)-8a-(methyl)-decahydro-3a,5a,8a,10a-tetraaza-pyrenium diiodide (**13**)

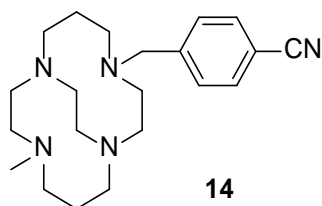


General procedure C was followed.

Amounts: 3a-(4-(Bromomethyl)benzyl)-decahydro-3a,5a,8a,10a-tetraaza-pyrenium bromide (**10**) (1.0 g, 2.38 mmol), dry acetonitrile (60 mL), iodomethane (16.9 g, 120.5 mmol, 7.42 mL, then 5.6 g, 40.1 mmol, 2.47 mL), diethyl ether (2 x 50 mL). To yield a white solid, 3a-(4-cyanobenzyl)-8a-(methyl)-decahydro-3a,5a,8a,10a-tetraaza-pyrenium diiodide (**13**), (0.89 g, 2.03 mmol, 85.3%).

^1H NMR (400 MHz, D_2O , δ): 1.78 (d, $J = 16.0$ Hz, N- β - CH_2 , 2H), 1.89 (d, $J = 16.0$ Hz, N- β - CH_2 , 2H), 2.08-2.26 (m, CH_3 , 3H), 2.54-2.73 (m, N- α - CH_2 , 2H), 2.77-2.80 (m, N- α - CH_2 , 1H), 2.81-2.93 (m, N- α - CH_2 , 1H), 3.02-3.11 (m, N- α - CH_2 , 3H), 3.12-3.28 (m, N- α - CH_2 , 2H), 3.26-3.28 (m, N- α - CH_2 , 1H), 3.40-3.50 (m, N- α - CH_2 , 2H), 3.52-3.60 (m, H_{aminal} , 1H), 3.75-3.79 (m, N- α - CH_2 , 1H), 4.25-4.37 (m, N- α - CH_2 , 2H), 4.70 (s, H_{aminal} , 1H), 4.82 (d, $J = 12.0$ Hz, N- α - CH_2 , 1H), 5.10 (m, CH_2 -Ar, 2H), 7.76 (d, $J = 8.0$ Hz, Ar-H, 2H), 8.09 (d, $J = 8.0$ Hz, Ar-H, 2H). ^{13}C NMR (100 MHz, DMSO-d_6 , δ): 17.23 (N- β - CH_2), 18.48 (N- β - CH_2), 22.87 (CH_3), 44.98 (N- α - CH_2), 45.63 (N- α - CH_2), 46.82 (N- α - CH_2), 48.00 (N- α - CH_2), 50.11 (N- α - CH_2), 50.21 (N- α - CH_2), 56.78 (N- α - CH_2), 58.54 (N- α - CH_2), 63.47 (CH_2 -Ar), 77.51 (C_{aminal}), 111.29 (C-Ar), 120.04 (CN), 130.88 (Ar-H), 131.76 (Ar-H), 133.28 (C-Ar). MS (ES-MS): m/z 176.70 (M-2I, 253.8). Anal. calcd for $\text{C}_{21}\text{H}_{31}\text{I}_2\text{N}_5 \cdot 0.4\text{MeI}$: expected: C, 38.70; H, 4.89; N, 10.55. Found: C, 38.60; H, 4.86; N, 10.60.

9.3.17 Synthesis of 1-(4-cyanobenzyl)-8-(methyl)-1,4,8,11-tetraazabicyclo[6.6.2]-hexadecane (14)



Method 1:

3a-(4-Cyanobenzyl)-8a-(methyl)-decahydro-3a,5a,8a,10a-tetraaza-pyrenium diiodide (**12**) (0.89 g, 1.86 mmol) was dissolved in ethanol (100 mL) and sodium borohydride (2.8 g, 74.5 mmol) was added in small portions under ice cooling. The mixture was stirred for 14 days at RT. Water was added to decompose excess sodium borohydride and the solvents were removed *in vacuo*. The residue was taken up into water and made strongly basic (pH 14, KOH). The basic solution was extracted with dichloromethane, the combined organic extracts were dried (Na₂SO₄), filtered and solvent removed *in vacuo* to yield a clear/yellow oil, 1-(4-cyanobenzyl)-8-(methyl)-1,4,8,11-tetraazabicyclo[6.6.2]-hexadecane (**14**), (325.4 mg, 0.92 mmol, 49.6%).

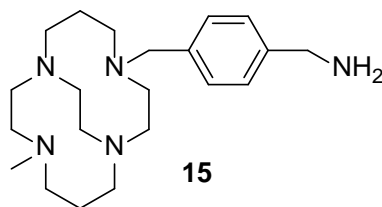
Method 2 – Preferred:

General procedure F was followed.

Amounts: 3a-(4-Cyanobenzyl)-8a-(methyl)-decahydro-3a,5a,8a,10a-tetraaza-pyrenium diiodide (**12**) (0.50 g, 1.04 mmol), ethanol (10 mL), sodium borohydride (24.0 mg, 7.5 mmol), microwaved (100°C, 300 W, 4 hours), water (100 mL, 150 mL), dichloromethane (5 x 50 mL). To yield a clear/yellow oil, 1-(4-cyanobenzyl)-8-(methyl)-1,4,8,11-tetraazabicyclo[6.6.2]-hexadecane (**14**), (0.32 g, 0.90 mmol, 86.5%).

¹H NMR (400 MHz, CDCl₃, δ): 1.72-1.89 (m, N-β-CH₂, 4H), 2.18-2.47 (br m, N-α-CH₂, 16H), 2.58-2.80 (m, CH₃, 3H), 2.83-2.91 (m, N-α-CH₂, 2H), 3.11 (d, *J* = 8.0 Hz, N-α-CH₂, 1H), 3.20 (d, *J* = 12.0 Hz, N-α-CH₂, 1H), 4.60-4.75 (m, CH₂-Ar, 2H), 7.44 (d, *J* = 8.0 Hz, Ar-H, 2H), 7.60 (d, *J* = 8.0 Hz, Ar-H, 2H). ¹³C NMR (100 MHz, CDCl₃, δ): 22.88 (N-α-CH₂), 25.41 (N-α-CH₂), 42.04 (CH₃), 49.64 (N-α-CH₂), 50.83 (N-α-CH₂), 53.47 (N-α-CH₂), 54.01 (N-α-CH₂), 54.18 (N-α-CH₂), 55.40 (N-α-CH₂), 55.73 (N-α-CH₂), 56.17 (N-α-CH₂), 58.37 (N-α-CH₂), 59.02 (N-α-CH₂), 59.13 (CH₂-Ar), 109.84 (C-Ar), 118.71 (CN), 130.48 (Ar-H), 132.43 (Ar-H), 146.96 (C-Ar). MS (ES-MS): *m/z* 356.3 (M⁺). Anal. calcd for C₂₁H₃₃N₅·2.5H₂O·0.8Na: expected: C, 60.20; H, 9.14; N, 16.72. Found: C, 60.66; H, 9.39; N, 16.14.

9.3.18 Synthesis of 1-(4-aminomethylbenzyl)-8-(methyl)-1,4,8,11-tetraazabicyclo[6.6.2]-hexadecane (**15**)

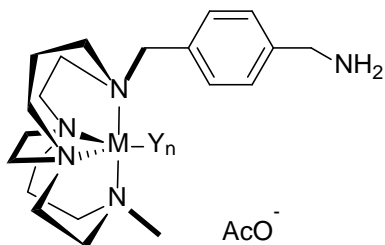


General procedure G was followed.

Amounts: 11-(4-cyanobenzyl)-8-(methyl)-1,4,8,11-tetraazabicyclo[6.6.2]-hexadecane (**14**), (325.4 mg, 0.88 mmol), anhydrous THF (20 mL), lithium aluminium hydride (133.6 mg, 3.52 mmol), anhydrous THF (20 mL), water (1 mL), 15% sodium hydroxide solution (1 mL), THF (2 x 20 mL), water (2 x 10 mL), THF (5 x 25 mL). To yield a pale yellow oil, 1-(4-aminomethylbenzyl)-8-(methyl)-1,4,8,11-tetraazabicyclo[6.6.2]-hexadecane (**15**), (231.4 mg, 0.64 mmol, 73.1%).

^1H NMR (400 MHz, CDCl_3 , δ): 1.55-1.80 (m, $\text{N-}\beta\text{-CH}_2$, 4H), 1.88-2.00 (m, $\text{N-}\alpha\text{-CH}_2$, 6H), 2.21-2.36 (m, $\text{N-}\alpha\text{-CH}_2$ + NH_2 , 8H), 2.40-2.82 (m, $\text{N-}\alpha\text{-CH}_2$ + CH_3 , 7H), 3.07-3.24 (m, $\text{N-}\alpha\text{-CH}_2$, 4H), 3.61-3.72 (m, $\text{CH}_2\text{-Ar}$, 2H), 4.11-4.37 (m, $\text{CH}_2\text{-Ar}$, 2H), 7.16-7.29 (br ov, Ar H, 4H). ^{13}C NMR (100 MHz, CDCl_3 , δ): 26.76 ($\text{N-}\beta\text{-CH}_2$), 34.32 ($\text{N-}\beta\text{-CH}_2$), 46.25 (CH_3), 52.24 ($\text{N-}\alpha\text{-CH}_2$), 52.48 ($\text{N-}\alpha\text{-CH}_2$), 53.25 ($\text{N-}\alpha\text{-CH}_2$), 54.39 ($\text{N-}\alpha\text{-CH}_2$), 55.10 ($\text{N-}\alpha\text{-CH}_2$), 56.36 ($\text{N-}\alpha\text{-CH}_2$), 56.53 ($\text{N-}\alpha\text{-CH}_2$), 56.55 ($\text{N-}\alpha\text{-CH}_2$), 58.08 ($\text{N-}\alpha\text{-CH}_2$), 59.69 ($\text{N-}\alpha\text{-CH}_2$), 59.75 ($\text{CH}_2\text{-Ar}$), 74.34 ($\text{CH}_2\text{-NH}_2$), 125.61 (C-Ar), 126.87 (Ar-H), 128.32 (Ar-H), 129.10 (C-Ar). MS (ES-MS): m/z 361.5 (M^+). Anal. calcd for $\text{C}_{21}\text{H}_{37}\text{N}_5 \cdot 1.1\text{THF} \cdot 0.8\text{H}_2\text{O}$: expected: C, 64.88; H, 10.35; N, 14.89. Found: C, 64.90; H, 10.41; N, 14.88.

9.3.19 Synthesis of metal complexes of ligands 1-(4-aminomethylbenzyl)-8-(methyl)-1,4,8,11-tetraazabicyclo[6.6.2]hexadecane ([Ni**15**(OAc)](OAc), [Cu**15**(OAc)](OAc) and [Zn**15**(OAc)](OAc))



M = Ni²⁺, Y = AcO⁻, (n = 1/2); [Ni**15**(OAc)](OAc)
M = Cu²⁺, Y = AcO⁻, (n = 1); [Cu**15**(OAc)](OAc)
M = Zn²⁺, Y = AcO⁻, (n = 1/2); [Zn**15**(OAc)](OAc)

General procedure E was followed.

1-(4-Aminomethylbenzyl)-8-(methyl)-1,4,8,11-tetraazabicyclo[6.6.2]-hexadecane nickel(II) acetate [Ni15**(OAc)](OAc)**

Amounts: 1-(4-Aminomethylbenzyl)-8-(methyl)-1,4,8,11-tetraazabicyclo[6.6.2]-hexadecane (**15**) (141.6 mg, 410.0 μ mol), methanol (5 mL, 40 mL), nickel(II) acetate (102.1 mg, 410.0 μ mol), to yield a pale green solid 1-(4-aminomethylbenzyl)-8-(methyl)-1,4,8,11-tetraazabicyclo[6.6.2]-hexadecane nickel (II) acetate, ([Ni**15**(OAc)](OAc)) (69.0 mg, 121.0 μ mol, 32.0% yield).

MS (ES-MS): *m/z* 476.6 (M-CH₃CO₂, 34). Anal. calcd for C₂₅H₄₃NiN₅O₄·1 H₂O·2.3MeOH: expected: C, 52.21; H, 8.70; N, 1.15. Found: C, 52.45; H, 8.89; N, 11.10.

1-(4-Aminomethylbenzyl)-8-(methyl)-1,4,8,11-tetraazabicyclo[6.6.2]-hexadecane copper(II) acetate [Cu15(OAc)](OAc)

Amounts: 1-(4-Aminomethylbenzyl)-8-(methyl)-1,4,8,11-tetraazabicyclo[6.6.2]-hexadecane (15) (217.3 mg, 0.61 mmol), methanol (5 mL, 50 mL), copper(II) acetate monohydrate (302.1 mg, 1.51 mmol) to yield a blue solid, 1-(4-aminomethylbenzyl)-8-(methyl)-1,4,8,11-tetraazabicyclo[6.6.2]-hexadecane copper(II) acetate ([Cu15(OAc)](OAc)), (257 mg, 0.48 mmol, 78.6% yield).

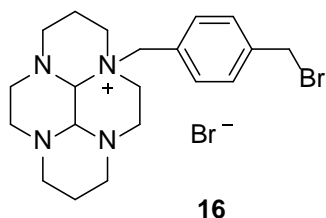
MS (ES-MS): m/z 481.3 (M-CH₃CO₂, 34). Anal. calcd for C₂₅H₄₃CuN₅O₄·2.0H₂O: expected: C, 51.93; H, 8.37; N, 12.11. Found,: C, 51.93; H, 8.42; N, 11.99.

1-(4-Aminomethylbenzyl)-8-(methyl)-1,4,8,11-tetraazabicyclo[6.6.2]-hexadecane zinc(II) acetate [Zn15(OAc)](OAc)

Amounts: 1-(4-Aminomethylbenzyl)-8-(methyl)-1,4,8,11-tetraazabicyclo[6.6.2]-hexadecane (15) (169.4 mg, 0.470 mmol), methanol (5mL, 40 mL), zinc(II) acetate (216.4 mg, 1.18 mmol), to yield an off-white solid, 1-(4-aminomethylbenzyl)-8-(methyl)-1,4,8,11-tetraazabicyclo[6.6.2]-hexadecane zinc(II) acetate ([Zn15(OAc)](OAc)), (187.0 mg, 0.346 mmol, 73.3% yield).

MS (ES-MS): m/z 482.2 (M-CH₃CO₂, 34). Anal. calcd for C₂₅H₄₃ZnN₅O₄·2H₂O: expected: C, 52.47; H, 8.71; N, 10.85. Found,: C, 52.23; H, 8.67; N, 10.72.

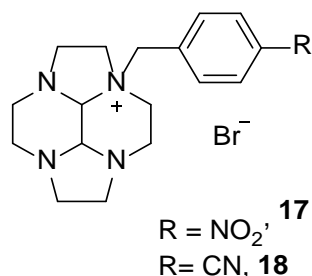
9.3.20 Synthesis of 3a-(4-(bromomethyl)benzyl)dodecahydro-6H-3a,5a,8a,10a-tetraazapyren-3a-ium bromide (**16**)



cis-3,5,8,10-Tetraazaperhydropyrene (**1**) (3.00 g, 13.49 mmol) and dibromo-*p*-xylene (7.12 g, 26.97) were dissolved in dry THF (80 mL) and stirred at R.T under argon for 3 days. The resulting precipitate was filtered and washed with THF (4 x 25 mL) and dried *in vacuo* to leave a white solid, 3a-(4-(bromomethyl)benzyl)dodecahydro-6H-3a,5a,8a,10a-tetraazapyren-3a-ium bromide (**16**), (2.641 g, 40.0% yield).

^1H NMR (400 MHz, D_2O , δ): 1.18-1.22 (m, N- β - CH_2 , 2H), 1.34-1.45 (m, N- β - CH_2 , 2H), 1.75-3.82 (br m, N- α - CH_2 , 16H), 4.55 (s, CH_2 -Ar, 2H), 4.72 (s, CH_2 -Br, 2H), 4.88-5.11 (m, H_{aminal} , 2H), 7.42-7.56 (m, Ar-H, 4H). ^{13}C NMR (100 MHz, D_2O , δ): 17.99 (N- β - CH_2), 18.55 (N- β - CH_2), 42.14 (CH_2 -Br), 46.89 (N- α - CH_2), 50.87 (N- α - CH_2), 53.74 (N- α - CH_2), 54.11 (N- α - CH_2), 54.78 (N- α - CH_2), 60.35 (N- α - CH_2), 61.88 (N- α - CH_2), 69.62 (CH_2 -Ar), 75.95 (C_{aminal}), 84.45 (C_{aminal}), 128.24 (Ar-H), 128.55 (Ar-H), 132.82 (Ar), 133.17 (Ar). MS (ES-MS): m/z 405.3 (M-Br, 79.9). Anal. calcd for $\text{C}_{20}\text{H}_{30}\text{Br}_2\text{N}_4 \cdot 2.2\text{H}_2\text{O} \cdot 0.4\text{THF}$: C, 46.80; H, 6.76; N, 10.11. Found: C, 46.60; H, 6.36; N, 9.99.

9.3.21 Synthesis of 2a-(4-nitrobenzyl)-decahydro-2a,4a,6a,8a-tetraaza-pyrenium bromide (**17**), and 2a-(4-cyanobenzyl)-decahydro-2a,4a,6a,8a-tetraaza-pyrenium bromide (**18**)



General procedure B was followed.

2a-(4-Nitrobenzyl)-decahydro-2a,4a,6a,8a-tetraaza-pyrenium bromide (**17**)

Amounts: *cis*-13-1,4,7,10-Tetraazatetracyclo[5.5.1.0^{4,14}.0^{10,13}]tetradecane (**2**) (2.00 g, 10.29 mmol), 4-nitrobenzyl bromide (2.22 g, 10.29 mmol), dry acetonitrile (100 mL), diethyl ether (2 x 25 mL). To yield a yellow solid 2a-(4-nitrobenzyl)-decahydro-2a,4a,6a,8a-tetraaza-pyrenium bromide (**17**), (3.457 g, 84.0% yield).

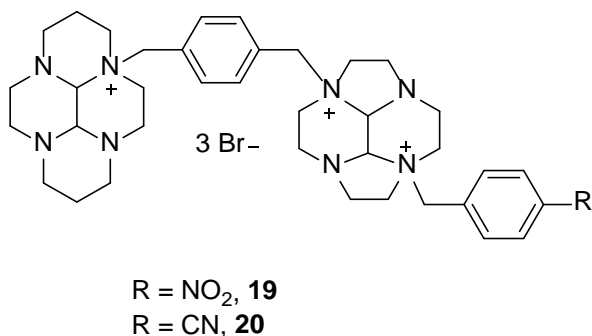
¹H NMR (400 MHz, D₂O, δ): 2.33-2.45 (m, N-α-CH₂, 2H), 2.61-2.85 (m, N-α-CH₂, 4H), 2.95-3.21 (m, N-α-CH₂, 5H), 3.33-3.50 (m, N-α-CH₂, 4H), 3.63 (m, N-α-CH₂, 1H), 3.91-3.94 (m, CH₂-Ar, 1H), 4.05-4.12 (m, CH₂-Ar, 1H), 4.68 (s, H_{aminal}, 1H), 4.88 (d, *J* = 13.5 Hz, H_{aminal}, 1H), 7.68 (d, *J* = 8.8 Hz, Ar-H, 2H), 8.20 (d, *J* = 8.0 Hz, Ar-H, 2H). ¹³C NMR (100 MHz, D₂O, δ): 43.87 (N-α-CH₂), 47.72 (N-α-CH₂), 48.23 (N-α-CH₂), 48.56 (N-α-CH₂), 51.57 (N-α-CH₂), 57.36 (N-α-CH₂), 60.35 (N-α-CH₂), 61.85 (N-α-CH₂), 71.77 (C_{aminal}), 83.33 (C_{aminal}), 110.53 (C-Ar), 124.70 (C-Ar), 133.97 (C-Ar), 149.26 (C-Ar). MS (ES-MS): *m/z* 330.2 (M-Br, 79.9). Anal. calcd for C₁₇H₂₄BrN₅O₂: C, 49.76; H, 5.90; N, 17.07. Found.: C, 49.92; H, 6.09; N, 16.28.

2a-(4-Cyanobenzyl)-decahydro-2a,4a,6a,8a-tetraaza-pyrenium bromide (**18**)

Amounts: *Cis*-13-1,4,7,10-tetraazatetracyclo[5.5.1.0^{4,14}.0^{10,13}]tetradecane (**2**) (3.4 g, 17.5 mmol), 4-(Bromomethyl)benzonitrile (3.4 g, 17.5 mmol), dry acetonitrile (100 mL), diethyl ether (2 x 25 mL). To yield the white solid, 2a-(4-cyanobenzyl)-decahydro-2a,4a,6a,8a-tetraaza-pyrenium bromide (**18**), (5.2 g, 16.7 mmol, 95.4% yield).

¹H NMR (400 MHz, D₂O, δ): 1.20-1.25 (m, N-β-CH₂, 2H), 1.42-1.50 (m, N-β-CH₂, 2H), 2.39 (d, *J* = 6.1 Hz, N-α-CH₂, 2H), 2.49-2.79 (m, N-α-CH₂, 4H), 2.83-2.88 (m, N-α-CH₂, 4H), 2.90 (s, N-α-CH₂, 1H), 2.96-3.19 (m, N-α-CH₂, 4H), 3.23-3.08 (m, N-α-CH₂, 5H), 3.52-3.31 (m, N-α-CH₂, 6H), 3.64-3.82 (m, N-α-CH₂, 4H), 3.64 (t, *J* = 5.9 Hz, N-α-CH₂, 1H), 3.93 (t, *J* = 6.0 Hz, N-α-CH₂, 1H), 4.07 (d, *J* = 11.9 Hz, H_{aminal}, 1H), 4.21-4.27 (m, H_{aminal}, 2H), 4.40-4.62 (m, CH₂-Ar, 6H), 4.84 (d, *J* = 13.4 Hz, H_{aminal}, 1H), 7.55-7.68 (m, A4-H, 4H), 7.71 (d, *J* = 8.0 Hz, Ar-H, 2H), 7.87 (d, *J* = 8.0 Hz, Ar-H, 2H). ¹³C NMR (100 MHz, D₂O, δ): 17.55 (N-β-CH₂), 18.60 (N-β-CH₂), 42.92 (N-α-CH₂), 43.75 (N-α-CH₂), 47.54 (N-α-CH₂), 48.20 (N-α-CH₂), 51.30 (N-α-CH₂), 57.21 (N-α-CH₂), 60.62 (N-α-CH₂), 61.60 (N-α-CH₂), 62.22 (N-α-CH₂), 62.45 (N-α-CH₂), 68.18 (N-α-CH₂), 68.69 (N-α-CH₂), 71.65 (C_{aminal}), 83.20 (C_{aminal}), 113.82 (CN), 132.08 (C-Ar), 133.19 (C-Ar), 133.51 (Ar-H). MS (ES-MS): *m/z* 310.8 (M-CH₃CO₂, 79.9). Anal. calcd for C₁₈H₂₄BrN₅·0.5H₂O·0.3MeCN: C, 54.27; H, 6.34; N, 18.03. Found: C, 54.00; H, 6.32; N, 18.05.

9.3.23 Synthesis of 2a-(4-nitrobenzyl)-6a-(4-((decahydro-3a,5a,8a,10a-tetraaza-pyren-3a-ium)methyl)benzyl) tribromide (**19**), and 2a-(4-cyanobenzyl)-6a-(4-((decahydro-3a,5a,8a,10a-tetraaza-pyren-3a-ium)methyl)benzyl)-decahydro-2a,4a,6a,8a-tetraazapyrenium tribromide (**20**)



General procedure B was followed.

2a-(4-Nitrobenzyl)-6a-(4-((decahydro-3a,5a,8a,10a-tetraaza-pyren-3a-ium)methyl)benzyl) tribromide (19**)**

Amounts: 3a-(4-(Bromomethyl)benzyl)-decahydro-3a,5a,8a,10a-tetraazapyrenium bromide (**16**) (5.576 g, 11.46 mmol), 2a-(4-nitrobenzyl)-decahydro-2a,4a,6a,8a-tetraazapyrenium bromide (**17**) (4.69 g, 11.46 mmol), dry acetonitrile (120 mL), diethyl ether (4 x 30 mL). To yield a white solid, 2a-(4-nitrobenzyl)-6a-(4-((decahydro-3a,5a,8a,10a-tetraaza-pyren-3a-ium)methyl)benzyl) tribromide (**19**), (7.37 g, 8.25 mmol, 72.0%).

¹H NMR (400 MHz, D₂O, δ): 1.03 (t, *J* = 7.0 Hz, N-β-CH₂, 1H), 1.39 (d, *J* = 13.6 Hz, N-β-CH₂, 1H), 1.64 (d, *J* = 14.5 Hz, N-β-CH₂, 2H), 2.00 (d, *J* = 14.5 Hz, N-α-CH₂, 2H), 2.09-2.11 (m, N-α-CH₂, 4H), 2.24 (t, *J* = 11.9 Hz, N-α-CH₂, 1H), 2.34-2.46 (m, N-α-CH₂, 2H), 2.59-2.61 (m, N-α-CH₂, 2H), 2.73-3.11 (m, N-α-CH₂, 12H), 3.20-3.51 (m, N-α-CH₂, 4H), 3.60 (s, N-α-CH₂, 1H), 3.71-3.82 (m, N-α-CH₂, 4H), 4.10 (m, H_{aminal}, 1H), 4.17 (m, H_{aminal}, 1H), 4.44 (s, H_{aminal}, 1H), 4.74-4.79 (m, CH₂-Ar, 4H), 4.93 (d, *J* = 13.3 Hz, H_{aminal}, 1H), 4.98-5.13 (m, CH₂-Ar, 2H), 7.53-7.63 (m, Ar-H, 4H), 7.75 (d, 7.7 Hz, Ar-H, 2H), 8.22 (d, *J* = 7.8 Hz, Ar-H, 2H). ¹³C NMR (100 MHz, D₂O, δ): 17.99 (N-β-CH₂), 18.48 (N-β-CH₂), 42.15 (N-α-CH₂), 42.81 (N-α-CH₂), 46.24 (N-α-CH₂), 46.61 (N-α-CH₂), 48.43 (N-α-CH₂), 52.06 (N-α-CH₂), 53.13 (N-α-

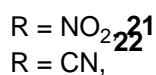
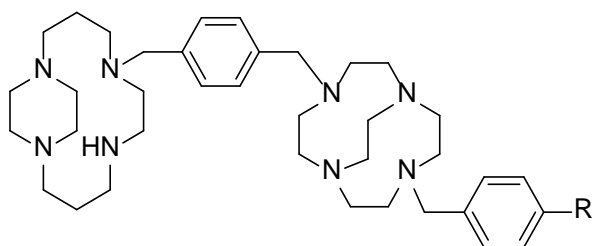
CH₂), 54.09 (N- α -CH₂), 55.11 (N- α -CH₂), 59.90 (N- α -CH₂), 60.37 (N- α -CH₂), 61.19 (N- α -CH₂), 61.49 (N- α -CH₂), 61.98 (N- α -CH₂), 66.30 (N- α -CH₂), 70.02 (N- α -CH₂), 77.96 (CH₂-Ar), 82.23 (CH₂-Ar), 124.87 (Ar-H), 128.94 (C-Ar), 129.42 (C-Ar), 133.37 (C-Ar), 133.57 (Ar-H), 133.99 (Ar-H), 134.78 (Ar-NO₂). MS (ES-MS): *m/z* 816.31 (M-Br, 79.9). Anal. calcd for C₃₈H₅₄N₉O₂Br₃·3.7H₂O: C, 45.14; H, 6.43; N, 13.09. Found, : C, 45.91; H, 6.07; N: 12.86.

2a-(4-Cyanobenzyl)-6a-(4-((decahydro-3a,5a,8a,10a-tetraaza-pyren-3a-ium)methyl)benzyl)-decahydro-2a,4a,6a,8a-tetraaza-pyrenium tribromide (20)

Amounts: 3a-(4-(Bromomethyl)benzyl)-decahydro-3a,5a,8a,10a-tetraaza-pyrenium bromide (**16**) (1.94 g, 4.01 mmol), 2a-(4-cyanobenzyl)-decahydro-2a,4a,6a,8a-tetraaza-pyrenium bromide (**18**) (1.56 g, 4.01 mmol), dry acetonitrile (200 mL), diethyl ether (4 x 30 mL). To yield a white solid, 2a-(4-cyanobenzyl)-6a-(4-((decahydro-3a,5a,8a,10a-tetraaza-pyren-3a-ium)methyl)benzyl)-decahydro-2a,4a,6a,8a-tetraaza-pyrenium tribromide (**20**), (1.95 g, 3.05 mmol, 76.1% yield).

¹H NMR (400 MHz, D₂O, δ): 1.10 (t, *J* = 7.0 Hz, N- β -CH₂, 1H), 1.47 (d, *J* = 13.5 Hz, N- β -CH₂, 1H), 1.77 (d, *J* = 14.5 Hz, N- β -CH₂, 1H), 1.84 (s, H, N- β -CH₂, 1H), 2.09-2.17 (m, N- α -CH₂, 2H), 2.39 (m, N- α -CH₂, 1H), 2.42-2.54 (m, N- α -CH₂, 2H), 2.77-2.79 (m, N- α -CH₂, 1H), 2.92-3.01 (m, N- α -CH₂, 2H), 3.15 (m, N- α -CH₂, 4H), 3.37-3.41 (m, N- α -CH₂, 4H), 3.44-3.49 (m, N- α -CH₂, 5H), 3.51-3.66 (m, N- α -CH₂, 6H), 3.77-3.80 (m, N- α -CH₂, 2H), 4.17-4.30 (m, N- α -CH₂, 3H), 4.53 (s, H_{aminal}, 1H), 4.77 (d, *J* = 13.5 Hz, C-ArH₂, 2H), 4.81-4.89 (m, C-ArH₂, 4H), 4.95-5.00 (m, H_{aminal}, 2H), 5.42 (d, *J* = 13.0 Hz, H_{aminal}, 1H), 7.62-7.68 (m, Ar-H, 4H), 7.72 (d, *J* = 8.0 Hz, Ar-H, 2H), 7.84 (d, *J* = 7.5 Hz, Ar-H, 2H). ¹³C NMR (100 MHz, D₂O, δ): 17.55 (N- β -CH₂), 18.12 (N- β -CH₂), 42.12 (CH₂-Br), 42.55 (N- α -CH₂), 46.22 (N- α -CH₂), 46.48 (N- α -CH₂), 48.27 (N- α -CH₂), 51.58 (N- α -CH₂), 52.09 (N- α -CH₂), 53.11 (N- α -CH₂), 54.09 (N- α -CH₂), 54.84 (N- α -CH₂), 60.22 (N- α -CH₂), 60.44 (N- α -CH₂), 61.00 (N- α -CH₂), 61.27 (N- α -CH₂), 61.87 (N- α -CH₂), 66.14 (N- α -CH₂), 69.81 (N- α -CH₂), 77.41 (C_{aminal}), 78.44 (C_{aminal}), 85.03 (C_{aminal}), 115.37 (CN), 118.01 (C-Ar), 128.88 (Ar-H), 129.54 (Ar-H), 132.14 (C-Ar), 132.82 (Ar-H), 133.24 (Ar-H), 133.94 (Ar-H), 135.21 (C-Ar). MS (ES-MS): *m/z* 357.7 (M-2Br, 159.8). Anal. calcd for C₃₈H₅₄Br₃N₉·7H₂O·0.2Na·0.5THF: C, 44.31; H, 6.92; N, 11.32. Found, C, 44.56; H, 6.65; N, 11.32.

9.3.24 Synthesis 1-(4-nitrobenzyl)-7-(4-((1,4,8,11-tetraazabicyclo[10.2.2]hexadecane)methyl)benzyl)-1,4,7,10-tetraazabicyclo[5.5.2]dodecane (**21**), and 1-(4-cyanobenzyl)-7-(4-((1,4,8,11-tetraazabicyclo[10.2.2]hexadecane)methyl)benzyl)-1,4,7,10-tetraazabicyclo[5.5.2]dodecane (**22**)



Synthesis of 1-(4-nitrobenzyl)-7-(4-((1,4,8,11-tetraazabicyclo[10.2.2]hexadecane)methyl)benzyl)-1,4,7,10-tetraazabicyclo[5.5.2]dodecane (21**)**

2a-(4-Nitrobenzyl)-6a-(4-((decahydro-2a,4a,6a,8a-tetraazapyren-2a-ium)methyl)benzyl)-decahydro-2a,4a,6a,8a-tetraazapyrenium tribromide (**19**) (7.37 g, 8.25 mmol) was added to dry ethanol (200 mL) and sodium borohydride (12.47 g, 330 mmol) was added in small portions over 1 h. The resulting pale yellow solution was stirred at rt for 10 d under argon. Aqueous hydrochloric acid (1 M, 20 mL) was added until pH 3-4 was reached to decompose excess sodium borohydride and the solvents were removed *in vacuo*. The residue was taken up in water (100 mL) and made strongly basic (pH 13.5, KOH pellets). The basic solution was extracted with dichloromethane (5 x 60 mL), the combined organic extracts were dried over anhydrous magnesium sulphate and the solvents were removed *in vacuo*. To yield the white solid 1-(4-nitrobenzyl)-7-(4-((1,4,8,11-tetraazabicyclo[10.2.2]hexadecane)methyl)benzyl)-1,4,7,10-tetraazabicyclo[5.5.2]dodecane (**21**), (3.28 g, 4.96 mmol, 60.0%).

¹H NMR (400 MHz, CD₃OD, δ): 1.66-1.84 (m, N-β-CH₂, 4H), 2.16-3.36 (br m, N-α-CH₂, 40H), 3.47-4.89 (m, CH₂-Ar, 6H), 4.52-4.58 (br s, NH, 1H), 7.11-7.31 (m, Ar-H, 4H), 7.45-7.55 (m, Ar-H, 2H), 8.16-8.33 (m, Ar-H, 2H). ¹³C NMR (100 MHz, CD₃OD, δ): 19.41 (N-β-CH₂), 20.28 (N-β-CH₂), 22.16 (N-β-CH₂), 23.17 (N-β-CH₂), 25.35 (N-α-CH₂), 25.56 (N-α-CH₂), 46.87 (N-α-CH₂), 50.26 (N-α-CH₂), 50.76 (N-α-

CH₂), 51.02 (N- α -CH₂), 51.33 (N- α -CH₂), 51.71 (N- α -CH₂), 53.90 (N- α -CH₂), 55.39 (N- α -CH₂), 56.04 (N- α -CH₂), 56.17 (N- α -CH₂), 56.29 (N- α -CH₂), 56.39 (N- α -CH₂), 56.89 (N- α -CH₂), 57.17 (N- α -CH₂), 57.40 (N- α -CH₂), 57.54 (N- α -CH₂), 59.22 (N- α -CH₂), 60.40 (N- α -CH₂), 61.69 (N- α -CH₂), 62.95 (N- α -CH₂), 123.41 (Ar-H), 123.69 (Ar-H), 127.19 (Ar-H), 129.28 (Ar-H), 129.50 (C-Ar), 129.85 (Ar-H), 130.21 (Ar-H), 139.28 (C-Ar), 146.66 (Ar-H), 147.30 (Ar-H), 147.62 (C-Ar), 148.64 (C-Ar). MS (ES-MS): *m/z* 662.42 (M⁺). Anal. calcd for C₃₈H₅₉N₉·2·H₂O: C, 67.14; H, 8.98; N, 19.04. Found, : C, 66.88; H, 8.59; N: 19.01.

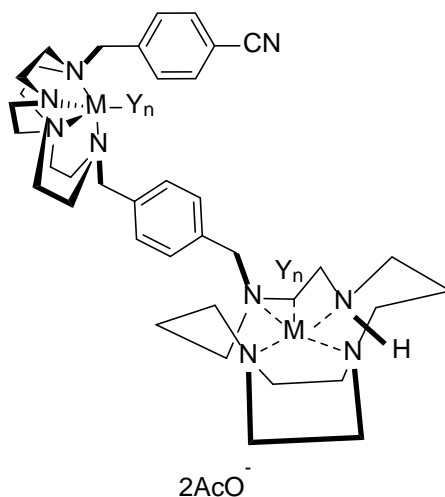
1-(4-Cyanobenzyl)-7-(4-((1,4,8,11-tetraazabicyclo[10.2.2]hexadecane)methyl)benzyl)-1,4,7,10-tetraazabicyclo[5.5.2]dodecane (22)

General procedure F was followed.

Amounts: 2a-(4-Cyanobenzyl)-6a-(4-((decahydro-3a,5a,8a,10a-tetraaza-pyren-3a-ium)methyl)benzyl)-decahydro-2a,4a,6a,8a-tetraaza-pyrenium tribromide (**19**) (0.5 g, 0.77 mmol), sodium borohydride (0.44 g, 11.52 mmol), ethanol (10 mL), microwaved (8 hours) water (100mL, 150 mL), dichloromethane (5 x 50 mL). To yield the white solid. 1-(4-cyanobenzyl)-7-(4-((1,4,8,11-tetraazabicyclo[10.2.2]hexadecane)methyl)benzyl)-1,4,7,10-tetraazabicyclo[5.5.2]dodecane (**22**), (0.45 g, 0.70 mmol, 91.3% yield).

¹H NMR (400 MHz, CD₃OD, δ): 1.32-1.55 (m, N- β -CH₂, 4H), 2.44-3.55 (m, N- β -CH₂, 38H), 3.87-3.91 (m, N- α -CH₂, 1H), 4.16-4.19 (m, N- α -CH₂, 1H), 4.66-4.72 (br s, NH, 1H), 4.79-4.88 (m, CH₂-Ar, 6H), 7.44-7.55 (m, Ar-H, 4H), 7.62-7.73 (m, Ar-H, 4H). ¹³C NMR (100 MHz, CD₃OD, δ): 21.46 (N- β -CH₂), 24.25 (N- β -CH₂), 44.27 (N- α -CH₂), 47.11 (N- α -CH₂), 49.89 (N- α -CH₂), 50.12 (N- α -CH₂), 50.56 (N- α -CH₂), 51.04 (N- α -CH₂), 51.72 (N- α -CH₂), 52.94 (N- α -CH₂), 55.14 (N- α -CH₂), 55.19 (N- α -CH₂), 55.77 (N- α -CH₂), 55.89 (N- α -CH₂), 56.44 (N- α -CH₂), 56.51 (N- α -CH₂), 56.87 (N- α -CH₂), 56.98 (N- α -CH₂), 57.05 (N- α -CH₂), 57.77 (N- α -CH₂), 58.02 (N- α -CH₂), 58.43 (N- α -CH₂), 59.21 (N- α -CH₂), 62.64 (N- α -CH₂), 119.01 (CN), 125.83 (Ar-H), 129.07 (Ar-H), 129.42 (Ar-H), 129.82 (Ar-H), 129.99 (Ar-H), 130.11 (Ar-H), 130.21 (C-Ar), 131.75 (Ar-H), 132.01 (Ar-H), 134.98 (C-Ar), 145.05 (C-Ar), 146.33 (C-Ar). MS (ES-MS): *m/z* 321.9 (M²⁺). Anal. calcd for C₃₈H₅₉N₉·2.7CH₂Cl₂·1.9H₂O: C, 53.99; H, 7.59; N, 13.92. Found, : C, 54.02; H, 7.42; N, 14.01.

9.3.25 Synthesis of metal complexes of 1-(4-(aminomethyl)benzyl)-7-(4-((1,4,8,11-tetraazabicyclo[10.2.2]hexadecane)methyl)benzyl)-1,4,7,10-tetraazabicyclo[5.5.2]dodecane ($[\text{Ni}_2\mathbf{22}(\text{OAc})_2](\text{OAc})_2$, $[\text{Cu}_2\mathbf{22}(\text{OAc})_2](\text{OAc})_2$ and $[\text{Zn}_2\mathbf{22}(\text{OAc})_2](\text{OAc})_2$)



$M = \text{Ni}^{2+}$, $Y = \text{AcO}^-$, ($n = 1/2$); $[\text{Cu}_2\mathbf{22}(\text{OAc})_2](\text{OAc})_2$
 $M = \text{Cu}^{2+}$, $Y = \text{AcO}^-$, ($n = 1$); $[\text{Cu}_2\mathbf{22}(\text{OAc})_2](\text{OAc})_2$
 $M = \text{Zn}^{2+}$, $Y = \text{AcO}^-$, ($n = 1/2$); $[\text{Cu}_2\mathbf{22}(\text{OAc})_2](\text{OAc})_2$

General procedure E was followed.

N-(4-(1,4,7-Triazonan-1-yl)methyl)benzyl)-2-(2-((4-((10-(4-((1,5,8,12-tetraazabicyclo[10.2.2]hexadecan-5-yl)methyl)benzyl)-1,4,7,10-tetraazabicyclo[5.5.2]tetradecan-4-yl)methyl)benzyl)amino)-2-oxoethoxy)acetamide nickel(II) acetate ($[\text{Ni}_2\mathbf{22}(\text{OAc})_2](\text{OAc})_2$)

Amounts: N-(4-(1,4,7-triazonan-1-yl)methyl)benzyl)-2-(2-((4-((10-(4-((1,5,8,12-tetraazabicyclo[10.2.2]hexadecan-5-yl)methyl)benzyl)-1,4,7,10-tetraazabicyclo[5.5.2]tetradecan-4-yl)methyl)benzyl)amino)-2-oxoethoxy)acetamide (**22**) (99.6 mg, 160.0 μmol), dry methanol (20 mL), nickel(II) acetate (85.0 mg, 340.0 μmol). To yield a blue green, N-(4-(1,4,7-triazonan-1-yl)methyl)benzyl)-2-(2-((4-((10-(4-((1,5,8,12-tetraazabicyclo[10.2.2]hexadecan-5-yl)methyl)benzyl)-1,4,7,10-tetraazabicyclo[5.5.2]tetradecan-4-yl)methyl)benzyl)amino)-2-oxoethoxy)acetamidnickel(II) acetate ($[\text{Ni}_2\mathbf{22}(\text{OAc})_2](\text{OAc})_2$), (66.6 mg, 49.2 μmol , 31.6% yield).

MS (ES-MS; run with formic acid): m/z 424.4 ($M-4CH_3CO_2+2HCO_2$). Anal. calcd for $C_{46}H_{70}N_9O_8Ni_2 \cdot 2.8H_2O \cdot 0.3MeOH$: C, 51.49; H, 7.83; N, 11.01. Found, : C, 51.55; H, 7.72; N, 11.08.

N-(4-((1,4,7-Triazonan-1-yl)methyl)benzyl)-2-(2-((4-((10-(4-((1,5,8,12-tetraazabicyclo[10.2.2]hexadecan-5-yl)methyl)benzyl)-1,4,7,10-tetraazabicyclo[5.5.2]tetradecan-4-yl)methyl)benzyl)amino)-2-oxoethoxy)acetamide copper(II) acetate ($[Cu_2\mathbf{22}(OAc)_2](OAc)_2$)

Amounts: 4-((10-(4-((1,5,8,12-Tetraazabicyclo[10.2.2]hexadecan-5-yl)methyl)benzyl)-1,4,7,10-tetraazabicyclo[5.5.2]tetradecan-4-yl)methyl)benzyl)benzyl)benzyl)amino)-2-oxoethoxy)acetamide (22) (113.8 mg, 180.0 μ mol), dry methanol (15 mL), copper(II) acetate (78.0 mg, 390.0 μ mol). To yield a blue solid, N-(4-(1,4,7-triazonan-1-yl)methyl)benzyl)-2-(2-((4-((10-(4-((1,5,8,12-tetraazabicyclo[10.2.2]hexadecan-5-yl)methyl)benzyl)-1,4,7,10-tetraazabicyclo[5.5.2]tetradecan-4-yl)methyl)benzyl)amino)-2-oxoethoxy)acetamide copper(II) acetate ($[Cu_2\mathbf{22}(OAc)_2](OAc)_2$), (152.0 mg, 112.2 μ mol, 63.2% yield).

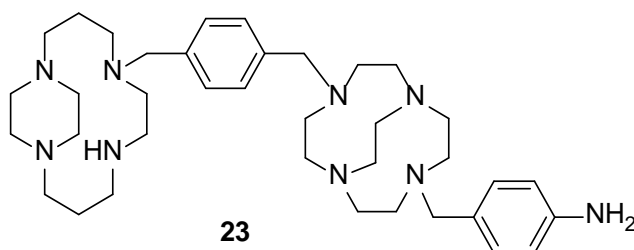
MS (ES-MS; run with formic acid): m/z 428.8 ($M-4CH_3CO_2+2HCO_2$). Anal. calcd for $C_{46}H_{70}N_9O_8Cu_2 \cdot 7.8H_2O \cdot 1.5MeCN$: C, 49.04; H, 7.58; N, 12.25. Found, : C, 48.98; H, 7.49; N, 12.33.

N-(4-(1,4,7-Triazonan-1-yl)methyl)benzyl)-2-(2-((4-((10-(4-((1,5,8,12-tetraazabicyclo[10.2.2]hexadecan-5-yl)methyl)benzyl)-1,4,7,10-tetraazabicyclo[5.5.2]tetradecan-4-yl)methyl)benzyl)amino)-2-oxoethoxy)acetamide zinc(II) acetate ($[Zn_2\mathbf{22}(OAc)_2](OAc)_2$)

Amounts: N-(4-(1,4,7-triazonan-1-yl)methyl)benzyl)-2-(2-((4-((10-(4-((1,5,8,12-tetraazabicyclo[10.2.2]hexadecan-5-yl)methyl)benzyl)-1,4,7,10-tetraazabicyclo[5.5.2]tetradecan-4-yl)methyl)benzyl)amino)-2-oxoethoxy)acetamide (22) (145.8 mg, 230.0 μ mol), dry methanol (15 mL), zinc(II) acetate (91.81 mg, 500.0 μ mol), To yield an off-white solid, N-(4-(1,4,7-triazonan-1-yl)methyl)benzyl)-2-(2-((4-((10-(4-((1,5,8,12-tetraazabicyclo[10.2.2]hexadecan-5-yl)methyl)benzyl)-1,4,7,10-tetraazabicyclo[5.5.2]tetradecan-4-yl)methyl)benzyl)amino)-2-oxoethoxy)acetamidezinc(II) acetate ($[Ni_2\mathbf{22}(OAc)_2](OAc)_2$), (189.0 mg, 139.5 μ mol, 61.3% yield).

MS (ES-MS; run with formic acid): m/z 430.8 ($M-4CH_3CO_2+2HCO_2$). Anal. calcd for $C_{46}H_{70}N_9O_8Zn_2 \cdot 3.8H_2O \cdot 1.9MeOH$: C, 50.59; H, 7.55; N, 11.09. Found, : C, 50.51; H, 7.77; N, 11.08.

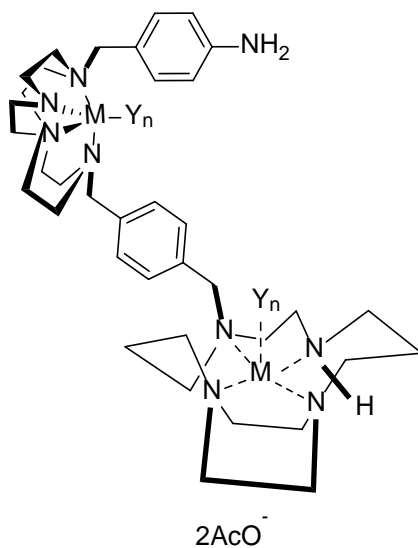
9.3.26 Synthesis of 1-(4-aminobenzyl)-7-(4-((1,4,8,11-tetraazabicyclo[10.2.2]hexadecane)methyl)benzyl)-1,4,7,10-tetraazabicyclo[5.5.2]dodecane (**23**)



1-(4-Nitrobenzyl)-7-(4-((1,4,8,11-tetraazabicyclo[10.2.2]hexadecane)methyl)benzyl)-1,4,7,10-tetraazabicyclo[5.5.2]dodecane (**21**) (3.28 g, 4.96 mmol) was dissolved in ethanol (200 mL) and degassed with the hydrogenator then put under a hydrogen atmosphere. Palladium on carbon (0.32 mL, 3.08 mmol) was added quickly, the solution was degassed and put under hydrogen again and left for 4 h. The mixture was filtered through high flow super cell to remove the catalyst and washed with ethanol (3 x 40 mL). The solvent was removed *in vacuo* to yield an orange powder, 1-(4-aminobenzyl)-7-(4-((1,4,8,11-tetraazabicyclo[10.2.2]hexadecane)methyl)benzyl)-1,4,7,10-tetraazabicyclo[5.5.2]dodecane (**23**), (2.27 g, 3.60 mmol, 73.0%).

^1H NMR (400 MHz, CD_3OD , δ): 1.72 (br s, N- β - CH_2 , 4H), 2.36-3.16 (br m, N- α - CH_2 , 40H), 3.62-3.98 (br m, CH_2 -Ar, 6H), 4.00-4.16 (m, NH_2 , 2H), 4.40-4.65 (br m, NH, 1H), 7.15-7.69 (m, Ar-H, 8H). ^{13}C NMR (100 MHz, CD_3OD , δ): 22.47 (N- β - CH_2), 24.87 (N- β - CH_2), 44.90 (N- α - CH_2), 46.42 (N- α - CH_2), 49.22 (N- α - CH_2), 50.11 (N- α - CH_2), 51.50 (N- α - CH_2), 52.62 (N- α - CH_2), 52.84 (N- α - CH_2), 53.99 (N- α - CH_2), 55.01 (N- α - CH_2), 55.75 (N- α - CH_2), 56.42 (N- α - CH_2), 58.17 (N- α - CH_2), 114.22 (Ar-H), 125.34 (C-Ar), 128.28 (Ar-H), 129.67 (Ar-H), 143.05 (C-Ar). MS (ES-MS): m/z 316.90 (M^{2+}). Anal. calcd for $\text{C}_{37}\text{H}_{61}\text{N}_9 \cdot 4.2\text{H}_2\text{O} \cdot 0.37\text{EtOH}$: C, 60.73; H, 10.52; N, 14.36. Found: C, 60.56; H, 10.57; N, 14.06.

9.3.27 Synthesis of metal complexes of 1-(4-(aminomethyl)benzyl)-7-(4-((1,4,8,11-tetraazabicyclo[10.2.2]hexadecane)methyl)benzyl)-1,4,7,10-tetraazabicyclo[5.5.2]dodecane ([Cu₂**23**(OAc)₂](OAc)₂ and [Zn₂**23**(OAc)₂](OAc)₂)



M = Cu²⁺, Y = AcO⁻, (n = 1); [Cu₂**23**(OAc)₂](OAc)₂
 M = Zn²⁺, Y = AcO⁻, (n = 1/2); [Zn₂**23**(OAc)₂](OAc)₂

General procedure E was followed.

Synthesis of 1-(4-aminobenzyl)-7-(4-((1,4,8,11-tetraazabicyclo[10.2.2]hexadecane)methyl)benzyl)-1,4,7,10-tetraazabicyclo[5.5.2]dodecane copper(II) acetate ([Cu₂23**(OAc)₂](OAc)₂)**

Amounts: 1-(4-Aminobenzyl)-7-(4-((1,4,8,11-tetraazabicyclo[10.2.2]hexadecane)methyl)benzyl)-1,4,7,10-tetraazabicyclo[5.5.2]dodecane (**23**) (0.40 g, 0.63 mmol), copper(II) acetate monohydrate (0.25 g, 1.7 mmol), methanol (25 mL). To yield a blue solid, bis copper [Cu₂**43**(OAc)₂](OAc)₂ copper(II) acetate ([Cu₂**23**(OAc)₂](OAc)₂), (0.22 g, 0.22 mmol, 34.9%).

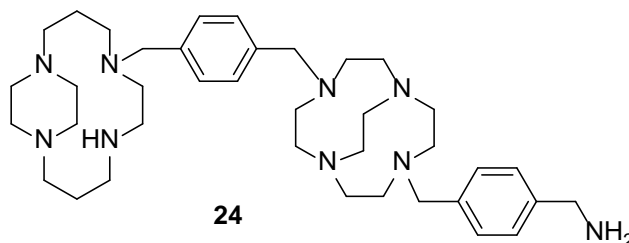
MS (ES-MS; run with formic acid): *m/z* 423.4 (M-4CH₃CO₂+2HCO₂).

Synthesis of 1-(4-aminobenzyl)-7-(4-((1,4,8,11-tetraazabicyclo[10.2.2]hexadecane)methyl)benzyl)-1,4,7,10tetraazabicyclo[5.5.2]dodecane zinc(II) acetate ([Zn₂23(OAc)₂](OAc)₂)

Amounts: 1-(4-Aminobenzyl)-7-(4-((1,4,8,11-tetraazabicyclo[10.2.2]hexadecane)methyl)benzyl)-1,4,7,10-tetraazabicyclo[5.5.2]dodecane (**23**) (0.40 g, 0.63 mmol), zinc(II) acetate (0.24 g, 1.33 mmol), methanol (25 mL). To yield an orange solid, bis zinc 1-(4-Aminobenzyl)-7-(4-((1,4,8,11-tetraazabicyclo[10.2.2]hexadecane)methyl)benzyl)-1,4,7,10tetraazabicyclo[5.5.2]dodecane zinc(II) acetate ([Zn₂**23**(OAc)₂](OAc)₂), (0.18 g, 0.18 mmol, 28.0%).

ES-MS (run with formic acid); (*m/z*): [M-4OAc+2CHO₂]²⁺ = 425.2.

9.3.28 Synthesis of 1-(4-(aminomethyl)benzyl)-7-(4-((1,4,8,11-tetraazabicyclo[10.2.2]hexadecane)methyl)benzyl)-1,4,7,10-tetraazabicyclo[5.5.2]dodecane (24)

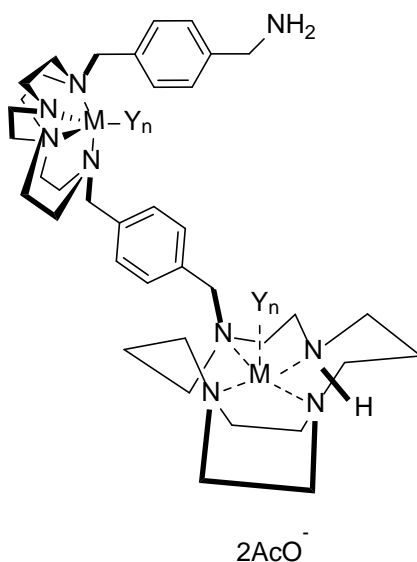


General procedure G was followed.

Amounts: 1-(4-Cyanobenzyl)-7-(4-((1,4,7,10-tetraazabicyclo[8.2.2]dodecane)methyl)benzyl)-1,4,7,10-tetraazabicyclo[5.5.2]dodecane (**22**) (6.50 g, 10.13 mmol), anhydrous tetrahydrofuran (100 mL), lithium aluminium hydride (1.54 g, 40.5 mmol), anhydrous THF (50 mL), water (1 mL), 15% sodium hydroxide solution (1 mL), THF (2 x 20 mL), water (2 x 10 mL), THF (5 x 25 mL). To yield a yellow oil, 1-(4-(aminomethyl)benzyl)-7-(4-((1,4,8,11-tetraazabicyclo[10.2.2]hexadecane)methyl)benzyl)-1,4,7,10-tetraazabicyclo[5.5.2]dodecane (**24**), (3.11 g, 4.82 mmol, 47.6% yield).

^1H NMR (400 MHz, CD_3OD , δ): 1.72 (br s, N- β - CH_2 , 4H), 2.36-3.16 (br m, N- α - CH_2 , 40H), 3.52-3.58 (m, CH_2 -Ar, 2H), 3.62-3.98 (br m, CH_2 -Ar, 6H), 4.00-4.16 (m, NH_2 , 2H), 4.40-4.65 (br m, NH, 1H), 7.15-7.69 (m, Ar-H, 8H). ^{13}C NMR (100 MHz, CD_3OD , δ): 23.11 (N- β - CH_2), 28.89 (N- β - CH_2), 44.63 (N- α - CH_2), 45.12 (N- α - CH_2), 49.02 (N- α - CH_2), 50.28 (N- α - CH_2), 51.20 (N- α - CH_2), 53.45 (N- α - CH_2), 54.37 (N- α - CH_2), 54.95 (N- α - CH_2), 55.12 (N- α - CH_2), 55.57 (N- α - CH_2), 56.11 (N- α - CH_2), 56.42 (N- α - CH_2), 56.76 (N- α - CH_2), 57.11 (N- α - CH_2), 57.27 (N- α - CH_2), 58.67 (N- α - CH_2), 60.22 (N- α - CH_2), 63.54 (N- α - CH_2), 123.45 (Ar-H), 127.05 (Ar-H), 127.80 (Ar-H), 128.75 (Ar-H), 128.87 (Ar-H), 129.20 (Ar-H), 129.31 (Ar-H), 129.64 (Ar-H), 130.01 (Ar-H), 134.95 (Ar-H), 136.55 (C-Ar), 137.77 (C-Ar), 139.08 (C-Ar), 142.71 (C-Ar). MS (ES-MS): m/z 316.90 (M^{2+}). Anal. calcd for $\text{C}_{38}\text{H}_{63}\text{N}_9 \cdot 5.6\text{H}_2\text{O} \cdot 1.3\text{THF}$: C, 61.78; H, 9.82; N, 15.03. Found.: C, 61.82; H, 10.00; N, 15.02.

9.3.29 Synthesis of metal complexes of 1-(4-(aminomethyl)benzyl)-7-(4-((1,4,8,11-tetraazabicyclo[10.2.2]hexadecane)methyl)benzyl)-1,4,7,10-tetraazabicyclo[5.5.2]dodecane ([Cu₂**24**(OAc)₂](OAc)₂ and [Zn₂**24**(OAc)₂](OAc)₂)



M = Cu²⁺, Y = AcO⁻, (n = 1); [Cu₂**24**(OAc)₂](OAc)₂
 M = Zn²⁺, Y = AcO⁻, (n = 1/2); [Zn₂**24**(OAc)₂](OAc)₂

General procedure E was followed.

1-(4-(Aminomethyl)benzyl)-7-(4-((1,4,8,11-tetraazabicyclo[10.2.2]hexadecane)methyl)benzyl)-1,4,7,10-tetraazabicyclo[5.5.2]dodecane copper(II) acetate ([Cu₂24**(OAc)₂](OAc)₂)**

Amounts: 1-(4-(Aminomethyl)benzyl)-7-(4-((1,4,8,11-tetraazabicyclo[10.2.2]hexadecane)methyl)benzyl)-1,4,7,10-tetraazabicyclo[5.5.2]dodecane (**24**) (2.29 g, 3.55 mmol), copper(II) acetate monohydrate (1.42 g, 7.10 mmol), methanol (50 mL, 50 mL) to yield a blue solid, 1-(4-(aminomethyl)benzyl)-7-(4-((1,4,8,11-tetraazabicyclo[10.2.2]hexadecane)methyl)benzyl)-1,4,7,10-tetraazabicyclo[5.5.2]dodecane copper(II) acetate ([Cu₂**24**(OAc)₂](OAc)₂), (1.87 g, 2.42 mmol, 68.2% yield).

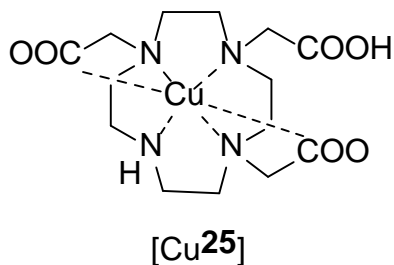
MS (ES-MS): *m/z* 444.7 (M-2CH₃CO₂, 68). Anal. calcd for C₄₆H₇₅Cu₂N₉O₈·2.8H₂O·0.5MeOH: C, 52.14; H, 7.67; N, 11.90. Found,: C, 52.09; H, 7.70; N, 11.58.

1-(4-(Aminomethyl)benzyl)-7-(4-((1,4,8,11-tetraazabicyclo[10.2.2]hexadecane)methyl)benzyl)-1,4,7,10-tetraazabicyclo[5.5.2]dodecane copper(II) acetate ([Zn₂24(OAc)₂](OAc)₂)

Amounts: 1-(4-(Aminomethyl)benzyl)-7-(4-((1,4,8,11-tetraazabicyclo[10.2.2]hexadecane)methyl)benzyl)-1,4,7,10-tetraazabicyclo[5.5.2]dodecane, (**24**) (81.0 mg, 130.0 μmol), methanol (5 mL, 20 mL), zinc(II) acetate (46.01 mg, 250.0 μmol) to yield a white solid 1-(4-(aminomethyl)benzyl)-7-(4-((1,4,8,11-tetraazabicyclo[10.2.2]hexadecane)methyl)benzyl)-1,4,7,10-tetraazabicyclo[5.5.2]dodecane copper(II) acetate ([Zn₂24(OAc)₂](OAc)₂), (89.0 mg, 88.0 μmol, 70.26% yield).

MS (ES-MS): *m/z* 446.2 (M-2CH₃CO₂, 68). Anal. calcd for C₄₆H₇₅Zn₂N₉O₈.3.0THF: C, 56.81; H, 7.89; N, 10.28. Found,: C, 57.02; H, 8.10; N, 10.31.

9.3.30 Synthesis of 2,2',2''-(1,4,7,10-tetraazacyclododecane-1,4,7-triyl)triacetic acid copper(II) acetate ([Cu25])

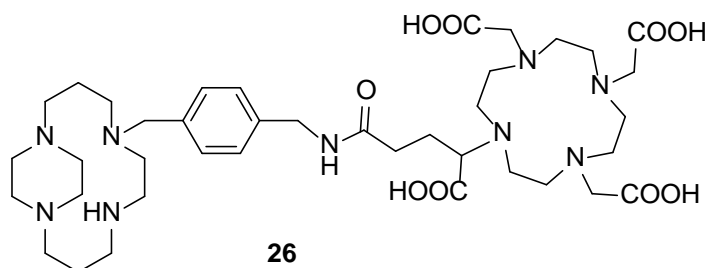


General procedure E was followed.

Amounts: 2,2',2''-(1,4,7,10-Tetraazacyclododecane-1,4,7-triyl)triacetic acid (173.8 mg, 0.50 mmol, supplied by past member of the Archibald group), copper(II) acetate (91.1 mg, 0.50 mmol), methanol (200 μ L). To yield the blue solid 2,2',2''-(1,4,7,10-tetraazacyclododecane-1,4,7-triyl)triacetic acid copper(II) acetate ([Cu25]), (126.0 mg, 0.31 mmol, 62.0% yield).

MS (ES-MS): m/z 406.1 (M^+). Anal. calcd for $C_{14}H_{21}CuN_4O_6 \cdot 0.5MeOH$: C, 41.28; H, 5.75; N, 13.28. Found,: C, 41.20; H, 5.89; N, 12.98.

9.3.31 Synthesis of 2,2',2''-(10-(4-((4-((1,5,8,12-tetraazabicyclo[10.2.2]hexadecan-5-yl)methyl)benzyl)amino)-1-carboxy-4-oxobutyl)-1,4,7,10-tetraazacyclododecane-1,4,7-triyl)triacetic acid (**26**)



General procedure H

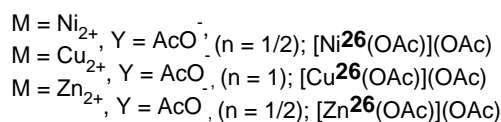
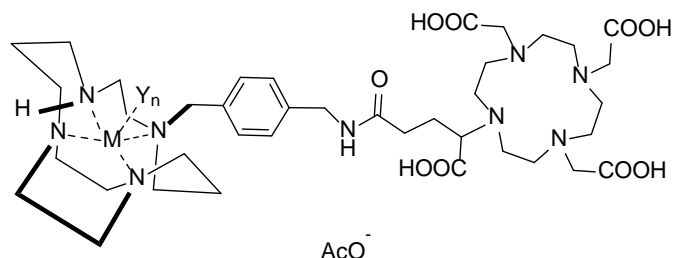
The macrocycle was dissolved in anhydrous amine-free DMF and combined with 2,2',2''-(10-(2,6-dioxotetrahydro-2H-pyran-3-yl)-1,4,7,10-tetraazacyclododecane-1,4,7-triyl)triacetic acid with the presence of bases. The reaction was shaken (550 RPM) overnight at RT before being reduced *in vacuo* before being purified by HPLC conditions.

2,2',2''-(10-(4-((4-((1,5,8,12-Tetraazabicyclo[10.2.2]hexadecan-5-yl)methyl)benzyl)amino)-1-carboxy-4-oxobutyl)-1,4,7,10-tetraazacyclododecane-1,4,7-triyl)triacetic acid (**26**)

Amounts: 1-(4-Aminomethylbenzyl)-1,4,8,11-tetraazabicyclo[10.2.2]-hexadecane (**12**) (11.8 mg, 34.0 μmol), DMF (2 mL), 2,2',2''-(10-(2,6-dioxotetrahydro-2H-pyran-3-yl)-1,4,7,10-tetraazacyclododecane-1,4,7-triyl)triacetic acid (40.0 mg, 85.0 μmol) and triethylamine (4.7 μL , 3.43 mg, 34.0 μmol). To yield a white solid, 2,2',2''-(10-(4-((4-((1,5,8,12-tetraazabicyclo[10.2.2]hexadecan-5-yl)methyl)benzyl)amino)-1-carboxy-4-oxobutyl)-1,4,7,10-tetraazacyclododecane-1,4,7-triyl)triacetic acid (**26**), (7.8 mg, 9.0 μmol , 62.5%).

Purified using RP semi-preparative HPLC System 4 (Section 9.2.2.4) (single peaks, $t_r = 15:20$ min). ^1H NMR (400 MHz, D_2O , δ): 1.23-1.29 (m, N- β - CH_2 , 4H), 1.72-2.13 (m, N- α - CH_2 , 12H), 2.67-2.97 (m, N- α - CH_2 , 6H), 3.01-3.67 (m, N- α - CH_2 , 18H), 3.22-3.38 (m, CH_2 -CO + CH_2 -CCO, 4H), 4.01-4.18 (m, CH_2 -Ar, 4H), 4.31 (br s, CH, 1H), 4.46-4.72 (m, CH_2 -CO, 6H), 7.18-7.23 (m, Ar, 4H), 8.01 (s, NH, 1H), 8.32 (s, OH, 1H), 8.65 (s, OH, 1H). MS (HRMS): m/z (M^+) calcd for $\text{C}_{39}\text{H}_{64}\text{N}_9\text{O}_9$: 802.4820 found, 802.4832.

9.3.32 Synthesis of metal complexes of 2,2',2''-(10-(4-((4-((1,5,8,12-tetraazabicyclo[10.2.2]hexadecan-5-yl)methyl)benzyl)amino)-1-carboxy-4-oxobutyl)-1,4,7,10-tetraazacyclododecane-1,4,7-triyl)triacetic acid ([Ni²⁶(OAc)](OAc), [Cu²⁶(OAc)](OAc), and [Zn²⁶(OAc)](OAc))



General procedure H was followed

2,2',2''-(10-(4-((4-((1,5,8,12-Tetraazabicyclo[10.2.2]hexadecan-5-yl)methyl)benzyl)amino)-1-carboxy-4-oxobutyl)-1,4,7,10-tetraazacyclododecane-1,4,7-triyl)triacetic acid nickel(II) acetate ([Ni²⁶(OAc)](OAc))

Amounts: 1-(4-Aminomethylbenzyl)-1,4,8,11-tetraazabicyclo[10.2.2]-hexadecane nickel(II) acetate ([Ni¹²(OAc)](OAc) (6.0 mg, 0.011 mmol), anhydrous DMF (2 mL), 2,2',2''-(10-(2,6-dioxotetrahydro-2H-pyran-3-yl)-1,4,7,10-tetraazacyclododecane-1,4,7-triyl)triacetic acid 13.13 mg, 0.028 mmol) and triethylamine (1 equiv.). To yield a green solid, 2,2',2''-(10-(4-((4-((1,5,8,12-tetraazabicyclo[10.2.2]hexadecan-5-yl)methyl)benzyl)amino)-1-carboxy-4-oxobutyl)-1,4,7,10-tetraazacyclododecane-1,4,7-triyl)triacetic acid nickel(II) acetate ([Ni²⁶(OAc)](OAc)), (4.7 mg, 4.88 μmol, 43.6%). No purification attempted.

MS (ES-MS): *m/z* 859.4 (M-2CH₃CO₂, 68).

2,2',2''-(10-(4-((4-((1,5,8,12-Tetraazabicyclo[10.2.2]hexadecan-5-yl)methyl)benzyl)amino)-1-carboxy-4-oxobutyl)-1,4,7,10-tetraazacyclododecane-1,4,7-triyl)triacetic acid copper(II) acetate ([Cu26(OAc)](OAc))

Amounts: 1-(4-Aminomethylbenzyl)-1,4,8,11-tetraazabicyclo[10.2.2]-hexadecane copper(II) acetate ([Cu12(OAc)](OAc)) (5.3 mg, 10.0 μ mol), anhydrous DMF (2 mL), 2,2',2''-(10-(2,6-dioxotetrahydro-2H-pyran-3-yl)-1,4,7,10-tetraazacyclododecane-1,4,7-triyl)triacetic acid (12.4 mg, 25.0 μ mol), and triethylamine (1 equiv.). To yield a light blue solid, 2,2',2''-(10-(4-((4-((1,5,8,12-tetraazabicyclo[10.2.2]hexadecan-5-yl)methyl)benzyl)amino)-1-carboxy-4-oxobutyl)-1,4,7,10-tetraazacyclododecane-1,4,7-triyl)triacetic acid copper(II) acetate ([Cu26(OAc)](OAc)) (5.2 mg, 6.0 μ mol, 60.1%).

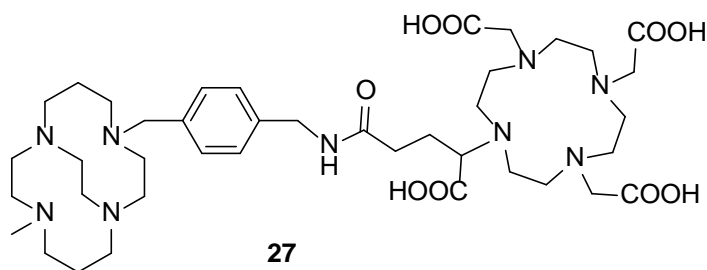
Purified using RP semi-preparative HPLC System 4 (Section 9.2.2.4) (single peaks, t_r = 10:20 min). MS (ES-MS): m/z 942.4 (M-CH₃CO₂+H₂O, 50).

2,2',2''-(10-(4-((4-((1,5,8,12-tetraazabicyclo[10.2.2]hexadecan-5-yl)methyl)benzyl)amino)-1-carboxy-4-oxobutyl)-1,4,7,10-tetraazacyclododecane-1,4,7-triyl)triacetic acid zinc(II) acetate ([Zn26(OAc)](OAc))

Amounts: 1-(4-Aminomethylbenzyl)-1,4,8,11-tetraazabicyclo[10.2.2]-hexadecane zinc(II) acetate ([Zn12(OAc)](OAc)) (5.10 mg, 9.0 μ mol), anhydrous DMF (2 mL), 2,2',2''-(10-(2,6-dioxotetrahydro-2H-pyran-3-yl)-1,4,7,10-tetraazacyclododecane-1,4,7-triyl)triacetic acid (11.06 mg, 24.0 μ mol) and triethylamine (1 equiv.). To yield a white solid, 2,2',2''-(10-(4-((4-((1,5,8,12-tetraazabicyclo[10.2.2]hexadecan-5-yl)methyl)benzyl)amino)-1-carboxy-4-oxobutyl)-1,4,7,10-tetraazacyclododecane-1,4,7-triyl)triacetic acid ([Zn26(OAc)](OAc)), (6.50 mg, 6.59 μ mol, 68.0%).

Purified using RP semi-preparative HPLC System 4 (Section 9.2.2.4) (single peaks, t_r = 11:05 min). MS (ES-MS): m/z 865.4 (M-2CH₃CO₂, 68).

9.3.33 Synthesis of 2,2',2''-(10-(1-carboxy-4-((4-((11-methyl-1,4,8,11-tetraazabicyclo[6.6.2]hexadecan-4-yl)methyl)benzyl)amino)-4-oxobutyl)-1,4,7,10-tetraazacyclododecane-1,4,7-triyl)triacetic acid (**27**)



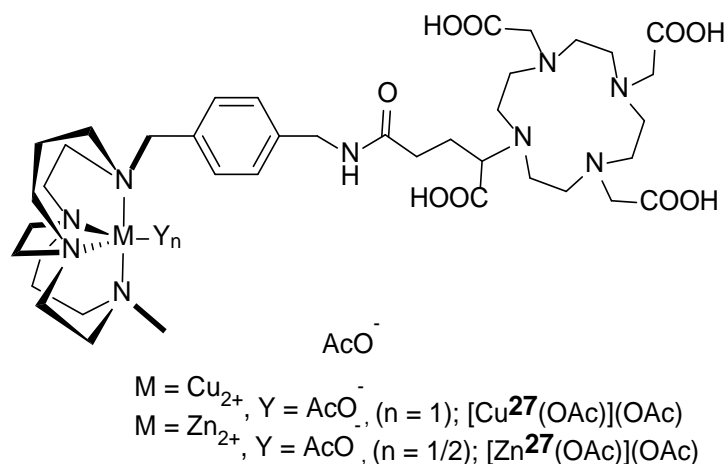
General procedure H was followed.

2,2',2''-(10-(1-Carboxy-4-((4-((11-methyl-1,4,8,11-tetraazabicyclo[6.6.2]hexadecan-4-yl)methyl)benzyl)amino)-4-oxobutyl)-1,4,7,10-tetraazacyclododecane-1,4,7-triyl)triacetic acid (27**)**

Amounts: 1-(4-Cyanobenzyl)-8-(methyl)-1,4,8,11-tetraazabicyclo[6.6.2]-hexadecane (**15**) (10.30 mg, 0.028 mmol), anhydrous DMF (2 mL), 2,2',2''-(10-(2,6-dioxotetrahydro-2H-pyran-3-yl)-1,4,7,10-tetraazacyclododecane-1,4,7-triyl)triacetic acid (17.00 mg, 0.034 mmol) and triethylamine (1 equiv.). To yield a white solid, 2,2',2''-(10-(1-carboxy-4-((4-((11-methyl-1,4,8,11-tetraazabicyclo[6.6.2]hexadecan-4-yl)methyl)benzyl)amino)-4-oxobutyl)-1,4,7,10-tetraazacyclododecane-1,4,7-triyl)triacetic acid (**27**), (4.2 mg, 4.91 μ mol, 17.5%).

Purified using RP semi-preparative HPLC System 4 (Section 9.2.2.4) (single peaks, t_r = 14:50 min). ^1H NMR (400 MHz, D_2O , δ): 1.24-1.56 (m, N- β - CH_2 , 2H), 2.71 (s, CH_3 , 3H) 2.93-2.99 (m, N- β - CH_2 + N- α - CH_2 , 6H), 3.18-3.24 (m, CH_2 -CO + CH_2 -CCO, 4H), 3.46 – 3.80 (m, N- α - CH_2 , 22H), 3.27-3.32 (m, N- α - CH_2 , 10H), 4.08-4.20 (m, CH_2 -Ar, 4H), 4.25 (s, CH, 1H), 4.40-4.80 (m, CH_2 -CO, 6H), 7.32-7.34 (m, Ar-H, 2H), 7.41-7.48 (m, Ar-H, 2H), 8.06 (s, OH, 1H), 8.45 (s, OH, 1H). MS (HRMS): m/z (M^+) calcd. for $\text{C}_{40}\text{H}_{66}\text{N}_9\text{O}_9^-$, 816.4989 found, 816.4984.

9.3.34 Synthesis of 2,2',2''-(10-(1-carboxy-4-((4-((11-methyl-1,4,8,11-tetraazabicyclo[6.6.2]hexadecan-4-yl)methyl)benzyl)amino)-4-oxobutyl)-1,4,7,10-tetraazacyclododecane-1,4,7-triyl)triacetic acid metal derivatives ([Cu]**27** and [Zn]**27**)



2,2',2''-(10-(1-Carboxy-4-((4-((11-methyl-1,4,8,11-tetraazabicyclo[6.6.2]hexadecan-4-yl)methyl)benzyl)amino)-4-oxobutyl)-1,4,7,10-tetraazacyclododecane-1,4,7-triyl)triacetic acid copper(II) acetate ([Cu²⁷(OAc)](OAc))

Amounts: 1-(4-Cyanobenzyl)-8-(methyl)-1,4,8,11-tetraazabicyclo[6.6.2]-hexadecane copper(II) acetate ([Cu¹⁵(OAc)](OAc)) (7.70 mg, 0.015 mmol), anhydrous DMF (2 mL), 2,2',2''-(10-(2,6-dioxotetrahydro-2H-pyran-3-yl)-1,4,7,10-tetraazacyclododecane-1,4,7-triyl)triacetic acid (18.07 mg, 0.037 mmol) and triethylamine (1 equiv.). To yield a light blue solid, 2,2',2''-(10-(1-carboxy-4-((4-((11-methyl-1,4,8,11-tetraazabicyclo[6.6.2]hexadecan-4-yl)methyl)benzyl)amino)-4-oxobutyl)-1,4,7,10-tetraazacyclododecane-1,4,7-triyl)triacetic acid copper(II) acetate ([Cu²⁷(OAc)](OAc)), (6.1 mg, 5.91 μmol, 39.4%).

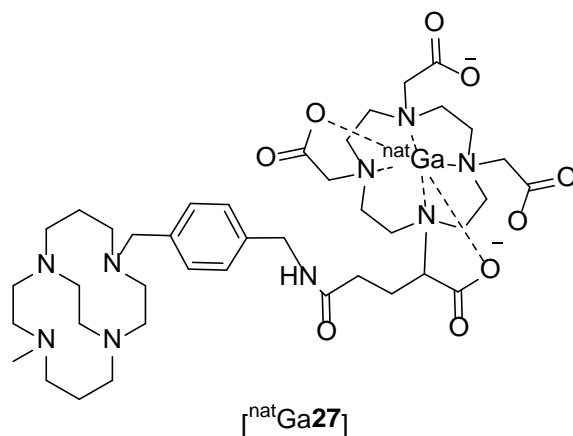
Purified using RP semi-preparative HPLC System 4 (Section 9.2.2.4) (single peaks, *t_r* = 09:10 min). MS (ES-MS): *m/z* 938.4 (M-CH₃CO₂, 34).

2,2',2''-(10-(1-Carboxy-4-((4-((11-methyl-1,4,8,11-tetraazabicyclo[6.6.2]hexadecan-4-yl)methyl)benzyl)amino)-4-oxobutyl)-1,4,7,10-tetraazacyclododecane-1,4,7-triyl)triacetic acid zinc(II) acetate ([Zn27(OAc)](OAc))

Amounts: 1-(4-Cyanobenzyl)-8-(methyl)-1,4,8,11-tetraazabicyclo[6.6.2]-hexadecane zinc(II) acetate, ([Zn15(OAc)](OAc)) (9.54 mg, 0.017 mmol), anhydrous DMF (2 mL), 2,2',2''-(10-(2,6-dioxotetrahydro-2H-pyran-3-yl)-1,4,7,10-tetraazacyclododecane-1,4,7-triyl)triacetic acid (21.73 mg, 0.0044 mmol) and triethylamine (1 equiv.). To yield a white solid, 2,2',2''-(10-(1-carboxy-4-((4-((11-methyl-1,4,8,11-tetraazabicyclo[6.6.2]hexadecan-4-yl)methyl)benzyl)amino)-4-oxobutyl)-1,4,7,10-tetraazacyclododecane-1,4,7-triyl)triacetic acid zinc(II) acetate ([Zn27(OAc)](OAc)), (6.2 mg, 6.00 μ mol, 35.3%).

Purified using RP semi-preparative HPLC System 4 (Setion 7.2.2.4) (single peaks, t_r = 10:20 min). MS (ES-MS): m/z 477.5 (M-CH₃CO₂+OH, 49).

9.3.35 Synthesis of 2,2',2''-(10-(1-carboxy-4-((4-((11-methyl-1,4,8,11-tetraazabicyclo[6.6.2]hexadecan-4-yl)methyl)benzyl)amino)-4-oxobutyl)-1,4,7,10-tetraazacyclododecane-1,4,7-triyl)triacetic acid (**27**) with gallium(III) to form ($[\text{natGa27}]$)



General procedure I

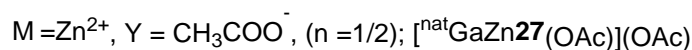
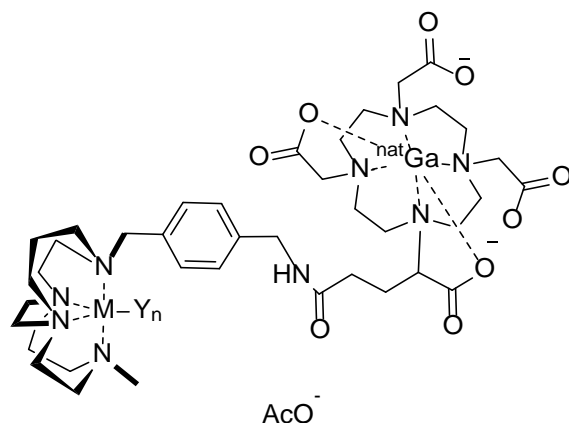
The macrocycle and a solution of gallium(III) nitrate hydrate in water were dissolved in HEPES buffer (2mL, pH = 3.5, 0.1 M). The reaction mixture was stirred (550 RPM) for 16 hours night at 35°C on a thermomixer. Compound was purified by semi-preparative chromatography, before being lyophilised.

2,2',2''-(10-(1-Carboxy-4-((4-((11-methyl-1,4,8,11-tetraazabicyclo[6.6.2]hexadecan-4-yl)methyl)benzyl)amino)-4-oxobutyl)-1,4,7,10-tetraazacyclododecane-1,4,7-triyl)triacetic acid gallium(III) complex ($[\text{natGa27}]$)

Amounts: 2,2',2''-(10-(1-Carboxy-4-((4-((11-methyl-1,4,8,11-tetraazabicyclo[6.6.2]hexadecan-4-yl)methyl)benzyl)amino)-4-oxobutyl)-1,4,7,10-tetraazacyclododecane-1,4,7-triyl)triacetic acid (**27**) (2.mg, 2.5 μmol), HEPES buffer (2mL, pH = 3.5, 0.1 M), gallium(III) nitrate hydrate (0.76 mg, 3.0 μmol). To yield a white solid, 2,2',2''-(10-(1-carboxy-4-((4-((11-methyl-1,4,8,11-tetraazabicyclo[6.6.2]hexadecan-4-yl)methyl)benzyl)amino)-4-oxobutyl)-1,4,7,10-tetraazacyclododecane-1,4,7-triyl)triacetic acid gallium(III) complex ($[\text{natGa27}]$), (1.80 mg, 2.0 μmol , 82.4% yield).

Purified using reverse phase semi-preparative HPLC System 4 (Section 9.2.2.4) (single peaks, t_r = 07:50 min, <90% incorporation by HPLC). MS (ES-MS): m/z 883.4 (M^+).

9.3.36 Synthesis of metal complexes of 2,2',2''-(10-(1-carboxy-4-((4-((11-methyl-1,4,8,11-tetraazabicyclo[6.6.2]hexadecan-4-yl)methyl)benzyl)amino)-4-oxobutyl)-1,4,7,10-tetraazacyclododecane-1,4,7-triyl)triacetic acid zinc(II) acetate ([Zn27(OAc)](OAc)) with gallium(III) to form ([^{nat}GaZn27(OAc)](OAc))



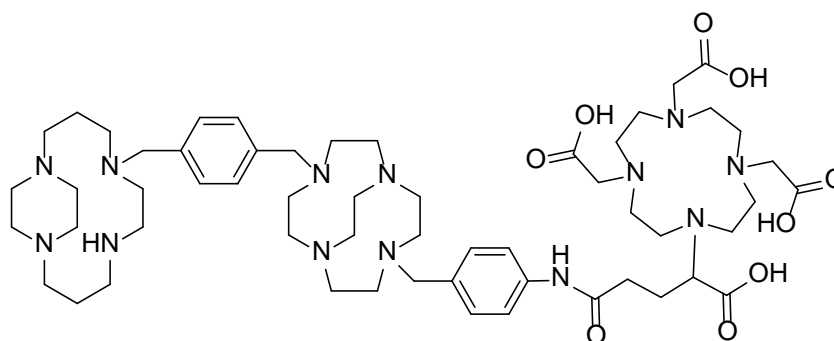
General procedure I was followed.

2,2',2''-(10-(1-Carboxy-4-((4-((11-methyl-1,4,8,11-tetraazabicyclo[6.6.2]hexadecan-4-yl)methyl)benzyl)amino)-4-oxobutyl)-1,4,7,10-tetraazacyclododecane-1,4,7-triyl)triacetic acid zinc(II) acetate gallium(III) complex ([^{nat}GaZn27(OAc)](OAc))

Amounts: 2,2',2''-(10-(1-Carboxy-4-((4-((11-methyl-1,4,8,11-tetraazabicyclo[6.6.2]hexadecan-4-yl)methyl)benzyl)amino)-4-oxobutyl)-1,4,7,10-tetraazacyclododecane-1,4,7-triyl)triacetic acid zinc acetate ([Zn27(OAc)](OAc)) (2.00 mg, 2.0 μmol), HEPES buffer (2mL, pH = 3.5, 0.1 M), gallium(III) nitrate hydrate (0.61 mg, 2.4 μmol). To yield a white solid, 2,2',2''-(10 (1-carboxy-4-((4-((11-methyl-1,4,8,11-tetraazabicyclo[6.6.2]hexadecan-4-yl)methyl)benzyl)amino)-4-oxobutyl)-1,4,7,10-tetraazacyclododecane-1,4,7-triyl)triacetic acid zinc(II) acetate gallium(III) complex ([^{nat}GaZn27(OAc)](OAc)), (2.00 mg, 1.9 μmol, 94.0% yield).

Purified using RP semi-preparative HPLC System 4 (7.2.2.4) (single peaks, t_r = 07:40 min, <90% incorporation by HPLC). MS (ES-MS; run with formic acid): m/z 993.4 (M-2CH₃CO₂+CHO₂+H, 22).

9.3.37 Attempted synthesis of 2,2',2''-(10-(4-((4-((10-(4-((1,5,8,12-tetraazabicyclo[10.2.2]hexadecan-5-yl)methyl)benzyl)-1,4,7,10-tetraazabicyclo[5.5.2]tetradecan-4-yl)methyl)phenyl)amino)-1-carboxy-4-oxobutyl)-1,4,7,10-tetraazacyclododecane-1,4,7-triyl)triacetic acid (**28**)

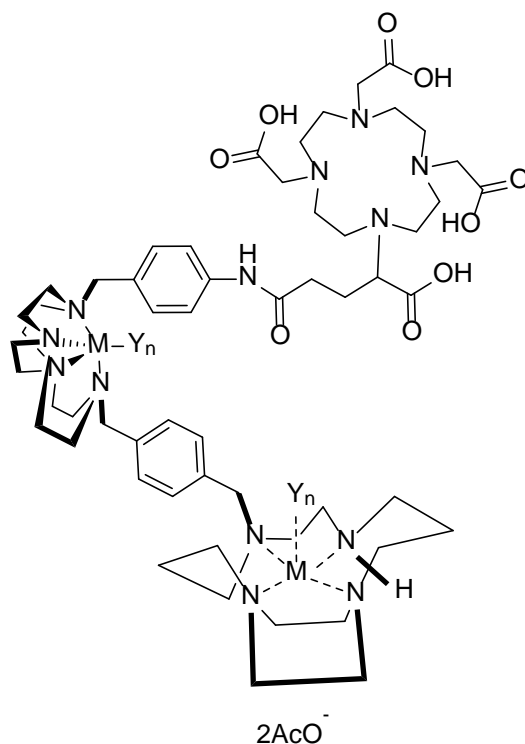


28

Attempted synthesis of 2,2',2''-(10-(4-((4-((10-(4-((1,5,8,12-Tetraazabicyclo[10.2.2]hexadecan-5-yl)methyl)benzyl)-1,4,7,10-tetraazabicyclo[5.5.2]tetradecan-4-yl)methyl)phenyl)amino)-1-carboxy-4-oxobutyl)-1,4,7,10-tetraazacyclododecane-1,4,7-triyl)triacetic acid (28**)**

Amounts: 1-(4-Aminobenzyl)-7-(4-((1,4,8,11tetraazabicyclo[10.2.2]hexadecane)methyl)benzyl)-1,4,7,10-tetraazabicyclo[5.5.2]dodecane (**23**) (5.41 mg, 8.6 μmol), 2,2',2''-(10-(2,6-dioxotetrahydro-2H-pyran-3-yl)-1,4,7,10-tetraazacyclododecane-1,4,7-triyl)triacetic acid (4.71 mg, 10.3 μmol), anhydrous DMF (1 mL). To yield an orange solid. The desired product was not isolated using this synthetic procedure.

9.3.38 Attempted synthesis of 2,2',2''-(10-(4-((4-((10-(4-((1,5,8,12-tetraazabicyclo[10.2.2]hexadecan-5-yl)methyl)benzyl)-1,4,7,10-tetraazabicyclo[5.5.2]tetradecan-4-yl)methyl)phenyl)amino)-1-carboxy-4-oxobutyl)-1,4,7,10-tetraazacyclododecane-1,4,7-triyl)triacetic acid metal complexes ($[\text{Cu}_2\mathbf{28}(\text{OAc})_2](\text{OAc})_2$ and $[\text{Zn}_2\mathbf{28}(\text{OAc})_2](\text{OAc})_2$)



$M = \text{Cu}^{2+}$, $Y = \text{AcO}^-$, ($n = 1$); $[\text{Cu}_2\mathbf{28}(\text{OAc})_2](\text{OAc})_2$
 $M = \text{Zn}^{2+}$, $Y = \text{AcO}^-$, ($n = 1/2$); $[\text{Zn}_2\mathbf{28}(\text{OAc})_2](\text{OAc})_2$

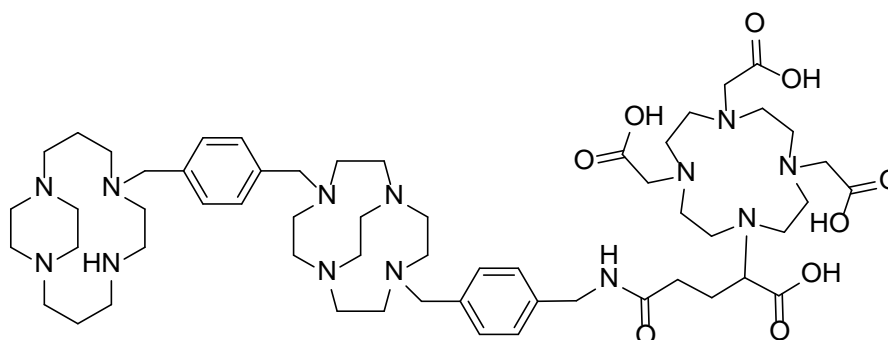
Attempted synthesis of 2,2',2''-(10-(4-((4-((10-(4-((1,5,8,12-tetraazabicyclo[10.2.2]hexadecan-5-yl)methyl)benzyl)-1,4,7,10-tetraazabicyclo[5.5.2]tetradecan-4-yl)methyl)phenyl)amino)-1-carboxy-4-oxobutyl)-1,4,7,10-tetraazacyclododecane-1,4,7-triyl)triacetic acid copper(II) acetate ($[\text{Cu}_2\mathbf{28}(\text{OAc})_2](\text{OAc})_2$)

Amounts: 1-(4-Aminobenzyl)-7-(4-((1,4,8,11-tetraazabicyclo[10.2.2]hexadecane)methyl)benzyl)-1,4,7,10-tetraazabicyclo[5.5.2]dodecane copper(II) acetate ($[\text{Cu}_2\mathbf{23}(\text{OAc})_2](\text{OAc})_2$) (7.00 mg, 9.2 μmol), 2,2',2''-(10-(2,6-dioxotetrahydro-2H-pyran-3-yl)-1,4,7,10-tetraazacyclododecane-1,4,7-triyl)triacetic acid (5.07 mg, 11.1 μmol), anhydrous DMF (340 μL). To yield a blue solid. The desired product was not isolated using this synthetic procedure.

Attempted synthesis of 2,2',2''-(10-(4-((4-((10-(4-((1,5,8,12-tetraazabicyclo[10.2.2]hexadecan-5-yl)methyl)benzyl)-1,4,7,10-tetraazabicyclo[5.5.2]tetradecan-4-yl)methyl)phenyl)amino)-1-carboxy-4-oxobutyl)-1,4,7,10-tetraazacyclododecane-1,4,7-triyl)triacetic acid zinc(II) acetate ([Zn]28)

Amounts: 1-(4-Aminobenzyl)-7-(4-((1,4,8,11-tetraazabicyclo[10.2.2]hexadecane)methyl)benzyl)-1,4,7,10tetraazabicyclo[5.5.2]dodecane zinc(II) acetate ([Zn₂23(OAc)₂](OAc)₂) (5.90 mg, 7.7 μmol), 2,2',2''- (10- (2,6-dioxotetrahydro-2H-pyran-3-yl)-1,4,7,10-tetraazacyclododecane-1,4,7-triyl)triacetic acid (4.26 mg, 9.3 μmol), dry DMF (1 mL). To yield an orange solid. The desired product was not isolated using this synthetic procedure.

9.3.39 Synthesis of 2,2',2''-(10-(4-((4-((10-(4-((1,5,8,12-tetraazabicyclo[10.2.2]hexadecan-5-yl)methyl)benzyl)-1,4,7,10-tetraazabicyclo[5.5.2]tetradecan-4-yl)methyl)benzyl)amino)-1-carboxy-4-oxobutyl)-1,4,7,10-tetraazacyclododecane-1,4,7-triyl)triacetic acid (**29**)



29

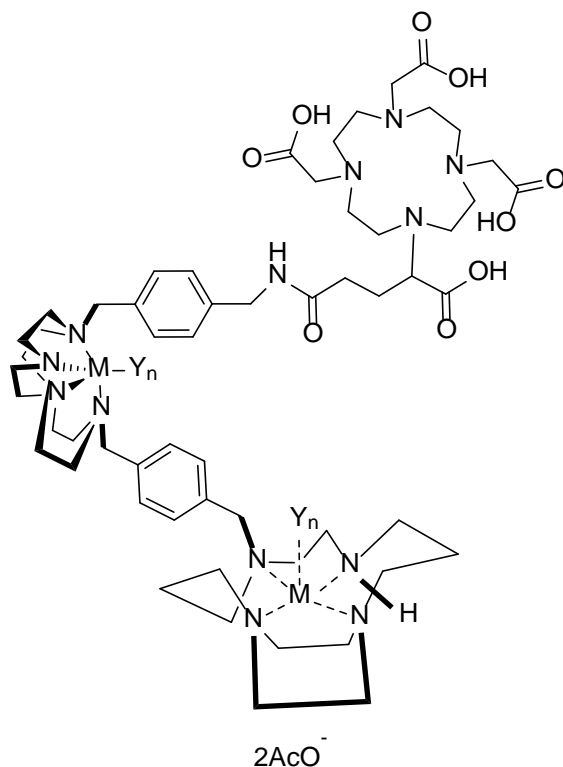
General procedure H was followed.

2,2',2''-(10-(4-((4-((10-(4-((1,5,8,12-Tetraazabicyclo[10.2.2]hexadecan-5-yl)methyl)benzyl)-1,4,7,10-tetraazabicyclo[5.5.2]tetradecan-4-yl)methyl)benzyl)amino)-1-carboxy-4-oxobutyl)-1,4,7,10-tetraazacyclododecane-1,4,7-triyl)triacetic acid (29**)**

Amounts: 1-(4-(Aminomethyl)benzyl)-7-(4-((1,4,8,11-tetraazabicyclo[10.2.2]hexadecane)methyl)benzyl)-1,4,7,10-tetraazabicyclo[5.5.2]dodecane (**24**) (48.5 mg, 0.080 mmol); 2,2',2''-(10-(2,6-dioxotetrahydro-2H-pyran-3-yl)-1,4,7,10-tetraazacyclododecane-1,4,7-triyl)triacetic acid (34.41 mg, 0.080 mmol), anhydrous DMF (2 mL). To yield a white solid, 2,2',2''-(10-(4-((4-((10-(4-((1,5,8,12-tetraazabicyclo[10.2.2]hexadecan-5-yl)methyl)benzyl)-1,4,7,10-tetraazabicyclo[5.5.2]tetradecan-4-yl)methyl)benzyl)amino)-1-carboxy-4-oxobutyl)-1,4,7,10-tetraazacyclododecane-1,4,7-triyl)triacetic acid (**29**) (42.0 mg, 3.8 μ mol, 50.6% yield).

Purified using RP semi-preparative HPLC System 5 (Section 9.2.2.5) (single peaks, t_r = 17:18 min). Analytical RP-HPLC Systems C (Section 9.2.1.3) (single peaks, t_r = 17:27 min). MS (HRMS): calcd for (M^+) $C_{57}H_{93}N_{13}O_9^+$: 1104.7292 found, 1104.7294

9.3.40 Synthesis of 2,2',2''-(10-(4-((4-((10-(4-((1,5,8,12-tetraazabicyclo[10.2.2]hexadecan-5-yl)methyl)benzyl)-1,4,7,10-tetraazabicyclo[5.5.2]tetradecan-4-yl)methyl)benzyl)amino)-1-carboxy-4-oxobutyl)-1,4,7,10-tetraazacyclododecane-1,4,7-triyl)triacetic acid metal complexes ($[\text{Cu}_2\mathbf{29}(\text{OAc})_2](\text{OAc})_2$ and $[\text{Zn}_2\mathbf{29}(\text{OAc})_2](\text{OAc})_2$)



$M = \text{Cu}^{2+}$, $Y = \text{AcO}^-$, ($n = 1/2$); $[\text{Cu}_2\mathbf{29}(\text{OAc})_2](\text{OAc})_2$
 $M = \text{Zn}^{2+}$, $Y = \text{AcO}^-$, ($n = 1$); $[\text{Zn}_2\mathbf{29}(\text{OAc})_2](\text{OAc})_2$

2,2',2''-(10-(4-((4-((10-(4-((1,5,8,12-Tetraazabicyclo[10.2.2]hexadecan-5-yl)methyl)benzyl)-1,4,7,10-tetraazabicyclo[5.5.2]tetradecan-4-yl)methyl)benzyl)amino)-1-carboxy-4-oxobutyl)-1,4,7,10-tetraazacyclododecane-1,4,7-triyl)triacetic acid copper(II) acetate ($[\text{Cu}_2\mathbf{29}(\text{OAc})_2](\text{OAc})_2$)

Amounts: 1-(4-(Aminomethyl)benzyl)-7-(4-((1,4,8,11-tetraazabicyclo[10.2.2]hexadecane)methyl)benzyl)-1,4,7,10-tetraazabicyclo[5.5.2]dodecane copper acetate ($[\text{Cu}_2\mathbf{24}(\text{OAc})_2](\text{OAc})_2$) (7.1 mg, 10.0 μmol), 2,2',2''-(10-(2,6-dioxotetrahydro-2H-pyran-3-yl)-1,4,7,10-tetraazacyclododecane-1,4,7-triyl)triacetic acid (3.26 mg, 10.0 μmol), anhydrous DMF (2 mL). To yield a blue solid, 2,2',2''-(10-(4-((4-((10-(4-((1,5,8,12-tetraazabicyclo[10.2.2]hexadecan-5-yl)methyl)benzyl)-1,4,7,10-tetraazabicyclo[5.5.2]tetradecan-4-yl)methyl)benzyl)amino)-1-carboxy-4-oxobutyl)-1,4,7,10-tetraazacyclododecane-1,4,7-triyl)triacetic acid copper(II) acetate ($[\text{Cu}_2\mathbf{29}(\text{OAc})_2](\text{OAc})_2$), (42.0 mg, 3.8 μmol , 50.6% yield).

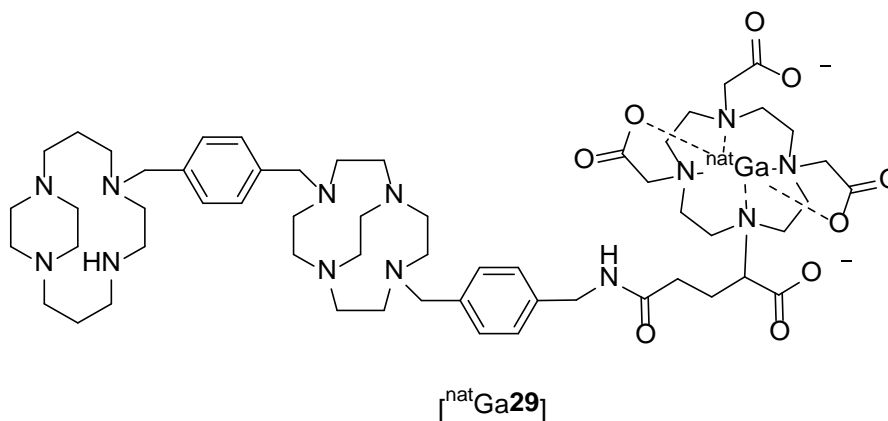
Purified using RP semi-preparative HPLC System 5 (Section 9.2.2.5) (single peaks, $t_r = 19:20$ min). MS (ES-MS): m/z 674.7 (M-2CH₃CO₂, 68).

2,2',2''-(10-(4-((4-((10-(4-((1,5,8,12-Tetraazabicyclo[10.2.2]hexadecan-5-yl)methyl)benzyl)-1,4,7,10-tetraazabicyclo[5.5.2]tetradecan-4-yl)methyl)benzyl)amino)-1-carboxy-4-oxobutyl)-1,4,7,10-tetraazacyclododecane-1,4,7-triyl)triacetic acid zinc(II) acetate ([Zn₂29(OAc)₂](OAc)₂)

Amounts: 1-(4-(Aminomethyl)benzyl)-7-(4-((1,4,8,11-tetraazabicyclo[10.2.2]hexadecane)methyl)benzyl)-1,4,7,10-tetraazabicyclo[5.5.2]dodecane zinc acetate ([Zn₂24(OAc)₂](OAc)₂) (15.00 mg, 10.0 μmol), 2,2',2''-(10-(2,6-dioxotetrahydro-2H-pyran-3-yl)-1,4,7,10-tetraazacyclododecane-1,4,7-triyl)triacetic acid (6.82 mg, 10.0 μmol), anhydrous DMF (2 mL). To yield a white solid, 2,2',2''-(10-(4-((4-((10-(4-((1,5,8,12-tetraazabicyclo[10.2.2]hexadecan-5-yl)methyl)benzyl)-1,4,7,10-tetraazabicyclo[5.5.2]tetradecan-4-yl)methyl)benzyl)amino)-1-carboxy-4-oxobutyl)-1,4,7,10-tetraazacyclododecane-1,4,7-triyl)triacetic acid zinc(II) acetate ([Zn₂29(OAc)₂](OAc)₂), (6.8 mg, 5.3 μmol, 35.6% yield).

Purified using RP semi-preparative HPLC System 5 (Section 9.2.2.5) (single peaks, $t_r = 15:21$ min). MS (ES-MS): m/z 790.5 (M-2CH₃CO₂+2TFA+2H).

9.3.41 Synthesis of metal complexes of 2,2',2''-(10-(4-((4-((10-(4-((1,5,8,12-tetraazabicyclo[10.2.2]hexadecan-5-yl)methyl)benzyl)-1,4,7,10-tetraazabicyclo[5.5.2]tetradecan-4-yl)methyl)benzyl)amino)-1-carboxy-4-oxobutyl)-1,4,7,10-tetraazacyclododecane-1,4,7-triyl)triacetic acid of (**29**) with gallium(III) nitrate to form ($[^{nat}\text{Ga}29]$)



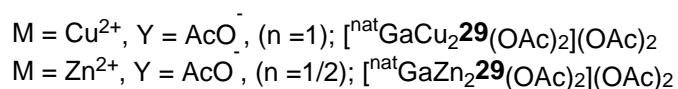
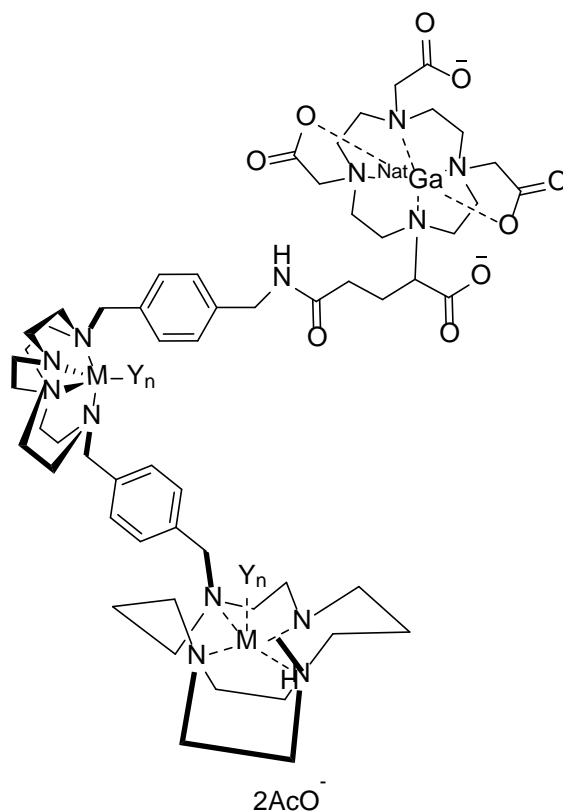
General procedure I was followed.

2,2',2''-(10-(4-((4-((10-(4-((1,5,8,12-Tetraazabicyclo[10.2.2]hexadecan-5-yl)methyl)benzyl)-1,4,7,10-tetraazabicyclo[5.5.2]tetradecan-4-yl)methyl)benzyl)amino)-1-carboxy-4-oxobutyl)-1,4,7,10-tetraazacyclododecane-1,4,7-triyl)triacetic acid gallium(III) ($[^{nat}\text{Ga}29]$)

Amounts: 2,2',2''-(10-(4-((4-((10-(4-((1,5,8,12-Tetraazabicyclo[10.2.2]hexadecan-5-yl)methyl)benzyl)-1,4,7,10-tetraazabicyclo[5.5.2]tetradecan-4-yl)methyl)benzyl)amino)-1-carboxy-4-oxobutyl)-1,4,7,10-tetraazacyclododecane-1,4,7-triyl)triacetic acid (**29**) (0.5mg, 0.4 μmol), HEPES buffer (2mL, pH = 3.5, 0.1 M), gallium(III) nitrate hydrate (0.14 mg, 0.5 μmol), to yield a white solid 2,2',2''-(10-(4-((4-((10-(4-((1,5,8,12-tetraazabicyclo[10.2.2]hexadecan-5-yl)methyl)benzyl)-1,4,7,10-tetraazabicyclo[5.5.2]tetradecan-4-yl)methyl)benzyl)amino)-1-carboxy-4-oxobutyl)-1,4,7,10-tetraazacyclododecane-1,4,7-triyl)triacetic acid gallium(III) ($[^{nat}\text{Ga}29]$), (0.34 mg, 0.3 μmol , 62.5% yield).

Analytical RP-HPLC Systems C (Section 9.2.1.3) (Single peaks, t_r = 12:50 min). MS (ES-MS): m/z 1172.5 (M^+).

9.3.42 Synthesis of metal complexes of 2,2',2''-(10-(4-((4-((10-(4-((1,5,8,12-tetraazabicyclo[10.2.2]hexadecan-5-yl)methyl)benzyl)-1,4,7,10-tetraazabicyclo[5.5.2]tetradecan-4-yl)methyl)benzyl)amino)-1-carboxy-4-oxobutyl)-1,4,7,10-tetraazacyclododecane-1,4,7-triyl)triacetic acid of $[\text{Cu}_2\mathbf{29}(\text{OAc})_2](\text{OAc})_2$ and $[\text{Zn}_2\mathbf{29}(\text{OAc})_2](\text{OAc})_2$ with gallium(III) nitrate to form $([\text{natGaCu}_2\mathbf{29}(\text{OAc})_2](\text{OAc})_2)$, and $([\text{natGaZn}_2\mathbf{29}(\text{OAc})_2](\text{OAc})_2)$



General procedure I was followed.

2,2',2''-(10-(4-((4-((10-(4-((1,5,8,12-Tetraazabicyclo[10.2.2]hexadecan-5-yl)methyl)benzyl)-1,4,7,10-tetraazabicyclo[5.5.2]tetradecan-4-yl)methyl)benzyl)amino)-1-carboxy-4-oxobutyl)-1,4,7,10-tetraazacyclododecane-1,4,7-triyl)triacetic acid copper(II) acetate gallium(III) $([\text{natGaCu}_2\mathbf{29}(\text{OAc})_2](\text{OAc})_2)$

Amounts: 2,2',2''-(10-(4-((4-((10-(4-((1,5,8,12-tetraazabicyclo[10.2.2]hexadecan-5-yl)methyl)benzyl)-1,4,7,10-tetraazabicyclo[5.5.2]tetradecan-4-yl)methyl)benzyl)amino)-1-carboxy-4-oxobutyl)-1,4,7,10-tetraazacyclododecane-1,4,7-triyl)triacetic acid copper(II) acetate ($[\text{Cu}_2\mathbf{29}(\text{OAc})_2](\text{OAc})_2$) (0.064 mg, 0.38 μmol), HEPES buffer (2mL, pH = 3.5, 0.1 M), and gallium nitrate (0.011 mg, 0.38 μmol). To yield copper(II) acetate 2,2',2''-(10-(4-((4-((10-(4-((1,5,8,12-tetraazabicyclo[10.2.2]hexadecan-5-yl)methyl)benzyl)-1,4,7,10-tetraazabicyclo[5.5.2]tetradecan-4-yl)methyl)benzyl)amino)-1-carboxy-4-oxobutyl)-1,4,7,10-tetraazacyclododecane-1,4,7-triyl)triacetic acid gallium(III) ($[\text{natGaCu}_2\mathbf{29}(\text{OAc})_2](\text{OAc})_2$), (0.040 mg, 0.26 μmol , 67.1% yield).

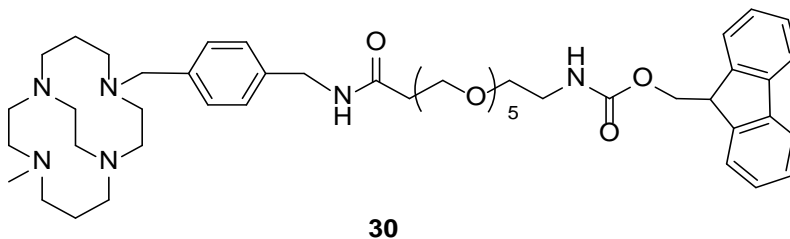
Analytical RP-HPLC Systems C (section 9.2.1.3) (Single peaks, $t_r = 12:28$ min). MS (HRMS): calcd for $[\text{M}-3\text{CH}_3\text{CO}_2+2\text{Na}]^{2+}$ for $\text{C}_{59}\text{H}_{88}\text{Cu}_2\text{GaN}_{13}\text{O}_9\text{Na}_2^{2+}$, 697.7179; found, 697.7175.

2,2',2''-(10-(4-((4-((10-(4-((1,5,8,12-tetraazabicyclo[10.2.2]hexadecan-5-yl)methyl)benzyl)-1,4,7,10-tetraazabicyclo[5.5.2]tetradecan-4-yl)methyl)benzyl)amino)-1-carboxy-4-oxobutyl)-1,4,7,10-tetraazacyclododecane-1,4,7-triyl)triacetic acid zinc(II) acetate gallium(III) ($[\text{natGaZn}_2\mathbf{29}(\text{OAc})_2](\text{OAc})_2$)

Amounts: 2,2',2''-(10-(4-((4-((10-(4-((1,5,8,12-tetraazabicyclo[10.2.2]hexadecan-5-yl)methyl)benzyl)-1,4,7,10-tetraazabicyclo[5.5.2]tetradecan-4-yl)methyl)benzyl)amino)-1-carboxy-4-oxobutyl)-1,4,7,10-tetraazacyclododecane-1,4,7-triyl)triacetic acid zinc(II) acetate ($[\text{natGaZn}_2\mathbf{29}(\text{OAc})_2](\text{OAc})_2$) (4.0 mg, 3.6 μmol), HEPES buffer (2mL, pH = 3.5, 0.1 M), and gallium(III) nitrate hydrate (1.12 mg, 4.8 μmol). To yield a white solid Zinc (II) acetate 2,2',2''-(10-(4-((4-((10-(4-((1,5,8,12-tetraazabicyclo[10.2.2]hexadecan-5-yl)methyl)benzyl)-1,4,7,10-tetraazabicyclo[5.5.2]tetradecan-4-yl)methyl)benzyl)amino)-1-carboxy-4-oxobutyl)-1,4,7,10-tetraazacyclododecane-1,4,7-triyl)triacetic acid gallium(III) ($[\text{natGaCu}_2\mathbf{29}(\text{OAc})_2](\text{OAc})_2$), (0.87 mg, 0.6 μmol , 15.6% yield).

Analytical RP-HPLC Systems C (Section 9.2.1.3) (Single peaks, $t_r = 12:38$ min). MS (ES-MS): m/z 1499.0 ($\text{M}-\text{CH}_3\text{CO}_2+\text{Na}$, 11).

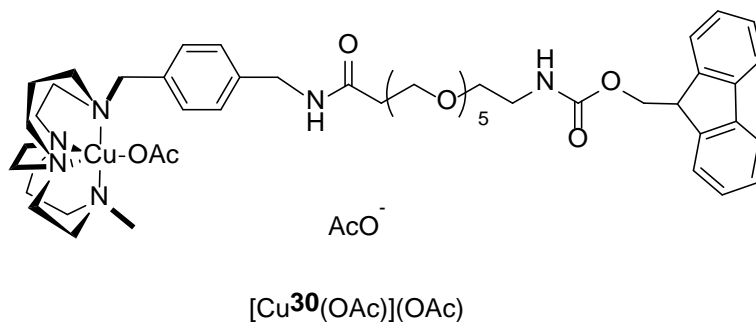
9.3.43 Synthesis of (9H-fluoren-9-yl)methyl(1-(4-((11-methyl-1,4,8,11-tetraazabicyclo[6.6.2]hexadecan-4-yl)methyl)phenyl)-3-oxo-6,9,12,15,18-pentaoxa-2-azaicosan-20-yl)carbamate (**30**)



(4-((11-Methyl-1,4,8,11-tetraazabicyclo[6.6.2]hexadecan-4-yl)methyl)phenyl)methanamine (**15**) (7.1 mg, 20.0 μmol), Fmoc-NH-PEG₅-COOH (10.4 mg, 20.0 μmol) and triethylamine (300 μL , 20.0 μmol) were combined in amine-free dimethylformide (700 mL) and shaken at RT for 1 hour. The resulting solution was reduced *in vacuo* to yield the white solid (9H-fluoren-9-yl)methyl(1-(4-((11-methyl-1,4,8,11-tetraazabicyclo[6.6.2]hexadecan-4-yl)methyl)phenyl)-3-oxo-6,9,12,15,18-pentaoxa-2-azaicosan-20-yl)carbamate (**30**), (12.2 mg, 18.8 μmol , 95.8% yield).

NMR analysis completed after Fmoc deprotection. MS (ES-MS): m/z 873.1 (M^+).

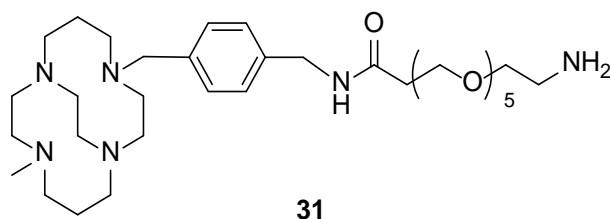
9.3.44 Synthesis of (9H-fluoren-9-yl)methyl(1-(4-((11-methyl-1,4,8,11-tetraazabicyclo[6.6.2]hexadecan-4-yl)methyl)phenyl)-3-oxo-6,9,12,15,18-pentaoxa-2-azaicosan-20-yl)carbamate copper(II) acetate ([Cu**30**(OAc)](OAc))



4-((11-Methyl-1,4,8,11-tetraazabicyclo[6.6.2]hexadecan-4-yl)methyl)phenyl)methanamine ([Cu**15**(OAc)](OAc)) (37.3 mg, 0.070 mmol), Fmoc-NH-PEG₅-COOH (36.54 mg, 0.070 mmol) and triethylamine (95.7 μ L, 0.690 mmol) were combined in amine-free dimethylformide (700 mL) and shaken at RT for 1 hour. The resulting solution was reduced *in vacuo* to yield the white solid (9H-fluoren-9-yl)methyl (1-(4-((11-methyl-1,4,8,11-tetraazabicyclo[6.6.2]hexadecan-4-yl)methyl)phenyl)-3-oxo-6,9,12,15,18-pentaoxa-2-azaicosan-20-yl)carbamate copper(II) acetate ([Cu**30**(OAc)](OAc)), (68.4 mg, 0.0649 mmol, 94.3% yield).

NMR analysis completed after Fmoc deprotection. ES-MS (*m/z*): MS (ES-MS): *m/z* 952.5 (M-2CH₃CO₂+OH, 51).

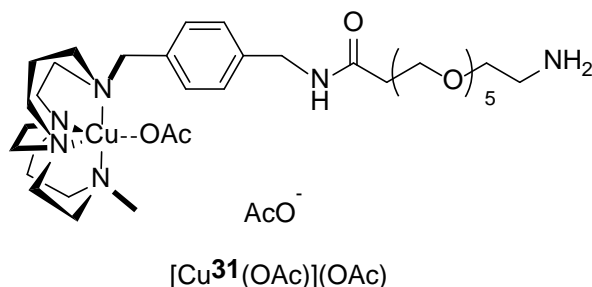
9.3.45 Synthesis of 1-amino-N-(4-((11-methyl-1,4,8,11-tetraazabicyclo[6.6.2]hexadecan-4-yl)methyl)benzyl)-3,6,9,12,15-pentaoxaoctadecan-18-amide (**31**)



(9H-Fluoren-9-yl)methyl(1-(4-((11-methyl-1,4,8,11-tetraazabicyclo[6.6.2]hexadecan-4-yl)methyl)phenyl)-3-oxo-6,9,12,15,18-pentaoxa-2-azaicosan-20-yl)carbamate (**30**) (12.2 mg, 18.8 μ mol) was taken up in dimethylformide (500 mL) and combined with a 1:1 volume of piperidine, the solution was shaken at 550 RPM at RT for an hour. The resulting was reduced *in vacuo* before being taken up in methanol (400 μ L) before being purified by LH20 sephradex. Mass spectrometry was used to combine the correct fraction before being recused *in vacuo* to yield 1-amino-N-(4-((11-methyl-1,4,8,11-tetraazabicyclo[6.6.2]hexadecan-4-yl)methyl)benzyl)-3,6,9,12,15-pentaoxaoctadecan-18-amide (**31**), (10.8 mg, 16.7 μ mol, 89.6%).

Analytical RP-HPLC Systems D (section 9.2.1.4) (single peaks, t_r = 21:50 min). ^1H NMR (100 MHz, CDCl_3 , δ): 1.50-3.51 (m, CH_2 , NH_2 + NH , 53H), 4.31-4.36 (m, CH_2 -Ar, 2H), 4.52-4.55 (m, CH_2 -Ar, 2H), 7.21 (d, J = 8.0 Hz, Ar-H, 2H), 7.26 (d, J = 8.0 Hz, Ar-H, 2H). ^{13}C NMR (100 MHz, CDCl_3 , δ): 26.61 (N- β - CH_2), 27.02 (N- β - CH_2), 32.11 ($\underline{\text{C}}$ -CO), 41.43 (C-NH $_2$), 48.27 (CH_3), 50.08 (N- α - CH_2), 50.11(N- α - CH_2), 53.69 (N- α - CH_2), 53.99 (N- α - CH_2), 54.21 (N- α - CH_2), 54.44 (N- α - CH_2), 55.31 (N- α - CH_2), 55.66 (N- α - CH_2), 56.08 (N- α - CH_2), 56.31 (N- α - CH_2), 62.41 (N- α - CH_2), 56.41 (N- α - CH_2), 65.81 ($\underline{\text{C}}\text{H}_2$ -Ar), 65.94 ($\underline{\text{C}}\text{H}_2$ -Ar), 69.71 (C-O), 70.04 (C-O), 71.83 (C-O), 73.16 (C-O), 125.10 (Ar-H), 126.80 (Ar-H), 128.33 (C-Ar), 128.97 (C-Ar), 132.08 (C=O), 181.23. MS (ES-MS): m/z 650.9 (M^+).

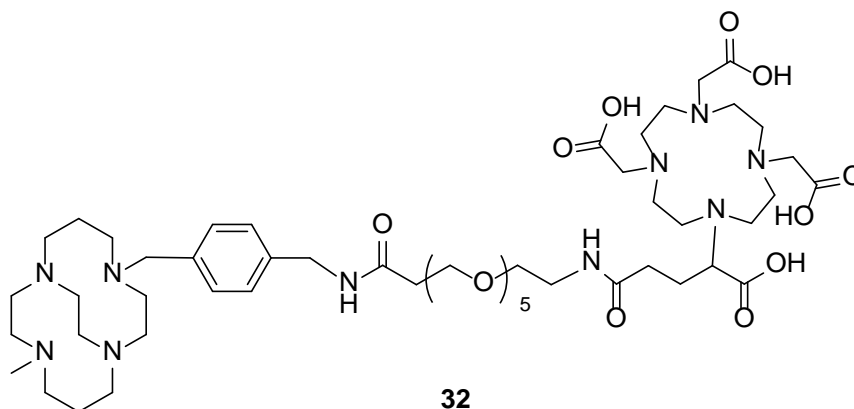
9.3.46 Synthesis of 1-amino-N-(4-((11-methyl-1,4,8,11-tetraazabicyclo[6.6.2]hexadecan-4-yl)methyl)benzyl)-3,6,9,12,15-pentaoxaoctadecan-18-amide copper(II) acetate ([Cu₂**31**(OAc)](OAc))



(9H-Fluoren-9-yl)methyl-(1-(4-((11-methyl-1,4,8,11-tetraazabicyclo[6.6.2]hexadecan-4-yl)methyl)phenyl)-3-oxo-6,9,12,15,18-pentaoxa-2-azaicosan-20-yl)carbamate copper(II) acetate ([Cu₂**30**(OAc)](OAc)) (68.4 mg, 64.9 μmol) was taken up in dimethylformide (500 mL) and combined with a 1:1 volume of piperidine, the solution was shaken at 550 RPM at RT for an hour. The resulting was reduced *in vacuo* before being taken up in methanol (400 μL) before being purified by LH20 sephradex. Mass spectrometry was used to combine the correct fraction before being reduced *in vacuo* to yield the blue solid, 1-amino-N-(4-((11-methyl-1,4,8,11-tetraazabicyclo[6.6.2]hexadecan-4-yl)methyl)benzyl)-3,6,9,12,15-pentaoxaoctadecan-18-amide ([Cu₂**31**(OAc)](OAc)) (10.8 mg, 16.7 μmol, 25.7%).

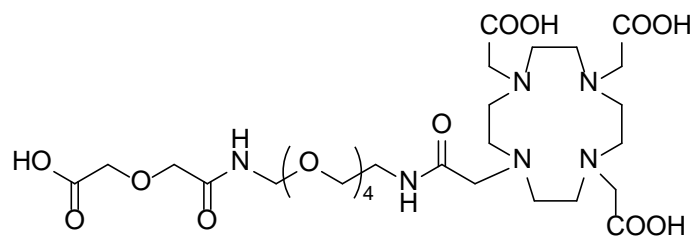
Analytical RP-HPLC Systems D (section 9.2.1.4) (single peaks, $t_r = 18:20$ min). MS (HRMS): m/z (M-2CH₃CO₂, 68) calcd for C₃₆H₆₅CuN₆O₈⁺, 722.4154; found, 722.4138.

9.3.47 Attempted synthesis of 2,2',2''-(10-(25-carboxy-1-(4-((11-methyl-1,4,8,11-tetraazabicyclo[6.6.2]hexadecan-4-yl)methyl)phenyl)-3,22-dioxo-6,9,12,15,18-pentaoxa-2,21-diazapentacosan-25-yl)-1,4,7,10-tetraazacyclododecane-1,4,7-triyl)triacetic acid (**32**)



1-Amino-N-(4-((11-methyl-1,4,8,11-tetraazabicyclo[6.6.2]hexadecan-4-yl)methyl)benzyl)-3,6,9,12,15-pentaoxaoctadecan-18-amide (**31**) (3.5 mg, 5.4 μmol) was dissolved in amine-free DMF and combined with 2,2',2''-(10-(2,6-dioxotetrahydro-2H-pyran-3-yl)-1,4,7,10-tetraazacyclododecane-1,4,7-triyl)triacetic acid (2.7 mg, 5.4 μmol) with triethylamine (1 μL , 7.2 μmol). The reaction was shaken (550 RPM) overnight at RT before being reduced *in vacuo* to yield a white solid (4.5 mg). The desired product was not isolated using this synthetic procedure.

9.3.48 Synthesis of 2,2',2''-(10-(1-carboxy-4,21-dioxo-2,8,11,14,17-pentaoxa-5,20-diazadocosan-22-yl)-1,4,7,10-tetraazacyclododecane-1,4,7-triyl)triacetic acid (**33**)

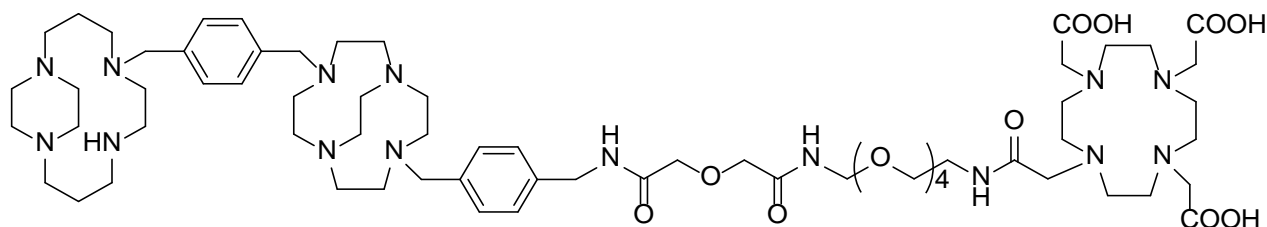


33

Diglycolic anhydride (8.22 mg, 0.070 mmol) and 2,2',2''-(10-(17-amino-2-oxo-6,9,12,15-tetraoxa-3-azaheptadecyl)-1,4,7,10-tetraazacyclododecane-1,4,7-triyl)triacetic acid (44.11 mg, 0.070 mmol) were combined in amine free DMF (300 μ L) to which triethylamine (19.7 μ L, 0.140 mmol) was added. The reaction was shaken (550 RPM) for 24 hours at RT before being reduced *in vacuo* to yield a yellow solid, 2,2',2''-(10-(1-carboxy-4,21-dioxo-2,8,11,14,17-pentaoxa-5,20-diazadocosan-22-yl)-1,4,7,10-tetraazacyclododecane-1,4,7-triyl)triacetic acid (**33**), (45.0 mg, 0.058 mmol, 81.1% yield).

^1H NMR (400 MHz, D_2O , δ): 1.12 (t, $J = 7.3$ Hz, N- α - CH_2 , 6H), 2.07 (s, N- α - CH_2 , 18H), 3.06 (m, N- α - CH_2 , 2H), 3.32 (t, $J = 5.4$ Hz, NH, 1H), 3.50-3.47 (m, CH_2 -NH, 2H), 3.54 (s, CH_2 -O, 6H), 4.00 (s, NH, 1H), 4.09 (s, NH, 1H), 4.65-4.67 (m, CH_2 -O, 14H), 7.76 (s, OH, 1H). ^{13}C NMR (100 MHz, D_2O , δ): 8.21 (NH- CH_2), 30.22 (N- CH_2), 46.66 (N- CH_2 -C=O), 68.36 (CH_2 -O), 69.61 (CH_2 -O), 69.69 (CH_2 -O), 69.73 (CH_2 -O), 69.82 (CH_2 -O), 191.20 (C=O), 213.77 (C=O), 214.57 (C=O), 215.41 (C=O). MS (ES-MS): m/z 739.9 (M^+).

9.3.49 Synthesis of 2,2',2''-(10-(1-(4-((10-(4-((1,5,8,12-tetraazabicyclo[10.2.2]hexadecan-5-yl)methyl)benzyl)-1,4,7,10-tetraazabicyclo[5.5.2]tetradecan-4-yl)methyl)phenyl)-3,7,24-trioxo-5,11,14,17,20-pentaoxa-2,8,23-triazapentacosan-25-yl)-1,4,7,10-tetraazacyclododecane-1,4,7-triyl)triacetic acid (**34**)

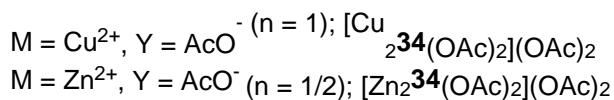
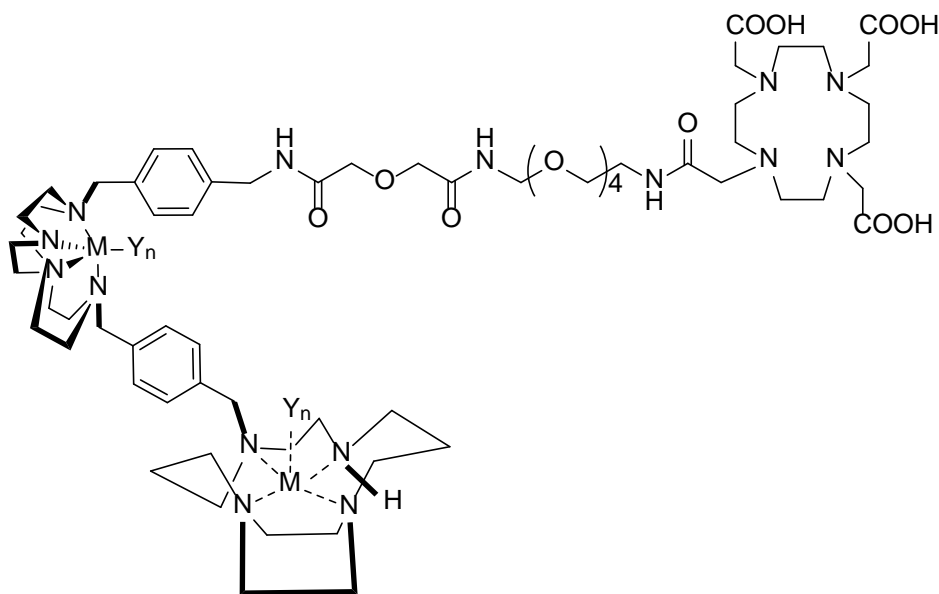


34

2,2',2''-(10-(1-Carboxy-4,21-dioxo-2,8,11,14,17-pentaoxa-5,20-diazadocosan-22-yl)-1,4,7,10-tetraazacyclododecane-1,4,7-triyl)triacetic acid (**33**) (24.0 mg, 30.0 μmol), 1-(4-(aminomethyl)benzyl)-7-(4-((1,4,8,11-tetraazabicyclo[10.2.2]hexadecane)methyl)benzyl)-1,4,7,10-tetraazabicyclo[5.5.2]dodecane (**24**) (21.0 mg, 30.0 μmol) and HATU (12.36mg, 30.0 μmol) were dissolved in anhydrous amine-free DMF (200 μL) with triethylamine (9.0 μL , 0.070 mmol). The reaction was shaken for 24 hours before being reduced *in vacuo*. The reaction was purified by reverse-phase C18 semi-preparative HPLC to yield a white solid, 2,2',2''-(10-(1-(4-((10-(4-((1,5,8,12-tetraazabicyclo[10.2.2]hexadecan-5-yl)methyl)benzyl)-1,4,7,10-tetraazabicyclo[5.5.2]tetradecan-4-yl)methyl)phenyl)-3,7,24-trioxo-5,11,14,17,20-pentaoxa-2,8,23-triazapentacosan-25-yl)-1,4,7,10-tetraazacyclododecane-1,4,7-triyl)triacetic acid (**34**), (5.2 mg, 0.0038 mmol, 11.7% yield).

Purified using RP semi-preparative HPLC System 6 (Section 9.2.2.6), (Single peaks, t_r = 8:45 min). Analytical reverse phase HPLC Systems E (Section 9.2.1.5) (single peaks, t_r = 09:40 min). MS (HRMS): ($\text{M}+\text{H}_2\text{O}+2\text{NH}_4$) calcd for $\text{C}_{68}\text{H}_{125}\text{N}_{17}\text{O}_{15}^{2+}$, 709.9765; found, 709.9245. MS (ES-MS): m/z 701.5 ($\text{M}+\text{H}+\text{K}$, 40), m/z 777.4 ($\text{M}+2\text{K}+\text{TFA}$).

9.3.50 Attempted synthesis of metal complexes of 2,2',2''-(10-(1-(4-((10-(4-((1,5,8,12-tetraazabicyclo[10.2.2]hexadecan-5-yl)methyl)benzyl)-1,4,7,10-tetraazabicyclo[5.5.2]tetradecan-4-yl)methyl)phenyl)-3,7,24-trioxo-5,11,14,17,20-pentaoxa-2,8,23-triazapentacosan-25-yl)-1,4,7,10-tetraazacyclododecane-1,4,7-triyl)triacetic acid ([Cu₂**34**(OAc)₂](OAc)₂ and [Zn₂**34**(OAc)₂](OAc)₂)



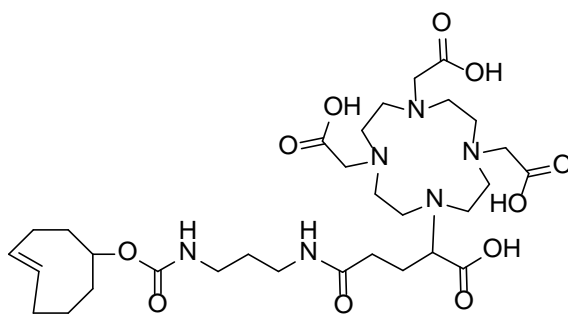
Attempted synthesis of 2,2',2''-(10-(1-(4-((10-(4-((1,5,8,12-tetraazabicyclo[10.2.2]hexadecan-5-yl)methyl)benzyl)-1,4,7,10-tetraazabicyclo[5.5.2]tetradecan-4-yl)methyl)phenyl)-3,7,24-trioxo-5,11,14,17,20-pentaoxa-2,8,23-triazapentacosan-25-yl)-1,4,7,10-tetraazacyclododecane-1,4,7-triyl)triacetic acid copper(II) acetate ([Cu₂34**(OAc)₂](OAc)₂)**

2,2',2''-(10-(1-Carboxy-4,21-dioxo-2,8,11,14,17-pentaoxa-5,20-diazadocosan-22-yl)-1,4,7,10-tetraazacyclododecane-1,4,7-triyl)triacetic acid (**33**) (13.05 mg, 0.020 mmol), 1-(4-(aminomethyl)benzyl)-7-(4-((1,4,8,11-tetraazabicyclo[10.2.2]hexadecane)methyl)benzyl)-1,4,7,10-tetraazabicyclo[5.5.2]dodecane copper(II) acetate ([Cu₂**24**(OAc)₂](OAc)₂) (17.8mg, 0.020 mmol), HATU (6.72mg, 0.0200mmol) and triethylamine (12.28 μL, 0.090 mmol) were combined in anhydrous amine-free DMF (200 μL). The reaction was shaken for 24 hours before being reduced *in vacuo*. Purification was attempted using reverse-phase C18 semi-preparative HPLC. The desired product was not isolated using this synthetic procedure.

Attempted synthesis of 2,2',2''-(10-(1-(4-((10-(4-((1,5,8,12-tetraazabicyclo[10.2.2]hexadecan-5-yl)methyl)benzyl)-1,4,7,10-tetraazabicyclo[5.5.2]tetradecan-4-yl)methyl)phenyl)-3,7,24-trioxo-5,11,14,17,20-pentaoxa-2,8,23-triazapentacosan-25-yl)-1,4,7,10-tetraazacyclododecane-1,4,7-triyl)triacetic acid zinc(II) acetate ([Zn₂34(OAc)₂](OAc)₂)

2,2',2''-(10-(1-Carboxy-4,21-dioxo-2,8,11,14,17-pentaoxa-5,20-diazadocosan-22-yl)-1,4,7,10-tetraazacyclododecane-1,4,7-triyl)triacetic acid (**33**) (13.05 mg, 0.020 mmol), 1-(4-(aminomethyl)benzyl)-7-(4-((1,4,8,11-tetraazabicyclo[10.2.2]hexadecane)methyl)benzyl)-1,4,7,10-tetraazabicyclo[5.5.2]dodecane copper(II) acetate ([Zn₂24(OAc)₂](OAc)₂) (22.68 mg, 0.020 mmol), HATU (7.84 mg, 0.020 mmol), triethylamine (14.3 μL, 0.100 mmol) were combined in anhydrous amine-free DMF (200 μL). The reaction was shaken for 24 hours before being reduced *in vacuo*. Purification was attempted using reverse-phase C18 semi-preparative HPLC. The desired product was not isolated using this synthetic procedure.

9.3.51 Synthesis of (*E*)-2,2',2''-(10-(1-carboxy-4-((3-(((cyclooct-4-en-1-yloxy)carbonyl)amino)propyl)amino)-4-oxobutyl)-1,4,7,10-tetraazacyclododecane-1,4,7-triyl)triacetic acid (**35**)

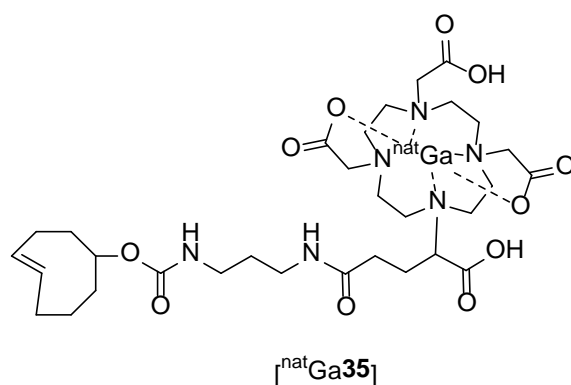


35

Trans-cyclooctene amine HCl salt (16.4 mg, 60.0 μmol) and 2,2',2''-(10-(2,6-dioxotetrahydro-2H-pyran-3-yl)-1,4,7,10-tetraazacyclododecane-1,4,7-triyl)triacetic acid (30.8 mg, 60.0 μmol) were combined in dry DMF (2.5 mL) and shaken at RT for 48 hours. The resulting mixture was reduced *in vacuo* before being purified on semi-preparative C18 HPLC. To yield a white solid 2,2',2''-(10-(1-carboxy-4-((3-(((cyclooct-4-en-1-yloxy)carbonyl)amino)propyl)amino)-4-oxobutyl)-1,4,7,10-tetraazacyclododecane-1,4,7-triyl)triacetic acid (**35**) (8.2 mg, 12.0 μmol , 19.2% yield).

Purified using reverse phase semi-preparative HPLC System 7 (section 9.2.2.7) (single peaks, t_r = 14:35 min). Analytical reverse phase HPLC Systems F (section 9.2.1.6) (single peaks, t_r = 14:40 min). $^1\text{H-NMR}$ (400 MHz, CD_3Cl , δ): 1.27-1.49 (m, CH_2 , 4H), 1.55-1.63 (m, CH_2 , 2H), 1.78-1.89 (m, CH_2 , 4H), 2.48-2.52 (m, CH_2 + NH, 6H), 2.56-2.71 (m, N- α - CH_2 , 8H), 2.79-2.82 (m, N- α - CH_2 , 6H), 2.88-2.98 (m, N- α - CH_2 , 2H), 3.18-3.22 (m, CH_2 -CO, 2H), 3.43-3.56 (m, CH_2 -CO, 8H), 3.69-3.71 (m, CH_2 -N, 3H), 4.67 (Br s, CH, 1H), 5.22 (s, CH, 1H), 5.48 (Br s, CH, 1H), 5.57 (Br s, CH, 1H). MS (HRMS): m/z (M^+) calcd. for $\text{C}_{31}\text{H}_{53}\text{N}_6\text{O}_{11}^+$, 685.3767; found, 685.3765

9.3.52 Synthesis of metal complexes of (E)-2,2',2''-(10-(1-carboxy-4-((3-(((cyclooct-4-en-1-yloxy)carbonyl)amino)propyl)amino)-4-oxobutyl)-1,4,7,10-tetraazacyclododecane-1,4,7-triyl)triacetic acid (**35**) with gallium(III) to form ($^{nat}\text{Ga35}$)

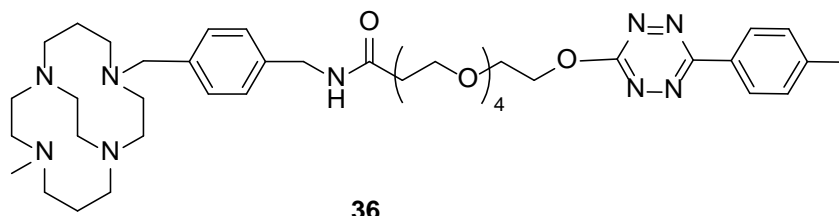


General procedure I was followed.

Amounts: Gallium(III) nitrate (0.41 mg, 1.6 μmol), (E)-2,2',2''-(10-(1-carboxy-4-((3-(((cyclooct-4-en-1-yloxy)carbonyl)amino)propyl)amino)-4-oxobutyl)-1,4,7,10-tetraazacyclododecane-1,4,7-triyl)triacetic acid (**35**) (1.1mg, 1.3 μmol), and HEPES buffer (2mL, pH = 3.5, 0.1 M). To yield a white solid, (E)-2,2',2''-(10-(1-carboxy-4-((3-(((cyclooct-4-en-1-yloxy)carbonyl)amino)propyl)amino)-4-oxobutyl)-1,4,7,10-tetraazacyclododecane-1,4,7-triyl)triacetic acid gallium ($^{nat}\text{Ga35}$) (0.99 mg, 1.3 μmol , 81.9% yield).

Analytical RP-HPLC Systems F (section 9.2.1.6) (single peaks, $t_r = 20:04$ min). MS (HRMS): m/z (M^+) calcd. for $\text{C}_{31}\text{H}_{50}\text{N}_6\text{GaO}_{11}^+$, 752.2844; found, 752.2843.

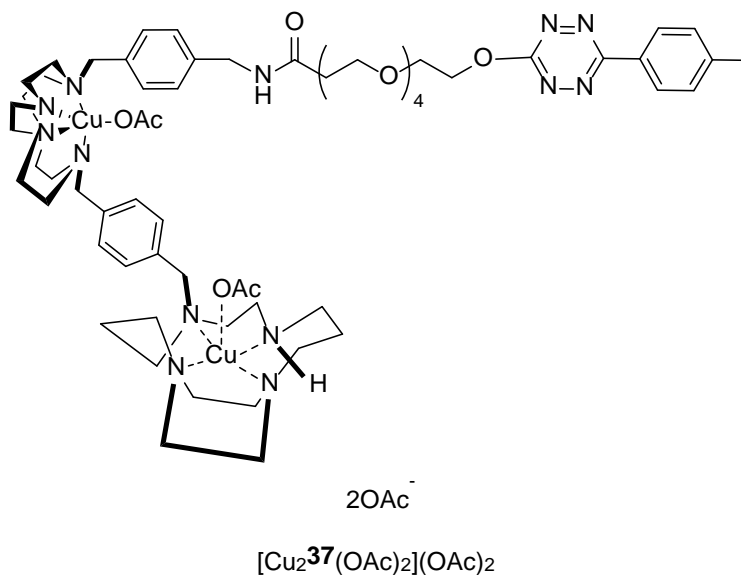
9.3.53 Synthesis of N-(4-((11-methyl-1,4,8,11-tetraazabicyclo[6.6.2]hexadecan-4-yl)methyl)benzyl)-1-((6-(p-tolyl)-1,2,4,5-tetrazin-3-yl)oxy)-3,6,9,12-tetraoxapentadecan-15-amide (36)



Tetrazine-PEG₄-NHS ester (5.0 mg, 10.0 μmol), 1-(4-aminomethylbenzyl)-8-(methyl)-1,4,8,11-tetraazabicyclo[6.6.2]hexadecane (**15**) (3.3 mg, 10.0 μmol), 1-(bis(dimethylamino)methylene)-1H-1,2,3-triazolo[4,5-b]pyridinium 3-oxid hexafluorophosphate (3.4 mg, 10.0 μmol) and triethylamine (12.57 μL, 9.0 μmol) were combined together in amine-free dry amine (1 mL) and shaken at RT for 1 hour. The resulting solution was reduced *in vacuo* to yield pink oil, N-(4-((11-methyl-1,4,8,11-tetraazabicyclo[6.6.2]hexadecan-4-yl)methyl)benzyl)-1-((6-(p-tolyl)-1,2,4,5-tetrazin-3-yl)oxy)-3,6,9,12-tetraoxapentadecan-15-amide (**36**), (6.8 mg, 96.8%).

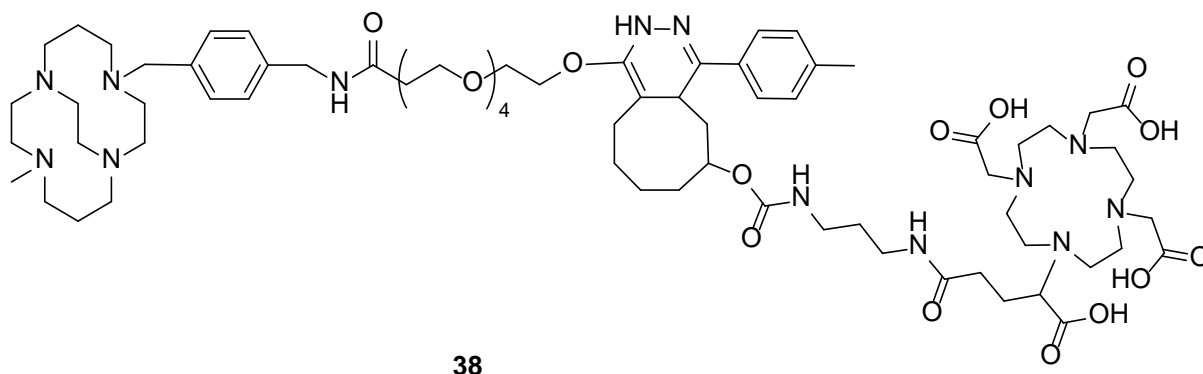
Purified using RP semi-preparative HPLC System E (section 9.2.2.6) (single peaks, $t_r = 17:50$ min). ¹H-NMR (400 MHz, CD₃Cl, δ): 1.51-1.68 (m, N-β-CH₂ + N-α-CH₂ 8H), 1.80-1.84 (s, CH₃, 3H), 2.27-2.37 (m, N-α-CH₂, 8H), 2.48-2.54 (m, N-α-CH₂, 2H), 2.58-2.73 (m, N-α-CH₂, 4H), 3.00 (s, Ar-CH₂, 2H), 3.04 (s, Ar-CH₂, 2H), 3.21-3.24 (s, CH₃, 3H), 3.47-3.87 (m, CH₂-O, 18H), 4.11-4.24 (m, CH₂-CO, 2H), 4.44 (Br s, NH, 1H), 7.13-7.15 (m, Ar, 4H), 8.13-8.15 (m, Ar, 2H), 8.41-8.43 (m, Ar, 2H). MS (HRMS): m/z (M⁺) calcd. for C₄₁H₆₆N₉O₆⁺, 778.4974; found, 778.4972.

9.3.54 Attempted synthesis of N1-(4-((10-(4-((1,5,8,12-tetraazabicyclo[10.2.2]hexadecan-5-yl)methyl)benzyl)-1,4,7,10-tetraazabicyclo[5.5.2]tetradecan-4-yl)methyl)benzyl)-N19-(4-(6-methyl-1,2,4,5-tetrazin-3-yl)benzyl)-4,7,10,13,16-pentaoxonadecanediamide copper(II) acetate ($[\text{Cu}_2\mathbf{37}(\text{OAc})_2](\text{OAc})_2$)



1-(4-Aminobenzyl)-7-(4-((1,4,8,11-tetraazabicyclo[10.2.2]hexadecane)methyl)benzyl)-1,4,7,10tetraazabicyclo[5.5.2]dodecane copper(II) acetate ($[\text{Cu}_2\mathbf{23}(\text{OAc})_2](\text{OAc})_2$) (8.96 mg, 0.010 mmol), HATU (3.08 mg, 0.010 mmol), tetrazine-PEG₅-NHS ester (50. mg, 0.0100 mmol), and triethylamine (5.63 μL , 0.040 mmol) were combined in anhydrous amine-free DMF (1.5 mL) and shaken (550 RPM) at RT for 3 days. The reaction was monitored by MS, and the colour of the solution changed from purple to green. Upon which the reaction was reduced *in vacuo* and purified by semi-preparative HPLC to yield a light green solid. Purification was attempted using reverse-phase C18 semi-preparative HPLC. The desired product was not isolated using this synthetic procedure.

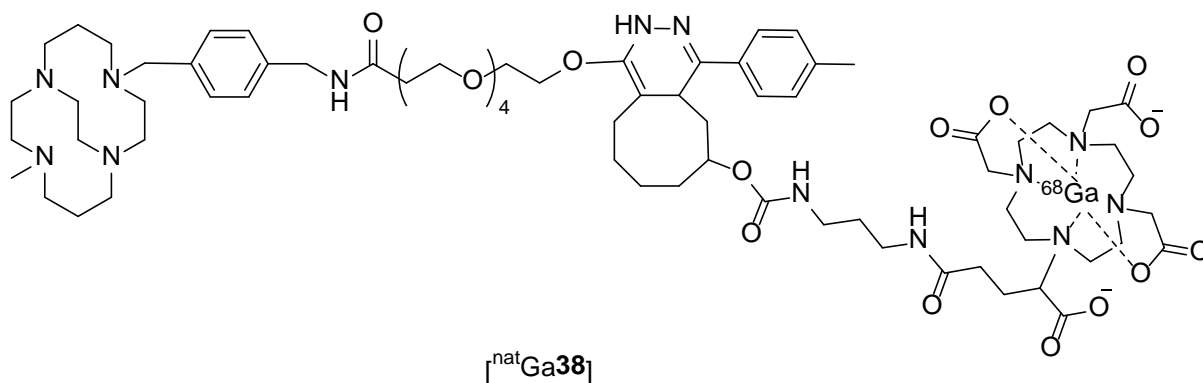
9.3.55 Attempted syntheses of 2-(4-(1-carboxy-4-((3-(((1-((1-(4-((11-methyl-1,4,8,11-tetraazabicyclo[6.6.2]hexadecan-4-yl)methyl)phenyl)-3-oxo-6,9,12,15-tetraoxa-2-azaheptadecan-17-yl)oxy)-4-(p-tolyl)-2,4a,5,6,7,8,9,10-octahydrocycloocta[d]pyridazin-6-yl)oxy)carbonyl)amino)propyl)amino)-4-oxobutyl)-7,10-bis(carboxymethyl)-1,4,7,10-tetraazacyclododecan-1-yl)acetate (**38**)



N-(4-((11-methyl-1,4,8,11-tetraazabicyclo[6.6.2]hexadecan-4-yl)methyl)benzyl)-1-((6-(p-tolyl)-1,2,4,5-tetrazin-3-yl)oxy)-3,6,9,12-tetraoxapentadecan-15-amide (**36**) (2.0 mg, 2.6 μmol) and (*E*)-2,2',2''-(10-(1-carboxy-4-((3-(((cyclooct-4-en-1-yloxy)carbonyl)amino)propyl)amino)-4-oxobutyl)-1,4,7,10-tetraazacyclododecane-1,4,7-triyl)triacetic acid (**35**), (1.8 mg, 2.6 μmol) were dissolved in 0.2 M sodium acetate buffer (pH 4.6, 200 μL) and shaken for one hour at room temperature. The resulting solution was reduced *in vacuo* and analysed by HPLC.

Mass spec unable to identify peaks. Analytical RP-HPLC Systems G (section 9.2.1.7) (single peaks, t_r = 14:40 min). MS (ES-MS): m/z highest peak at 1289.9. The peaks could not be assigned to expected molecular ions.

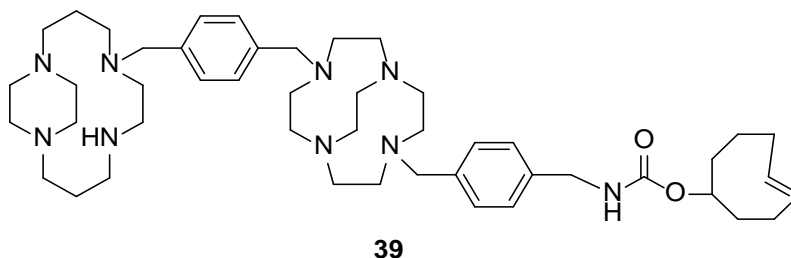
9.3.56 Attempted syntheses of gallium metallated 2-(4-(1-carboxy-4-((3-(((1-((1-(4-((11-methyl-1,4,8,11-tetraazabicyclo[6.6.2]hexadecan-4-yl)methyl)phenyl)-3-oxo-6,9,12,15-tetraoxa-2-azaheptadecan-17-yl)oxy)-4-(p-tolyl)-2,4a,5,6,7,8,9,10-octahydrocycloocta[d]pyridazin-6-yl)oxy)carbonyl)amino)propyl)amino)-4-oxobutyl)-7,10-bis(carboxymethyl)-1,4,7,10-tetraazacyclododecan-1-yl)acetate ($[^{nat}\text{Ga}38]$)



N-(4-((11-methyl-1,4,8,11-tetraazabicyclo[6.6.2]hexadecan-4-yl)methyl)benzyl)-1-((6-(p-tolyl)-1,2,4,5-tetrazin-3-yl)oxy)-3,6,9,12-tetraoxapentadecan-15-amide (**36**) (2.1 mg, 2.7 μmol) and (E)-2,2',2''-(10-(1-carboxy-4-((3-(((cyclooct-4-en-1-yloxy)carbonyl)amino)propyl)amino)-4-oxobutyl)-1,4,7,10-tetraazacyclododecane-1,4,7-triyl)triacetic acid (**35**) (1.9 mg, 2.7 μmol) were combined in 0.2 M sodium acetate buffer (pH 4.6, 200 μL). A solution of gallium nitrate (0.7 mg, 2.7 μmol) in 0.2 M sodium acetate buffer (pH 4.6, 50 μL) was added and the solution shaken at 550 RPM at 90°C for an hour. The reaction was reduced *in vacuo* and purification attempted by HPLC.

MS (ES-MS): m/z highest peak at 1289.9. The peaks could not be assigned to expected molecular ions.

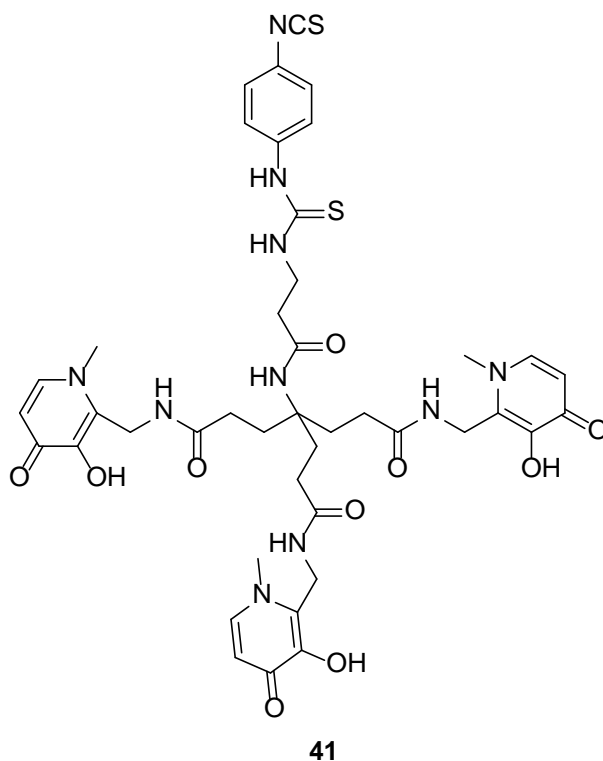
9.3.57 Synthesis of (*E*)-cyclooct-4-en-1-yl(4-((10-(4-((1,5,8,12-tetraazabicyclo[10.2.2]hexadecan-5-yl)methyl)benzyl)-1,4,7,10-tetraazabicyclo[5.5.2]tetradecan-4-yl)methyl)benzyl)carbamate (**39**)



Trans-cyclooctene-NHS ester (10.44 mg, 39.1 μ mol), 1-(4-aminobenzyl)-7-(4-((1,4,8,11-tetraazabicyclo[10.2.2]hexadecane)methyl)benzyl)-1,4,7,10-tetraazabicyclo[5.5.2]dodecane (**24**) (25.19 mg, 39.1 μ mol) and triethyl amine (5.43 μ L, 39.1 μ mol) were combined in anhydrous amine free DMF and shaken at RT for 48 hours, with progress monitored by analytical RP- HPLC. The reaction was then reduced *in vacuo* to yield the cream solid, (*E*)-cyclooct-4-en-1-yl(4-((10-(4-((1,5,8,12-tetraazabicyclo[10.2.2]hexadecan-5-yl)methyl)benzyl)-1,4,7,10-tetraazabicyclo[5.5.2]tetradecan-4-yl)methyl)benzyl)carbamate, (**39**) (20.0 mg, 16.4 μ mol, 42.0% yield).

Purified using RP semi-preparative HPLC System 8 (section 9.2.2.8) (single peaks, t_r = 12:50 min). $^1\text{H-NMR}$ (400 MHz, CD_3OD , δ): 1.34-1.87 (m, CH_2 , 6H), 1.95-2.10 (m, CH_2 , 4H), 2.25-2.40 (m, $\text{N-}\beta\text{-CH}_2$, 4H), 2.43-2.48 (m, CH_2 , 2H), 2.69-3.85 (m, $\text{N-}\alpha\text{-CH}_2$, 32H), 3.97-4.32 (m, $\text{N-}\alpha\text{-CH}_2$, 4H), 4.16-4.24 (m, $\text{N-}\alpha\text{-CH}_2$, 4H), 4.64 (s, NH, 2H), 4.47 (s, CH, 1H), 5.00-5.11 (m, Ar- CH_2 , 2H), 5.61-5.45 (m, CH, 2H), 6.55-6.45 (m, Ar- CH_2 , 4H), 6.61-6.75 (m, Ar- CH_2 , 2H), 8.47-8.49 (m, Ar-H, 2H), 9.04-9.06 (m, Ar-H, 2H), 9.54-9.56 (m, Ar-H, 2H), 9.64-9.65 (m, Ar-H, 2H). MS (hrMS): m/z (M^+) calcd. for $\text{C}_{47}\text{H}_{57}\text{N}_9\text{O}_2^+$, 798.6114 found, 798.6116.

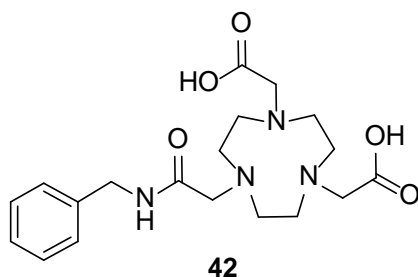
9.3.59 Synthesis of deprotected tris(hydroxypyridinone)-phenyl isothiocyanate (**41**)



A solution of chilled boron trichloride in dichloromethane (3 mL, 1M) was added to a sealed vial of benzyl protected tris(hydroxypyridinone)-phenyl isothiocyanate (8 mg, 7.3 μmol), and the reaction stirred at ambient temperature for 1 hour. The reaction vial was then cooled in an ice bath, and methanol (1 mL) was added dropwise. The reaction solution was evaporated to dryness under reduced pressure, and acetone (50 mL) was added to the residue, resulting in a white precipitate. This suspension was transferred to 50 mL falcon tube, and the mixture centrifuged at 3000 rpm for 10 mins. After this, the solution was decanted and discarded, action added (50 mL), the suspensions agitates, and centrifuged again for ten mins. This process was repeated a third time. Finally, the product was dissolved in water/acetonitrile (50/50), filtered, frozen and lyophilised, to yield an off-white solid, tris(hydroxypyridinone)-phenyl isothiocyanate (**41**), (3.4 mg, 3.1 μmol , 42.5%).

^1H NMR (400 MHz, CD_3OD , δ): 2.04-2.09 (m, CH_3 , 6H), 2.32-2.34 (m, CH_2 , 6H), 2.58-2.64 (m, NH, 2H), 2.71 (s, $\text{CH}_2\text{-CO}$, 9H), 3.86-3.95 (br s, NH, 2H), 4.01 (s, $\text{CH}_2\text{-NH}$, 9H), 4.78 (s, $\text{CH}=\text{CH}$, 6H), 7.01 (s, OH, 3H), 7.34 (dd, $J = 8.5$, Ar-H, 2H), 7.54 (dd, $J = 8.5$, Ar-H, 2H). ^{13}C NMR (100 MHz, CDCl_3 , δ): 20.05 (CH_2), 29.55 ($\text{CH}_2\text{-CO}$), 35.00 ($\text{CH}_2\text{-CO}$), 35.04 ($\text{CH}_2\text{-CO}$), 38.16 (N- $\alpha\text{-CH}_2$), 39.95(N- $\alpha\text{-CH}_2$), 57.88 ($\text{C}(\text{CH}_2)\text{NH}$), 112.96 (C-Ar), 124.86 (C-Ar), 126.07 (C-Ar), 127.75 (C-Ar), 137.96 (C-Ar), 139.99 (C-Ar), 141.02 (C-Ar), 144.55 (C-Ar), 149.05 (C-Ar), 162.27 (C=O), 171.87 (C=O), 175.14 (C=O), 184.91 (C=S). MS (ES-MS): m/z 460.9 (M^{2+}).

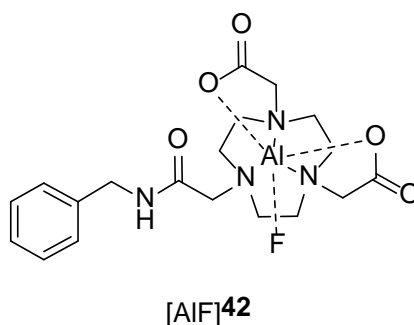
9.3.60 Synthesis of 2,2'-(7-(2-(benzylamino)-2-oxoethyl)-1,4,7-triazonane-1,4-diyl)diacetic acid (**42**)



2,2'-(7-(2-((2,5-Dioxopyrrolidin-1-yl)oxy)-2-oxoethyl)-1,4,7-triazonane-1,4-diyl)diacetic acid (37.0 mg, 60.0 μmol) was dissolved in amine-free dimethylformamide (200 μL). To which triethylamine (7.8 μL , 60.0 μmol) and benzyl amine (6.0 mg, 60.0 μmol) were added. The reaction was shaken at 550 RPM at room temperature for 24 hours. The solvent was removed *in vacuo* to yield the white solid, 2,2'-(7-(2-(benzylamino)-2-oxoethyl)-1,4,7-triazonane-1,4-diyl)diacetic acid (**42**), (17.5 mg, 44.6 μmol , 79.6% yield).

Analytical RP-HPLC System H (Section 9.2.1.7) (single peak, $t_r = 12:70$ min). Semi-preparative HPLC System 9 (Section 9.2.2.9) (single peak; $t_r = ca. 12:00$ min). ^1H NMR (400 MHz, D_2O , δ): 2.23-2.49 (m, N- α - CH_2 , 12H), 3.07-3.33 (m, N- α - CH_2 , 6H), 4.29-4.56 (m, CH_2 -Ar, 2H), 7.19-7.29 (m, Ar, 5H). ^{13}C NMR (100 MHz, CD_3OD , δ): 37.02 (N- α - CH_2), 49.02 (N- α - CH_2), 55.10 (N- α - CH_2), 55.67 (N- α - CH_2), 56.09 (N- α - CH_2), 56.31 (N- α - CH_2), 59.42 (N- α - CH_2), 60.13 (N- α - CH_2), 61.92 (C-Ar H_2), 119.82 (C-Ar), 120.19 (C-Ar), 120.75 (C-Ar), 138.11 (C-Ar), 166.01 (C=O), 169.59 (C=O). MS (ES-MS): m/z 393.0 (M^+).

9.3.61 Aluminium fluoride complexation with 2,2'-(7-(2-(benzylamino)-2-oxoethyl)-1,4,7-triazonane-1,4-diyl)diacetic acid with aluminium chloride ([AlF]42)



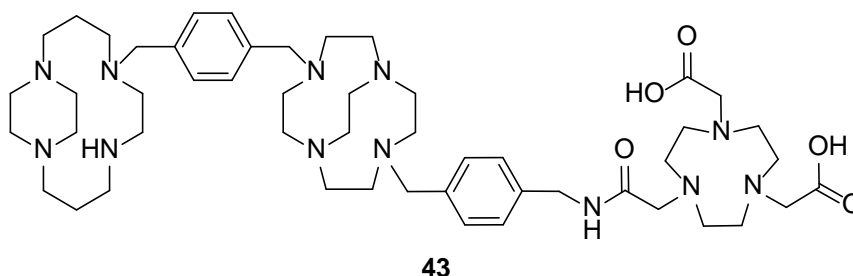
General procedure J

The macrocyclic chelator was combined with aluminium chloride (1.2 equivalents) and sodium fluoride (1.2 equivalents) in 0.5 M sodium acetate buffer (pH 4 adjusted with high grade metal-free glacial acetic acid) and ethanol (50%, volume/volume, *v/v*). The reaction was heated at 90 °C for an hour before being reduced *in vacuo* to yield a solid.

Amounts: 2,2'-(7-(2-(Benzylamino)-2-oxoethyl)-1,4,7-triazonane-1,4-diyl)diacetic acid (**42**) (13.4 mg, 30.0 μmol), aluminium chloride (4.56 mg, 30.0 μmol) and sodium fluoride (1.27 mg, 30.0 μmol); dissolved in 0.5 M sodium acetate buffer (400 μL , pH 4) and ethanol (400 μL). Yielding a white solid, 2,2'-(7-(2-(benzylamino)-2-oxoethyl)-1,4,7-triazonane-1,4-diyl)diacetic acid aluminium fluoride ([AlF42]), (7.2 mg, 17.7 μmol , 49.1% yield).

Analytical reverse phase HPLC System H (Section 9.2.1.7) (single peak, t_r = 13.10 min). MS (ES-MS): m/z 437.4 (M^+).

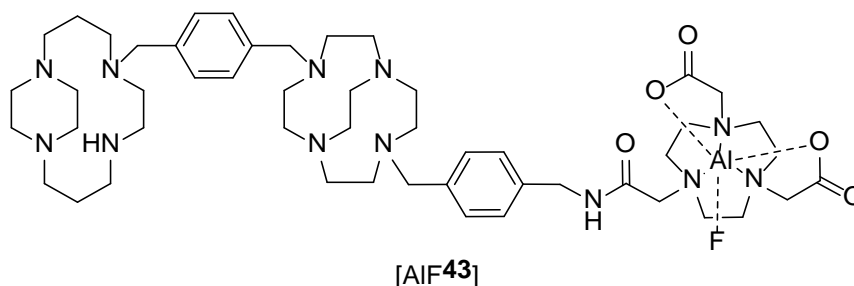
9.3.62 Synthesis of 2,2'(7-(2-((4-((10-(4-((1,5,8,12-tetraazabicyclo[10.2.2]hexadecan-5-yl)methyl)benzyl)-1,4,7,10-tetraazabicyclo[5.5.2]tetradecan-4-yl)methyl)benzyl)amino)-2-oxoethyl)-1,4,7-triazonane-1,4-diyl)diacetic acid (**43**)



2,2'(7-(2-(benzylamino)-2-oxoethyl)-1,4,7-triazonane-1,4-diyl)diacetic acid (9.4 mg, 10.0 μmol) was combined with (4-((10-(4-((1,5,8,12-tetraazabicyclo[10.2.2]hexadecan-5-yl)methyl)benzyl)-1,4,7,10-tetraazabicyclo[5.5.2]tetradecan-4-yl)methyl)phenyl)methanamine (**24**) (9.2 mg, 10.0 μmol) in amine-free dimethylformamide (1.5 mL) in the presence of pyridine (1.1 μL , 10.0 μmol). The reaction was shaken at 550 RPM at RT for 24 hours. The resulting solution was reduced *in vacuo* to yield a yellow oil, 2,2'(7-(2-((4-((10-(4-((1,5,8,12-tetraazabicyclo[10.2.2]hexadecan-5-yl)methyl)benzyl)-1,4,7,10-tetraazabicyclo[5.5.2]tetradecan-4-yl)methyl)benzyl)amino)-2-oxoethyl)-1,4,7-triazonane-1,4-diyl)diacetic acid (**43**), (10.2 mg, 10.0 μmol , 76.8% yield).

Further purification achieved using reverse phase semi-preparative HPLC System 9 (Section 9.2.2.9) (broad peak, t_r = 12-13 min). Analytical RP-HPLC System I (Section 9.2.1.8) (broad peak, t_r = 13 min). ^1H NMR (400 MHz, CDCl_3 , δ): 1.13-1.27 (m, N- β - CH_2 , 4H), 1.41-1.51 (m, N- α - CH_2 , 4H), 1.86-2.00 (m, N- α - CH_2 , 2H), 2.06-2.32 (m, N- α - CH_2 , 10H), 2.39-2.79 (m, N- α - CH_2 , 24H), 2.86 (s, N- α - CH_2 , 4H), 2.94-3.02 (m, N- α - CH_2 , 8H), 3.13-3.29 (m, CH_2 -Ar, 6H), 3.50-4.95 (m, N- α - CH_2 + CH_2 -Ar, 8H), 7.29-7.34 (m, Ar-H, 8H), 7.69-7.78 (m, NH, 1H), 8.00 (s, NH, 1H). ^{13}C NMR (100 MHz, CDCl_3 , δ): 16.87 (N- β - CH_2), 17.53 (N- β - CH_2), 30.25 (N- α - CH_2), 33.58 (N- α - CH_2), 36.45 (N- α - CH_2), 42.58 (N- α - CH_2), 45.55 (N- α - CH_2), 46.88 (N- α - CH_2), 50.36 (N- α - CH_2), 53.82 (N- α - CH_2), 56.90 (N- α - CH_2), 63.04 ($\underline{\text{C}}\text{H}_2$ -Ar), 63.92 ($\underline{\text{C}}\text{H}_2$ -Ar), 87.88 ($\underline{\text{C}}\text{H}_2$ -Ar), 110.73 (Ar-H), 115.39 (Ar-H), 116.68 (Ar-H), 123.84 (Ar-H), 129.44 (C-Ar), 129.83 (C-Ar), 130.58 (C-Ar), 138.10 (C-Ar), 147.36 (C-Ar), 168.63 (C=O), 169.03 (C=O), 182.84 (C=O). MS (HRMS): m/z (M^+) calcd. for $\text{C}_{50}\text{H}_{83}\text{N}_{12}\text{O}_5^+$, 931.6604; found, 931.6607.

9.3.63 Aluminium fluoride complexation of 2,2'-(7-(2-((4-((10-(4-((1,5,8,12-tetraazabicyclo[10.2.2]hexadecan-5-yl)methyl)benzyl)-1,4,7,10-tetraazabicyclo[5.5.2]tetradecan-4-yl)methyl)benzyl)amino)-2-oxoethyl)-1,4,7-triazonane-1,4-diyl)diacetic acid with aluminium fluoride ([AlF $\mathbf{43}$])

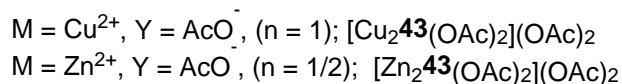
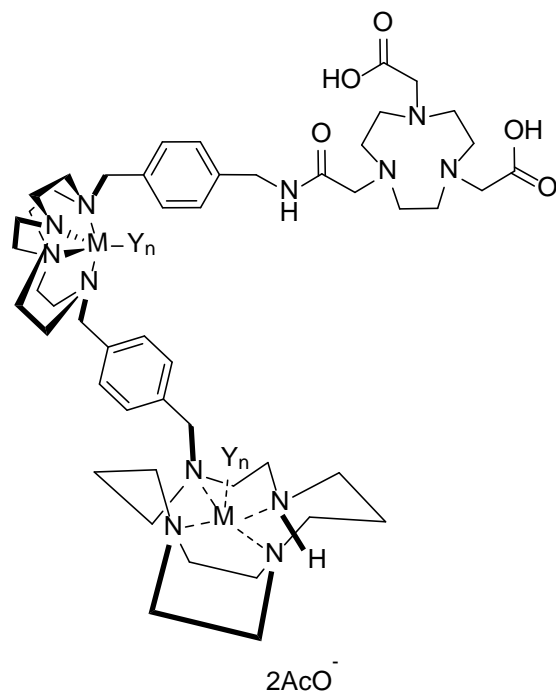


General procedure J was followed.

Amounts: 2,2'-(7-(2-((4-((10-(4-((1,5,8,12-Tetraazabicyclo[10.2.2]hexadecan-5-yl)methyl)benzyl)-1,4,7,10-tetraazabicyclo[5.5.2]tetradecan-4-yl)methyl)benzyl)amino)-2-oxoethyl)-1,4,7-triazonane-1,4-diyl)diacetic acid (**43**) (0.50 mg, 0.5 μ mol), aluminium chloride (0.09 mg, 0.6 μ mol) and sodium fluoride (0.03 mg, 0.6 μ mol); dissolved in 0.5 M sodium acetate buffer (400 μ L, pH 4) and ethanol (400 μ L). Yielding a white solid, 2,2'-(7-(2-((4-((10-(4-((1,5,8,12-tetraazabicyclo[10.2.2]hexadecan-5-yl)methyl)benzyl)-1,4,7,10-tetraazabicyclo[5.5.2]tetradecan-4-yl)methyl)benzyl)amino)-2-oxoethyl)-1,4,7-triazonane-1,4-diyl)diacetic acid aluminium fluoride ([AlF $\mathbf{43}$]) (0.42 mg, 0.4 μ mol, 80.3% yield).

Analytical RP-HPLC System I (Section 9.2.1.8) (single peak, t_r = 13:20 min). MS (ES-MS): m/z 974.80 (M^+).

9.3.64 Synthesis of 2,2'-(7-(2-((4-((10-(4-((1,5,8,12-tetraazabicyclo[10.2.2]hexadecan-5-yl)methyl)benzyl)-1,4,7,10-tetraazabicyclo[5.5.2]tetradecan-4-yl)methyl)benzyl)amino)-2-oxoethyl)-1,4,7-triazonane-1,4-diyl)diacetic acid with copper or zinc acetate ($[\text{Cu}_2\mathbf{43}(\text{OAc})_2](\text{OAc})_2$ and $[\text{Zn}_2\mathbf{43}(\text{OAc})_2](\text{OAc})_2$)



Synthesis of 2,2'-(7-(2-((4-((10-(4-((1,5,8,12-tetraazabicyclo[10.2.2]hexadecan-5-yl)methyl)benzyl)-1,4,7,10-tetraazabicyclo[5.5.2]tetradecan-4-yl)methyl)benzyl)amino)-2-oxoethyl)-1,4,7-triazonane-1,4-diyl)diacetic acid copper(II) acetate ($[\text{Cu}_2\mathbf{43}(\text{OAc})_2](\text{OAc})_2$)

1-(4-(aminomethyl)benzyl)-7-(4-((1,4,8,11-tetraazabicyclo[10.2.2]hexadecane)methyl)benzyl)-1,4,7,10-tetraazabicyclo[5.5.2]dodecane copper(II) acetate ($[\text{Cu}_2\mathbf{24}]$) (40.0 mg, 40.0 μmol) and 2,2'-(7-(2-(benzylamino)-2-oxoethyl)-1,4,7-triazonane-1,4-diyl)diacetic acid (26.2 mg, 40.0 μmol) were combined in amine-free dimethylformamide (10.0 mL) and stirred at RT for 48 hours. The resulting solution was reduced *in vacuo* to yield a blue solid, bis copper metallated 2,2'-(7-(2-((4-((10-(4-((1,5,8,12-tetraazabicyclo[10.2.2]hexadecan-5-yl)methyl)benzyl)-1,4,7,10-tetraazabicyclo[5.5.2]tetradecan-4-yl)methyl)benzyl)amino)-2-oxoethyl)-1,4,7-triazonane-1,4-diyl)diacetic acid ($[\text{Cu}_2\mathbf{43}(\text{OAc})_2](\text{OAc})_2$) (36.0 mg, 27.9 μmol , 70.2% yield).

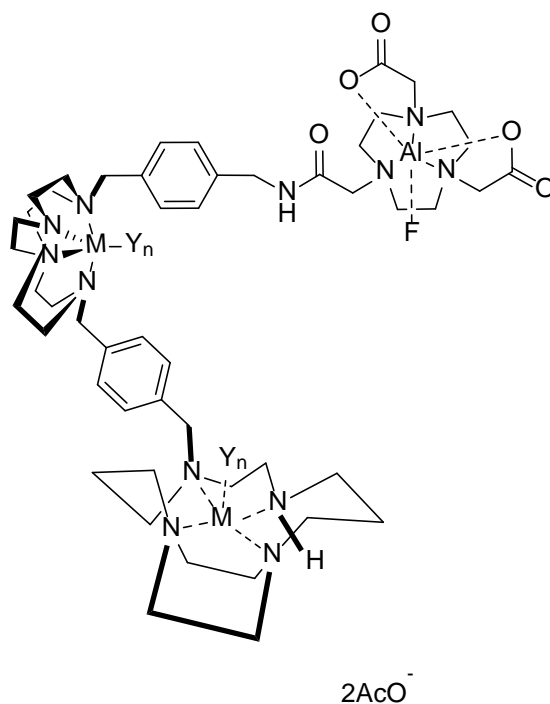
Purified using RP semi-preparative HPLC System 10 (Section 9.2.2.10) (single peak, $t_r = 15:30$). MS (HRMS): m/z ($M-CH_2CO_2$) calcd. for $C_{56}H_{91}N_{12}Cu_2O_{11}^+$, 1233.5177; found, 1233.5132.

Synthesis of 2,2'-(7-(2-((4-((10-(4-((1,5,8,12-tetraazabicyclo[10.2.2]hexadecan-5-yl)methyl)benzyl)-1,4,7,10-tetraazabicyclo[5.5.2]tetradecan-4-yl)methyl)benzyl)amino)-2-oxoethyl)-1,4,7-triazonane-1,4-diyl)diacetic acid copper(II) acetate ($Zn_2\mathbf{43}(OAc)_2](OAc)_2$)

1-(4-(aminomethyl)benzyl)-7-(4-((1,4,8,11-tetraazabicyclo[10.2.2]hexadecane)methyl)benzyl)-1,4,7,10-tetraazabicyclo[5.5.2]dodecane zinc(II) acetate ($[Zn_2\mathbf{24}(OAc)_2](OAc)_2$) (12.4 mg, 10.0 μ mol) and 2,2'-(7-(2-(benzylamino)-2-oxoethyl)-1,4,7-triazonane-1,4-diyl)diacetic acid (8.1 mg, 10.0 μ mol) were combined in amine-free dimethylformamide (1.5 mL) with pyridine (1.0 μ L, 10.0 μ mol) and shaken at 550 RPM at RT for 24 hours. The resulting solution was reduced *in vacuo* to yield 2,2'-(7-(2-((4-((10-(4-((1,5,8,12-tetraazabicyclo[10.2.2]hexadecan-5-yl)methyl)benzyl)-1,4,7,10-tetraazabicyclo[5.5.2]tetradecan-4-yl)methyl)benzyl)amino)-2-oxoethyl)-1,4,7-triazonane-1,4-diyl)diacetic acid ($[Zn_2\mathbf{43}(OAc)_2](OAc)_2$), (5.6 mg, 4.3 μ mol, 35.2% yield).

Purified using RP semi-preparative HPLC System 10 (Section 9.2.2.10) (Single peak, $t_r = 18:06$ min). MS (HRMS): m/z ($M+Na$, 23) calcd. for $C_{58}H_{94}N_{12}Zn_2NaO_{11}^+$, 1321.9842; found, 1321.9842.

9.3.65 Aluminium fluoride complexation of 2,2'-(7-(2-((4-((10-(4-((1,5,8,12-tetraazabicyclo[10.2.2]hexadecan-5-yl)methyl)benzyl)-1,4,7,10-tetraazabicyclo[5.5.2]tetradecan-4-yl)methyl)benzyl)amino)-2-oxoethyl)-1,4,7-triazonane-1,4-diyl)diacetic acid with copper or zinc acetate ($[\text{Cu}_2\text{AlF43}(\text{OAc})_2](\text{OAc})_2$ and $[\text{Zn}_2\text{AlF43}(\text{OAc})_2](\text{OAc})_2$)



$\text{M} = \text{Cu}^{2+}$, $\text{Y} = \text{AcO}^-$, ($n = 1$); $[\text{Cu}_2\text{AlF43}(\text{OAc})_2](\text{OAc})_2$
 $\text{M} = \text{Zn}^{2+}$, $\text{Y} = \text{AcO}^-$, ($n = 1/2$); $[\text{Zn}_2\text{AlF43}(\text{OAc})_2](\text{OAc})_2$

General procedure J was followed.

Synthesis of 2,2'-(7-(2-((4-((10-(4-((1,5,8,12-tetraazabicyclo[10.2.2]hexadecan-5-yl)methyl)benzyl)-1,4,7,10-tetraazabicyclo[5.5.2]tetradecan-4-yl)methyl)benzyl)amino)-2-oxoethyl)-1,4,7-triazonane-1,4-diyl)diacetic acid copper(II) acetate aluminium fluoride ($[\text{Cu}_2\text{AlF43}(\text{OAc})_2](\text{OAc})_2$)

Amounts: 2,2'-(7-(2-((4-((10-(4-((1,5,8,12-Tetraazabicyclo[10.2.2]hexadecan-5-yl)methyl)benzyl)-1,4,7,10-tetraazabicyclo[5.5.2]tetradecan-4-yl)methyl)benzyl)amino)-2-oxoethyl)-1,4,7-triazonane-1,4-diyl)diacetic acid copper(II) acetate ($[\text{Cu}_2\text{43}(\text{OAc})_2](\text{OAc})_2$) (3.2 mg, 2.5 μmol), aluminium chloride (0.4 mg, 3.0 μmol) and sodium fluoride (0.12 mg, 3.0 μmol); dissolved in 0.5 M sodium acetate buffer (400 μL , pH 4) and ethanol (400 μL). To yield a blue solid, 2,2'-(7-(2-((4-((10-(4-

((1,5,8,12-tetraazabicyclo[10.2.2]hexadecan-5-yl)methyl)benzyl)-1,4,7,10-tetraazabicyclo[5.5.2]tetradecan-4-yl)methyl)benzyl)amino)-2-oxoethyl)-1,4,7-triazonane-1,4-diyl)diacetic acid copper(II) acetate aluminium fluoride ($[\text{Cu}_2\text{AlF}_4(\text{OAc})_2](\text{OAc})_2$) (2.9 mg, 2.2 μmol , 87.67% yield).

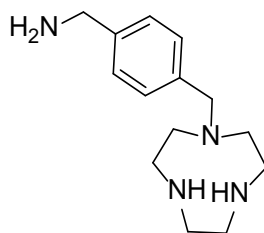
Analytical RP-HPLC System 7 (Section 9.2.1.9) (single peak, $t_r = 12:47$ min). MS (ES-MS): m/z 1177.56 (M-2CH₂CO₂+OH, 51).

2,2'-(7-(2-((4-((10-(4-((1,5,8,12-Tetraazabicyclo[10.2.2]hexadecan-5-yl)methyl)benzyl)-1,4,7,10-tetraazabicyclo[5.5.2]tetradecan-4-yl)methyl)benzyl)amino)-2-oxoethyl)-1,4,7-triazonane-1,4-diyl)diacetic acid zinc(II) acetate aluminium fluoride ($[\text{Zn}_2\text{AlF}_4(\text{OAc})_2](\text{OAc})_2$)

Amounts: 2,2'-(7-(2-((4-((10-(4-((1,5,8,12-tetraazabicyclo[10.2.2]hexadecan-5-yl)methyl)benzyl)-1,4,7,10-tetraazabicyclo[5.5.2]tetradecan-4-yl)methyl)benzyl)amino)-2-oxoethyl)-1,4,7-triazonane-1,4-diyl)diacetic acid zinc(II) acetate ($[\text{Cu}_2\text{AlF}_4(\text{OAc})_2](\text{OAc})_2$) (2.8 mg, 2.2 μmol), aluminium chloride (0.35 mg, 2.6 μmol) sodium fluoride (0.11 mg, 2.6 μmol) dissolved in 0.5 M sodium acetate buffer (400 μL , pH 4) and ethanol (400 μL). To yield an off-white solid, 2,2'-(7-(2-((4-((10-(4-((1,5,8,12-tetraazabicyclo[10.2.2]hexadecan-5-yl)methyl)benzyl)-1,4,7,10-tetraazabicyclo[5.5.2]tetradecan-4-yl)methyl)benzyl)amino)-2-oxoethyl)-1,4,7-triazonane-1,4-diyl)diacetic acid zinc(II) acetate aluminium fluoride ($[\text{Zn}_2\text{AlF}_4(\text{OAc})_2](\text{OAc})_2$) (2.5 mg, 1.9 μmol , 86.4% yield).

Purification attempted using RP analytical HPLC System K, (Section 9.2.1.10) (single peak, suspected peak $t_r = 15:38$ min). MS unable to identified.

9.3.66 Synthesis of (4-((1,4,7-triazonan-1-yl)methyl)phenyl)methanamine (**44**)

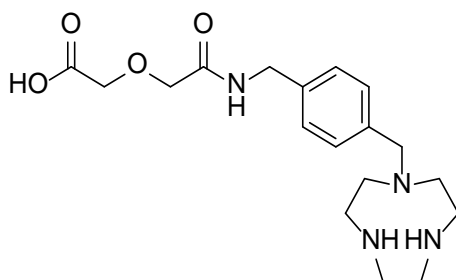


44

Di-*tert*-butyl 7-(4-(aminomethyl)benzyl)-1,4,7-triazonane-1,4-dicarboxylate (provided by Ms. Zainab Al-Ali, 20.0 mg, 40.0 μmol) was dissolved in 5 mL of hydrochloric acid (3M). The reaction was stirred under argon for 16 hours, upon which the reaction was reduced *in vacuo* to yield a white precipitate (4-((1,4,7-triazonan-1-yl)methyl)phenyl)methanamine (**44**), (10.0 mg, 40.0 μmol , 90.3% yield).

^1H NMR (400 MHz, CD_3OD , δ): 2.84-2.86 (m, N- α - CH_2 , 4H), 3.06-3.18 (m, N- α - CH_2 , 6H), 3.75 (s, N- α - CH_2 + NH, 5H), 4.02 (s, CH_2 -Ar, 2H) 4.52 (s, CH_2 -Ar, 2H), 7.31 (s, Ar-H, 4H). ^{13}C NMR (100 MHz, CDCl_3 , δ): 42.26 (N- α - CH_2), 42.70 (N- α - CH_2), 43.70 (N- α - CH_2), 47.54 (N- α - CH_2), 58.36 (CH_2 -Ar), 59.56 (CH_2 -Ar), 129.13 (C-Ar), 129.18 (C-Ar), 130.85 (C-Ar), 130.92 (C-Ar). MS (ES-MS): m/z 248.7 (M^+).

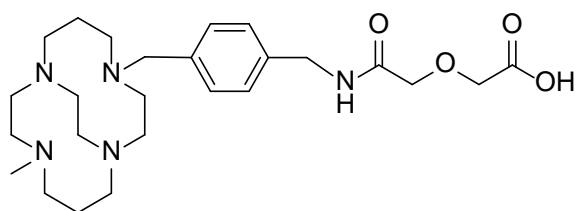
9.3.67 Attempted synthesis of 2-(2-((4-((1,4,7-triazonan-1-yl)methyl)benzyl)amino)-2-oxoethoxy)acetic acid (**45**)



45

(4-((1,4,7-Triazonan-1-yl)methyl)phenyl)methanamine (**44**) (31.0 mg, 0.120 mmol) and diglycolic anhydride (14.5 mg, 0.120 mmol) were dissolved in dry (amine-free) DMF (0.5 mL) with the addition of 5 equivalents of triethylamine (87.0 μ L, 0.620 mmol). The mixture was shaken for 16 hours, and reduced *in vacuo* to yield a pale yellow solid (**45**), (31.0 mg). The desired product was not isolated using this synthetic procedure.

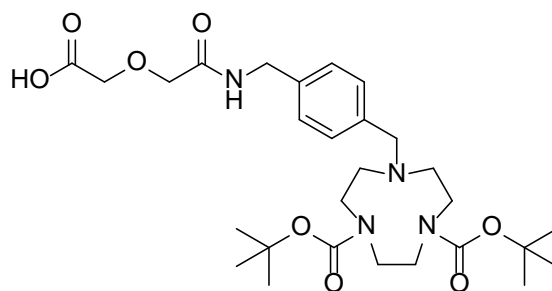
9.3.68 Synthesis of 2-(2-((4-((11-methyl-1,4,8,11-tetraazabicyclo[6.6.2]hexadecan-4-yl)methyl)benzyl)amino)-2-oxoethoxy)acetic acid (**46**)



46

1-(4-Aminomethylbenzyl)-8-(methyl)-1,4,8,11-tetraazabicyclo[6.6.2]-hexadecane (**15**) (189.0 mg, 0.530 mmol) and diglycolic anhydride (61.0 mg, 0.530 mmol) were dissolved in dry methanol (10 mL) and at room temperature for 16 hours. The solvents was removed *in vacuo* to yield a brown solid, 2-(2-((4-((11-methyl-1,4,8,11-tetraazabicyclo[6.6.2]hexadecan-4-yl)methyl)benzyl)amino)-2-oxoethoxy)acetic acid (**46**), (221.0 mg, 0.465 mmol, 88.4% yield).

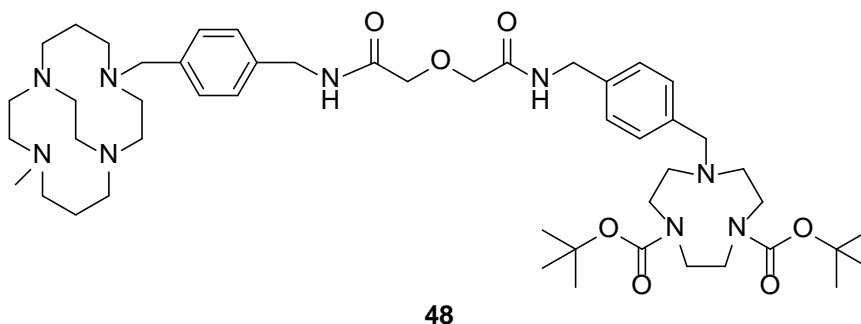
^1H NMR (400 MHz, D_2O , δ): 1.61-1.86 (m, N- β - CH_2 , 4H), 2.40-2.50 (m, N- α - CH_2 , 2H), 2.52-3.14 (m, N- α - CH_2 , 14H), 3.03-3.35 (m, N- α - CH_2 , 6H), 2.67 (s, CH_3 , 3H), 3.63-3.72 (m, CH_2 -O, 2H), 3.90-3.94 (m, CH_2 -O, 2H), 4.03 (s, CH_2 -Ar, 2H), 4.18 (s, NH, 1H), 4.35 (s, CH_2 -Ar, 2H), 4.43 (br s, OH, 1H), 7.21-7.53 (m, Ar-H, 4H). ^{13}C NMR (100 MHz, CD_3OD , δ): 22.73 (N- β - CH_2), 24.65 (N- β - CH_2), 41.90 (N- α - CH_2), 53.60 (N- α - CH_2), 53.77 (N- α - CH_2), 57.06 (N- α - CH_2), 57.94 (N- α - CH_2), 58.19 (N- α - CH_2), 58.66 (N- α - CH_2), 63.81 (N- α - CH_2), 67.10 (N- α - CH_2), 69.48 (CH_2 -Ar), 69.84 (CH_2 -Ar), 70.74 ($\underline{\text{C}}$ -CO), 70.77 ($\underline{\text{C}}$ -CO), 86.15 ($\underline{\text{C}}$ H_2 -Ar), 127.53 (C-Ar), 129.82 (Ar-H), 140.42 (Ar-H), 161.92 (C=O), 171.45 (C=O). MS (HRMS): m/z (M^+) calcd. for $\text{C}_{25}\text{H}_{42}\text{N}_5\text{O}_4^+$, 476.3231; found, 476.3224.

**47**

Diglycolic anhydride (8.05 mg, 0.070 mmol) and di-*tert*-butyl-7-(4-(aminomethyl)benzyl)-1,4,7-triazonan-1,4-dicarboxylate (provided by Ms. Zainab Al-Ali, 31.1 mg, 70.0 μ mol) were dissolved in dry (amine-free) DMF (0.5 mL) with triethylamine (96.6 μ L, 69.0 μ mol) and stirred at room temperature for 16 hours. The solution was reduced in *vacuo* to yield clear oil, 2-(2-((4-((4,7-bis(*tert*-butoxycarbonyl)-1,4,7-triazonan-1-yl)methyl)benzyl)amino)-2-oxoethoxy)acetic acid (**47**), (35.0 mg, 62.0 μ mol, 89.4% yield).

^1H NMR (400 MHz, CD_3OD , δ): 1.45-1.52 (m, CH_3 , 18H), 2.69-2.93 (m, $\text{N-}\alpha\text{-CH}_2$, 6H), 2.99 (s, $\text{N-}\alpha\text{-CH}_2$, 2H), 3.36-3.48 (m, $\text{N-}\alpha\text{-CH}_2 + \text{CH}_2\text{-O}$, 6H), 3.73-3.89 (m, $\text{CH}_2\text{-O}$, 2H), 4.09-4.17 (m, $\text{CH}_2\text{-Ar}$, 4H), 4.43 (br s, NH, 2H), 7.25-7.44 (m, Ar-H, 4H), 7.96 (br s, OH, 1H). ^{13}C NMR (100 MHz, CD_3OD , δ): 27.41 (C-CH_3), 30.28 (C-CH_3), 35.61 ($\text{CH}_2\text{-Ar}$), 41.88 ($\text{N-}\alpha\text{-CH}_2$), 49.08 ($\text{CH}_2\text{-Ar}$), 51.09 ($\text{CH}_2\text{-Ar}$), 68.38 ($\text{CH}_2\text{-Ar}$), 69.99 ($\text{CH}_2\text{-O}$), 129.91 (Ar-H), 155.64 (Ar-H), 158.06 (C-Ar), 163.44 (C-Ar), 164.37 (N-C=O), 169.70 (C=O), 172.53 (C=O). MS (HRMS): m/z (M^+) calcd. for $\text{C}_{28}\text{H}_{43}\text{N}_4\text{O}_8^+$, 536.3086; found, 563.3074.

9.3.70 Synthesis of di-*tert*-butyl-7-(4-((2-(2-((4-((11-methyl-1,4,8,11-tetraazabicyclo[6.6.2]hexadecan-4-yl)methyl)benzyl)amino)-2-oxoethoxy)acetamido)methyl)benzyl)-1,4,7-triazonane-1,4-dicarboxylate (**48**)



General procedure K

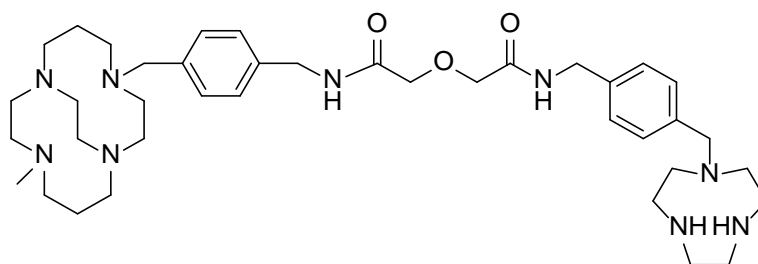
The macrocycle and 2-(2-((4-((4,7-bis(*tert*-butoxycarbonyl)-1,4,7-triazonan-1-yl)methyl)benzyl)amino)-2-oxoethoxy)acetic acid were dissolved in dry (amine free DMF) in the presence of base and HATU. The reaction was shaken at room temperature for 16 hour. The solvent was reduced *in vacuo*.

Amounts: 1-(4-Aminomethylbenzyl)-8-(methyl)-1,4,8,11-tetraazabicyclo[6.6.2]-hexadecane (**15**) provided by Ms. Zainab Al-Ali provided by Ms. Zainab Al-Ali (21.0 mg, 60.0 μmol), 2-(2-((4-((4,7-bis(*tert*-butoxycarbonyl)-1,4,7-triazonan-1-yl)methyl)benzyl)amino)-2-oxoethoxy)acetic acid (33.0 mg, 60.0 μmol), DMF (0.5 mL), triethylamine (76.6 μL , 0.550 mmol), HATU (22.2 mg, 60.0 μmol) to yield a yellow precipitate, di-*tert*-butyl-7-(4-((2-(2-((4-((11-methyl-1,4,8,11-tetraazabicyclo[6.6.2]hexadecan-4-yl)methyl)benzyl)amino)-2-oxoethoxy)acetamido)methyl)benzyl)-1,4,7-triazonane-1,4-dicarboxylate (**48**), (43.0 mg, 48.0 μmol , 81.2% yield).

^1H NMR (400 MHz, CDCl_3 , δ): 1.25-1.53 (m, CH_3 , 18H), 2.02-2.51 (m, $\text{N-}\beta\text{-CH}_2$, $\text{N-}\alpha\text{-CH}_2$, 16H), 2.77-2.96 (m, $\text{N-}\alpha\text{-CH}_2$, 12H), 3.09-3.18 (m, $\text{N-}\alpha\text{-CH}_2$, 2H), 3.35-3.50 (m, $\text{N-}\alpha\text{-CH}_2$, 6H), 3.68-3.82 (m, CH_3 , 3H), 4.04-4.19 (m, $\text{CH}_2\text{-Ar}$, 6H), 4.21-4.28 (m, $\text{CH}_2\text{-Ar}$, 2H), 4.32-4.44 (m, $\text{CH}_2\text{-O}$, 4H), 6.66 (br s, NH, 1H), 7.39-7.41 (m, Ar-H, 2H), 7.74-7.87 (m, Ar-H, 2H), 8.01 (br s, NH, 1H), 8.19-8.29 (d, $J = 8.4$ Hz, Ar-H, 2H), 8.49-8.50 (d, $J = 8.4$ Hz, Ar-H, 2H). ^{13}C NMR (100 MHz, CD_3OD , δ): 16.80 ($\text{N-}\beta\text{-CH}_2$), 17.25 ($\text{N-}\beta\text{-CH}_2$), 18.44 (CH_3), 28.07 ($\text{N-}\alpha\text{-CH}_2$), 28.37 ($\text{N-}\alpha\text{-CH}_2$), 28.63 ($\text{N-}\alpha\text{-CH}_2$), 29.18 ($\text{N-}\alpha\text{-CH}_2$), 29.51 ($\text{N-}\alpha\text{-}$

CH₂), 29.79 (N- α -CH₂), 30.40 (N- α -CH₂), 36.61 (N- α -CH₂), 45.73 (N- α -CH₂), 46.01 (N- α -CH₂), 53.95 (CH₂-Ar), 54.66 (CH₂-Ar), 56.28 (CH₂-Ar), 59.30 (CH₂-Ar), 70.37 (C-O), 71.20 (C-O), 72.33 (C-CH₃), 114.57 (Ar-H), 115.90 (Ar-H), 120.00 (Ar-H), 120.04 (Ar-H), 127.78 (C-Ar), 127.83 (C-Ar), 128.11 (C-Ar), 129.64 (C-Ar), 149.03 (C=O), 180.41 (C=O). MS (ES-MS): *m/z* 907.7 (M⁺).

9.3.71 Synthesis of N-(4-((1,4,7-triazonan-1-yl)methyl)benzyl)-2-(2-((4-((11-methyl-1,4,8,11-tetraazabicyclo[6.6.2]hexadecan-4-yl)methyl)benzyl)amino)-2-oxoethoxy)acetamide (**49**)



49

Method 1- Attempted synthesis

(4-((1,4,7-Triazonan-1-yl)methyl)phenyl)methanamine (12.8 mg, 50.0 μmol) and 2-(2-((4-((11-methyl-1,4,8,11-tetraazabicyclo[6.6.2]hexadecan-4-yl)methyl)benzyl)amino)-2-oxoethoxy)acetic acid (**46**) (24.5 mg, 50.0 μmol) were combined in dry (amine-free) DMF (0.5 mL) in the presence of HATU (19.58 mg, 50.0 μmol) and triethylamine (71.7 μL , 0.520 mmol). The reaction was shaken at room temperature for 16 hours. The resulting solution was reduced *in vacuo* to yield a brown precipitate. The desired product was not isolated using this synthetic procedure.

Method 2 – Preferred synthesis

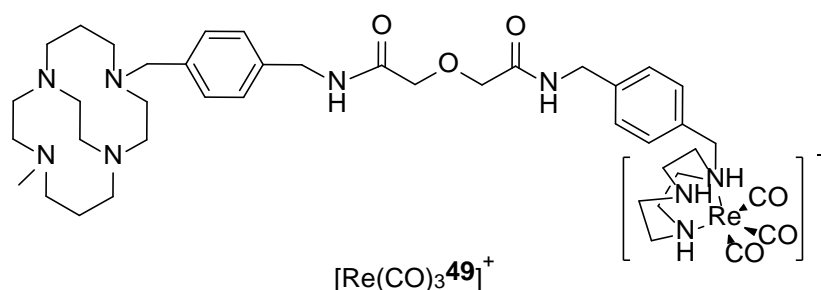
General procedure L

The macrocycle was dissolved in hydrochloric acid (3M) and stirred under argon for 16 hours. The reaction was reduced *in vacuo* to yield a solid which was then purified using reverse phase semi-preparative HPLC.

Amounts: Di-*tert*-butyl-7-(4-((2-(2-((4-((11-methyl-1,4,8,11-tetraazabicyclo[6.6.2]hexadecan-4-yl)methyl)benzyl)amino)-2-oxoethoxy)acetamido)methyl)benzyl)-1,4,7-triazonan-1,4-dicarboxylate (**48**) (36.0 mg, 40.0 μmol), 5 mL of hydrochloric acid (3M). To yield the white solid, N-(4-((1,4,7-triazonan-1-yl)methyl)benzyl)-2-(2-((4-((11-methyl-1,4,8,11-tetraazabicyclo[6.6.2]hexadecan-4-yl)methyl)benzyl)amino)-2-oxoethoxy)acetamide (**49**), (12.0 mg, 17.0 μmol , 37.5% yield).

Purified by reverse phase C18 semi-preparative HPLC System 11 (Section 9.2.2.11) (broad single peak, $t_r = 04:40$ min). ^1H NMR (400 MHz, CD_3OD , δ): 1.14 (s, CH_3 , 3H), 1.62-1.69 (m, $\text{N-}\beta\text{-CH}_2$, 4H), 2.06 (m, $\text{N-}\alpha\text{-CH}_2$, 10H), 2.28-2.37 (m, $\text{N-}\alpha\text{-CH}_2$, 6H), 2.39-2.65 (m, $\text{N-}\alpha\text{-CH}_2$, 6H), 2.72 (s, NH, 3H), 2.83-2.93 (m, $\text{N-}\alpha\text{-CH}_2$, 6H), 3.44-3.86 (m, $\text{N-}\alpha\text{-CH}_2$, 4H), 4.14-4.28 (m, $\text{CH}_2\text{-O}$, 4H), 5.89-5.95 (m, $\text{CH}_2\text{-Ar}$, 2H), 6.01 (s, $\text{CH}_2\text{-Ar}$, 1H), 6.01 (s, $\text{CH}_2\text{-Ar}$, 1H), 6.08-6.13 (m, $\text{CH}_2\text{-Ar}$, 3H), 6.86 (dd, $J = 3.5, 1.0$ Hz, Ar-H, 2H), 7.19 (d, $J = 4.5, 1.3$ Hz, Ar-H, 2H), 7.19-7.25 (m, Ar-H, 4H). ^{13}C NMR (100 MHz, CD_3OD , δ): 16.42 ($\text{N-}\beta\text{-CH}_2$), 17.58 ($\text{N-}\beta\text{-CH}_2$), 18.12 (CH_3), 30.01 ($\text{N-}\alpha\text{-CH}_2$), 30.06 ($\text{N-}\alpha\text{-CH}_2$), 30.11 ($\text{N-}\alpha\text{-CH}_2$), 30.16 ($\text{N-}\alpha\text{-CH}_2$), 35.53 ($\text{N-}\alpha\text{-CH}_2$), 35.66 ($\text{N-}\alpha\text{-CH}_2$), 35.75 ($\text{N-}\alpha\text{-CH}_2$), 40.72 ($\text{N-}\alpha\text{-CH}_2$), 40.84 ($\text{N-}\alpha\text{-CH}_2$), 42.09 ($\text{N-}\alpha\text{-CH}_2$), 42.18 ($\text{N-}\alpha\text{-CH}_2$), 46.28 (C-O), 52.57 ($\text{CH}_2\text{-Ar}$), 53.76 ($\text{CH}_2\text{-Ar}$), 55.16 ($\text{CH}_2\text{-Ar}$), 57.21 ($\text{CH}_2\text{-Ar}$), 121.93 (Ar-H), 122.08 (Ar-H), 126.19 (Ar-H), 126.29 (Ar-H), 129.22 (C-Ar), 130.89 (C-Ar), 148.75 (C-Ar), 163.58 (C-Ar), 170.38 (C=O). MS (HRMS): m/z (M^+) calcd. for $\text{C}_{39}\text{H}_{65}\text{N}_9\text{O}_3^+$, 707.3775; found, 707.3770.

9.3.72 Synthesis of the rhenium complexation of N-(4-((1,4,7-triazonan-1-yl)methyl)benzyl)-2-(2-((4-((11-methyl-1,4,8,11-tetraazabicyclo[6.6.2]hexadecan-4-yl)methyl)benzyl)amino)-2-oxoethoxy)acetamide ([Re(CO)₃**49**]⁺)



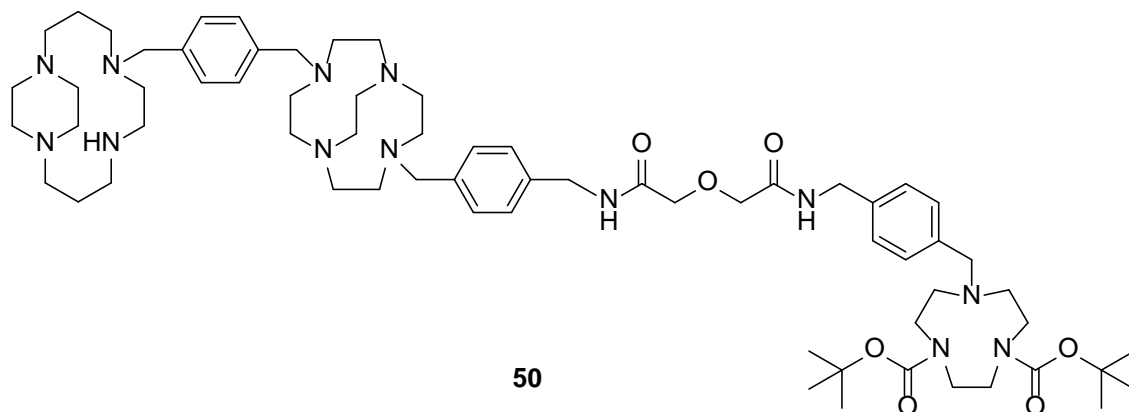
General procedure M

The macrocycle was combined with [NEt₄]₂[ReBr₃(CO)₃] in dry DMF, the reaction was heated at 50°C for 4 hours, before being reduced *in vacuo* and purified by reverse phase C18 semi-preparative HPLC.

Amounts: N-(4-((1,4,7-triazonan-1-yl)methyl)benzyl)-2-(2-((4-((11-methyl-1,4,8,11-tetraazabicyclo[6.6.2]hexadecan-4-yl)methyl)benzyl)amino)-2-oxoethoxy)acetamide (**49**) (7.0 mg, 10.0 μmol), [NEt₄]₂[ReBr₃(CO)₃] (11.38 mg, 10.0 μmol). To yield compound an off-white solid, ([Re(CO)₃**49**]⁺) (5.5 mg, 5.6 μmol, 57.0% yield).

Purified by RP= semi-preparative HPLC System 12 (Section 9.2.2.12) (broad single peak, t_r = 07:20 min). MS (ES-MS): *m/z* 526.2 (M+2K, 78).

9.3.73 Synthesis of di-*tert*-butyl-7-(4-((2-(2-((4-((10-(4-((1,5,8,12-tetraazabicyclo[10.2.2]hexadecan-5-yl)methyl)benzyl)-1,4,7,10-tetraazabicyclo[5.5.2]tetradecan-4-yl)methyl)benzyl)amino)-2-oxoethoxy)acetamido)methyl)benzyl)-1,4,7-triazonane-1,4-dicarboxylate (**50**)

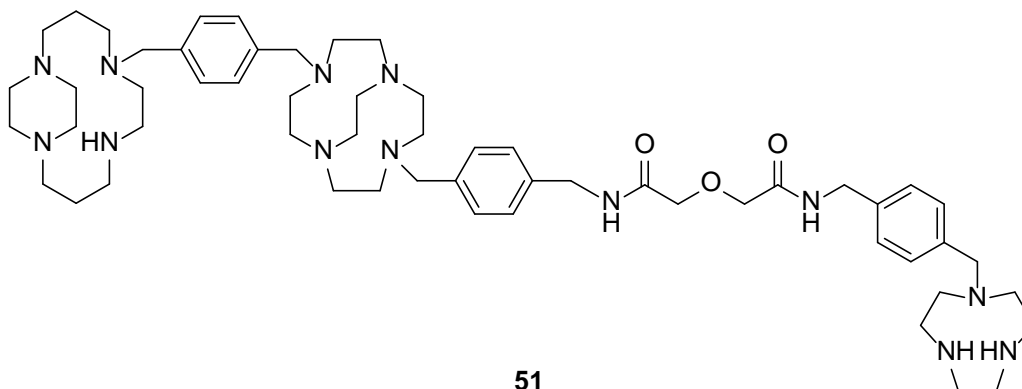


General procedure K was followed.

Amounts: (4-((10-(4-((1,5,8,12-Tetraazabicyclo[10.2.2]hexadecan-5-yl)methyl)benzyl)-1,4,7,10-tetraazabicyclo[5.5.2]tetradecan-4-yl)methyl)phenyl)methanamine (**24**) (40.03 mg, 60.0 μ mol), 2-(2-((4-((4,7-bis(*tert*-butoxycarbonyl)-1,4,7-triazonane-1-yl)methyl)benzyl)amino)-2-oxoethoxy)acetic acid (**24**) (35. mg, 60.0 μ mol), triethylamine (93.16 μ L, 0.670 mmol), HATU (23.6 mg, 60.0 μ mol) to yield a yellow precipitate, di-*tert*-butyl-7-(4-((2-(2-((4-((10-(4-((1,5,8,12-tetraazabicyclo[10.2.2]hexadecan-5-yl)methyl)benzyl)-1,4,7,10-tetraazabicyclo[5.5.2]tetradecan-4-yl)methyl)benzyl)amino)-2-oxoethoxy)acetamido)methyl)benzyl)-1,4,7-triazonane-1,4-dicarboxylate (**50**), (69.0 mg, 0.058 mmol, 93.3% yield).

^1H NMR (400 MHz, CD_3OD , δ): 1.42-1.48 (m, CH_3 , 18H), 1.54-1.58 (m, NH, 3H), 2.26-2.36 (m, N- β - CH_2 , 4H), 2.51-2.67 (m, N- α - CH_2 , 12H), 2.67-3.14 (m, N- α - CH_2 , 28H), 3.18-3.26 (m, N- α - CH_2 , 4H), 3.42-3.49 (m, N- α - CH_2 , 6H), 3.53-3.56 (m, CH_2 -O, 4H), 3.69-3.82 (m, CH_2 -Ar, 4H), 3.91-4.04 (m, CH_2 -Ar, 6H), 4.33-4.43 (m, CH_2 -Ar, 2H), 7.13-7.50 (m, Ar-H, 12H). MS (HRMS): m/z (M^{2+}) calcd. for $\text{C}_{66}\text{H}_{107}\text{N}_{13}\text{O}_7^{2+}$, 596.9203; found, 596.9193.

9.3.74 Synthesis of N-(4-((1,4,7-triazonan-1-yl)methyl)benzyl)-2-(2-((4-((10-(4-((1,5,8,12-tetraazabicyclo[10.2.2]hexadecan-5-yl)methyl)benzyl)-1,4,7,10-tetraazabicyclo[5.5.2]tetradecan-4-yl)methyl)benzyl)amino)-2-oxoethoxy)acetamide (**51**)

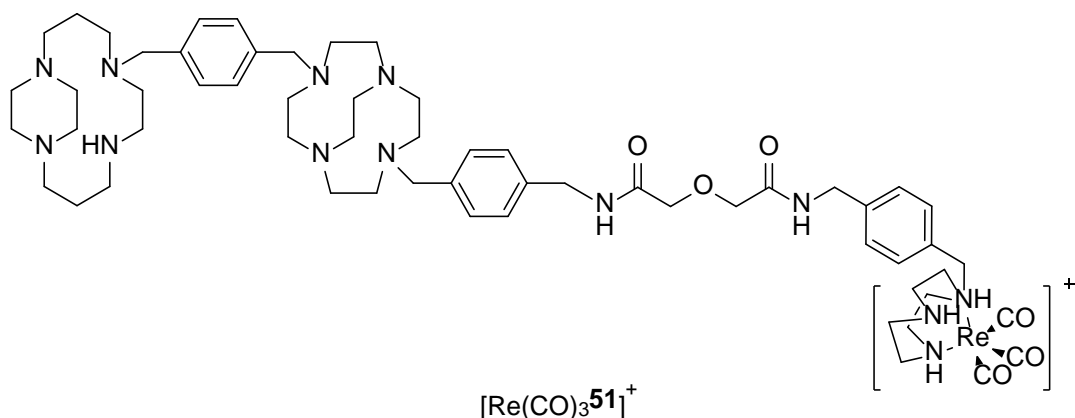


General procedure L was followed.

Amounts: Di-*tert*-butyl-7-(4-((2-(2-((4-((10-(4-((1,5,8,12-tetraazabicyclo[10.2.2]hexadecan-5-yl)methyl)benzyl)-1,4,7,10-tetraazabicyclo[5.5.2]tetradecan-4-yl)methyl)benzyl)amino)-2-oxoethoxy)acetamido)methyl)benzyl)-1,4,7-triazonane-1,4-dicarboxylate (**50**) (69.0 mg, 60.0 μ mol), 5 mL of hydrochloric acid (3M). To yield the white precipitate N-(4-((1,4,7-triazonan-1-yl)methyl)benzyl)-2-(2-((4-((10-(4-((1,5,8,12-tetraazabicyclo[10.2.2]hexadecan-5-yl)methyl)benzyl)-1,4,7,10-tetraazabicyclo[5.5.2]tetradecan-4-yl)methyl)benzyl)amino)-2-oxoethoxy)acetamide (**51**), (24.0 mg, 26.3 μ mol, 45.0% yield).

Purified by reverse phase C18 semi-preparative System 13, (Section 9.2.2.13), (broad single peak, t_r = 16:20 min). ¹H NMR (400 MHz, CD₃OD, δ): 1.44-1.56 (m, NH, 3H), 2.62-2.71 (m, N- β -CH₂, 4H), 2.93-2.99 (m, N- α -CH₂, 10H), 3.18-3.24 (m, N- α -CH₂, 4H), 3.24-3.30 (m, N- α -CH₂, 10H), 3.34-3.40 (m, N- α -CH₂, 4H), 3.46-3.80 (m, N- α -CH₂, 24H), 3.90-3.94 (m, CH₂-O, 4H), 4.10-4.20 (m, CH₂-Ar, 4H), 4.22-4.25 (m, CH₂-Ar, 2H), 4.40-4.80 (m, CH₂-Ar, 6H), 7.33 (d, J = 7.9 Hz, Ar-H, 2H), 7.41-7.65 (m, Ar-H, 6H), 7.74-7.97 (m, Ar-H, 2H), 8.45 (s, NH, 1H), 8.74 (s, NH, 1H). MS (HRMS): m/z (M⁺) calcd. for C₅₆H₉₀N₁₃O₃⁺, 992.7284; found, 992.7162.

9.3.75 Synthesis of the rhenium complexation of N-(4-((1,4,7-triazonan-1-yl)methyl)benzyl)-2-(2-((4-((10-(4-((1,5,8,12-tetraazabicyclo[10.2.2]hexadecan-5-yl)methyl)benzyl)-1,4,7,10-tetraazabicyclo[5.5.2]tetradecan-4-yl)methyl)benzyl)amino)-2-oxoethoxy)acetamide ([Re(CO)₃**51**]⁺)

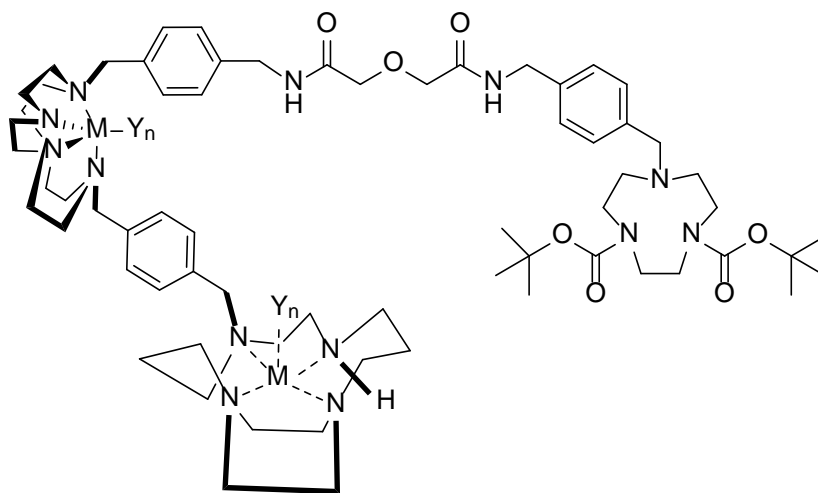


General procedure M was followed.

Amounts: N-(4-((1,4,7-triazonan-1-yl)methyl)benzyl)-2-(2-((4-((10-(4-((1,5,8,12-tetraazabicyclo[10.2.2]hexadecan-5-yl)methyl)benzyl)-1,4,7,10-tetraazabicyclo[5.5.2]tetradecan-4-yl)methyl)benzyl)amino)-2-oxoethoxy)acetamide (**51**) (4.2mg, 4.6 μmol), dry DMF (1 mL), [NEt₄]₂[ReBr₃ (CO)₃] (5.3 mg, 4.6 μmol). To yield the white solid, N-(4-((1,4,7-triazonan-1-yl)methyl)benzyl)-2-(2-((4-((10-(4-((1,5,8,12-tetraazabicyclo[10.2.2]hexadecan-5-yl)methyl)benzyl)-1,4,7,10-tetraazabicyclo[5.5.2]tetradecan-4-yl)methyl)benzyl)amino)-2-oxoethoxy)acetamide rhenium complex ([Re(CO)₃**51**]⁺) (0.8 mg, 0.6 μmol, 13.8% yield).

Purified by RP semi-preparative HPLC System 13 (Section 9.2.2.14) (broad multiple peak, t_r = 17-19 min). MS (ES-MS): m/z 708.6 (M+TFA+K).

9.3.76 Synthesis of metal complexes of di-*tert*-butyl-7-(4-((2-(2-((4-((10-(4-((1,5,8,12-tetraazabicyclo[10.2.2]hexadecan-5-yl)methyl)benzyl)-1,4,7,10-tetraazabicyclo[5.5.2]tetradecan-4-yl)methyl)benzyl)amino)-2-oxoethoxy)acetamido)methyl)benzyl)-1,4,7-triazonane-1,4-dicarboxylate ([Cu₂50(OAc)₂](OAc)₂ and [Zn₂50(OAc)₂](OAc)₂)



2AcO⁻

M = Cu²⁺, Y = AcO⁻, (n = 1); [Cu₂50(OAc)₂](OAc)₂
 M = Zn²⁺, Y = AcO⁻, (n = 1/2); [Zn₂50(OAc)₂](OAc)₂

General procedure N

The macrocycle and 2-(2-((4-((4,7-bis(*tert*-butoxycarbonyl)-1,4,7-triazonan-1-yl)methyl)benzyl)amino)-2-oxoethoxy)acetic acid were dissolved in dry (amine free DMF) in the presence of HATU. The reaction was shaken at room temperature for 16 hour. The solvent was reduced *in vacuo*.

Di-*tert*-butyl-7-(4-((2-(2-((4-((10-(4-((1,5,8,12-tetraazabicyclo[10.2.2]hexadecan-5-yl)methyl)benzyl)-1,4,7,10-tetraazabicyclo[5.5.2]tetradecan-4-yl)methyl)benzyl)amino)-2-oxoethoxy)acetamido)methyl)benzyl)-1,4,7-triazonane-1,4-dicarboxylate copper acetate ([Cu₂50(OAc)₂](OAc)₂)

Amounts: 1-(4-(Aminomethyl)benzyl)-7-(4-((1,4,8,11-tetraazabicyclo[10.2.2]hexadecane)methyl)benzyl)-1,4,7,10-tetraazabicyclo[5.5.2]dodecane copper acetate ($[\text{Cu}_2\mathbf{24}(\text{OAc})_2](\text{OAc})_2$) (8.0 mg, 10.0 μmol), 2-(2-((4-((4,7-bis(*tert*-butoxycarbonyl)-1,4,7-triazonan-1-yl)methyl)benzyl)amino)-2-oxoethoxy)acetic acid (**47**) (4.5 mg, 10.0 μmol), HATU (3.0 mg, 10.0 μmol), DMF (2 mL), to yield bis copper di-*tert*-butyl-7-(4-((2-(2-((4-((10-(4-((1,5,8,12-tetraazabicyclo[10.2.2]hexadecan-5-yl)methyl)benzyl)-1,4,7,10-tetraazabicyclo[5.5.2]tetradecan-4-yl)methyl)benzyl)amino)-2-oxoethoxy)acetamido)methyl)benzyl)-1,4,7-triazonane-1,4-dicarboxylate ($[\text{Cu}_2\mathbf{50}(\text{OAc})_2](\text{OAc})_2$) (10.2 mg, 6.6 μmol , 82.7% yield).

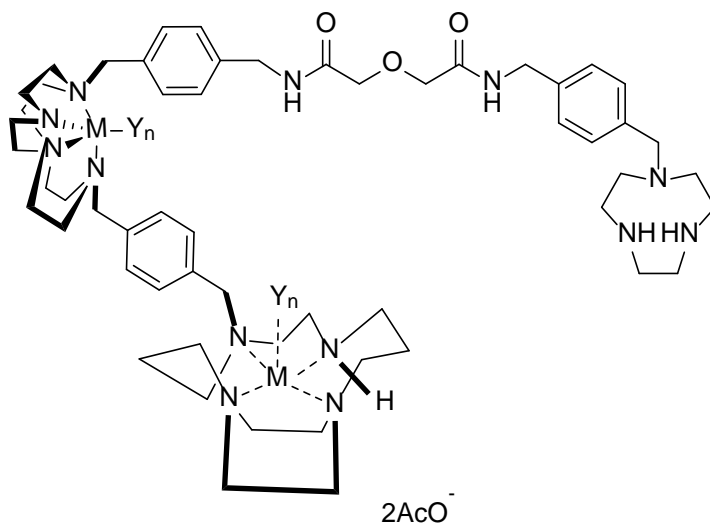
No analysis taken at this stage.

Di-*tert*-butyl-7-(4-((2-(2-((4-((10-(4-((1,5,8,12-tetraazabicyclo[10.2.2]hexadecan-5-yl)methyl)benzyl)-1,4,7,10-tetraazabicyclo[5.5.2]tetradecan-4-yl)methyl)benzyl)amino)-2-oxoethoxy)acetamido)methyl)benzyl)-1,4,7-triazonane-1,4-dicarboxylate zinc acetate ($[\text{Zn}_2\mathbf{50}(\text{OAc})_2](\text{OAc})_2$)

Amounts: 1-(4-(Aminomethyl)benzyl)-7-(4-((1,4,8,11-tetraazabicyclo[10.2.2]hexadecane)methyl)benzyl)-1,4,7,10-tetraazabicyclo[5.5.2]dodecane zinc acetate ($[\text{Zn}_2\mathbf{24}(\text{OAc})_2](\text{OAc})_2$) (48.5 mg, 50.0 μmol), 2-(2-((4-((4,7-bis(*tert*-butoxycarbonyl)-1,4,7-triazonan-1-yl)methyl)benzyl)amino)-2-oxoethoxy)acetic acid (**47**) (27.0 mg, 50.0 μmol), HATU (18.3 mg, 50.0 μmol), DMF (10 mL) to yield bis zinc di-*tert*-butyl-7-(4-((2-(2-((4-((10-(4-((1,5,8,12-tetraazabicyclo[10.2.2]hexadecan-5-yl)methyl)benzyl)-1,4,7,10-tetraazabicyclo[5.5.2]tetradecan-4-yl)methyl)benzyl)amino)-2-oxoethoxy)acetamido)methyl)benzyl)-1,4,7-triazonane-1,4-dicarboxylate ($[\text{Zn}_2\mathbf{50}(\text{OAc})_2](\text{OAc})_2$), (35.0 mg, 22.6 μmol , 46.9% yield).

No analysis taken at this stage.

9.3.77 Synthesis of metal complexes of N-(4-((1,4,7-triazonan-1-yl)methyl)benzyl)-2-(2-((4-((10-(4-((1,5,8,12-tetraazabicyclo[10.2.2]hexadecan-5-yl)methyl)benzyl)-1,4,7,10-tetraazabicyclo[5.5.2]tetradecan-4-yl)methyl)benzyl)amino)-2-oxoethoxy)acetamide ([Cu₂**51**(OAc)₂](OAc)₂ and [Cu₂**51**(OAc)₂](OAc)₂)



M = Cu²⁺, Y = CH₃COO⁻, (n = 1); [Cu₂**51**(AcO)₂](AcO)₂
M = Zn²⁺, Y = CH₃COO⁻, (n = 1/2); [Zn₂**51**(AcO)₂](AcO)₂

General procedure N was followed.

N-(4-((1,4,7-triazonan-1-yl)methyl)benzyl)-2-(2-((4-((10-(4-((1,5,8,12-tetraazabicyclo[10.2.2]hexadecan-5-yl)methyl)benzyl)-1,4,7,10-tetraazabicyclo[5.5.2]tetradecan-4-yl)methyl)benzyl)amino)-2-oxoethoxy)acetamide copper acetate ([Cu₂51**(OAc)₂](OAc)₂)**

Amounts: Di-*tert*-butyl-7-(4-((2-(2-((4-((10-(4-((1,5,8,12-tetraazabicyclo[10.2.2]hexadecan-5-yl)methyl)benzyl)-1,4,7,10-tetraazabicyclo[5.5.2]tetradecan-4-yl)methyl)benzyl)amino)-2-oxoethoxy)acetamido)methyl)benzyl)-1,4,7-triazonan-1,4-dicarboxylate copper(II) acetate ([Cu₂**50**(OAc)₂](OAc)₂) (10.3 mg, 10.0 μmol), HCl solution (3M, 5 mL). To yield the blue solid, N-(4-((1,4,7-triazonan-1-yl)methyl)benzyl)-2-(2-((4-((10-(4-((1,5,8,12-tetraazabicyclo[10.2.2]hexadecan-5-yl)methyl)benzyl)-1,4,7,10-tetraazabicyclo[5.5.2]tetradecan-4-yl)methyl)benzyl)amino)-2-oxoethoxy)acetamide copper(II) acetate ([Cu₂**51**(OAc)₂](OAc)₂), (4.0 mg, 5.5 μmol, 41.5% yield).

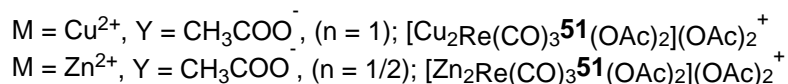
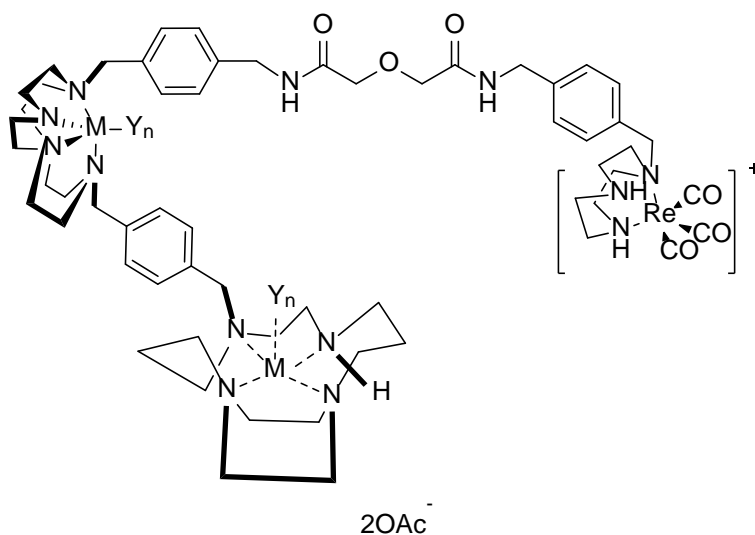
Purified by RP semi-preparative HPLC System 13 (Section 9.2.2.13) (single peak, $t_r = 10:17$ min). MS (ES-MS): m/z 448.2 (M-4CH₂CO₂+TFA).

N-(4-((1,4,7-triazonan-1-yl)methyl)benzyl)-2-(2-((4-((10-(4-((1,5,8,12-tetraazabicyclo[10.2.2]hexadecan-5-yl)methyl)benzyl)-1,4,7,10-tetraazabicyclo[5.5.2]tetradecan-4-yl)methyl)benzyl)amino)-2-oxoethoxy)acetamide zinc acetate ([Zn₂51(OAc)₂](OAc)₂)

Amounts: Di-*tert*-butyl-7-(4-((2-(2-((4-((10-(4-((1,5,8,12-tetraazabicyclo[10.2.2]hexadecan-5-yl)methyl)benzyl)-1,4,7,10-tetraazabicyclo[5.5.2]tetradecan-4-yl)methyl)benzyl)amino)-2-oxoethoxy)acetamido)methyl)benzyl)-1,4,7-triazonane-1,4-dicarboxylate zinc acetate ([Zn₂50(OAc)₂](OAc)₂) (30.2 mg, 20.0 μmol), HCl solution (3M, 5 mL). To yield the off-white solid, N-(4-((1,4,7-triazonan-1-yl)methyl)benzyl)-2-(2-((4-((10-(4-((1,5,8,12-tetraazabicyclo[10.2.2]hexadecan-5-yl)methyl)benzyl)-1,4,7,10-tetraazabicyclo[5.5.2]tetradecan-4-yl)methyl)benzyl)amino)-2-oxoethoxy)acetamide zinc acetate ([Zn₂51(OAc)₂](OAc)₂), (6.6 mg, 4.9 μmol, 25.1% yield).

Purified by RP semi-preparative HPLC system 13 (Section 9.2.2.13) (single peak, $t_r = 16:20$ min). MS (ES-MS): m/z 704.3 (M-2CH₂CO₂+K+H₂O+TFA).

9.3.78 Synthesis of the rhenium complexation of the metal complexed of N-(4-((1,4,7-triazonan-1-yl)methyl)benzyl)-2-(2-((4-((10-(4-((1,5,8,12-tetraazabicyclo[10.2.2]hexadecan-5-yl)methyl)benzyl)-1,4,7,10-tetraazabicyclo[5.5.2]tetradecan-4-yl)methyl)benzyl)amino)-2-oxoethoxy)acetamide ($[\text{Cu}_2\text{Re}(\text{CO})_3\mathbf{51}(\text{AcO})_2](\text{AcO})_2^+$ and $[\text{Zn}_2\text{Re}(\text{CO})_3\mathbf{51}(\text{AcO})_2](\text{AcO})_2^+$)



General procedure M was followed.

Rhenium complexation of N-(4-((1,4,7-triazonan-1-yl)methyl)benzyl)-2-(2-((4-((10-(4-((1,5,8,12-tetraazabicyclo[10.2.2]hexadecan-5-yl)methyl)benzyl)-1,4,7,10-tetraazabicyclo[5.5.2]tetradecan-4-yl)methyl)benzyl)amino)-2-oxoethoxy)acetamide copper acetate ($[\text{Cu}_2\text{Re}\mathbf{51}(\text{AcO})_2](\text{AcO})_2$)

Amounts: N-(4-((1,4,7-triazonan-1-yl)methyl)benzyl)-2-(2-((4-((10-(4-((1,5,8,12-tetraazabicyclo[10.2.2]hexadecan-5-yl)methyl)benzyl)-1,4,7,10-tetraazabicyclo[5.5.2]tetradecan-4-yl)methyl)benzyl)amino)-2-oxoethoxy)acetamide copper acetate ($[\text{Cu}_2\mathbf{51}(\text{AcO})_2](\text{AcO})_2$) (2.1 mg, 1.7 μmol), $[\text{NEt}_4]_2[\text{ReBr}_3(\text{CO})_3]$ (1.95 mg, 1.7 μmol) to yield the blue solid, rhenium complexed N-(4-((1,4,7-triazonan-1-yl)methyl)benzyl)-2-(2-((4-((10-(4-((1,5,8,12-tetraazabicyclo[10.2.2]hexadecan-5-yl)methyl)benzyl)-1,4,7,10-tetraazabicyclo[5.5.2]tetradecan-4-yl)methyl)benzyl)amino)-2-oxoethoxy)acetamide copper acetate ($[\text{Cu}_2\text{Re}(\text{CO})_3\mathbf{51}(\text{AcO})_2](\text{AcO})_2^+$) (1.8 mg, 1.4 μmol , 84.0% yield).

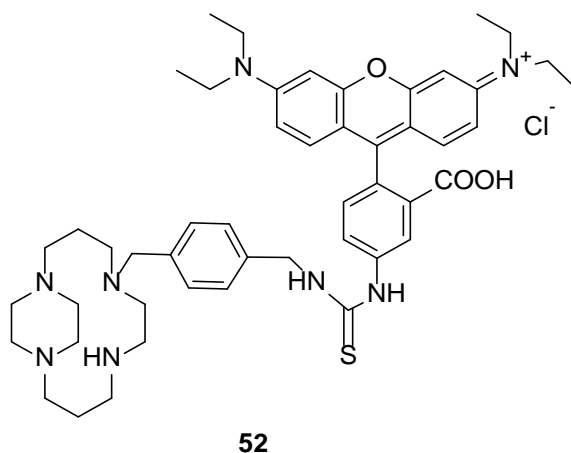
Analytical analysis carried out using RP-HPLC System L (Section 9.2.1.11) (single peak, $t_r = 14.50$ min).
Amounts: MS data unable to be interpreted.

Rhenium complexation of N-(4-((1,4,7-triazonan-1-yl)methyl)benzyl)-2-(2-((4-((10-(4-((1,5,8,12-tetraazabicyclo[10.2.2]hexadecan-5-yl)methyl)benzyl)-1,4,7,10-tetraazabicyclo[5.5.2]tetradecan-4-yl)methyl)benzyl)amino)-2-oxoethoxy)acetamide zinc acetate ($[\text{Zn}_2\text{Re}(\text{CO})_3\mathbf{51}(\text{AcO})_2](\text{AcO})_2^+$)

Amounts: N-(4-((1,4,7-triazonan-1-yl)methyl)benzyl)-2-(2-((4-((10-(4-((1,5,8,12-tetraazabicyclo[10.2.2]hexadecan-5-yl)methyl)benzyl)-1,4,7,10-tetraazabicyclo[5.5.2]tetradecan-4-yl)methyl)benzyl)amino)-2-oxoethoxy)acetamide zinc acetate ($[\text{Zn}_2\mathbf{51}(\text{AcO})_2](\text{AcO})_2$) (1.2mg, 1.0 μmol) $[\text{NEt}_4]_2[\text{ReBr}_3(\text{CO})_3]$ (1.12mg, 1.0 μmol) to yield the off-white solid, rhenium complexed N-(4-((1,4,7-triazonan-1-yl)methyl)benzyl)-2-(2-((4-((10-(4-((1,5,8,12-tetraazabicyclo[10.2.2]hexadecan-5-yl)methyl)benzyl)-1,4,7,10-tetraazabicyclo[5.5.2]tetradecan-4-yl)methyl)benzyl)amino)-2-oxoethoxy)acetamide zinc acetate ($[\text{Zn}_2\text{Re}(\text{CO})_3\mathbf{51}(\text{AcO})_2](\text{AcO})_2^+$), (0.8 mg, 0.6 μmol , 65.3% yield).

Analytical analysis carried out using RP-HPLC System L (Section 9.2.1.11) (single peak, $t_r = 13.45$ min).
MS data unable to be interpreted.

9.3.79 Synthesis of N-(9-(4-(3-(4-((1,5,8,12-tetraazabicyclo[10.2.2]hexadecan-5-yl)methyl)benzyl)thioureido)-2-carboxyphenyl)-6-(diethylamino)-3H-xanthen-3-ylidene)-N-ethylethanaminium chloride (**52**)



General procedure O

The macrocycles and the fluorescent dye are combined in anhydrous amine-free DMF (1 mL) in a glass vial under argon and shaken at RT for 24 hours. The reaction is reduced *in vacuo* and re-suspended in methanol (2 mL) and purified by sephradex column (LH20). The correct fraction identified by mass spectroscopy are combined to yield the strongly coloured product.

N-(9-(4-(3-(4-((1,5,8,12-tetraazabicyclo[10.2.2]hexadecan-5-yl)methyl)benzyl)thioureido)-2-carboxyphenyl)-6-(diethylamino)-3H-xanthen-3-ylidene)-N-ethylethanaminium chloride (**52**)

Amounts: 1-(4-Aminomethylbenzyl)-1,4,8,11-tetraazabicyclo[10.2.2]hexadecane (**12**) (11.0 mg, 30.0 μmol), rhodamine B isothiocyanate (26.0 mg, 50.0 μmol) and anhydrous amine-free DMF (1 mL). To yield a purple solid, N-(9-(4-(3-(4-((1,5,8,12-tetraazabicyclo[10.2.2]hexadecan-5-yl)methyl)benzyl)thioureido)-2-carboxyphenyl)-6-(diethylamino)-3H-xanthen-3-ylidene)-N-ethylethanaminium chloride (**52**), (40 mg, 45.0 μmol , 98.0% yield).

UV/vis (H_2O): ($E_{m_{\max}}$: 555 nm/ $E_{x_{\max}}$: 580 nm). MS (HRMS): m/z (M^+) calcd. for $\text{C}_{49}\text{H}_{65}\text{N}_8\text{O}_3\text{S}^+$, 845.4895; found, 845.4886.

N-(9-(4-(3-(4-((1,5,8,12-tetraazabicyclo[10.2.2]hexadecan-5-yl)methyl)benzyl)thioureido)-2-carboxyphenyl)-6-(diethylamino)-3H-xanthen-3-ylidene)-N-ethylethanaminium chloride copper acetate ([Cu52(OAc)](OAc))

Amounts: 1-(4-Aminomethylbenzyl)-1,4,8,11-tetraazabicyclo[10.2.2]hexadecane copper(II) acetate ([Cu12(OAc)](OAc)) (2.7 mg, 10.0 μ mol), rhodamine B isothiocyanate (3.84 mg, 10.0 μ mol) and anhydrous amine-free DMF (1 mL). To yield a purple solid, N-(9-(4-(3-(4-((1,5,8,12-tetraazabicyclo[10.2.2]hexadecan-5-yl)methyl)benzyl)thioureido)-2-carboxyphenyl)-6-(diethylamino)-3H-xanthen-3-ylidene)-N-ethylethanaminium chloride copper acetate ([Cu52(OAc)](OAc)), (3.6 mg, 3.4 μ mol, 66.2% yield).

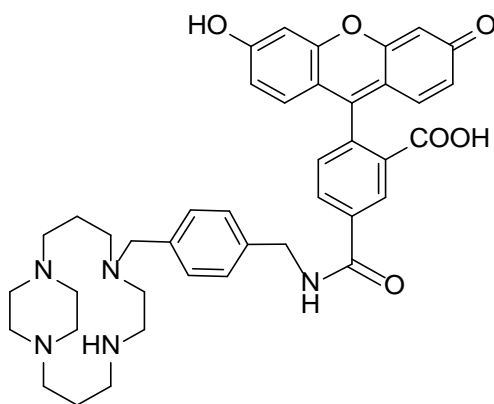
UV/vis (H₂O): (Em_{max}: 555 nm/Ex_{max}: 580 nm). MS (HRMS): *m/z* (M-CH₂CO₂+K) calcd. for C₅₃H₇₈ClCuN₈O₅KS⁺: 1075.7116 found, 1075.7117. MS (HRMS): *m/z* (M-2CH₂CO₂-Cl+2OH) calcd. for C₅₁H₇₄CuN₈O₄S⁺, 957.4544; found, 957.4542.

N-(9-(4-(3-(4-((1,5,8,12-tetraazabicyclo[10.2.2]hexadecan-5-yl)methyl)benzyl)thioureido)-2-carboxyphenyl)-6-(diethylamino)-3H-xanthen-3-ylidene)-N-ethylethanaminium chloride zinc acetate ([Zn52(OAc)](OAc))

Amounts: 1-(4-Aminomethylbenzyl)-1,4,8,11-tetraazabicyclo[10.2.2]hexadecane zinc(II) acetate ([Zn12(OAc)](OAc)) (4.86 mg, 10.0 μ mol), rhodamine B isothiocyanate (7.76 mg, 10.0 μ mol) and anhydrous amine-free DMF (1 mL). To yield a purple solid, N-(9-(4-(3-(4-((1,5,8,12-tetraazabicyclo[10.2.2]hexadecan-5-yl)methyl)benzyl)thioureido)-2-carboxyphenyl)-6-(diethylamino)-3H-xanthen-3-ylidene)-N-ethylethanaminium chloride zinc acetate ([Zn52(OAc)](OAc)) (4.3 mg, 4.0 μ mol, 43.9% yield).

UV/vis (H₂O): (Em_{max}: 555 nm/Ex_{max}: 580 nm). MS (HRMS): *m/z* (M-CH₂CO₂+K) for C₅₁H₇₄N₈O₃ZnS⁺, 1096.4851; found, 1096.4857.

9.3.81 Synthesis of 5-((4-((1,5,8,12-tetraazabicyclo[10.2.2]hexadecan-5-yl)methyl)benzyl)carbamoyl)-2-(6-hydroxy-3-oxo-3H-xanthen-9-yl)benzoic acid (**53**)



53

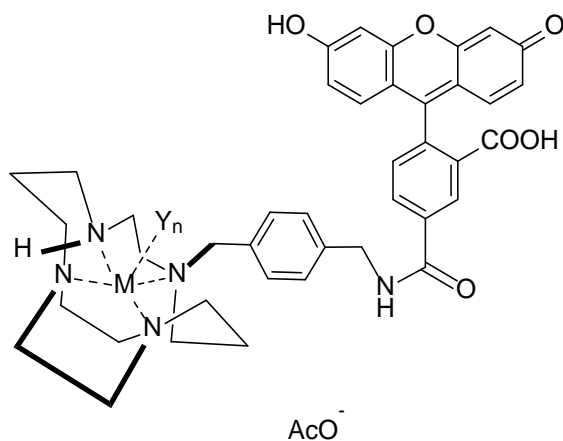
General method O was followed.

5-((4-((1,5,8,12-tetraazabicyclo[10.2.2]hexadecan-5-yl)methyl)benzyl)carbamoyl)-2-(6-hydroxy-3-oxo-3H-xanthen-9-yl)benzoic acid (53**)**

Amounts: 1-(4-Aminomethylbenzyl)-1,4,8,11-tetraazabicyclo[10.2.2]hexadecane (**12**) (11.0 mg, 30.0 μmol), 5/6-carboxyfluorescein succinimidyl ester (30.14 mg, 60.0 μmol) and anhydrous amine-free DMF (1 mL). To yield a yellow solid, 5-((4-((1,5,8,12-tetraazabicyclo[10.2.2]hexadecan-5-yl)methyl)benzyl)carbamoyl)-2-(6-hydroxy-3-oxo-3H-xanthen-9-yl)benzoic acid (**53**), (9.1 mg, 12.9 μmol , 40.7% yield).

UV/vis (H_2O): ($E_{m_{\max}}$: 485 nm/ $E_{x_{\max}}$: 519 nm). MS (HRMS): m/z (M^+) calcd. for $\text{C}_{41}\text{H}_{45}\text{N}_5\text{O}_6^+$, 704.3370; found, 704.3421.

9.3.82 Synthesis of 5-((4-((1,5,8,12-tetraazabicyclo[10.2.2]hexadecan-5-yl)methyl)benzyl)carbamoyl)-2-(6-hydroxy-3-oxo-3H-xanthen-9-yl)benzoic acid metal derivatives, ([Cu53(OAc)](OAc), and [Zn53(OAc)](OAc)



M = Cu²⁺, Y = AcO⁻, (n = 1); [Cu53(OAc)](OAc)
 M = Zn²⁺, Y = AcO⁻, (n = 1/2); [Zn53(OAc)](OAc)

5-((4-((1,5,8,12-tetraazabicyclo[10.2.2]hexadecan-5-yl)methyl)benzyl)carbamoyl)-2-(6-hydroxy-3-oxo-3H-xanthen-9-yl)benzoic acid copper acetate ([Cu53(OAc)](OAc))

Amounts: 1-(4-Aminomethylbenzyl)-1,4,8,11-tetraazabicyclo[10.2.2]hexadecane copper acetate, ([Cu12(OAc)](OAc)) (4.2 mg, 10.0 μmol), 5/6-carboxyfluorescein succinimidyl ester (5.66 mg, 10.0 μmol) and anhydrous amine-free DMF (1 mL). To yield a yellow solid, 5-((4-((1,5,8,12-tetraazabicyclo[10.2.2]hexadecan-5-yl)methyl)benzyl)carbamoyl)-2-(6-hydroxy-3-oxo-3H-xanthen-9-yl)benzoic acid copper acetate ([Cu53(OAc)](OAc)), (6.1 mg, 6.9 μmol, 86.6% yield).

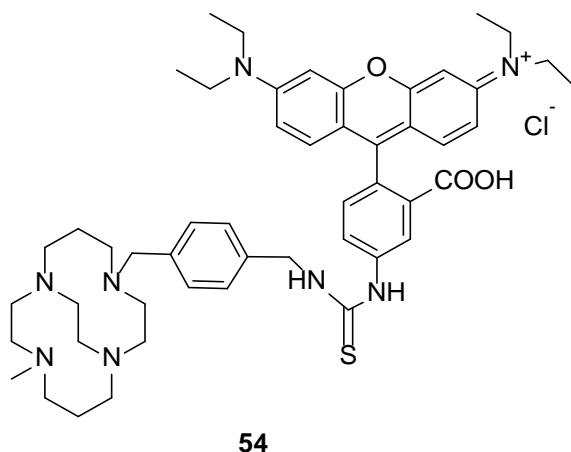
UV/vis (H₂O): (Em_{max}: 485 nm/Ex_{max}: 520 nm). MS (ES-MS; in formic acid): m/z 813.6 (M-2CH₂CO₂+CHO₂).

5-((4-((1,5,8,12-tetraazabicyclo[10.2.2]hexadecan-5-yl)methyl)benzyl)carbamoyl)-2-(6-hydroxy-3-oxo-3H-xanthen-9-yl)benzoic acid zinc acetate ([Zn53(OAc)](OAc))

Amounts: 1-(4-Aminomethylbenzyl)-1,4,8,11-tetraazabicyclo[10.2.2]hexadecane ([Zn12(OAc)](OAc)) (15.2 mg, 20.0 μ mol), 5/6-carboxyfluorescein succinimidyl ester (10.24 mg, 20.0 μ mol) and anhydrous amine-free DMF (1 mL). To yield a yellow solid, 5-((4-((1,5,8,12-tetraazabicyclo[10.2.2]hexadecan-5-yl)methyl)benzyl)carbamoyl)-2-(6-hydroxy-3-oxo-3H-xanthen-9-yl)benzoic acid zinc acetate ([Zn53(OAc)](OAc)), (24.5 mg, 27.7 μ mol, 92.0% yield).

UV/vis (H₂O): (Em_{max}: 485 nm/Ex_{max}: 520 nm). MS (ES-MS): *m/z* 433.6 (M-CH₃CO₂+K).

9.3.83 Synthesis of N-(9-(2-carboxy-4-(3-(4-((11-methyl-1,4,8,11-tetraazabicyclo[6.6.2]hexadecan-4-yl)methyl)benzyl)thioureido)phenyl)-6-(diethylamino)-3H-xanthen-3-ylidene)-N-ethylethanaminium chloride (**54**)



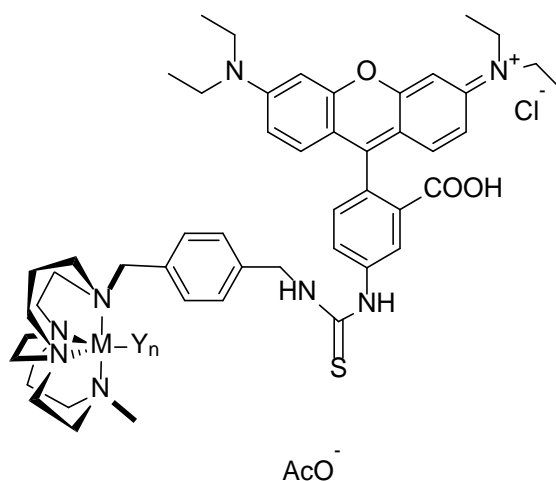
General method O was followed.

N-(9-(2-carboxy-4-(3-(4-((11-methyl-1,4,8,11-tetraazabicyclo[6.6.2]hexadecan-4-yl)methyl)benzyl)thioureido)phenyl)-6-(diethylamino)-3H-xanthen-3-ylidene)-N-ethylethanaminium chloride (54**)**

Amounts: 1-(4-aminomethylbenzyl)-8-(methyl)-1,4,8,11-tetraazabicyclo[6.6.2]-hexadecane (**15**) (20.0 mg, 0.040 mmol), rhodamine B isothiocyanate (33.9 mg, 0.060 mmol) and anhydrous amine-free DMF (1 mL). To yield a pink solid, N-(9-(2-carboxy-4-(3-(4-((11-methyl-1,4,8,11-tetraazabicyclo[6.6.2]hexadecan-4-yl)methyl)benzyl)thioureido)phenyl)-6-(diethylamino)-3H-xanthen-3-ylidene)-N-ethylethanaminium chloride (**54**) (7.1 mg, 8.0 μ mol, 18.9% yield).

UV/vis (H₂O): (Em_{max}: 555 nm/Ex_{max}: 580 nm). MS (HRMS): *m/z* (M-Cl) calcd. for C₅₀H₆₇N₈O₃S⁺, 859.5051; found, 859.5032.

9.3.84 Synthesis of N-(9-(2-carboxy-4-(3-(4-((11-methyl-1,4,8,11-tetraazabicyclo[6.6.2]hexadecan-4-yl)methyl)benzyl)thioureido)phenyl)-6-(diethylamino)-3H-xanthen-3-ylidene)-N-ethylethanaminium chloride metal derivatives ([Cu $\mathbf{54}$ (OAc)](OAc), and [Zn $\mathbf{54}$ (OAc)](OAc))



M = Cu $^{2+}$, Y = AcO $^{-}$, (n = 1); [Cu $\mathbf{54}$ (OAc)](OAc)
M = Zn $^{2+}$, Y = AcO $^{-}$, (n = 1/2); [Zn $\mathbf{54}$ (OAc)](OAc)

General method O was followed.

N-(9-(2-carboxy-4-(3-(4-((11-methyl-1,4,8,11-tetraazabicyclo[6.6.2]hexadecan-4-yl)methyl)benzyl)thioureido)phenyl)-6-(diethylamino)-3H-xanthen-3-ylidene)-N-ethylethanaminium chloride copper acetate ([Cu $\mathbf{54}$ (OAc)](OAc))

Amounts: 1-(4-aminomethylbenzyl)-8-(methyl)-1,4,8,11-tetraazabicyclo[6.6.2]-hexadecane copper acetate ([Cu $\mathbf{15}$ (OAc)](OAc)) (4.89 mg, 10.0 μ mol), rhodamine B isothiocyanate (12.6 mg, 10.0 μ mol) and anhydrous amine-free dry DMF (1 mL). To yield a pink solid, N-(9-(2-carboxy-4-(3-(4-((11-methyl-1,4,8,11-tetraazabicyclo[6.6.2]hexadecan-4-yl)methyl)benzyl)thioureido)phenyl)-6-(diethylamino)-3H-xanthen-3-ylidene)-N-ethylethanaminium chloride copper acetate ([Cu $\mathbf{54}$ (OAc)](OAc)), (1.3 mg, 1.2 μ mol, 13.0% yield).

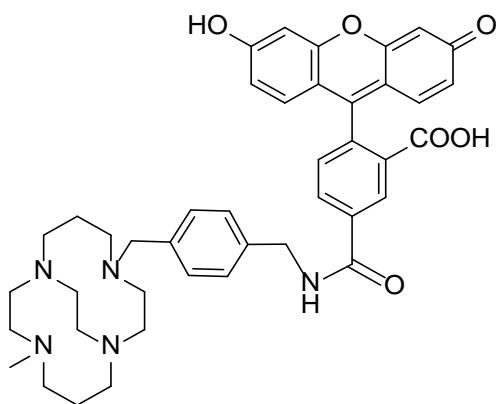
UV/vis (H $_2$ O): (Em $_{\max}$: 555 nm/Ex $_{\max}$: 580 nm). MS (HRMS): m/z (M-CH $_2$ CO $_2$ -Cl) calcd. for C $_{50}$ H $_{68}$ N $_8$ O $_3$ SCu $^{+}$, 923.4392; found, 923.4420.

N-(9-(2-carboxy-4-(3-(4-((11-methyl-1,4,8,11-tetraazabicyclo[6.6.2]hexadecan-4-yl)methyl)benzyl)thioureido)phenyl)-6-(diethylamino)-3H-xanthen-3-ylidene)-N-ethylethanaminium chloride zinc acetate ([Zn54(OAc)](OAc))

Amounts: 1-(4-aminomethylbenzyl)-8-(methyl)-1,4,8,11-tetraazabicyclo[6.6.2]-hexadecane copper acetate ([Zn15(OAc)](OAc)) (4.89 mg, 10.0 μ mol), rhodamine B isothiocyanate (6.41 mg, 10.0 μ mol) and anhydrous amine-free DMF (1 mL). To yield a pink precipitate N-(9-(2-carboxy-4-(3-(4-((11-methyl-1,4,8,11-tetraazabicyclo[6.6.2]hexadecan-4-yl)methyl)benzyl)thioureido)phenyl)-6-(diethylamino)-3H-xanthen-3-ylidene)-N-ethylethanaminium chloride zinc acetate ([Zn54(OAc)](OAc)) (2.2 mg, 2.0 μ mol, 22.6% yield).

UV/vis (H₂O): (Em_{max}: 555 nm/Ex_{max}: 580 nm). MS (HRMS): *m/z* 393.0 (M-CH₂CO₂-Cl) calcd. for C₅₀H₆₆N₈O₃SZn⁺, 922.4259; found, 922.4255.

9.3.85 Synthesis of 2-(6-hydroxy-3-oxo-3H-xanthen-9-yl)-5-(2-((4-((11-methyl-1,4,8,11-tetraazabicyclo[6.6.2]hexadecan-4-yl)methyl)benzyl)amino)-2-oxoethyl)benzoic acid (**55**)



55

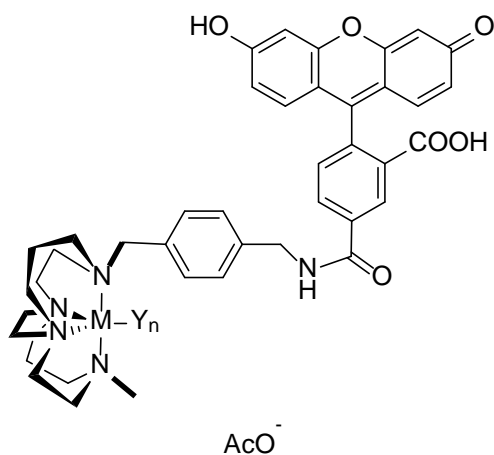
General method O was followed.

2-(6-Hydroxy-3-oxo-3H-xanthen-9-yl)-5-(2-((4-((11-methyl-1,4,8,11-tetraazabicyclo[6.6.2]hexadecan-4-yl)methyl)benzyl)amino)-2-oxoethyl)benzoic acid (55**)**

Amounts: 1-(4-Aminomethylbenzyl)-8-(methyl)-1,4,8,11-tetraazabicyclo[6.6.2]-hexadecane (**15**) (9.5 mg, 30.0 μ mol), 5/6-carboxyfluorescein succinimidyl ester (15.63 mg, 30.0 μ mol) and anhydrous amine-free DMF (1 mL). To yield the yellow solid, 2-(6-hydroxy-3-oxo-3H-xanthen-9-yl)-5-(2-((4-((11-methyl-1,4,8,11-tetraazabicyclo[6.6.2]hexadecan-4-yl)methyl)benzyl)amino)-2-oxoethyl)benzoic acid (**55**), (5.1 mg, 7.0 μ mol, 26.9% yield).

UV/vis (H_2O): ($E_{m_{max}}$: 460 nm/ $E_{x_{max}}$: 490 nm). MS (HRMS): m/z cald. (M^+) for $C_{42}H_{48}O_6^+$, 718.3599; found, 718.3578.

9.3.86 Synthesis of 2-(6-hydroxy-3-oxo-3H-xanthen-9-yl)-5-(2-((4-((11-methyl-1,4,8,11-tetraazabicyclo[6.6.2]hexadecan-4-yl)methyl)benzyl)amino)-2-oxoethyl)benzoic acid metal derivatives ([Cu55(OAc)](OAc) and [Zn55(OAc)](OAc))



M = Cu²⁺, Y = AcO⁻, (n = 1); [Cu55(OAc)](OAc)
M = Zn²⁺, Y = AcO⁻, (n = 1/2); [Zn55(OAc)](OAc)

2-(6-Hydroxy-3-oxo-3H-xanthen-9-yl)-5-(2-((4-((11-methyl-1,4,8,11-tetraazabicyclo[6.6.2]hexadecan-4-yl)methyl)benzyl)amino)-2-oxoethyl)benzoic acid copper acetate [Cu55(OAc)](OAc)

Amounts: 1-(4-Aminomethylbenzyl)-8-(methyl)-1,4,8,11-tetraazabicyclo[6.6.2]-hexadecane copper acetate ([Cu15(OAc)](OAc)) (5.83 mg, 10.0 μmol), 5/6-carboxyfluorescein succinimidyl ester (10.22 mg, 20.0 μmol) and anhydrous amine free DMF (1 mL). To yield the yellow solid, 2-(6-hydroxy-3-oxo-3H-xanthen-9-yl)-5-(2-((4-((11-methyl-1,4,8,11-tetraazabicyclo[6.6.2]hexadecan-4-yl)methyl)benzyl)amino)-2-oxoethyl)benzoic acid copper acetate ([Cu55(OAc)](OAc)), (4.5 mg, 5.0 μmol, 46.3% yield).

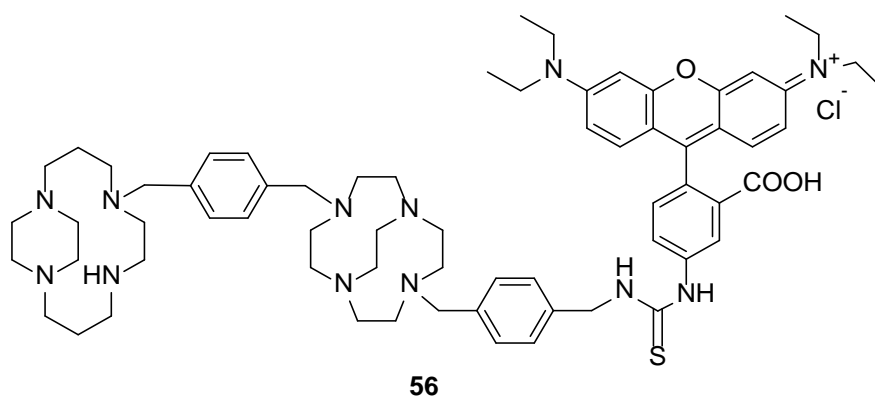
UV/vis (H₂O): (Em_{max}: 455 nm/Ex_{max}: 470 nm). MS (HRMS): *m/z* (M-2CH₂CO₂)²⁺ calcd. for C₄₃H₄₉CuN₅O₆²⁺, 397.1484; found, 397.1521.

(2-(6-Hydroxy-3-oxo-3H-xanthen-9-yl)-5-(2-((4-((11-methyl-1,4,8,11-tetraazabicyclo[6.6.2]hexadecan-4-yl)methyl)benzyl)amino)-2-oxoethyl)benzoic acid zinc acetate ([Zn55(OAc)](OAc))

Amounts: 1-(4-Aminomethylbenzyl)-8-(methyl)-1,4,8,11-tetraazabicyclo[6.6.2]-hexadecane zinc(II) acetate ([Zn55(OAc)](OAc)) (4.89 mg, 10.0 μmol), 5/6-carboxyfluorescein succinimidyl ester (6.41 mg, 10.0 μmol) and anhydrous amine-free DMF (1 mL). To yield the yellow solid, 2-(6-hydroxy-3-oxo-3H-xanthen-9-yl)-5-(2-((4-((11-methyl-1,4,8,11-tetraazabicyclo[6.6.2]hexadecan-4-yl)methyl)benzyl)amino)-2-oxoethyl)benzoic acid copper acetate ([Zn55(OAc)](OAc)), (2.2 mg, 2.2 μmol , 22.6% yield).

UV/vis (H_2O): ($E_{m_{\max}}$: 455 nm/ $E_{x_{\max}}$: 470 nm). MS (ES-MS): m/z 307.4 ($M+\text{Na}+2\text{H}^{3+}$).

9.3.87 Synthesis of N-(9-(4-(3-(4-((10-(4-((1,5,8,12-tetraazabicyclo[10.2.2]hexadecan-5-yl)methyl)benzyl)-1,4,7,10-tetraazabicyclo[5.5.2]tetradecan-4-yl)methyl)benzyl)thioureido)-2-carboxyphenyl)-6-(diethylamino)-3H-xanthen-3-ylidene)-N-ethylethanaminium chloride (**56**)



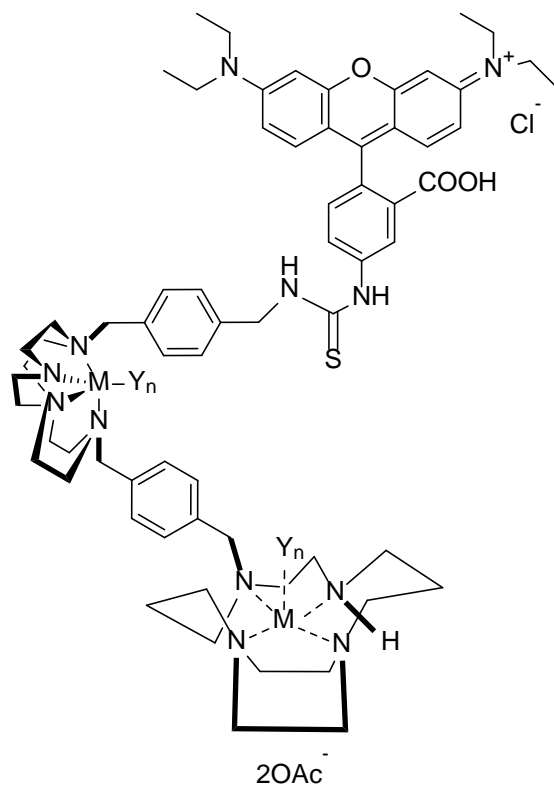
General method O was followed.

N-(9-(4-(3-(4-((10-(4-((1,5,8,12- | Tetraazabicyclo[10.2.2]hexadecan-5-yl)methyl)benzyl)-1,4,7,10-tetraazabicyclo[5.5.2]tetradecan-4-yl)methyl)benzyl)thioureido)-2-carboxyphenyl)-6-(diethylamino)-3H-xanthen-3-ylidene)-N-ethylethanaminium chloride (56**)**

Amounts: 1-(4-(Aminomethyl)benzyl)-7-(4-((1,4,8,11-tetraazabicyclo[10.2.2]hexadecane)methyl)benzyl)-1,4,7,10-tetraazabicyclo[5.5.2]dodecane (**24**) (23.9 mg, 40.0 μmol), rhodamine B isothiocyanate (21.8 mg, 40.0 μmol) and anhydrous amine-free DMF (1 mL). To yield the pink solid, N-(9-(4-(3-(4-((10-(4-((1,5,8,12-tetraazabicyclo[10.2.2]hexadecan-5-yl)methyl)benzyl)-1,4,7,10-tetraazabicyclo[5.5.2]tetradecan-4-yl)methyl)benzyl)thioureido)-2-carboxyphenyl)-6-(diethylamino)-3H-xanthen-3-ylidene)-N-ethylethanaminium chloride (**56**), (35.0 mg, 32.0 μmol , 80.1% yield).

UV/vis (H_2O): ($E_{m_{\max}}$: 545 nm/ $E_{x_{\max}}$: 559 nm). MS (HRMS): m/z . ($M-\text{Cl}^+$) calcd. for $\text{C}_{67}\text{H}_{95}\text{N}_{12}\text{O}_3\text{S}^+$, 1145.7209; found, 1145.7239.

9.3.88 Synthesis of N-(9-(4-(3-(4-((10-(4-((1,5,8,12-tetraazabicyclo[10.2.2]hexadecan-5-yl)methyl)benzyl)-1,4,7,10-tetraazabicyclo[5.5.2]tetradecan-4-yl)methyl)benzyl)thioureido)-2-carboxyphenyl)-6-(diethylamino)-3H-xanthen-3-ylidene)-N-ethylethanaminium chloride metal derivatives ($[\text{Cu}_2\mathbf{56}(\text{OAc})_2](\text{OAc})_2$ and $[\text{Zn}_2\mathbf{56}(\text{OAc})_2](\text{OAc})_2$)



$M = \text{Cu}^{2+}, Y = \text{AcO}^-$, ($n = 1$); $[\text{Cu}\mathbf{56}(\text{OAc})_2](\text{OAc})_2$
 $M = \text{Zn}^{2+}, Y = \text{AcO}^-$, ($n = 1/2$); $[\text{Zn}\mathbf{56}(\text{OAc})_2](\text{OAc})_2$

General method O was followed.

(N-(9-(4-(3-(4-((10-(4-((1,5,8,12-Tetraazabicyclo[10.2.2]hexadecan-5-yl)methyl)benzyl)-1,4,7,10-tetraazabicyclo[5.5.2]tetradecan-4-yl)methyl)benzyl)thioureido)-2-carboxyphenyl)-6-(diethylamino)-3H-xanthen-3-ylidene)-N-ethylethanaminium chloride copper(II) acetate ($[\text{Cu}_2\mathbf{56}(\text{OAc})_2](\text{OAc})_2$)

Amounts: 1-(4-(Aminomethyl)benzyl)-7-(4-((1,4,8,11-tetraazabicyclo[10.2.2]hexadecane)methyl)benzyl)-1,4,7,10-tetraazabicyclo[5.5.2]dodecane copper acetate ($[\text{Cu}_2\mathbf{24}(\text{OAc})_2](\text{OAc})_2$) (5.21 mg, 10.0 μmol), rhodamine B isothiocyanate (4.32 mg, 10.0 μmol) and anhydrous amine-free DMF (1 mL). To yield the pink solid, (N-(9-(4-(3-(4-((10-(4-

((1,5,8,12-tetraazabicyclo[10.2.2]hexadecan-5-yl)methyl)benzyl)-1,4,7,10-tetraazabicyclo[5.5.2]tetradecan-4-yl)methyl)benzyl)thioureido)-2-carboxyphenyl)-6-(diethylamino)-3H-xanthen-3-ylidene)-N-ethylethanaminium chloride copper acetate ([Cu₂56(OAc)₂](OAc)₂), (9.1 mg, 6.0 μmol, 76.0% yield).

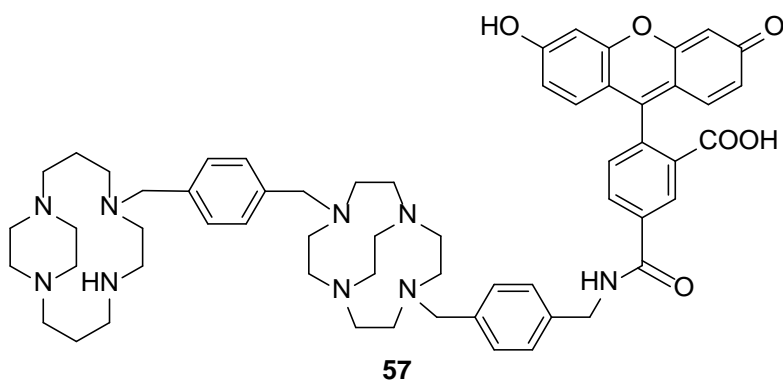
UV/vis (H₂O): (Em_{max}: 545 nm/Ex_{max}: 570 nm). MS (ES-MS): *m/z* 742.6 (M-CH₂CO₂).

(N-(9-(4-(3-(4-((10-(4-((1,5,8,12-Tetraazabicyclo[10.2.2]hexadecan-5-yl)methyl)benzyl)-1,4,7,10-tetraazabicyclo[5.5.2]tetradecan-4-yl)methyl)benzyl)thioureido)-2-carboxyphenyl)-6-(diethylamino)-3H-xanthen-3-ylidene)-N-ethylethanaminium chloride zinc(II) acetate ([Zn₂56(OAc)₂](OAc)₂)

Amounts: 1-(4-(Aminomethyl)benzyl)-7-(4-((1,4,8,11-tetraazabicyclo[10.2.2]hexadecane)methyl)benzyl)-1,4,7,10-tetraazabicyclo[5.5.2]dodecane zinc(II) acetate ([Zn₂24(OAc)₂](OAc)₂) (7.69 mg, 10.0 μmol), rhodamine B isothiocyanate (6.38 mg, 10.0 μmol) and anhydrous amine-free DMF (1 mL). To yield the pink solid, (N-(9-(4-(3-(4-((10-(4-((1,5,8,12-tetraazabicyclo[10.2.2]hexadecan-5-yl)methyl)benzyl)-1,4,7,10-tetraazabicyclo[5.5.2]tetradecan-4-yl)methyl)benzyl)thioureido)-2-carboxyphenyl)-6-(diethylamino)-3H-xanthen-3-ylidene)-N-ethylethanaminium chloride copper acetate ([Zn₂56(OAc)₂](OAc)₂), (2.6 mg, 1.7 μmol, 14.2% yield).

UV/vis (H₂O): (Em_{max}: 545 nm/Ex_{max}: 570 nm). MS (ES-MS, run with formic acid): *m/z* 295.9 (M-2CH₂CO₂-Cl+H).

9.3.89 Synthesis of 5-((4-((10-(4-((1,5,8,12-tetraazabicyclo[10.2.2]hexadecan-5-yl)methyl)benzyl)-1,4,7,10-tetraazabicyclo[5.5.2]tetradecan-4-yl)methyl)benzyl)carbamoyl)-2-(6-hydroxy-3-oxo-3H-xanthen-9-yl)benzoic acid (**57**)



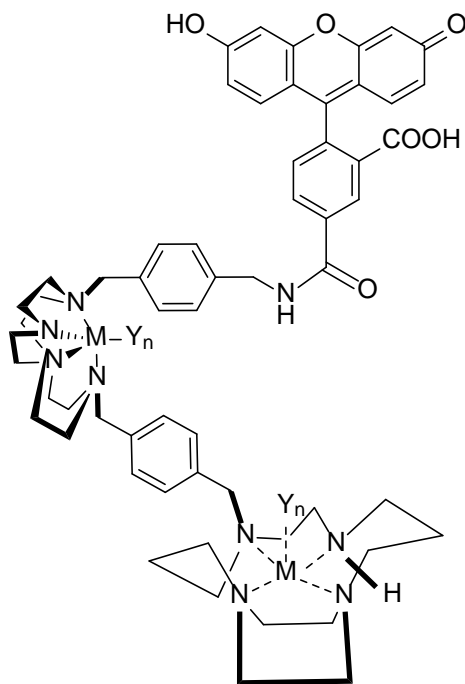
General method O was followed.

5-((4-((10-(4-((1,5,8,12-Tetraazabicyclo[10.2.2]hexadecan-5-yl)methyl)benzyl)-1,4,7,10-tetraazabicyclo[5.5.2]tetradecan-4-yl)methyl)benzyl)carbamoyl)-2-(6-hydroxy-3-oxo-3H-xanthen-9-yl)benzoic acid (57**)**

Amounts: 1-(4-(Aminomethyl)benzyl)-7-(4-((1,4,8,11-tetraazabicyclo[10.2.2]hexadecane)methyl)benzyl)-1,4,7,10-tetraazabicyclo[5.5.2]dodecane (**24**) (68.7 mg, 0.110 mmol), 5/6-carboxyfluorescein succinimidyl ester (50.37 mg, 0.110 mmol) and anhydrous amine-free DMF (1 mL). To yield the yellow solid, 5-((4-((10-(4-((1,5,8,12-tetraazabicyclo[10.2.2]hexadecan-6-yl)methyl)benzyl)-1,4,7,10-tetraazabicyclo[5.5.2]tetradecan-4-yl)methyl)benzyl)carbamoyl)-2-(6-hydroxy-3-oxo-3H-xanthen-9-yl)benzoic acid (**57**), (25.3 mg, 21.4 μ mol, 20.1% yield).

UV/vis (H₂O): (Em_{max}: 495 nm/Ex_{max}: 526 nm). MS (ES-MS): *m/z* 1005.6 (M⁺).

9.3.90 Synthesis of 5-((4-((10-(4-((1,5,8,12-tetraazabicyclo[10.2.2]hexadecan-5-yl)methyl)benzyl)-1,4,7,10-tetraazabicyclo[5.5.2]tetradecan-4-yl)methyl)benzyl)carbamoyl)-2-(6-hydroxy-3-oxo-3H-xanthen-9-yl)benzoic acid metal derivatives ($[\text{Cu}_2\mathbf{57}(\text{OAc})_2](\text{OAc})_2$ and $[\text{Zn}_2\mathbf{57}(\text{OAc})_2](\text{OAc})_2$)



2OAc⁻

M = Cu²⁺, Y = AcO⁻, (n = 1); $[\text{Cu}\mathbf{57}(\text{OAc})_2](\text{OAc})_2$
M = Zn²⁺, Y = AcO⁻, (n = 1/2); $[\text{Zn}\mathbf{57}(\text{OAc})_2](\text{OAc})_2$

General method O was followed.

5-((4-((10-(4-((1,5,8,12-tetraazabicyclo[10.2.2]hexadecan-5-yl)methyl)benzyl)-1,4,7,10-tetraazabicyclo[5.5.2]tetradecan-4-yl)methyl)benzyl)carbamoyl)-2-(6-hydroxy-3-oxo-3H-xanthen-9-yl)benzoic acid copper acetate ($[\text{Cu}_2\mathbf{57}(\text{OAc})_2](\text{OAc})_2$)

Amounts: 1-(4-(Aminomethyl)benzyl)-7-(4-((1,4,8,11-tetraazabicyclo[10.2.2]hexadecane)methyl)benzyl)-1,4,7,10-tetraazabicyclo[5.5.2]dodecane copper acetate ($[\text{Cu}_2\mathbf{24}(\text{OAc})_2](\text{OAc})_2$) (8.03 mg, 10.0 μmol), 5/6-carboxyfluorescein succinimidyl ester (3.78 mg, 10.0 μmol) and anhydrous amine-free DMF (1 mL). To yield the yellow solid, 5-((4-((10-(4-((1,5,8,12-tetraazabicyclo[10.2.2]hexadecan-5-yl)methyl)benzyl)-1,4,7,10-

tetraazabicyclo[5.5.2]tetradecan-4-yl)methyl)benzyl)carbamoyl)-2-(6-hydroxy-3-oxo-3H-xanthen-9-yl)benzoic acid copper acetate ($[\text{Cu}_2\mathbf{57}(\text{OAc})_2](\text{OAc})_2$), (1.9 mg, 1.4 μmol , 17.4% yield).

UV/vis (H_2O): ($E_{m_{\max}}$: 495 nm/ $E_{x_{\max}}$: 525 nm). MS (ES-MS): m/z 676.7 ($\text{M}+\text{H}+\text{CH}_3\text{CH}_2\text{OH}-2\text{CH}_2\text{CO}_2$).

5-((4-((10-(4-((1,5,8,12-Tetraazabicyclo[10.2.2]hexadecan-5-yl)methyl)benzyl)-1,4,7,10-tetraazabicyclo[5.5.2]tetradecan-4-yl)methyl)benzyl)carbamoyl)-2-(6-hydroxy-3-oxo-3H-xanthen-9-yl)benzoic acid zinc acetate ($[\text{Zn}_2\mathbf{57}(\text{OAc})_2](\text{OAc})_2$)

Amounts: 1-(4-(Aminomethyl)benzyl)-7-(4-((1,4,8,11-tetraazabicyclo[10.2.2]hexadecane)methyl)benzyl)-1,4,7,10-tetraazabicyclo[5.5.2]dodecane zinc(II) acetate ($[\text{Cu}_2\mathbf{24}(\text{OAc})_2](\text{OAc})_2$) (11.4 mg, 10.0 μmol), 5/6-carboxyfluorescein succinimidyl ester (5.34 mg, 10.0 μmol) and anhydrous amine-free DMF (1 mL). To yield the yellow solid, 5-((4-((10-(4-((1,5,8,12-tetraazabicyclo[10.2.2]hexadecan-5-yl)methyl)benzyl)-1,4,7,10-tetraazabicyclo[5.5.2]tetradecan-4-yl)methyl)benzyl)carbamoyl)-2-(6-hydroxy-3-oxo-3H-xanthen-9-yl)benzoic acid zinc acetate ($[\text{Cu}_2\mathbf{24}(\text{OAc})_2](\text{OAc})_2$) (1.5 mg, 0.1 μmol , 9.7% yield).

UV/vis (H_2O): ($E_{m_{\max}}$: 495 nm/ $E_{x_{\max}}$: 525 nm). MS (ES-MS): m/z 534.6 ($\text{M}-\text{Zn}-4\text{CH}_2\text{CO}_2$).

9.4 Peptide synthesis

9.4.1 Stages of peptide synthesis

The peptide synthesis procedure reported herein has been modified from that reported by Wester and co-workers in synthesising Pentixafor.¹⁷⁰

9.4.1.1 Swelling of TCP-Resin

Peptide synthesis was carried out using Fmoc-Gly-2-Cl-Trt Resin, 100-200 Mesh (0.54 mmol/g) which has swollen in anhydrous dichloromethane (0.8 mL/g resin) followed by anhydrous DMF (0.8 mL/g resin) at room temperature for 1 h, respectively.

9.4.1.2 Orn-Resin Fmoc Deprotection

The resin-bound Fmoc peptide was treated with 20% piperidine in DMF (v/v) for 1 minutes and a second time for 5 minutes. The resin was washed 5 times with DMF.

9.4.1.3 HBTU Coupling

A solution of Fmoc-Xaa-OH (4 eq.), HBTU (4 eq.), DIPEA (4 eq.) in DMF (1 mL/g resin) was added to the resin-bound free amine peptide and shaken for 45 min at room temperature and washed 5 times with DMF.

9.4.1.4 o-NBS Protection

A solution of o-NBS-Cl (4 eq.) and collidine (10 eq.) in NMP (1 mL/g resin) was added to the resin-bound free amine peptide and shaken for 15 min at room temperature. The resin was washed once with NMP and reaction repeated for another 15 min using fresh reagents.

9.4.1.5 N-Methylation

A solution of DBU (3 eq.) in NMP was added to the resin-bound o-Ns protected peptides and shaken for 3 mins followed by addition of dimethylsulfate (10. eq) NMP solution followed by 2 min shaking. The resin was washed once with NMP and N-methylation was repeated twice.

9.4.1.6 On-Resin o-NBSs Deprotection

For o-NBSs deprotection, the resin-bound o-Ns-peptides were stirred in a solution of mercaptoethanol (10 eq.) and DBU (5 eq.) in NMP (1 mL/g resin) for 5 minutes. The deprotection procedure was repeated twice and the resin was washed 5 times with NMP.

9.4.1.7 HATU Coupling

A solution of Fmoc-Xaa-OH (4 eq.), HATU (4 eq.) DIEPA (6 eq.) in DMF (4 mL/g resin) was added to the resin-bound N-methylamine peptides and shaken for an hour at room temperature. This step was repeated a second time before finally being washed 5 times with NMP.

9.4.1.8 Alloc Deprotection

Pd(PPh₃)₄ (0.3 eq.) in dry degassed dichloromethane (6 mL/g resin) was added to the resin-bound Alloc peptide followed by an addition of phenylsilane in dry dichloromethane (6 mL/g resin) and shaken for 1 hour in the dark. The resin was washed 5 times with dichloromethane.

9.4.1.9 Peptide Cleavage

For complete cleavage from the resin the peptides were treated three times with a solution of dichloromethane and HFIP (4:1; v:v 20%) at room temperature for an hour. This step was repeated a second time before the solvent evaporated under reduced pressure.

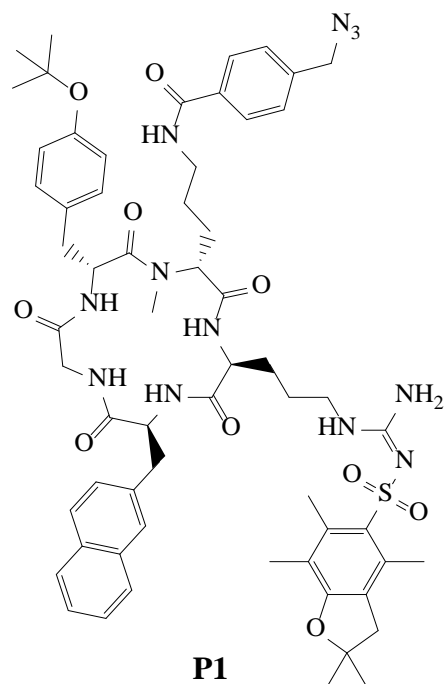
9.4.1.10 Cyclisation

Peptide and NaHCO₃ (10 eq.) DPPA (6 eq.) DMF (20 mL) was added at room temperature and stirred overnight. The solvent was evaporated under reduced pressure. The peptide was taken up in dichloromethane and extracted with water before being reduced under reduced pressure.

9.4.1.11 Side chain deprotection

To deprotect Tyrosine and Arginine residues' side chains, the cyclised peptide was treated for 2 h with 95% TFA solution complemented with 2.5% of water and 2.5% of triethylsilane. At the end, the solution was reduced under vacuum and deprotected peptide was precipitated as TFA salt upon addition of diethyl ether. The solution was spun down, washed (3 x diethyl ether) before being air dried.

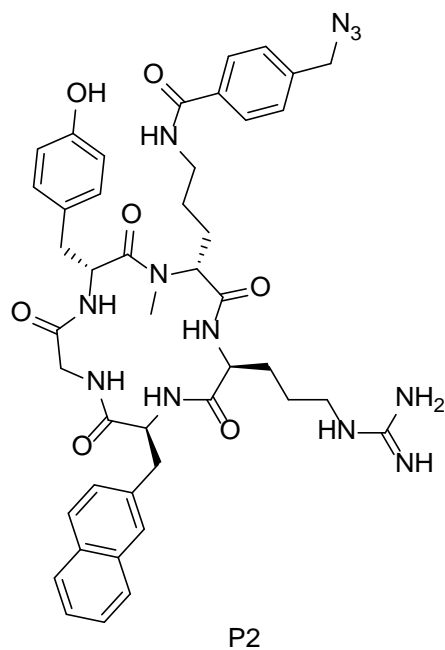
9.4.2 Synthesis of protected CPCr4.2 AzMBA, (**P1**)



Solid phase peptide synthesis (SPPS) was used to build cyclo (D-Tyr-D-[NMe]Orn-Arg-Nal-Gly) cyclic peptides functionalised on ϵ -Ornithine amine with an aromatic azide. The procedure outlined in section 9.4.1.1-9.4.1.7 was followed. The reaction was reduced *in vacuo*, before being taken up in water and lyophilised to give CPCr4.2 AzMBA (**P1**).

ES-MS (m/z): $[M+H]^+$ calcd. for $C_{61}H_{77}N_{12}O_{10}S^+$ = 1169.64.

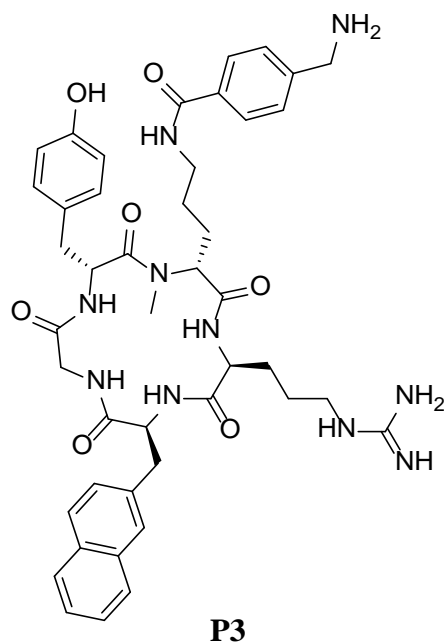
9.4.3 Synthesis of deprotected CPCr4.2-AzMBA, (**P2**)



Deprotection was performed as stated in section 9.4.1.8. The reaction was reduced *in vacuo*, before being taken up in water and lyophilised to give deprotected CPCr4.2-AzMBA, (**P2**).

HRMS (m/z): [M+H]⁺ calcd. for C₄₄H₅₃N₁₂O₇⁺, 861.4155; found, 861.4154.

9.4.4 Synthesis of CPR4.2-AMBA, (P3)

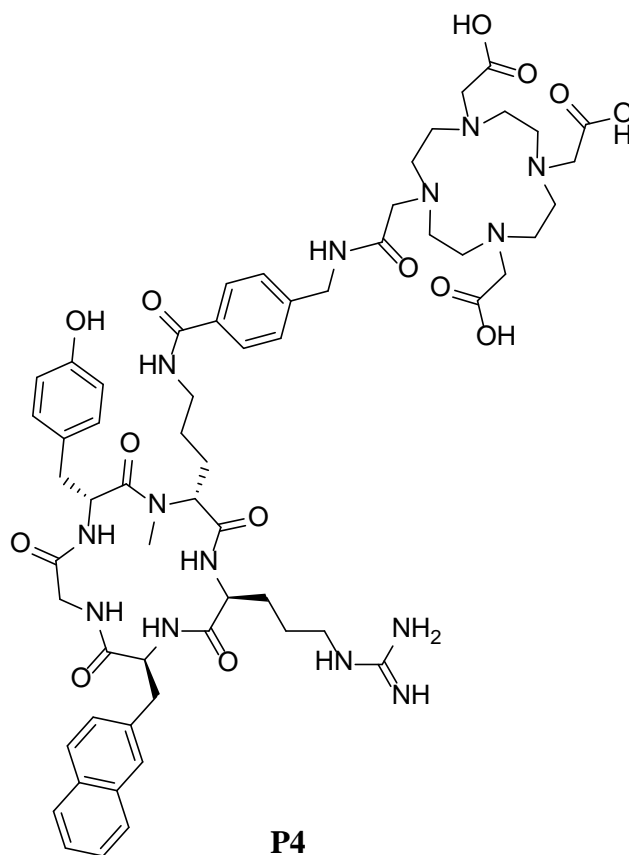


Synthesising using modified procedure reported by Wester and co-workers in synthesising Pentixafor.¹⁷⁰

Solid phase peptide synthesis (SPPS) will be used to build cyclo (D-Tyr-D-[NMe]Orn-Arg-Nal-Gly) cyclic peptides functionalised on ϵ -Ornithine amine with an aromatic acid. The procedure outlined in section 7.4.1.1-7.4.1.7. The reaction was reduced *in vacuo*, before being taken up in water and lyophilised to give CPR4.2-AMBA, (P3).

Purified using semi-preparative HPLC System 15 (Section 9.2.2.15) (single peak, t_r = 18:10 min). HRMS (m/z): [M+H]⁺ calcd. for C₄₄H₅₅N₁₀O₇⁺, 835.4250; found, 835.4251.

9.4.5 Synthesis of CPCR4.2-AMBA-DOTA, (**P4**)

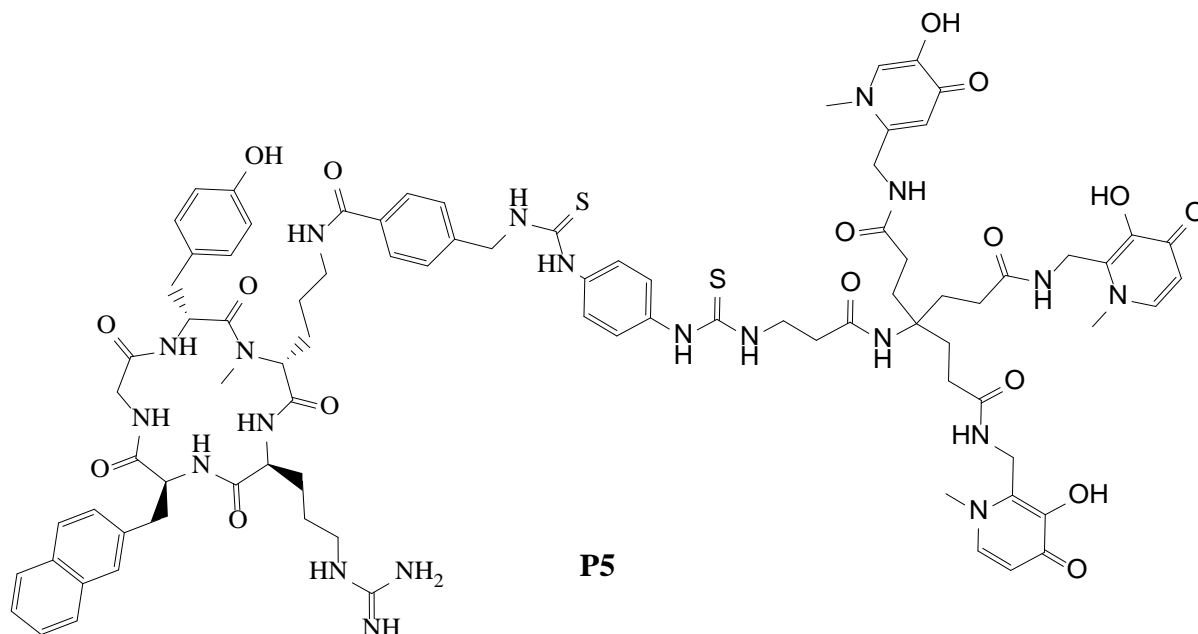


Synthesising using modified procedure reported by Wester and co-workers in synthesising Pentixafor.¹⁷⁰

CPCR4.2-AMBA **P3** (20.0 mg, 20.0 μmol) was dissolved in dry amine-free DMF (200 μL) and combined with 1,4,7,10-Tetraazacyclododecane-1,4,7,10-tetracarboxylic acid mono-N-hydroxysuccinimide ester (21.9 mg, 30.0 μmol) and triethylamine (3.34 μL , 20.0 μmol) in dry amine-free DMF (100 μL). The reaction was shaken for 18 hours at 500 RPM at room temperature. The reaction was reduced *in vacuo*, before being taken up in water and lyophilised to give CPCR4.2-AMBA-DOTA, **P4** (20.0 mg, 16.4 μmol , 68.4% yield).

Purified using semi-preparative HPLC system 16 (Section 9.2.2.16) (single peak, $t_r = 10:40$ min). ES-MS (m/z): $[\text{M}+2\text{H}]^{2+}$ calcd. for $\text{C}_{60}\text{H}_{82}\text{N}_{14}\text{O}_{14}^{2+} = 611.4$.

9.4.7 Synthesis of CPCr4.2-AMBA conjugated with tris(hydroxypyridinone)-phenyl isothiocyanate (P5)



Method 1

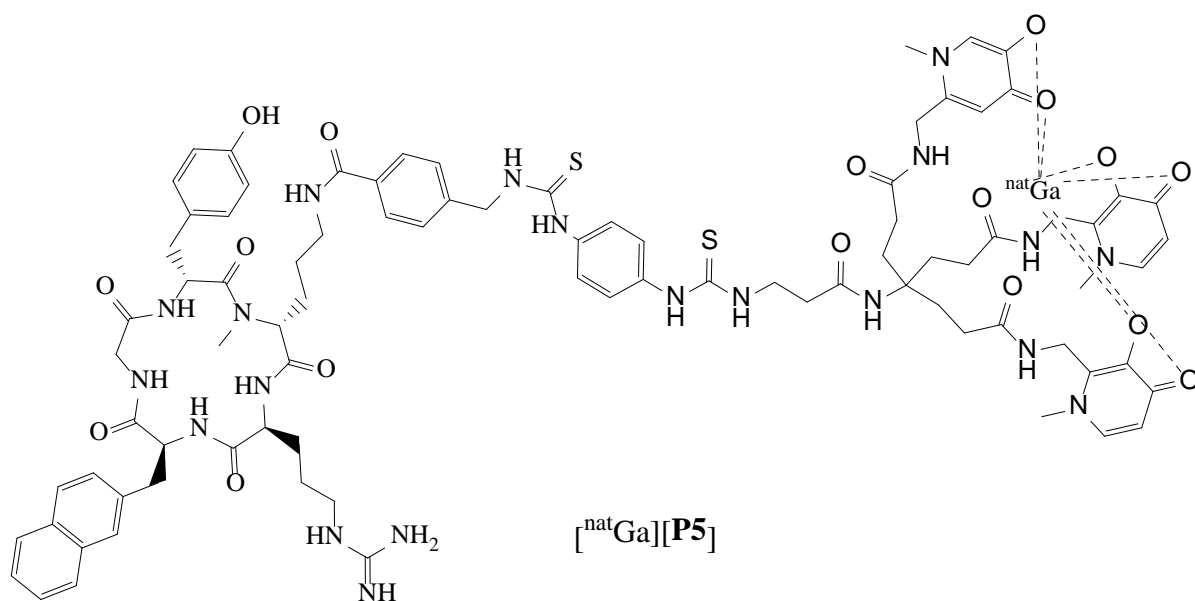
CPCr4.2-AMBA (**P3**) (2.91 mg, 2.7 μmol) was dissolved in dimethyl sulfoxide (200 μL) and added to a solution of tris(hydroxypyridinone)-phenyl isothiocyanate, **41**, (2.5 mg, 2.7 μmol) in dimethyl sulfoxide (100 μL), and diisopropylethylamine (2.43 μL , 13.7 μmol) was added. The reaction solutions were heated in a microwave (120°C, 300 W, 30 min) and then applied to a reverse-phase HPLC column. The resulting mixture was lyophilised and purification attempted on semi-prep HPLC. The desired product was not isolated using this synthetic procedure.

Method 2 – preferred approach

Reaction carried out as above.

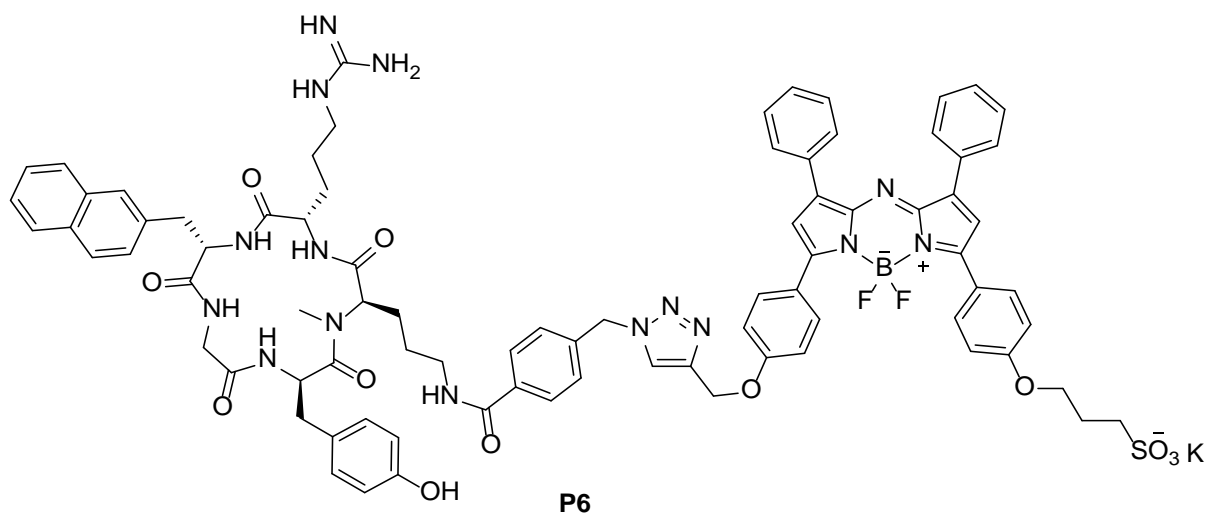
Semi preparative HPLC used to obtain a pure product using (Section 9.2.2.22) (single peak, $t_r = 10:30$ min). ES-MS (m/z): $[M+\text{Na}]^{2+}$ calcd for $\text{C}_{89}\text{H}_{104}\text{N}_{20}\text{O}_{17}\text{Na}_2\text{S}_2^{2+} = 899.0$.

9.4.8 Complexation of P5 with gallium(III) nitrate



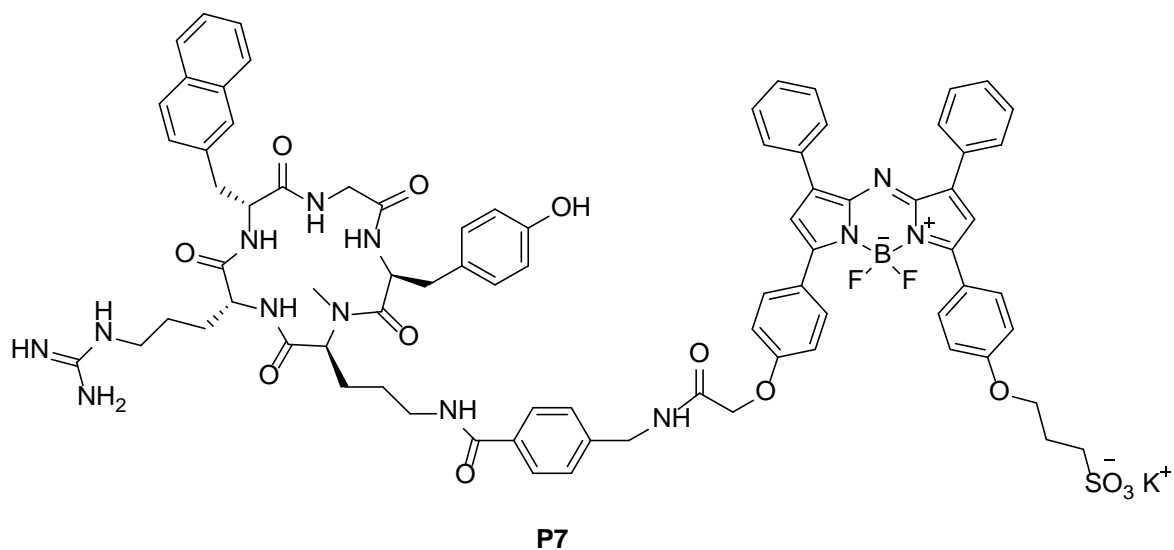
Semi preparative HPLC used to obtain a pure product using system 22 (Section 9.2.2.22) (single peak, $t_r = 8:54$ min). ES-MS (m/z): $[\text{M}+2\text{H}]^{2+}$ calcd for $\text{C}_{89}\text{H}_{134}\text{N}_{20}\text{GaO}_{17}\text{S}_2^{2+} = 910.5$

9.4.9 Attempted synthesis of CPCr4.2-AzMBA conjugated BODIPY (**P6**)



CPCr4.2-AzMBA (**P2**) (9.48 mg, 10.0 μmol) and aza-BODIPY (8.00 mg, 11.0 μmol , provided by Ms. Miffy Cheng) were dissolved in anhydrous amine-free DMF and *t*-butanol (2:1 ratio). In addition copper (II) sulfate pentahydrate (0.7 mg, 2.48 μmol), sodium ascorbate (3.43 mg, 18.0 mmol) and tris (3-hydroxypropyltriazolylmethyl)amine (1.07 mg, 2.48 μmol) were dissolved in water (0.25 mL) and added to the reaction vial. The mixture was stirred at RT for 18 hours. The resulting mixture was lyophilised and purification attempted on semi-prep HPLC. The desired product was not isolated using this synthetic procedure.

9.4.10 Synthesis of CPCr4.2-AMBA conjugated BODIPY (**P7**)



CPCr4.2-AMBA (**P3**) (5.58 mg, 5.2 μmol) and aza-BODIPY (4.16 mg, 5.8 μmol , provided by Ms. Miffy Cheng) were combined with 2-(1H-benzotriazol-1-yl)-1,1,3,3-tetramethyluronium hexafluorophosphate (HBTU) (2.39 mg, 6.3 μmol) and triethylamine (4.39 μL , 31.5 μmol) in amine-free DMF (0.5 mL) resulting in a dark blue solution. The reaction was shaken (550 RPM) at room temperature for 16 hours. The reaction was then diluted with water (20 mL). The obtained aqueous solution containing the product was flushed through a preconditioned C18 cartridge. A fraction was eluted off the cartridge using 10 mL solution of 80% acetonitrile: 20% water. A second fraction was collected using 10 mL of acetonitrile. TLC and analytical HPLC was used to identify the correct fractions which were combined and lyophilised to yield CPCr4.2-AMBA-BODIPY (**P7**) (6.3 mg, 4.1 μmol , 77.5% yield).

TLC conditions; RP silica eluted with 1:1:8 $\text{KNO}_3(aq.)\text{:H}_2\text{O:MeCN}$. Analytical RP-HPLC System N (Section 7.2.1.13) (single peak, $t_r = 08:35$ min). Initial purification achieved with RP semi preparative using system 17 (Section 9.2.2.17) (single peak, $t_r = 11:46$ min). ES-MS (m/z): $[\text{M}+\text{H}]^+$ calcd for $\text{C}_{81}\text{H}_{83}\text{BF}_2\text{KN}_{13}\text{O}_{13}\text{S}^+$, = 1566.6.

9.5 Radiolabelling conditions

9.5.1 Radiolabelling with copper-64

9.5.1.1 Standard optimised method for radiolabelling with copper-64

[⁶⁴Cu]chloride (1.64-2.2 GBq, ~250 μL) upon arrival is in an extremely acidic state, the solution is brought to a neutral pH range (6-8) by the addition of sodium hydroxide solutions of varying concentrations (0.1 - 10 M). If the solution becomes too basic the pH is adjusted by the addition of small amounts of hydrochloric acid solution (0.1 - 1 M). An equal volume of 0.4 M sodium acetate (pH 5.5) is added to the activity and heated at 60°C for 15 minutes.

9.5.1.2 Radiolabelling conditions for [⁶⁴Cu][Cu₅(OAc)](OAc)

A portion of the [⁶⁴Cu]acetate stock (60-120 μL, 100-560 MBq) is combined with the required amount of 1,4-bis((11-methyl-1,4,8,11-tetraazabicyclo[6.6.2]hexadecan-4-yl)methyl)benzene (**5**) (1 mg/1 mL, 0.4 M sodium acetate, pH 5.5) in a 1 mL glass vial. The reaction is shaken (500 RPM) and heated at 90°C for 15 mins. Radio-TLC (neutral alumina, eluting in MeOH:H₂O; 95:5 with excess NaCl) is taken after the reaction is allowed to cool for 5 mins to monitor the progress of the reaction. If the reaction has not gone to completion the reaction can be heated for an additional 15 mins. [⁶⁴Cu₅] was purified by semi-preparative HPLC (Section 7.5.5). The major product peak was collected and concentrated by heating and the flow of argon and the addition of ethanol. The final product was then formulated in PBS, sterile filtered, and used for *in vitro* and *in vivo* experiments.

9.5.1.3 Radiolabelling conditions for [⁶⁴Cu][Cu₂5(OAc)₂](OAc)₂

To form [⁶⁴Cu₅(OAc)](OAc) a known amount of the purified [⁶⁴Cu][Cu₂5(OAc)₂](OAc)₂ was combined with ~ 10 μL of a 10 mg/mL solution of copper(II) acetate into a 1 mL glass vial. The reaction was shaken (500 RPM) and heated at 90°C for 60+ minutes. The reaction was allowed to cool before formulated in PBS, sterile filtered, and used for *in vitro* and *in vivo* experiments.

9.5.1.4 Radiolabelling conditions for [⁶⁴Cu**8**(OAc)](OAc)

An adapted procedure reported by Nimmagadda *et al.* was used to label AMD3100.¹⁸⁹ 50 µL of a 1 mg/mL solution of 1,1'-(1,4-phenylenebis(methylene))bis-1,4,8,11-tetraazacyclotetradecane octahydrochloride (**8**) was added to ~ 100 MBq of [⁶⁴Cu]acetate buffered with 25 µL of 0.4 M sodium acetate (pH 5.5) in a 1 mL glass vial. The reaction was heated at 60°C for 15 minutes. Radio-TLC (RP silica eluted with 6% w/v EDTA in H₂O) confirmed 100% conversion with complexation shown on the baseline. [⁶⁴Cu**8**(OAc)](OAc) was purified via semi-preparative HPLC (Section 7.5.5). The major product peak was collected and concentrated by heating and the flow of argon and the addition of ethanol. The final product was then formulated in PBS, sterile filtered, and used for *in vitro* and *in vivo* experiments.

9.5.1.5 Radiolabelling conditions for [⁶⁴Cu**9**(OAc)](OAc)

50 µL of a 1 mg/mL of AMD3465 was added to ~ 100 MBq of [⁶⁴Cu]acetate buffered with 25 µL of 0.4 M sodium acetate (pH 5.5) and heated at 60°C for 15 minutes. RadioTLC (RP silica eluted with 6% w/v EDTA in H₂O) was used to monitor the reaction. [⁶⁴Cu**9**(OAc)](OAc) purified via semi-preparative HPLC (Section 7.5.5). The major product peak was collected and concentrated by heating and the flow of argon and the addition of ethanol. The final product was then formulated in PBS, sterile filtered, and used for *in vitro* and *in vivo* experiments.

9.5.2 Radiolabelling with gallium-68

9.5.2.1 Processing of gallium-68

A ⁶⁸Ge/⁶⁸Ga generator (IDB Holland BV/ iThemba, South Africa) was eluted with 3 mL of 0.6 M aq. HCl solution and diluted by a factor of 5. The activity (200-1800 MBq) was loaded onto a Pheomenex Strata X-C solid-phase extraction cartridge. The cartridge was washed with a solution consisting of acetone: 0.1 M HCl (80:20; 1 mL) as washing which is then discarded, before being eluted with a solution of acetone: 0.1 M HCl (98:2, 1 mL) into a 1 mL glass vial. The activity was then dried to completeness by air flow at 90°C for 5 minutes before being re-suspended in the chosen buffer.

9.5.2.2 Radiolabelling conditions for **P4**

The processing of the activity is carried out as described in section 9.5.2.1. The peptide CPCr4.2-AMBA-DOTA (**P4**) (20-25 µg, 10 nmol) was re-suspended in methanol (20 µL) and HEPES buffer (0.1 M, 4-(2-hydroxyethyl)-1-piperazineethanesulfonic acid, pH 3.5, 180 µL). The peptide solution was then combined to a vial containing the dried gallium-68 (100-400 MBq). The reaction was heated

and stirred (550 RPM) for 10 min at 95°C. The reaction is then left to cool for 5 mins, before a radio-TLC (RP silica eluted with 0.1 M sodium citrate buffer) is taken to determine reactions progress. If the reaction is high yielding, the majority of the activity remains on the baseline. If the yield is looking low (>50% conversion) the reaction can be heated at 95°C for a further 5 mins. [⁶⁸Ga][Ga**P4**] purified via semi-preparative HPLC (Section 9.5.5). The major product peak was collected and concentrated by heating and the flow of argon and the addition of ethanol. The final product was then formulated in PBS, sterile filtered, and used for *in vitro* and *in vivo* experiments.

9.5.2.3 Standard optimised method for radiolabelling with gallium-68

The processing of the activity is carried out as described in Section 9.5.2.1. The compound of known concentration was dissolved in 0.2 M sodium acetate buffer (pH 4.6) (50-100 µL). The solution is then transferred into a champagne vial (1.5 mL) containing an aliquoted amount of known activity. The reaction volume should not exceed 200 µL and remain at pH 4.6. Approximately the activity in a labelling test experiment was typically 5-30 MBq. For *in vivo* and *in vitro* experiments typically between 100 – 1800 MBq of activity was used. The reaction was stirred (550 RPM) and heated for the desired duration as stated in Table 29. The reaction is then left to cool for 5 mins, before a radio-TLC (RP silica eluted with 0.1 M sodium citrate buffer) is taken to determine reactions progress. Depending on the experiment further method development, purification, characterisation and formulation could then be completed. Section 9.5.5 details the purification methods used.

9.5.2.4 Radiolabelling of pretargeted compound **35**

The processing of the activity is carried out as described in section 9.5.2.1. Compound **35** of known concentration was dissolved in 0.2 M sodium acetate buffer (pH 4.6) (100 µL). The solution is then transferred into a champagne vial (1.5 mL) containing an aliquoted amount of known activity (~ 200 MBq). The reaction was heated and stirred at 60°C, 550 RPM for 40 min. The reaction is then left to cool for 5 mins, before a radio-TLC (RP silica eluted with 0.1 M sodium citrate buffer) is taken to determine reactions progress. [⁶⁸Ga][Ga**35**] was then combined to a 1:1 ratio of antagonist **36** dissolved in in 0.2 M sodium acetate buffer (pH 4.6) (100 µL). The reaction was left for 5 min at 37.5°C, before being re-analysed by radio-HPLC and TLC.

9.5.2.5 Radiolabelling conditions for **P5**

The processing of the activity is carried out as described in Section 9.5.2.1. Peptide **P5** (25 µg) was dissolved in 200 µL of 50:50 v/v EtOH/deionised water solution. 100 µL of that solution was

combined with the dried ^{68}Ga activity followed by 100 μL of 0.2 M sodium acetate solution (pH 6-7). After 5 mins of the reaction shaking at 500 RPM at 95°C , the reaction is then left to cool for 5 mins, before a radio-TLC (RP silica eluted with 0.1 M sodium citrate buffer) is taken to determine reactions progress. [^{68}Ga][GaP5] purified via semi-preparative HPLC (Section 9.5.23). The major product peak was collected and concentrated by heating and the flow of argon and the addition of ethanol. The final product was then formulated in PBS, sterile filtered, and used for *in vitro* and *in vivo* experiments.

9.5.3 Radiolabelling with fluorine-18

9.5.3.1 Preparation of fluorine-18

The [^{18}F]fluoride (non-carrier added) received from the cyclotron was trapped on a preconditioned anion-exchange (QMA) cartridge. The cartridge was subsequently washed with metal-free water (10-15 mL) before the [^{18}F]fluoride (0.5-1.1 GBq) was eluted using 0.4 M KHCO_3 solution (0.2 mL) into a HPLC vial.

9.5.3.2 Standard optimised method for radiolabelling with [^{18}F]Al complex

The pH of the stock [^{18}F]fluoride solution was adjusted to *ca.* 4 using metal free glacial acetic acid (15-20 μL). An aliquot of this [^{18}F]fluoride stock (5-100 MBq) was combined with 2 mM AlCl_3 solution (3-25 μL , 0.1 M sodium acetate buffer, pH 4) as well as the antagonists of a known concentration (in 25 μL , 0.5 M sodium acetate buffer, pH 4) in ethanol (50 μL (v/v)). The mixture was shaken (550 RPM) at 100°C for 20 min. After the given period of time the reaction vial was allowed to cool before being diluted with water (20 mL). The obtained aqueous solution containing the labelled product was flushed through a preconditioned C18 cartridge followed by an additional 10 mL of water to remove left over [^{18}F]fluoride from the cartridge. The product was subsequently eluted with ethanol (0.3-0.5 mL) and analysed for purity using radio-HPLC.

9.5.4 Radiolabelling with technetium-99m

9.5.4.1 Elution for $^{99}\text{Mo}/^{99\text{m}}\text{Tc}$ generator

Technetium-99m was produced from an UltraTechnekow FM generator (Mallinckrodt Medical Cat. No. DRN 4329). The generator contains the parent isotope molybdenum-99 absorbed to an aluminium oxide column. Instructions provided by the manufacture were followed with sterile saline used to elute sodium pertechnetate ($\text{Na}[^{99\text{m}}\text{TcO}_4]$).

9.5.4.2 Synthesis of $[^{99m}\text{Tc}(\text{CO})_3(\text{H}_2\text{O})_3]^+$

$[^{99m}\text{Tc}(\text{CO})_3(\text{H}_2\text{O})_3]^+$ was prepared according to literature method, starting from sodium pertechnetate ($\text{Na}[^{99m}\text{TcO}_4]$) from a $^{99}\text{Mo}/^{99m}\text{Tc}$ generator. Approximately 300-600 MBq of $\text{Na}[^{99m}\text{TcO}_4]$ was added to a mixture of sodium tetraborate decahydrate (2.9 mg, 7.6 μmol), sodium carbonate (7.8 mg, 73.6 μmol), potassium sodium tartrate tetrahydrate (9.0 mg, 31.9 μmol) and disodium boranocarbonate (4.5 mg, 43.3 μmol) purged with argon for 10 minutes the heated. The degassed mixture was heated at 90°C for 20 minutes. A 20 μl portion containing typically ~20 MBq of the reaction mixture is injected into the HPLC to monitor progress of the reduction. Analytical HPLC run on C18 150 x 4.6 mm column using isocratic conditions with 2% [MeOH + 0.1% TFA] and 98% $[\text{H}_2\text{O}]$; with the reduced technetium(I) species eluting at 25-28 min in a broad peak. Alternatively radio-TLC can be used (solvent: saline solution, technetium(I) stays on baseline, technetium(VII) $R_f = 0.6$).

9.5.4.3 Standard optimised method for radiolabelling with technetium-99m

The corresponding ligand was dissolved in a 1 mL glass vial with 150 μL of basic water (pH 11). The reaction vial was then tightly closed, and flushed with argon for 10 minutes. Freshly prepared $[^{99m}\text{Tc}(\text{CO})_3(\text{H}_2\text{O})_3]^+$ (50 μL) was added to the reaction and the mixture heated at 90°C while being shaken at 500 RPM for 30 mins. Depending on the experiment further method development, purification, characterisation and formulation could then be completed. Section 7.5.5 details the purification methods used.

9.5.5 Radiolabelling and purification of ligands

Following the general procedure outlined in section 7.5; below details the radiolabelling and purification of ligands.

Table 28: Copper-64 radiolabelling conditions and information.

Ligand	Concentration	Buffer	Radiolabelling procedure	Reaction duration (min)	Reaction Temperature (°C)	TLC conditions and R _f value	Purification method	Partition coefficient	Decay Corrected RCY (%)
5	0.5 mg/mL	Sodium acetate (0.4 M, pH 7)	9.5.1.2	15	90	Neutral alumina, eluted with MeOH:H ₂ O 95:5 with excess NaCl; R _f = 0.46	System 1 (Section 9.2.2.1); multiple peaks, t _r = 3-4 min	-2.38 ± 0.25	41.6 ± 4.6
[⁶⁴ Cu][Cu5(OAc)](OAc)	0.5 mg/mL	Sodium acetate (0.4 M, pH 7)	9.5.1.3	60-240	99	Neutral alumina, eluted with MeOH:H ₂ O 95:5 with excess NaCl; R _f = 0.46	-	-2.45 ± 0.31	75.4 ± 1.5
8	~25 mM	Sodium acetate (0.4 M, pH 7)	9.5.1.4	15	60	RP silica eluted with 6% w/v EDTA in H ₂ O; R _f = 0	System 2 (Section 9.2.2.2); multiple peaks, t _r = 19-20 min	-	12.7
9	~20 mM	Sodium acetate (0.4 M, pH 7)	9.5.1.5	15	60	RP silica eluted with 6% w/v EDTA in H ₂ O; R _f = 0	System 3 (Section 9.2.2.3); multiple peaks, t _r = 18-20 min	-	35.1

Table 29: Gallium-68 radiolabelling conditions and information.

Ligand	Concentration	Buffer	Radiolabelling procedure	Reaction duration (min)	Reaction Temperature (°C)	TLC conditions and R _f value	Purification	Partition coefficient	Decay Corrected RCY (%)
P4	0.01 mM (25 µg)	HEPES (0.1 M, pH 3.5)	9.5.2.2	10	95	RP silica eluted with citric acid (0.1 M); R _f = 0	System 18 (9.2.2.18); single peak, t _r = 12:50 min	-	22.4 ± 19.5
25	N/A	Sodium acetate (0.2 M, pH 4.6)	9.5.2.3	20	95	RP silica eluted with citric acid (0.1 M); R _f = 0.3	-	-	-
26	10 mM	Sodium acetate (0.2 M, pH 4.6)	9.5.2.3	20	95	RP silica eluted with citric acid (0.1 M); R _f = 0	System 4 (Section 9.2.2.4); single peak, t _r = 7:2 min	- 2.63 ± 0.20	-
27	10 mM	Sodium acetate (0.2 M, pH 4.6)	9.5.2.3	20	95	RP silica eluted with citric acid (0.1 M); R _f = 0	System 4 (Section 9.2.2.4); single peak, t _r = 7:45 min	- 2.66 ± 0.12	32.2 ± 14.1
[Cu 27 (OAc)](OAc)	0.1 mM	Sodium acetate (0.2 M, pH 4.6)	9.5.2.3	20	95	RP silica eluted with citric acid (0.1 M); R _f = 0	System 4 (Section 9.2.2.4); single peak, t _r = 8:00 min	- 2.59 ± 0.20	41.7 ± 5.6
29	22 µM	Sodium acetate (0.2 M, pH 4.6)	9.5.2.3	20	95	RP silica eluted with citric acid (0.1 M); R _f = 0	System 20 (9.2.2.20); single peaks, t _r = 18:20 min. System O (9.2.1.14) single peaks, t _r = 14:49 min.	- 2.29 ± 0.18	25.0 ± 9.0
[Cu ₂ 29 (OAc) ₂](OAc) ₂	50 µM	Sodium acetate (0.2 M, pH 4.6)	9.5.2.3	20	95	RP silica eluted with citric acid (0.1 M); R _f = 0	System 19 (Section 9.2.2.19); single peak, t _r = 12:30 min. System O (9.2.1.14) single peaks, t _r = 14:45 min.	- 2.55 ± 0.19	14.2 ± 4.1
[Zn ₂ 29 (OAc) ₂](OAc) ₂	50 µM	Sodium acetate (0.2 M, pH 4.6)	9.5.2.3	20	95	RP silica eluted with citric acid (0.1 M); R _f = 0	System 19 (Section 7.2.2.19); single peak, t _r = 10:55 min. System O (9.2.1.14) single peaks, t _r = 14:46 min.	- 2.63 ± 0.20	21.3 ± 7.0

34	~0.1 mM	Sodium acetate (0.2 M, pH 4.6)	9.5.2.3	20	60	RP silica eluted with citric acid (0.1 M); R _f = 0	System 21 (Section 9.2.2.21); single peak, t _r = 12:30 min. System E (Section 9.2.1.5); single peak, t _r = 17:50 min	-	42.9
35	~0.1 mM	Sodium acetate (0.2 M, pH 4.6)	9.5.2.3	40	60	RP silica eluted with citric acid (0.1 M); R _f = 0	Systems F (Section 9.2.1.6); Single peaks, (t _r = 14:54 min).	-	21.7
38	~0.1 mM	Sodium acetate (0.2 M, pH 4.6)	9.5.2.4	20	99	RP silica eluted with citric acid (0.1 M); R _f = 0	Systems F (Section 9.2.1.6); Single peaks, (t _r = 14:54 min).	-	-
P5	25 µg	50:50 v/v ethanol/deionised water	9.5.2.5	5	95	RP silica eluted with citric acid (0.1 M); R _f = 0	System 23 (Section 9.2.2.23) (single peak, t _r = 10:16 min)	-	76.6

Table 30: Fluorine-18 radiolabelling conditions and information.

Ligand	Concentration	Buffer	Radiolabelling procedure	Reaction duration (min)	Reaction Temperature (°C)	TLC conditions and R _f value	Purification	Partition coefficient	Decay Corrected RCY (%)
42	0.1 mM	0.1 M sodium acetate buffer, (pH 4)	9.5.3.2	20	100	RP silica eluted in acidified methanol, (R _f = 0.22)	System H (Section 9.2.1.7); single peak (t _r = 13:20 min)	-	25.7 ± 6.4
43	100 μM	0.1 M sodium acetate buffer, (pH 4)	9.5.3.2	20	100	RP silica eluted in acidified methanol, (R _f = 0.22)	System I (Section 9.2.1.8)	-	-
[Cu ₂ 43 (OAc) ₂](OAc) ₂	100 - 500 μM	0.1 M sodium acetate buffer, (pH 4)	9.5.3.2	20-40	100	RP silica eluted in acidified methanol, (R _f = 0.22)	System 7 (Section 9.2.1.9)	-	-

Table 31: Technetium-99m radiolabelling conditions and information.

Ligand	Concentration	Buffer	Radiolabelling procedure	Reaction duration (min)	Reaction Temperature (°C)	TLC conditions and R _f value	Purification	Partition coefficient	Decay Corrected RCY (%)
44	0.5 μM	Aqueous (pH 11)	9.5.4.2	30	90	RP silica eluted in saline solution, compound R _f = 0, technetium(VII) R _f = 0.66	System 11 (Section 9.2.2.11); single peak (t _r = 10:20 min)	-	-
49	0.5 μM	Aqueous (pH 11)	9.5.4.2	30	90	RP silica eluted in saline solution, compound R _f = 0, technetium(VII) R _f = 0.66	System 11 (Section 9.2.2.11); single peak (t _r = 07:15 min)	-1.48 ± 0.04	39.8 ± 2.8
51	0.5 μM	Aqueous (pH 11)	9.5.4.2	30	90	RP silica eluted in saline solution, compound R _f = 0, technetium(VII) R _f = 0.66	System 14 (Section 9.2.2.14); single peak, t _r = 12:45	-1.50 ± 0.04	43.3 ± 7.1
[Cu ₂ 51 (OAc) ₂](OAc) ₂	0.5 μM	Aqueous (pH 11)	9.5.4.2	30	90	RP silica eluted in saline solution, compound R _f = 0, technetium(VII) R _f = 0.66	System 11 (Section 9.2.2.11); single peak, t _r = 6.88	0.59 ± 0.22	46.0

9.5.6 Calculating the partition coefficient (LogP)

To a solution of ~2 kBq of radiolabelled ligand in 500 µl of PBS (pH 7.4), 500 µL of octanol were added (n = 3). Vials were vortexed vigorously for 5 min. To achieve quantitative phase separation, the vials were centrifuged at 800 rpm for 5 min. Due to the lipophilic nature of the compound 50 µL of the octanol layer and 10 µL of the aqueous layer were separated and made up to 1 mL in a gamma tube. Both the partition coefficient logP, which is defined as the molar concentration ratio of a single species A between octanol and water at equilibrium which is an important parameter used to characterize lipophilicity of a compounds were calculated.

9.5.7 Stability studies in serum/PBS

The radiolabelled tracer, was dissolved in phosphate buffer (400 µL, 1 M, pH 7.4) and foetal bovine serum (400 µL) in an Eppendorf and vortexed vigorously for 1 min to ensure mixing. This solution was incubated at 37°C for 0-180 min. Each aliquots (50 µL) taken at the correct time point was then combined with methanol (50 µL, v/v) to denature the proteins and vortexed vigorously for 1 min to ensure mixing. The aliquoted Eppendorf was centrifuged at 800 rpm for 5 min to give a protein pellet. 25 µL from the supernatant was then carefully extracted for further analytical analysis.

9.5.8 Stability studies in apo-transferrin

Procedure modified by that reported by Ma *et al.*²⁶⁸ The radiolabelled tracer, was dissolved in phosphate buffer (800 µL, 1 M, pH 7.4) containing 6 mg of apo-transferrin. This solution was incubated at 37°C for 0-180 min. Each aliquots (50 µL) taken at the correct time point, were centrifuged at 800 rpm for 5 min and 25 µL from the surface of the Eppendorf subjected to HPLC analysis. TLC analysis (0.1 M citrate buffer): Tracer typically ($R_f > 0.1$), [⁶⁸Ga]transferrin, broad tailing ($R_f = 0.5$)/

9.5.9 Radiochemical decay corrected

Decay corrected radiochemical quantities were calculated using RadPro Calculator. The Decay corrected RCY was calculated from the point of start of the reaction, to when the reaction was purified and formulated ready for biological evaluation or further chemical characterisation.

9.5.10 Column recovery

To determine column recovery, the amount of radioactivity injected and the amount of radioactivity recovered are quantified. The column recovery is then defined as:

Column recovery = (decay corrected activity post-column/ decay corrected activity pre-column) x 100

9.5.10.1 Pre-column quantification

Before injection the activity in the radioactive sample was recorded. The solvent flow from the HPLC was split before the column to allow collection. The solvent flow was set appropriately for the sample under analysis. The gradient initial conditions was used with a run time of *ca.* 5 minutes used. After the injection was made a pre-weight vial was used to collect the sample flow with the exact time and activity.

9.5.10.2 Post-column quantification

For the post-column quantification the second injection of a known amount of activity should be collected directly after the column before the detector into a pre-weighed vessel. The collection in the vessel was weighted and a representative aliquot taken to record the amount of activity that passed through the column.

9.6 Biological Experiments

9.6.1 *In vivo* experiments

All animal procedures were carried out in accordance with the Scientific Procedures Act 1986 and in line with the NCRI guidelines under Home Office License Number 60/4549 (held by Dr C. Cawthorne at the University of Hull).

9.6.2 Experimental for competition binding assay

Cells at 60% to 80% confluence were washed twice with cold phosphate-saline buffer (PBS), flasks were placed on ice to prevent receptor internalization. Cells were centrifuged at 200 g for 5 minutes and then 5×10^5 cells were resuspended with cold PBS containing 0.25% BSA to block non-specific binding. 50 μL of cell suspension were incubated with 10 μL of 200 μM of the compound for one hour at 4°C. A high concentration of compound was used to ensure saturation of the receptors.

Thereafter, cells were washed thrice with 1 mL of the buffer 0.25% BSA-PBS to remove the excess of compound that did not bind to cells' receptors, centrifuged. Cells were then incubated with 10 μL of either phycoerythrin (PE)-conjugated anti-human CXCR4 monoclonal antibody (clone 12G5) or PE-conjugated mouse IgG2A isotype control antibody (R&D systems, Minnesota, USA) for 60 minutes on ice. Unbound antibody was separated from the cells by three washes with 0.25% BSA-PBS using centrifugation at 200 g for 5 minutes. The pellet was re-suspended in 300 μL of PBS and the cell suspension transferred into polypropylene FACS tubes (Falcon 2054) and analysed by a FACScan flow cytometer (BD Biosciences Europe, Erembodegem, 15 Belgium). Dot plot was used to gate cells and the FL-2 channel was used to measure variation in fluorescence intensities. Ten thousand events were acquired and data were analysed using Cellquest software.

9.6.3 Experimental for fluorescent ligand binding assays

Cells were primarily washed in 5mL of PBS+ 0.25% BSA to remove any unwanted media and spun at 200xg for 5 minutes, additional steps of cells scrapping were taken for adherent cell lines. The cell pellet was then resuspended and aliquoted into eppendorf tubes at 5.0×10^5 cells/ 50 μ l with the addition of 20 μ M of fluorescent compound in one eppendorf, covered by tinfoil and left on ice. After 1 hour cells were washed in 1 mL PBS + 0.25% BSA and centrifuged at 200xg for 5 minutes at 4°C, 10 μ l of PE unconjugated 12G5 Ab was then added to the eppendorf containing the fluorescent compound. At this point positive and negative controls were also prepared: unconjugated antibody, conjugated antibody, isotype, fluorescent compound, added to separate eppendorfs all containing the aforementioned cells, another negative control of just cells was also prepared. These were then all incubated in ice for 1 hour covered by tinfoil. Samples were then washed under the same conditions as before three times. The pellet was re-suspended in 300 μ L of PBS and the cell suspension transferred into polypropylene FACS tubes (Falcon 2054) and analysed by a FACScan flow cytometer (BD Biosciences Europe, Erembodegem, 15 Belgium). Dot plot was used to gate cells and the FL-2 channel was used to measure variation in fluorescence intensities. Ten thousand events were acquired and data were analysed using Cellquest software.

9.6.4 Experimental for confocal microscopy

General Procedure:

U87-CXCR4 or U87 cells were seeded onto glass base petri dishes (35 mm; Thermo Scientific, Nunc™) and incubated overnight. The cells were washed with medium, incubated with 5, 10 or 20 μM of antagonist in medium for 30 min at 4°C and washed again with chilled phosphate buffered saline (PBS). Live cell images were obtained using ZEN software on a Zeiss LSM 710 inverted confocal microscope. The laser used was adapted to the absorption maximum of the antagonists (HeNe 633 nm laser). Images were obtained using a Zeiss 63x water objective.

9.6.5 Experimental for determination of CXCR4 radioligand binding *in vitro*

Cells grown to 60% to 80% confluence were used for receptor binding assays. Cells were washed with cold PBS buffer and flasks were placed on ice to prevent receptor internalization. Cells were detached using a cell scraper. Cells were incubated with 37 kBq/mL (1 μCi/mL) of radiotracer in PBS for 60 minutes at 4°C. After incubation, cells were washed quickly three times with cold PBS and cell-associated radioactivity was determined in a gamma spectrometer (Automatic Gamma counter, Wizard 3" Wallac).

Data are expressed as the accumulation ratio (%) ± SEM calculated by dividing the radioactivity in the pellet by the total radioactivity (supernatant + pellet). For blocking studies, Jurkat cells were pre-incubated with a saturation concentration of cold CXCR4 antagonist (20μM) for one hour. Cells were then washed to remove excess of unbound ligand and incubated with 37 kBq of [⁶⁴Cu][Cu₂5(OAc)(OAc)] , before further incubation for one hour and determination of tracer uptake as above.

10. Appendix

10.1 Z-stacking confocal images of peptide **P7** in U87-CXCR4 cells

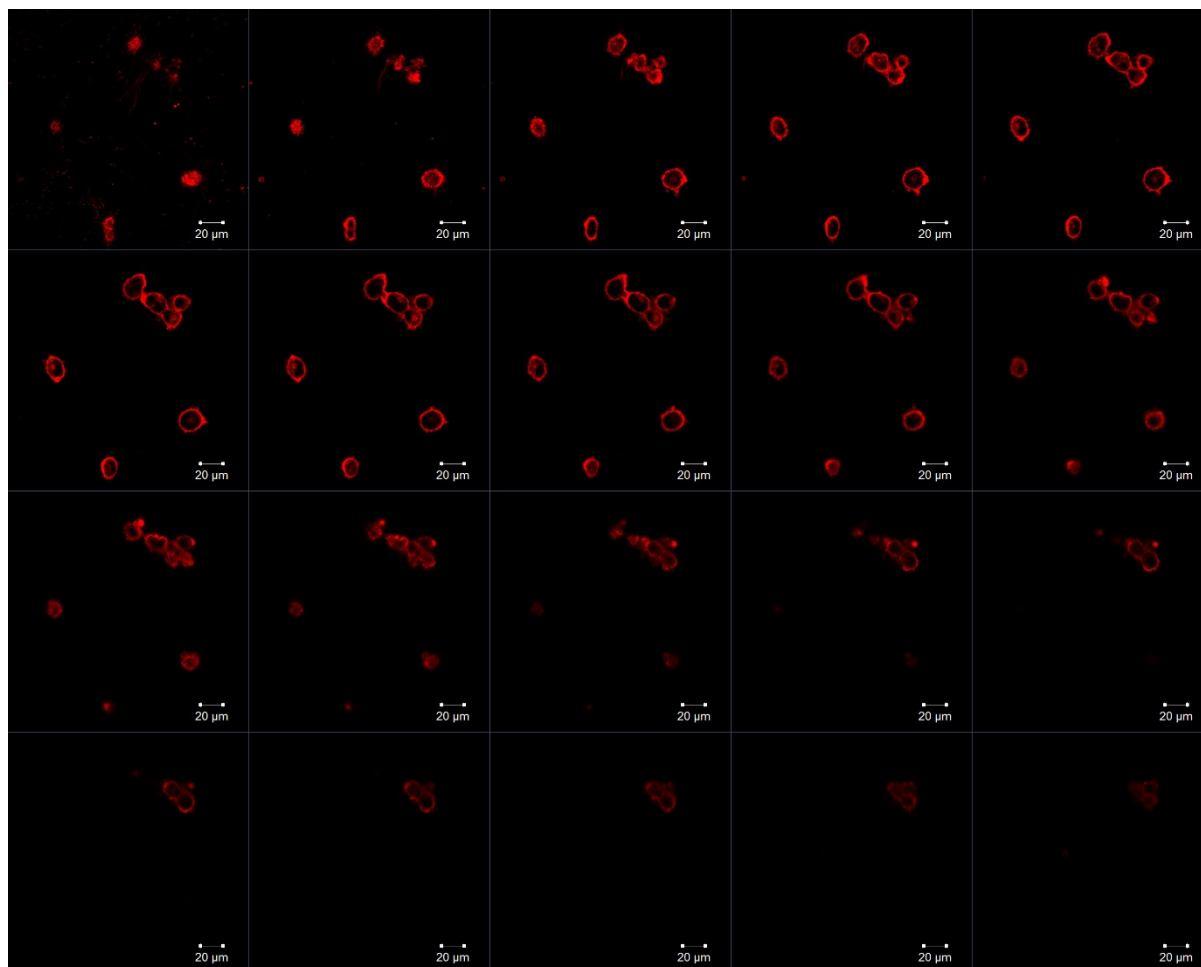


Figure 133: Confocal microscopy Z-stack (20-slices) images of peptide **P7** (10 μ M) in U87-CXCR4 cells.

Figure 133 shows an examples of the images collect in U87-CXCR4 cells using 10 μ M of **P7**. The image shows that none of the **P7** peptide is internalised or taken into the cell by non-specific uptake.

10.2 Comparison confocal images of peptide **P7** in U87 and U87-CXCR4 cells

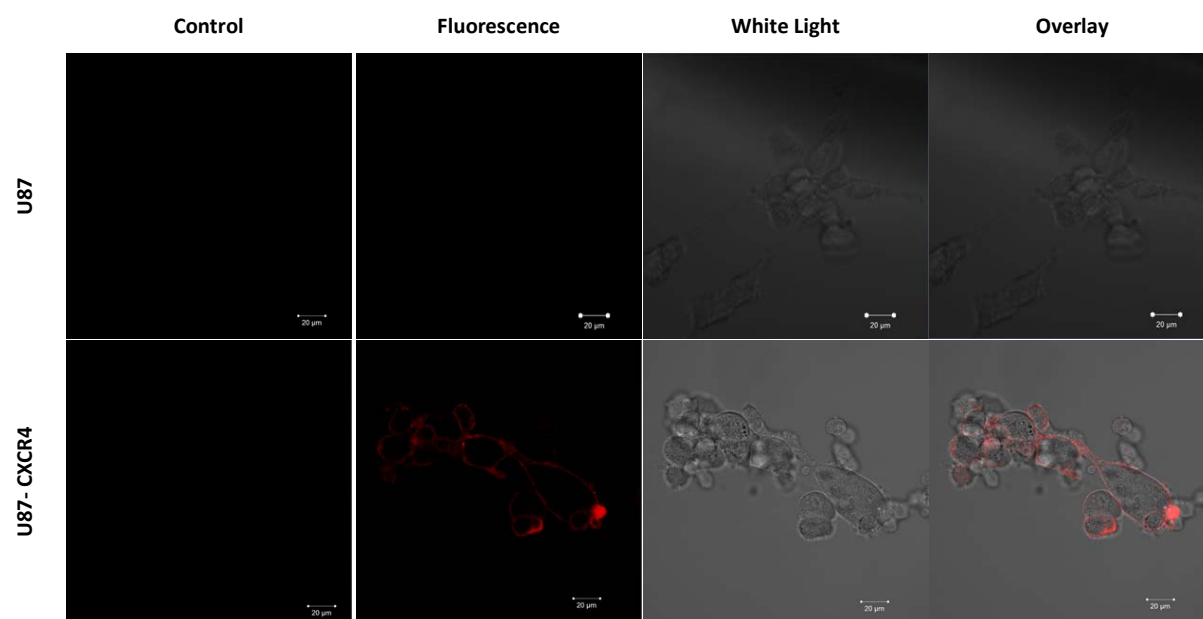


Figure 134: Confocal microscopy images of peptide **P7** in U87 and U87-CXCR4 cell, along with a control autofluorescence image of cells alone.

10.3 Confocal blocking images of peptide **P7** in U87-CXCR4 cells treated with $[\text{Cu}_2\text{5}(\text{OAc})_2](\text{OAc})_2$

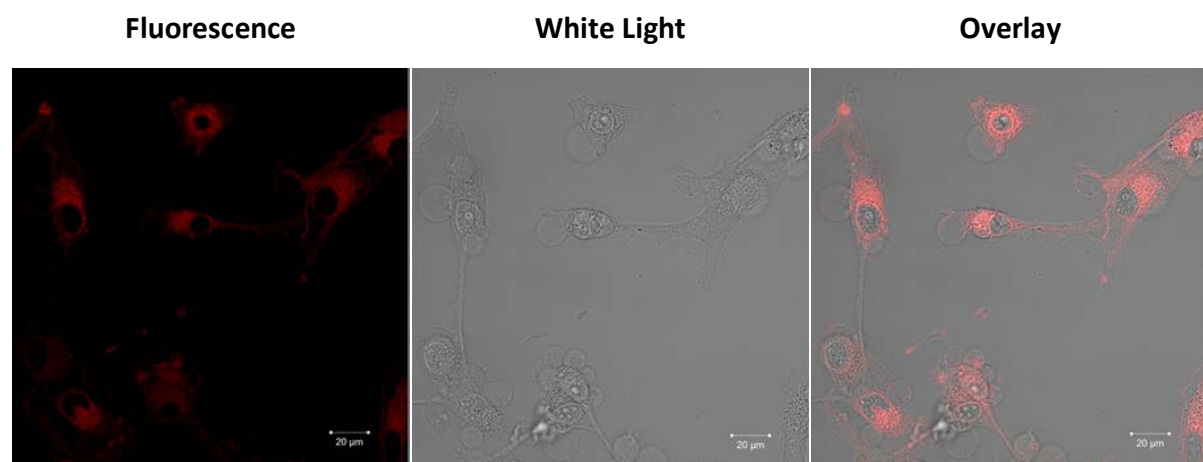


Figure 135: Confocal images of competition/blocking experiment of peptide **P7** with $[\text{Cu}_2\text{5}(\text{OAc})_2](\text{OAc})_2$ in U87 CXCR4 cells.

11. References

1. S. Werner and E. Quimby, *J. Clin. Endocrinol. Metab.*, 1948, **8**, 597-597.
2. F. J. Bonte, *J. Nucl. Med.*, 1995, **36**, 26-27.
3. C. N. Guy, *An introduction to the principles of medical imaging*, Imperial College Press, London, 2000, ch. 1, pp. 1-22.
4. N. J. Long and W. Wong, *The Chemistry of Molecular Imaging*, John Wiley & sons, New Jersey, 2015, ch. 1, pp. 1-25.
5. J. Key and J. F. Leary, *Int. J. Nanomedicine*, 2014, **9**, 711-726.
6. E. W. Price and C. Orvig, *Chem. Soc. Rev.*, 2014, **43**, 260-290.
7. <http://medical.toshiba.com/products/ct/celesteion/>, Toshiba America Medical Systems, (accessed May 2015).
8. J. C. Waterton, *Biomedical Imaging: The Chemistry of Labels, Probes and Contrast Agents*, The Royal Society of Chemistry, London, 2012, ch. 3, pp. 49-143.
9. T. N. Tozer and M. Rowland, *Introduction to Pharmacokinetics and Pharmacodynamics: The Quantitative Basis of Drug Therapy*, Lippincott Williams & Wilkins, Philadelphia, 2006, ch. 1, pp. 1-13.
10. R. Weissleder, *Science*, 2006, **312**, 1168-1171.
11. M. Braddock, D. E. Thurston and D. Rotella, *Biomedical Imaging: The Chemistry of Labels, Probes and Contrast Agents*, Royal Society of Chemistry, Cambridge, 2011, ch. 2, pp. 21-48.
12. A. Y. Rulev and M. G. Voronkov, *New J. Chem.*, 2013, **37**, 3826-3832.
13. J. T. Bushberg and J. M. Boone, *The Essential Physics of Medical Imaging*, Wolters Kluwer Health, Philadelphia, 2011, ch. 1-3, pp. 3-60.
14. P. J. Blower, *Dalton Trans.*, 2015, **44**, 4819-4844.
15. S. Vallabhajosula, in *Mol. Image*, Springer New York, 2014, ch. 1, pp. 1-27.
16. D. Di Pierro, A. Rizzello, G. Cicoria, F. Lodi, M. Marengo, D. Pancaldi, S. Trespidi and S. Boschi, *Appl. Radiat. Isot.*, 2008, **66**, 1091-1096.
17. P. W. L. Miller, N. J.; Vilar, R.; Gee, A. D, *Angew. Chem., Int. Ed. Engl.*, 2008, **2008**, 8998-9033.
18. C. B. Sampson, *Textbook Radiopharmacy*, Taylor & Francis, Cambridge, 1994, ch. 1,2,4,5, pp. 1-110.
19. C. A. Lipinski, F. Lombardo, B. W. Dominy and P. J. Feeney, *Adv. Drug Deliv. Rev.*, 2012, **64**, 4-17.
20. W. D. Loveland, D. J. Morrissey and G. T. Seaborg, *Modern Nuclear Chemistry*, Wiley, 2005.
21. L. R. Bernstein, *Pharmacol. Rev.*, 1998, **50**, 665-682.
22. P. E. Valk, *Positron Emission Tomography: Basic Sciences*, Springer, Singapore, 2003, ch. 1, 2, 3, pp. 1-54.
23. P. W. Atkins and D. F. Shriver, *Shriver & Atkins' inorganic chemistry*, Oxford University Press, Oxford, 5 edn., 2010 ch. 13-23, pp. 325-597.
24. T. J. Wadas, E. H. Wong, G. R. Weisman and C. J. Anderson, *Chem. Rev.*, 2010, **110**, 2858-2902.
25. S. R. Banerjee and M. G. Pomper, *Appl. Radiat. Isot.*, 2013, **76**, 2-13.
26. L. Lang, W. Li, H.-M. Jia, D.-C. Fang, S. Zhang, X. Sun, L. Zhu, Y. Ma, B. Shen, D. O. Kiesewetter, G. Niu and X. Chen, *Theranostics*, 2011, **1**, 341-353.
27. M. Conti and L. Eriksson, *EJNMMI Phys.*, 2016, **3**, 8-16.
28. G. B. Saha, *Fundamentals of Nuclear Pharmacy*, Springer New York, New York, 2013, ch. 4, pp. 33-66.
29. F. Roesch, *Curr. Radiopharm.*, 2012, **5**, 202-211.
30. M. D. Bartholomä, *Inorg. Chim. Acta*, 2012, **389**, 36-51.
31. Z. Cai and C. J. Anderson, *J. Label. Compd. Radiopharm.*, 2014, **57**, 224-230.
32. P. J. Blower, J. S. Lewis and J. Zweit, *Nucl. Med. Biol.*, 1996, **23**, 957-980.
33. D. S. Ma, F. Lu, T. Overstreet, D. E. Milenic and M. W. Brechbiel, *Nucl. Med. Biol.*, 2002, **29**, 91-105.

-
34. T. J. Wadas, E. H. Wong, G. R. Weisman and C. J. Anderson, *Curr. Pharm. Des.*, 2007, **13**, 3-16.
 35. C. J. Anderson, T. J. Wadas, E. H. Wong and G. R. Weisman, *Q. J. Nucl. Med. Mol. Imaging*, 2008, **52**, 185-192.
 36. T. J. Hubin, P. N. A. Amoyaw, K. D. Roewe, N. C. Simpson, R. D. Maples, T. N. C. Freeman, A. N. Cain, J. G. Le, S. J. Archibald, S. I. Khan, B. L. Tekwani and M. O. F. Khan, *Bioorg. Med. Chem.*, 2014, **22**, 3239-3244.
 37. J. D. Silversides, R. Smith and S. J. Archibald, *Dalton Trans.*, 2011, **40**, 6289-6297.
 38. J. D. Silversides, B. P. Burke and S. J. Archibald, *C. R. Chim.*, 2013, **16**, 524-530.
 39. H. A. Williams, S. Robinson, P. Julyan, J. Zweit and D. Hastings, *Eur. J. Nucl. Med. Mol. Imaging*, 2005, **32**, 1473-1480.
 40. F. F. Dyer and G. W. Leddicotte, *The Radiochemistry of Copper*, Subcommittee on Radiochemistry, National Academy of Sciences, National Research Council, 1961, ch. 1, pp. 1-20.
 41. M. M. King, *Nuclear Data Sheets*, 1993, **69**, 1-67.
 42. M. R. Bhat, *Nuclear Data Sheets*, 1999, **88**, 417-532.
 43. H. Junde and B. Singh, *Nuclear Data Sheets*, 2000, **91**, 317-422.
 44. B. Singh, *Nuclear Data Sheets*, 1996, **78**, 395-546.
 45. F. Szelecsényi, G. Blessing and S. M. Qaim, *Appl. Radiat. Isot.*, 1993, **44**, 575-580.
 46. D. W. McCarthy, R. E. Shefer, R. E. Klinkowstein, L. A. Bass, W. H. Margeneau, C. S. Cutler, C. J. Anderson and M. J. Welch, *Nucl. Med. Biol.*, 1997, **24**, 35-43.
 47. B. P. Burke, G. S. Clemente and S. J. Archibald, *Contrast Media Mol. Imaging*, 2015, **10**, 96-110.
 48. M. J. Welch and C. S. Redvanly, *Handbook of Radiopharmaceuticals: Radiochemistry and Applications*, Wiley, 2003, ch. 1-3, pp. 1-87.
 49. D. Le Bars, *J. Fluorine Chem.*, 2006, **127**, 1488-1493.
 50. H. H. Coenen, P. H. Elsinga, R. Iwata, M. R. Kilbourn, M. R. A. Pillai, M. G. R. Rajan, H. N. Wagner, Jr. and J. J. Zaknun, *Nucl. Med. Biol.*, **37**, 727-740.
 51. O. Jacobson, D. O. Kiesewetter and X. Chen, *Bioconjugate Chem.*, 2015, **26**, 1-18.
 52. M. Lin, M. J. Welch and S. E. Lapi, *Mol. Imaging Biol.*, 2013, **15**, 606-613.
 53. S. Poty, P. Desogere, C. Goze, F. Boschetti, T. D'Huys, D. Schols, C. Cawthorne, S. J. Archibald, H. R. Maecke and F. Denat, *Dalton Trans.*, 2015, **44**, 5004-5016.
 54. R. D. Hancock, *J. Chem. Educ.*, 1992, **69**, 615.
 55. R. M. Smith and A. E. Martell, *Sci. Total Environ.*, 1987, **64**, 125-147.
 56. M. Hofmann, H. Maecke, A. R. Borner, E. Weckesser, P. Schoffski, M. L. Oei, J. Schumacher, M. Henze, A. Heppeler, G. J. Meyer and W. H. Knapp, *Eur. J. Nuc. Med.*, 2001, **28**, 1751-1757.
 57. A. E. Martell, R. J. Motekaitis, E. T. Clarke, R. Delgado, Y. Z. Sun and R. Ma, *Supramol. Chem.*, 1996, **6**, 353-363.
 58. I. Velikyan, A. L. Sundberg, O. Lindhe, A. U. Hoglund, O. Eriksson, E. Werner, J. Carlsson, M. Bergstrom, B. Langstrom and V. Tolmachev, *J. Nucl. Med.*, 2005, **46**, 1881-1888.
 59. A. Dimitrakopoulou-Strauss, P. Hohenberger, U. Haberkorn, H. R. Maecke, M. Eisenhut and L. G. Strauss, *J. Nucl. Med.*, 2007, **48**, 1245-1250.
 60. G. Kramer-Marek, N. Shenoy, J. Seidel, G. L. Griffiths, P. Choyke and J. Capala, *Eur. J. Nucl. Med. Mol. Imaging*, 2011, **38**, 1967-1976.
 61. C. Decristoforo, I. H. Gonzalez, J. Carlsen, M. Rupprich, M. Huisman, I. Virgolini, H.-J. Wester and R. Haubner, *Eur. J. Nucl. Med. Mol. Imaging*, 2008, **35**, 1507-1515.
 62. M. Gabriel, C. Decristoforo, D. Kendler, G. Dobrozemsky, D. Heute, C. Uprimny, P. Kovacs, E. Von Guggenberg, R. Bale and I. J. Virgolini, *J. Nucl. Med.*, 2007, **48**, 508-518.
 63. L. Wei, Y. Miao, F. Gallazzi, T. P. Quinn, M. J. Welch, A. L. Vavere and J. S. Lewis, *Nucl. Med. Biol.*, 2007, **34**, 945-953.
 64. Y. Z. Sun, C. J. Anderson, T. S. Pajeau, D. E. Reichert, R. D. Hancock, R. J. Motekaitis, A. E. Martell and M. J. Welch, *J. Med. Chem.*, 1996, **39**, 458-470.

-
65. J.-F. Morfin and E. Toth, *Inorg. Chem.*, 2011, **50**, 10371-10378.
 66. S. Liu, J. Pietryka, C. E. Ellars and D. S. Edwards, *Bioconjugate Chem.*, 2002, **13**, 902-913.
 67. W. A. P. Breeman, M. de Jong, T. J. Visser, J. L. Erion and E. P. Krenning, *Eur. J. Nucl. Med. Mol. Imaging*, 2003, **30**, 917-920.
 68. G. A. Bailey, E. W. Price, B. M. Zeglis, C. L. Ferreira, E. Boros, M. J. Lacasse, B. O. Patrick, J. S. Lewis, M. J. Adam and C. Orvig, *Inorg. Chem.*, 2012, **51**, 12575-12589.
 69. C. L. Ferreira, D. T. Yapp, E. Lamsa, M. Gleave, C. Bensimon, P. Jurek and G. E. Kiefer, *Nucl. Med. Biol.*, 2008, **35**, 875-882.
 70. M. S. Cooper, M. T. Ma, K. Sunassee, K. P. Shaw, J. D. Williams, R. L. Paul, P. S. Donnelly and P. J. Blower, *Bioconjugate Chem.*, 2012, **23**, 1029-1039.
 71. S. Chaves, R. Delgado and J. Dasilva, *Talanta*, 1992, **39**, 249-254.
 72. R. Delgado and J. Dasilva, *Talanta*, 1982, **29**, 815-822.
 73. P. McQuade, Y. B. Miao, J. Yoo, T. P. Quinn, M. J. Welch and J. S. Lewis, *J. Med. Chem.*, 2005, **48**, 2985-2992.
 74. S. H. Hausner, D. L. Kukis, M. K. J. Gagnon, C. E. Stanecki, R. Ferdani, J. F. Marshall, C. J. Anderson and J. L. Sutcliffe, *Mol. Image*, 2009, **8**, 111-121.
 75. G. B. Biddlecombe, B. E. Rogers, M. de Visser, J. J. Parry, M. de Jong, J. L. Erion and J. S. Lewis, *Bioconjugate Chem.*, 2007, **18**, 724-730.
 76. S. Eigner, D. R. B. Vera, M. Fellner, N. S. Loktionova, M. Piel, O. Lebeda, F. Roesch, T. L. Ross and K. E. Henke, *Mol. Imaging Biol.*, 2013, **15**, 79-86.
 77. D. V. Filosofov, N. S. Loktionova and F. Roesch, *Radiochim. Acta.*, 2010, **98**, 149-156.
 78. A. Majkowska-Pilip and A. Bilewicz, *J. Inorg. Biochem.*, 2011, **105**, 313-320.
 79. L. R. Perk, G. W. M. Visser, M. Vosjan, M. Stigter-van Walsum, B. M. Tijnink, C. R. Leemans and G. van Dongen, *J. Nucl. Med.*, 2005, **46**, 1898-1906.
 80. P. McQuade, Y. Miao, J. Yoo, T. P. Quinn, M. J. Welch and J. S. Lewis, *J. Med. Chem.*, 2005, **48**, 2985-2992.
 81. M. Shokeen and C. J. Anderson, *Acc. Chem. Res.*, 2009, **42**, 832-841.
 82. J. D. Silversides, C. C. Allan and S. J. Archibald, *Dalton Trans.*, 2007, 971-978.
 83. E. T. Clarke and A. E. Martell, *Inorg. Chim. Acta*, 1991, **190**, 27-36.
 84. C. J. Anderson, F. Dehdashti, P. D. Cutler, S. W. Schwarz, R. Laforest, L. A. Bass, J. S. Lewis and D. W. McCarthy, *J. Nucl. Med.*, 2001, **42**, 213-221.
 85. E. T. Clarke and A. E. Martell, *Inorg. Chim. Acta*, 1991, **190**, 37-46.
 86. E. Boros, C. L. Ferreira, J. F. Cawthray, E. W. Price, B. O. Patrick, D. W. Wester, M. J. Adam and C. Orvig, *J. Am. Chem. Soc.*, 2010, **132**, 15726-15733.
 87. I. Velikyan, H. Maecke and B. Langstrom, *Bioconjugate Chem.*, 2008, **19**, 569-573.
 88. E. T. Clarke and A. E. Martell, *Inorg. Chim. Acta*, 1991, **181**, 273-280.
 89. J. Strand, H. Honarvar, A. Perols, A. Orlova, R. K. Selvaraju, A. E. Karlstrom and V. Tolmachev, *Plos One*, 2013, **8**, 1-10.
 90. A. Fuchs, I. Greguric and G. Roe, *Nucl. Med. Biol.*, 2010, **37**, 692-692.
 91. C. J. Broan, J. P. L. Cox, A. S. Craig, R. Katakay, D. Parker, A. Harrison, A. M. Randall and G. Ferguson, *Perkin Trans. 2*, 1991, **1**, 87-99.
 92. T. J. McMurry, M. Brechbiel, C. C. Wu and O. A. Gansow, *Bioconjugate Chem.*, 1993, **4**, 236-245.
 93. K. P. Eisenwiener, M. I. M. Prata, I. Buschmann, H. W. Zhang, A. C. Santos, S. Wenger, J. C. Reubi and H. R. Macke, *Bioconjugate Chem.*, 2002, **13**, 530-541.
 94. V. Tolmachev, M. Altai, M. Sandstrom, A. Perols, A. E. Karlstrom, F. Boschetti and A. Orlova, *Bioconjugate Chem.*, 2011, **22**, 894-902.
 95. Y. Zhang, H. Hong, J. W. Engle, J. Bean, Y. Yang, B. R. Leigh, T. E. Barnhart and W. Cai, *Plos One*, 2011, **6**, 1-7.
 96. A. Bevilacqua, R. I. Gelb, W. B. Hebard and L. J. Zompa, *Inorg. Chem.*, 1987, **26**, 2699-2706.

-
97. K. Suzuki, N. Shimmura, K. Thipyapong, T. Uehara, H. Akizawa and Y. Arano, *Inorg. Chem.*, 2008, **47**, 2593-2600.
98. E. Cole, D. Parker, G. Ferguson, J. F. Gallagher and B. Kaitner, *Chem. Commun.*, 1991, **0**, 1473-1475.
99. C. Royston and A. Judith, *Dalton Trans.*, 1994, **11**, 1619-1629.
100. J. Notni, P. Hermann, J. Havlíčková, J. Kotek, V. Kubíček, J. Plutnar, N. Loktionova, P. J. Riss, F. Rösch and I. Lukeš, *Chem. Eur. J.*, 2010, **16**, 7174-7185.
101. J. Šimeček, M. Schulz, J. Notni, J. Plutnar, V. Kubíček, J. Havlíčková and P. Hermann, *Inorg. Chem.*, 2012, **51**, 577-590.
102. L. Camera, S. Kinuya, K. Garmestani, C. C. Wu, M. W. Brechbiel, L. H. Pai, T. J. McMurry, O. A. Gansow, I. Pastan, C. H. Paik and J. A. Carrasquillo, *J. Nucl. Med.*, 1994, **35**, 882-889.
103. D. J. Berry, Y. Ma, J. R. Ballinger, R. Tavaré, A. Koers, K. Sunassee, T. Zhou, S. Nawaz, G. E. D. Mullen, R. C. Hider and P. J. Blower, *Chem. Commun.*, 2011, **47**, 7068-7070.
104. M. T. Ma, L. K. Meszaros, B. M. Paterson, D. J. Berry, M. S. Cooper, Y. Ma, R. C. Hider and P. J. Blower, *Dalton Trans.*, 2015, **44**, 4884-4900.
105. M. T. Ma, C. Cullinane, K. Waldeck, P. Roselt, R. J. Hicks and P. J. Blower, *EJNMMI Res.*, 2015, **5**, 1-11.
106. B. P. Burke, G. S. Clemente and S. J. Archibald, *J. Label. Compd. Radiopharm.*, 2014, **57**, 239-243.
107. M. T. Ma, L. K. Meszaros, B. M. Paterson, D. J. Berry, M. S. Cooper, Y. M. Ma, R. C. Hider and P. J. Blower, *Dalton Trans.*, 2015, **44**, 4884-4900.
108. G. J. Kontoghiorghes, K. Pattichi, M. Hadjigavriel and A. Kolnagou, *Transfus. Sci.*, 2000, **23**, 211-223.
109. F. Balkwill, *Nat. Rev. Cancer*, 2004, **4**, 540-550.
110. A. Zlotnik, O. Yoshie and H. Nomiyama, *Genome Biol.*, 2006, **7**, 243-254.
111. S. Chatterjee, B. B. Azad and S. Nimmagadda, in *Emerging Applications of Molecular Imaging to Oncology*, eds. M. G. Pomper and P. B. Fisher, Elsevier Academic Press Inc, San Diego, 2014, vol. 124, pp. 31-82.
112. T. N. C. Wells, C. A. Power, J. P. Shaw and A. E. I. Proudfoot, *Trends Pharmacol. Sci.*, **27**, 41-47.
113. A. E. I. Proudfoot, *Nat. Rev. Immunol.*, 2002, **2**, 106-115.
114. K. Balabanian, B. Lagane, S. Infantino, K. Y. C. Chow, J. Harriague, B. Moepps, F. Arenzana-Seisdedos, M. Thelen and F. Bachelier, *J. Biol. Chem.*, 2005, **280**, 35760-35766.
115. E. A. Berger, P. M. Murphy and J. M. Farber, *Annu. Rev. Immunol.*, 1999, **17**, 657-700.
116. E. De Clercq, *Nat. Rev. Drug Discov.*, 2003, **2**, 581-587.
117. S. Fruehauf, W. J. Zeller and G. Calandra, *Novel Developments in Stem Cell Mobilization: Focus on CXCR4*, Springer, Boston, 2012, ch. 1, pp. 3-23.
118. D. Raman, P. J. Baugher, Y. M. Thu and A. Richmond, *Cancer Letts.*, 2007, **256**, 137-165.
119. J. Vandercappellen, J. Van Damme and S. Struyf, *Cancer Letts.*, 2008, **267**, 226-244.
120. C. L. Richard and J. Blay, *PPAR Res.*, 2008, **2008**, 19.
121. G. A. Donzella, D. Schols, S. W. Lin, J. A. Este, K. A. Nagashima, P. J. Maddon, G. P. Allaway, T. P. Sakmar, G. Henson, E. De Clercq and J. P. Moore, *Nat. Med.*, 1998, **4**, 72-77.
122. C. C. Bleul, L. Wu, J. A. Hoxie, T. A. Springer and C. R. Mackay, *Proc. Nat. Acad. Sci. USA*, 1997, **94**, 1925-1930.
123. X. Liang and P. J. Sadler, *Chem. Soc. Rev.*, 2004, **33**, 246-266.
124. B. Wu, E. Y. T. Chien, C. D. Mol, G. Fenalti, W. Liu, V. Katritch, R. Abagyan, A. Brooun, P. Wells, F. C. Bi, D. J. Hamel, P. Kuhn, T. M. Handel, V. Cherezov and R. C. Stevens, *Science*, 2010, **330**, 1066-1071.
125. C. R. UK, <http://www.cancerresearchuk.org/health-professional/cancer-statistics>, (accessed May 2015).

-
126. A. Muller, B. Homey, H. Soto, N. Ge, D. Catron, M. E. Buchanan, T. McClanahan, E. Murphy, W. Yuan, S. N. Wagner, J. L. Barrera, A. Mohar, E. Verastegui and A. Zlotnik, *Nature*, 2001, **410**, 50-56.
127. C. J. Scotton, J. L. Wilson, K. Scott, G. Stamp, G. D. Wilbanks, S. Fricker, G. Bridger and F. R. Balkwill, *Cancer Res.*, 2002, **62**, 5930-5938.
128. D. Milliken, C. Scotton, S. Raju, F. Balkwill and J. Wilson, *Clin. Cancer Res.*, 2002, **8**, 1108-1114.
129. M. Shakir, D. L. Tang, H. J. Zeh, S. W. Tang, C. J. Anderson, N. Bahary and M. T. Lotze, *Pancreas*, 2015, **44**, 528-534.
130. F. Marchesi, P. Monti, B. E. Leone, A. Zerbi, A. Vecchi, L. Piemonti, A. Mantovani and P. Allavena, *Cancer Res.*, 2004, **64**, 8420-8427.
131. M. Neagu, C. Constantin and C. Longo, *J. Immunoassay Immunochem.*, 2015, **36**, 559-566.
132. S. Scala, A. Ottaiano, P. A. Ascierto, M. Cavalli, E. Simeone, P. Giuliano, M. Napolitano, R. Franco, G. Botti and G. Castello, *Clin. Cancer Res.*, 2005, **11**, 1835-1841.
133. M. Terasaki, Y. Sugita, F. Arakawa, Y. Okada, K. Ohshima and M. Shigemori, *Brain Tumor Pathol.*, 2011, **28**, 89-97.
134. J. T. Kaifi, E. F. Yekebas, P. Schurr, D. Obonyo, R. Wachowiak, P. Busch, A. Heinecke, K. Pantel and J. R. Izbicki, *J. Natl. Cancer Inst.*, 2005, **97**, 1840-1847.
135. Y. Z. Ding, Y. Shimada, M. Maeda, A. Kawabe, J. Kaganoi, I. Komoto, Y. Hashimoto, M. Miyake, H. Hashida and M. Imamura, *Clin. Cancer Res.*, 2003, **9**, 3406-3412.
136. R. J. Phillips, M. D. Burdick, M. Lutz, J. A. Belperio, M. P. Keane and R. M. Strieter, *Am. J. Respir. Crit. Care Med.*, 2003, **167**, 1676-1686.
137. A. Muller, E. Sonkoly, C. Eulert, P. A. Gerber, R. Kubitzka, K. Schirlau, P. Franken-Kunkel, C. Poremba, C. Snyderman, L.-O. Klotz, T. Ruzicka, H. Bier, A. Zlotnik, T. L. Whiteside, B. Homey and T. K. Hoffmann, *Int. J. Cancer*, 2006, **118**, 2147-2157.
138. A. Eisenhardt, U. Frey, M. Tack, D. Roskopf, G. Lümmen, H. Rübber and W. Siffert, *Eur. Uro.*, 2005, **47**, 111-117.
139. M. M. Retz, S. S. Sidhu, E. Blaveri, S. C. Kerr, G. M. Dolganov, J. Lehmann, P. Carroll, J. Simko, F. M. Waldman and C. Basbaum, *Int. J. Cancer*, 2005, **114**, 182-189.
140. T. Murakami, K. Kawada, M. Iwamoto, M. Akagami, K. Hida, Y. Nakanishi, K. Kanda, M. Kawada, H. Seno, M. M. Taketo and Y. Sakai, *Int. J. Cancer*, 2013, **132**, 276-287.
141. K. Rupertus, J. Sinistra, C. Scheuer, R. M. Nickels, M. K. Schilling, M. D. Menger and O. Kollmar, *Clin. Exp. Metastasis*, 2014, **31**, 447-459.
142. L. Lombardi, F. Tavano, F. Morelli, T. P. Latiano, P. Di Sebastiano and E. Maiello, *Crit. Rev. Oncol./Hematol.*, 2013, **88**, 696-705.
143. I. von Luetlichau, S. Segerer, A. Wechselberger, M. Notohamiprodjo, M. Nathrath, M. Kremer, A. Henger, R. Djafarzadeh, S. Burdach, R. Huss and P. J. Nelson, *BMC Cancer*, 2008, **8**, 10.
144. D. Baumhoer, J. Smida, S. Zillmer, M. Rosemann, M. J. Atkinson, P. J. Nelson, G. Jundt, I. von Luetlichau and M. Nathrath, *Mod. Pathol.*, 2012, **25**, 522-528.
145. N. Gross and R. Meier, *Semin. Cancer Biol.*, 2009, **19**, 103-110.
146. J. Sun, C. Feng, W. W. Liao, H. Zhang and S. Q. Tang, *Oncol. Lett.*, 2014, **7**, 2083-2088.
147. C. Faaij, A. J. Willemze, T. Revesz, M. Balzarolo, C. P. Tensen, M. Hoogeboom, M. H. Vermeer, E. van Wering, C. M. Zwaan, G. J. L. Kaspers, C. Story, A. G. S. van Halteren, J. M. Vossen, R. M. Egeler, M. J. D. van Tol and N. E. Annels, *Pediatr. Blood Cancer*, 2010, **55**, 344-348.
148. A. Corcione, N. Arduino, E. Ferretti, A. Pistorio, M. Spinelli, L. Ottonello, F. Dallegri, G. Basso and V. Pistoia, *Leukemia Res.*, 2006, **30**, 365-372.
149. J. A. Burger and A. Peled, *Leukemia*, 2009, **23**, 43-52.
150. D. Zagzag, B. Krishnamachary, H. Yee, H. Okuyama, L. Chiriboga, M. A. Ali, J. Melamed and G. L. Semenza, *Cancer Res.*, 2005, **65**, 6178-6188.

-
151. W. Mo, J. Chen, A. Patel, L. Zhang, V. Chau, Y. J. Li, W. Cho, K. Lim, J. Xu, A. J. Lazar, C. J. Creighton, S. Bolshakov, R. M. McKay, D. Lev, L. Q. Le and L. F. Parada, *Cell*, 2013, **152**, 1077-1090.
152. A. Zlotnik, *Int. J. Cancer*, 2006, **119**, 2026-2029.
153. H. Nakashima, T. Murakami, N. Yamamoto, H. Sakagami, S.-i. Tanuma, T. Hatano, T. Yoshida and T. Okuda, *Antiviral Res.*, 1992, **18**, 91-103.
154. H. Tamamura, Y. Xu, T. Hattori, X. Zhang, R. Arakaki, K. Kanbara, A. Omagari, A. Otaka, T. Ibuka, N. Yamamoto, H. Nakashima and N. Fujii, *Biochem. Biophys. Res. Commun.*, 1998, **253**, 877-882.
155. J. O. Trent, Z.-x. Wang, J. L. Murray, W. Shao, H. Tamamura, N. Fujii and S. C. Peiper, *J. Biol. Chem.*, 2003, **278**, 47136-47144.
156. H. Tamamura, A. Omagari, K. Hiramatsu, K. Gotoh, T. Kanamoto, Y. Xu, E. Kodama, M. Matsuoka, T. Hattori, N. Yamamoto, H. Nakashima, A. Otaka and N. Fujii, *Bioorg. Med. Chem. Letts.*, 2001, **11**, 1897-1902.
157. T. Hirokazu, T. Hiroshi and F. Nobutaka, *Mini Rev. Med. Chem.*, 2006, **6**, 989-995.
158. H. Hanaoka, T. Mukai, H. Tamamura, T. Mori, S. Ishino, K. Ogawa, Y. Iida, R. Doi, N. Fujii and H. Saji, *Nucl. Med. Biol.*, 2006, **33**, 489-494.
159. O. Jacobson, I. D. Weiss, D. O. Kiesewetter, J. M. Farber and X. Chen, *J. Nucl. Med.*, 2010, **51**, 1796-1804.
160. I. D. Weiss and O. Jacobson, *Theranostics*, 2013, **3**, 76-84.
161. X.-X. Zhang, Z. Sun, J. Guo, Z. Wang, C. Wu, G. Niu, Y. Ma, D. O. Kiesewetter and X. Chen, *Mol. Imaging Biol.*, 2013, **15**, 758-767.
162. O. Jacobson, I. D. Weiss, L. P. Szajek, G. Niu, Y. Ma, D. O. Kiesewetter, A. Peled, H. S. Eden, J. M. Farber and X. Chen, *J. Control. Release*, 2012, **157**, 216-223.
163. U. Hennrich, L. Seyler, M. Schäfer, U. Bauder-Wüst, M. Eisenhut, W. Semmler and T. Bäuerle, *Bioorg. Med. Chem.*, 2012, **20**, 1502-1510.
164. O. Jacobson, I. D. Weiss, L. P. Szajek, G. Niu, Y. Ma, D. O. Kiesewetter, J. M. Farber and X. Chen, *Theranostics*, 2011, **1**, 251-262.
165. O. Demmer, I. Dijkgraaf, U. Schumacher, L. Marinelli, S. Cosconati, E. Gourni, H.-J. Wester and H. Kessler, *J. Med. Chem.*, 2011, **54**, 7648-7662.
166. E. Gourni, O. Demmer, M. Schottelius, C. D'Alessandria, S. Schulz, I. Dijkgraaf, U. Schumacher, M. Schwaiger, H. Kessler and H.-J. Wester, *J. Nucl. Med.*, 2011, **52**, 1803-1810.
167. O. Åberg, F. Pisaneschi, G. Smith, Q.-D. Nguyen, E. Stevens and E. O. Aboagye, *J. Fluorine Chem.*, 2012, **135**, 200-206.
168. G. P. C. George, F. Pisaneschi, E. Stevens, Q.-D. Nguyen, O. Åberg, A. C. Spivey and E. O. Aboagye, *J. Label. Compd. Radiopharm.*, 2013, **56**, 679-685.
169. I. Dijkgraaf, O. Demmer, U. Schumacher, N. Koglin, M. Anton, W. Brandau, M. Schwaiger, H. Kessler and H. Wester, *Eur. J. Nucl. Med. Mol. Imag.*, 2008, **35**, S318-S318.
170. E. Gourni, O. Demmer, M. Schottelius, C. D'Alessandria, S. Schulz, I. Dijkgraaf, U. Schumacher, M. Schwaiger, H. Kessler and H. J. Wester, *J. Nucl. Med.*, 2011, **52**, 1803-1810.
171. K. Herrmann, C. Lapa, H. J. Wester, M. Schottelius, C. Schiepers, U. Eberlein, C. Bluemel, U. Keller, S. Knop, S. Kropf, A. Schirbel, A. K. Buck and M. Lassmann, *J. Nucl. Med.*, 2015, **56**, 410-416.
172. K. Philipp-Abbrederis, K. Herrmann, S. Knop, M. Schottelius, M. Eiber, K. Luckerath, E. Pietschmann, S. Habringer, C. Gerngross, K. Franke, M. Rudelius, A. Schirbel, C. Lapa, K. Schwamborn, S. Steidle, E. Hartmann, A. Rosenwald, S. Kropf, A. J. Beer, C. Peschel, H. Einsele, A. K. Buck, M. Schwaiger, K. Gotze, H. J. Wester and U. Keller, *EMBO Mol. Med.*, 2015, **7**, 477-487.
173. A. Poschenrieder, M. Schottelius, M. Schwaiger, H. Kessler and H.-J. Wester, *EJNMMI Res.*, 2016, **6**, 1-8.
174. A. Poschenrieder, M. Schottelius, M. Schwaiger and H.-J. Wester, *EJNMMI Res.*, 2016, **6**, 70.

-
175. K. Herrmann, M. Schottelius, C. Lapa, T. Osl, A. Poschenrieder, H. Haenscheid, K. Lueckerath, M. Schreder, C. Bluemel, M. Knott, U. Keller, A. Schirbel, S. Samnick, M. Lassmann, S. Kropf, A. K. Buck, H. Einsele, H.-J. Wester and S. Knop, *J. Nucl. Med.*, 2016, **57**, 248-251.
176. W. Rozenbaum, D. Dormont, B. Spire, E. Vilmer, M. Gentilini, C. Griscelli, L. Montagnier, F. Barre-Sinoussi and J. C. Chermann, *Lancet*, 1985, **325**, 450-451.
177. F. Giuntini, C. M. A. Alonso and R. W. Boyle, *Photochem. Photobiol. Sci.*, 2011, **10**, 759-791.
178. E. De Clercq, *Mol. Pharm.*, 2000, **57**, 833-839.
179. V. I. Pérez-Nueno, D. W. Ritchie, O. Rabal, R. Pascual, J. I. Borrell and J. Teixidó, *J. Chem. Inf. Model.*, 2008, **48**, 509-533.
180. L. O. Gerlach, R. T. Skerlj, G. J. Bridger and T. W. Schwartz, *J. Biol. Chem.*, 2001, **276**, 14153-14160.
181. R. S. Y. Wong, V. Bodart, M. Metz, J. Labrecque, G. Bridger and S. P. Fricker, *Mol. Pharm.*, 2008, **74**, 1485-1495.
182. G. J. Bridger, R. T. Skerlj, P. E. Hernandez-Abad, D. E. Bogucki, Z. Wang, Y. Zhou, S. Nan, E. M. Boehringer, T. Wilson, J. Crawford, M. Metz, S. Hatse, K. Princen, E. De Clercq and D. Schols, *J. Med. Chem.*, 2010, **53**, 1250-1260.
183. S. L. F. G. A. Cahen, R. MacFarland, K. Badel, J. DiPersio, *Biol. Blood Marrow Transplant*, 2008, **14**, 1253.
184. R. R. Bai, Z. X. Liang, Y. Yoon, S. P. Liu, T. Gaines, Y. Oum, Q. Shi, S. R. Mooring and H. Shim, *Eur. J. Med. Chem.*, 2016, **118**, 340-350.
185. A. Khan, J. Greenman and S. J. Archibald, *Curr. Med. Chem.*, 2007, **14**, 2257-2277.
186. L. O. J. Gerlach, J. S.; Jensen, K. P.; Rosenkilde, M. R.; Skerlj, R. T.; Ryde, U.; Bridger, G. J.; Schwartz, T. W., *Biochem.*, 2002, **42** 710-717.
187. T. Tanaka, T. Narumi, T. Ozaki, A. Sohma, N. Ohashi, C. Hashimoto, K. Itotani, W. Nomura, T. Murakami, N. Yamamoto and H. Tamamura, *Chem. Med. Chem.*, 2011, **6**, 834-839.
188. O. Jacobson, I. D. Weiss, L. Szajek, J. M. Farber and D. O. Kiesewetter, *Bioorg. Med. Chem.*, 2009, **17**, 1486-1493.
189. S. Nimmagadda, M. Pullambhatla, K. Stone, G. Green, Z. M. Bhujwalla and M. G. Pomper, *Cancer Res.*, 2010, **70**, 3935-3944.
190. A. Cabrera, E. Alonzo, E. Sauble, Y. L. Chu, M. C. Linder, D. S. Sato and A. Z. Mason, *Biometals : an international journal on the role of metal ions in biology, biochemistry, and medicine*, 2008, **21**, 525-543.
191. I. D. Weiss, O. Jacobson, D. O. Kiesewetter, J. P. Jacobus, L. P. Szajek, X. Chen and J. M. Farber, *Mol. Imaging Biol.*, 2012, **14**, 106-114.
192. A. Aghanejad, A. R. Jalilian, Y. Fazaeli, B. Alirezapoor, M. Pouladi, D. Beiki, S. Maus and A. Khalaj, *Sci. Pharm.*, 2014, **82**, 29-42.
193. A. R. J. Ayuob Aghanejad, Yousef Fazaeli, Ali Khalaj, *J. Radioanal. Nucl. Chem.*, 2014, **299**, 1635-1644.
194. S. Hatse, K. Princen, E. D. Clercq, M. M. Rosenkilde, T. W. Schwartz, P. E. Hernandez-Abad, R. T. Skerlj, G. J. Bridger and D. Schols, *Biochem. Pharmacol.*, 2005, **70**, 752-761.
195. R. A. De Silva, K. Peyre, M. Pullambhatla, J. J. Fox, M. G. Pomper and S. Nimmagadda, *J. Nucl. Med.*, 2011, **52**, 986-993.
196. S. V. Hartimath, R. Dierckx and E. d. Vries, *Eur. J. Nucl. Med. Mol. Imaging*, 2013, **40**, 570-577.
197. S. V. Hartimath, M. A. Khayum, A. van Waarde, R. A. J. O. Dierckx and E. F. J. de Vries, *Mol. Imaging Biol.*, 2017, **19**, 570-577.
198. A. Khan, G. Nicholson, J. Greenman, L. Madden, G. McRobbie, C. Pannecouque, E. De Clercq, R. Ullom, D. L. Maples, R. D. Maples, J. D. Silversides, T. J. Hubin and S. J. Archibald, *J. Am. Chem. Soc.*, 2009, **131**, 3416-3147.

-
199. R. Smith, D. Huskens, D. Daelemans, R. E. Mewis, C. D. Garcia, A. N. Cain, T. N. C. Freeman, C. Pannecouque, E. De Clercq, D. Schols, T. J. Hubin and S. J. Archibald, *Dalton Trans.*, 2012, **41**, 11369-11377.
200. G. C. Valks, G. McRobbie, E. A. Lewis, T. J. Hubin, T. M. Hunter, P. J. Sadler, C. Pannecouque, E. De Clercq and S. J. Archibald, *J. Med. Chem.*, 2006, **49**, 6162-6165.
201. T. J. Hubin, N. W. Alcock and D. H. Busch, *Acta Cryst. C*, 2000, **56**, 37-39.
202. R. D. Maples, A. N. Cain, B. P. Burke, J. D. Silversides, R. E. Mewis, T. D'Huys, D. Schols, D. P. Linder, S. J. Archibald and T. J. Hubin, *Chem. Eur. J.*, 2016, **22**, 12916-12930.
203. L. E. Woodard, R. A. De Silva, B. B. Azad, A. Lisok, M. Pullambhatla, W. G. Lesniak, R. C. Mease, M. G. Pomper and S. Nimmagadda, *Nucl. Med. Biol.*, 2014, **41**, 552-561.
204. G. J. Bridger, R. T. Skerlj, D. Thornton, S. Padmanabhan, S. A. Martellucci, G. W. Henson, M. J. Abrams, N. Yamamoto and K. D. Vreese, *J. Med. Chem.*, 1995, **38**, 366-378.
205. A. Khan, G. Nicholson, G. McRobbie, J. Greenman, C. Pannecouque, D. Daelemans, D. Schols, E. De Clercq, T. J. Hubin and S. J. Archibald, *Antiviral Res.*, 2009, **82**, 59-60.
206. G. McRobbie, G. C. Valks, C. J. Empson, A. Khan, J. D. Silversides, C. Pannecouque, E. De Clercq, S. G. Fiddy, A. J. Bridgeman, N. A. Young and S. J. Archibald, *Dalton Trans.*, 2007, **43**, 5008-5018.
207. M. Le Baccon, F. Chuburu, L. Toupet, H. Handel, M. Soibinet, I. Dechamps-Olivier, J.-P. Barbier and M. Aplincourt, *New J. Chem.*, 2001, **25**, 1168-1174.
208. B. H. Abdulwahaab, B. P. Burke, J. Domarkas, J. D. Silversides, T. J. Prior and S. J. Archibald, *J. Org. Chem.*, 2016, **81**, 890-898.
209. J. Dessolin, P. Galea, P. Vlieghe, J.-C. Chermann and J.-L. Kraus, *J. Med. Chem.*, 1999, **42**, 229-241.
210. M. Ciampolini, L. Fabbrizzi, A. Perotti, A. Poggi, B. Seghi and F. Zanobini, *Inorg. Chem.*, 1987, **26**, 3527-3533.
211. L. Fabbrizzi, F. Foti, M. Licchelli, P. M. Maccarini, D. Sacchi and M. Zema, *Chem. Eur. J.*, 2002, **8**, 4965-4972.
212. E. H. Wong, G. R. Weisman, D. C. Hill, D. P. Reed, M. E. Rogers, J. S. Condon, M. A. Fagan, J. C. Calabrese, K.-C. Lam, I. A. Guzei and A. L. Rheingold, *J. Am. Chem. Soc.*, 2000, **122**, 10561-10572.
213. O. Demmer, I. Dijkgraaf, M. Schottelius, H. J. Wester and H. Kessler, *Org. Lett.*, 2008, **10**, 2015-2018.
214. J. Mungalpara, S. Thiele, O. Eriksen, J. Eksteen, M. M. Rosenkilde and J. Vabeno, *J. Med. Chem.*, 2012, **55**, 10287-10291.
215. P. Gomez-Martinez, M. Dessolin, F. Guibe and F. Albericio, *Perkin Trans.*, 1999, **20**, 2871-2874.
216. M. Sakaitani and Y. Ohfuné, *J. Org. Chem.*, 1990, **21**, 870-876.
217. T. Fukuyama, C.-K. Jow and M. Cheung, *Tetrahedron Lett.*, 1995, **36**, 6373-6374.
218. E. Biron, J. Chatterjee and H. Kessler, *J. Pept. Sci.*, 2006, **12**, 213-219.
219. G. R. Weisman, M. E. Rogers, E. H. Wong, J. P. Jasinski and E. S. Paight, *J. Am. Chem. Soc.*, 1990, **112**, 8604-8605.
220. T. J. Hubin, J. M. McCormick, N. W. Alcock, H. J. Clase and D. H. Busch, *Inorg. Chem.*, 1999, **38**, 4435-4446.
221. W. Niu, E. H. Wong, G. R. Weisman, L. N. Zakharov, C. D. Incarvito and A. L. Rheingold, *Polyhedron*, 2004, **23**, 1019-1025.
222. X. Sun, M. Wuest, G. R. Weisman, E. H. Wong, D. P. Reed, C. A. Boswell, R. Motekaitis, A. E. Martell, M. J. Welch and C. J. Anderson, *J. Med. Chem.*, 2002, **45**, 469-477.
223. K. J. Heroux, K. S. Woodin, D. J. Tranchemontagne, P. C. B. Widger, E. Southwick, E. H. Wong, G. R. Weisman, S. A. Tomellini, T. J. Wadas, C. J. Anderson, S. Kassel, J. A. Golen and A. L. Rheingold, *Dalton Trans.*, 2007, **21**, 2150-2162.
224. E. A. Lewis, R. W. Boyle and S. J. Archibald, *Chem. Commun*, 2004, **19**, 2212-2213.

225. T. M. Jones-Wilson, K. A. Deal, C. J. Anderson, D. W. McCarthy, Z. Kovacs, R. J. Motekaitis, A. D. Sherry, A. E. Martell and M. J. Welch, *Nucl. Med. Biol.*, 1998, **25**, 523-530.
226. T. J. Wadas and C. J. Anderson, *Nat. Protocols*, 2007, **1**, 3062-3068.
227. C. A. Boswell, C. A. S. Regino, K. E. Baidoo, K. J. Wong, A. Bumb, H. Xu, D. E. Milenic, J. A. Kelley, C. C. Lai and M. W. Brechbiel, *Bioconjugate Chem.*, 2008, **19**, 1476-1484.
228. J. E. Sprague, Y. Peng, A. L. Fiamengo, K. S. Woodin, E. A. Southwick, G. R. Weisman, E. H. Wong, J. A. Golen, A. L. Rheingold and C. J. Anderson, *J. Med. Chem.*, 2007, **50**, 2527-2535.
229. R. Ferdani, D. J. Stigers, A. L. Fiamengo, L. Wei, B. T. Y. Li, J. A. Golen, A. L. Rheingold, G. R. Weisman, E. H. Wong and C. J. Anderson, *Dalton Trans.*, 2012, **41**, 1938-1950.
230. O. Demmer, E. Gourni, U. Schumacher, H. Kessler and H.-J. Wester, *Chem. Med. Chem.*, 2011, **6**, 1789-1791.
231. C. S. Miranda, PhD thesis, University of Hull, 2018, ch. 1-3, pp. 1-63.
232. S. R. Banerjee and M. G. Pomper, *Appl. Radiat. Isot.*, 2013, **76**, 2-13.
233. I. Velikyan, *Theranostics*, 2014, **4**, 47-80.
234. M. Hofmann, H. Maecke, A. Börner, E. Weckesser, P. Schöffski, M. Oei, J. Schumacher, M. Henze, A. Heppeler and G. Meyer, *Eur. J. Nuc. Med.*, 2001, **28**, 1751-1757.
235. M. Gabriel, C. Decristoforo, D. Kendler, G. Dobrozemsky, D. Heute, C. Uprimny, P. Kovacs, E. Von Guggenberg, R. Bale and I. J. Virgolini, *J. Nucl. Med.*, 2007, **48**, 508-518.
236. T. Jindal, A. Kumar, B. Venkitaraman, R. Dutta and R. Kumar, *The Korean journal of internal medicine*, 2010, **25**, 386-391.
237. I. Velikyan, A. Sundin, J. Sörensen, M. Lubberink, M. Sandström, U. Garske-Román, H. Lundqvist, D. Granberg and B. Eriksson, *J. Nucl. Med.*, 2014, **55**, 204-210.
238. Z. Wang, M. Zhang, L. Wang, S. Wang, F. Kang, G. Li, O. Jacobson, G. Niu, W. Yang, J. Wang and X. Chen, *Theranostics*, 2015, **5**, 882-889.
239. M. Mitterhauser, S. Toegel, W. Wadsak, R. R. Lanzenberger, L.-K. Mien, C. Kuntner, T. Wanek, H. Eidherr, D. E. Ettliger, H. Viernstein, R. Kluger, R. Dudczak and K. Kletter, *Nucl. Med. Biol.*, 2007, **34**, 391-397.
240. V. Beylergil, P. G. Morris, P. M. Smith-Jones, S. Modi, D. Solit, C. A. Hudis, Y. Lu, J. O'Donoghue, S. K. Lyashchenko, J. A. Carrasquillo, S. M. Larson and T. J. Akhurst, *Nucl. Med. Commun.*, 2013, **34**, 1157-1165.
241. M. Eiber, T. Maurer, M. Souvatzoglou, A. J. Beer, A. Ruffani, B. Haller, F.-P. Graner, H. Kübler, U. Haberhorn, M. Eisenhut, H.-J. Wester, J. E. Gschwend and M. Schwaiger, *J. Nucl. Med.*, 2015, **56**, 668-674.
242. S. Poty, E. Gourni, P. Désogère, F. Boschetti, C. Goze, H. R. Maecke and F. Denat, *Bioconjugate Chem.*, 2016, **27**, 752-761.
243. H. C. Kolb, M. G. Finn and K. B. Sharpless, *Angew. Chem., Int. Ed. Engl.*, 2001, **40**, 2004-2021.
244. J. C. Knight and B. Cornelissen, *Am. J. Nucl. Med. Mol. Imaging*, 2014, **4**, 96-113.
245. E. M. Sletten and C. R. Bertozzi, *Acc. Chem. Res.*, 2011, **44**, 666-676.
246. R. V. L. J. R. A. Carboni, *J. Am. Chem. Soc.*, 1959, **81**, 4342-4346.
247. L. Carroll, H. L. Evans, E. O. Aboagye and A. C. Spivey, *Org. Biomol. Chem.*, 2013, **11**, 5772-5781.
248. M. L. Blackman, M. Royzen and J. M. Fox, *J. Am. Chem. Soc.*, 2008, **130**, 13518-13519.
249. M. Royzen, G. P. A. Yap and J. M. Fox, *J. Am. Chem. Soc.*, 2008, **130**, 3760-3761.
250. P. Thirumurugan, D. Matosiuk and K. Jozwiak, *Chem. Rev.*, 2013, **113**, 4905-4979.
251. M. S. J. Schoch, A. Samanta, M. Wiessler, A. Jachke., *Bioconjugate Chem.*, 2012, **23**, 1382-1386.
252. R. Selvaraj, B. Giglio, S. Liu, H. Wang, M. Wang, H. Yuan, S. R. Chintala, L.-P. Yap, P. S. Conti, J. M. Fox and Z. Li, *Bioconjugate Chem.*, 2015, **26**, 435-442.
253. R. Rossin, S. M. van den Bosch, W. ten Hoeve, M. Carvelli, R. M. Versteegen, J. Lub and M. S. Robillard, *Bioconjugate Chem.*, 2013, **24**, 1210-1217.

-
254. P. R. V. R. Rossin, S. M van den Bosch, C. M. Vulders, I. Verel, J. Lub, M. S. Robillard, *Angew. Chem., Int. Ed. Engl.*, 2010, **49**, 3375-3378.
255. R. A. Kolinski, *Pol. J. Chem.*, 1995, **69**, 1039-1045.
256. L. Lukešová, J. Ludvík, I. Císařová and P. Štěpnička, *Collection of Czechoslovak Chemical Communications*, 2000, **65**, 1897-1910.
257. R. Smith, PhD thesis, University of Hull, 2012, ch. 1-4, pp. 1-123.
258. A. Hackling, R. Ghosh, S. Perachon, A. Mann, H.-D. Höltje, C. G. Wermuth, J.-C. Schwartz, W. Sippl, P. Sokoloff and H. Stark, *J. Med. Chem.*, 2003, **46**, 3883-3899.
259. K.-P. Eisenwiener, P. Powell and H. R. Mäcke, *Bioorg. Med. Chem. Letts.*, 2000, **10**, 2133-2135.
260. C. Bernhard, M. Moreau, D. Lhenry, C. Goze, F. Boschetti, Y. Rousselin, F. Brunotte and F. Denat, *Chem. Eur. J.*, 2012, **18**, 7834-7841.
261. M. Moreau, O. Raguin, J.-M. Vrigneaud, B. Collin, C. Bernhard, X. Tizon, F. Boschetti, O. Duchamp, F. Brunotte and F. Denat, *Bioconjugate Chem.*, 2012, **23**, 1181-1188.
262. K. Nicholson, PhD thesis, University of Hull, 2014, ch. 1-3, pp. 1-93.
263. T. M. Hunter, S. J. Paisey, H.-s. Park, L. Cleghorn, A. Parkin, S. Parsons and P. J. Sadler, *J. Inorg. Biochem.*, 2004, **98**, 713-719.
264. Z. Varasteh, B. Mitran, U. Rosenström, I. Velikyan, M. Rosestedt, G. Lindeberg, J. Sörensen, M. Larhed, V. Tolmachev and A. Orlova, *Nucl. Med. Biol.*, **42**, 446-454.
265. D. J. Berry, Y. M. Ma, J. R. Ballinger, R. Tavare, A. Koers, K. Sunassee, T. Zhou, S. Nawaz, G. E. D. Mullen, R. C. Hider and P. J. Blower, *Chem. Commun*, 2011, **47**, 7068-7070.
266. J. Notni, K. Pohle and H.-J. Wester, *EJNMMI Res.*, 2012, **2**, 28-28.
267. W. R. Harris and V. L. Pecoraro, *Biochem.*, 1983, **22**, 292-299.
268. M. T. Ma, O. C. Neels, D. Denoyer, P. Roselt, J. A. Karas, D. B. Scanlon, J. M. White, R. J. Hicks and P. S. Donnelly, *Bioconjugate Chem.*, 2011, **22**, 2093-2103.
269. R. Cusnir, C. Imberti, R. C. Hider, P. J. Blower and M. T. Ma, *Int. J. Mol. Sci.*, 2017, **18**, 1-23.
270. K. Philipp-Abbrederis, K. Herrmann, M. Schottelius, M. Eiber, C. Gerngross, E. Pietschmann, K. Luckerath, K. Franke, M. Rudelius, S. Knop, K. Gotze, K. Schwamborn, S. Steidle, A. Beer, C. Peschel, H. Einsele, A. Buck, M. Schwaiger, H. J. Wester and U. Keller, *Blood*, 2014, **124**, 3-9.
271. V. Kumar and D. K. Boddeti, in *Theranostics, Gallium-68, and Other Radionuclides*, Springer, 2013, pp. 189-219.
272. P. G. M. Wuts and T. W. Greene, *Greene's Protective Groups in Organic Synthesis*, Wiley, 2006.
273. C. Bailly, C. Bodet-Milin, C. Rousseau, A. Faivre-Chauvet, F. Kraeber-Bodéré and J. Barbet, *EJNMMI Radiopharmacy and Chemistry*, 2017, **2**, 6-14.
274. H. L. Evans, Q. D. Nguyen, L. S. Carroll, M. Kaliszczak, F. J. Twyman, A. C. Spivey and E. O. Aboagye, *Chem. Commun*, 2014, **50**, 9557-9560.
275. J. P. Meyer, J. L. Houghton, P. Kozlowski, D. Abdel-Atti, T. Reiner, N. V. K. Pillarsetty, W. W. Scholz, B. M. Zeglis and J. S. Lewis, *Bioconjugate Chem.*, 2016, **27**, 298-301.
276. S. Heskamp, R. Hernandez, J. D. M. Molkenboer-Kuenen, M. Essler, F. Bruchertseifer, A. Morgenstern, E. J. Steenbergen, W. B. Cai, C. Seidl, W. J. McBride, D. M. Goldenberg and O. C. Boerman, *J. Nucl. Med.*, 2017, **58**, 926-933.
277. M. F. Debets, J. C. M. van Hest and F. Rutjes, *Org. Biomol. Chem.*, 2013, **11**, 6439-6455.
278. A. Vito, H. Alarabi, S. Czorny, O. Beiraghi, J. Kent, N. Janzen, A. R. Genady, S. A. Alkarmi, S. Rathmann, Z. Naperstkow, M. Blacker, L. Llano, P. J. Berti and J. F. Valliant, *Plos One*, 2016, **11**, 1-15.
279. R. Selvaraj, S. Liu, M. Hassink, C.-w. Huang, L.-p. Yap, R. Park, J. M. Fox, Z. Li and P. S. Conti, *Bioorg. Med. Chem. Letts.*, 2011, **21**, 5011-5014.
280. A. Darko, S. Wallace, O. Dmitrenko, M. M. Machovina, R. A. Mehl, J. W. Chin and J. M. Fox, *Chem. Sci.*, 2014, **5**, 3770-3776.

-
281. J. P. Meyer, P. Adumeau, J. S. Lewis and B. M. Zeglis, *Bioconjugate Chem.*, 2016, **27**, 2791-2807.
282. M. Patra, K. Zarschler, H.-J. Pietzsch, H. Stephan and G. Gasser, *Chem. Soc. Rev.*, 2016, **45**, 6415-6431.
283. J. D. Young, V. Abbate, C. Imberti, L. K. Meszaros, M. T. Ma, S. Y. A. Terry, R. C. Hider, G. E. Mullen and P. J. Blower, *J. Nucl. Med.*, 2017, **58**, 1270-1277.
284. D. Lobeek, S. Terry, G. Franssen, M. Rijpkema, M. Ma, H. Wester, C. Decristoforo, W. Oyen and O. Boerman, *J. Nucl. Med.*, 2017, **58**, 920-927.
285. C. Imberti, S. Y. A. Terry, C. Cullinane, F. Clarke, G. H. Cornish, N. K. Ramakrishnan, P. Roselt, A. P. Cope, R. J. Hicks, P. J. Blower and M. T. Ma, *Bioconjugate Chem.*, 2017, **28**, 481-495.
286. M. T. Ma, C. Cullinane, C. Imberti, J. Baguna Torres, S. Y. A. Terry, P. Roselt, R. J. Hicks and P. J. Blower, *Bioconjugate Chem.*, 2016, **27**, 309-318.
287. P. G. M. Wuts, *Greene's Protective Groups in Organic Synthesis*, Wiley, 2014, ch. 5, pp. 533-646.
288. M. T. Ma, C. Cullinane, C. Imberti, J. Baguña Torres, S. Y. A. Terry, P. Roselt, R. J. Hicks and P. J. Blower, *Bioconjugate Chem.*, 2015, **27**, 309-318.
289. E. L. Cole, M. N. Stewart, R. Littich, R. Hoareau and P. J. H. Scott, *Curr. Top. Med. Chem.*, 2014, **14**, 875-900.
290. K. Chansaenpak, B. Vabre and F. P. Gabbai, *Chem. Soc. Rev.*, 2016, **45**, 954-971.
291. O. Jacobson, D. O. Kiesewetter and X. Y. Chen, *Bioconjugate Chem.*, 2015, **26**, 1-18.
292. G. E. Smith, H. L. Sladen, S. C. G. Biagini and P. J. Blower, *Dalton Trans.*, 2011, **40**, 6196-6205.
293. Y.-R. Luo, *Comprehensive handbook of chemical bond energies*, CRC press, 2007.
294. W. J. McBride, R. M. Sharkey and D. M. Goldenberg, *EJNMMI Res.*, 2013, **3**.
295. W. J. McBride, R. M. Sharkey, H. Karacay, C. A. D'Souza, E. A. Rossi, P. Laverman, C. H. Chang, O. C. Boerman and D. M. Goldenberg, *J. Nucl. Med.*, 2009, **50**, 991-998.
296. P. Laverman, W. J. McBride, R. M. Sharkey, A. Eek, L. Joosten, W. J. Oyen, D. M. Goldenberg and O. C. Boerman, *J. Nucl. Med.*, 2010, **51**, 454-461.
297. C. A. D'Souza, W. J. McBride, R. M. Sharkey, L. J. Todaro and D. M. Goldenberg, *Bioconjugate Chem.*, 2011, **22**, 1793-1803.
298. D. Shetty, S. Y. Choi, J. M. Jeong, J. Y. Lee, L. Hoigebazar, Y.-S. Lee, D. S. Lee, J.-K. Chung, M. C. Lee and Y. K. Chung, *Chem. Commun*, 2011, **47**, 9732-9734.
299. W. J. McBride, C. A. D'Souza, R. M. Sharkey and D. M. Goldenberg, *Appl. Radiat. Isot.*, 2012, **70**, 200-204.
300. C. Da Pieve, L. Allott, C. D. Martins, A. Vardon, D. M. Ciobota, G. Kramer-Marek and G. Smith, *Bioconjugate Chem.*, 2016, **27**, 1839-1849.
301. H. J. Chen, G. Niu, H. Wu and X. Y. Chen, *Theranostics*, 2016, **6**, 78-92.
302. J. L. Zeng, J. Wang and J. A. Ma, *Bioconjugate Chem.*, 2015, **26**, 1000-1003.
303. Q. Xu, C. Zhu, Y. P. Xu, D. H. Pan, P. Liu, R. L. Yang, L. Z. Wang, F. Chen, X. C. Sun, S. N. Luo and M. Yang, *J. Drug Targ.*, 2015, **23**, 813-820.
304. Q. H. Liu, D. H. Pan, C. Cheng, D. Z. Zhang, A. Y. Zhang, L. Z. Wang, H. D. Jiang, T. Wang, H. R. Liu, Y. P. Xu, R. L. Yang, F. Chen, M. Yang and C. J. Zuo, *PLoS One*, 2015, **10**.
305. G. Carlucci, A. Kuipers, H. J. K. Ananias, D. D. Faria, R. Dierckx, W. Helfrich, R. Rink, G. N. Moll, I. J. de Jong and P. H. Elsinga, *Peptides*, 2015, **67**, 45-54.
306. R. Bhalla, W. Levason, S. K. Luthra, G. McRobbie, G. Sanderson and G. Reid, *Chem. Eur. J.*, 2015, **21**, 4688-4694.
307. D. H. Pan, Y. J. Yan, R. H. Yang, Y. P. Xu, F. Chen, L. Z. Wang, S. N. Luo and M. Yang, *Contrast Media Mol. Imaging*, 2014, **9**, 342-348.
308. J. X. Guo, L. X. Lang, S. Hu, N. Guo, L. Zhu, Z. C. Sun, Y. Ma, D. O. Kiesewetter, G. Niu, Q. G. Xie and X. Y. Chen, *Mol. Imaging Biol.*, 2014, **16**, 274-283.

-
309. K. L. S. Chatalic, G. M. Franssen, W. M. van Weerden, W. J. McBride, P. Laverman, E. de Blois, B. Hajjaj, L. Brunel, D. M. Goldenberg, J. A. Fehrentz, J. Martinez, O. C. Boerman and M. de Jong, *J. Nucl. Med.*, 2014, **55**, 2050-2056.
310. D. O. Kiesewetter, N. Guo, J. X. Guo, H. K. Gao, L. Zhu, Y. Ma, G. Niu and X. Y. Chen, *Theranostics*, 2012, **2**, 999-1009.
311. W. Wan, N. Guo, D. Pan, C. Yu, Y. Weng, S. Luo, H. Ding, Y. Xu, L. Wang, L. Lang, Q. Xie, M. Yang and X. Chen, *J. Nucl. Med.*, 2013, **54**, 691-698.
312. X. F. Yan, G. Niu, Z. Wang, X. Y. Yang, D. O. Kiesewetter, O. Jacobson, B. Z. Shen and X. Y. Chen, *Mol. Imaging Biol.*, 2016, **18**, 135-142.
313. A. Poschenrieder, T. Osl, M. Schottelius, F. Hoffmann, M. Wirtz, M. Schwaiger and H.-J. Wester, *Tomography*, 2016, **2**, 85-93.
314. S. L. Liu, H. G. Liu, H. Jiang, Y. D. Xu, H. Zhang and Z. Cheng, *Eur. J. Nucl. Med. Mol. Imaging*, 2011, **38**, 1732-1741.
315. F. Cleeren, J. Lecina, E. M. F. Billaud, M. Ahamed, A. Verbruggen and G. M. Bormans, *Bioconjugate Chem.*, 2016, **27**, 790-798.
316. S. Liu, H. Liu, H. Jiang, Y. Xu, H. Zhang and Z. Cheng, *Eur. J. Nucl. Med. Mol. Imaging*, 2011, **38**, 1732-1741.
317. R. A. Yokel, *Coord. Chem. Rev.*, 2002, **228**, 97-113.
318. P. Laverman, C. A. D'Souza, A. Eek, W. J. McBride, R. M. Sharkey, W. J. G. Oyen, D. M. Goldenberg and O. C. Boerman, *Tumor Biol.*, 2012, **33**, 427-434.
319. K. S. Rajan, S. Mainer, N. L. Rajan and J. M. Davis, *J. Inorg. Biochem.*, 1981, **14**, 339-350.
320. M. Lipowska, J. Klenc, D. Shetty, J. A. Nye, H. Shim and A. T. Taylor, *Nucl. Med. Biol.*, 2014, **41**, 248-253.
321. S. E. Stanton, J. F. Eary, E. A. Marzbani, D. Mankoff, L. G. Salazar, D. Higgins, J. Childs, J. Reichow, Y. Dang and M. L. Disis, *J. Immunother. Cancer*, 2016, **4**, 27-33.
322. S. R. Cherry, *Semin. Nucl. Med.*, 2009, **39**, 348-353.
323. H. Shanoudy, P. Raggi, G. A. Beller, A. Soliman, E. G. Ammermann, R. J. Kastner and D. D. Watson, *J. Am. Coll. Cardiol.*, 1998, **31**, 331-337.
324. K. Ogasawara, A. Ogawa, M. Ezura, H. Konno, M. Suzuki and T. Yoshimoto, *Am. J. Neuroradiol.*, 2001, **22**, 48-54.
325. I. Ilias, C. Divgi and K. Pacak, *Semin. Nucl. Med.*, 2011, **41**, 364-368.
326. S. Boyd, R. Nour, R. Quinn, E. McKay and S. Butler, *Eur. J. Nucl. Med. Mol. Imaging*, 1993, **20**, 201-206.
327. J. Kuil, T. Buckle, J. Oldenburg, H. Yuan, L. Josephson and F. W. B. van Leeuwen, *Mol. Pharm.*, 2011, **8**, 2444-2453.
328. J. Kuil, H. Yuan, T. Buckle, S. Oishi, N. Fujii, L. Josephson and F. W. B. van Leeuwen, *Bioconjugate Chem.*, 2011, **22**, 859-864.
329. W. Gan, L. Wei, J. Petryk, C. Gaudet, M. Kamkar, Y. Duan and T. Ruddy, *J. Nucl. Med.*, 2015, **56**, 205-212.
330. T. Buckle, N. S. van Berg, J. Kuil, A. Bunschoten, J. Oldenburg, A. D. Borowsky, J. Wesseling, R. Masada, S. Oishi, N. Fujii and F. W. van Leeuwen, *Am. J. Nucl. Med. Mol. Imaging*, 2012, **2**, 99-109.
331. A. Aghanejad, A. R. Jalilian, Y. Fazaeli, B. Alirezapoor, M. Pouladi, D. Beiki, S. Maus and A. Khalaj, *Sci. Pharm.*, 2014, **82**, 29-42.
332. S. V. Hartimath, U. M. Domanska, A. M. E. Walenkamp, D. Rudi A.J.O and E. F. J. de Vries, *Nucl. Med. Biol.*, 2013, **40**, 507-517.
333. T. Perera, P. A. Marzilli, F. R. Fronczek and L. G. Marzilli, *Inorg. Chem.*, 2010, **49**, 2123-2131.
334. J. Klenc, M. Lipowska, A. T. Taylor and L. G. Marzilli, *Eur. J. Inorg. Chem.*, 2012, **2012**, 325-339.
335. U. Abram and R. Alberto, *J. Braz. Chem. Soc.*, 2006, **17**, 1486-1500.
336. K. Ogawa and K. Washiyama, *Curr. Med. Chem.*, 2012, **19**, 3290-3300.

-
337. F. Liberal, A. A. S. Tavares and J. Tavares, *Appl. Radiat. Isot.*, 2016, **110**, 87-99.
338. G. Rubini, A. Nicoletti, D. Rubini and A. N. Asabella, *Cancer Biother. Radiopharm.*, 2014, **29**, 1-11.
339. J. H. Turner, *Ann. Nucl. Med.*, 2012, **26**, 289-297.
340. R. Schibli and A. P. Schubiger, *Eur. J. Nucl. Med. Mol. Imaging*, 2002, **29**, 1529-1542.
341. R. T. M. de Rosales, C. Finucane, J. Foster, S. J. Mather and P. J. Blower, *Bioconjugate Chem.*, 2010, **21**, 811-815.
342. R. Alberto, R. Schibli, A. Egli, A. P. Schubiger, U. Abram and T. A. Kaden, *J. Am. Chem. Soc.*, 1998, **120**, 7987-7988.
343. R. Alberto, R. Schibli, A. P. Schubiger, U. Abram, H. J. Pietzsch and B. Johannsen, *J. Am. Chem. Soc.*, 1999, **121**, 6076-6077.
344. I. Zolle, *Technetium-99m Pharmaceuticals: Preparation and Quality Control in Nuclear Medicine*, Springer Berlin Heidelberg, 2007, ch. 2, pp. 7-27.
345. A. Egli, R. Alberto, L. Tannahill and R. Schibli, *J. Nucl. Med.*, 1999, **40**, 1913-1917.
346. R. Alberto, J. Kyong Pak, D. van Staveren, S. Mundwiler and P. Benny, *J. Pept. Sci.*, 2004, **76**, 324-333.
347. H. J. Pietzsch, A. Gupta, M. Reisgys, A. Drews, S. Seifert, R. Syhre, H. Spies, R. Alberto, U. Abram, P. A. Schubiger and B. Johannsen, *Bioconjugate Chem.*, 2000, **11**, 414-424.
348. S. Alves, A. Paulo, J. D. G. Correia, L. Gano, C. J. Smith, T. J. Hoffman and I. Santos, *Bioconjugate Chem.*, 2005, **16**, 438-449.
349. S. Imstepf, V. Pierroz, P. Raposinho, M. Felber, T. Fox, C. Fernandes, G. Gasser, I. R. Santos and R. Alberto, *Dalton Trans.*, 2016, **45**, 13025-13033.
350. B. B. Kasten, X. Ma, K. Cheng, L. Bu, W. S. Slocumb, T. R. Hayes, S. Trabue, Z. Cheng and P. D. Benny, *Bioconjugate Chem.*, 2016, **27**, 130-142.
351. R. R. Conry and J. M. Mayer, *Inorg. Chem.*, 1990, **29**, 4862-4867.
352. J. Y. K. Cheng, K.-K. Cheung, M. C. W. Chan, K.-Y. Wong and C.-M. Che, *Inorg. Chim. Acta*, 1998, **272**, 176-187.
353. F. Wai-Hong, C. Wing-Chi, P. Shie-Ming and C. Chi-Ming, *Polyhedron*, 1995, **14**, 1791-1794.
354. C. Pomp and K. Wieghardt, *Polyhedron*, 1988, **7**, 2537-2542.
355. G. Boehm, K. Wieghardt, B. Nuber and J. Weiss, *Inorg. Chem.*, 1991, **30**, 3464-3476.
356. K. Wieghardt, C. Pomp, B. Nuber and J. Weiss, *Inorg. Chem.*, 1986, **25**, 1659-1661.
357. H. Vanbilloen, K. Eraets, N. Evens, C. Terwinghe, D. Rattat, G. Bormans, L. Mortelmans and A. Verbruggen, *J. Label. Compd. Radiopharm.*, 2005, **48**, 1003-1011.
358. R. Alberto, W. A. Herrmann, P. Kiprof and F. Baumgartner, *Inorg. Chem.*, 1992, **31**, 895-899.
359. H. Braband, *CHIMIA International Journal for Chemistry*, 2011, **65**, 776-781.
360. H. Braband and U. Abram, *Inorg. Chem.*, 2006, **45**, 6589-6591.
361. H. Braband, Y. Tooyama, T. Fox, R. Simms, J. Forbes, J. F. Valliant and R. Alberto, *Chem. Eur. J.*, 2011, **17**, 12967-12974.
362. H. Braband, S. Imstepf, M. Benz, B. Spingler and R. Alberto, *Inorg. Chem.*, 2012, **51**, 4051-4057.
363. P. Misra, D. Lebeche, H. Ly, M. Schwarzkopf, G. Diaz, R. J. Hajjar, A. D. Schecter and J. V. Frangioni, *J. Nucl. Med.*, 2008, **49**, 963-969.
364. P. Fu, L. Tian, X. Cao, L. Li, P. Xu and C. Zhao, *Mol. Imaging Biol.*, 2016, **18**, 353-359.
365. J. M. Zhang, J. H. Tian, T. R. Li, H. Y. Guo and L. Shen, *Chin. Chem. Lett.*, 2010, **21**, 461-463.
366. D. E. Troutner, J. Simon, A. R. Ketring, W. Volkert and R. A. Holmes, *J. Nucl. Med.*, 1980, **21**, 443-448.
367. A. R. Ketring, D. E. Troutner, T. J. Hoffman, D. K. Stanton, W. A. Volkert and R. A. Holmes, *Int. J. Nucl. Med. Biol.*, 1984, **11**, 113-119.
368. S. A. Zuckman, G. M. Freeman, D. E. Troutner, W. A. Volkert, R. A. Holmes, D. G. Van Derveer and E. K. Barefield, *Inorg. Chem.*, 1981, **20**, 2386-2389.
369. D. Troutner, W. Volkert, J. Simon, A. Ketring and R. Holmes, *J. Nucl. Med.*, 1979, **20**, 641-642.

-
370. W. Volkert, J. Simon, D. Troutner and R. Holmes, *J. Nucl. Med.*, 1980, **21**, 14-15.
371. L. Y. Martin, L. J. DeHayes, L. J. Zompa and D. H. Busch, *J. Am. Chem. Soc.*, 1974, **96**, 4046-4048.
372. A. Marchi, L. Marvelli, M. Cattabriga, R. Rossi, M. Neves, V. Bertolasi and V. Ferretti, *Dalton Trans.*, 1999, 1937-1944.
373. M. Lipowska, H. He, E. Malveaux, X. Xu, L. G. Marzilli and A. Taylor, *J. Nucl. Med.*, 2006, **47**, 1032-1040.
374. G. Liu, S. Dou, J. He, J.-L. Vanderheyden, M. Rusckowski and D. J. Hnatowich, *Bioconjugate Chem.*, 2004, **15**, 1441-1446.
375. J. R. Dilworth and S. J. Parrott, *Chem. Soc. Rev.*, 1998, **27**, 43-55.
376. C. J. Coghlan, E. M. Campi, S. R. Batten, W. R. Jackson and M. T. W. Hearn, *Polyhedron*, 2016, **105**, 246-252.
377. P. Florio, E. M. Campi, M. K. Potdar, W. R. Jackson and M. T. W. Hearn, *Green Chem. Lett. Rev.*, 2012, **5**, 251-254.
378. L. Tjioe, A. Meininger, T. Joshi, L. Spiccia and B. Graham, *Inorg. Chem.*, 2011, **50**, 4327-4339.
379. R. Alberto, A. Egli, U. Abram, K. Hegetschweiler, V. Gramlich and P. A. Schubiger, *Dalton Trans.*, 1994, 2815-2820.
380. K. E. Bullok, M. Dyszlewski, J. L. Prior, C. M. Pica, V. Sharma and D. Piwnica-Worms, *Bioconjugate Chem.*, 2002, **13**, 1226-1237.
381. R. Alberto, K. Ortner, N. Wheatley, R. Schibli and A. P. Schubiger, *J. Am. Chem. Soc.*, 2001, **123**, 3135-3136.
382. O. O. Sogbein, A. E. C. Green and J. F. Valliant, *Inorg. Chem.*, 2005, **44**, 9585-9591.
383. M. Lipowska, J. Klenc, L. G. Marzilli and A. T. Taylor, *J. Nucl. Med.*, 2012, **53**, 1277-1283.
384. G. Mees, R. Dierckx, K. Mertens, S. Vermeire, M. Van Steenkiste, C. Reutelingsperger, Y. D'Asseler, K. Peremans, N. Van Damme and C. Van de Wiele, *J. Nucl. Med.*, 2012, **53**, 464-471.
385. J.-H. Kim, S.-J. Choi and Y.-D. Hong, *J. Radioanal. Nucl. Chem.*, 2012, **292**, 203-209.
386. A. Badar, J. Williams, R. T. M. de Rosales, R. Tavare, F. Kampmeier, P. J. Blower and G. E. D. Mullen, *EJNMMI Res.*, 2014, **4**.
387. P. J. Sadler and A. Tucker, *Eur. J. Biochem.*, 1993, **212**, 811-817.
388. J. R. Cann, R. A. Brown and J. G. Kirkwood, *J. Am. Chem. Soc.*, 1949, **71**, 1609-1614.
389. R. A. Simon and C. H. Jeremy, *Phys. Med. Biol.*, 1997, **42**, 841.
390. K. E. Adams, S. Ke, S. Kwon, F. Liang, Z. Fan, Y. Lu, K. Hirschi, M. E. Mawad, M. A. Barry and E. M. Sevick-Muraca, *J. Biomed. Opt.*, 2007, **12**, 024017-024019.
391. N. Kosaka, M. Ogawa, P. L. Choyke and H. Kobayashi, *Future Oncol.*, 2009, **5**, 1501-1511.
392. M. M. Rosenkilde, L.-O. Gerlach, S. Hatse, R. T. Skerlj, D. Schols, G. J. Bridger and T. W. Schwartz, *J. Biol. Chem.*, 2007, **282**, 27354-27365.
393. N. Fujii, S. Oishi, K. Hiramatsu, T. Araki, S. Ueda, H. Tamamura, A. Otaka, S. Kusano, S. Terakubo, H. Nakashima, J. A. Broach, J. O. Trent, Z.-x. Wang and S. C. Peiper, *Angew. Chem., Int. Ed. Engl.*, 2003, **42**, 3251-3253.
394. S. Nimmagadda, M. Pullambhatla and M. G. Pomper, *J. Nucl. Med.*, 2009, **50**, 1124-1130.
395. A. Dar, P. Goichberg, V. Shinder, A. Kalinkovich, O. Kollet, N. Netzer, R. Margalit, M. Zsak, A. Nagler, I. Hardan, I. Resnick, A. Rot and T. Lapidot, *Nat. Immunol.*, 2005, **6**, 1038-1046.
396. O. Kollet, A. Dar, S. Shivtiel, A. Kalinkovich, K. Lapid, Y. Sztainberg, M. Tesio, R. M. Samstein, P. Goichberg, A. Spiegel, A. Elson and T. Lapidot, *Nat. Med.*, 2006, **12**, 657-664.
397. M. Meincke, S. Tiwari, K. Hattermann, H. Kalthoff and R. Mentlein, *Clin. Exp. Metastasis*, 2011, **28**, 713-720.
398. K. E. Luker, M. Gupta, J. M. Steele, B. R. Foerster and G. D. Luker, *Neoplasia (New York, N.Y.)*, 2009, **11**, 1022-1035.

-
399. S. Oishi, R. Masuda, B. Evans, S. Ueda, Y. Goto, H. Ohno, A. Hirasawa, G. Tsujimoto, Z. X. Wang, S. C. Peiper, T. Naito, E. Kodama, M. Matsuoka and N. Fujii, *Chem. Bio. Chem.*, 2008, **9**, 1154-1158.
400. N. S. van den Berg, T. Buckle, J. Kuil, J. Wesseling and F. W. B. van Leeuwen, *Transl. Oncol.*, 2011, **4**, 234-240.
401. W. Nomura, Y. Tanabe, H. Tsutsumi, T. Tanaka, K. Ohba, N. Yamamoto and H. Tamamura, *Bioconjugate Chem.*, 2008, **19**, 1917-1920.
402. K. Nishizawa, H. Nishiyama, S. Oishi, N. Tanahara, H. Kotani, Y. Mikami, Y. Toda, B. J. Evans, S. C. Peiper, R. Saito, J. Watanabe, N. Fujii and O. Ogawa, *Int. J. Cancer*, 2010, **127**, 1180-1187.
403. Y. L. Yang, Q. H. Zhang, M. Gao, X. H. Yang, Z. W. Huang and J. An, *Biochem.*, 2014, **53**, 4881-4883.
404. L. Albertazzi, M. Serresi, A. Albanese and F. Beltram, *Mol. Pharm.*, 2010, **7**, 680-688.
405. T. Tanaka, W. Nomura, T. Narumi, A. Masuda and H. Tamamura, *J. Am. Chem. Soc.*, 2010, **132**, 15899-15901.
406. H. L. Handl, R. Sankaranarayanan, J. S. Josan, J. Vagner, E. A. Mash, R. J. Gillies and V. J. Hruby, *Bioconjugate Chem.*, 2007, **18**, 1101-1109.
407. O. Tietz, N. Kamaly, G. Smith, E. Shamsaei, K. K. Bhakoo, N. J. Long and E. O. Aboagye, *Am. J. Nucl. Med. Mol. Imaging*, 2013, **3**, 372-383.
408. W. Nomura, H. Aikawa, S. Taketomi, M. Tanabe, T. Mizuguchi and H. Tamamura, *Bioorg. Med. Chem.*, 2015, **23**, 6967-6973.
409. S. Santagata, L. Portella, M. Napolitano, A. Greco, C. D'Alterio, M. V. Barone, A. Luciano, M. Gramanzini, L. Auletta, C. Arra, A. Zannetti and S. Scala, *Sci. Rep.*, 2017, **7**, 1-9.
410. L. Portella, R. Vitale, S. De Luca, C. D'Alterio, C. Ieranò, M. Napolitano, A. Riccio, M. N. Polimeno, L. Monfregola, A. Barbieri, A. Luciano, A. Ciarmiello, C. Arra, G. Castello, P. Amodeo and S. Scala, *PLOS ONE*, 2013, **8**, 1-11.
411. K. Kuder and K. Kiec-Kononowicz, *Curr. Med. Chem.*, 2008, **15**, 2132-2143.
412. U. S. Eggert and T. J. Mitchison, *Curr. Opin. Chem. Biol.*, 2006, **10**, 232-237.
413. L. D. Lavis and R. T. Raines, *ACS Chem. Biol.*, 2008, **3**, 142-155.
414. D. Oltmanns, S. Zitzmann-Kolbe, A. Mueller, U. Bauder-Wuest, M. Schaefer, M. Eder, U. Haberkorn and M. Eisenhut, *Bioconjugate Chem.*, 2011, **22**, 2611-2624.
415. A. Khan, J. D. Silversides, L. Madden, J. Greenman and S. J. Archibald, *Chem. Commun*, 2007, **4**, 416-418.
416. J. C. Knight, A. J. Hallett, A. Brancale, S. J. Paisey, R. W. E. Clarkson and P. G. Edwards, *Chem. Bio. Chem.*, 2011, **12**, 2692-2698.
417. R. Sjöback, J. Nygren and M. Kubista, *Spectrochim. Acta Mol. Biomol. Spectrosc.*, 1995, **51**, 7-21.
418. M. M. Martin and L. Lindqvist, *J. Lumin.*, 1975, **10**, 381-390.
419. N. Klonis and W. H. Sawyer, *J. Fluoresc.*, 1996, **6**, 147-157.
420. Q. T. Nguyen and R. Y. Tsien, *Nat. Rev. Cancer*, 2013, **13**, 653-662.
421. H. J. Wester, U. Keller, M. Schottelius, A. Beer, K. Philipp-Abbrederis, F. Hoffmann, J. Simecek, C. Gerngross, M. Lassmann, K. Herrmann, N. Pellegata, M. Rudelius, H. Kessler and M. Schwaiger, *Theranostics*, 2015, **5**, 618-630.
422. K. Herrmann, C. Lapa, H. J. Wester, M. Schottelius, C. Schiepers and U. Eberlein, *J. Nucl. Med.*, 2015, **56**, 410-416.
423. K. Philipp-Abbrederis, K. Herrmann, S. Knop, M. Schottelius, M. Eiber and K. Luckerath, *EMBO Mol. Med.*, 2015, **7**, 477-487.
424. C. Lapa, K. Luckerath, M. Rudelius, J. S. Schmid, A. Schoene and A. Schirbel, *Oncotarget.*, 2016, **7**, 9288-9295.
425. S. L. Gibbs, *Quant. Imaging Med. Surg.*, 2012, **2**, 177-187.
426. S. Gioux, H. S. Choi and J. V. Frangioni, *Mol. Image*, 2010, **9**, 237-255.
427. G. Ulrich, R. Ziessel and A. Harriman, *Angew. Chem., Int. Ed. Engl.*, 2008, **47**, 1184-1201.

-
428. N. Boens, V. Leen and W. Dehaen, *Chem. Soc. Rev.*, 2012, **41**, 1130-1172.
429. M. H. Y. Cheng, H. Savoie, F. Bryden and R. W. Boyle, *Photochem. Photobiol. Sci.*, 2017, **16**, 1260-1267.
430. M. Zevon, V. Ganapathy, H. Kantamneni, M. Mingozzi, P. Kim, D. Adler, Y. Sheng, M. C. Tan, M. Pierce, R. E. Riman, C. M. Roth and P. V. Moghe, *Small*, 2015, **11**, 6347-6357.
431. G. Fan, L. Yang and Z. Chen, *Front. Chem. Sci. Eng.*, 2014, **8**, 405-417.
432. A. Kamkaew and K. Burgess, *Chem. Commun*, 2015, **51**, 10664-10667.
433. L. Liang and D. Astruc, *Coord. Chem. Rev.*, 2011, **255**, 2933-2945.
434. E. J. Keliher, J. A. Klubnick, T. Reiner, R. Mazitschek and R. Weissleder, *Chem. Med. Chem.*, 2014, **9**, 1368-1373.
435. N. Kondo, T. Temma, J. Deguchi, K. Sano, M. Ono and H. Saji, *J. Control. Release*, 2015, **220**, 476-483.
436. Z. Li, T.-P. Lin, S. Liu, C.-W. Huang, T. W. Hudnall, F. P. Gabbai and P. S. Conti, *Chem. Commun*, 2011, **47**, 9324-9326.
437. S. Liu, T.-P. Lin, D. Li, L. Leamer, H. Shan, Z. Li, F. P. Gabbai and P. S. Conti, *Theranostics*, 2013, **3**, 181-189.
438. A. Al-Zirgani, PhD Thesis, University Of Hull, 2016, ch. 5.